

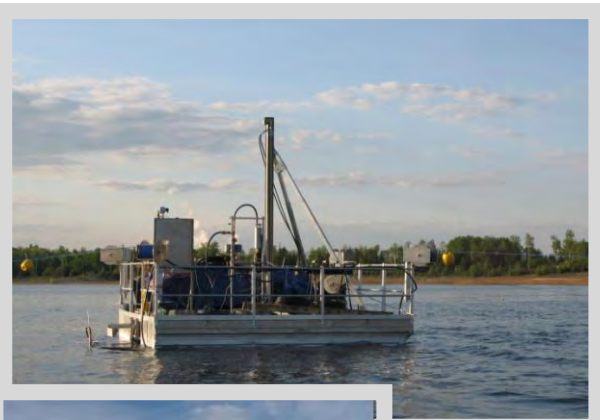
FOG



Freiberg Online Geology

FOG is an electronic journal registered under **ISSN 1434-7512**

2011, Volume 29



M. Schipek

Treatment of acid mine lakes - Lab and field studies -

381 pages, 143 figures, 81 tables, 343 references

Treatment of acid mine lakes

- Lab and field studies -

Von der Fakultät für Geowissenschaften, Geotechnik und Bergbau
der Technischen Universität Bergakademie Freiberg
genehmigte

DISSERTATION

zur Erlangung des akademischen Grades

doctor rerum naturalium
(Dr. rer. nat.)

vorgelegt

von Dipl.-Geoökol. Mandy Schipek
geboren am 11.12.1981 in Zeitz

Gutachter: Prof. Dr. Broder Merkel, TU Bergakademie Freiberg
Dr. Kurt Friese, Helmholtz-Zentrum für Umweltforschung (UFZ), Magdeburg

Tag der Verleihung: 22.11.2011

Acknowledgement

I would like to gratefully and sincerely thank Prof. Dr. habil. Broder Merkel, Head of the Geology Department and Chair of Hydrogeology, for his invaluable guidance, encouragement, patience, and most importantly, his friendship during my work on this thesis at TU Bergakademie Freiberg. He encouraged me to not only grow as a geoscientist and a chemist but also as an instructor and independent thinker.

Special thanks go to Dr. habil. Kurt Friese from the Helmholtz Centre for Environmental Research, Department Lake Research, for his fruitful comments during the preparation of this thesis.

I would also like to thank all of the members of the Chair of Hydrogeology, especially the laboratory team – Sascha Kummer, Hans-Joachim Peter and Karina Taupadel – who provided great help in analyzing amounts of samples. Many thanks go to Mrs. Anja Obst for her help in SEM-EDX measurements, Dr. Reinhard Kleeberg for XRD analysis and PD Jens Götze for CL measurements. I would like to express my thanks to PD Volkmar Dunger, Dipl.-Geoökol. Robert Sieland, Dipl.-Geol. Andrea Berger, and Dipl.-Geol. Yvonne Lindig who helped and advised me through the course of my study and research.

Many thanks go to Rheinkalk GmbH, Germany, for supplying me with different neutralizing products and advice during column experiments. Special thanks also to the team of MOVAB-D GmbH, Germany, for help in sampling and monitoring during the field experiments.

Finally, and most importantly, I would like to thank my husband Jenö. His support, encouragement, quiet patience and unwavering love were undeniably the bedrock upon which the past years of my life have been built. I thank my parents, Carola and Hans-Jürgen, for their faith in me and allowing me to be as ambitious as I wanted. Also, I thank Jenö's parents, Elisabeth and Hartmut, who provided me with unending encouragement and support.

Table of Contents

TABLE OF CONTENTS	VII
LIST OF FIGURES.....	IX
LIST OF TABLES	XVII
LIST OF TEXT BOXES	XIX
LIST OF APPENDICES	XXI
ABBREVIATIONS.....	XXIII
ABSTRACT	XXV
ZUSAMMENFASSUNG	XXVII
1 STATE OF ART	1
1.1 AMD – ACID MINE DRAINAGE	1
1.1.1 Open pit mining problems - worldwide	1
1.1.2 Major lignite mining districts in Germany.....	4
1.2 AMD TREATMENT.....	10
1.2.1 <i>In situ</i> remediation	11
1.3 CO ₂ SEQUESTRATION	12
1.3.1 CCS Concept.....	13
1.3.2 Capture of CO ₂	13
1.3.3 Transport of CO ₂	13
1.3.4 Storage of CO ₂	13
1.4 LAKE LIMING.....	14
1.4.1 General information	14
1.4.2 Solution and precipitation of carbonates	15
1.4.3 Advanced Mobile Inlake Technology (AMIT).....	20
1.5 FLY ASH	21
1.5.1 Coal combustion by-products (CCBs)	21
1.5.2 Use of fly ash for treatment of AMD affected waters.....	22
1.5.3 Weathering products.....	22
1.5.4 Mineral CO ₂ sequestration by carbonation of fly ash.....	23
1.6 KINETICS.....	24
1.6.1 General	24
1.6.2 Batch reactors.....	25
1.6.3 Flow-Through Reactors	25
2 INVESTIGATION AREA	27
2.1 MINING LAKES IN THE LAUSITZ AREA	27
2.2 FLOODING CONCEPT	27
2.3 LAKE BURGHAMMER	28
2.3.1 Groundwater	31
2.3.2 Lake water	33
3 METHODS	35
3.1 SAMPLING	35
3.2 LAB METHODS	36
3.2.1 Solids Analysis and Mineralogy.....	36
3.2.2 Water chemistry Analysis	39
3.2.3 Porewater chemistry	39
3.2.4 Batch experiments (CO ₂ sequestration)	40
3.2.5 Kinetic experiments	42
3.2.6 Column experiments	45
3.3 FIELD METHODS.....	48

Table of Contents

3.3.1	<i>Technical description</i>	48
3.3.2	<i>Monitoring</i>	48
3.4	MODELS AND VISUALISATION.....	55
3.4.1	<i>Hydrochemical modelling</i>	55
3.4.2	<i>Visualisation</i>	59
4	RESULTS AND DISCUSSION.....	61
4.1	SOLID CHARACTERISTICS	61
4.1.1	<i>Fly ash</i>	61
4.1.2	<i>Liming products</i>	73
4.2	RESULTS USING FLY ASH FOR COMBINING PIT LAKE TREATMENT AND CO ₂ STORAGE	77
4.2.1	<i>Contamination risk using fresh and settled fly ash</i>	77
4.2.2	<i>Increase of buffering capacity</i>	89
4.2.3	<i>Carbonate Precipitation</i>	91
4.3	RESULTS OF KINETIC EXPERIMENTS USING LIMING AGENTS	92
4.3.1	<i>General results</i>	92
4.3.2	<i>Influence of CO₂ partial pressure</i>	95
4.3.3	<i>Influence of inhibiting ions</i>	98
4.3.4	<i>Comparision of synthetic marble powder and industrial calcite (KSM Beroun)</i>	101
4.4	COLUMN EXPERIMENTS - LIMING.....	102
4.4.1	<i>General results</i>	102
4.4.2	<i>Experimental series 1 (water type: Burghammer)</i>	102
4.4.3	<i>Experimental series 2 (water type: Lohsa)</i>	106
4.4.4	<i>Experimental series 3 (water type: Scheibe)</i>	108
4.5	FIELD STUDY (CO ₂ SEQUESTRATION)	111
4.5.1	<i>Aim of the field study</i>	111
4.5.2	<i>Theoretical considerations</i>	111
4.5.3	<i>Site description</i>	111
4.5.4	<i>Results</i>	113
4.6	RESULTS OF ADVANCED MOBILE INLAKE TECHNOLOGY WITHIN THE TREATMENT SHEME OF LAKE BURGHAMMER.....	142
5	EVALUATION AND MODELING	145
5.1	ASSESSMENT OF CARBONATE PRECIPITATION AND CO ₂ FIXATION THROUGH PRELIMINARY INVESTIGATIONS AND BATCH EXPERIMENTS	145
5.2	ASSESSMENT OF CARBONATE PRECIPITATION AND CO ₂ FIXATION THROUGH THE PILOT EXPERIMENT.....	146
5.2.1	<i>Hydrochemical modeling</i>	146
5.2.2	<i>Calculation and Visualisation</i>	149
5.3	RISK ASSESSMENT OF RE-DISSOLUTION OF PRECIPITATED CARBONATE DUE TO GROUNDWATER AND LAKE WATER	154
5.4	LAKE LIMING.....	155
6	CONCLUSION	157
	REFERENCES.....	161

APPENDIX A: Additional Figures

APPENDIX B: Tables

APPENDIX C: Matlab© Scripts (Visualisation Lake Modeling)

List of figures

Figure 1. Reaction pathways for pyrite oxidation (after (Banks et al., 1997), modified after (Lottermoser, 2003)).....	2
Figure 2. The self-sustaining, cyclic destruction of pyrite simplified as the “AMD engine”. The oxidation of pyrite is initiated through oxygen (“starter switch”). Pyrite, oxygen and iron (“fuel”) combust in the waste (“engine room”), and release Fe-hydroxides, sulfuric acid and heat into mine waters (“exhaust pipe”) (Lottermoser, 2003).....	2
Figure 3. (a) Distribution of CO ₂ -species plotted as function of pH; (b) titration curve for H ₂ O/CO ₂ system. Dashed arrows show equivalence points x, y, z (for explanation; see text) (Kirby and Cravotta, 2005a).....	4
Figure 4. Major lignite mining districts in Germany (Schreck and Glässer, 1998).	5
Figure 5. Major opencast mines in the Lower Rhine District (RWE, 2011).	6
Figure 6. The future lake district in the Central German mining district (Linke and Schiffer, 2002).....	8
Figure 7. Active open pits in the Lusatian mining district (brown). Dark blue areas represent already flooded mining lakes. Light blue areas represent planned mining lakes. Green areas are remediation areas of the LMBV. (source: (LMBV, 2008)).....	10
Figure 8. Log rate of calcite dissolution (mmoles dissolved cm ⁻² sec ⁻¹) as a function of bulk fluid pH and CO ₂ in stirred solutions at 25°C. Region 1 and 2 are far from equilibrium and rate depends only on forward reaction (see text). Dissolution rate in region 3 is a function of both forward and reverse rates of reaction (Plummer et al., 1978).	16
Figure 9. Model for Alkaline Fly Ash weathering (EPRI - Electric Power Research Institute & Southern Company Services, 2006).....	23
Figure 10. Topographical map of the investigation area surrounding lake Burghammer (TK25, Sheet 4551 Hoyerswerda, 4552 Weißkollm; issue date 1990).	29
Figure 11. Storage system Lohsa II, topographical map (Zschiedrich, 2011).....	30
Figure 12. Digital Terrain Model of lake Burghammer; drawn triangles clarify sampling points (Gauß-Krueger (zones are only 3° apart, as opposed to 6° in UTM), RD 83, Rauenberg, Bessel).	31
Figure 13. Topographical map of the investigation area around Lake Burghammer (TK25, Sheet 4552 / Weißkollm; issue date 1990). Red circles mark observation wells.	32
Figure 14. Development of selected water quality parameters in Lake Burghammer (data source: LMBV, own data collection)	34
Figure 15. Digital Terrain Model of Lake Burghammer; drawn triangles clarify sampling points (Gauß-Krueger (zones are only 3° apart, as opposed to 6° in UTM), RD 83, Rauenberg, Bessel).	35
Figure 16. Schematic experimental setup for mineral trapping.	40
Figure 17. Comparison of IC measurements with different treatment (0 & 1 symbolize “normal” acidified samples in combination with acidified calibration; 2 shows non-acidified samples and calibration; 3 shows non-acidified samples and standard solutions in NaHCO ₃ matrix).....	44
Figure 18. Comparison of calcium contractions measured by ion chromatography and ICP-MS, n = 27.....	45

Figure 19. Schematic drawing of the column experiment set-up. 6 sampling ports provided sampling in different water depths.....	46
Figure 20: Base of the pilot experiment in lake Burghammer: Floating platform, CO ₂ injection technology.....	48
Figure 21: Tank of liquid CO ₂ (provided by Linde), Heat exchanger based vaporizer. The gas was transported from the shore to the platform at a pressure of 8 – 9 bar.....	48
Figure 22. CO ₂ gas injection lance. White buoys in background mark monitoring installations.	49
Figure 23. System of flowmeters and manual valves.....	49
Figure 24. View on monitoring equipment. On the left side: micropumps for CO ₂ monitoring. Right side: controll board (IR sensor). Power supply was provided by 12 V batteries.	50
Figure 25. pH probe WQ201 and CTD diver for monitoring on-site parameters during the pilot experiment	50
Figure 26. Plan of monitoring setup (not to scale).....	50
Figure 27. Schematic diagram of monitoring setup consisting of pH probes (Type WQ 201) and CO ₂ sensors.....	51
Figure 28. Schematic sketch of the sensor set-up.	52
Figure 29. Digital Terrain Model of Lake Burghammer. Red square shows CO ₂ injection point. Blue dots represent sampling points before and afte CO ₂ treatment (Gauß-Krueger (zones are only 3° apart, as opposed to 6° in UTM), RD 83, Rauenberg, Bessel).	54
Figure 30. Distribution of water content in drilling cores BGH-131206-P1, -P2, -P3.....	61
Figure 31. Particle size distribution of ash sediment, sample BGH-131205-P1, different depths.....	62
Figure 32. Particle size distribution of ash sediment, sample BGH-141205-P2, different depths.....	62
Figure 33. Particle size distribution of ash sediment, sample BGH-141205-P3, different depths.....	63
Figure 34. Thinsection of drilling core BGH-141205-P2-3.50.....	65
Figure 35. Thinsection of drilling core BGH-131205-P2-4.50.....	65
Figure 36. Sample P2-141205-3.5 (3.75-4.00): (a), (b) Main fraction consisting of coal-like, dark substance (probably Fe-Oxides). Besides, quartz (blue-purple luminescent) and feldspar (white luminescent) is visible. Organic particles surrounded by few orange-luminescent carbonates.	66
Figure 37. Sample P2-141205-3.5 (3.75-4.00): (a), (b) Preserved organic structure (unburned). Orange-luminescent carbonates filling existent fractures.	67
Figure 38. Sample P2-141205-6.5 (6.75-8.00): (a) Spherical particles show inclusions. (b) Main fraction consisting of coal-like, dark substance (probably Fe-Oxides). White aggregates represent feldspar minerals. Only few carbonate can be identified in / at organic constituents.	67
Figure 39. Sample P2-141205-6.5 (6.75-8.00): (a), (b) Preserved organic structure surrounded by orange-luminescent carbonates. Background: Probably Fe-oxides with feldspar minerals (white) and quartz (blue-purple luminescent).....	67

Figure 40. Eluent-dependet cation release from the deposited ash sediment.....	69
Figure 41. Extractable calcium concentrations of the drilling core BGH-131206-P1, BGH-141206-P2, and BGH-141206-P3	70
Figure 42. Extractable magnesium concentrations of the drilling core BGH-131206-P1, BGH-141206-P2, and BGH-141206-P3	71
Figure 43. SEM image of marble powder.....	75
Figure 44. SEM image of KSM Beroun. 11 – 18 indicate mainly Ca-rich phases (CaO_{calc} 97.8 wt.-%). Minor constituents contain Si (SiO_2 , calc 0.85 wt.-%), Mg (MgO_{calc} 0.53 wt.-%), Sr (SrO_{calc} 0.50 wt.-%), Al (Al_2O_3 , calc 0.26 wt.-%) and Fe (Fe_{calc} 0.07 wt.-%).	75
Figure 45. SEM image of DSM Borna. 1 – 5 indicate mainly Ca- and Mg-rich phases (Ca 23.43 (2) – 55.26 (5) wt.-%, Mg 10.99 (5) – 16.89 wt.-%, average Ca = 37.05 wt.-%, Mg = 14.68 wt.-%. Minor constituents are Si (2.56 wt.-%) and Fe (1.39 wt.-%) and Al (0.11 wt.-%).....	75
Figure 46. SEM image of KSM Borna. 1 – 5 indicate areas which are rich in Ca (37.22 wt.-%). Minor constituents are rich in Mg (wide range 0.6 (3) – 7.87 (5) wt.-%, in average 3.49 wt.-%), Si (0.78 (3) – 9.79 wt.-%, in average 2.97), Al (0.25 (3) – 4.72 (5), in average 1.41 wt.-%. Further elements are Fe (in average 1 wt.-%), Mn (in average 0.37 wt.-%), and K (0.54 wt.-%).....	76
Figure 47. SEM image of Mischkalk Borna. This sample contains mainly Calcium (in average 38.73 wt.-%). Si (in average 2.80 wt.-%), Mg (in average 1.59 wt.-%), Al (in average 1.03 wt.-%), Fe (in average 0.83 wt.-%) and K (in average 0.83 wt.-%) were found in lower concentrations.	76
Figure 48. SEM image of WFK (Weissfeinkalk) CaO. WFK CaO mainly consists of Ca (52.67 wt.-%). Further elements were Fe (in average 0.56 wt.-%), Mg (in average 0.43 wt.-%), Si (in average 0.28 wt.-%) and Al (in average 0.24 wt.-%).....	76
Figure 49. SEM image of Weisskalkhydrat WKH 2-4. Calcium was detected with in average 45.33 wt.-%. Si and Mg were minor constituents with 1.42 and 1.13 wt.-%. Lower concentrations of Fe (in average 0.74 wt.-%), Al (in average 0.57 wt.-%), and Mn (in average 0.43 wt.-%) had been measured.	77
Figure 50. Variation of pH, TIC during batch experiments with fresh fly ash (Boxberg). Error bar presents variation between number of experiments ($n_{\text{DI}} = 2$; $n_{\text{AMD}} = 3$)	79
Figure 51. Variation of Ca^{2+} , SO_4^{2-} , Cl^- , Sr^{2+} , Fe_{total} and Mn during batch experiments with fresh fly ash (Boxberg). Error bar presents variation between number of experiments ($n_{\text{DI}} = 2$; $n_{\text{AMD}} = 3$)	80
Figure 52. Variation of the trace elements As and Sb during batch experiments with fresh fly ash (Boxberg). Error bar presents variation between number of experiments ($n_{\text{DI}} = 2$; $n_{\text{AMD}} = 3$).....	82
Figure 53. Variation of the trace elements Mo, Cr, Cu, Se, Co and Zn during batch experiments with fresh fly ash (Boxberg). Error bar presents variation between number of experiments ($n_{\text{DI}} = 2$; $n_{\text{AMD}} = 3$)	83
Figure 54. Variation of pH, TIC, Ca^{2+} , SO_4^{2-} during batch experiments with settled fly ash (Lake Burghammer). Error bar presents variation between number of experiments ($n_{\text{DI}} = 1$; $n_{\text{AMD}} = 3$)	85
Figure 55. Variation of Cl^- , Sr^{2+} , Fe_{total} and Mn during batch experiments with settled fly ash (Lake Burghammer). Error bar presents variation between number of experiments ($n_{\text{DI}} = 1$; $n_{\text{AMD}} = 3$)	86

Figure 56. Variation of trace elements As, Sb, Mo, Cu during batch experiments with fly ash sediment (Lake Burghammer). Error bar presents variation between number of experiments ($n_{DI} = 1$; $n_{AMD} = 3$)	87
Figure 57. Variation of trace elements Cr, Co, and Zn during batch experiments with fly ash sediment (Lake Burghammer). Error bar presents variation between number of experiments ($n_{DI} = 1$; $n_{AMD} = 3$)	88
Figure 58. Batch experiment with sediment from Lake Burghammer (experiment U191206, 30 % CO ₂ , lake water, mixed sediment sample: BGH-1312-P2-6.50 (6.95-7.10), BGH-1312-P2-3.5 (4.25-4.50), BGH-1312-P2-6.5 (6.65-6.80)).....	90
Figure 59. Typical development of the pH during a titration with a strong acid. The green line represents the curve of the titration from distilled water – water with little buffering capacity (modelled by the use of PhreeqC, Version 2.0); the blue line was modeled for the buffering capacity of the treated lake water.....	91
Figure 60. Development of pH over time. Boundary conditions: pure water, $p_{CO_2} 3.8 * 10^{-4}$ bar.....	93
Figure 61. Development of electrical conductivity over time. Boundary conditions: pure water, $p_{CO_2} 3.8 * 10^{-4}$ bar.....	93
Figure 62. Development of the calcium concentration over time. Boundary conditions: pure water, $p_{CO_2} 3.8 * 10^{-4}$ bar.	94
Figure 63. Development of pH in kinetic experiment influenced by different p_{CO_2} . Boundary conditions: pure water, 5-times saturated.....	95
Figure 64. Development of pH in kinetic experiment influenced by different p_{CO_2} . Boundary conditions: pure water, 5-times saturated.....	96
Figure 65. Development of calcium concentration in kinetic experiment influenced by different p_{CO_2} . Boundary conditions: pure water, 5-times saturated.....	96
Figure 66. Development of calcium concentration in kinetic experiment influenced by different p_{CO_2} . Boundary conditions: pure water, 5-times saturated.....	97
Figure 67. SEM images of marble powder before (A) and after (B - F) experimental use. Boundary conditions: pure water, 5-times saturated, B – $p_{CO_2} 3.8 * 10^{-4}$ bar, C – $p_{CO_2} 0.05$ bar, D – $p_{CO_2} 0.3$ bar, E – $p_{CO_2} 0.5$ bar, F – $p_{CO_2} 1$ bar.....	98
Figure 68. Development of the calcium concentration in kinetic experiment influenced by manganese ions ($c_{Mn^{2+}} = 8.98 * 10^{-4}$ mmol/L). Boundary conditions: pure water, $p_{CO_2} 3.8 * 10^{-4}$ bar, 5-times saturated / 20 times saturated. Plotted curves represent best-fit curves (polynomial).....	99
Figure 69. Development of the calcium concentration in kinetic experiment influenced by cadmium ions ($c_{SO_{42-}} = 1.04 * 10^{+1}$ mmol/L). Boundary conditions: pure water, $p_{CO_2} 3.8 * 10^{-4}$ bar, 5-times saturated / 20 times saturated. Plotted curves represent best-fit curves (polynomial).....	100
Figure 70. Development of the calcium concentration in kinetic experiment influenced by cadmium ions ($c_{Cd} = 7.65 * 10^{-6}$ mmol/L). Boundary conditions: pure water, $p_{CO_2} 3.8 * 10^{-4}$ bar, 5-times saturated / 20 times saturated. Plotted curves represent best-fit curves (polynomial).....	100
Figure 71. SEM image of synthetic marble powder.....	101
Figure 72. SEM image of an industrial calcite KSM Beroun.....	101
Figure 73. pH curve using different neutralizing agents. The yellow arrows represent the time of adding of the neutralizing agent.....	103

Figure 74. Modelled vs. experimental determined pH values after adding CaO	104
Figure 75. Modelled vs. experimental determined pH values after adding CaCO ₃	104
Figure 76. Graph of the efficiency in dependence on the existing H ⁺ -acitivity.	105
Figure 77. pH curve using different neutralizing agents in experimental series 2. The yellow arrows represent the time of adding of the neutralizing agent.....	107
Figure 78. pH curve using different neutralizing agents in experimental series 3. The yellow arrows represent the time of adding of the neutralizing agent.....	109
Figure 79. Digital terrain model of the lake bottom from mining Lake Burghammer. The marked square indicated the boundary of the test site (Gauß-Krueger (zones are only 3° apart, as opposed to 6° in UTM), RD 83, Rauenberg, Bessel).....	112
Figure 80. Application of CO ₂ during pilot experiment. Grey bars indicate periods of no CO ₂ injection through technical problems (05/30/2008 to 06/01/2008; 06/24/2008; 07/06/2008).....	115
Figure 81. pH-values of Lake Burghammer in the area of CO ₂ injection.	116
Figure 82. Total inorganic carbon concentration of different sampling sites in Lake Burghammer within the area of CO ₂ injection.	116
Figure 83. Development of base neutralization capacity in the water body during CO ₂ injection.....	117
Figure 84. Pore water distribution in sediment cores of Lake Burghammer before and after CO ₂ injection. BGH-290408-P0 shows data before CO ₂ injection; BGH-300708-P1 / P2 / P3 show data after CO ₂ injection.	118
Figure 85. pH of the pore water in sediment cores of Lake Burghammer before and after CO ₂ . BGH-290408-P0 shows data before CO ₂ injection; BGH-300708-P1 / P2 / P3 show data after CO ₂ injection.....	118
Figure 86. TIC-content of the pore water in sediment cores of Lake Burghammer before (BGH-290408-P0) and after CO ₂ injection (BGH-300708-P1, BGH-300708-P2, BGH-310708-P3)	119
Figure 87. Depth profiles of major ions in the porewater before (left hand, BGH-290408-P1) and after CO ₂ treatment (right hand, BGH-310708-P3)	120
Figure 88. Depth profile of sulfate in the porewater before (left hand, BGH-290408-P1) and after CO ₂ treatment (right hand, BGH-310708-P3)	121
Figure 89. X-ray diffractogram of fly ash before CO ₂ treatment (BGH-300408-P0, depth 4.90 – 4.95 m).....	123
Figure 90. Comparision of X-ray diffractograms of fly ash before CO ₂ treatment (BGH-300408-P0, depth 4.90 – 4.95 m, red coloured) and after CO ₂ treatment (BGH-310708-P3, depth 5.08 – 5.20 m, black coloured)	124
Figure 91 (A – F). Scanning electron micrographs of deposited lignite-ash particles (Sample BGH-290408-P0). Squares mark the areas where EDX microprobe analyses were taken (for element identification cf. appendix B, Table B.36).....	126
Figure 92 (A – F). Scanning electron micrographs of deposited lignite-ash particles (Sample BGH-290408-P0). Squares mark the areas where EDX microprobe analyses were taken (for element identification cf. Appendix B, Table B.36)	127
Figure 93 (A – C). Scanning electron micrographs of deposited lignite-ash particles (Sample BGH-290408-P0). Squares mark the areas of which EDX microprobe analyses were taken (for element identification cf. Appendix B, Table B.36)	128

Figure 94 (A – F). Scanning electron micrographs of deposited lignite-ash particles ((A) - Sample BGH-300708-P1; (B – F) – Sample BGH-310708-P3). Squares mark the areas where EDX microprobe analyses were performed (for element identification cf. appendix B, Table B.37)	130
Figure 95 (A – F). Scanning electron micrographs of deposited lignite-ash particles ((B – F) – Sample BGH-310708-P3). Squares mark the areas where EDX microprobe analyses were taken (for element identification cf. appendix B, Table B.37).....	131
Figure 96. Image made by polarization microscopy (left: xPol, right: II Pol). Sample BGH-290408-P0	134
Figure 97. Image made by polarization microscopy (left: xPol, right: II Pol). Sample BGH-290408-P0	135
Figure 98. Image made by polarization microscopy (left: xPol, right: II Pol). Sample BGH-300708-P1	136
Figure 99. Optical micrographs made by polarization microscopy (left: xPol, right: II Pol). Sample BGH-300708-P3.....	137
Figure 100 (A – F). Cathodoluminescence (left) and transmission microscopy photographs. Sample BGH-290408-P0 (qz = quarz, fsp = alkali feldspar, c = carbonate)	139
Figure 101 (A – F). Cathodoluminescence (left) and transmission microscopy photographs. Sample BGH-300708-P1 and BGH-310708-P3 (qz = quarz, fsp = alkali feldspar, c = carbonate).	140
Figure 102 (A – F). Cathodoluminescence (left) and transmission microscopy photographs. Sample BGH-310708-P3 (qz = quarz, fsp = alkali feldspar, c = carbonate).	141
Figure 103. Course of in-situ parameters pH and alkalinity during the water treatment in lake Burghammer.	143
Figure 104. (a) Swedish treatment ship during application of $\text{Ca}(\text{OH})_2$ in lake Burghammer. (b) Aerial view of lake Burghammer during the initial neutralization phase. (c) Visual distribution within the lake (copyright: G. Scholz, MOVAB-D GmbH). (d) Transport of the treatment ship.	144
Figure 105. Calculated saturation indices for calcite (before CO_2 treatment)	147
Figure 106. Calculated saturation indices for calcite (after CO_2 treatment)	149
Figure 107. Distribution of TIC in dependency of sediment depth and distance to point of injection. Interpolation method: Kriging, linear (slope = 1, anisotropy = 1, angle = 0)	151
Figure 108. Calcite distribution based on calculations of TIC in dependency of sediment depth and distance to point of injection. Interpolation method: Kriging, linear (slope = 1, anisotropy = 1, angle = 0)	152
Figure 109. Variation in Calcite contents after CO_2 treatment. Interpolation method: Kriging, linear (slope = 1, anisotropy = 1, angle = 0)	153
Figure 110. a – Visualisation of the lake bathymetry. b – Visualisation of the measuring points. c/d – Animated 2D-plots showing the distribution of specified parameters (pH, electrical conductivity, etc.) in time and depth. e – Animated 3D-slices of specified parameters (pH, electrical conductivity, etc.) in time and depth. f – 3D-slices of specified parameters (pH, electrical conductivity, etc.) in specified depths and along user-defined slices through the lake body.	156
Figure 111. Treatment sheme of an optimized in-lake liming by vessels under consideration of weather conditions and wind-induced currents (Merkel et al., 2010) . For further description, see text.	159

Figure 112. Treatment sheme of an optimized in-lake liming by a pipeline-based system under consideration of weather conditions and wind-induced currents (Merkel et al., 2010). For further description, see text.....159

List of tables

Table 1. Lignite reserves in bn t (Bundesverband, 2011)	5
Table 2. Overview about conducted experiments of different authors regarding calcite dissolution rates with respect to different parameters (experimental set-up, p_{CO_2} , temperature etc.)	18
Table 3. Overview about published investigations of authors regarding different inhibiting ions affecting calcite dissolution rates.	20
Table 4. Water quality goals according to official approval and according to the working committee for water quality (Zschiedrich et al., 2007).....	28
Table 5. Morphological parameters of the mining lake Burghammer (source:(LUG, 2005)) ..	30
Table 6. Water quality of a groundwater sample in the surrounding of Lake Burghammer....	32
Table 7. Chemical composition of the acid mine lake water (11/2007).....	34
Table 8. Gauß-Krueger-Coordinates of the sampling points from December 2005 (RD 83, Rauenberg, Bessel). Depth means depth of sediment.....	35
Table 9. General outline of the sequential extraction procedure and the acquired metals and metalloid binding forms (modified after (Zeien, 1995)).....	38
Table 10. Overview of varying experimental conditions	41
Table 11. Overview of varying experimental conditions	43
Table 12. Heights of the sampling ports within the column experiment set-up.	46
Table 13. Overview about conducted column experiments to improve liming technology in acidified mining lakes.	47
Table 14. Overview about the monitoring system used during CO_2 injection.	49
Table 15. Photometrical methods: measuring ranges and detection limits.....	53
Table 16. Coordinates of sampling points (drilling cores) before and after CO_2 treatment (Gauß-Krueger-Coordinates, RD 83, Rauenberg, Bessel).....	54
Table 17. Overview about developed m-files and function of the script. As well, variable parameters are listed.....	59
Table 18. Calculated hydraulic conductivities of Lake Burghammer sediments (drilling cores from 12/05).....	63
Table 19. Analyzed mineral phases of the brown coal filter ash (power plant Boxberg).....	64
Table 20: Mineral phases containing Calcium	66
Table 21. Elemental contents of investigated liming agents. Contents are given in wt.-%. For full analysis see Appendix B.....	74
Table 22. Comparison of the buffering capacity of initial lake water and after batch reactions	89
Table 23. Description of the buffering capacity of the original acid mine lake water	90
Table 24. Carbonate precipitation in batch experiments with fly ash ($n = 10$) and lake sediment ($n = 16$).	92
Table 25. Calcium concentrations at the thermodynamic equilibrium state during calcite dissolution	97

Table 26. Efficiency calculation based on experimental and modeled results, liming agent: CaO	105
Table 27. Efficiency calculation based of experimental and modeled results, liming agent: CaCO ₃	105
Table 28. Chemical composition of the mining lake Lohsa II, 11/2009.....	106
Table 29. Chemical composition of the mining lake Scheibe, 06/2010.....	108
Table 30. Calculation of effective efficiencies.....	110
Table 31. Coordinates of the different test sites during pilot experiment of passive treatment (Gauß-Krueger-Coordinates, RD 83, Rauenberg, Bessel).....	112
Table 32. Application of CO ₂ : measured gas flow and applied pressure of CO ₂ during the pilot experiment.....	114
Table 33. Trace element mobilisation before and after pilot experiment [ppb]	122
Table 34. Mineral alterations through CO ₂ injection	124
Table 35. Temporal course and amounts of liming agents.....	142
Table 36. Valuation of uncertainties concerning physical and chemical parameters and consequential calculated CO ₂ amounts	145
Table 37. Calculated saturation indices for selected mineral phases before CO ₂ treatment	147
Table 38. Calculated saturation indices for selected mineral phases after CO ₂ treatment...	149
Table 39. Precipitated amounts of total carbon (TC), total inorganic carbon (TIC), Calcite during field experiment.....	150
Table 40. Calculation of theoretical captured CO ₂ amounts and precipitated CaCO ₃ based on the results of the field experiment.....	153

List of Text boxes

Text box 1. PhreeqC-input file – Modeling the amount of calcite in equilibrium, preparation for kinetic experiments (lake liming)	56
Text box 2. Efficiency estimation of the results of column experiments (lake liming).....	57
Text box 3. PhreeqC-input file – Modeling kinetic experiments using the empirical model of Plummer & Busenberg (1982)	58

List of appendices

APPENDIX A: Additional Figures

APPENDIX B: Tables

APPENDIX C: Matlab[©] Scripts

Abbreviations

AMD	Acid mine drainage
AMIT	Advanced mobile inlake technology
ASE	Accelerated solvent extraction
bn	billion
BSE	Backscattered Scanning Electron Microscopy
c	carbonates
CCBs	Coal combustion by-products
CCS	Carbon capture and storage
CL	Cathodoluminescence
CO ₂	Carbon dioxide
CSTR	Continuously stirred tank reactor, flow-through reactor
dist.	Disturbed
EC	Electrical conductivity
DL	detection limit
ELCOM	Estuary and Lake Computer Model
EPA-PAH	PAH according to Environmental Protection Agency
fsp	feldspar
IC	Ion chromatography
ICP-MS	Inductive coupled plasma mass spectrometry
LDO	Luminescent dissolved oxygen
LMBV	Lausitzer und Mitteldeutsche Bergbau-Verwaltungsgesellschaft mbH
M	Molar
MSWI	Municipal solid waste incineration fly ash
n.d.	not determined
NN	Normalnull
NPOC	non-purgable organic carbon
ORP	redox
PAH	Polycyclic aromatic hydrocarbon
p _{CO₂}	CO ₂ partial pressure
PFR	Plug flow reactor, packed bed reactor, column reactor
qz	quartz

Abbreviations

RD 83	Rauenberg Datum (1983)
ROI	Radius of influence
rpm	Rounds per minute
S4	Elution with distilled water
SE	Scanning Electron Microscopy
SEM-EDX	Energy dispersive X-ray spectroscopy coupled with Scanning Electron Microscope
SI	Saturation index
SpCond	Specific Conductivity
TC	Total carbon
TIC	Total inorganic carbon
TOC	Total organic carbon
TK 25	Topographical map, scale 1:25000
TU BAF	Technische Universität Bergakademie Freiberg
UTM	Universal Transverse Mercator
wt.-%	Percent by weight
WTW	WTW Wissenschaftlich-Technische Werkstätten GmbH
XANES	X-ray absorption near-edge structure
Xpol	Crossed polarized microscopy
XRD	X-ray diffraction
IIpol	parallel polarized microscopy

Abstract

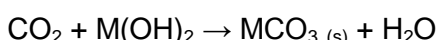
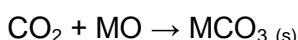
Mining of lignite in Lusatia has a long history of over 100 years. The extracted brown coal is utilized to generate electricity in three large power plants: Jänschwalde, Boxberg, and Schwarze Pumpe. With an annual carbon dioxide (CO_2) output of approximately 50 million tons, these power plants are among Germany's large-scale CO_2 emitters.

The environmental impact from open-pit mining is of a considerable degree and currently poses a challenging problem. The groundwater deficit in 1990 was 7 billion m^3 over a surface area of approximately 2100 km^2 (Luckner, 2006a) and was bisected in value until today. Due to the decline of mining activity and the termination of mine drainage at most open pits in the Lusatian region, the groundwater table has recovered forming 28 pit lakes (Zschiedrich, 2011). The majority of the post mining lakes do not meet the quality standards for pH, iron or sulfate parameters; because of pyrite oxidation that produces acid mine drainage (Luckner, 2006b, Klapper and Schultze, 1995, Schultze et al., 2010). The post mining lakes in Lusatia have low pH values (3 – 4), high sulfate contents (up to 2800 ppm) as well as high iron concentrations (100 – 150 ppm).

Lakes are flooded by groundwater and using surface water from Spree and Neisse River to achieve fast filling and dilution; however, due to the limited availability of surface water, further rehabilitation strategies for the region had to be investigated.

Between 1970 and 1990, approximately 26 million m^3 of suspended fly ash were deposited in the lake Burghammer and settled as an ash body at its base; where it may be used for rehabilitation. In a first experiment conducted in 2001 material from the ash body was picked up and redistributed throughout the lake. By this treatment the pH of the lake was raised temporarily; however, a sustainable remediation was not achieved.

Based on these experiments it was investigated whether the ash reacts more sufficiently through additional CO_2 injection or not. Aim was to combine the rehabilitation of acid mine lakes with the utilization of atmospheric carbon dioxide emissions from coal-fired power plants. The CO_2 sequestration is achieved through the generation and accumulation of carbonates in the lake. The following equations describe the precipitation of carbonate by using CO_2 and alkaline earth cations M:



Therefore, neutral pH conditions are necessary for the long-term accumulation of carbonates in the lakes.

In laboratory investigations it was shown, that the 20 to 30 years old fly ash deposits of lake Burghammer can be used for carbonate sequestration and lake water treatment. Bivalent ions (Ca^{2+} , Mg^{2+}) are elutable and available for carbonate precipitation; on average we assumed 1 wt.-% of reactive calcium to be contained in the settled ash sediments. Settled fly ash sediments are less reactive than fresh fly ash from a power plant (e.g. Schwarze Pumpe). During batch experiments, we increased the buffering capacity to maximum values of 7 mmol/L. Beforehand no buffering capacity exists due to the low pH of 2.9 in the lake. Batch investigations provided a sequestration potential of 17 g CO_2/kg ash sediment; in comparison fresh fly ash results in a sequestration potential of 33 g CO_2/kg ash (Schipek and Merkel, 2008b, Schipek and Merkel, 2008a, Schipek, 2009).

Abstract

Based on the laboratory results a field experiment was conducted. In this field experiment gas injection lances were installed to a sediment depth of 12 m. Gaseous CO₂ was applied with a pressure of 2.2 bar and 2.2 m³/h for 3 months and lake water was monitored during injection. Variations in total inorganic carbon due to diffusion processes of CO₂ saturated pore waters could be observed. As the pilot experiment comprised only a small area of lake Burghammer no initial neutralisation (e.g. by a suction excavator) was possible. Thus, no further changes in water chemistry were observed.

Drilling cores in the vicinity of the injection area provided mineralogical and geochemical conditions before and after CO₂ treatment. No trace metal mobilization was found during CO₂ injection. Most elements showed decreasing trends or didn't change significantly. Calculated saturation indices for calcite indicated equilibrium conditions or slightly oversaturated conditions (SI_{Calcite,average} +0.12; SI_{Calcite,median} +0.31). Geochemical and mineralogical investigations proved that CO₂ sequestration is possible with an average precipitation rate of 0.5 wt.-% (2.2 g CO₂/kg). The maximum rate for carbonate precipitation was determined with 7.4 wt.-% Calcite, according to 32.6 g CO₂ per kilogram treated ash.

Besides the use of the settled fly ash as neutralizing agent in acidic mining lakes, laboratory and field investigations were conducted in order to improve in-lake liming. In batch and columns experiments, different liming agents (synthetic marble powder and industrial products) were tested and investigated. Significant differences in reactivity were obvious at p_{CO₂} > 3.8 • 10⁻⁴ atm. Ions typical for acid mine drainage (e.g. Mn²⁺, Cd²⁺, SO₄²⁻) do have different effects on the kinetic of carbonate dissolution. Manganese concentrations typical for acidic mining lakes inhibit calcite dissolution. Cadmium has as well a significant influence on dissolution and kinetics. Only circa 50 % of the calcium concentration was reached with cadmium as inhibitor compared to the dissolution in pure water. Increased CO₂ partial pressure might be used to compensate inhibition by material impurities and/or water constituents.

Column experiments showed that a multi-stage application of liming agent increases the efficiency of a lake treatment. The combination of a first application of calcite (up to pH 4.5) and further application of Ca(OH)₂ seemed to be the most promising method. This treatment scheme was successfully applied in lake Burghammer from March 2009 – December 2010 (initial neutralisation and 6 follow-up treatments).

Finally, it can be concluded, that in lignite mining districts in-lake treatment of acidic mining lakes is a seminal method to handle water quality problems. Using gaseous CO₂ in combination with industrial by-products can be accounted as sustainable method for CO₂ sequestration and for treatment of AMD. The advantage for mining areas lays in the prevention during treatment of acid mine lakes. Nevertheless, this method presents only a niche solution due to the dependence on alkaline materials, e.g. fly ash.

The development of further strategies and optimization during lake water treatment by in-lake liming might improve the effectiveness of the method. Using calcite instead of NaOH or CaO as liming agent will provide advantages in being more economic and ecological (CO₂ balance). In order to enhance efficiency the use of calcite in combination with CO₂ can be a worth considering suggesting. If meteorological parameters (wind) and lake specific characteristics (morphology, currents, etc.) will be considered efforts and costs for in-lake liming will be minimized.

Zusammenfassung

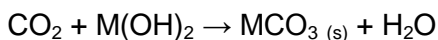
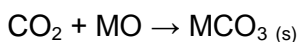
Der Abbau von Braunkohle im Lausitzer Bergbaurevier hat seit über 100 Jahren Tradition. Die abgebaute Braunkohle wird dabei hauptsächliche zur Energieerzeugung in den drei großen Kraftwerken Jänschwalde, Boxberg und Schwarze Pumpe genutzt. Mit einem jährlichen Kohlenstoffdioxid (CO_2) – Ausstoß von circa 50 Millionen Tonnen gehören diese Kraftwerke zu Deutschlands größten CO_2 -Emittenten.

Der Einfluss auf die Umwelt durch Tagebau-Betrieb ist von beträchtlichem Ausmaß und bringt große Probleme mit sich. Im Jahr 1990 betrug das Grundwasser-Defizit im Lausitzer Bergbaurevier 7 Milliarden m^3 auf einer Fläche von circa 2100 km^2 (Luckner, 2006a). Dieses Defizit hat sich bis zum heutigen Zeitpunkt halbiert. Durch den Rückgang der Bergbauaktivitäten und die Beendigung der Wasserhaltungsmaßnahmen in den meisten Tagebauen, hat der ansteigende Grundwasserspiegel 28 Tagebaufolgeseen geschaffen (Zschiedrich, 2011). Der überwiegende Teil der Tagebaufolgeseen ist aufgrund der Pyritoxidation, welche AMD (acid mine drainage) produziert, hinsichtlich der Wasserqualitätsparameter stark beeinflusst (Luckner, 2006b, Klapper and Schultze, 1995, Schultze et al., 2010). Die Tagebaufolgeseen im Lausitzer Bergbaurevier sind durch niedrige pH-Werte (3 – 4), hohe Sulfat-Konzentrationen (bis zu 2800 ppm) und hohe Eisengehalte (100 – 150 ppm) gekennzeichnet.

Die entstehenden Seen sind hauptsächlich durch aufsteigendes Grundwasser und Oberflächenwasser aus den Flüssen Spree und Neisse geflutet. Aufgrund der geringen Verfügbarkeit von Oberflächenwasser mussten weitere Sanierungsmaßnahmen für die Region untersucht werden.

Zwischen 1970 und 1990 wurden im Tagebaufolgesee Burghammer circa 26 Millionen m^3 Flugasche-Suspension als Aschekörper abgelagert, wobei eine Nutzung zu Sanierungszwecken angedacht war. Im Rahmen einer Aschesedimentumlagerung im Jahr 2001 wurde der pH-Wert des Seewassers kurzzeitig angehoben, eine nachhaltige Sanierung fand jedoch nicht statt.

Auf Grundlage dieser Ergebnisse wurde im Rahmen dieser Dissertation untersucht, ob die abgelagerten Aschesedimente nachhaltiger durch Einsatz von CO_2 reagieren. Ziel war es die Sanierung von Tagebaufolgeseen mit der Reduktion von CO_2 -Emissionen aus Kohlekraftwerken zu kombinieren. Diese CO_2 -Sequestrierung sollte durch die Bildung und Ablagerung von Carbonaten im Seesediment erfolgen. Die Gleichungen (1) und (2) beschreiben dabei die Fällungsreaktion von Carbonaten aus CO_2 mit dem Alkalimetall M (aus Oxiden bzw. Hydroxiden):



Zur Carbonatfällung und nachhaltigen Ablagerung sind neutrale pH-Bedingungen notwendig.

In Laboruntersuchungen konnte gezeigt werden, dass die 20 bis 30 Jahre alten Flugaschesedimente zur CO_2 -Sequestrierung in Kombination mit Seewasserbehandlung genutzt werden können. Zweiwertige Ionen (Ca^{2+} , Mg^{2+}) sind aus den Aschesedimenten eluierbar und stehen für die Fällungsreaktion zur Verfügung. Durchschnittlich 1 Masse-% reaktives Calcium befindet sich in den Sedimenten. Die abgelagerten Aschesedimente sind dabei weniger reaktiv als frische Flugaschen aus Kohlekraftwerken (z.B. Schwarze Pumpe). In Batch-Versuchen mit Tagebaufolgesee-Wasser konnte die Säure-Pufferkapazität auf

maximal 7 mmol/L erhöht werden. Sequestrierungs-Raten von 17 g CO₂/kg Aschesediment wurden im Rahmen der Versuche erreicht. Im Vergleich dazu betragen die Sequestrierungs-Raten in Versuchen mit frischen Flugaschen bis 33 g CO₂/kg Asche (Schipek and Merkel, 2008b, Schipek and Merkel, 2008a, Schipek, 2009).

Auf Grundlage dieser Laborergebnisse wurde ein Feldversuch im Tagebaufolgesee Burghammer geplant. Während diesem wurden Gasinjektionslanzen bis in eine Sedimenttiefe von 12 m im abgelagerten Aschesediment installiert. Gasförmiges CO₂ wurde mit einem durchschnittlichen Druck von 2.2 bar und 2.2 m³/h für eine Dauer von 3 Monaten injiziert. Während dieser Zeit fand ein kontinuierliches Monitoring des Seewassers im Bereich der Injektion statt. Veränderungen des Gehaltes an TIC (total inorganic carbon) aufgrund von Diffusionprozessen von CO₂-gesättigtem Porenwasser aus dem Aschekörper waren beobachtbar. Da der Feldversuch nur in einem begrenzten Bereich des Tagebaufolgesees Burghammer stattfand und keine Initialneutralisierung vorsah, konnten keine weiteren, großmaßstäblichen Veränderungen im Wasserkörper festgestellt werden.

Bohrkernentnahmen im Umfeld des Behandlungsgebietes lieferten Aussagen bezüglich der mineralogischen und geochemischen Beschaffenheit vor und nach CO₂-Injektion. Im Porenwasser wurde keine Spurenmetall-(re)-mobilisierung durch die Behandlung mit CO₂ festgestellt. Nahezu alle Elemente zeigten einen abnehmenden Trend durch die Behandlung mit CO₂, bzw. keine signifikanten Veränderungen. Modellierte Sättigungsindizes für Calcit wiesen auf Gleichgewichtsbedingungen oder leichte Übersättigung bzgl. Calcit hin (SI_{Calcit}, Mittelwert +0.12; SI_{Calcit}, Median +0.31). Geochemische und mineralogische Untersuchungen zeigten, daß CO₂-Sequestrierung mit einer durchschnittlichen Fällungsrate von 0.5 Masse-% (2.2 g CO₂/kg Aschesediment) erreicht wurde. Die maximale Fällungsrate wurde mit 7.4 Masse-% Calcit bestimmt, dies entspricht einer Festlegung von 32.6 g CO₂/ kg Aschesediment.

Neben der Nutzung der abgelagerten Aschesedimente zur Behandlung des Tagebaufolgesewassers wurden desweiteren Labor- und Feldversuche durchgeführt um In-Lake-Behandlungen mit industriellen Kalkprodukten zu optimieren. In Batch- und Säulenversuchen wurden verschiedene Kalkprodukte (synthetisches Marmorpulver und industrielle Produkte) getestet und untersucht. Signifikante Unterschiede auf die Reaktivität wurde bei erhöhten CO₂-Partialdrücken ($p_{CO_2} > 3.8 \cdot 10^{-4}$ bar) beobachtet. Wasserinhaltsstoffe, die typisch für AMD sind (z.B.. Mn²⁺, Cd²⁺, SO₄²⁻) zeigten einen signifikanten Einfluss auf die Calcit-Lösungskinetik. Mangankonzentrationen, wie sie in Lausitzer Tagebaufolgeseen vorkommen, zeigten – ebenso wie Cadmium – eine inhibitierende Wirkung auf die Kinetik. Im Vergleich zu Versuchen mit destilliertem Wasser wurden nur ungefähr 50 % der Calcium-Gleichgewichtskonzentration mit Cadmium als Inhibitor erreicht. Erhöhte CO₂-Partialdrücke könnten genutzt werden, um die inhibitierende Wirkung von vorhanden Materialverunreinigungen und/oder Wasserinhaltsstoffen zu kompensieren.

Säulenversuche zeigten, dass der mehrstufige Einsatz von Kalkprodukten die Effizienz während einer Seewasserbehandlung erhöht. Die Kombination einer Erstbehandlung mit Kalksteinmehl (bis pH 4.5), und einer Behandlungsfortsetzung mit Ca(OH)₂ erwies sich als wirkungsvollste Methode. Dieses Behandlungsschema (Initialneutralisation, 6 Nachfolgebehandlungen) wurde im Tagebaufolgesee Burghammer von März 2009 – Dezember 2010 erfolgreich angewandt.

Zusammenfassend lässt sich sagen, dass in ehemaligen Bergbaurevieren die In-Lake-Behandlung von Tagebaufolgeseen eine zukunftsträchtige Methode zur Behandlung von Wasserqualitätsproblemen darstellt. Die Nutzung von gasförmigen CO₂ in Kombination mit industriellen „Abfall-Produkten“ kann als nachhaltige Methode zur CO₂-Sequestrierung und zur Behandlung von AMD bezeichnet werden. Der Vorteil in Bergbaurevieren liegt dabei in der Vorbeugung der Entstehung von Wasserqualitätsproblemen. Dennoch stellt diese Methode nur eine Nischenlösung aufgrund der Verfügbarkeit der alkalischen Materialien (Flugasche) dar.

Die Entwicklung und Optimierung weiterführender Strategien zur In-Lake-Behandlung durch Kalkung wird zur Effizienzerhöhung beitragen. Die Nutzung von Kalksteinmehl anstelle von NaOH bzw. CaO als Neutralisationsprodukt wird Vorteile hinsichtlich ökonomischer und ökologischer Sicht (CO₂-Bilanz) mit sich führen. Um die Effizienz beim Einsatz von Kalksteinmehl zu steigern, kann der Einsatz von CO₂ in Betracht gezogen werden. Sobald meteorologische Parameter (Wind) und see-spezifische Merkmale (Morphologie, Strömungen, etc.) berücksichtigt werden, kann der Aufwand und die Kosten für In-Lake-Behandlungen minimiert werden.

1 State of Art

1.1 AMD – Acid mine drainage

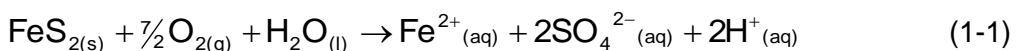
1.1.1 Open pit mining problems - worldwide

1.1.1.1 General processes

Acid mine drainage is an environmental problem often produced as a direct result of mining operations. If mining progresses below the water table water must be constantly pumped from the mine to prevent flooding. With the removal of ore from the ground exposure of sulfides to air takes place; in turn, the oxidation processes of pyrite (FeS_2) associated with lignite deposits produces an acidic environment (Stottmeister et al., 2002). Sulfides are stable under strongly reducing conditions, but presence of oxygen will destabilize them (Lottermoser, 2003).

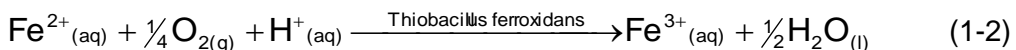
The main processes can be described in the following way (Skousen et al., 1998):

There is an initial weathering of iron-disulfide (pyrite) when its layers come in contact with the atmosphere (Klapper and Schultze, 1995). Pyrite is oxidized by oxygen to produce dissolved ferrous iron (Fe^{2+}), sulfate and hydrogen ions:

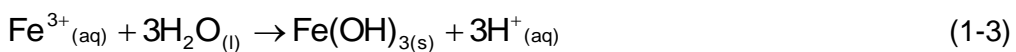


The release of hydrogen ions with the sulfate anions results in an acidic solution unless other reactions occur to neutralize the hydrogen ions (Lottermoser, 2003).

The emerging Fe^{2+} ions are further oxidized to Fe^{3+} (ferric iron) by air-oxygen:



The following step – the formation of ferrihydroxide – takes place mainly during the movement of solution, from the heaps to the open water, and is connected with the highest share of proton delivery (Mudroch et al., 2002):



Under very acidic conditions (< pH 3.5), the ferric hydroxide prevails in solution.

In addition to pyrites atmospheric oxidation further processes occur. Ferric iron (Fe^{3+}) acts as an oxidant for pyrite and causes an essential proportion for proton delivery:



Reaction (1-3) and (1-4) form a continuing cycle of Fe^{2+} conversion to Fe^{3+} and subsequent oxidation of pyrite by Fe^{3+} to produce Fe^{2+} (Lottermoser, 2003).

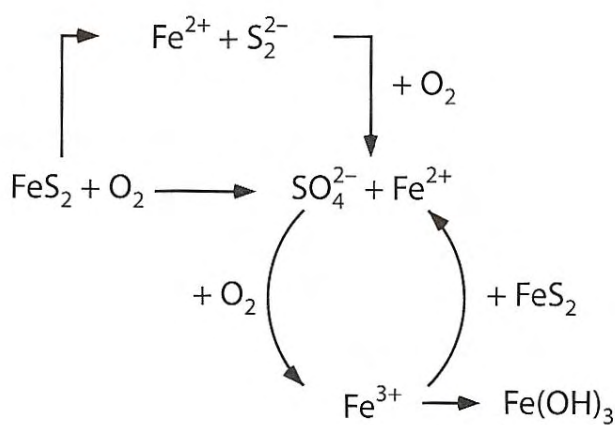
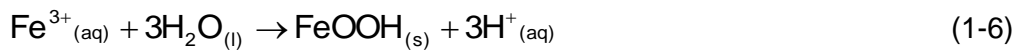
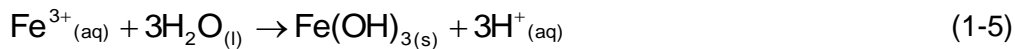


Figure 1. Reaction pathways for pyrite oxidation (after (Banks et al., 1997), modified after (Lottermoser, 2003).

The cyclic reaction pathway continues until the supply of pyrite or Fe^{3+} to the reaction system is exhausted. According to Lottermoser (2003) the abundance of the oxidising agent Fe^{3+} is influenced by the pH. Regarding the predominance diagram of iron, the solubility of Fe^{3+} is very low in neutral to alkaline waters due to the precipitation of ferric hydroxides (Fe(OH)_3) and oxyhydroxides (FeOOH). Thus, in these waters pyrite oxidation by Fe^{3+} is insignificant.



Both reactions provide acidity in form of hydrogen ions in the water, thus, lowers the pH and allows more Fe^{3+} to stay in solution and support reaction 1-4.

The reactions (1-2) to (1-6) is described by some authors as self-sustaining cyclic destruction of pyrite, simplified as the “AMD engine” (Lottermoser, 2003) (Figure 2).

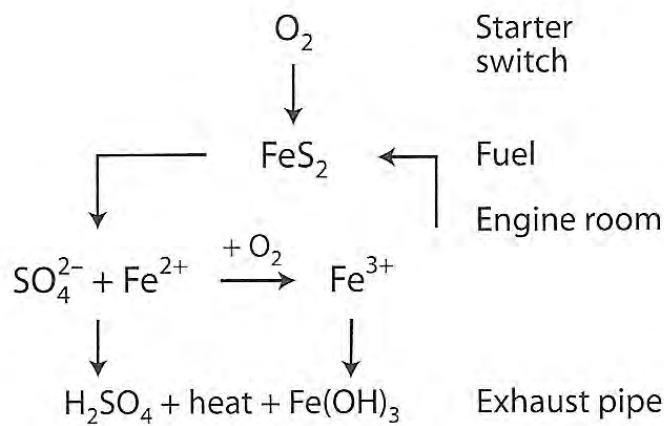
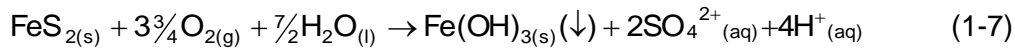


Figure 2. The self-sustaining, cyclic destruction of pyrite simplified as the “AMD engine”. The oxidation of pyrite is initiated through oxygen (“starter switch”). Pyrite, oxygen and iron (“fuel”) combust in the waste (“engine room”), and release Fe-hydroxides, sulfuric acid and heat into mine waters (“exhaust pipe”) (Lottermoser, 2003).

The overall process of geogenic sulfur acidification can be simplified by the following equation:



The oxidation of sulfide minerals does not only create acid, it also liberates metals into waters and accelerates the leaching of other elements (Lottermoser, 2003). Acid mine drainage (AMD), in addition to being highly acidic, often contains high concentrations of metals and ions such as iron, manganese, aluminum, and sulfate, elements like zinc, cobalt, lead, chromium and copper are often found in trace concentrations (Gitari et al., 2008b). For further reference AMD problems are contronted in a wide birth of publications (Gitari et al., 2008b, Aykol et al., 2003, Blodau, 2006, Gray, 1997, Kuyucak, 1998, Gitari et al., 2006, Sheoran and Sheoran, 2006, Chen et al., 1997, Schroeter and Glasser, 2011, Verburg et al., 2009, Brassard et al., 1996, Robb and Robinson, 1995, Pratt et al., 1994, Sullivan and Yelton, 1988, Kendrick, 1977, Barnes and Romberger, 1968, Temple and Colmer, 1951, Hoffert, 1947).

1.1.1.2 Effect on water chemistry

Besides pH and the content of metals and ions such as iron, manganese, aluminum and sulfate, acidity and alkalinity describe relevant parameters for the characterization of mine drainage (Kirby and Cravotta, 2005a).

There are different definitions on the term „alkalinity“. Total alkalinity is defined classically as

$$[\text{Alk}] = [\text{HCO}_3^{-}] + 2[\text{CO}_3^{2-}] + [\text{OH}^{-}] - [\text{H}^{+}] \quad (1-8)$$

(e.g. (Sigg and Stumm, 1996)).

For example, Appelo and Postma (1996) and Kirby and Cravotta (2005a) state that “alkalinity of a water sample is equal to the number of equivalents of dissociated weak acids”. It is determined by titration, with HCl or H₂SO₄, towards an endpoint pH of 4.2. Kirby and Cravotta (2005a) investigated theoretical definitions and laboratory practices for alkalinity and acidity determinations.

Equivalence points shown in Figure 3 equate the definite end pH points: pH of 4.2, 8.3 and 11 (see Figure 3). At these points, particular components in the H₂O / CO₂ system are at equal concentrations (Kirby and Cravotta, 2005a):

$$[\text{H}^{+}] = [\text{HCO}_3^{-}] \quad (1-9)$$

$$[\text{H}_2\text{CO}_3^*] = [\text{CO}_3^{2-}] \quad (1-10)$$

$$[\text{HCO}_3^{-}] = [\text{OH}^{-}] \quad (1-11)$$

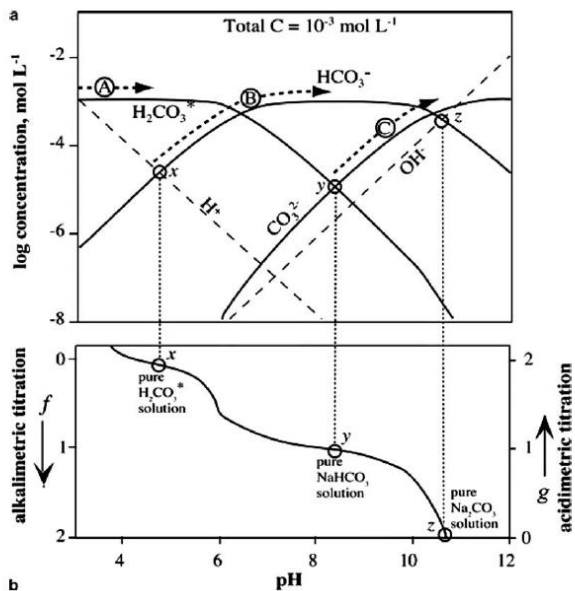


Figure 3. (a) Distribution of CO₂-species plotted as function of pH; **(b)** titration curve for H₂O/CO₂ system. Dashed arrows show equivalence points x, y, z (for explanation; see text) (Kirby and Cravotta, 2005a)

Some of the authors (e.g. (Stumm and Morgan, 1996) do not include H⁺ or some other negative contributions to alkalinity. For further details see literature (Kirby and Cravotta, 2005a, Kirby and Cravotta, 2005b).

For mining waters alkalinity is defined as follows (Kirby and Cravotta, 2005a):

$$\begin{aligned} [\text{Alk}] = & 2[\text{CO}_3^{2-}] + [\text{HCO}_3^-] + [\text{OH}^-] \\ & - [\text{H}^+] - [\text{HSO}_4^-] - 2[\text{Mn}^{2+}] - 2[\text{Fe}^{2+}] - 2[\text{Cu}^{2+}] - 3[\text{Al}^{3+}] - \text{HUS} \end{aligned} \quad (1-12)$$

1.1.2 Major lignite mining districts in Germany

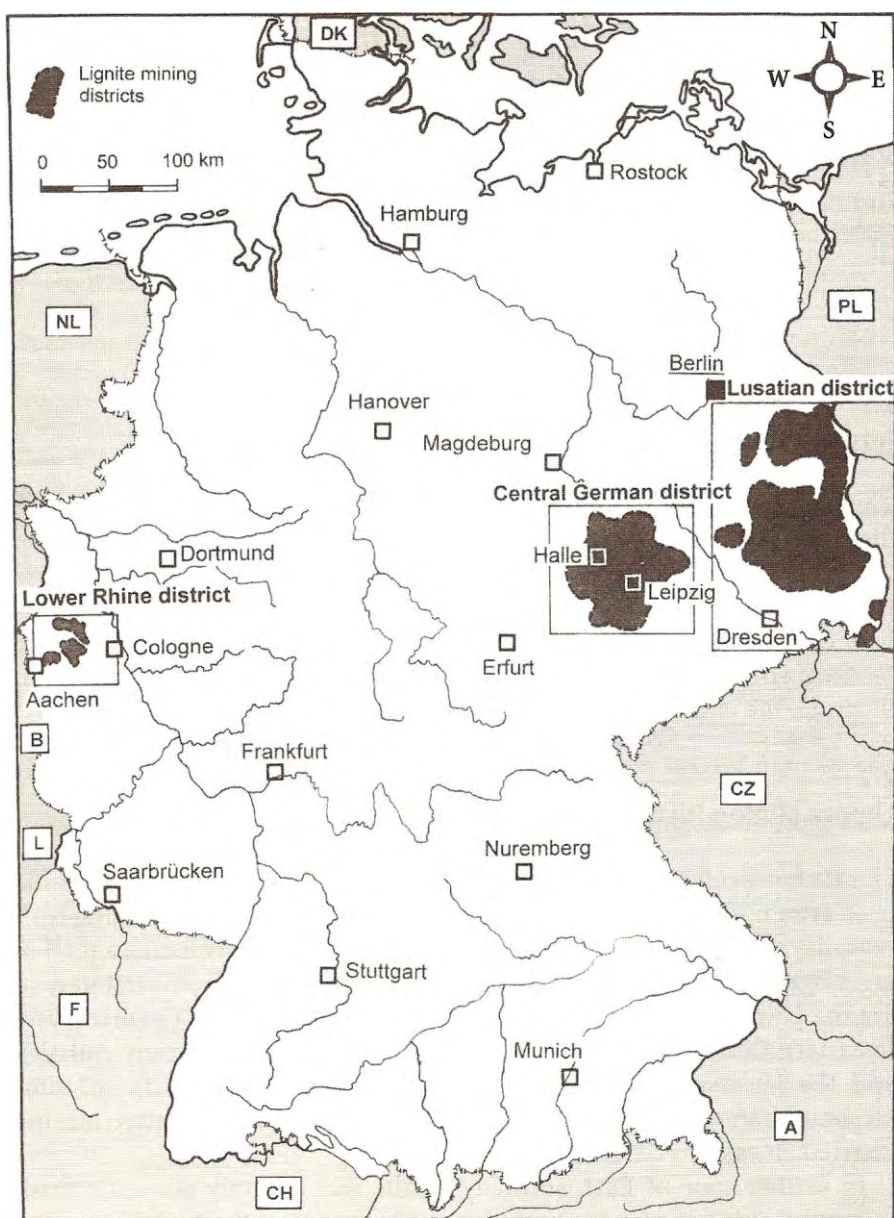
Germany has three large lignite-mining districts: the Lower Rhine basin, the Central German lignite district, and the Lusatia district. Despite decreasing mining activities, Germany is by far the biggest producer of lignite (2008: 180 million t., 40.8 % of European lignite production) (EURACOAL, 2009). Since lignite is the youngest variety of all coals and thus close to the surface, it is mined in opencast mining.

Total lignite resources in Germany can be estimated with 77 billion tons (Bundesverband, 2011). Of these, about 40.5 billion tons are classified as economically minable (according to state of mining techniques and energy prices; based on an internationally agreed definition for the evaluation of deposits). At the moment 6.3 billion tons are available in developed and approved mines.

Table 1. Lignite reserves in bn t (Bundesverband, 2011)

Mining area	Geological reserves	Economically minable reserves	Approved and developed opencast mines
Rhineland	55.0	35.0	3.3
Lusatia	12.0	3.5	1.2 (+0.8)
Central Germany	10	2.0	0.5
Germany, total	77.0	40.5	5.0

Lignite mining in other German districts (e.g. Oberpfalz, Bavaria) had been stopped for decades, since lignite was not economically minable (Bundesverband, 2000).

**Figure 4. Major lignite mining districts in Germany (Schreck and Glässer, 1998).**

1.1.2.1 Lower Rhine district

The Lower Rhine district is a mining area in the Cologne Bay (Kölner Bucht), and builds the northern border of the Rhenish Slate Mountains (Rheinisches Schiefergebirge). Lignite strip mining formed the landscape within this area. In the 17th century, first mining activities were reported. Industrial activities started 1850 – 1905 by the use of steam-heated dewatering pumps, automatic compactors, and overburden excavators. First power plants were built 1892 (Schüler and Coenen, 2005).

Extraction of pit coal in the Lower Rhine district reached 1984 a maximum of 120.6 million tons. According to EURACOAL (2005), in the Rhineland a total of 100.3 million tons of lignite were produced in 2004. Three opencast mines exist: Hambach, Garzweiler and Inden.

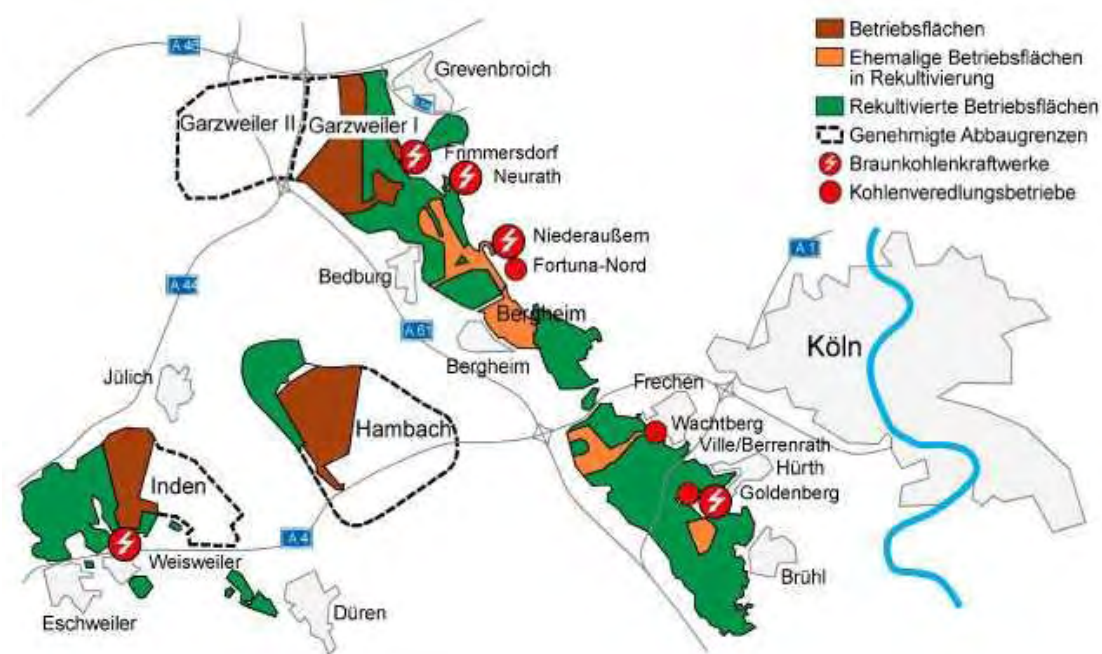


Figure 5. Major opencast mines in the Lower Rhine District (RWE, 2011).

The open pits Hambach and Garzweiler II will be finally mined in 2040 – 2045, the open pit Inden will be closed approximately 10 years earlier.

Within this area, it was and is necessary to pump the groundwater from depths up to of 500 m below surface. Environmental problems concerning dewatering, particulate matter emissions are of actual political interest.

The three currently operated open pits are very large compared to other mining districts. Due to the mined lignite and the formed dumps, the existing holes cannot be filled completely by material. Developing lakes will have the size of ca. 4200 ha and comprise a volume of 3.6 billion m³ (RWE, 2011).

1.1.2.2 The Central German mining district

According to Stottmeister et al. (2002) the states of Saxony and Saxony-Anhalt in Central Germany have a long history of heavy industry. These industries greatly relied on lignite. It

was used in power stations producing electricity needed for the chlorine-based chemical industry and steelworks. Lignite was also decomposed by heating under exclusion of air (pyrolysis) to produce raw materials for the chemical industry. Lignite mining resulted not only in tremendous destruction of the landscape, but also in the massive contamination of surface water and groundwater (Stottmeister et al., 2002). After German reunification, lignite mining was drastically reduced. The Central German mining area around Leipzig yielded a total lignite output of 20.3 million t in 2004 (EURACOAL, 2005).

Stottmeister et al. (2002) describe three scenarios that typify the current state of abandoned lignite mines in eastern Germany.

- Open pits are being or have been flooded to form recreational lakes, resulting in a new type of landscape. Problems described include mechanical slope erosion in the shore zones and the acidification of water by natural oxidation processes (forming "acidic lakes")
- Opencast mines are being naturally flooded, normally by the rising groundwater table and by rainfall [...].
- Opencast mines were used after mining for waste disposal, especially industrial waste without any safety measures. The nature of the material dumped is often unknown and so it must first be analyzed [...].

"Lignite mining has fundamentally changed the water balance in Central Germany – both quantitatively and qualitatively" (Linke and Schiffer, 2002). Main problems include the dramatic reduction of the water table (> 100 m) and the resulting shortage of groundwater. The Central German coalfield covers diverse hydrological areas (Linke and Schiffer, 2002):

- the mining district south of Leipzig (White Elster catchment area) with at least five aquifers and thus a relatively complicated hydrogeological situation,
- mining areas north of Leipzig (Mulde catchment area) with only two main aquifers,
- the western part of the Central German coalfield with local lignite deposits in Geiseltal and Röblingen (Amsdorf) (Saale catchment area), which in turn composes a series of hydrogeological separate areas each with their own water balance.

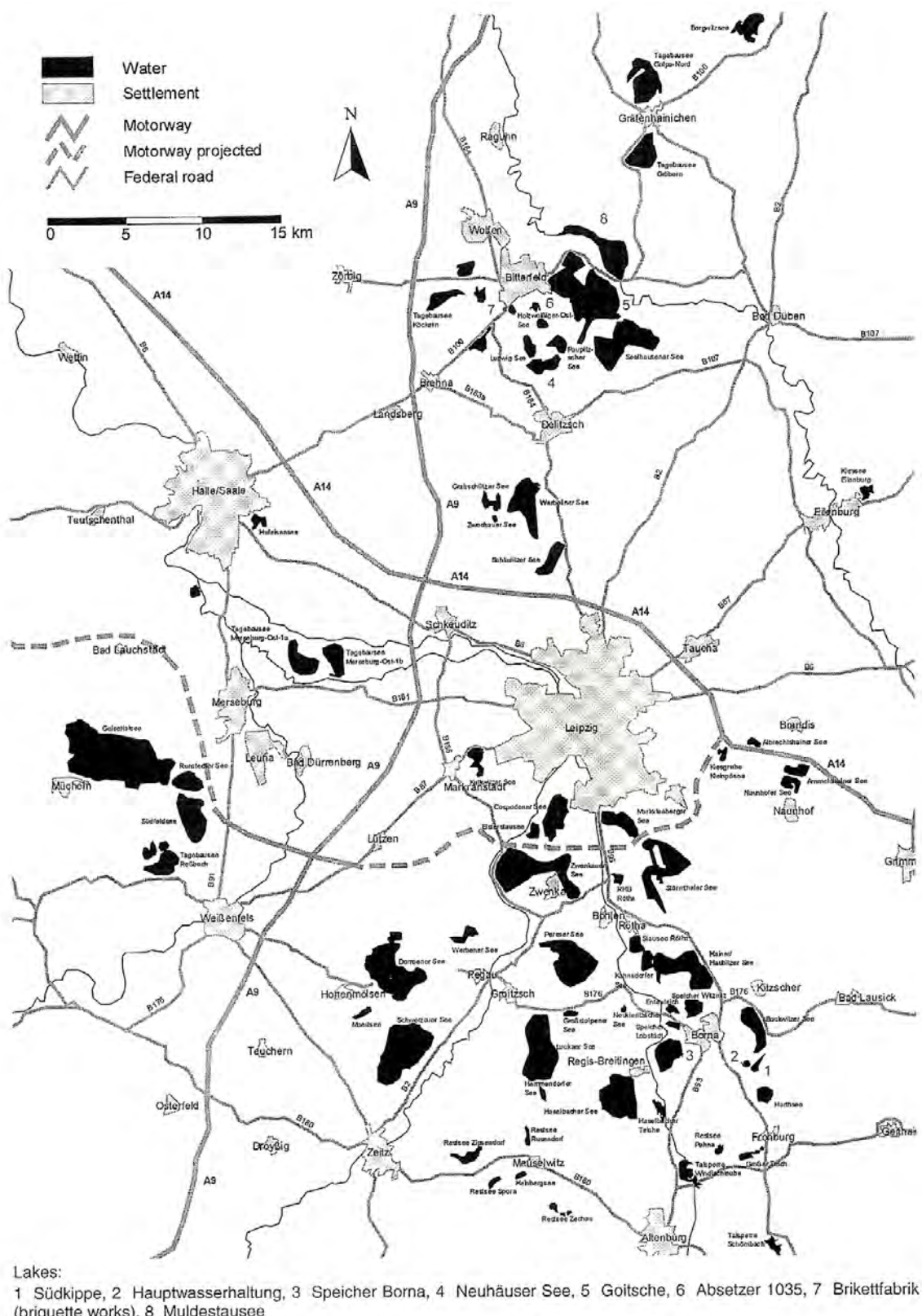


Figure 6. The future lake district in the Central German mining district (Linke and Schiffer, 2002).

Each of these three areas has specific problems in flooding of the open pits and the hydrogeochemical quality of the upcoming lakes. These problems stem from the way in

which flooding is carried out (Linke and Schiffer, 2002, Schultze et al., 2010): either natural rising of the groundwater level or external flooding with river water or drainage water. Advantages and disadvantages of both approaches are described in Klapper (2002). External flooding is the main approach used as flooding concept in the northern and western parts of the Central German coalfield.

In total 41 new lakes will be formed in the former mining district of Central Germany by 2050. They will comprise a total area of about 150 km² and a volume of nearly 3 billion m³ (Linke and Schiffer, 2002).

1.1.2.3 *The Lusatian mining district*

AMD in the Lusatian area originates from sulfide weathering taking place during active and inactive periods of the local brown coal mining industry. In general, the Lusatian lignite district is especially affected by geogenic acidification (Mudroch et al., 2002, Banwart and Evans, 2002). Large open-pits in this district are chiefly being filled with uprising acidic groundwater.

Active coal mining in Lausitz was reduced from 28 (1989) to 4 open pits (1990), which are all managed by Vattenfall Europe Mining AG. In 2008 the Lusatian mines produced 58 million t of lignite (EURACOAL, 2009). Currently, the four surface mines Jänschwalde, Cottbus-North, Welzow South and Nohchten are operated by Vattenfall Europe Mining, producing coal mainly for three large power plants in the region (Jänschwalde, Schwarze Pumpe and Boxberg) (EURACOAL, 2009).

The geology of the Lausitz area can be characterised by two important aquifers, the quaternary and the tertiary aquifer (Nowel et al., 1994). Within the latter, pyrite and marcasite (FeS₂) are present in an anoxic environment. It can be stated that pyrite is the dominant mineral; therefore, explanations of section 1.1.1 can be applied to understand the environment.

After dewatering, the mine site an enormous amount of overburden was moved and deposited prior to excavation of coal seams. With the coal seam excavation, the sediments from quaternary and tertiary layers were mixed and deposited. This resulted in waste rock piles with varying total sulphur content, which left varying acidity release potentials in response to pyrite oxidation. As long as pyrite is in an oxic environment, the weathering process is progressing, but to what degree is difficult to calculate exactly.

Heaps and pits form a part of the developing artificial landscape after mine closure. Heaps are the major AMD source and pits start to fill with acid water. Lake Burghammer is one of the 19 lakes out of 28 in the Lausitz region needing treatment to achieve a standard water quality according to the EU water directive (Koch and Zundel, 2005).

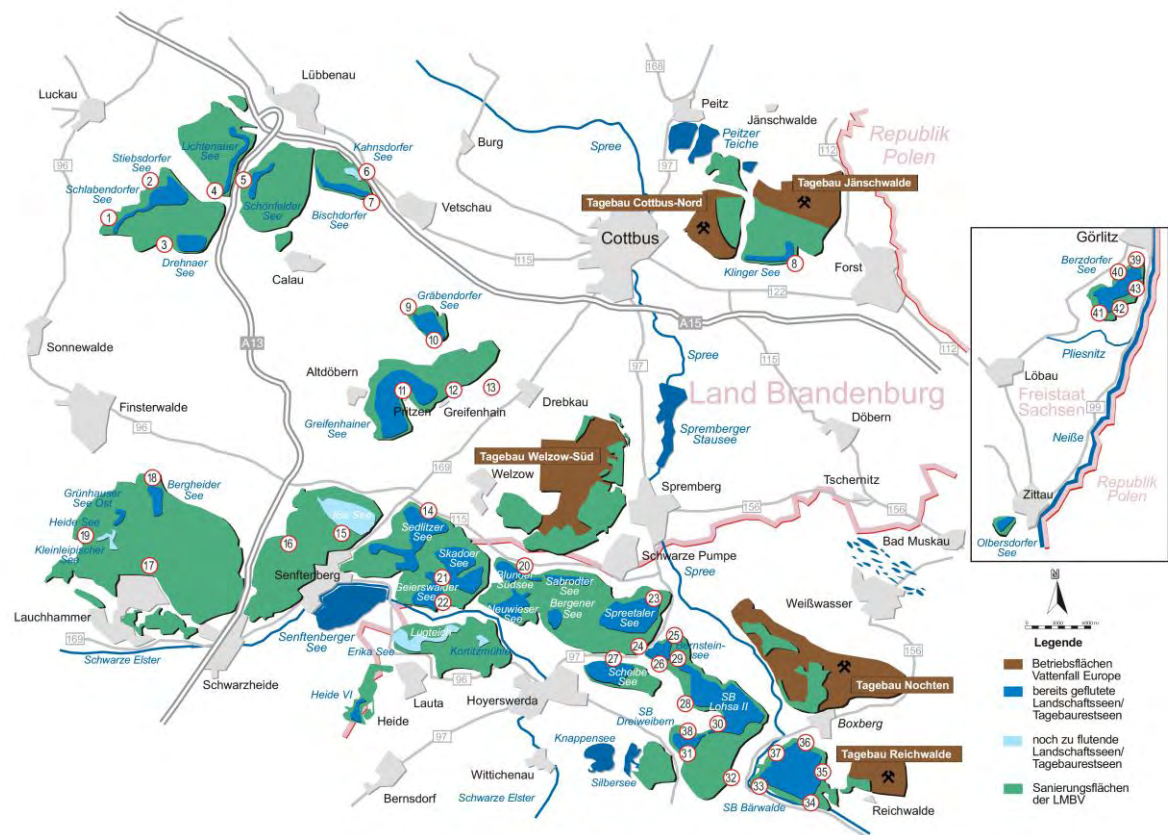


Figure 7. Active open pits in the Lusatian mining district (brown). Dark blue areas represent already flooded mining lakes. Light blue areas represent planned mining lakes. Green areas are remediation areas of the LMBV. (source: (LMBV, 2008))

Groundwater in the Lausitz mining area is characterized by slightly acid pH (5.1 to 6.0), elevated sulfate concentrations (up to 21 mmol/L) as well as the presence of iron(II) species (1.2 - 4.5 mmol/L), aluminum (up to 1 mmol/L), and zinc (up to 0.31 mmol/L) (Grünwald, 2002). The composition is typical for AMD affected groundwater. It is expected that AMD will influence the region for decades or even centuries. Due to AMD, the majority of the lakes cannot achieve water quality standards for pH, sulfate, and iron concentration. Lakes are characterised by low pH (3 - 4) and sulfate concentrations of up to 25 mmol/L. The use of the lakes is limited due to legal restrictions. An economical use is not likely.

1.2 AMD Treatment

Acidification of surface waters is a worldwide problem; major impact areas are rivers, lakes, estuaries, and coastal waters (Gray, 1997). Atmospheric deposition is one contributor to the acidification of surface waters; especially in catchment areas with low acid buffer capacities (Dickson et al., 1995, Svenson et al., 1995). Mining of lignite and / or metals is also responsible for acid mine drainage. Diverse concepts exist for the remediation of acidified waters; each depending on the geochemical parameters and boundaries as well as on water type. Due to the number of publications on the remediation of acidified lakes, this literature research focuses mainly on remediation of acidified lakes. However, the remediation of acidified lakes does not affect the source (Merkel, 2005). In mining areas, remediation

strategies can also be addressed to dump material, but this is often cost and work intensive (Merkel, 2005).

Different studies deal with remediation concepts in bench-scale such as batch experiments (e.g. (Fauville et al., 2004)), in microcosm and mesocosm studies (e.g. (Becerra et al., 2009); (Fyson et al., 2006); (Froemmichen et al., 2004); (Castro et al., 1999) (Crusius et al., 2003, Brugam et al., 1995, Koschorreck et al., 2007a, Bozau et al., 2007b, Totsche et al., 2006)) and in In-Lake reactors (e.g.(Koschorreck et al., 2007a, Koschorreck et al., 2002)).

1.2.1 In situ remediation

1.2.1.1 Liming

As a strategy of acid deposition mitigation, the application of neutralizing agents has received substantial attention (Cirmo et al., 2000). The enhancement of sulfate reducing microorganisms to decrease sulfate concentration is a further strategy. In addition to acidification, the release of metal(oid)s is also a problem for water quality; particularly in mining areas. The application of clay for adsorptive metal binding, the addition of sludge and the addition of nutrients to enhance biological activity can prevent this problem (Crusius et al., 2003). Brouwer and Roelofs (2002) describe the controlled supply of calcareous groundwater as an alternative method of restoring the pH and the alkalinity of lake water. Numerous publications have been addressed to liming of surface waters and soils (e.g. (Blette and Newton, 1996); (Yavitt and Fahey, 1996)). In principle, liming of the lake body is different to the application of CaCO_3 to lake sediments (Gubala and Driscoll, 1991). Comber et al. (1999) suggest liming of sediment in combination with lake water. Cirmo and Driscoll (1996) and Driscoll (1996) describe the liming of soil in the catchment area as an indirect alternative for lake treatment. Watershed treatment results in a gradual change in pH and alkalinity, in contrast to the direct application of CaCO_3 to water bodies, which is characterized by abrupt increases in pH following liming and subsequent rapid reacidification (Driscoll et al., 1996). Even though liming is successful in raising pH; reacidification often occurs and kills much of the flora and fauna that encroached upon the environment during limed conditions (Dickson et al., 1995). Reacidification may lead to remobilization of metal(oid)s (Lydersen et al., 2002). Brouwer and Roelofs (2002) describe the eutrophication of lakes caused by liming. Cirmo and Driscoll (1996) demonstrated that dissolution of applied CaCO_3 may be accelerated by increased microbial processing resulting in higher partial pressure of CO_2 . Similar results could be obtained for AMD treatment in limestone beds along with elevated p_{CO_2} (e.g. (Sibrell et al., 2006, Watten et al., 2007, Watten et al., 2005, Watten et al., 2004, Hedin et al., 1994)). However, the reacidification in this instance is due to the AMD replenishment from the waste rock piles that need to be taken into account. Thus, either a lake has to be treated on a regular basis before reacidification occurs or the source of AMD has to be rehabilitated or isolated from the lake. Adding carbon dioxide in addition to liming increases the alkalinity buffer and thus limits the reacidification speed (Schipek et al., 2006b, Schipek et al., 2006a, Schipek et al., 2007).

1.2.1.2 Alkalinity production by sulfate reducing organisms

Alkalinity may also be generated through natural or enhanced microbial sulfate reduction (Bailey et al., 1995, Friese et al., 1998). Due to microbial activity, base cations were released resulting in an increase in pH (Kopacek et al., 2003). Furthermore, microbial sulfate reduction leads to an enhanced retention of aluminum (Bailey et al., 1995) and reduction of ferric iron to ferrous iron (Vile and Wieder, 1993). Measures to prevent oxidation of mining waste and to promote anoxic conditions, including measures to fill pits quickly with water may minimize the formation of acids and dissolved metals (Castro and Moore, 2000); however, in some regions quick flooding of pits is impossible and organic material is often used to accelerate bacterial sulfate reduction. Fauville et al. (2004) tested pyruvate, glucose, succinic acid, lactate, ethanol, acetate, and various industrial by-products to create anoxic conditions in bottle experiments. In general, the addition of selected organic carbon compounds sufficiently enhanced bacterial sulfate reduction in order to generate enough alkalinity for raising the pH to near-neutral values (Fauville et al., 2004). Castro et al. (1999) used organic waste products (waste from a potato-processing plant and composted steer manure) in microcosm studies; discovering populations of sulfate reducing bacteria could be increased and pH approached neutrality (Castro et al., 1999). Vile and Wieder (1993) constructed wetlands with different organic substrates (Sphagnum peat with limestone and fertilizer, Sphagnum peat, sawdust, straw/manure, mushroom compost). Koschorrek et al. (2007b) added Carbokalk and straw in field mesocosms; although, the neutral sediment layer became thicker during the experiment, reacidification of the sediment surface was observed. The neutralization rate was limited by the precipitation of iron sulfides rather than sulfate reduction(Koschorreck et al., 2007a). Further microcosm studies had been conducted by (Frommichen et al., 2004, Frommichen et al., 2003). To determine the efficiency of controlled in-situ organic carbon amendments as a possible neutralization method, sediment and water were treated with ethanol and Carbokalk with and without wheat straw (Frommichen et al., 2004, Frommichen et al., 2003). Carbokalk and wheat straw seemed to be most suitable for stimulating growth of sulfate-reducing bacteria. pH increased from 2.6 to 6.5 within the whole microcosm.

1.3 CO₂ sequestration

Three options to reduce total CO₂ emissions into the atmosphere are known: reducing energy consumption, reducing carbon dioxide emitting, and enhancing sequestration of CO₂ (Yang et al., 2008). The first option requires efficient use of energy. The second option requires an energy supply based on non-fossil fuels such as hydrogen and renewable energy. To enhance the sequestration of CO₂, different options are under investigation; natural sinking processes: afforestation (Dixon et al., 1994, Schroeder and Ladd, 1991), ocean fertilization ((Ritschard, 1992), (Markels and Barber, 2002)) and mineral carbonation; or direct artificial CO₂ sequestration: injection into geological formations and the ocean (Yang et al., 2008).

1.3.1 CCS Concept

Carbon dioxide capture and storage (CCS) is one of the main options for reducing atmospheric emissions of CO₂ (IPCC, 2005). The three main components of CCS are capture, transport, and storage.

1.3.2 Capture of CO₂

The purpose of CO₂ capture is to separate CO₂ from other gas components, so that CO₂ can be transported to a storage site. There are different capture systems available: post combustion systems, pre-combustion systems (e.g. oxy-fuel combustion systems), and gasification.

Post combustion systems separate CO₂ from the flue gas by using different sorption materials. Conventional adsorbents (e.g. monoethanolamine) operate according to the principles of physisorption (Chaffee et al., 2007). Therefore, Chaffee et al. (2007) developed inorganic-organic hybrid adsorbents, whose adsorption mechanism involves chemical bonding. Ives et al. (2008) compared different natural sorbents (chicken eggshells, mussel shells, and limestone) for removing CO₂ from combustion gases. In this study, it was found that eggshells and mussel shells have a minor capturing potential in comparison with limestone. Liang et al. (2004) used regenerable Na₂CO₃ as sorbent material for post-combustion processes.

Other authors conducted experiments with natural gas in air and in mixture with oxygen and recycled flue gas; termed O₂/CO₂ recycle combustion to enrich the flue gas with CO₂ (Tan et al., 2002).

The so called oxy-fuel combustion (e.g. (Wang et al., 2008), (Buhre et al., 2005)) system uses oxygen instead of air for combustion. Gasification of coal is a method to produce power, liquid fuels, chemicals, and hydrogen (Supp, 2007, Pichler and Hector, 1965, Häussinger et al., 2007, Dai et al., 2008, Grabner et al., 2007, Lucas et al., 1988).

However, CO₂ capture systems require significant amounts of energy for their operation (IPCC, 2005). This additional energy has to be produced and might emit further CO₂; therefore, the process might not be sustainable or ecologically balanced.

1.3.3 Transport of CO₂

The transport step may be required to carry captured CO₂ to a suitable storage site. The most common method for transporting CO₂ are pipelines; however, transportation as liquid in ships, road or rail tankers is also possible (IPCC, 2005).

1.3.4 Storage of CO₂

The most often published CO₂ storage concept is the sequestration of CO₂ in geological formations. Different formations such as depleted oil and gas reservoirs (e.g. (Beccaluva et al., 2001); (Stevens et al., 2001); (Braccini et al., 2005)), deep saline aquifers (e.g. (Palandri et al., 2005); (Bachu and Adams, 2003)), and deep and unmineable coal beds (e.g. (Prusty,

2008); (Stevens et al., 1999); (Hamelinck et al., 2002); (White et al., 2005)). Geological sinks for CO₂ do not really need any major technological development; the challenge is rather to identify the best methods and sites for long-term CO₂ sequestration (Bachu, 2000). Apart from that Huijts et al (2007) pinpoint that the social acceptance of CO₂ storage is not definite. People judge the idea of storage in general as slightly positive, but when the technology enters people's daily lives, as in storage nearby, the attitude becomes more negative ("not in my backyard") (Huijts et al., 2007).

Marchetti (1977) and subsequent studies (e.g. (Herzog et al., 1991); (Ohsumi, 1995); (Hirai et al., 1999)) proposed CO₂ sequestration into the deep ocean. However, recent studies show that ocean CO₂ sequestration (e.g. (Ishimatsu et al., 2006); (Thistle et al., 2007)) may have negative influence on marine organisms such as reduced rates of calcification, reproduction, growth, mobility as well as increased mortality over time (IPCC, 2005).

A more sustainable concept for CO₂ sequestration is mineral carbonation, which involves converting CO₂ to solid inorganic carbonates using chemical reactions (IPCC, 2005). For the mineral carbonation process, many different alkaline materials may be used. Teir et al. (2007), Teir et al. (2009), Haenchen et al. (2008), and Park et al. (2003) propose the precipitation of magnesium carbonates using Mg-bearing silicate rocks like olivine or serpentinite. Uibu et al. (2009) investigated ash formed during oil-shale combustion, which contains free Ca and Mg oxides and could show that free CaO is the main CO₂ binding component in ash, but other components such as MgO and Ca-silicates may also participate in the carbonation process. Montes-Hernandez et al. (2009) propose the use of ash from coal combustion for the mineral carbonation process. Stolaroff et al.(2005)), Eloneva et al. (2008), and Huijgen et al. (2005) used Ca(OH)₂ and CaO from steel slag and concrete waste to react with CO₂ to form stable carbonate minerals. Koljonen et al. (2004) investigated the industrial reuse potential of CO₂ in Finland, since sequestration of CO₂ in geologic formations or in the ocean is not suitable. CO₂ consuming industries such as pulp and paper, beverage, food processing and metal industries offer niches, wherein CO₂ capture processes could become economical (Koljonen et al., 2004).

1.4 Lake Liming

1.4.1 General information

Compared to the above-mentioned restoration methods direct liming of acidified surface waters seems to be the most cost effective treatment method. Experiences in direct liming of lakes over more than three decades can be found mainly in Sweden, Norway and Finland.

In Northern European lakes, the acidic load originates mainly from the atmosphere and is not influenced by pyrite weathering. Since more than 30 years, direct liming in catchment areas, or of lakes by boat or helicopter, was applied (Henrikson et al., 1995, Sverdrup, 1985). A number of publications exists dealing with the properties of the neutralizing agents and their influence on the success of the remediation strategy (Nyberg and Thornelof, 1988). Positive effects resulted not only in terms of water quality aspects but also for the whole ecosystem (Driscoll et al., 1996, Guhrén et al., 2007, Iivonen et al., 1995). Furthermore, there are considerations and experiences in the rehabilitation of mining lakes by liming, in the United States (Castro and Moore, 2000, Dowling et al., 2004), Finland (Ahtiainen et al., 1983). Despite considerable research only little information is available in international literature for

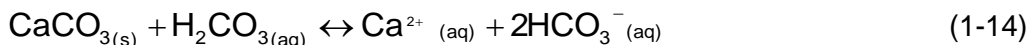
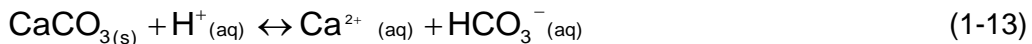
acidic lakes in Germany (Bozau et al., 2007a, Koschorreck et al., 2007a, Hemm et al., 2002). In order to optimize direct liming of acidified surface water, there are several considerations (Merkel et al., 2010).

1.4.2 Solution and precipitation of carbonates

The solution and precipitation of carbonates has been studied by various scientists (Plummer et al., 1978, Dreybrodt et al., 1996, Liu and Dreybrodt, 1997, Reddy, 1980, Rickard and Sjoberg, 1983, Svensson and Dreybrodt, 1992).

Dissolution rates of carbonates in natural waters were determined experimentally by various authors (Weyl, 1958, Terjesen et al., 1961, Berner, 1967, Nestaas and Terjesen, 1969). Carbonate mineral dissolution rates are influenced by varying solution composition (Arvidson et al., 2006, Vinson et al., 2007). Investigations of the solution kinetic in sea water was carried out by Berner and Morse (1974).

The first mechanistic rate law of the calcite dissolution kinetic was formulated by Plummer et al. (1978) as a function of the surface activity of the involved species. The following reactions occur in parallel during carbonate dissolution under ambient conditions:



The dissolution process is described to be controlled by different rate limiting steps, dependent on pH. The overall reaction expression can be described as follows:

$$R = k_1 a_{\text{H}^+} + k_2 a_{\text{H}_2\text{CO}_3^*} + k_3 a_{\text{H}_2\text{O}} - k_4 a_{\text{Ca}^{2+}} a_{\text{HCO}_3^-} \quad (1-16)$$

where

$$k_4 = \frac{K_2}{K_c} \left(k_1' + \frac{1}{a_{\text{H}^+}} [k_2 a_{\text{H}_2\text{CO}_3^*} + k_3 a_{\text{H}_2\text{O}}] \right) \quad (1-17)$$

k_1 , k_2 and k_3 are first-order rate constants dependent on the temperature. k_4 is the backward rate constant. K_2 is the second dissociation constant for carbonic acid. K_c is the solubility product of calcite, and H_2CO_3^* is the sum of undissociated carbonic acid and dissolved aqueous CO_2 . The value H^+ represents the H^+ -activity at the calcite surface. Transport and interface reactions occur consecutively, thus, the slowest reaction is rate limiting (Brantley, 2008). Two regions of dissolution were distinguished based on pH and p_{CO_2} : for $\text{pH} < 3.5$, dissolution is controlled by transport (rate $\sim a_{\text{H}^+}$), while for $\text{pH} > 3.5$ surface reaction is slower than the transport and the rate becomes more surface-controlled. At still higher pH, the third reaction ((1-15), hydrolysis of calcite, see above) becomes important.

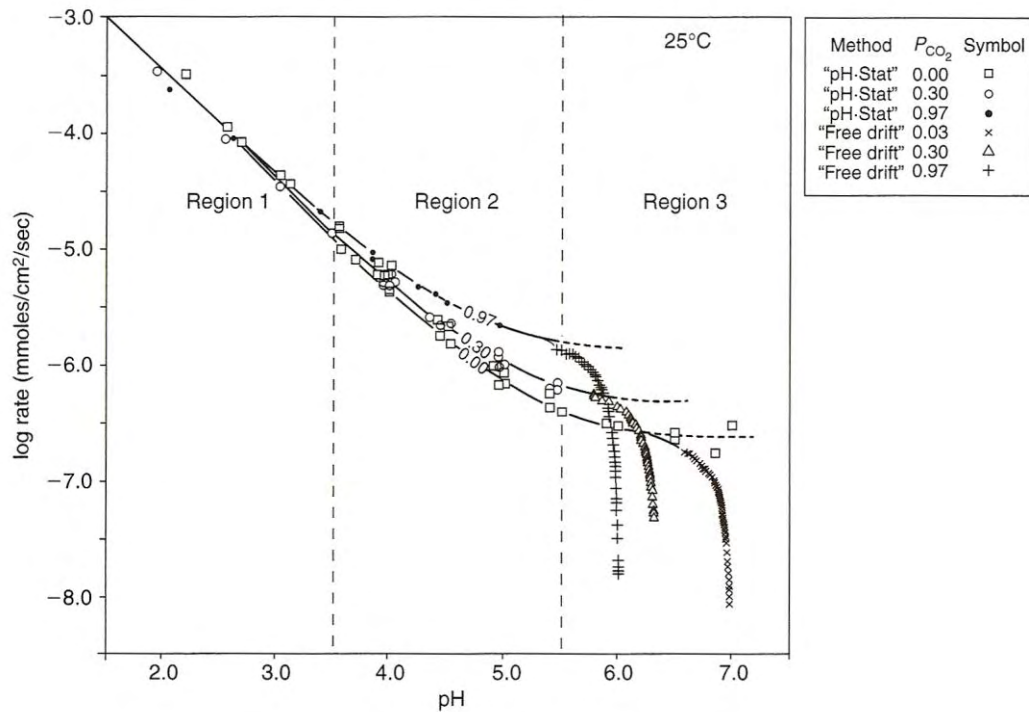


Figure 8. Log rate of calcite dissolution (mmoles dissolved $\text{cm}^{-2} \text{ sec}^{-1}$) as a function of bulk fluid pH and CO_2 in stirred solutions at 25°C. Region 1 and 2 are far from equilibrium and rate depends only on forward reaction (see text). Dissolution rate in region 3 is a function of both forward and reverse rates of reaction (Plummer et al., 1978).

Chou et al. (1989) formulated a mechanistic rate law for various carbonates (calcite, aragonite, witherite, magnesite, and dolomite) similar to Plummer et al. (1978). Elementary steps during the dissolution reactions are:



M represents the metal ion (Ca^{2+} , Mg^{2+} , or Ba^{2+}). The total forward and backward rates can be expressed as follows (Chou et al., 1989):

$$R_{\text{forward}} = k_1 a_{\text{H}^+} + k_2 a_{\text{H}_2\text{CO}_3^*} + k_3 \quad (1-21)$$

$$R_{\text{backward}} = k_{-1} a_{\text{M}^{2+}} a_{\text{HCO}_3^-} + k_{-2} a_{\text{M}^{2+}} a_{\text{HCO}_3^-}^2 + k_{-3} a_{\text{M}^{2+}} a_{\text{CO}_3^{2-}} \quad (1-22)$$

For calcite, the following net rate can be formulated:

$$R = k_1 a_{\text{H}^+} + k_2 a_{\text{H}_2\text{CO}_3^*} + k_3 - k_{-3} a_{\text{Ca}^{2+}} a_{\text{CO}_3^{2-}} \quad (1-23)$$

A number of studies dealt with empirical laws to describe the solution kinetics of calcite (Berner and Morse, 1974, Eisenlohr et al., 1997, Palmer, 1991, Svensson and Dreybrodt, 1992). Some publications dealt with the description of the solution kinetics of synthetic, high-purity calcite (Sjoberg, 1978, Gutjahr et al., 1996b, Compton et al., 1986, Chou et al., 1989).

Due to the differences in solution kinetics of natural calcite and synthetic calcite, results of these laboratory studies are not compatible with natural systems (Svensson and Dreybrodt, 1992). Literature studies showed a direct influence on the solution kinetics of calcite by conditions such as CO₂ partial pressure, temperature, turbulence of a system, and other ions.

According to Svensson and Dreybrodt (1992) natural limestone contains impurities that accumulate at the mineral surface during the dissolution process and interact with Ca²⁺/HCO₃⁻ ions absorbed from the solution on the surface. As mentioned above numerous publications deal with the study of solutions kinetics of synthetic, highly pure calcite. These results are not applicable to natural systems as natural limestone differs in its solution behavior (Svensson and Dreybrodt, 1992). Furthermore a great variance between natural carbonate rocks exists (Eisenlohr et al., 1999).

Different processes depending on pH dominate the calcite-solution kinetics (Berner and Morse, 1974, Buhmann and Dreybrodt, 1985, Dreybrodt et al., 1996, Liu and Dreybrodt, 1997). Solution kinetics at low pH (pH < 4) is dominated by the diffusion rate of available protons to the calcite surface (Berner and Morse, 1974). If the pH increases, boundary conditions get dominant (thickness of the diffusion boundary layer, thickness of the turbulent water film). Natural calcites showed a change in their solution behavior as the water was near the equilibrium. A change of the reaction kinetics established by the inhibition of surface reactions occurs (Dreybrodt et al., 1996, Svensson and Dreybrodt, 1992).

1.4.2.1 Influence of varying CO₂ partial pressure

As described above at low pH calcite dissolution rates are transport-controlled and are not dependent upon CO₂ partial pressures, whereas at pH > 3.5, dissolution becomes interface-controlled. Diffusion processes across the boundary layer on a mineral particle is fast compared to the rate of the interface reaction, so the concentration of solutes in the layer equals the bulk concentration. Hence, dissolution in the high pH region is more dependent upon p_{CO₂} (Brantley, 2008).

Considering increased CO₂ partial pressures during the dissolution process of calcite, the overall reaction can be described as follows (Appelo and Postma, 1996):



An increase of CO₂ results in enhanced dissolution of CaCO₃. Different authors investigated varying CO₂ partial pressures during the dissolution of calcites. Table 2 shows an overview about relevant publications dealing with calcite dissolution. Experimental conditions, type of used solid, temperature, p_{CO₂} are also shown. The last column gives a hint on the measured parameters to estimate the equilibrium state of the dissolution reaction.

Table 2. Overview about conducted experiments of different authors regarding calcite dissolution rates with respect to different parameters (experimental set-up, p_{CO_2} , temperature etc.)

Source	Experimental set-up	Material	p_{CO_2}	Temperature	pH	Measuring values
(Alkattan et al., 1998)	Free-drift, rotating disc	Single calcite crystals	-	25 / 50 / 80°C	1 – 3	
(Berner and Morse, 1974)	pH-stat	Synthetic calcite	$1 \cdot 10^{-4.5}$ atm	25°C	3.9 -7.5	
(Buhmann and Dreybrodt, 1985)	Open system	Carrara marble, pure limestone	$5 \cdot 10^{-3}$ atm, $3 \cdot 10^{-4}$ atm	10 / 20°C		Ca
(Buhmann and Dreybrodt, 1987)	Open system	Carrara marble	$5 \cdot 10^{-3}$ atm			Ca=f(EC)
(Busenberg and Plummer, 1986)	Open system		0 – 0.99 atm	25°C		
(Chou et al., 1989)	Fluidized bed reactor	Calcite, aragonite, magnesite, witherite, dolomite		25°C	3 - 10	pH, Ca, Mg, Ba, alkalinity
(Dreybrodt et al., 1997, Dreybrodt et al., 1996)	Free-drift, Closed system	Baker calcite, natural marble (Greece)	$5 \cdot 10^{-3}$, $1 \cdot 10^{-2}$, $1 \cdot 10^{-1}$ atm	20°C		Ca=f(EC)
(Eisenlohr et al., 1999)	Batch, closed system		0.05 atm	10°C		
(Gledhill and Morse, 2006a)	pH-Free-drift, open system		0.1 – 1 atm	25.0 – 82.5°C		Ca=f(pH)
(Gutjahr et al., 1996b)	pH-stat	Calcite, aragonite	0 atm	20 – 70°C		
(Herman, 1982)	Rotating disc	Calcite single crystals	1 atm	25°C		
(Inskeep and Bloom, 1985)	pH-stat		< 0.01 atm		> 8	
(Morse, 1978)	Closed system		0.0003	25°C		
(Palmer, 1991)	Open system		0.003 – 1 atm	20°C		
(Plummer and Busenberg, 1982)		dolomite, aragonite				
(Plummer and Wigley, 1976)	Free-drift	Iceland Spar	1 atm	25°C		Ca=f(pH)

Source	Experimental set-up	Material	pCO ₂	Temperature	pH	Measuring values
(Plummer et al., 1978)	pH-stat, free-drift	Iceland Spar	0.0 – 1.0 atm	5 – 60°C	2 - 7	pH (time), pCO ₂
(Pokrovsky et al., 2005)		Calcite, dolomite, magnesite		25°C		
(Pokrovsky et al., 2009a)	Rotating disk, closed system	Calcite, dolomite, magnesite	1 – 55 atm	25 – 150°C		Ca=f(pH)
(Rauch and White, 1977)	Recirculating water through tubes bored in limestone					
(Rickard and Sjoberg, 1983)	Rotating disc, pH-stat	Carrara marble		25°C		pH
(Sjoberg, 1976)	Rotating disc	Pure calcite	0	5-50°C		
(Svensson and Dreybrodt, 1992)	Free-drift, Open system	NBS calcite; natural calcites: marbles, limestones, marine pelagic sediments	0.005 atm	20°C		Ca=f(EC)
(Vosbeck, 2004)	Batch, closed system	Baker calcite	0.0003 – 0.1 atm	10°C		
(Wallin and Bjerle, 1989a, Wallin and Bjerle, 1989b)						

1.4.2.2 Influence of inhibiting ions

The composition of investigated calcite materials has a strong influence on the solution kinetics (Arvidson et al., 2006, Cubillas et al., 2005, Vinson et al., 2007). Natural lime products often contain trace ions such as magnesium, aluminum, silicates, phosphate, strontium, and iron. These ions are often bound by sorption on the surface of calcite minerals, and thus inhibit the solution of the limestone.

Additionally constituents in natural waters have a strong influence on the solution kinetics by changing the saturation state of the solution or by sorption processes on the mineral surface. Buhmann and Dreybrodt (1987) describe ionic-pairing effects, ionic-strength effect, common-ion effect, acid effect, and base effect.

Important mining-related water constituents include sulfate, manganese, cadmium, and iron. Only little information regarding the effect of dissolved sulfate on the dissolution kinetic of calcite is available. The results of different authors (Akinfiev and Diamond, 2003, Dreybrodt and Gabrovsek, 2000, Edenborn et al., 1986) provide inconsistent evidence for the inhibition

of the dissolution by sulfate ions. Other authors (Lea et al., 2001, Vinson et al., 2007) describe the inhibition by manganese and strontium. Table 3 shows an overview about published investigations under consideration of different inhibitors.

Table 3. Overview about published investigations of authors regarding different inhibiting ions affecting calcite dissolution rates.

Inhibitor	source
Ba ²⁺	(Gutjahr et al., 1996a)
Ca ²⁺	(Buhmann and Dreybrodt, 1987, Gledhill and Morse, 2006a, Gledhill and Morse, 2006b, Gledhill and Morse, 2004, Gutjahr et al., 1996b, Gutjahr et al., 1996a, Sjoberg, 1978, Sjoberg and Rickard, 1985)
Cl ⁻	(Gledhill and Morse, 2006a, Gledhill and Morse, 2004, Alkattan et al., 2002)
CO ₃ ²⁻	(Lea et al., 2001)
Cu ²⁺	(Gutjahr et al., 1996a)
Fe ²⁺	(Gutjahr et al., 1996a)
Mg ²⁺	(Akin and Lagerwer.Jv, 1965b, Berner, 1967, Berner and Morse, 1974, Morse et al., 1979, Morse et al., 1997, Reddy, 1980, Zhang and Dawe, 2000, Gledhill and Morse, 2006a, Gledhill and Morse, 2004, Burton and Walter, 1991, Arvidson et al., 2006, Lea et al., 2001, Alkattan et al., 2002, Gutjahr et al., 1996a, Compton and Brown, 1994, Sabbides and Koutsoukos, 1994)
Mn ²⁺	(Vinson et al., 2007, Franklin and Morse, 1983, Dromgoole and Walter, 1990, Terjesen et al., 1961, Gutjahr et al., 1996a, Lea et al., 2001)
Na ⁺	(Buhmann and Dreybrodt, 1987, Gledhill and Morse, 2006a, Gledhill and Morse, 2004, Alkattan et al., 2002)
Organics	(Inskeep and Bloom, 1986, Pokrovsky et al., 2009a, Lebron and Suarez, 1998)
PO ₄ ³⁻	(Walter and Hanor, 1979, Burton and Walter, 1990, Walter and Burton, 1986, Morse, 1974, Svensson and Dreybrodt, 1992, Sabbides and Koutsoukos, 1994, Sabbides and Koutsoukos, 1996)
Silica	(Klein and Walter, 1995)
SO ₄ ²⁻	(Mucci et al., 1989, Kushnir and Kastner, 1985, Akin and Lagerwer.Jv, 1965b, Dreybrodt and Gabrovsek, 2000, Vosbeck, 2004)
Sr ²⁺	(Lea et al., 2001, Gutjahr et al., 1996a)
Zn	(Gutjahr et al., 1996a)

Contradictory meanings of the authors in Table 3 can be reasoned by experimental and analytical methodology (free drift runs vs. flow cells, open vs. closed systems), different calcite materials (synthetic, ultra-pure material vs. natural materials), varying concentrations of inhibitors, varying pH values, or other factors.

1.4.3 Advanced Mobile Inlake Technology (AMIT)

To face the atmospheric immissions of acids in Swedish lakes, spreading techniques by boats have been developed in the 1970's. Boat technologies are able to distribute powdered limestone very equally over the surface of the lake in order to achieve a complete

neutralization of the water and to set up a buffer to prevent fast re-acidification (Sverdrup, 1985). Current boat technology is able to distribute up to 250 tons per day (Pust et al., 2010).

The Swedish technology worked reasonable fine for the past 30 years to treat acidified lakes with a pH value above 4. An important advantage of the boat technology is the comfortable transportability on a normal trailer and the possibility of a direct launching without an artificial slipway (Pust et al., 2010). As described, water chemistry in German mining lakes is different from those in Sweden. Therefore a special neutralization strategy was developed and proven for its applicability (Pust et al., 2010, Merkel and Schipek, 2008). Detailed results of conducted preliminary investigations and column experiments had been focus of this thesis and are shown in chapter 4.4. Results of AMIT itself are shown in chapter 4.6.

1.5 Fly ash

1.5.1 Coal combustion by-products (CCBs)

Coal combustion by-products (CCBs) are formed through high-temperature combustion of coal for power production (EPRI - Electric Power Research Institute & Southern Company Services, 2006). The mineralogy and the geochemical behaviour of fly ash is greatly influenced by the parent coal from which it is derived, as well as by the combustion technology. Fly ashes can be distinguished in 2 classes: class C (Brown Coal Fly Ash) and class F (e.g. (Tauber, 1988, Rostami and Brendley, 2003, Hoffman, 2002, Manz, 1999, Rao et al., 1998)). Class C fly ash is formed by the combustion of lignite. The amount of CaO in class C fly ash is about 20 wt.-% (Singh and Kolay, 2002). Class F fly ash contains less CaO (< 5 wt.-%) and consists of large amounts of unburned carbon. This ash is formed during the combustion of anthracite or hard coal (Singh and Kolay, 2002). Worldwide many fly ashes have been investigated mineralogically and geochemically (Hower et al., 1999, Hower et al., 2001, Koukouzas et al., 2007, Koukouzas et al., 2006, Perez-Lopez et al., 2007c, Prashanth et al., 2001, Querol et al., 2001, Singh and Kolay, 2002, Steenari et al., 1999, Vassilev and Vassileva, 2007, Vassilev and Vassileva, 2005, Vassilev and Vassileva, 1996, Vassilev et al., 2005). Despite variations in the constitution of these investigated ashes, the amount of amorphous glass phases is more than 50 wt.-%. The principal components of fly ash are quartz, lime (CaO), iron oxides (hematite, magnetite) and different silicates.

The thermic behavior of coal constituents and the resulting ash composition is described in detail by different authors (Münch, 1996, RWE and IfK, 1995). Tauber (1988) investigated the development of fly ash particles (cenospheres) with regard to trace element accumulations. The main components of the lignite filter ash are specified for the full analysis of the metal oxides. The Lusatian fly ash is mainly composed of: Al₂O₃, CaO, MgO, Fe₂O₃, MnO, K₂O, SiO₂, Na₂O, TiO₂, SO₃ (mbH and AG, 1995). Especially interesting pertaining to the goal of this thesis are the CaO and MgO that can be used for the carbonate formation and for the alkaline reaction in the aqueous phase.

The majority of the CCB materials produced in Germany are disposed in landfills and pond impoundments where meteoric water or groundwater may percolate through, and interact with metastable ash materials (Kayser et al., 1986). Metastable phases like coal ash may persist in weathering conditions for long time periods, but are thermodynamically unstable due to their high temperature of formation and composition (EPRI - Electric Power Research Institute & Southern Company Services, 2006). They will react with meteoric fluids and

convert to stable, low-temperature phases over time. Because of this the conversion elevated levels of many trace elements, as well as secondary minerals, that are more stable in the disposal environments will be found (see chapter 1.5.2).

1.5.2 Use of fly ash for treatment of AMD affected waters

The neutralization of AMD with various liming agents is described in chapter 1.2 and chapter 1.4. High costs are an important disadvantage of these chemical treatments of AMD (Gitari et al., 2008a); which has produced a search for cheaper and more effective liming agents. Alkaline industrial by-products that are gaining importance in the treatment of AMD include cement kiln dust, red mud bauxite, and the highly alkaline steel slag.

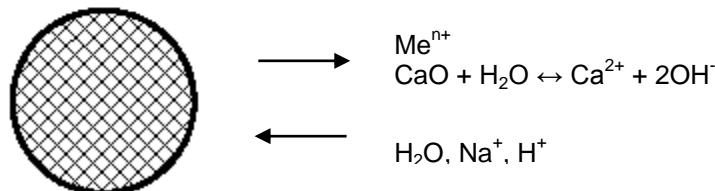
Several authors have investigated the capacity of fly ash to improve the quality of leachates generated by coal refuse (Wilson et al., 2001, Stewart et al., 1997, Daniels et al., 1993), by oxidation of sulfide-rich mining waste (Perez-Lopez et al., 2007c, Perez-Lopez et al., 2007b, Perez-Lopez et al., 2007a) and passive treatment of AMD (Gitari et al., 2008a). The prevention of acidic leachate generation and a significant reduction of inorganic contaminants were observed (Vadapalli et al., 2008, Gitari et al., 2008b, Gitari et al., 2006, Perez-Lopez et al., 2007c).

1.5.3 Weathering products

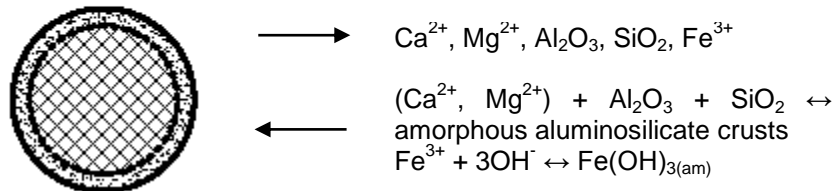
Zevenbergen et al. (1999, , 1994) indicated that the products of incineration ash weathering behave analogous to volcanic ashes; although, the kinetics are different. The new formation of well-ordered clay minerals such as illite and non-crystalline clay (allophones) from incineration ashes after about 10 years of weathering were described (Zevenbergen et al., 1999, Zevenbergen et al., 1994). Other authors investigated the conversion of fly ash into zeolites (Kasture et al., 2005, Lin and Hsi, 1995, Michihiro Miyake, 2002, Penilla et al., 2003). Long-term leaching behavior seems to be affected by the precipitation of clay and other secondary compounds such as Fe- and Al-Hydroxides.

Many authors have investigated mineral alterations (Weinberg and Hemmings, 1997, Warren and Dudas, 1985). The EPRI (2006) developed a model for alkaline fly ash weathering (Figure 9) where the main geochemical reactions during the formation of secondary minerals in CCB materials are: hydration, solution, hydrolysis, carbonation, oxidation, precipitation, adsorption and co-precipitation (EPRI - Electric Power Research Institute & Southern Company Services, 2006). During phase 1 (Figure 9) oxides and soluble salts existing on ash particle surfaces are dissolved when mixed with water. The ensuing hydrolysis of CaO results in a rapid increase in pH; the higher pH during phase 2 dissolves the more soluble glass, at the outer surfaces of ash, releasing cations. Supersaturation of these cations cause the formation of amorphous crusts (made of aluminosilicates and Fe-hydroxides). In phase 3, the formation of amorphous crusts continues and their initial transformation into more crystalline phases begins. The dissolution of cations from inner glass continues. Phase 4 involves the aging of amorphous phases into thermodynamically stable phases like Fe-oxides, clay minerals, and zeolites.

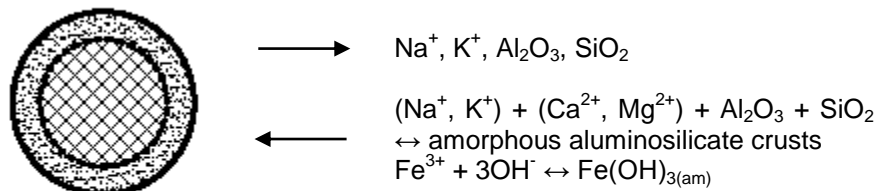
Phase 1: Fresh fly ash. Dissolution of soluble salts and oxides on particle surfaces.



Phase 2: Dissolution of outer glass from ash particles. Formation of amorphous crusts.



Phase 3: Continuing formation of amorphous crusts, aging of crusts. Diffusion-limited dissolution of inner glass from ash particles.



Phase 4: Transformation of amorphous crusts.

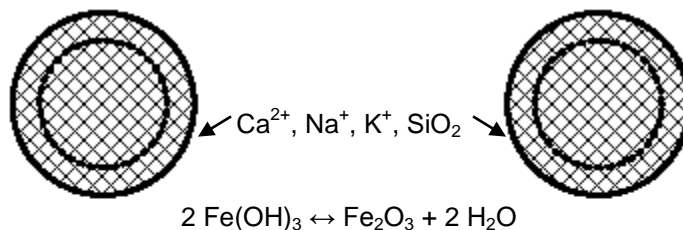


Figure 9. Model for Alkaline Fly Ash weathering (EPRI - Electric Power Research Institute & Southern Company Services, 2006)

The amorphous aluminosilicates formed during weathering are able to adsorb much larger quantities of cations and anions than crystalline glass because they have a much greater surface area and the surfaces possess greater charges (Haynes, 2009)

1.5.4 Mineral CO₂ sequestration by carbonation of fly ash

As mentioned in chapter 4.4, industrial by-products present alkaline materials that are usable for mineral CO₂ sequestration.

Abanades et al. (2004) investigated the carbonation reaction of CaO, as a potential method for CO₂ capture from combustion flue gases. Huijgen and Comans (2005) give an overview about mineral CO₂ sequestration by carbonation of industrial residues (MSWI bottom ash, coal fly ash, slag).

Industrial by-products are generally rich in calcium when Ca-minerals often control the pH (Meima and Comans, 1997). The carbonation of Ca-minerals is the main CO₂ sequestration reaction for residues.

According to Huijgen and Comans (2005) different reactions can be distinguished:

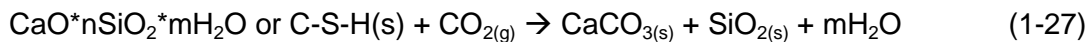
- i. Fly ash often contains portlandite, which controls the solubility of Ca as well as pH. Portlandite is carbonated relatively easily (Huijgen, 2003).



- ii. Ca-silicates (e.g. CaSiO₃, wollastonite) represent another group of Ca-minerals for carbonation:



Or in general (Huijgen and Comans, 2005):



- iii. Ettringite in CCBs. In fresh fly ash samples, a typical secondary mineral is ettringite ((CaO)₆(Al₂O₃)(SO₄)₃ · 26 H₂O). At low pH-values, ettringite is not stable; generally, there is no occurrence in carbonated residues.

The sequestration potential for MSWI fly ash was calculated to be 155 CO₂ g/kg and an acid neutralizing capacity of 55 g/kg was determined (Huijgen and Comans, 2005).

1.6 Kinetics

1.6.1 General

Rates of chemical reactions (e.g. water-rock interactions) can be determined by using reaction vessels (Brantley and Conrad, 2008). Chemical reactors to determine kinetic rates can be divided according their mode of operation (Dietzsch et al., 2007).

According to Brantley and Conrad (2008) a reactor is a perfectly stirred container (tank reactor) whose contents are always homogenous in concentration and temperature. Different modi seem possible: batch (no flow in/out, discontinuous mode) or flow mode (flow process, continuous mode). In contrast, tubular reactors exist, where a fluid moves through a tube, creating a continuous gradient in concentration of reactants and products. If reactants are

added or products are removed during investigation, reactors often are called semi-batch reactors (Brantley and Conrad, 2008).

1.6.2 Batch reactors

Brantley and Conrad (2008) describe batch reactors as “simplest reactors for use”, as they are “agitated or stirred tanks which are set up with all reactants either closed or open to the atmosphere”.

According to Dietzsch et al. (2007) advantages of batch reactors are low financial costs due to the use of beakers and low level of automation, preferentially for the production of low products, high flexibility, and usable for reactions with long reaction times.

Main disadvantages are as follows: time amount for filling and emptying, higher energy effort due to heating and cooling of the reaction mixture, low level of automation. If reaction progress cannot be monitored by in-situ sensors, aliquots of solution must be sampled sequentially. This makes calculation of reaction rate more complex. Interpretation might be complicated because the measured rate may change as a function of time as the solution chemistry changes (pH, ionic strength) in the reactor. If acid or base is added in order to suppress pH changes reactor type changes to semi-batch mode.

Additionally several publications deal with problems of using batch reactors for reactions where rate changes with time (Oelkers et al., 2001).

pH-stat and free drift methods can be used to measure dissolution rates of minerals. According to Sjöberg and Rickard (1983) powder runs have the advantage of making a large reactant surface area available. Particles less than 10 µm are very slow relative to the solution at normal stirring rates. This leads to the assumption of a stationary diffuse layer. Different authors report a stirring dependence of the dissolution rate of fine powders (Sjoberg, 1976).

Experiments using the rotating disk technique are said to be hydrodynamically well-defined (Sjoberg, 1976). Critical parameters include disc size, vessel size, and rotation speed.

1.6.3 Flow-Through Reactors

Mixed flow reactors, also called stirred flow-through reactors or continuously stirred tank reactors (CSTR), allow maintenance of constant solution chemistry during reaction (Brantley and Conrad, 2008). A mineral sample can be placed in a tank with a specified volume through which the fluid is continuously pumped with a constant flow rate. To obtain ideal conditions (homogenous concentration and temperature) in the vessel, the reactor is continuously stirred by a propeller or by agitation. Ideal mixing of solid and aqueous reactants is provided by using suspended powdered solid reactants. Mixed flow reactors provide direct measurements of the reaction rate. Experiments are run until the outlet concentration reaches constant values (steady-state value that represents the steady-state reaction rate).

Plug-flow reactors (PFR, packed bed reactors, column reactors) are tubular reactors that represent more closely natural systems. Due to possible precipitation of product phases and the non-ideality of flow through packed beds of particles. They are more complicated to

model than continuously stirred tank reactors. Interpretation of PFRs is difficult due to the changing chemical affinity as a function of position in the reactor, and the possibility of precipitation of secondary phases (Brantley and Conrad, 2008).

Advantages of continuous mode are high level of automation, equal product quality, and higher output. Main disadvantages comprise higher financial costs due to higher level of automation, and less flexibility due to the optimisation for specific reactions (Dietzsch et al., 2007).

2 Investigation area

2.1 Mining Lakes in the Lausitz area

As stated by Zschiedrich (2011) the water deficit in the Lusatian mining district had been restocked with a total amount of 5.3 billion m³ water. Nearly 3.4 billion m³ water were necessary to refill the groundwater body. Concerning surface waters, approximately 1.9 billion m³ have been utilized since 1990.

In total 28 mining lakes will form with an area of around 14.000 ha. At the very moment (12/2010), an area of 11,938 ha was flooded with 1.68 billion m³. This equals 84 % of the area and 74 % concerning water level (Zschiedrich, 2011).

2.2 Flooding concept

Immediately after stopping mining-related groundwater depression, recovering of groundwater forced the inflow of groundwater into the existing open pits. Additionally precipitation leads to groundwater rising in newly formed catchment areas. Problems concerning groundwater and surface water chemistry occurred as mentioned in chapter 1.1.1.

The current flooding and water treatment concept of Lausitzer and Mitteldeutsche Bergbau-Verwaltungsgesellschaft (LMBV) of the years 2003 and 2005 was recently renewed in 2007 on the basis of verified data for water resources, actualized information about geohydrological conditions in ground water horizons, on results in current remediation processes and change of use requirements (Zschiedrich et al., 2007).

Goals described in (Zschiedrich et al., 2007) include

- possibly balanced water level increase to avoid large differences between the single lakes and possible geotechnical risks
- consequently, relative low groundwater gradients within the flooding phase to avoid high loads of acidity and special treatment processes

Flooding of open pits will be reached by rising groundwater levels and – additionally flooding by other sources (water from rivers, treatment plants, etc.). The period of flooding of a developing lake will be 10 to 15 years (Zschiedrich, 2011).

Water quality aims for discharging water from the pit lakes had been fixed in an official approval and by the working committee for water quality (Arbeitskreis "Gewässergüte"), Table 4 shows quality goals for selected water constituents (Zschiedrich et al., 2007).

Table 4. Water quality goals according to official approval and according to the working committee for water quality (Zschiedrich et al., 2007)

Parameter	Dimension	Concentration in discharging water
pH	[-]	6.5 – 8.5
Fe _{total}	ppm	≤ 3.0
Fe _{dissolved}	ppm	≤ 1.0
Sulfate	ppm	≤ 800
Ammonia-N	ppm	≤ 1.5
Zinc	ppm	≤ 1.0
Copper _{dissolved}	ppm	≤ 0.04

In the end of the flooding phase the acidity in the Lausitz region comprises around 2500 million mol acidity (total summarized lake volume = 830 million m³_{water}, median of acidity in the end of the flooding phase = 3 mol_{acidity}/m³_{water}). Additionally there will be acidity provided by groundwater (300 million mol_{acidity}/a) (Zschiedrich et al., 2007).

2.3 Lake Burghammer

The Burghammer lignite mining field is located at the eastern foothill of the Spreetal lignite mining field, covering an area of about 8.8 km². It was situated in the northern part of the former Hoyerswerda district, in the south of the district town Spremberg and in the east of the open-cast mine Spreetal. In the north, the east and the south Burghammer was limited by leachings and in the western district it was bordered by the partially exhausted Spreetal mining field.

The western part of the Burghammer lignite mining field was intersected by the river "Kleine Spree" and the road Burg – Burghammer. Today, the mining lake is situated to the southeast of Burghammer, northeast of the site Burg and to the west of the diverted river "Kleine Spree".

The groundwater recession occurred from a ground level of +68 m NN. This maximal drawdown was maintained from 1963 – 1973; until the open-pit mining was terminated. The resulting cone of depression cannot be localised, because at that time other cones of depression from the surrounding open-pits Lohsa, Spreetal, and Scheibe, interfered with each other (Figure 10). In this respect, an own cone of depression cannot be associated to the Burghammer open-pit. The south, the southwest, the northwest and the north of the mining lake is restricted by the open pit's anthropogenic embankments; the east is lined by the mines dump system.

Regarding Burghammer in the sense of a water reservoir, the groundwater inflow develops accordingly to its dependence on the water levels of the surrounding open-pits (specifically Lohsa II). The largest difference between the water levels will exist during phases of low water between Dreiweibern and Lohsa II with 6.5 m, during the phase of maximum water level between Lohsa II and Burghammer with 7.4 m. Because of the relatively constant water level in Lohsa II and the rising water level in Burghammer, a lowering of the (potential-) gradient occurs, resulting in an obvious decrease of iron and sulfate.

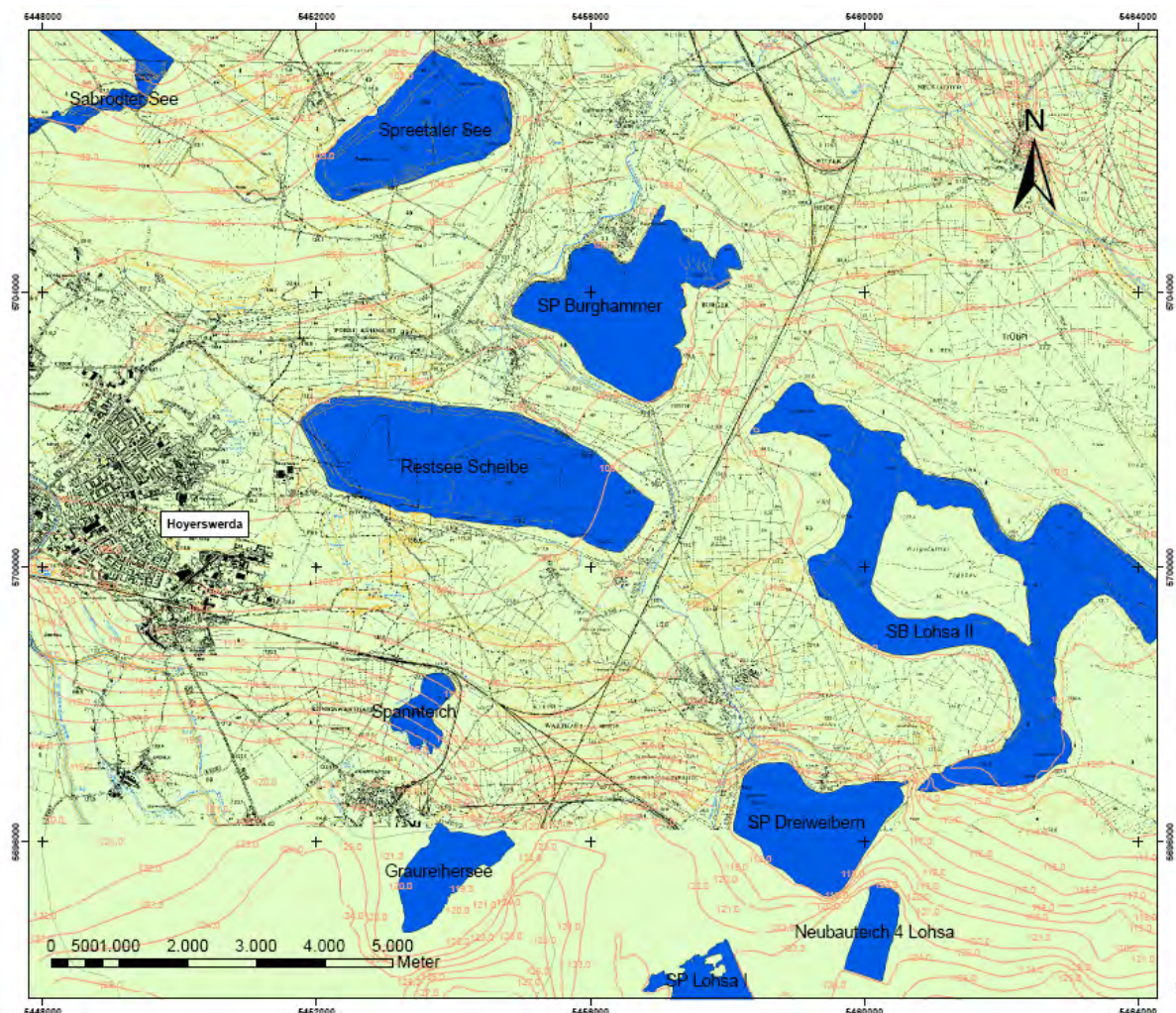


Figure 10. Topographical map of the investigation area surrounding Lake Burghammer (TK25, Sheet 4551 Hoyerswerda, 4552 Weißkollm; issue date 1990).

The mining lake Burghammer will be used as water reservoir and will be the last lake in the water storage chain Lohsa II. Tasks will be guaranteeing an ecological and hydrological necessary minimum flow to the river Kleine Spree and Spree (see Figure 11). This storage system will be realized by connecting the mining lakes Lohsa, Dreiweibern and Burghammer. Together with the mining lake Bärwalde a storage volume of 90 million m³ will be available (Zschiedrich, 2011).

Investigation area

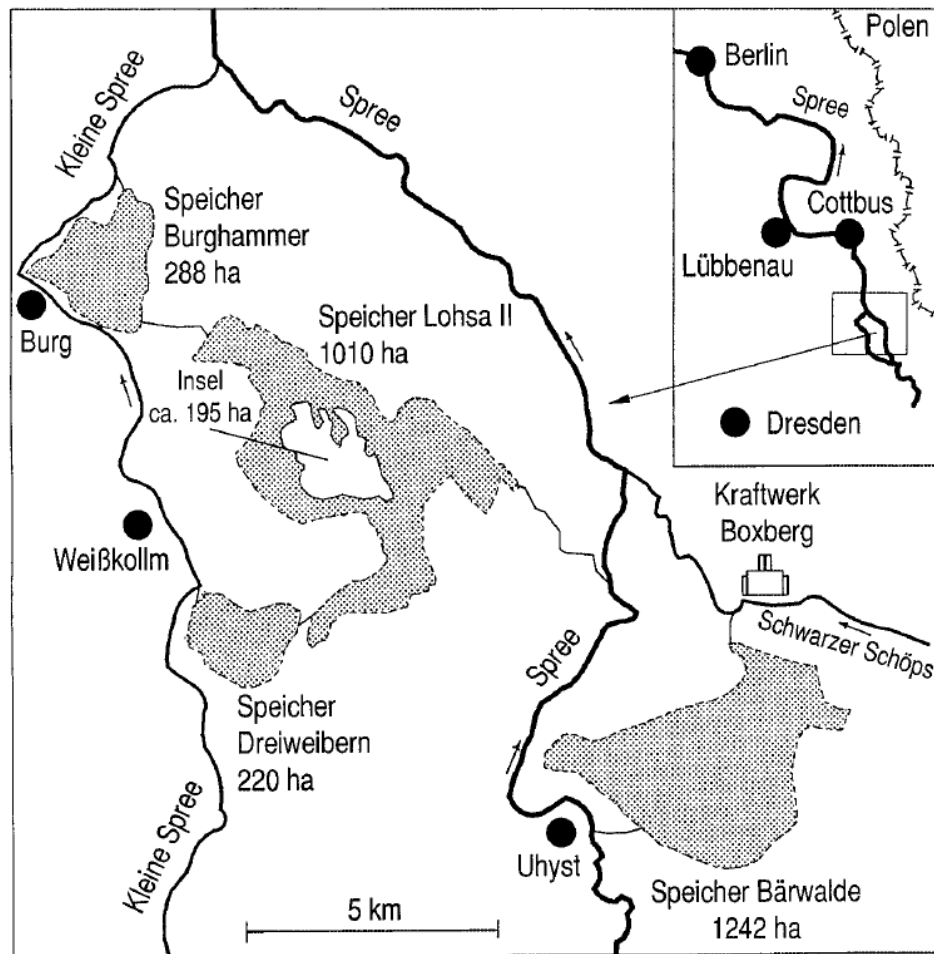


Figure 11. Storage system Lohsa II, topographical map (Zschiedrich, 2011)

Available morphological data of Lake Burghammer are shown in Table 5. The storage volume of Lake Burghammer will be 5 million m³ where the water level can vary between 107.5 – 109 m NN. A maximum of 10 m³/s will be discharged in the river Kleine Spree (Zschiedrich, 2011).

Table 5. Morphological parameters of the mining lake Burghammer (source:(LUG, 2005))

Parameter	Dimension	Final state
Water level, final	m NN	+109
Lake volume	million m ³	36.3
Lake area	million m ²	4.04
Ratio V _{hypolimnion} / V _{epilimnion}	-	0.40
Maximum length	m	4139
Maximum width	m	2674
Maximum depth	m	21.4
Average depth	m	9.0

As can be seen from Figure 12 the ash body is situated at the northern part of the lake (green areas). However, it cannot be excluded that ash sediments are distributed within the whole area of the lake. Only few data exist about the discharge of ash in the open pit. Uptake and relocation of ash sediments for neutralising the lake water are reported (Aktiengesellschaft, 2001).

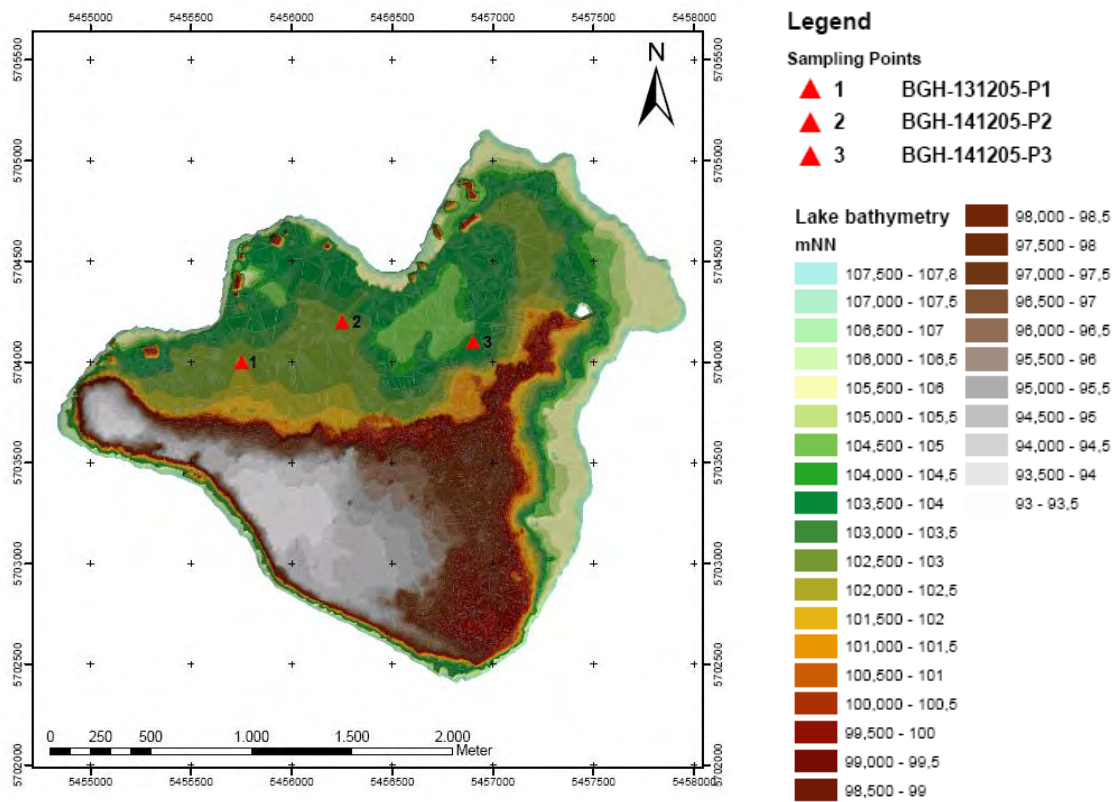


Figure 12. Digital Terrain Model of Lake Burghammer; drawn triangles clarify sampling points (Gauß-Krueger (zones are only 3° apart, as opposed to 6° in UTM), RD 83, Rauenberg, Bessel).

2.3.1 Groundwater

According to BTU (2005), the groundwater situation around lake Burghammer is best explained by dividing the aquifer into five different zones: southwest, northwest, north, south and the east bank (dump site). The groundwater originating from the south and east bank aquifers form Lake Burghammer's groundwater inflow. The other mentioned aquifer zones mainly form the outflow. This situation is plausible due to the 3.6 m water level difference between lake Burghammer and lake Lohsa II, which is located in the southeast of lake Burghammer. Elevated sulfate and iron concentration and moderate pH values are characteristic not only for the aquifer around Lake Burghammer but also for most aquifers in the mining area in the Lusatian district.

There are different observation wells surrounding Lake Burghammer and the other mining lakes. Figure 13 shows a map with the positions of the observation wells. Corresponding chemical data can be found in Table 6.

The groundwater is characterized by moderate pH values (varying between 4.35 and 5.84 as shown in Table 6), elevated sulfate concentrations (up to 3720 ppm) as well as iron (II)

Investigation area

concentrations (1220 ppm). The composition is typical for the groundwater coming from waste rock piles.

Table 6. Water quality of a groundwater sample in the surrounding of Lake Burghammer

Observation well	006012	006013	006067	006068	006080
sampling date	02/20/2006	02/20/2006	02/20/2006	02/28/2006	02/23/2006
	unit	value			
pH	-	5.84	5.18	5.04	5.14
TIC	ppm	43.4	12	3.3	89
K _S 4.3	mmol/L	1.1	0.25	0.10	1.15
EC	µS/cm	2220	1401	1190	5150
temperature	°C	11.1	10.2	10	12.7
potassium	ppm	14.3	18	14.6	14.1
sodium	ppm	75.7	28	30.2	39.4
calcium	ppm	381	155	124	478
magnesium	ppm	46.9	39.30	31.3	232
iron (III) species	ppm	0.7	4	1.6	240
iron (II) species	ppm	86.2	127	74.8	1220
aluminum	ppm	0.1	0.14	0.21.	0.27
manganese	ppm	2.44	3.62	2.38	16
sulfate	ppm	1200	785	632	3720
chloride	ppm	122	22.4	28.2	64.7
					85.7

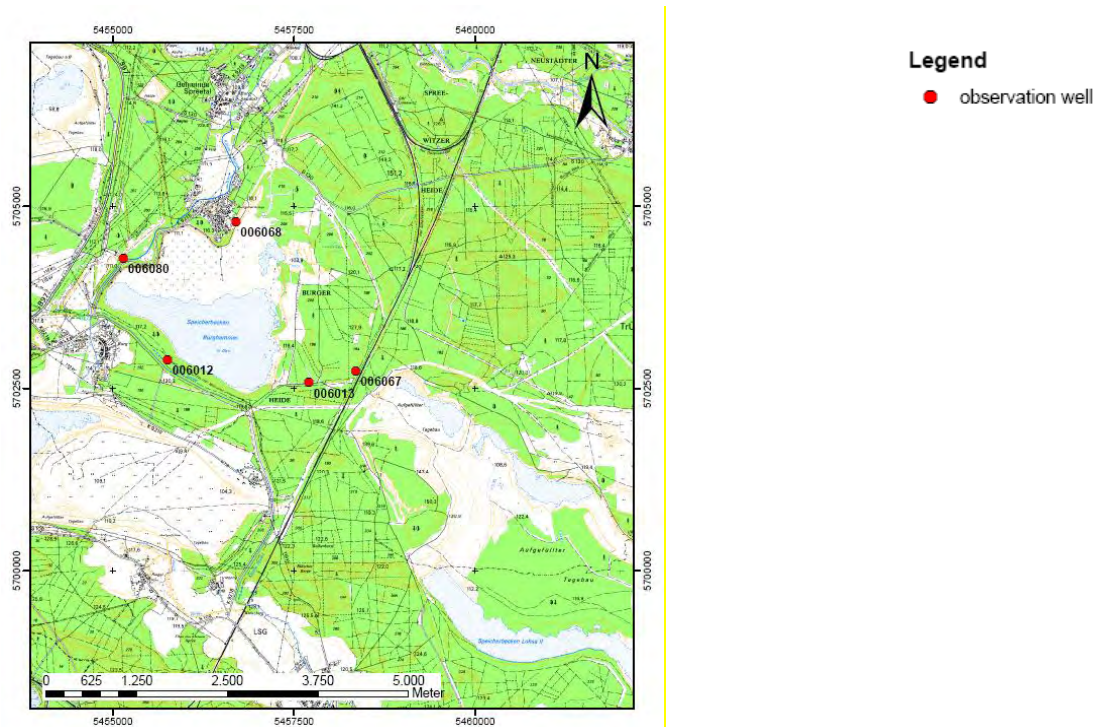


Figure 13. Topographical map of the investigation area around Lake Burghammer (TK25, Sheet 4552 / Weißkollm; issue date 1990). Red circles mark observation wells.

2.3.2 Lake water

Between 1970 and 1997, approximately 26 million m³ of suspended fly ash were deposited in the lake. The suspension of water and ash was characterised by a pH of 7.9. Because of this discharge and a negligible groundwater inflow, the water of the lake Burghammer was neutral. As one can see in Figure 14, during a period from July 1997 until October 1999, water of pumping wells of the open-pit Spreetal-NO was discharged into the lake Burghammer. The quality of the water corresponds to oxygen-free groundwater with high contents in iron. The pH was determined in a range from 5.5 to 6.1 (Grünewald, 2005). Due to the oxidizing conditions in the lake, oxidation took place and the dissolved iron (Fe (II)) precipitated. Hence, in the Burghammer mining lake, a decrease of Fe (II) was registered and pH reached 3.3.

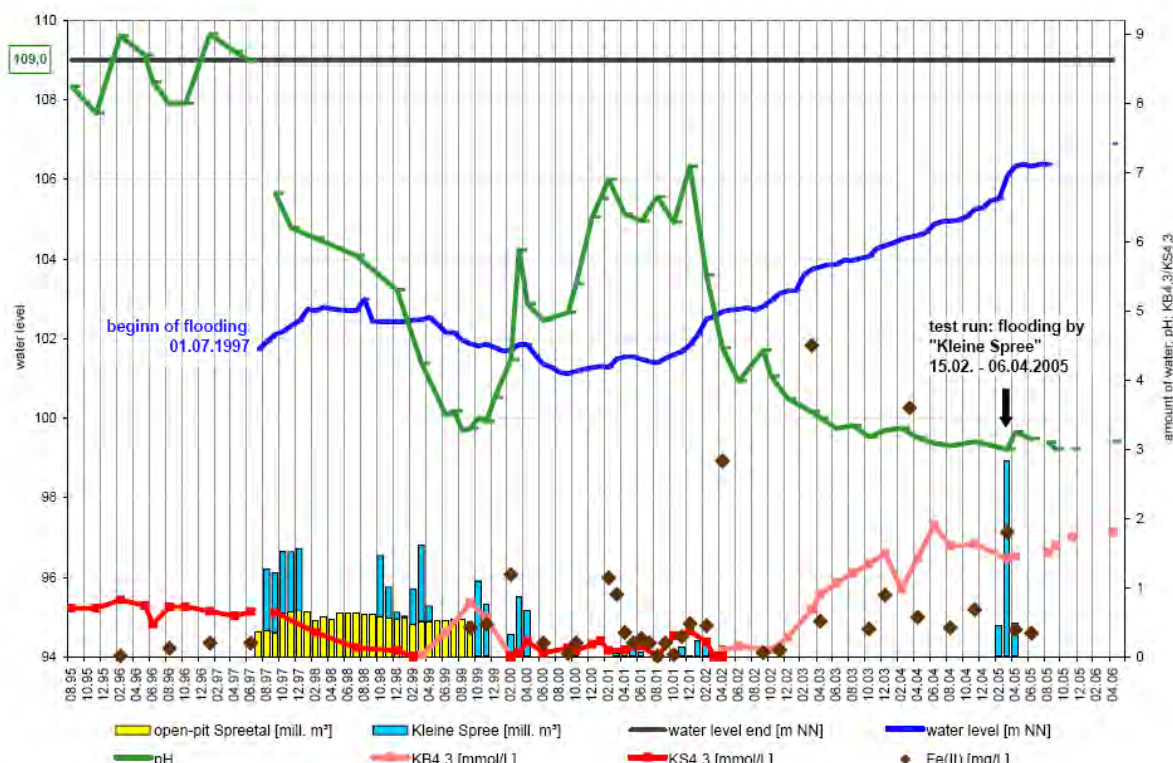
After water supply from the pumping well was terminated, Lake Burghammer was partly neutralised by surface water of the river "Kleine Spree" and alkalinity supplied by the lake sediments and ash sediments, which had been flooded by the rising water. The reservoir featured a pH of 5.0 - 5.5, but without any buffering capacities. Since 1999, the previous development of the water level in the Burghammer reservoir was influenced by flooding of Lohsa II. This caused elevated groundwater inflow (up to 30 m³/min, with high acidity) from the residual embankment between Lohsa II and Burghammer. The water composition deteriorated drastically (from a maximum pH of 7.1 to 2.9). In December 2000 (until October 2002), lake treatment by resuspension of ash took place. Nearly 3 million m³ of suspended sediment was reallocated by swimming pipelines. Figure 14 shows an increase of the pH (December 2000 – December 2001). The buffering capacity of the lake water was completely exhausted, the pH dipped to 3.2 ($K_{B4.3}$ 1.6 mmol/L) (eta, 2003).

Different samples taken throughout the course of the thesis have shown that the water body of the Burghammer acid mine lake is relatively uniform with respect to water quality. The lake water is characterized by a low pH and elevated electrical conductivity (Schipek et al., 2006b). Table 7 describes the most important anions and cations of the acid mine lake water.

Table 7. Chemical composition of the acid mine lake water (11/2007)

In-situ Parameters			
pH	[\cdot]	2.98	
Electrical conductivity	[$\mu\text{S}/\text{cm}$]	2310	
Redox potential	[mV]	624	
O ₂ -content	[ppm]	9.42	
Cations [ppm]	Anions [ppm]		
lithium	0.03	Fluoride	0.24
sodium	45.78	Chloride	72.45
Potassium	14.03	Nitrite	0.01
Calcium	264.42	Bromide	-
Magnesium	50.84	Nitrate	3.35
Iron (total)	26.9	Phosphate	0.21
manganese	6.21	Sulfate	1,264
Ammonia	3.01	TIC	0.97
aluminum	3.92		

The acidity of the lake water is approximately 1 mmol/L. Due to the extremely poor buffering capacity of the lake water, the pH dropped from approximately 8 in 1997 to approximately 2.9 (November 2007).

**Figure 14. Development of selected water quality parameters in Lake Burghammer (data source: LMBV, own data collection)**

3 Methods

3.1 Sampling

2 sampling campaigns were planned at the beginning of the investigations. In November 2005, surface samples of the flooded ash body were taken.

In December 2005 3 drilling cores were sampled to a maximum depth of 8 m (10.5 m below water table) with the help of an amphibious tank and a Cobra drilling unit. Figure 15 shows a digital terrain model of Lake Burghammer; the drawn triangles pinpoint the sampling points BGH-131205-P1, BGH-141205-P2 and BGH-141205-P3. The coordinates of the sampling points are listed in Table 8.

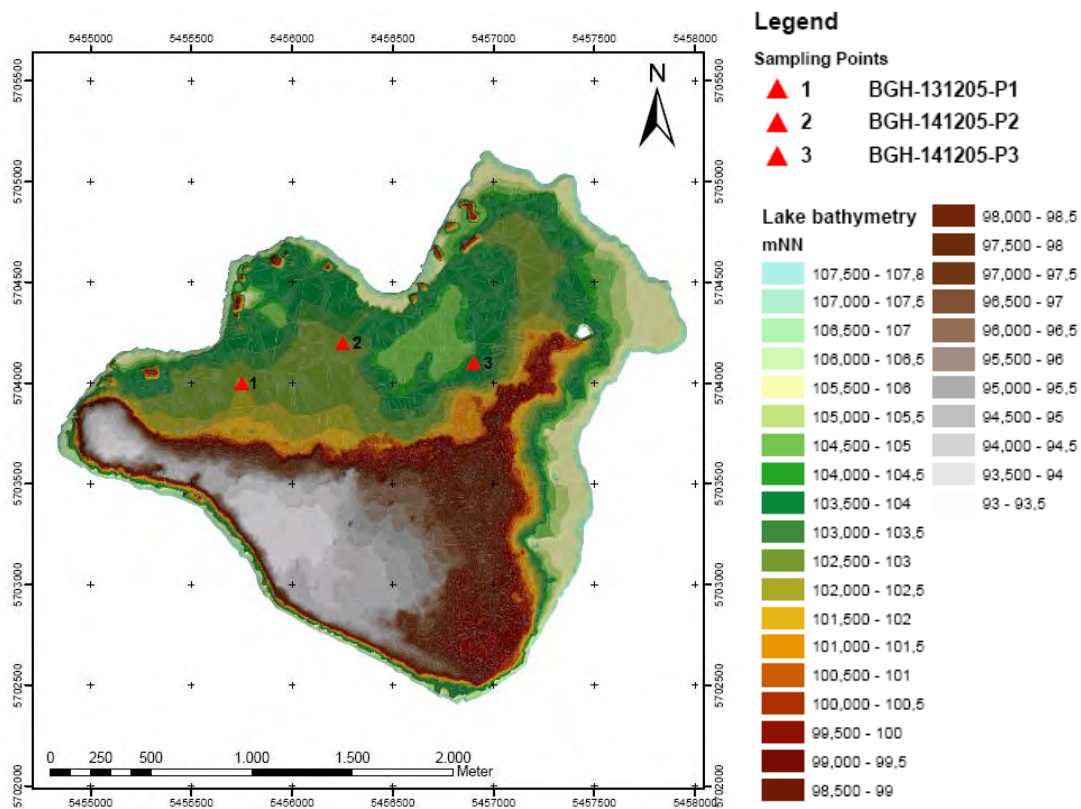


Figure 15. Digital Terrain Model of Lake Burghammer; drawn triangles clarify sampling points (Gauß-Krueger (zones are only 3° apart, as opposed to 6° in UTM), RD 83, Rauenberg, Bessel).

Table 8. Gauß-Krueger-Coordinates of the sampling points from December 2005 (RD 83, Rauenberg, Bessel). Depth means depth of sediment.

Sample ID	Easting	Northing	Depth [m]
BGH-131205-P1	5455750.3	5703999.6	6
BGH-141205-P2	5456250.5	5704199.7	6
BGH-141205-P3	5456899.7	5704099.7	8

3.2 Lab methods

3.2.1 Solids Analysis and Mineralogy

Solids investigated are lake sediment and fresh lignite filter ashes. They have been used in batch and column experiments. Before batch experiments a detailed analysis of sediments from the acid mine Lake Burghammer and the fly ash took place.

Liming agents for geochemical investigations, batch and column experiments were provided by different companies (e.g. Rheinkalk GmbH).

3.2.1.1 Physical Analysis

Evaluation of the grain size distribution for particle size range 63 – 2000 µm was carried out using dry sieving according to DIN 18123 (1996). The use of wet sieving was used to separate fractions < 63 µm in an earlier step. The determination of the grain size distribution for the particle range of < 63 µm was conducted with the help of a photosedimentometer LUMOSED (Retsch). Due to the strong generation of aggregates, a fifteen-minute treatment in an ultrasonic bath was carried out before wet sieving.

Determination of density of ash sediment from the Burghammer lake was performed with a pyknometer according to DIN 18124 (2007).

Water content of the sediment was determined according to DIN EN 12880 (2001). The unsettled ash sediment was dried at 105°C to constant weight. The water content was then evaluated over the given equations and respective mass differences.

3.2.1.2 Mineralogical Analysis

X-Ray diffraction analysis

The mineralogical composition of the investigated sediments was ascertained using roentgenography (XRD). Prior to this, the freeze-dried samples were grinded in a McCrone Micronesian mill; with sintered corundum grinding elements; in an ethanol suspension. To assess the content of amorphous phases, crystal ZnO was added as 10 % of the total mass, and the content of the crystal phases was based on this internal standard.

Step-scan XRD data (5 to 80° 2H, 0.03° 2H step width, 8 s/step) were collected using the X-Ray diffractometer URD-6 (Seifert-FPM, Germany), with Co-K α -radiation. Phase identification was then conducted by comparison to the line thicknesses of the powder diffractogram with the data bank PDF-2, Release 2004. The quantification was conducted with the Rietveld Procedure (Program BGMN-AUTOQUAN) on the basis of public crystal structure data for the identified phases (Kleeberg and Bergmann, 2002, Monecke et al., 2007, Ufer et al., 2004). The detection limits are between 0.5 and 5 wt.-%.

The mineralogical phase stock of fresh lignite ash was established using the diffractometer (XRD) SIEMENS D 5005 with Cu-radiation in 2-Theta-scope from 8 to 50°. The results were shown in an evaluated diffractogram. The quantity of crystal CaO and Portlandite (Ca(OH)₂) was determined with the calculation program Superquant. The limit of detection of this process is 0.5 wt.-%.

SEM-EDX

Small-scale alteration features of solid samples from Burghammer sediments were visualized by scanning electron microscopy (SEM); using a JEOL 6400 equipped with a Tracor (Noran) series II energy-dispersive X-ray (EDX) spectrometer. Routine operating conditions were 20 kV with a beam current of 600 pA, high-resolution back-scattered electron (BSE) images were collected at up to 4.5 nA.

The morphology of the liming agents (calcite, dolomite) was performed by a JEOL JSM 7001F (Zeiss AG). Evaluation of the data was done with the help of the software Esprit. Combined with an energy-dispersive X-ray analysis the chemical composition of special sample areas was investigated.

X-ray fluorescence analysis

X-ray fluorescence analysis was performed on powder samples (< 63 microns). The device XEPOS (Spectro) was used to determine the elements K to U (mass number 39 to 238). Occurring matrix effects had been taken into account by the Turbo Quant method. The excitation of the elements was performed by using different targets (K - V: HOPG Target; Cr - Zn, Pr - U: Mo secondary target, Y - Ce: Barkla-Al₂O₃-target).

Thinsection investigations

Microscopy

The microscopic analysis was used to determine both the qualitative and quantitative mineral inventory of fly ash by thinsections. For analysis a stereo microscope Discovery V12 (Zeiss) in combination with the software AxioVision Release 4.7 was used. Photographs were obtained by the microscope camera AxioCam MRC 5 (Zeiss).

The main mineral phases were determined in the course of qualitative analysis.

Cathodoluminescence

In addition to optical microscopy, Cathodoluminescence (CL) microscopy was conducted using the hot cathode CL microscope HC1-LM (Neuser et al., 1995) operated at 10 kV with a current density of 0.2 mA and an operating vacuum of < 10⁻⁶ bar. Photos were made with the help of a digital video camera Type CF20DXS (Peltier cooled). Accumulation times were 10s (a), 20 s (b), and 30s (c). The major focus was on the quantification of carbonates, which usually appear bright orange-yellow to yellow-orange luminescent colours.

Determination of TIC / TC

Total carbon (TC) was determined by the oxidative combustion of 100 to 200 mg of air-dried homogenized sample material in a 1300 °C furnace ; with subsequent NDIR detection of the resulting CO₂ with a multi EA 2000 device (analytic Jena, Germany) according to DIN EN 1484 H3 (1997). Total inorganic carbon (TIC) was analysed with the same device for detection of the resulting CO₂ after the sample was acidified with approximately 15 - 20 mL 40 % phosphoric acid in a separate reaction chamber. An oxygen carrier stream was used to purge the CO₂ from the reaction chamber or rather the furnace to the detector. The complete

system was rinsed by oxygen, to avoid the influence of atmospheric CO₂. Water vapor was removed from the combustion gas stream prior to detection by filtering the stream through a quartz wool filled pipe; avoiding interferences with water vapor, which absorbs IR radiation at the same wavelength as CO₂. Total organic carbon (TOC) was calculated by the difference of TC and TIC. According to the manufacturer the detection limit is approximately 0.1 wt.-%. For the calculation of TOC all results determined as < DL were replaced by 0.3 × DL.

3.2.1.3 Geochemical Analysis

S4 Elution and Sequential Extraction

The S4-Elution was executed according to DIN 38414-4 (1984).

A sequential extraction method according to Zeien (1995) was used to estimate the elutable amount of trace metals in the investigated sediments. The extraction steps are shown in Table 9. In each case, 2 g of freeze-dried sediment (< 63 µm) were mixed with an extraction agent and shaken upside down for 24 hours.

Following this step, the samples were centrifuged at 2000 rpm. The solution was transfused and analyzed using ICP-MS.

Table 9. General outline of the sequential extraction procedure and the acquired metals and metalloid binding forms (modified after (Zeien, 1995))

Fraction	Sequential Extraction Step and binding form	Extraction agent
1.	S4-elution	dist. H ₂ O
2.	Mobile fraction Water-soluble and exchangeable (non-specifically adsorbed) metals and easily soluble metal-organic complexes)	1 M NH ₄ NO ₃
3.	Easily mobilized fraction Specifically adsorbed, occluded close to the particle surfaces, bound to carbonates and extracted from metal- organic complexes of low stability	1 M NH ₄ OAc (pH 6.0)
4.	Residual fraction	HNO ₃ + HCl (3 : 1)
5.	Aqua regia	

To determine the total elemental content, DIN 38414-7 (1983) description of *aqua regia* digestion under back flow cooling was used. 2 g of freeze-dried sediment (<63 µm) were extracted with 12 mL HCl and 4 mL HNO₃.

ASE-Extraction for PAK-Determination

The polycyclic aromatic hydrocarbon content of different samples was determined by diluting the samples with sand in a ratio of 1:2.2 and extracting them with the help of ASE (instrument from Dionex). 50 mL of the extraction agent toluene was applied following the extraction. The constraints of the program are given by the following parameters: pressure: 100 bar, temperature program: step 1: heat-up phase up to 150°C, length of time period 7

min; Step 2: 150°C, 10 min. Each sample was extracted in duplicates and after the extraction, the contents were added to an internal standard (with 4 deuterated PAKs). Finally, the extracted contents were constricted into a rotary evaporator of about 5 mL. The measurement was then made with GC-MS.

3.2.2 Water chemistry Analysis

The determination of the **onsite parameters**: pH, electrical conductivity, redox potential and oxygen content, was carried out with instruments from WTW Mess- und Analysengeräte. The instruments included a pH single-rod measuring cell with integrated temperature sensor SenTix 97/T, an oxygen sensor CellOx 325, the standard-conductivity measuring probe TetraCon 325, and the redox single-rod measuring cell SenTix.

The evaluation of the acid/base capacity was conducted with a processor controlled titrator Basic Titrino (Metrohm).

NO_3^- , NO_2^- , NH_4^+ , Fe^{2+} , and Fe_{tot} content were each determined from water samples photometrically on site (Hach DR 890).

The cation determination (Li^+ , Na^+ , K^+ , Mg^{2+} , Ca^{2+} , Mn^{2+}) was conducted with a LC-System L 6000 (Merck-Hitachi) using an L 6000 A Interface, a L 5025 Column heater, a L 6200 A HPLC-Pump, and a L 3720 conductivity detector. A RT LiChrosil® IC CA 2 from Merck (length 125 mm, internal diameter 4.6 mm, Sorbens: spherical silica gel with polymer cation exchange phase, particle size 5 µm) was used as analytical column. A RT LiChrosil® IC CA 2 from Merck (length 10 mm, internal diameter 4.6 mm) served as a pre column.

Eppendorf Biotronik IC 2001 in combination with a Shimadzu Liquid Chromatograph LC-10 As was used for the determination of anions. The suppressor column used was a FGC BTS AG-P. The eluent for the anion separation was a solution of 2 mM NaCO_3 and 4 mM NaHCO_3 . The flow rate of the eluent amounted to 2 ml/min.

The total inorganic carbon was determined with the help of a liquiTOC (elementar Analysensysteme GmbH).

First trace element measurements of the samples were carried out using an ICP-MS-instrument Fisons PQ2+ from the company VG Elemental, Winsford (GB). Since 2009 measurements of trace elements (pore water) and batch experiments were carried out using an ICP-MS XSERIES 2 from Thermo Fisher Scientific. Detected isotopes, used modi, detection limits etc. can be found in Appendix B, Table B.1.

3.2.3 Porewater chemistry

Depth related variations in pore water chemistry were of particular interest in this work. Pore waters were obtained from the Burghammer drilling cores by the use of the MD 142/73 (Schleicher & Schuell) pressure filtration unit, in combination with cellulose-acetate-filters (pore size 100 nm).

Extracted porewater samples were divided into 3 aliquots; one for trace elements determination (acidified using HNO_3 suprapur), one for main anions/cations (untreated) and

one for TIC measurements (untreated). The pore water samples were then stored in a refrigerator to minimize biological activity before analysis.

Main anions and cations, total inorganic carbon and trace element concentrations were determined as described in chapter 3.2.2.

3.2.4 Batch experiments (CO_2 sequestration)

3.2.4.1 Aim of the batch experiments

The aim of the performed batch experiments was to confirm that an immobilization of CO_2 forming carbonates and a simultaneous improvement of water quality of the acid mine lake is possible. CO_2 should be mineralized when introduced to the ash coming either directly from the power plant or from the deposited sediment in the acid mine lake. The emerging product of the carbonate reaction will be deposited over the long term on the bottom of the acid mine lake.

To illustrate this goal from an engineering process point of view, it was necessary to acquire insight about the relationship between the aqueous phases (distilled water, tap water or lake water), solid phases (fresh ash and settled ash sediment) and gas phases (technical CO_2) in the batch experiments. In the beginning of the investigations, distilled water was used to gain a basic understanding of the CO_2 aeration under defined and controlled experimental conditions (without the influence of lake water).

In the following sections, the experimental layout and implementation will be presented and the determined technical process parameters will be derived from the experimental results.

3.2.4.2 Experimental layout and procedure

The batch experiments were conducted within a cylindrical acrylic container with an internal diameter of 100 mm and a height of 160 mm (Figure 16). The volume of the closed reactor was 1260 mL.

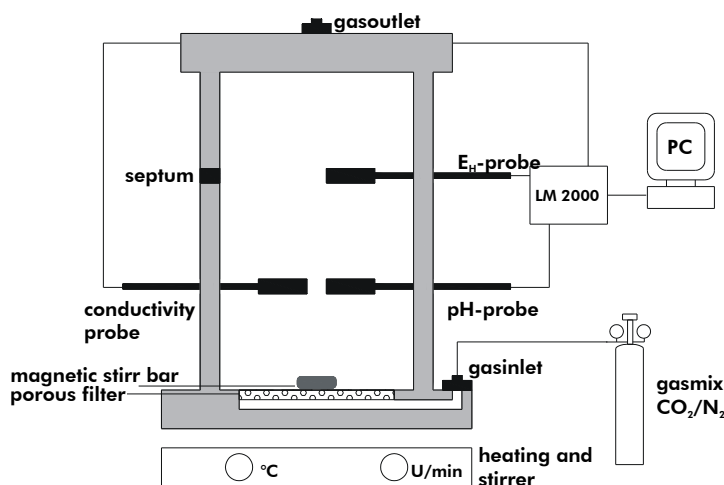


Figure 16. Schematic experimental setup for mineral trapping.

Gas exposure was realized by technical gas mixtures of carbon dioxide and nitrogen (5 %, 10 %, 30 %, 50 % and 100 %) and took place through a filter plate in the bottom of the batch column (pore size: 10 – 30 µm). Continuously recording pH, electrical conductivity, and temperature was maintained with a PC Laboratory Multiparameter System LM 2000 (Meinsberg). Water sampling took place over a gas tight septum with the help of a cannula and syringe.

The progression of each experiment is designed to enhance the reproducibility of results. Experimental conditions are shown in Table 10.

Table 10. Overview of varying experimental conditions

Parameter	Modification
Solid phase	
Type	Pure CaO / Fresh Fly Ash (power plant Boxberg) / Ash Sediment (lake Burghammer)
Amount	10 – 50 g
Solvent	
Type	Distilled water / Tap water / Lake water
Amount	1 L – 1.2 L
CO₂	
CO ₂ percentage	5, 10, 30, 50, 100%
Flow rate (total)	100 mL/min
Flow rate CO ₂	5 – 100 mL/min
Exposure to gas	
Type of injection	Injection from the base of the reactor
No of gas exposure intervals	1 – 3
Gassing periods	1 to 120 min
Pressure	
Temperature	1035 (atmosphere)
Turbulence	
Test arrangement	
A) <u>first step:</u> suspension of pure CaO / filter ash / lake sediments in the liquid phase (distilled water / tap water / lake water)	
<u>second step:</u> CO ₂ gassing of the assessed suspension	
<u>third step:</u> recovery	
B) <u>first step:</u> CO ₂ gassing of liquid phase (distilled water / tap water / lake water)	
<u>second step:</u> Addition of solids (pure CaO, ash, lake sediment)	

3.2.4.3 Chemical monitoring

During the batch experiments, pH, electrical conductivity [µS/cm], redox potential [mV], and temperature [°C] of the given and aerated suspension were recorded continuously by the Laboratory Multi-parameter System LM 2000 (Meinsberg).

Changes in the composition of the water phase were implemented by methods described in chapter 3.2.2 (ion chromatography, ICP-MS, TIC).

In order to confirm the formation of minerals, the concentration of total inorganic carbon in the solids was determined before and after each test. The solid samples were filtered (200 nm) at the end of the experiment and dried at 30°C until constant weight.

3.2.5 Kinetic experiments

3.2.5.1 Aim of the kinetic experiments

As described in chapter 1.4 calcite dissolution kinetics is well investigated. However, results from experimental set-ups often cannot be upscaled to natural systems due to large simplifications or different conditions in natural systems. Therefore, batch experiments were carried out in order to apply general results on dissolution rates of synthetic materials (marble powder) and industrial products used as liming agents.

Furthermore, experiments were carried out taking into account the inhibition of dissolution kinetics by water constituents typically for AMD affected waters. Therefore, chemical parameters had been observed, as well as non-dissolved carbonate particles by mineralogical analysis.

The literature review in chapter 1.4.2 shows that the dissolution of calcite is relatively fast at low pH, when the water is far away from the equilibrium. If a former mining lake is very acid, the first phase of neutralisation can be done with CaCO_3 . The final adjustment of the pH will be more efficient with Ca(OH)_2 due to its faster kinetic. Ca(OH)_2 might have negative effects on the ecosystem within a developing lake (Angeler and Goedkoop, 2010, Hakanson, 2003, Teien et al., 2006). Thus, re-treatment of mining lakes is usually recommended by using carbonates. As literature and first experiments showed, surface complexation will inhibit the dissolution kinetics. Using calcite in combination with gaseous CO_2 could be a solution to make liming of mining lakes more efficient.

3.2.5.2 Experimental layout and procedure

The experimental layout for determining the solution kinetics of selected neutralization products included a free-drift method in a batch experiment. According to Berner and Morse (1974) and Plummer et al. (1978) the advantage of these batch experiments is to provide a large number of dissolution sites at the calcite surface (kinks and steps), and thus a rapidly proceeding of the dissolution (Dreybrodt and Buhmann, 1991). But Dreybrodt and Buhmann (1991) also describe the undefined movement of calcite particles relative to surrounding water. In comparison, rotating disc experiments are hydrodynamically well known and suitable for calculations (Dreybrodt and Buhmann, 1991). Disadvantages appear in the small solid / fluid ration ($\sim 1 \text{ cm}^2 / 500 \text{ cm}^3$) (Dreybrodt and Buhmann, 1991).

We decided to use powdered samples in free-drift experiments particularly with regard to the technical application on a remediation ship used in liming campaigns (see chapter 1.4.3).

The batch system consisted of a 5-L beaker, filled with 4 L distilled water. CO_2 partial pressure and temperature was kept constant during the experiment. The amount of material

used in all experiments exceeded the solubility 5 times or 20 times, so that a constant particle surface can be assumed over the entire course of an experiment. Turbulent flow conditions were generated using a stirrer (700 rpm).

Varying CO₂ partial pressures were realized by using a glove box, technical CO₂-N₂ mixtures provided by Praxair had been used. Before the test, the p_{CO₂} of the water was adjusted by purging to the desired initial p_{CO₂}. The pH of the solution was chosen as indicator of the saturation state. The amount of liming agent added was modeled before using PhreeqC as shown in chapter 3.4.1.1. The amount of calcite to reach saturation was multiplicated by 5 or 20 in order to guarantee solid material in excess during the experiment.

Experimental conditions, used neutralizing agents and saturation states are shown in Table 11.

Table 11. Overview of varying experimental conditions

ID	Neutralizing product	saturation [-]	CO ₂ partial pressure [vol.-%]	inhibitor [mmol/L]
V1	marble powder	5x	0.038	-
V2	KSM	5x	0.03	-
V3	marble powder	5x	100	-
V4	KSM	5x	100	-
V5	marble powder	5x	5	-
V6	KSM	5x	5	-
V7	marble powder	5x	0.038	-
V8	marble powder	20x	0.038	
V9	marble powder	20x	0.038	8.98*10 ⁻⁴ Mn(II)
V10	marble powder	5x	0.038	8.98*10 ⁻⁴ Mn(II)
V11	marble powder	20x	0.038	9.10*10 ⁻² Mn(II)
V12	marble powder	5x	0.038	
V13	marble powder	5x	0.038	9.10*10 ⁻² Mn(II)
V14	KSM Beroun	5x	0.038	
V15	marble powder	5x	0.038	7.56*10 ⁻³ Cd
V16	marble powder	5x	0.038	7.65*10 ⁻⁶ Cd
V17	KSM Beroun	5x	50	-
V18	KSM Beroun	20x	50	-
V19	marble powder	5x	50	-
V20	marble powder	20x	50	-
V21	marble powder	5x	0.03	1.04*10 ⁺¹ SO ₄ ²⁻
V22	marble powder	20x	0.03	1.04*10 ⁺¹ SO ₄ ²⁻
V23	marble powder	5x	0.03	1.79*10 ⁻¹ Fe
V24	marble powder	20x	0.03	1.79*10 ⁻¹ Fe
V25	marble powder	5x	50	-
V26	KSM Beroun	5x	50	-
V27	marble powder	20x	50	-
V28	KSM Beroun	20x	50	-
V29	marble powder	5x	30	-
V30	KSM Beroun	5x	30	-
V31	marble powder	10x	30	-
V32	KSM Beroun	20x	30	-

3.2.5.3 Chemical monitoring

Chemical monitoring was done according to chapter 3.2.4.3. Due to the large number of samples calcium and trace element concentrations were determined by ICP-MS taking less time than IC. In order to exclude systematical errors during analytical procedures a comparison of both methods – ion chromatography vs. ICP-MS – was done. First, test runs were conducted with (i) acidified IC samples (normal procedure), (ii) non-acidified samples and calibration and (iii) non-acidified samples and standard solutions in NaHCO_3 matrix (see Figure 17). Different treatment was conducted due to nescience of effects of acidification (on dissolution of possible calcite particles). As well, an effect of different filter pore sizes (200 nm vs. 20 nm) was ruled out.

A good recovery rate for the analyte was proved for ICP-MS measured values (dilution 1:10) vs. IC measured values. The results showed no evidence of constant systematic errors. The chart for the recovery functions for Calcium is shown in Figure 18. Both statistical series show correlation coefficients of $r^2 = 0.9974$ and $r^2 = 0.999$ respectively. Undiluted samples using ICP-MS showed an over-estimation of about +10 % in comparison to ion chromatography. Based on these results all samples gained in kinetic experiments were diluted 1:10, and then measured by ICP-MS (Thermo Fisher Scientific).

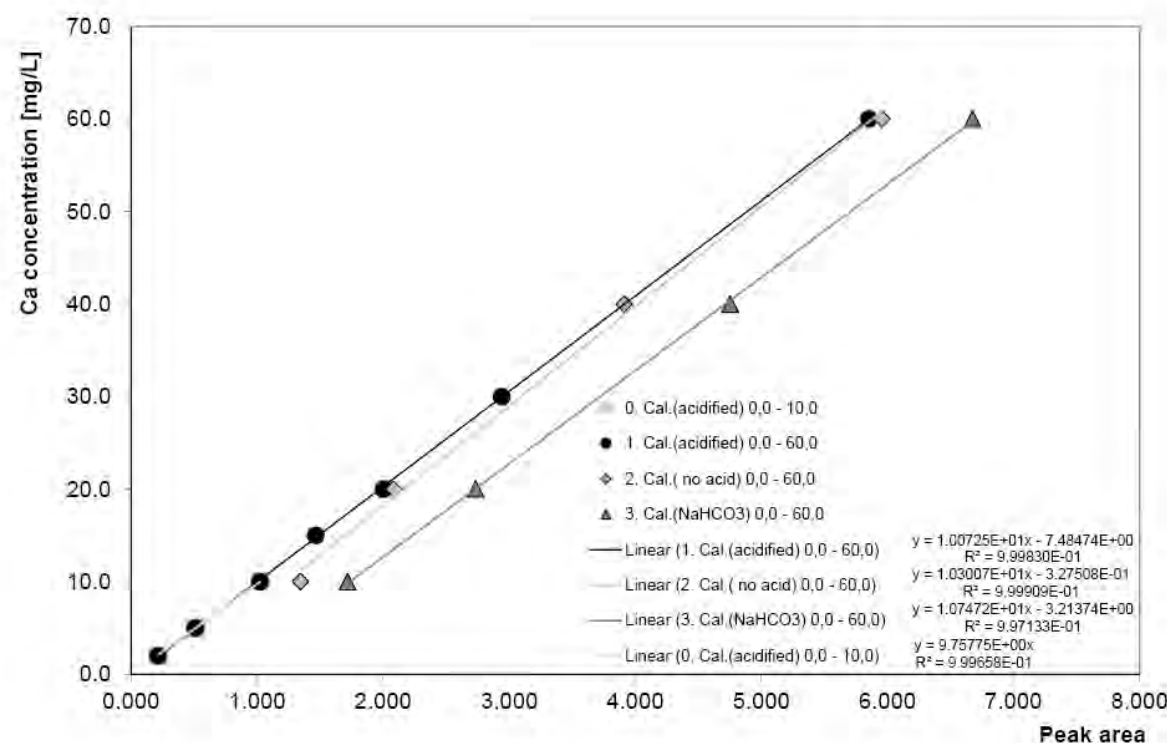


Figure 17. Comparison of IC measurements with different treatment (0 & 1 symbolize “normal” acidified samples in combination with acidified calibration; 2 shows non-acidified samples and calibration; 3 shows non-acidified samples and standard solutions in NaHCO_3 matrix).

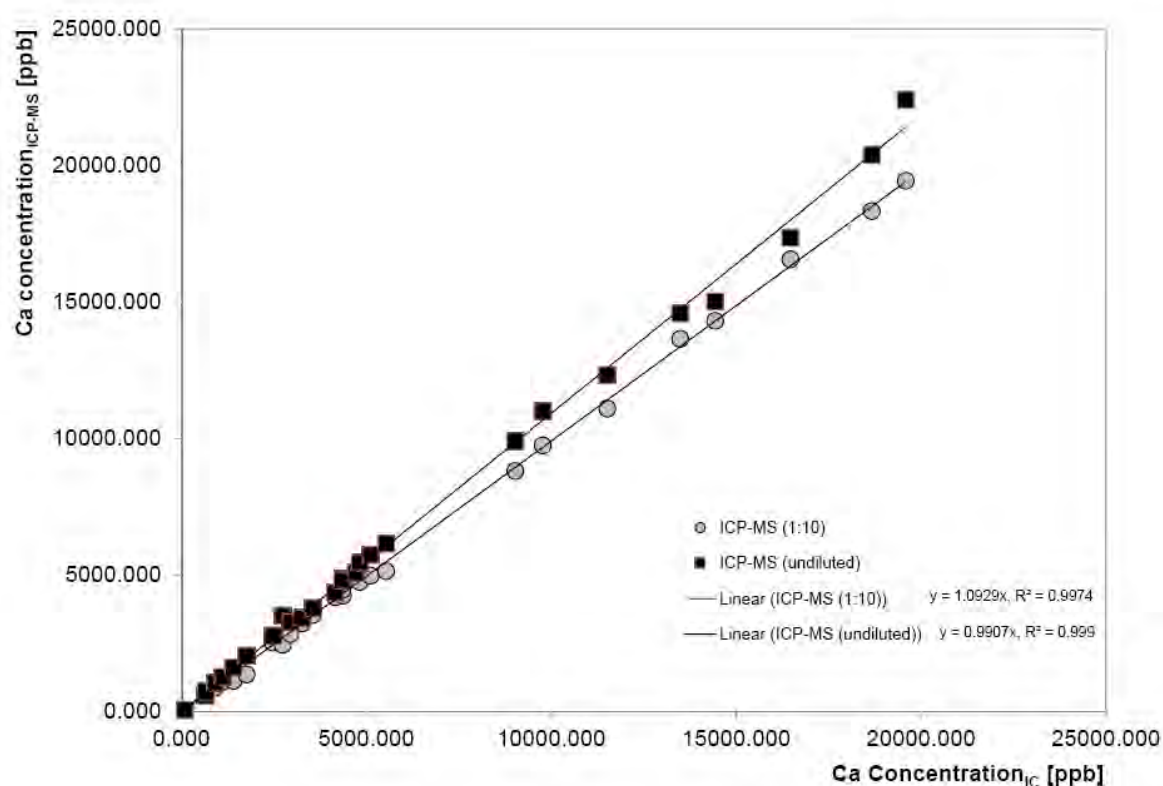


Figure 18. Comparison of calcium concentrations measured by ion chromatography and ICP-MS, n = 27.

3.2.6 Column experiments

3.2.6.1 Aim of the Column experiments

As described in chapter 1.4.3 Advanced Mobile Inlake Technology (AMIT) had been developed in the 1970's to treat acid lakes in Sweden. However, water chemistry in German open pit lakes is different from those in Sweden. Therefore, it was essential to develop a special neutralization strategy for open pit lakes and to prove its applicability.

Especially the number of liming intervals and their effect of the efficiency of liming campaigns was focus of research in this thesis.

3.2.6.2 Experimental layout and procedure

Since batch experiments cannot be directly applied to natural systems, it was necessary to develop larger-scale experiments to investigate the planned remediation method. Lakes in the Lusatian area provide an average water depth of 20 m. To investigate the behavior of different liming agents 2 m high columns made of Plexiglas were used Figure 19. Therefore, this experimental design was extremely conservative, as in a real lake the way of sinking of the liming agent would be 10 times longer.

The addition of liming agent was based on the water volume to treat.

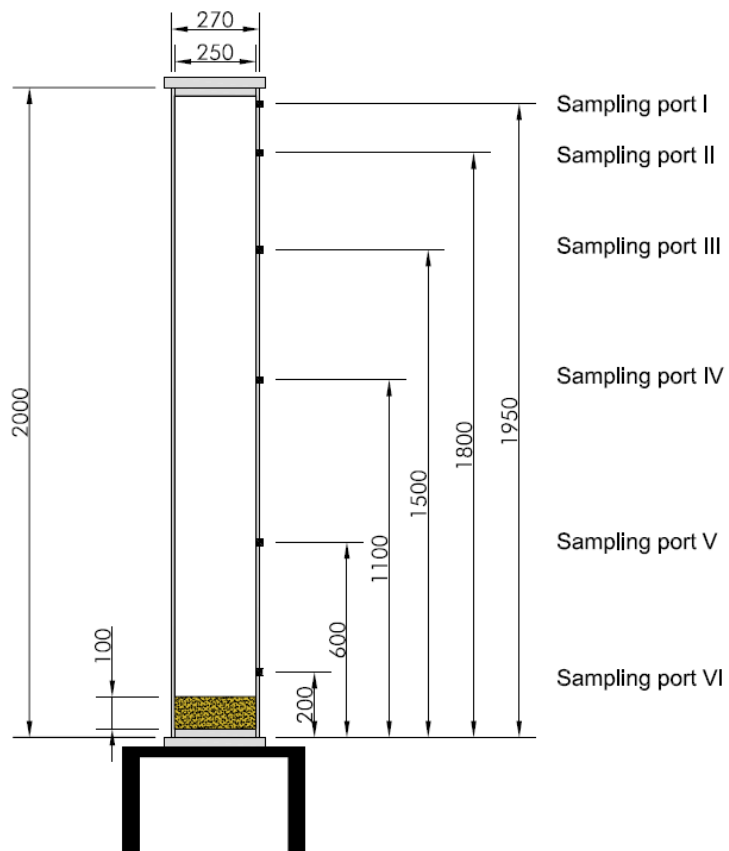


Figure 19. Schematic drawing of the column experiment set-up. 6 sampling ports provided sampling in different water depths.

Table 12. Heights of the sampling ports within the column experiment set-up.

Sampling Port	I	II	III	IV	V	VI
Height [mm]*	1950	1800	1500	1100	600	200

* distance from the bottom

The bottom of each column was filled with a 10 cm sand layer equaling circa 8 kg sand (Figure 19). Then approximately 92 L water from an open pit lake (see Table 13) was added. To avoid initial turbulences experiments started 1 or 2 days after preparation. Liming agents were added by the help of a plate that allows an equal distribution on the water surface of a column.

More than 30 column experiments had been conducted. Table 13 shows an overview about the most important experiments.

Table 13. Overview about conducted column experiments to improve liming technology in acidified mining lakes.

ID	Column Experiment	Liming agent	Chemical Formula	Water type	Liming interval	Range / average of grain size
1_1		KSM Beroun	CaCO ₃	BGH	5	< 63 µm 71 – 76 % < 125 µm 90 – 96 % > 90 µm 14-19%
1_2		Quick-lime “Weißfeinkalk”	CaO	BGH	5	< 90 µm 86.8 % < 200 µm 13.1 % > 200 µm 0.1 %
1_3		Branndolomit, Dolomitfeinkalk (Wünschendorf)	CaO, MgO	BGH	5	< 63 µm 90.5 % < 0.1 µm 9.5 % > 100 µm 0.1 %
1_4		KSM Ostrau 0- 0.09 mm (DSM)	CaCO ₃ , MgCO ₃	BGH	3	< 90 µm 42.5 % < 1000 µm 39.6 % < 3150 µm 15.6 % > 3150 µm 2.3 %
2_1		KSM Beroun	CaCO ₃	Lohsa	9	< 63 µm 71 – 76 % < 125 µm 90 – 96 % > 90 µm 14-19%
2_2		KSM Borna	CaCO ₃	Lohsa	9	$x_{50} = 24.43 \mu\text{m}$ $x_{\max} = < 174 \mu\text{m}$
2_3		„Mischkalk“ Borna	(Ca,Mg)CO ₃	Lohsa	9	$x_{50} = 33.62 \mu\text{m}$ $x_{\max} = < 174 \mu\text{m}$
2_4		DSM Borna	MgCO ₃	Lohsa	9	$x_{50} = 31.01 \mu\text{m}$ $x_{\max} = < 206 \mu\text{m}$
3_1		KSM Beroun	CaCO ₃	Scheibe	1	< 63 µm 71 – 76 % < 125 µm 90 – 96 % > 90 µm 14-19%
3_2		KSM Beroun	CaCO ₃	Scheibe	5	< 63 µm 71 – 76 % < 125 µm 90 – 96 % > 90 µm 14-19%
3_3		DSM Ostrau	MgCO ₃	Scheibe	1	-
3_4		DSM Ostrau	MgCO ₃	Scheibe	5	-
4_1		CaO	CaO	Scheibe	5	< 90 µm 86.8 % < 200 µm 13.1 % > 200 µm 0.1 %
4_2		KSM C20	CaCO ₃	Scheibe	5	< 20 µm 90% $x_{\text{med}} 3 – 8 \mu\text{m}$

3.2.6.3 Chemical monitoring

Sampling was carried out by the help of 6 sampling ports (for heights see Table 12). By using 20 mL syringes (Luer Omnifix Solo 20 mL, Braun) and needles (MIRAJECT 17x42, Hager works) samples for pH measurement and for measuring the electrical conductivity were obtained. The sample volume was 1.5 mL per sample; the pH value and electrical conductivity were measured daily. Sampling for the determination of major anions and cations were carried out at selected times.

Chemical analysis was done according to chapter 3.2.4.3.

3.3 Field methods

3.3.1 Technical description

For CO₂ injection, gas lances were installed to a sediment depth of 12 m by means of a heavy hydraulic hammer mounted on a floating platform (Figure 20). A tank with liquid CO₂ and a heat exchanger based vaporizer placed close to the shore of the lake was used as a carbon dioxide supply (Figure 21). CO₂ was transported as gas with a pressure of 8 - 9 bar by means of a floating pressure hose connected to the platform; from there the CO₂ was injected into the ash body. Gas injection took place through sections of integrated filter elements. In general, the length of an injection lance amounted to 10 to 12 m in sediment, whereas the last 2 meters of the injection lance consisted of integrated filter elements with a slot width of 0.5 or 0.7 mm.

3.3.2 Monitoring

3.3.2.1 Technical observation

The pilot gas injection experiment was controlled with flowmeters and manual valves. Under water observation via a submersed video camera allowed to monitor whether injected gas was released from the sediments in the vicinity of the injection ports (“controlling escape of bubbles”).



Figure 20: Base of the pilot experiment in lake Burghammer: Floating platform, CO₂ injection technology.



Figure 21: Tank of liquid CO₂ (provided by Linde), Heat exchanger based vaporizer. The gas was transported from the shore to the platform at a pressure of 8 – 9 bar.



Figure 22. CO₂ gas injection lance. White buoys in background mark monitoring installations.



Figure 23. System of flowmeters and manual valves.

3.3.2.2 Chemical monitoring (on-site), Sampling

As a result of monitoring, it was possible to determine how large the affected water body was, which is depending on the pressure applied and gas discharge via the rod into the sediment. This information is important for the design of an optimal treatment of the entire lake.

Onsite parameters

An online monitoring system was used for the parameters temperature, electrical conductivity, pH, and CO₂-content (Table 14, Figure 24 - Figure 26). These monitoring systems were installed in different water depths in order to recognize a stratification of the water body.

Table 14. Overview about the monitoring system used during CO₂ injection.

ID	Location	Water depth	Type	Interval
BGH 1	Lance	2 m	CTD Diver	T, EC, water level
BGH 2	Corner 1 platform	5 m	CTD Diver	T, EC, water level
BGH 3	Centre platform	5 m	CTD Diver	T, EC, water level
BGH 4	Lance	5 m	CTD Diver	T, EC, water level
BGH 5	Buoy 1	4.95 m	CTD Diver	T, EC, water level
BGH 6	Buoy 2	4.80 m	CTD Diver	T, EC, water level
BGH 7	Corner 2 platform	5 m	CTD Diver	T, EC, water level
pH probe1	Centre platform	5 m	pH	pH, T
pH probe 2	Lance / Corner 2	5 m	pH	pH, T
pH probe 3	Corner 3	5 m	pH	pH, T
CO ₂ - #1	Centre Platform	5 m		CO ₂
CO ₂ - #2	Lance	5 m		CO ₂

Methods

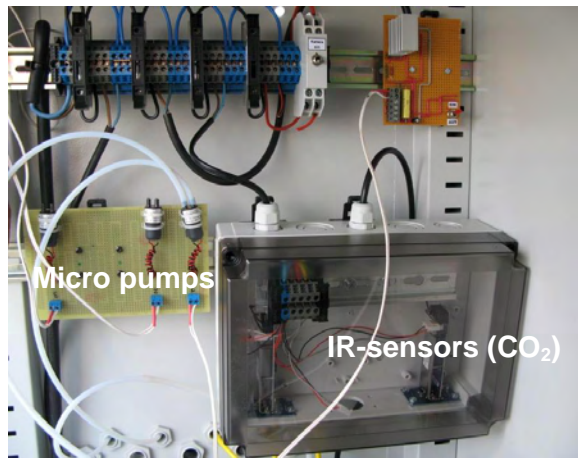


Figure 24. View on monitoring equipment. On the left side: micropumps for CO₂ monitoring. Right side: control board (IR sensor). 12 V batteries provided power supply.

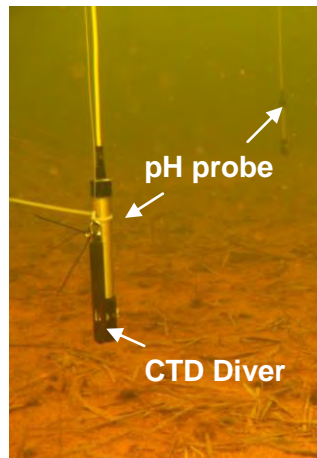


Figure 25. pH probe WQ201 and CTD diver for monitoring on-site parameters during the pilot experiment

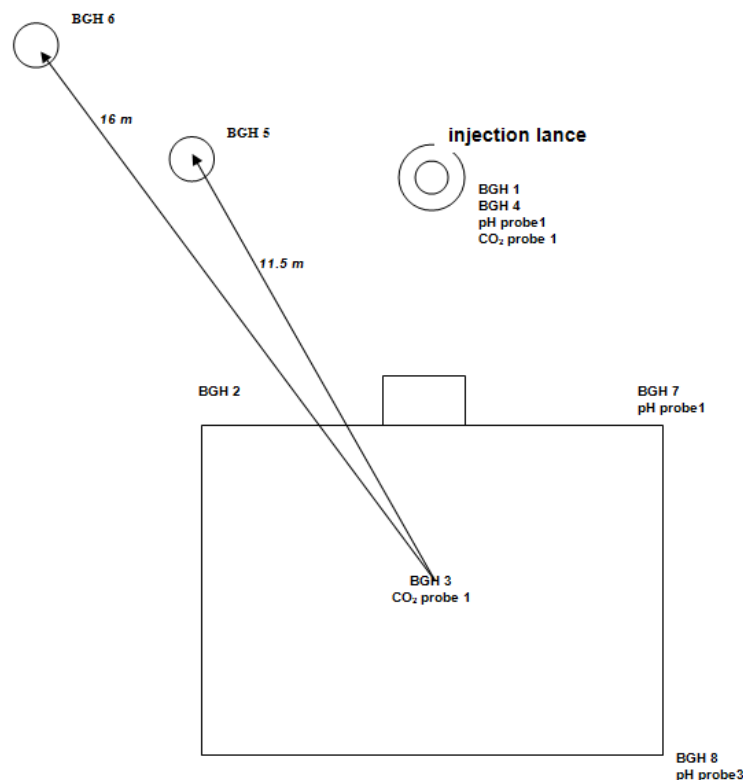


Figure 26. Plan of monitoring setup (not to scale)

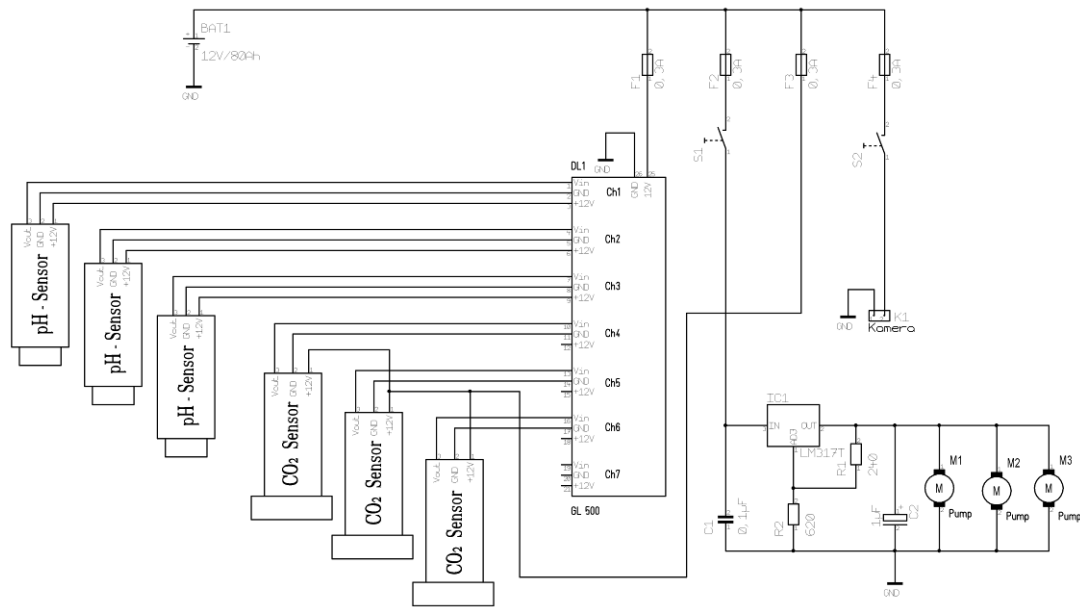


Figure 27. Schematic diagram of monitoring setup consisting of pH probes (Type WQ 201) and CO₂ sensors.

Water samples were taken in specific time intervals with an automatic sampling device (Type Liquiport 2000 RPT20; Endress and Hauser). Additionally, water-depth orientated samples were taken twice a week. On site the determination of pH, electrical conductivity, redox potential and oxygen content was carried out. Measurement devices and analytical procedures are described in chapter 3.2.2.

3.3.2.3 Methodological excurs: *in-situ-measurement of dissolved CO₂*

As described in Table 14 and in section 3.3.2.2 dissolved carbon dioxide was monitored by a self-constructed measuring system.

After sampling, the determination of CO₂ in aqueous systems can be done according to ISO standards (DIN 38409). Commercially available CO₂ meters [e.g. Model 503 pH / CO₂ Analyzer, Royce Instrument Cooperation, New Orleans, LA 70 129, USA] provide a direct reading of pH and temperature, while alkalinity of the water must be determined independently and provided as additional information. Sampling has to be at short intervals to evaluate short time-scale temporal modifications. Nevertheless, this may be tedious and costly if the sampling intervals are getting in the range of hours and minutes.

TDIC (total dissolved inorganic carbon) can be determined directly by the conversion of dissolved carbonate species in CO₂ by acidification. CO₂ can be separated by stripping or gas diffusion in an acceptor solution. CO₂ in the aqueous or gaseous phase can be as well determined by gas chromatography (GC), spectrometry, non-dispersive (IR) spectrometry, coulometric, potentiometric or conductometric methods.

Potentiometric electrochemical sensors are based on two membranes separating liquids (1 - sample solution, 2 - HCO₃⁻ containing solution). Due to diffusion of CO₂ pH-changes in the

electrolyte solution occur. The corresponding voltage of the sensor is proportional to the CO₂ concentration in the measured sample. Advantages of electrochemical sensors over other analytical methods are the easy use, low interferences with other ions, and in-situ determination in liquids. A disadvantage of electrochemical sensors is the need of regular calibration in order to avoid a drift of the sensor's signal.

Spectrometric measurements using fiber optic sensors have the advantage to be suitable for in-situ measurement, high sensitivity, accuracy, and low energy consumption. The principle is based on the detection of changes in an indicator solution within a membrane cell by fiber optic fibers. Major disadvantages are large sample amounts to reach equilibrium state, and the non-applicability for long-term readings.

Sensor arrays was designed, build, and tested based on commercially available sensors for gas monitoring. The sensor setup used is shown in Figure 28: separation of the aqueous solution (1) from the dissolved gas (3) using a gas-permeable membrane (silicon tube, outer diameter 4.0 mm, thickness 0.5 mm, Lindemann, Germany; (2)). Thus, water (and solids) cannot enter the sensor system itself. CO₂ molecules present in the water migrate by diffusion through the membrane reaching equilibrium between the surrounding water and the gas phase within the tube. The gas phase in this tube is continuously pumped (pump: type SP 135 FZ Fa., Schwarzer Precision, Germany; (4)) through the sensor array in order to accelerate the sensor's reaction and response time.

CO₂ is detected by a non-dispersive infrared two-channel detector (NDIR CO₂-Sensor Model 400, Digital Control Systems, (5)). This sensor emits two pulsed infrared signals, which are absorbed by CO₂ molecules. The intensity of the two beams reaching the detector is processed and expressed as CO₂ concentration. Due to the existence of pH-dependent species (CO₂ or H₂CO₃ / HCO₃⁻ / CO₃²⁻), a pH probe (7) is integrated in the sensor arrangement. All values are processed (9) and stored in a low cost data logger (Tinytag Plus, Gemini Data Loggers, UK), (10).

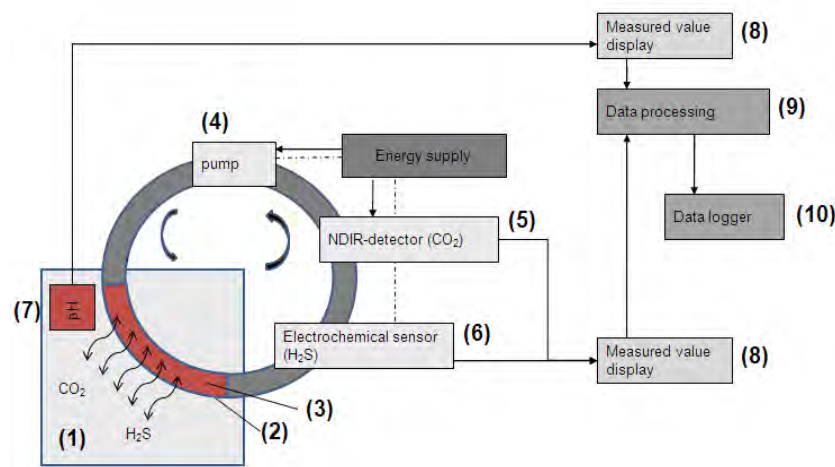


Figure 28. Schematic sketch of the sensor set-up.

A rechargeable battery (12 V / 20 Ah) provides power supply. Compression springs (VKM-13604, company Gutekunst &Co, Germany) were used to stabilize the semi-permeable membrane in the aqueous environment.

The measurement was designed and improved within a project with an industrial partner. For measurements in hydrothermal systems, the sensor set-up was extended by an electrochemical H₂S gas sensor (3001 SI, Analox Sensor Technology, 0 - 100 ppm).

Compared to prior setups, the combination of 2 or more commercial available gas sensors in combination with a gas-sensitive membrane and a pump in the array is an essential improvement because pumping the gas in the array improves the response time of the sensor by far. Compared to an application without pump, a 50 – 60 times higher response time was reached. Furthermore, by choosing a suitable membrane an enrichment of gas is reached in the membrane. Thus, an overall faster transport of the gas from the liquid to the gas phase takes place. Other advantages are the relatively simple construction, the possibility to combine different sensors, and the suitability for short- and long-term monitoring of fluids.

Concerning the field of application, the sensor was calibrated in different chemical/environmental conditions. The calibration showed no significant differences and interactions in pure 5 mM NaHCO₃ solutions, in solutions with higher ionic strength (5 mmol/L compared to 44 mmol/L), and with particular reference to other IR-sensitive gases (e.g. H₂S). During calibration pH was adjusted with 1 M HCl. The depending aquatic species of C and S were modeled by the hydrochemical code PhreeqC (Parkhurst & Appelo 1999) (database: wateq4f.dat). First results have been published in (Schipek et al., 2010).

3.3.2.4 Water chemistry Analysis

The analysis of the samples in the laboratory included main cations/anions, trace metals, and total inorganic carbon (TIC), as described in chapter 3.2.2. The evaluation of the acid/base capacity was conducted with a processor-controlled titrator Basic Titrino (Metrohm).

Additionally, filtered water samples were immediately analysed photometrically with respect to manganese (Mn_{tot}), phosphate (PO₄³⁻), nitrite (NO₂⁻), iron (Fe_{total}, Fe²⁺), and ammonia (NH₄⁺). This was realised using a DR/890 Colorimeter (HACH). The respective methods with their range of concentration, precision and estimated detection limit (EDL) are summarised in Table 15.

Table 15. Photometrical methods: measuring ranges and detection limits

	Method	Range [ppm]	precision	DL [ppm]
Fe _{total}	FerroVer method	0 – 3.00	±0.017 ppm	0.03
Fe ²⁺	1,10-Phenanthrolin method	0 – 3.00	±0.017 ppm	0.03
PO ₄ ³⁻	PhosVer 3 method	0 – 2.50	±0.05 ppm	0.05
NO ₂ ⁻	Diazotierungs method	0 – 0.350	±0.001 ppm	0.005
NH ₄ ⁺	Salicylate method	0 – 0.50	±0.02 ppm	0.02
Mn _{tot}	PAN method	0 – 0.7		0.007

3.3.2.5 Geochemical investigations (ash sediments, pore water)

In order to obtain changes in the geochemical and mineralogical composition of the settled ash sediment, before and after CO₂ treatment in the vicinity of the injection point, drilling cores were sampled. In the beginning and after the pilot experiment sediment cores were taken with the help of the Drilling Unit "Niederreiter 60" (Uwitec). A detailed description of the technology of the drilling process can be taken from (Clauß, 2008).

Before CO₂ treatment, one drilling core (BGH-290408-P0, sediment depth: 5 m) was taken. Due to technical problems at the end of the pilot experiment, only 3 drilling cores were taken after CO₂ treatment. Table 16 shows an overview about gained depths.

Table 16. Coordinates of sampling points (drilling cores) before and after CO₂ treatment (Gauß-Krueger-Coordinates, RD 83, Rauenberg, Bessel)

Labeling of the drilling core	Easting	Northing	Depth
BGH-290408-P0	5456269	5704237	5 m
BGH-300708-P1	5456316	5704232	4 m
BGH-300708-P2	5456257	5704236	2 m
BGH-310708-P3	5456254	5704243	8 m

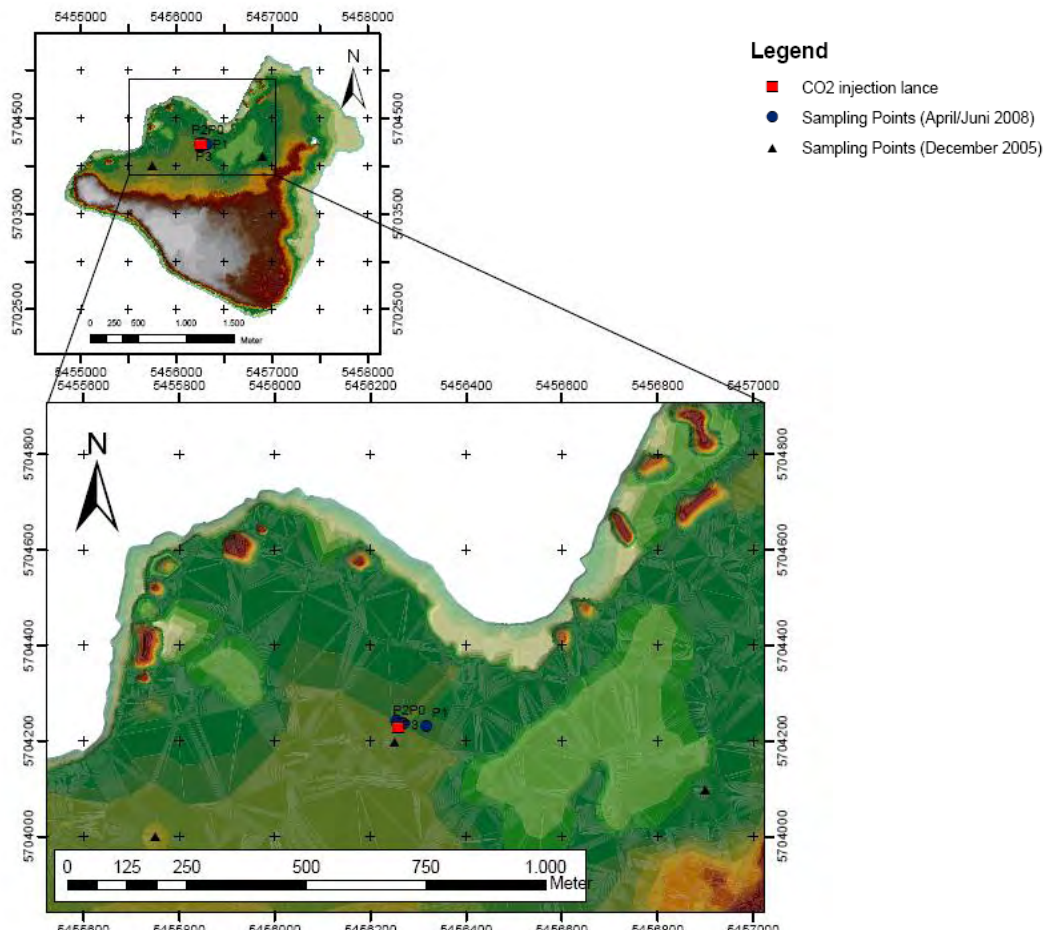


Figure 29. Digital Terrain Model of Lake Burghammer. Red square shows CO₂ injection point. Blue dots represent sampling points before and after CO₂ treatment (Gauß-Krueger (zones are only 3° apart, as opposed to 6° in UTM), RD 83, Rauenberg, Bessel).

3.4 Models and Visualization

3.4.1 Hydrochemical modelling

3.4.1.1 *Chemical thermodynamic modeling*

Modeling mineral saturation indices (SI) in (pore) water samples, and batch experiments (CO₂ sequestration)

Thermodynamic modeling was done using the hydrogeochemical modeling program PhreeqC (Parkhurst and Appelo, 1999). The program is based on the formation of equilibria in aqueous solutions with mineral phases, gases, ion exchangers and sorption surfaces. PhreeqC calculates among other options activity coefficients using Debye-Hückel-equations and ion dissociation theory (Parkhurst and Appelo, 1999).

Activities of aqueous species and mineral saturation indices (SI) of selected mineral phases were calculated using PhreeqC in combination with the Minteq.v4.dat database. Secondary minerals formed during weathering of CCBs have the potential to limit (or enhance) the mobility of trace elements in ash disposal facilities. Unfortunately, there are only few thermodynamic, kinetic or adsorption data, for many of these secondary minerals.

This Minteq.v4.dat database was modified to include minerals concerning fly ash sediments: ettringite ($\log K = 62.5632$; Lawrence Livermore National Library (LLNL) database), ferrihydrate (Fe(OH)_3 ($\log K = 4.891$, wateq.4f.dat database)), sillimanite (a mineral similar to mullite, main aluminosilicate matrix in fly ash), allophone-1.26 ($\log K = 11.27$, Su and Harsh 1998), calcium antimonite $\text{Ca}[\text{Sb}(\text{OH})_6]_2$ ($\log K = -12.55$; (Johnson et al., 2005)), halloysite ($\log K = 9.57$; (HydroGeoLogic, 1999)), illite ($\log K = 9.03$; LLNL database), imogolite ($\log K = 13.04$, (Su and Harsh, 1994)), boehmite ($\log K = 8.578$, (Hemingway et al., 1991)), gibbsite ($\log K = 8.02$, (Su and Harsh, 1994)), kaolinite ($\log K = 7.43$; (HydroGeoLogic, 1999)), K-mica ($\log K = 12.703$; wateq.4f.dat database), K-feldspar ($\log K = -20.573$; wateq.4f.dat database), and manganite ($\log K = 25.340$; wateq.4f.dat database).

The discussed minerals were selected based on different reasons: (i) their likeness to be present or formed in municipal solid waste incinerator ashes (e.g. (Johnson et al., 1999, Dijkstra et al., 2006a, Dijkstra et al., 2006b, Zevenbergen et al., 1996), (ii) calculated saturation indices (SI) that approach zero ($-1 < \log SI < 1$). The SI does not confirm whether or not a solid phase is actually present, but it indicates whether a given solid phase would have a tendency to precipitate ($SI > 0$) or dissolve ($SI < 0$) (Merkel and Planer-Friedrich, 2005).

Modeling of the equilibrium state to estimate the amount of liming agent for kinetic experiments (lake liming)

The following input script was used to model the amount of calcite to reach equilibrium in the kinetic experiments. Varying CO₂ partial pressures had been considered. The amount used in the experiments was 5 / 20 times oversaturated compared to modeling equilibrium.

Modeling was done using two databases: wateq4f.dat and llnl.dat.

Methods

Text box 1. PhreeqC-input file – Modeling the amount of calcite in equilibrium, preparation for kinetic experiments (lake liming)

```
TITLE Modeling the amount of calcite in equilibrium  
  
SOLUTION 1 distilled water  
units ppm  
pH 7  
temp 22  
  
EQUILIBRIUM_PHASES  
CO2(g) -3.42021 # 0.038 vol-%  
#CO2(g) -1.30103 # 5 vol-%, varying CO2 partial pressures according modelling step  
#CO2(g) -0.52288 # 30 vol-%  
#CO2(g) -0.30103 # 50 vol-%  
#CO2(g) 0 # 100 vol-%  
  
End
```

Modeling of the results of the column experiments in order to estimate the efficiency of the liming agents

The results of the column experiments were modeled using PhreeqC. Solution 1 represents the initial solution (water from lake Burghammer). By the help of the keyword REACTION a total of 2.71 mmol neutralizing agent (either CaCO₃ or CaO) was added in 42 steps. The possible precipitation of mineral phases was allowed using the keyword EQUILIBRIUM_PHASES.

Text box 2. Efficiency estimation of the results of column experiments (lake liming)

```

KNOBS
-iterations 5000
-pe_step_size 1.5

SOLUTION 1;
pH 2.89
temp 3.4
pe 12.86

units ppm
Li 0.05
Na 53.9
K 9.11
Ca 340.7 charge
Mg 47.65
Fe(+2) 2.22
Fe(+3) 20.9
Mn(2) 6.55
N(-3) 0.19 as NH4
N(+5) 1.40 as NO3
N(+3) 0.044 as NO2
P 0.25
F 1.34
Cl 81.3
S(+6) 1251 as SO4
C 1.70 as C(+4)

SELECTED_OUTPUT
-molalities
-file burghammer_CaCO3.csv
-pH
-reaction true

REACTION 1
CaCO3 #alternative: CaO
2.71E-03 in 42 steps
EQUILIBRIUM_PHASES
Calcite 0 0 #1.83e-3
Fe(OH)3(a) 0 0
Fe(OH)2.7Cl.3 0 0
Fluorite 0 0
Gypsum 0 0
MnHPO4 0 0
Jarosite(ss) 0 0
FCO3Apatite 0 0
Rhodochrosite(d) 0 0
Rhodochrosite 0 0
Strengite 0 0
CO2(g) -3.5

REACTION 2
Mn
-2e-5
Save solution 2
end

```

3.4.1.2 Kinetical modeling

Besides chemical thermodynamical modeling PhreeqC offers the possibility to implement any reaction kinetics. For the calculation of the calcite-solution kinetics, the empirical model of Plummer & Busenberg (1982) was used. As described by Plummer & Busenberg (1982), a

Methods

significant dependence on pH is visible: high dissolution rates at low pH values and a significant decrease with approach to the neutral point.

Text box 3. PhreeqC-input file – Modeling kinetic experiments using the empirical model of Plummer & Busenberg (1982)

```
TITLE defined reaction rate solution of calcite
SOLUTION 1 distilled water
units ppm
pH 7
temp 22

EQUILIBRIUM_PHASES
CO2(g) -3.42021 # 0.038 Vol%
#CO2(g) -1.30103 # 5 Vol%, varying CO2 partial pressure according to modeling step
#CO2(g) -0.52288 # 30 Vol%
#CO2(g) -0.30103 # 50 Vol%
#CO2(g) 0      # 100 Vol%

KINETICS 1
Calcite
-tol 1e-8
-m0    6.14.e-4
-m     6.14.e-4
-parms 50      0.6
-steps 1209600 in 5000 steps
-step_divide 1e-4

RATES
Calcite
-start
1 rem  parm(1) = A/V, 1/dm      parm(2) = exponent for m/m0

10 si_cc = si("Calcite")
20 if (m <= 0 and si_cc < 0) then goto 200
30 k1 = 10^(0.198 - 444.0 / (273.16 + tc) )
40 k2 = 10^(2.84 - 2177.0 / (273.16 + tc) )
50 if tc <= 25 then k3 = 10^(-5.86 - 317.0 / (273.16 + tc) )
60 if tc > 25 then k3 = 10^(-1.1 - 1737.0 / (273.16 + tc) )
70 t = 1
80 if m0 > 0 then t = m/m0
90 if t = 0 then t = 1
100 moles = parm(1) * 0.1 * (t)^parm(2)
110 moles = moles * (k1 * act("H+") + k2 * act("CO2") + k3 * act("H2O"))
120 moles = moles * (1 - 10^(2/3*si_cc))
130 moles = moles * time
140 if (moles > m) then moles = m
150 if (moles >= 0) then goto 200
160 temp = tot("Ca")
170 mc = tot("C(4)")
180 if mc < temp then temp = mc
190 if -moles > temp then moles = -temp
200 save moles
-end

SELECTED_OUTPUT
-file 0_CO2_Plummer.csv          # example
-saturation_indices calcite
-ph
-totals Ca
end
```

E Göransson et al. (2006) showed in a study that similar simple models for regional scale in Sweden were in good agreement with measurements in limed lakes.

The given input script (Text box 3) was used to model kinetic reactions.

3.4.2 Visualisation

Visualization of water quality development during liming campaigns was visualized and modeled with MATLAB® (Version 7.7.0.471, R2008b).

MATLAB® is a software package developed by The MathWorks Inc.. It was designed to perform mathematical calculations, to analyze and visualize data, and write new software programs.

Input parameters were

- Bathymetry of lake Burghammer
- Coordinates of multiprobe-measurements ($n = 1 - 24$) in lake Burghammer
- Multiprobe measurements of monitoring campaigns before, during and after addition of liming agents (temperature, pH, ORP, SpCond, depth, turbidity, LDO%, LDO)

Cubic-spline interpolation was used for interpolating the unevenly spaced data. Cubic splines are piecewise continuous curves, passing through at least four data points for each step (Trauth, 2007). According to Trauth (2007) this method has the advantage that it preserves the high-frequency information which is contained in the data. A median filter was applied to the data of multiprobe measurements in case of unexpected gaps in the plot.

Different visualization methods had been developed. Table 17 shows an overview about developed m-files and their script functions. m-files as described in Table 17 can be found in Appendix C.

Table 17. Overview about developed m-files and function of the script. As well, variable parameters are listed.

	Function of the script	Variable parameters
Hydro_topo.m	Plots the surface of the lake	<ul style="list-style-type: none"> ▪ surface height (according to flooding state, sampling date)
Hydro_plot_mp.m	Plots the surface of the lake and the multiprobe measurement profiles for a certain date	<ul style="list-style-type: none"> ▪ surface height (according to flooding state, sampling date)
Hydro_depth.m	Creates animated 2D-plots of parameter distributions for one date and different depths	<ul style="list-style-type: none"> ▪ surface height (according to flooding state, sampling date) ▪ depth spacing of vertical data interpolation
Hydro_time.m	Creates animated 2D-plots of parameter distributions in dependence of the date of measurement and for an user-defined depth	<ul style="list-style-type: none"> ▪ surface height (according to flooding state, sampling date) ▪ depth spacing of vertical data interpolation

Methods

	Function of the script	Variable parameters
Hydro_surface.m	Creates a 3D-plot of parameter distributions for the bottom of the lake	<ul style="list-style-type: none">▪ surface height (according to flooding state, sampling date)▪ depth spacing of vertical data interpolation
Hydro_surface_time.m	Creates animated 3D-plots of parameter distributions in dependence of the date of measurement and for the bottom of the lake	<ul style="list-style-type: none">▪ surface height (according to flooding state, sampling date)depth spacing of vertical data interpolation
Hydro_sclice.m	Creates 3D-slices of parameter distributions across the lake in different user-defined directions	<ul style="list-style-type: none">▪ surface height (according to flooding state, sampling date)▪ depth spacing of vertical data interpolation▪ type of slices (horizontal, vertical)
Hydro_slice_anim.m	Creates animated 3D-slices of parameter distributions across the lake and along a user-defined direction	<ul style="list-style-type: none">▪ surface height (according to flooding state, sampling date)▪ depth-spacing of vertical data interpolation▪ type of slices (horizontal, vertical)

4 Results and discussion

4.1 Solid characteristics

In total 31 samples were taken from 3 drilling cores (up to 8 m sediment depth, sampling date 12/2005). Additionally 11 disturbed samples of the lake sediment were taken (sampling date 11/2005 and 12/2005).

A total of 23 different neutralizing products were preliminary investigated.

4.1.1 Fly ash

4.1.1.1 Physical investigations

The sediment taken from the lake shows a water content of approximately 30 to 70 wt.-%, in average 50 wt.-%, and a net density of approximately 2.65 g/cm^3 (Figure 30).

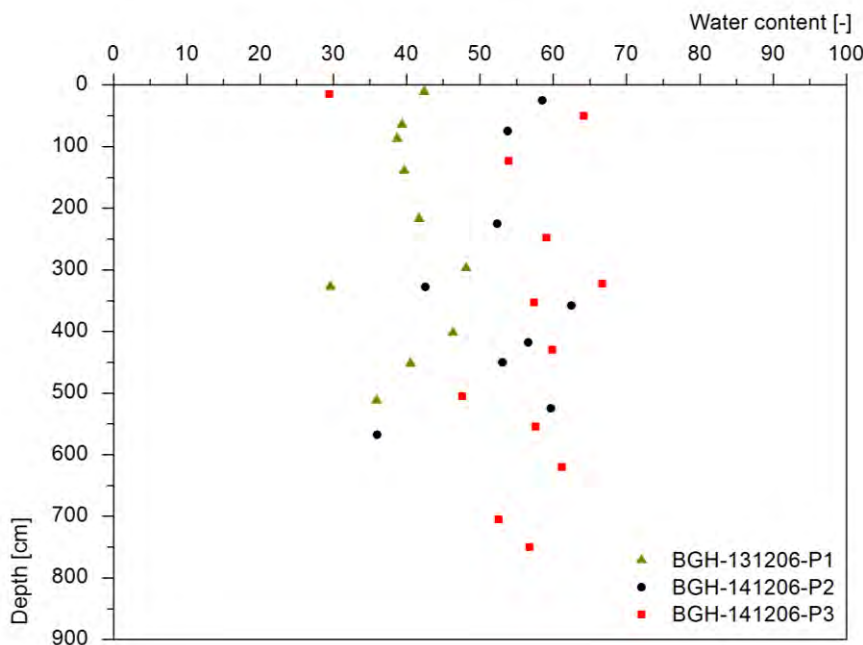


Figure 30. Distribution of water content in drilling cores BGH-131206-P1, -P2, -P3

Particle size distribution shows the predominance (60 wt.-%) of finer particles ($< 100 - 1000 \mu\text{m}$). The larger surface area of the smaller particles increases mobilisation of trace elements on the particle surfaces. Detailed studies on the element versus particle size distribution show an inverse dependence on concentration with respect to particle size distribution (Iyer, 2002). The smaller particle has a larger specific surface area, making a larger area susceptible to hydrolysis (Fisher et al., 1978). It has been shown that only about 1 - 3 wt.-% fly ash material is soluble in water with lignite fly ash (Keyser et al., 1978).

Results and discussion

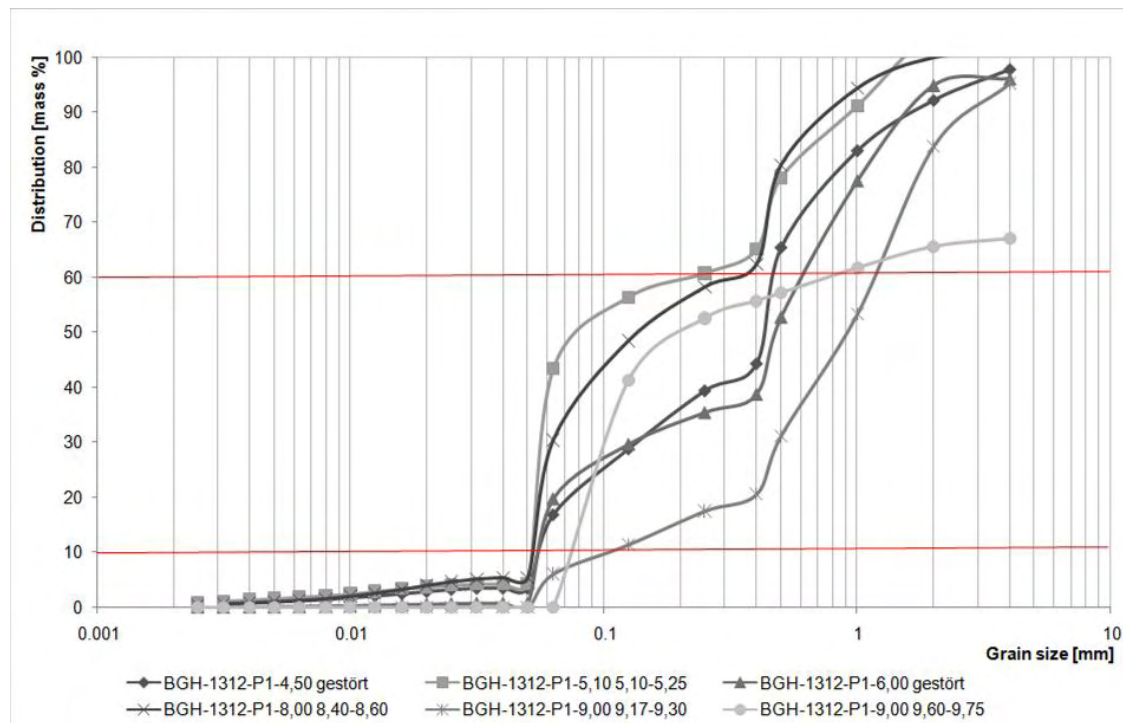


Figure 31. Particle size distribution of ash sediment, sample BGH-131205-P1, different depths.

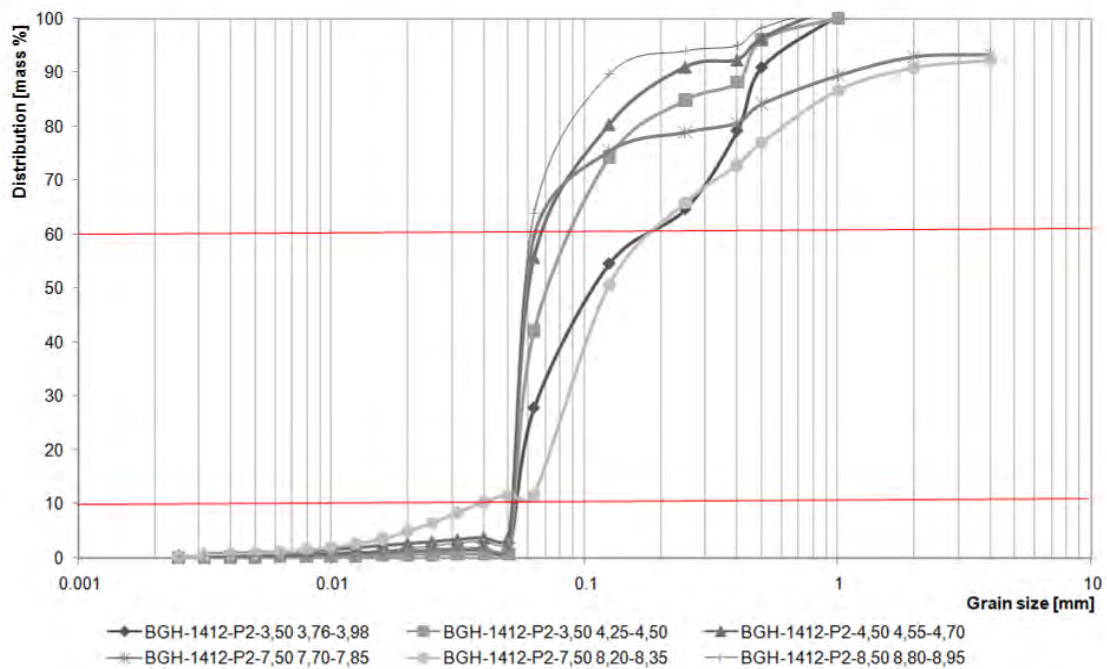


Figure 32. Particle size distribution of ash sediment, sample BGH-141205-P2, different depths.

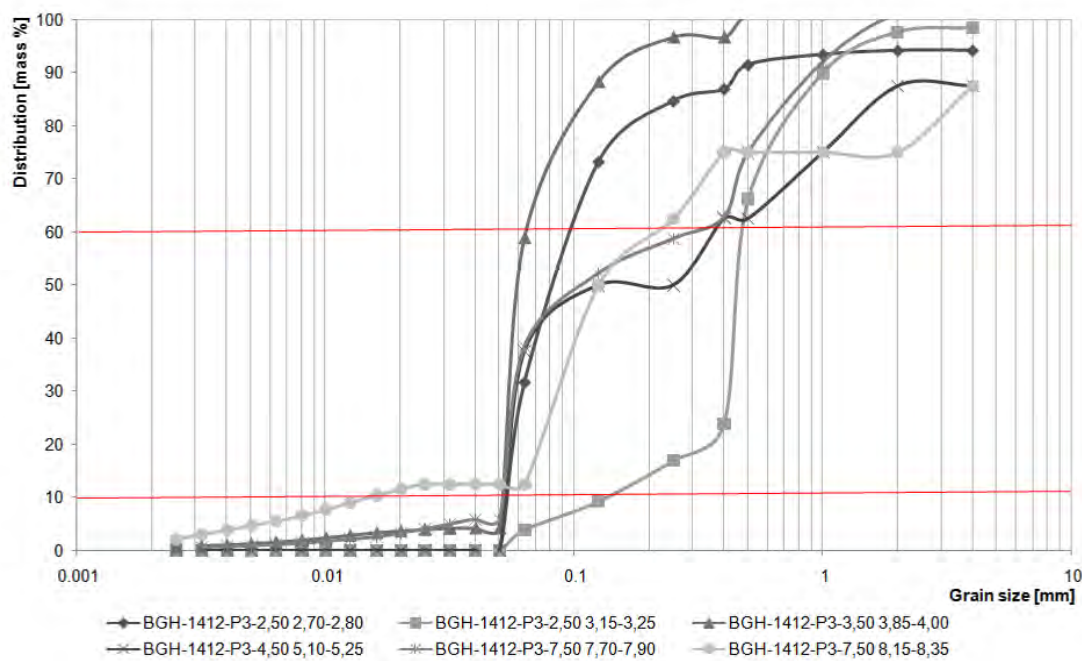


Figure 33. Particle size distribution of ash sediment, sample BGH-141205-P3, different depths.

Hydraulic conductivities were calculated according to Beyer (1964) and Kaubisch (1986) in a range of 10^{-5} – 10^{-8} m/s (see Table 18).

Table 18. Calculated hydraulic conductivities of Lake Burghammer sediments (drilling cores from 12/05)

	calculated hydraulic conductivity [m/s]	used formula*
BGH-1312-P1-4.00 (disturbed)	-	
BGH-1312-P1-4.50	5.28E-06	2
BGH-1312-P1-5.10 (5.10-5.25)	2.14E-08	2
BGH-1312-P1--6.00 (disturbed)	2.58E-06	2
BGH-1312-P1-7.00 (7.20-7.35)	-	
BGH-1312-P1-7.00 (7.50-7.65)	-	
BGH-1312-P1-8.40 (8.40-8.60)	2.77E-07	2
BGH-1312-P1-9.17 (9.17-9.30)	8.83E-05	1
BGH-1312-P1-9.60 (9.60-9.75)	4.11E-05	1
BGH-1412-P2-3.50 (3.76-3.98)	4.25E-07	2
BGH-1412-P2-3.50 (4.25-4.50)	3.73E-08	2
BGH-1412-P2-4.50 (4.55-4.70)	3.33E-09	2
BGH-1412-P2-4.50 (5.07-5.22)	-	
BGH-1412-P2-5.50 (5.85-6.00)	2.77E-07	2
BGH-1412-P2-6.50 (6.65-6.80)	3.31E-05	1
BGH-1412-P2-6.50 (6.95-7.10)	-	
BGH-1412-P2-7.50 (7.70-7.85)	2.44E-09	2
BGH-1412-P2-7.50 (8.20-8.35)	1.41E-05	2
BGH-1412-P2-8.50 (8.80-8.95)	1.36E-09	2
BGH-1412-P3-2.50 (2.70-2.80)	3.42E-07	2
BGH-1412-P3-2.50 (3.15-3.25)	1.88E-04	1
BGH-1412-P3-3.50 (3.85-4.00)	2.44E-09	2
BGH-1412-P3-4.50 (5.10-5.25)	6.65E-08	2

Results and discussion

	calculated hydraulic conductivity [m/s]	used formula*
BGH-1412-P3-5.50 (5.80-6.00)	-	
BGH-1412-P3-5.50 (6.15-6.30)	-	
BGH-1412-P3-6.50 (6.90-7.10)	3.24E-05	1
BGH-1412-P3-7.50 (7.70-7.90)	6.65E-08	2
BGH-1412-P3-7.50 (8.15-8.35)	1.10E-05	2
BGH-1412-P3-8.50 (8.80-9.00)	-	
BGH-1412-P3-9.50 (9.65-9.85)	-	
BGH-1412-P3-9.50 (10.10-10.30)	5.17E-08	1

* Calculation after ¹⁾ (Beyer, 1964), ²⁾ (Kaubisch, 1986)

4.1.1.2 Mineralogical analysis

Mineralogical investigations of fresh **fly ash from the power plant Boxberg** were carried out. Figure 19 sums up the mineralogical composition of the findings.

Table 19. Analyzed mineral phases of the brown coal filter ash (power plant Boxberg)

Mineral phases	Chemical formula
Quartz	SiO ₂
Ca-Mg-Fe-Silicate	Ca ₂ Fe _{1,2} Mg _{0,4} Si _{0,4} O ₅
Periclase	MgO
Anhydrite	CaSO ₄
Hematite	Fe ₂ O ₃
Gehlenite	Ca ₂ Al(Al, Si) ₂ O ₇
Free Lime	CaO & Ca(OH) ₂
Ca-Al-Oxide	Ca(AlO ₂) ₂
Orthoclase	KAlSi ₃ O ₈

The composition of the investigated **ash sediment** is rather varying. Coal, coke particles as well as quartz were determined in varying fractions.

Figure 34 and Figure 35 show micrographs of thinsections of the drilling cores BGH-131205-P2-3.50 and BGH-131205-P2-4.50. Mainly opaque substances with various particle shapes and sizes, partly transparent, are identifiable (1). Some of the larger clasts own a fine-grained matrix consisting partly of quartz fragments (2). Sporadically, brown to red colored wooden residues were found in the thin sections.

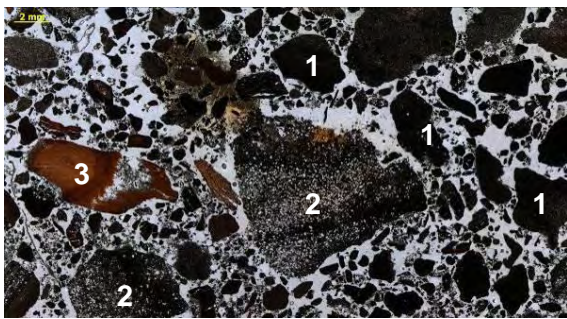


Figure 34. Thinsection of drilling core BGH-141205-P2-3.50.

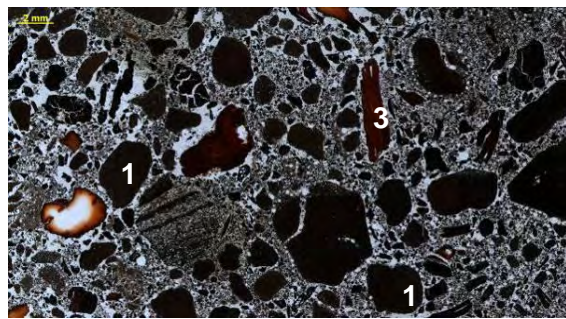


Figure 35. Thinsection of drilling core BGH-131205-P2-4.50.

As seen from the results in Table B.2 (Appendix B), the predominant part of the unsettled ash sediment is composed of amorphous, presumably, aluminosilicate glass.

The minerals quartz (SiO_2), calcite (CaCO_3), hematite ($\alpha\text{-Fe}_2\text{O}_3$), magnesian ferrite ($\text{MgFe}_2^{3+}\text{O}_4$) and brownmillerite ($\text{Ca}_2(\text{Al},\text{Fe})_2\text{O}_5$) could be identified in almost all particle ranges.

The quartz content was between 1 and 50 wt.-%. Calcite and brownmillerite could be identified in a range of 1 to 8 wt.-%. The hematite content ranged from 0.3 to 2 wt.-%. Magnesium rich ferrite was found to be up to 11 wt.-% in the drilled core sediment. In the trace range, the mineral phases akermanite ($\text{Ca}_2\text{Mg}[\text{Si}_2\text{O}_7]$), diopside ($\text{MgCaSi}_2\text{O}_6$), and rutile (TiO_2) also appeared. A number of other crystalline phases are very possible; however, they cannot be identified with sufficient certainty from the diffractograms.

Crystalline CaO did not prove to be in the unsettled sediment. Sporadically, but only prior to core drilling in BGH-1412-P3, ettringite und periclase were identified.

Ettringite ($(\text{CaO})_6(\text{Al}_2\text{O}_3)(\text{SO}_4)_3 \cdot 26 \text{ H}_2\text{O}$) is a typical mineral found in ash sediment. The maximum content of ettringite accounts for 8.6 wt.-%. Due to the fact that no pore water samples were available, thermodynamic modeling could not be done. Ettringite is supposed to be an artifact of sample preparation. Investigations of sediment samples before and after CO_2 injection showed sporadic appearances of ettringite, as well; whereas thermodynamical modeling, as well as pH conditions, results in undersaturation concerning the mineral ettringite.

EPRI (2006) describes weathering processes of alkaline fly ash. Common geochemical reactions include: hydration (anhydrite to gypsum, lime to portlandite), solution (dissolution of gypsum), hydrolysis (dissolution of glass), carbonation (portlandite to calcite), oxidation (magnetite to hematite / maghemite), precipitation (ettringite), adsorption from heavy metals on oxides and co-precipitation.

In summary, it can be concluded that 4 of the 10 identified mineral phases have calcium embedded in their crystal lattice, which will be mobilized by the different extraction measures. Münch (1996) indicates calcium to be available in the form of (Al)-(Mg)-ferrite, as well as amorphous structures of different composition and calcium silicates. Chemical and XRD analysis were conducted to gain information about the binding form of Ca in ashes.

Results and discussion

Table 20: Mineral phases containing Calcium

Mineral phases	Chemical composition
Akermanite	$\text{Ca}_2\text{MgSi}_2\text{O}_7$
Brownmillerite	$\text{Ca}_2(\text{Al},\text{Fe}^{3+})_2\text{O}_5$
Calcite	CaCO_3
Diopside	$\text{CaMgSi}_2\text{O}_6$
Ettringite	$\text{Ca}_6\text{Al}_2(\text{SO}_4)_3(\text{OH})_{12} \cdot 26 \text{ H}_2\text{O}$

TIC is in correspondence with the values of the XRD (Table B.2, Table B.3, appendix B). On average, the TIC content was about 3 – 4 g C/kg of ash sediment (Table B.3, appendix B).

Table 20 shows the calcium containing mineral phases. Slight variations between the XRD and TIC-determinations can be attributed to the instrument's conditional methods and the possible inhomogeneity of the samples.

5 Samples were investigated by Cathodoluminescence: P2-3.5 (3.75 – 4.00), P2-8.5 (9.25 – 9.5), P2-6.5 (6.75 – 8.0), P2-4.5 (5.25 – 5.5), and P2-7.5 (8.25-8.50). Figure 36 - Figure 39 show micrographs of ash sediment samples (left column shows polarization microscopy / transmission microscopy; right column shows Cathodoluminescence modus).

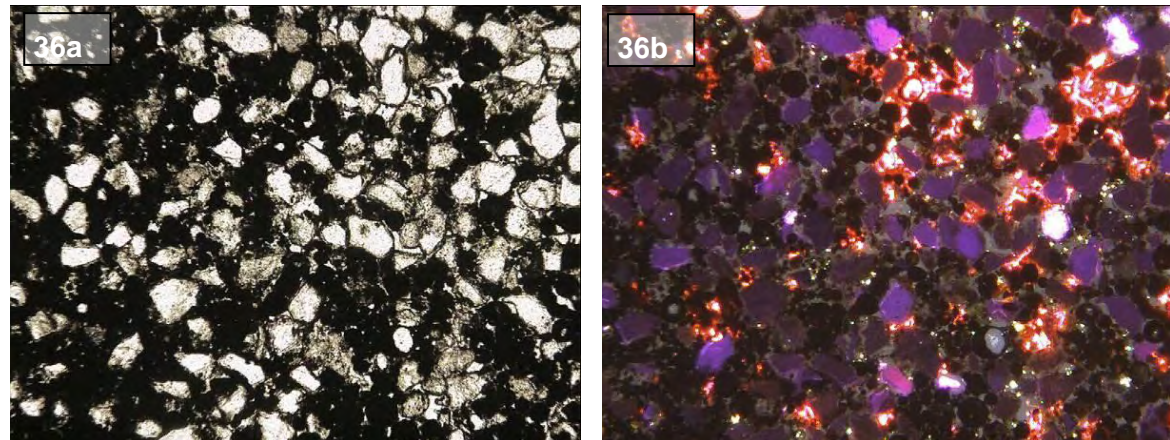


Figure 36. Sample P2-141205-3.5 (3.75-4.00): (a), (b) Main fraction consisting of coal-like, dark substance (probably Fe-Oxides). Besides, quartz (blue-purple luminescent) and feldspar (white luminescent) is visible. Organic particles surrounded by few orange-luminescent carbonates.

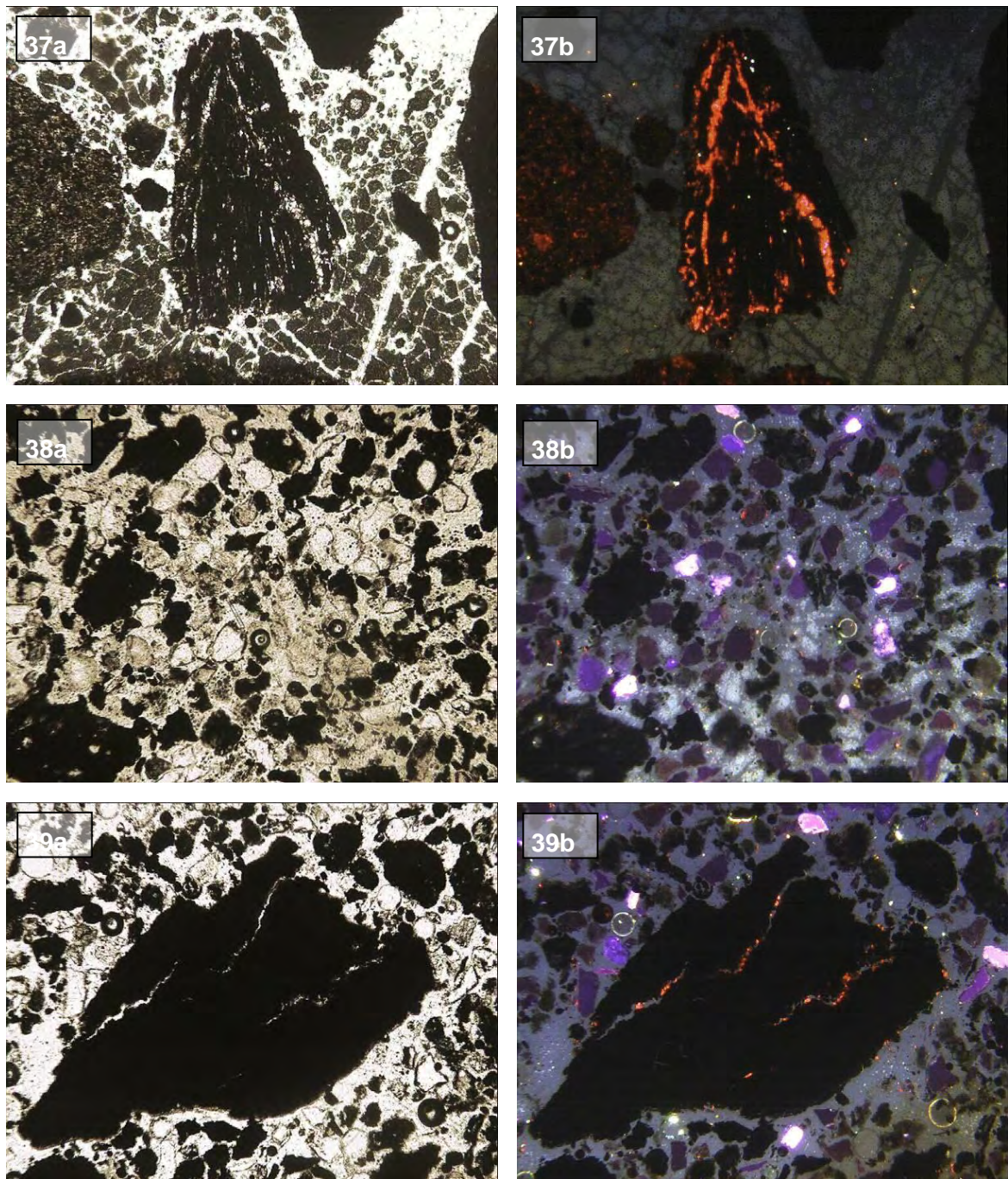


Figure 37. Sample P2-141205-3.5 (3.75-4.00): (a), (b) Preserved organic structure (unburned). Orange-luminescent carbonates filling existent fractures.

Figure 38. Sample P2-141205-6.5 (6.75-8.00): (a) Spherical particles show inclusions. (b) Main fraction consisting of coal-like, dark substance (probably Fe-Oxides). White aggregates represent feldspar minerals. Only few carbonate can be identified in / at organic constituents.

Figure 39. Sample P2-141205-6.5 (6.75-8.00): (a), (b) Preserved organic structure surrounded by orange-luminescent carbonates. Background: Probably Fe-oxides with feldspar minerals (white) and quartz (blue-purple luminescent).

Cathodoluminescence shows large, dark and coal-like areas which can be accounted as amorphous Fe-oxides (Figure 38). Blue purple luminescence shows the occurrence of quartz minerals, whereas white luminescence proves the occurrence of feldspars (Figure 36, Figure 38). In some samples isolated carbonate grains were detected (Figure 36). Besides isolated occurrence, larger amounts of calcite were detected in fractures and/or surroundings of organic constituents (Figure 37, Figure 39).

4.1.1.3 Geochemical results

In general, the investigated ash sediment reacted alkaline. All eluates were characterized by high electrical conductivities (137 – 656 µS/cm). pH of S4 elution was determined to be in average of 8.37 (median: 8.51); the absence of free CaO caused lower pH values than described in literature (e.g. 11.04 (Stewart et al., 2001), 11.4 – 12.7 (Münch, 1996), 11.55 (Ram et al., 2007)).

CCBs are enriched in trace elements such as cadmium, copper, lead and zinc, in comparison to natural materials (e.g. (Travar, 2006)). The effect of treatment with CO₂ has to be investigated concerning potential leaching and release of contaminants. A thorough characterization of the settled ash sediment and an investigation of their behavior under the expected exposure conditions are compulsory.

A general assessment of the eluability of chemical elements is not possible due to the diversity of ashes and extraction procedures (Münch, 1996). The limiting factors for eluability of elements are presence and solubility (van der Sloot et al., 1982).

The concentration of trace metals in the eluates varies (Table B.4 – B.7, appendix B). The purpose for the use of different elution processes was the determination of the mobility of trace metals during the planned rehabilitation process of the Burghammer Lake. The first two extraction steps from Zeien (1995) characterize the water soluble and exchangeable (unspecific adsorbed) metal/metalloid compounds; like the specifically sorbed, in the small-scale sense close to the surface occluded and metal organic complexes. The extraction steps, mentioned in 3.2.1.3, were performed to obtain more geochemical information of the samples.

The elution rates with respect to the elements calcium, magnesium, sodium and potassium were from 0.5 to 35 g/kg.

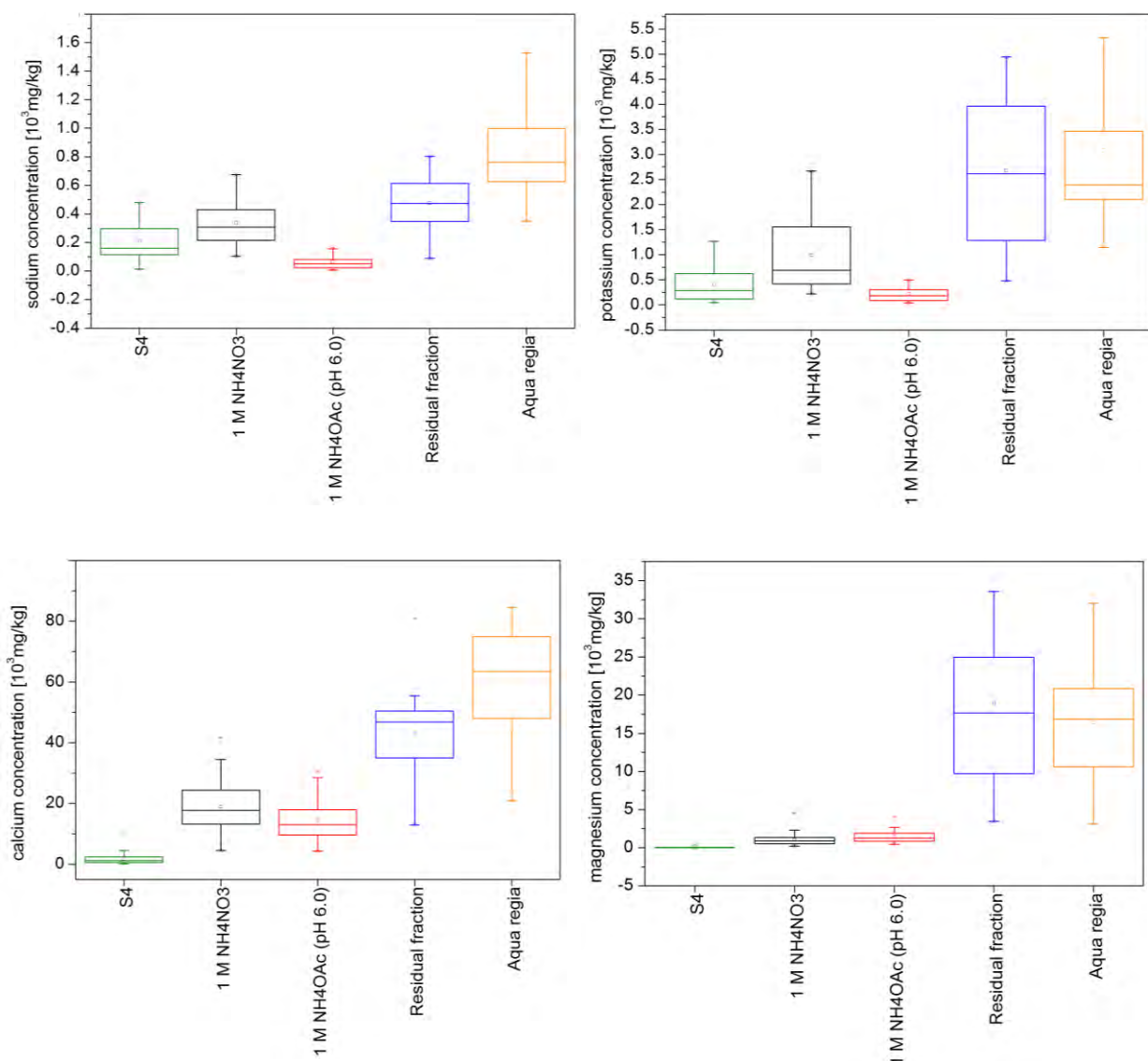


Figure 40. Eluent-dependent cation release from the deposited ash sediment.

Most notably, the released bivalent ions (**calcium, magnesium**) present potential cations for the carbonate precipitation. As can be seen from Figure 40, calcium and magnesium are the most important constituents of the eluates. In comparison with the easily mobilized fraction, from the mobile fraction more calcium can be eluted. The residual fractions provide a calcium content of 1 to 8 wt.-%. Prashanth (2001) report a calcium content of 3 to 9 wt.-%, and investigations from Zschiedrich et al. (2000) showed an average of 20 wt.-% CaO.

After the mineralogical investigations and the sequential extractions it was estimated, that approximately 40 - 50 wt.-% of the calcium in the mobile fraction can be used for the carbonate precipitation. The available calcium concentration corresponds to about 1 wt.-% of the total solid. Figure 41 shows the calcium content of the sampled drilling cores dependent on sediment depth.

Results and discussion

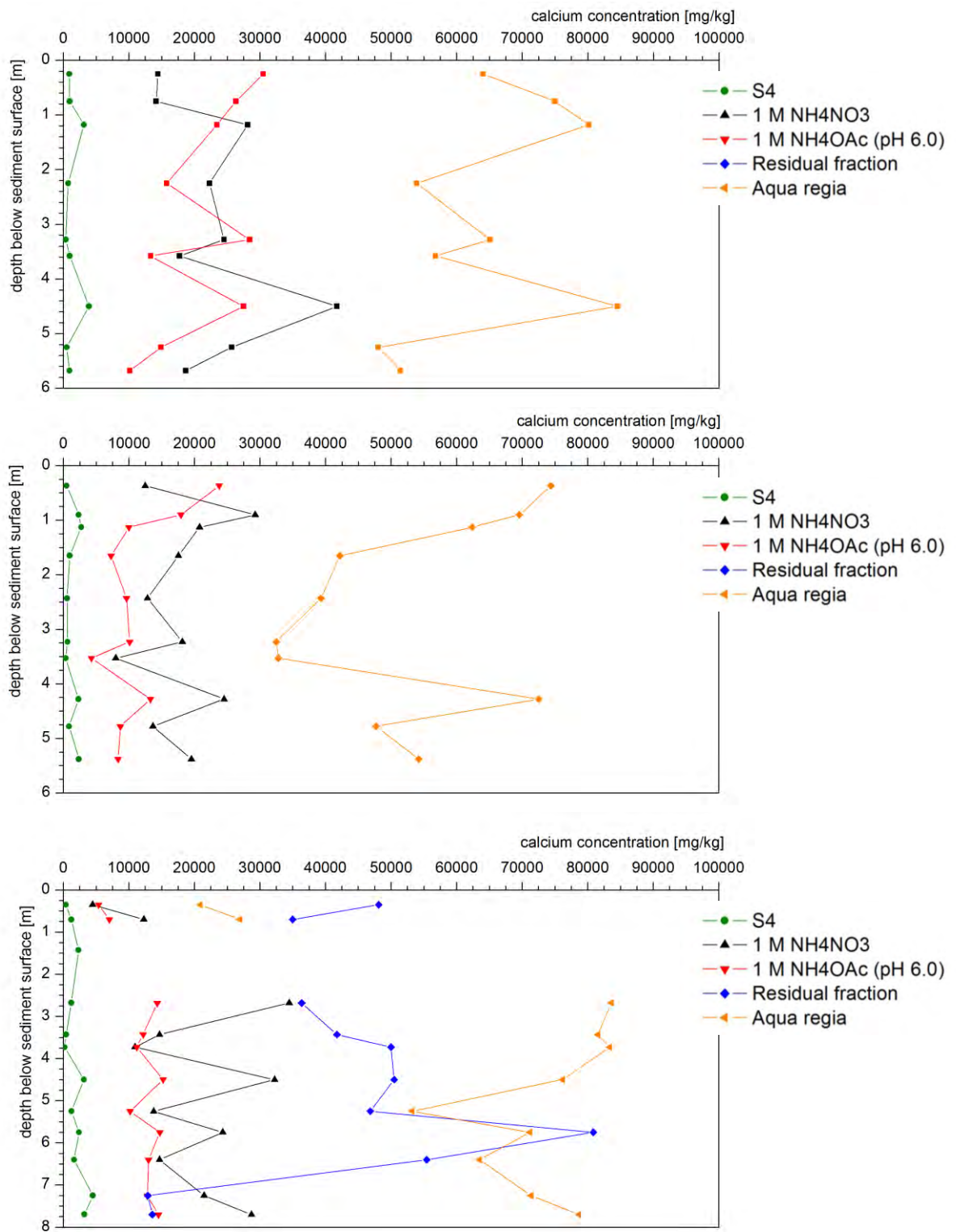


Figure 41. Extractable calcium concentrations of the drilling core BGH-131206-P1, BGH-141206-P2, and BGH-141206-P3

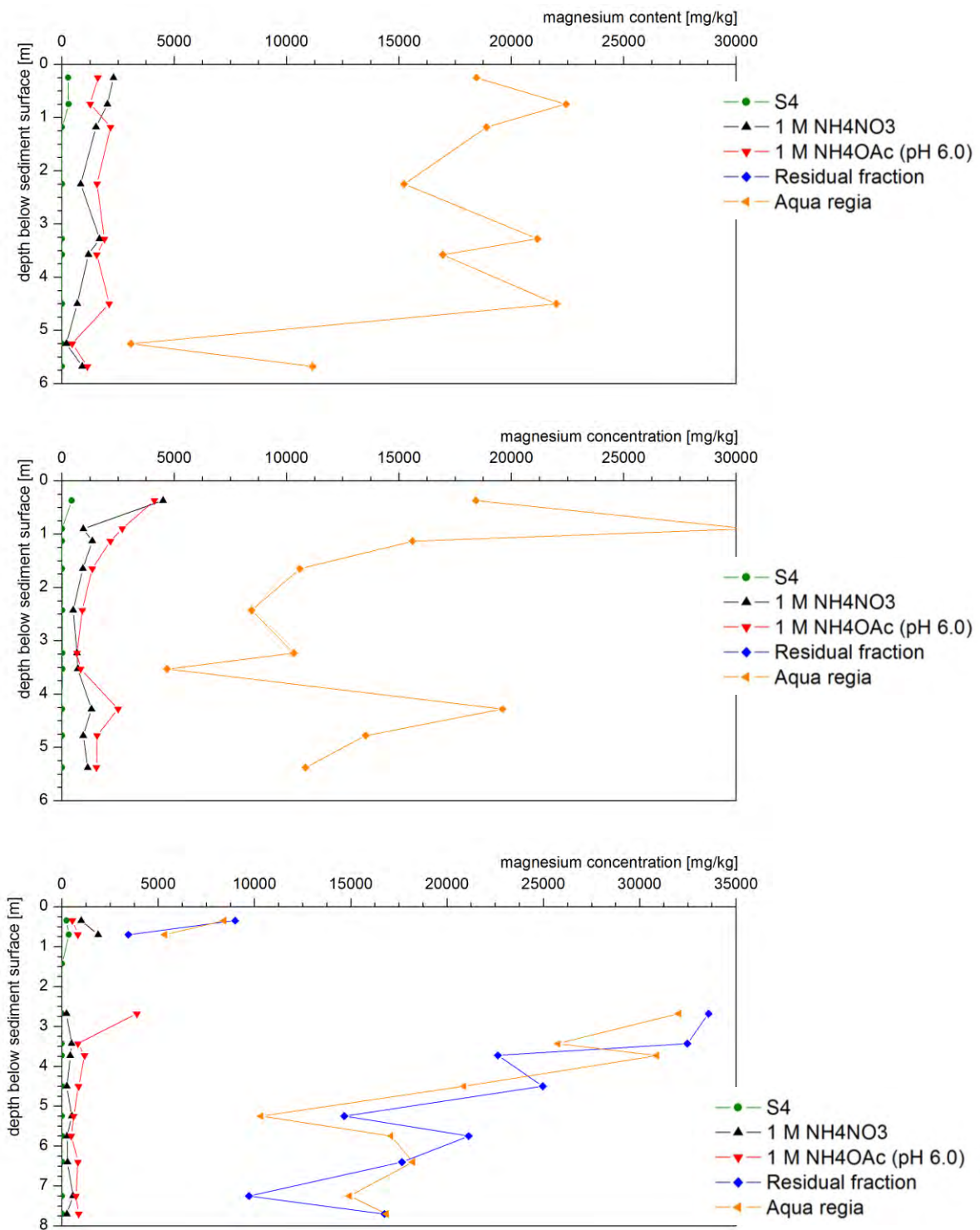


Figure 42. Extractable magnesium concentrations of the drilling core BGH-131206-P1, BGH-141206-P2, and BGH-141206-P3

The release of trace metals is graphically shown in Figure A.1 to Figure A.6, appendix A.

Zinc and **nickel** showed elevated mobility through the applied elutions/extractions process. With increased strength of the elution steps (aqua dist. (S4) < Ammonium nitrate <

Ammonium acetate) more zinc and nickel could be leached from the sediment. The S4-elution showed about 0.25 mg/kg Zn, while in the following steps the extractable zinc content surged up to 2 mg/kg. In both extraction steps from Zeien (1995), a mean value of approximately 1 mg/kg was reached. The residual fraction was determined with 65 mg/kg. Jegadeesan et al. (2008) reported a leachability of < 1 wt.-% of its total content within the labile fraction (sum of water soluble, exchangeable and carbonate fraction). It is important to note, that the sequential extraction procedure used by these authors differs in some steps.

The nickel in the fly ash sediment behaved similarly. The S4-Elution contains 1 mg/kg extractable nickel. In the second extraction step from Zeien (1995), a maximum content of 2.0 mg/kg was extracted. The solubility of both elements is dependent upon pH. With pH smaller than 6, the contents of water soluble and exchangeable nickel clearly gain; therefore, the availability rises with decreasing pH (Merkel and Sperling, 1998).

Molybdenum, arsenic, and chromium represent a group of trace elements whose highest extractability (with respect to step 1 to 3) lies within the range of the S4-Elution. With gradually progressing extraction strength, the content of extractable molybdenum, arsenic and chromium declined. With the S4-Elution, maximum contents of 0.7 mg/kg Mo, 0.3 mg/kg As and 1.1 mg/kg Cr could be detected. The mean values were around 0.15 mg/kg Mo, 0.5 mg/kg As and 0.6 mg/kg Cr. For molybdenum, the extractability decreased in extraction steps 1 and 3 to 0.1 mg/kg and 0.05 mg/kg, respectively. Arsenic was found to have a mean value of 0.05 mg/kg. The chromium concentration dropped in the second and third extraction steps to approximately 0.25 mg/kg. Referring to all extraction steps, the highest elutability of arsenic was determined in the residual fraction (0.92 mg/kg). Jegadeesan et al. (2008) reports a primary distribution of arsenic in the sulfidic/residual fraction and the iron oxide fraction. During coal combustion arsenic is embedded in fly ash samples; XANES spectra indicated that arsenic is primarily associated with iron minerals (Huggins et al., 2007, Zielinski and Budahn, 2007).

The data from the sequential extraction procedure indicated that **iron** appeared predominantly to be in the residual phases.

Based on the sequential extraction results of the ash sediments, it was observed that the 3 chosen extraction steps (aqua dist. (S4) < Ammonium nitrate < Ammonium acetate) revealed leachable amounts of only a few percent of the total content (for most trace elements). These results correspond with the published results (Jegadeesan et al., 2008). The results also indicated that the majority of the trace metals would be unavailable for leaching, and thus not released during CO₂ treatment.

Polycyclic aromatic hydrocarbons (PAH)

Polycyclic aromatic hydrocarbons (PAH) emerges as by-products from the partial combustion of organic substances like coal, heating oil, motor fuels, wood, and turf. The number and structure of the refined PAH depends upon both the temperature and the available amount of oxygen (Sims and Overcash, 1983, Giger et al., 1974). Deposited Burghammer fly ash sediments may as well release organic pollutants. PAH concentrations in the deposited sediment were investigated in µg/kg range. Total contents of up to 3.7 mg/kg results in the first line from the occurrence of naphthalene (Table B.8, appendix B). Naphthalene is the most water soluble of the 16 EPA-PAH. Other PAH were found at lower concentrations or were below the detection limit of 0.2 µg/kg. The applied extraction medium, toluene, led to an

intensive extraction and revealed results which were not comparable to release under natural conditions. The comparison of these results with results from Dominok and Kilz (1995) shows significant differences in the PAH-content of the ash. The sum of the EPA-PAH in the ash from the Neurath power plant amounts to 0.036 mg/kg. In the ash from Jänschwalde 0.29 mg/kg were found (Zschiedrich et al., 2000). According to chemical investigations, naphthalene is supposed to be responsible for PAH occurrence. Both results generally differ from each other by factors from 10 to 100. This is assumedly attributed to the differing elution methods: Dominok and Kilz (1995) report a “search test” (Gas chromatography/ mass spectrometry-screening – GC-MS-Screening).

4.1.2 Liming products

4.1.2.1 *Chemical composition*

A total of 23 different neutralization products of different manufacturers (calcite / dolomite / mixed products) had been investigated for their elemental contents.

X-ray fluorescence showed calcium as major element, in addition to minor elements. The calcium contents in the investigated products contained 398.54 g/kg \pm 133.89 g/kg calcium. Magnesium as a minor component in the samples was determined with 4.03 wt.-% (40.29 g/kg). Only one limestone (Dolomifeinkalk DL85) contained 192.9 g/kg magnesium. Silicon and aluminum were on average 14.02 g/kg and 3.26 g/kg. Contained trace metals in the neutralization products are shown in Table B.9 in appendix B. This table gives an overview about all liming chemicals investigated. Results observed by X-ray fluorescence correlate with data obtained by SEM-EDX (see chapter 4.1.2.2).

Main constituents of liming material used in kinetic and/or column experiments are listed in Table 21. In kinetic experiments, mainly marble powder and the limestone KSM Beroun were used. Chemical composition seems quite similar. The synthetic chemical marble powder contained small amounts of impurities (like magnesium, silicon, aluminum, iron, etc.). KSM Beroun is a limestone that was already used in liming of mining lakes (see chapter 4.6). Therefore, the content of minor constituents and trace metals is relevant to estimate a possible release into lake water.

Other limestone products (e.g. Borna KSM 90) had significantly lower calcium concentrations (30.3 wt.-%), but higher concentrations of magnesium (3.52 wt.-%) and silicon (5.65 wt.-%). Contents of trace metals like aluminum, iron, strontium and manganese were observed at higher concentrations than in KSM Beroun. Besides limestone, also dolomite products were used in columns experiments in order to estimate the neutralization efficiency of these products. They seem to be cheaper in production, so they may be an alternative for limestone. 2 dolomites were tested (DSM Ostrau and Borna DSM 90). Main constituents of both products were calcium and magnesium (22.42 / 25.04 wt.-%; 12.46 / 9.98 wt.-%). Additionally, higher concentrations of silicon, aluminum, iron and manganese were observed in these materials. Contents correlate with SEM-EDX results (Figure 45). Another product tested in column experiments was Mischkalk Borna (a mixture of limestone 60 wt.-% and dolomite 40 wt.-%). Chemically it is very similar to the limestone Borna KSM 90, but containing less magnesium than Borna KSM 90. Occurrence of minor constituents was in the same range. High reactivity CaO and Ca(OH)₂ was tested in column experiments, too. Both, rich in calcium (65.72 wt.-% for CaO, 51.1 wt.-% for Ca(OH)₂) contained only small amounts

of minor constituents (magnesium, silicon, strontium, ...). Detailed concentrations are given in Table 21 and in appendix B (Table B.9).

Table 21. Elemental contents of investigated liming agents. Contents are given in wt.-%. For full analysis, see Appendix B.

	Marble powder	KSM Beroun	DSM Ostrau	Borna DSM 90	Borna KSM 90	Mischkalk Borna	CaO_02/11	Ca(OH) ₂ _02/11
Ca	39.1	39.4	22.42	25.04	30.3	31.61	65.72	51.1
Mg	0.2497	0.2747	12.46	9.982	3.518	2.772	0.4563	0.4367
Si	0.08777	0.05579	1.0050	4.842	5.648	3.93	0.2454	0.04235
Al	0.03757	0.01392	0.4061	0.7719	0.9508	1.144	0.081	< 0.0020
Fe	0.02013	0.01979	0.4909	0.5045	0.5293	0.5691	0.07842	0.00545
Sr	0.01545	0.01546	0.0085	0.02077	0.03113	0.04012	0.02515	0.01938
Mn	0.00703	0.00524	0.2083	0.03309	0.1212	0.02627	0.00773	0.005
Ta	0.00611	0.00612	0.0056	0.00613	0.006	0.00583	0.00685	0.00694
Ti	0.0049	< 0.00020	0.0161	0.0452	0.0535	0.065	< 0.00020	< 0.00020
Cl	0.00298	0.00726	0.0155	0.00405	0.00516	0.00302	0.00261	0.0046
Ba	0.00287	< 0.00020	0.0018	0.00576	0.00327	0.00947	0.00413	< 0.00020
I	0.0015	0.00261	0.0004	0.00018	0.00075	< 0.00030	0.00387	0.00377
P	0.00132	0.00321	0.0120	0.01178	0.01191	0.02011	0.00535	0.00258
Sn	0.00116	0.00149	< 0.00030	< 0.00030	0.00053	0.00004	0.00451	0.00284
Sb	0.00102	0.00158	< 0.00030	< 0.00030	0.0003	0.00018	0.00419	0.00315
Mo	0.00096	0.00086	0.0004	0.00062	0.00069	0.00045	0.00217	0.00161
Zn	0.0008	0.00086	0.0334	0.00496	0.04446	0.00346	0.00146	0.00117
Te	0.00059	0.00141	< 0.00030	< 0.00030	0.00025	< 0.00030	0.00443	0.00376
Y	0.00032	0.00018	0.0004	0.00023	0.00029	0.00026	0.00047	0.00023
Th	0.00031	0.0003	0.0005	0.00018	0.00023	0.00028	0.00048	0.00032
Pb	0.00029	0.0004	0.0464	0.00072	0.00068	0.00104	0.00062	0.00032
Ga	0.00028	0.00026	< 0.00005	0.00019	0.00047	0.00048	0.00043	0.00035
Cu	0.00023	0.00022	0.0023	0.00068	0.00067	0.00058	< 0.00005	< 0.00005
Rb	0.0002	0.00013	0.0011	0.00058	0.0009	0.00123	0.00019	0.00013
Br	0.0001	0.00014	0.0006	0.00006	< 0.00005	0.00008	< 0.00005	0.00006
W	0.00009	0.00019	< 0.00010	0.00004	0.00015	0.00012	0.00016	0.00012
Tl	0.00009	0.00006	0.0001	0.00004	< 0.00010	< 0.00010	0.00014	< 0.00010
K	< 0.0010	< 0.0010	0.1217	0.0957	0.2008	0.2349	< 0.0010	< 0.0010
S	< 0.00020	0.00136	0.0419	0.05405	0.04222	0.05308	0.08396	0.01355

Further elements, detection limits and uncertainties are given in Table B.9, appendix B.

4.1.2.2 Mineralogical analysis

Figure 43 and Figure 44 show SEM images of particles of synthetic marble powder and a limestone powder (KSM Beroun) from Rheinkalk GmbH (Germany) with the typical rhombohedral structure of the particles. Moreover, the surface of the synthetic product is smoother than that of the industrial product. Visually, the geometry of industrial product

particles seems to be entirely different from that of the synthetic material. A significantly larger surface of the material can be estimated. Data obtained by SEM-EDX correlate very well with X-ray fluorescence measurements.

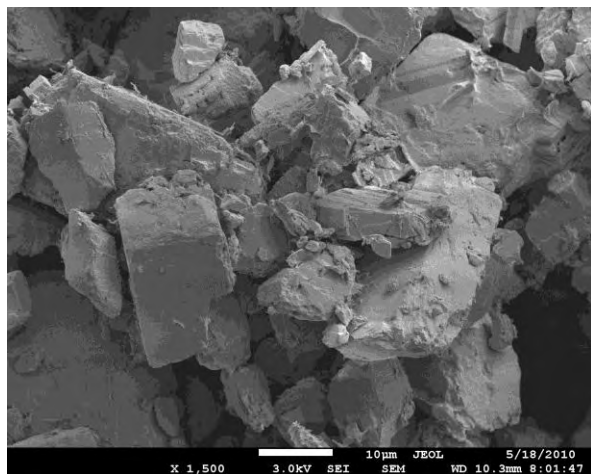


Figure 43. SEM image of marble powder.

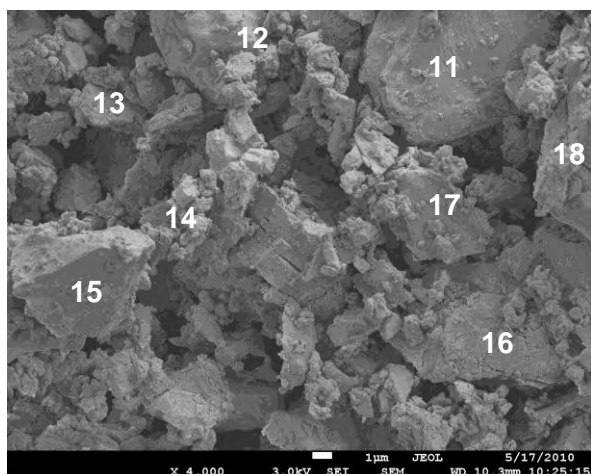


Figure 44. SEM image of KSM Beroun. 11 – 18 indicate mainly Ca-rich phases (CaO_{calc} 97.8 wt.-%). Minor constituents contain Si (SiO_2 , calc 0.85 wt.-%), Mg (MgO_{calc} 0.53 wt.-%), Sr (SrO_{calc} 0.50 wt.-%), Al (Al_2O_3 , calc 0.26 wt.-%) and Fe (Fe_{calc} 0.07 wt.-%).

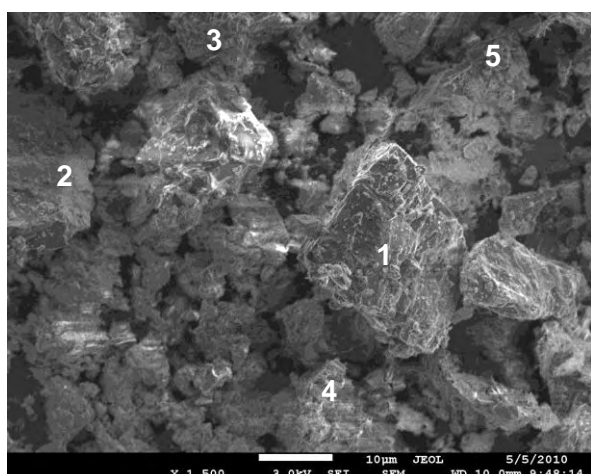


Figure 45. SEM image of DSM Bornia. 1 – 5 indicate mainly Ca- and Mg-rich phases (Ca 23.43 (2) – 55.26 (5) wt.-%, Mg 10.99 (5) – 16.89 wt.-%, average Ca = 37.05 wt.-%, Mg = 14.68 wt.-%. Minor constituents are Si (2.56 wt.-%) and Fe (1.39 wt.-%) and Al (0.11 wt.-%).

Results and discussion

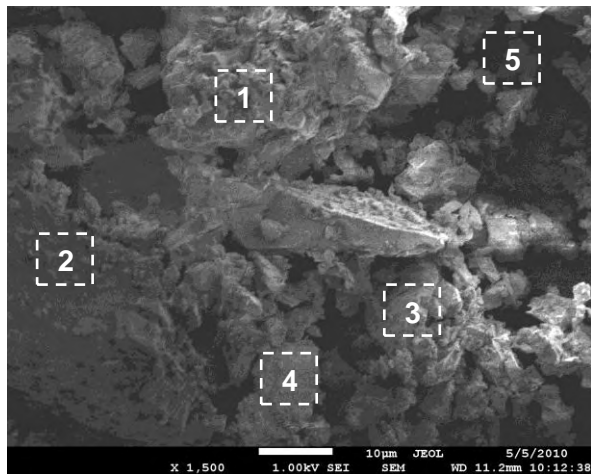


Figure 46. SEM image of KSM Bornia. 1 – 5 indicate areas which are rich in Ca (37.22 wt.-%). Minor constituents are rich in Mg (wide range 0.6 (3) – 7.87 (5) wt.-%, in average 3.49 wt.-%), Si (0.78 (3) – 9.79 wt.-%, in average 2.97), Al (0.25 (3) – 4.72 (5), in average 1.41 wt.-%). Further elements are Fe (in average 1 wt.-%), Mn (in average 0.37 wt.-%), and K (0.54 wt.-%).

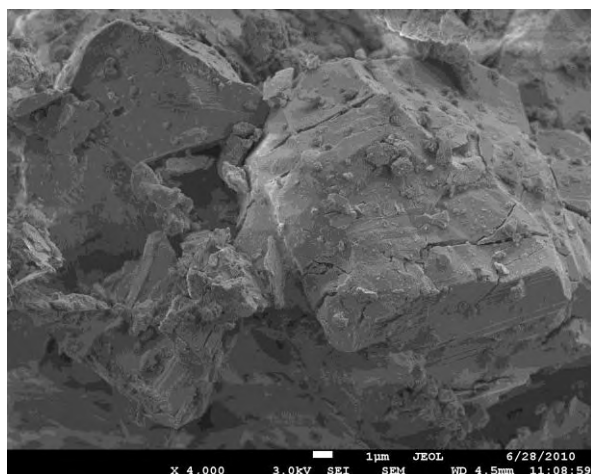


Figure 47. SEM image of Mischkalk Bornia. This sample contains mainly Calcium (in average 38.73 wt.-%). Si (in average 2.80 wt.-%), Mg (in average 1.59 wt.-%), Al (in average 1.03 wt.-%), Fe (in average 0.83 wt.-%) and K (in average 0.83 wt.-%) were found in lower concentrations.

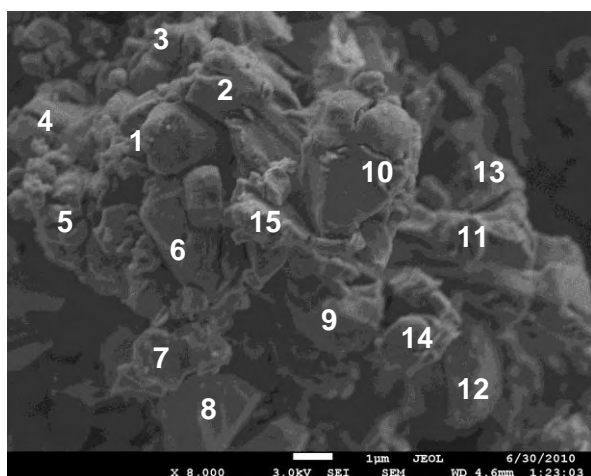


Figure 48. SEM image of WFK (Weissfeinkalk) CaO. WFK CaO mainly consists of Ca (52.67 wt.-%). Further elements were Fe (in average 0.56 wt.-%), Mg (in average 0.43 wt.-%), Si (in average 0.28 wt.-%) and Al (in average 0.24 wt.-%).

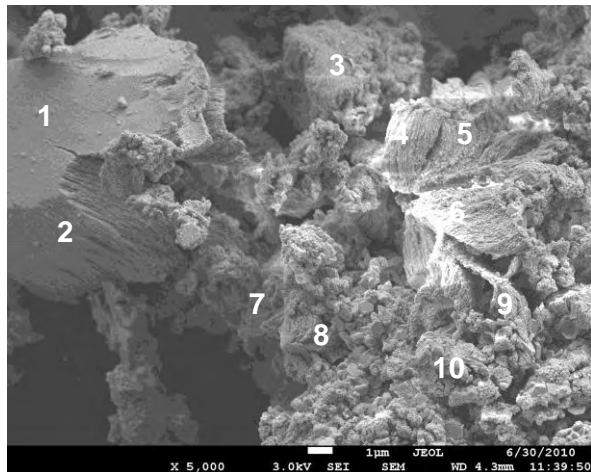


Figure 49. SEM image of Weisskalkhydrat WKH 2-4. Calcium was detected with an average 45.33 wt.-%. Si and Mg were minor constituents with 1.42 and 1.13 wt.-%. Lower concentrations of Fe (in average 0.74 wt.-%), Al (in average 0.57 wt.-%), and Mn (in average 0.43 wt.-%) had been measured.

Industrial products seem to provide larger surfaces of the material. Comparing the scales in Figure 44 and Figure 45 dolomite particles (DSM Ostrau) are significant larger than KSM Beroun. The surface of DSM Ostrau particles appears similar to KSM Beroun (Figure 45). KSM Borna is characterized by sharply formed particles (Figure 46). Figure 47 shows a SEM image of Mischkalk Borna that appears completely different from KSM and DSM Borna. The image shows a relatively large particle with a smooth surface (Figure 47). Only little unevenness can be seen, providing a significant smaller surface than the other products described. Additionally to calcite and dolomite products, Quicklime (CaO) was investigated. Compared to calcite/dolomite products the size of the particles appeared similar whereas the surface of the particles seemed to be smoother. Small unevenness was visible, but in total particles can be described to be well rounded. Figure 49 shows a SEM image of Weisskalkhydrat. Aggregated particles are visible with a highly structured surface, whereas simultaneously larger particles with smooth surface are visible.

Besides Figure 43 to Figure 49 further SEM images of industrial products can be found in appendix A, Figure A.7 – A.25. It can be concluded that there are some differences in size of the particles and especially in the specific surfaces of the industrial products, which might have significant influence on the kinetic in dissolution processes.

4.2 Results using fly ash for combining pit lake treatment and CO_2 storage

As described in chapter 3.2.4 various experiments with different experimental conditions were performed. In the following, only an assortment of experiments subdivided by the use of fresh fly ash (chapter 4.2.1.1) and settled fly ash (chapter 4.2.1.2) is shown.

4.2.1 Contamination risk using fresh and settled fly ash

Overall, a number of experiments were conducted, including different combinations of fresh fly ash, distilled water and AMD. In the first experiments, distilled water was used to study the reaction and formation of precipitates without the influence of the complex matrix of the AMD. Furthermore, varying gas partial pressures were applied.

4.2.1.1 Summary of conducted batch experiments with fresh fly ash

Due to the possible leaching of toxic trace elements (e.g. B, As, Se, Mo, V, and Cr) the general application of industrial by-products like fly ash for AMD treatment is not common (Vadapalli et al., 2008, Gitari et al., 2008b, Gitari et al., 2008a, Gitari et al., 2006). In order to determine the validity of this assumption batch experiments were performed, in order to check the release of toxic metals from fly ash during water treatment in combination with CO₂.

The following summarizes the results of all fresh fly ash batch experiments.

Development of **pH** during batch experiments is presented in Figure 51. The dissolution and hydrolysis of oxides like CaO and MgO from fresh fly ash on contact with DI or AMD is proposed to contribute to an increase in pH. As a consequence, an increase of Ca is observed.

The concentration of **calcium** initially showed an increase within the first 15 minutes. Geochemical modeling of the batch experiments showed, that the solution after the first phase of the experiments (mixing of the water phase with fresh fly ash) was undersaturated in regards to lime (CaO) (SI -16.51), periclase (MgO) (SI -6.73) and Anhydrite (CaSO₄) (SI -0.42).

Figure 51 shows the **sulfate** trends during batch reactions. In phase A, an increasing sulfate concentration to a maximum of 1561 ± 198 ppm was observed for AMD and 848 ± 52 for DI. During phase B1 and B2 (exposure to gas) an increase between 1,154.5 ± 120 ppm (DI) and 1,616 ± 174 ppm was monitored. After phase C the sulfate contents were determined to be 1134 ± 30 ppm (DI) and 1685 ± 207 ppm (AMD). Calculated saturation indices (SI) indicate that gypsum (CaSO₄*2H₂O) and anhydrite were undersaturated or near saturation (SI -0.45 / SI -0.17) anytime during the experiments. Barite (BaSO₄) was oversaturated during the entire experiment (SI 1.14). As the pH of solution increases in an alkaline range the OH⁻ ions compete with SO₄²⁻ for adsorption sites on the amorphous iron phases leading to desorption of SO₄²⁻ (Gitari et al., 2008b).

In all experiments, an increase in **TIC** of the aqueous phase could be reached. Concentrations in phase A were determined to be 1.32 ± 0.41 ppm for distilled water and 1.56 ± 0.56 ppm for AMD. Directly after CO₂ treatment the maximum values of 204 ± 69 ppm (DI) and 23.9 ± 17.44 ppm were determined. During phase C the TIC concentration decreased to 180 ± 47 ppm and 6.26 ± 1.84 ppm, for DI and AMD respectively. TIC contents show large variations due to different experiment conditions (CO₂ partial pressure, exposure to gas). The effect on the buffering capacity is described in chapter 4.2.2.

The content of **chlorine** remained almost constant during all phases of the batch experiments. Phase A was determined with 6.85 ± 0.64 ppm (DI) and 80.63 ± 5.76 ppm (AMD). After exposure to gas, chlorine contents were 6.16 ± 2.89 ppm and 83.17 ± 3.20 ppm.

Strontium concentrations increased from 0 to 6.2 ± 3.4 ppm in distilled water and from 1.6 ppm to 8.3 ± 1.2 ppm in phase A. CO₂ treatment led to a further increase to 8.1 ± 2.9 ppm (DI) and 10.1 ± 1.2 ppm. Celestite (SrSO₄) was calculated to be undersaturated (SI -0.23). Saturation indices for Strontianite (SrCO₃) showed slight undersaturation or near-saturation (SI -0.08), while after CO₂ treatment, it was oversaturated (SI +0.37). Merkel and Sperling (1998) describe a similar behavior in calcium, but report a relatively poor solubility in

comparison to Ca-minerals. During precipitation of carbonates Sr can be co-precipitated (Merkel and Sperling, 1998). Other Sr-containing mineral phases (SrF_2 , SrSeO_3 , SrSeO_4) showed undersaturation (SI -6.93, SI -5.85, SI -8.34) in all phases of the batch experiments. In general, the leaching behavior of strontium is not well investigated. So far, no publications about the release of strontium from fly ash are available.

The removal of **total iron** in AMD was investigated by treatment with fresh fly ash and CO_2 ; 95 % was removed. The initial concentration of total iron at pH 2.89 was 18.2 ppm. After adding fresh fly ash, an increase of pH was observed. Saturation indices indicate the removal of ferrous iron, probably as amorphous Fe(OH)_3 (SI +1.73), Hematite (Fe_2O_3) (SI +14.67), $\text{Fe(OH)}_{2.7}\text{Cl}_3$ (SI +5.88) or Goethite ($\alpha\text{-FeOOH}$) (SI +6.14). Siderite was undersaturated in all batch experiments because iron with the oxidation number 3 was dominant and redox conditions did not change to reducing conditions. Gitari et al. (2008b) report the probable precipitation of iron as Schwermannite due to the existence of high sulfate concentrations.

During some batch experiments, a release of **manganese** was observed. Using distilled water an increase of 280 ± 69 ppb (phase A) and 328.7 ± 268.8 ppb was seen. On contrary, during batch experiments with AMD, a significant decrease of manganese occurred. The initial concentration of 5916 ppb decreased by 99.9 % to 2.8 ± 2.5 ppb Mn (phase A), and 23.86 ± 17.80 ppb (phase C). PhreeqC calculations showed an oversaturation with respect to manganite (MnO(OH)) during phase A (SI +4.03) and a slight undersaturation of manganite during phase B (SI -0.28). Besides metal removal other processes like adsorption and co-precipitation are possible (Gitari et al., 2008b).

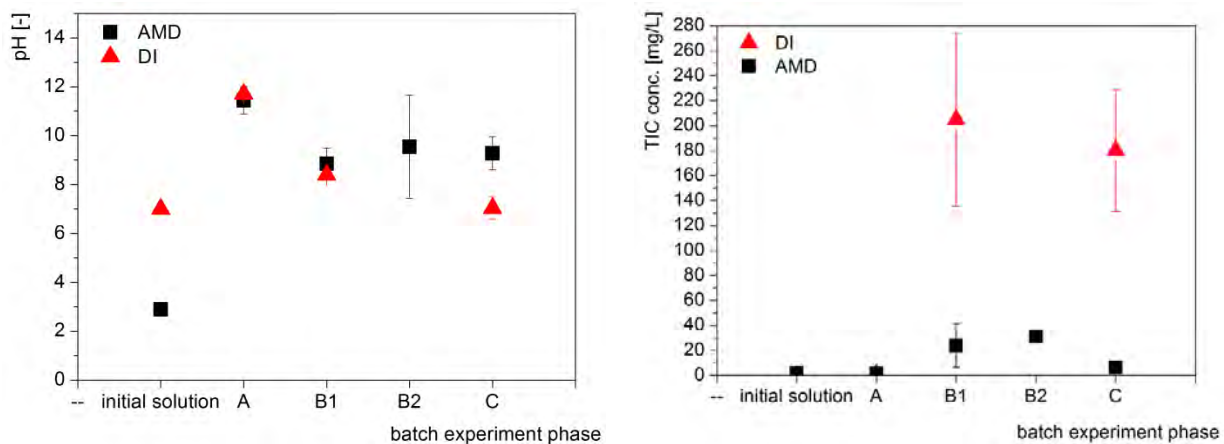


Figure 50. Variation of pH, TIC during batch experiments with fresh fly ash (Boxberg). Error bar presents variation between number of experiments ($n_{\text{DI}} = 2$; $n_{\text{AMD}} = 3$)

Results and discussion

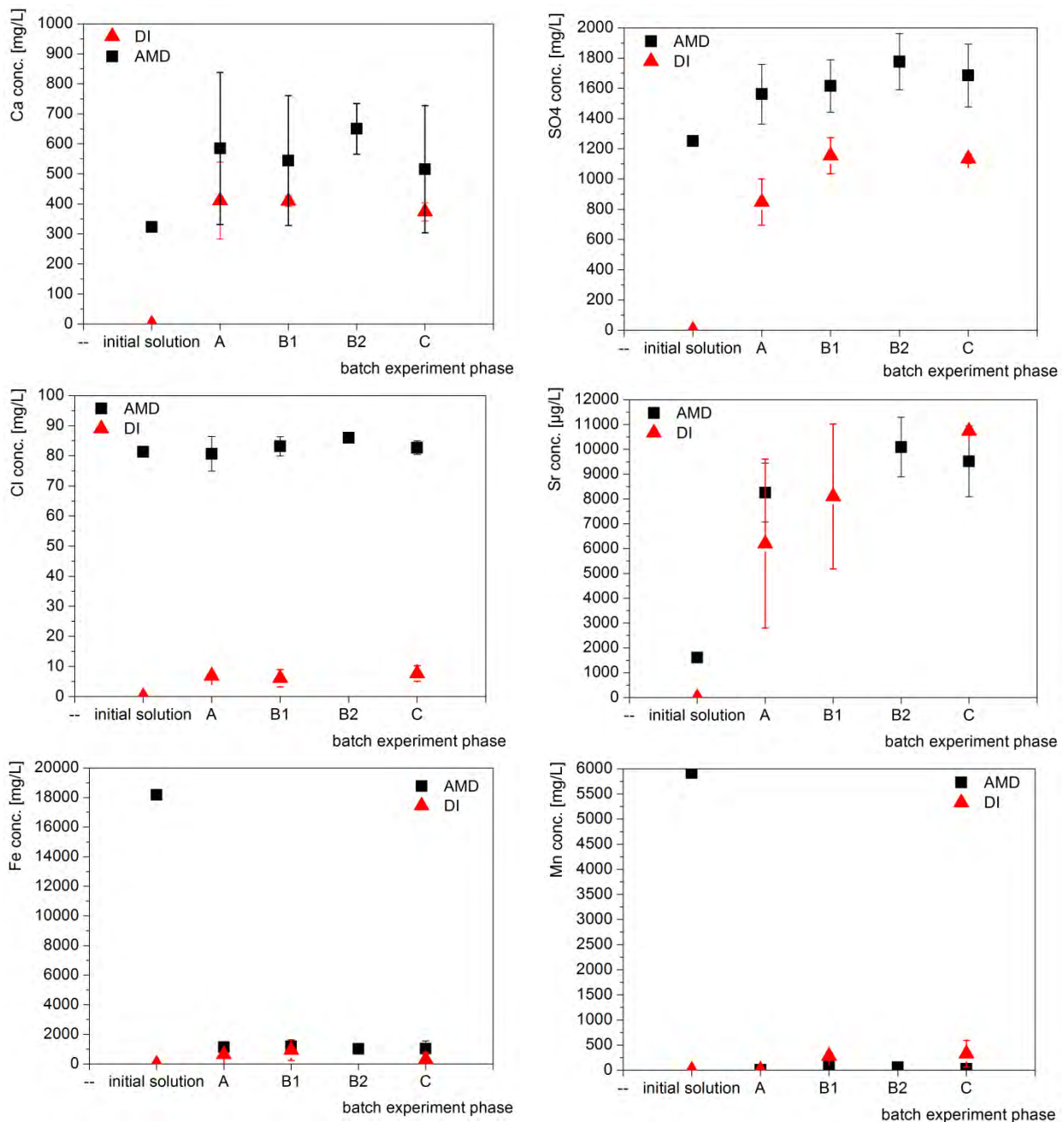


Figure 51. Variation of Ca^{2+} , SO_4^{2-} , Cl^- , Sr^{2+} , Fe_{total} and Mn during batch experiments with fresh fly ash (Boxberg). Error bar presents variation between number of experiments ($n_{\text{DI}} = 2$; $n_{\text{AMD}} = 3$)

As seen from total iron and manganese, the removal of metals is regulated by precipitation, co-precipitation and adsorption processes.

Arsenic was determined to be 2.35 ppb in the lake water. Within the batch experiments an increase to 15.56 ± 0.44 ppb (phase A) for distilled water, and 8.18 ± 3.34 ppb was observed. Treatment of the batch solution led to a further increase: 35.78 ± 13.22 ppb (DI) and 27.64 ± 8.10 ppb (AMD). According to Merkel and Sperling (1998) the equilibrium of arsenic minerals is regulated by sorption processes, and not limited by mineral phases. Due to that fact, solubility products of arsenic minerals do not play a significant role. Oxidizing

redox conditions indicate the occurrence of pentavalent arsenic; arsenate is subject to anion exchange and will be fixed by sorption on hydroxides.

Cobalt concentration decreases from 62 ppb (lake water) to 2.40 ± 0.33 ppb. As mentioned in Merkel and Sperling (1998) cobalt-containing chlorides, nitrates and sulfates are supposed to be very soluble. In the database used, minteq.4f.dat, few thermodynamic data concerning cobalt existed; the calculation of saturation indices for CoCO_3 results in undersaturation of the mineral phase (SI -3.72). Merkel and Sperling (1998) suppose co-precipitation with Fe and Mn-oxides to be the limiting factor of the occurrence of cobalt in aqueous solutions. After the adding of fly ash (phase A), CO_2 treatment (phase B), and the certain lag time (phase C) the concentration of cobalt remained nearly constant 2.80 ± 0.52 ppb (see Figure 53).

The concentration of **chromium** in the lake water was < 0.069 ppb (detection limit). By adding fresh fly ash, the concentration increased to 6.48 ± 3.80 ppb for distilled water and 9.51 ± 4.35 ppb for AMD. During CO_2 treatment, the concentration decreased below detection limit for distilled water; while, in an experiment with lake water concentrations around 9.26 ± 5.97 ppb were observed. After phase C the concentration was 1.95 ± 3.35 ppb. These low concentrations are described in literature to be caused by the sorption on Fe-, Al- or Mn-Oxyhydrates (e.g. (Merkel and Sperling, 1998))

The initial content of **copper** in the lake water was determined to be 17 ppb. In general, a decrease of concentration was observed. Batch experiments using lake water resulted in copper concentrations of maximum 1.24 ± 1.08 ppb (average content after phase C). Within the results of the batch experiments with distilled water, one point seems to be an outlier (see Figure 53). Various copper minerals are calculated to be undersaturated: Nantokite (CuCl) (SI -13.15), Cu_2SO_4 (Si -25.51), CuCO_3 (SI -4.45), Cu(OH)_2 (SI -1.20), and Malachite ($\text{Cu}_2(\text{OH})_2\text{CO}_3$) (SI -3.16). Only Cuprous ferrite (Cu_2O) occurred highly saturated (SI +11.64). Besides precipitation or co-precipitation, the adsorption of copper on Fe- and Al-oxides/hydroxides can be one reason for removal of copper from aqueous solutions (Gitari et al., 2008b, Gitari et al., 2006). As mentioned above, hematite was oversaturated during all phases of the batch experiments. Also, sorption of coal or lignite may be a limiting process (Merkel and Sperling, 1998).

By adding fresh fly ash to lake water, **zinc** concentrations decreased from 232 ppb to 27.70 ± 14.95 ppb. Similar to copper, zinc is supposed to be removed by adsorption onto precipitated iron(oxy)hydroxides and manganese oxides (Gitari et al., 2008b, Gitari et al., 2006, Merkel and Sperling, 1998). Calculated saturation indices indicate an undersaturation of selected zinc minerals: Smithsonite (ZnCO_3) (SI -3.51), Zincosite (Si -15.07), $\text{ZnCO}_3 \cdot 1\text{H}_2\text{O}$ (SI -3.24), and amorphous $\text{Zn}(\text{OH})_2$ (SI -2.64). According to Merkel and Sperling (1998) the precipitation of $\text{Zn}(\text{OH})_2$ depends on hydrogen activity ($> \text{pH } 6$ to 6.3); Zn is also known for co-precipitation with calcite (Merkel and Sperling, 1998). In general, these processes contribute to a decrease in zinc to 28.53 ± 8.27 ppb for both, distilled water and lake water.

Before treatment Burghammer lake water contained 0.16 ppb **molybdenum**. Due to the limiting minerals ferric molybdate ($\text{Fe}_2(\text{MoO}_4)_2$) and wulfenite (PbMoO_4) the occurrence of molybdenum in AMD affected waters is very low (Merkel and Sperling, 1998). At a pH range of 3 to 4 co-precipitation of negative charged molybdenum complexes influence the contents of molybdenum in water (Merkel and Sperling, 1998). During batch experiments, in combination with pH increase, the concentration of molybdenum increased. Maximum concentrations of 56.4 ± 28.87 ppb (DI) and 57.18 ± 35.00 ppb (AMD) after phase A, and 93.09 ± 0.15 ppb (DI) and 72.35 ± 44.66 ppb (AMD) after phase C were measured. Merkel

Results and discussion

and Sperling (1998) reported co-precipitation on calcium and magnesium hydroxides, as well as sorption on Fe and Mn-oxides, at pH > 9.5. After CO₂ treatment pH was lower than 9.5; thus, Mo concentrations increased.

The content of **antimony** in lake water was less than the detection limit (0.0039 ppb). After adding fly ash during the batch experiments with distilled water and AMD, the content of antimony increased slightly to 0.11 ± 0.15 ppb and 0.20 ± 0.18 ppb, respectively. After phase B and C the concentration reached maximum values of 1.86 ± 0.20 ppb (DI) and 1.31 ± 0.52 ppb (AMD).

Selenium in Burghammer Lake was below detection limit of ~1.12 ppb. During batch experiments, an increase of selenium concentration was obtained after phase B (CO₂ exposure), for distilled water (67.43 ± 8.03 ppb). The behavior of batch experiments with lake water differed; a maximum content of 71.28 ± 10.23 ppb (phase A) and 71.15 ± 0.56 ppb (phase B2) was determined. In experiments with only one gas exposure interval selenium concentrations were much lower (47.92 ± 43.11 ppb). After one hour of lag time (phase C), concentration decreased for both, distilled water and AMD. According to Merkel and Sperling (1998) selenium is controlled by sorption on goethite and amorphous Fe(OH)₃.

A number of elements showed very low concentrations that did not change significantly during CO₂ treatment: concentrations of mercury, cerium, lead, tellur, lanthanum, cesium, tin, cadmium and nickel were determined below detection limit. Detection limits are represented in brackets: Hg (0.12 ppb), Ce (0.01 ppb), Pb (0.0011 ppb), Tl (0.011 ppb), La (0.0035 ppb), Cs (1.82 ppb), Sn (0.0097 ppb), Cd (0.0064 ppb), and Ni (0.212 ppb).

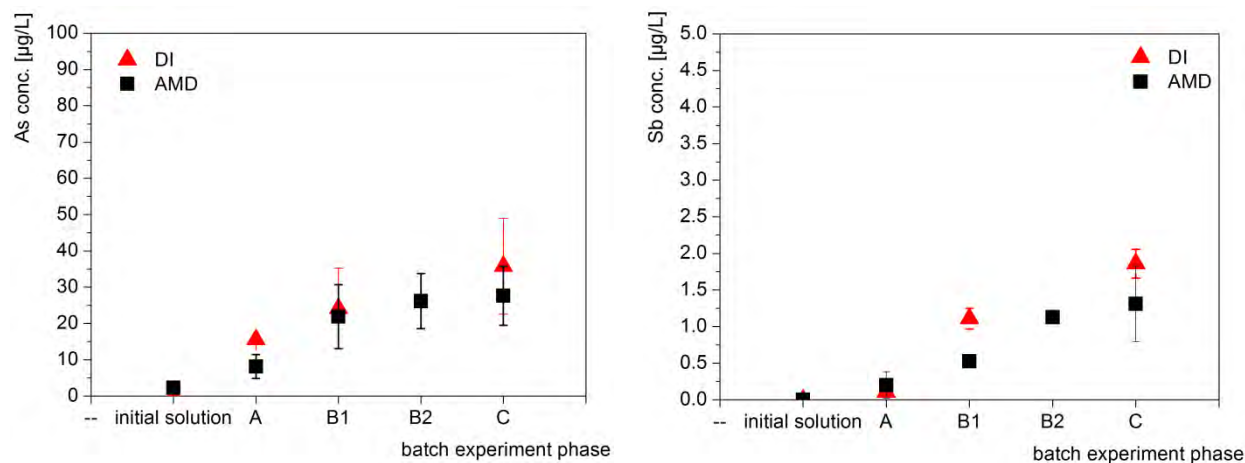


Figure 52. Variation of the trace elements As and Sb during batch experiments with fresh fly ash (Boxberg). Error bar presents variation between number of experiments ($n_{DI} = 2$; $n_{AMD} = 3$)

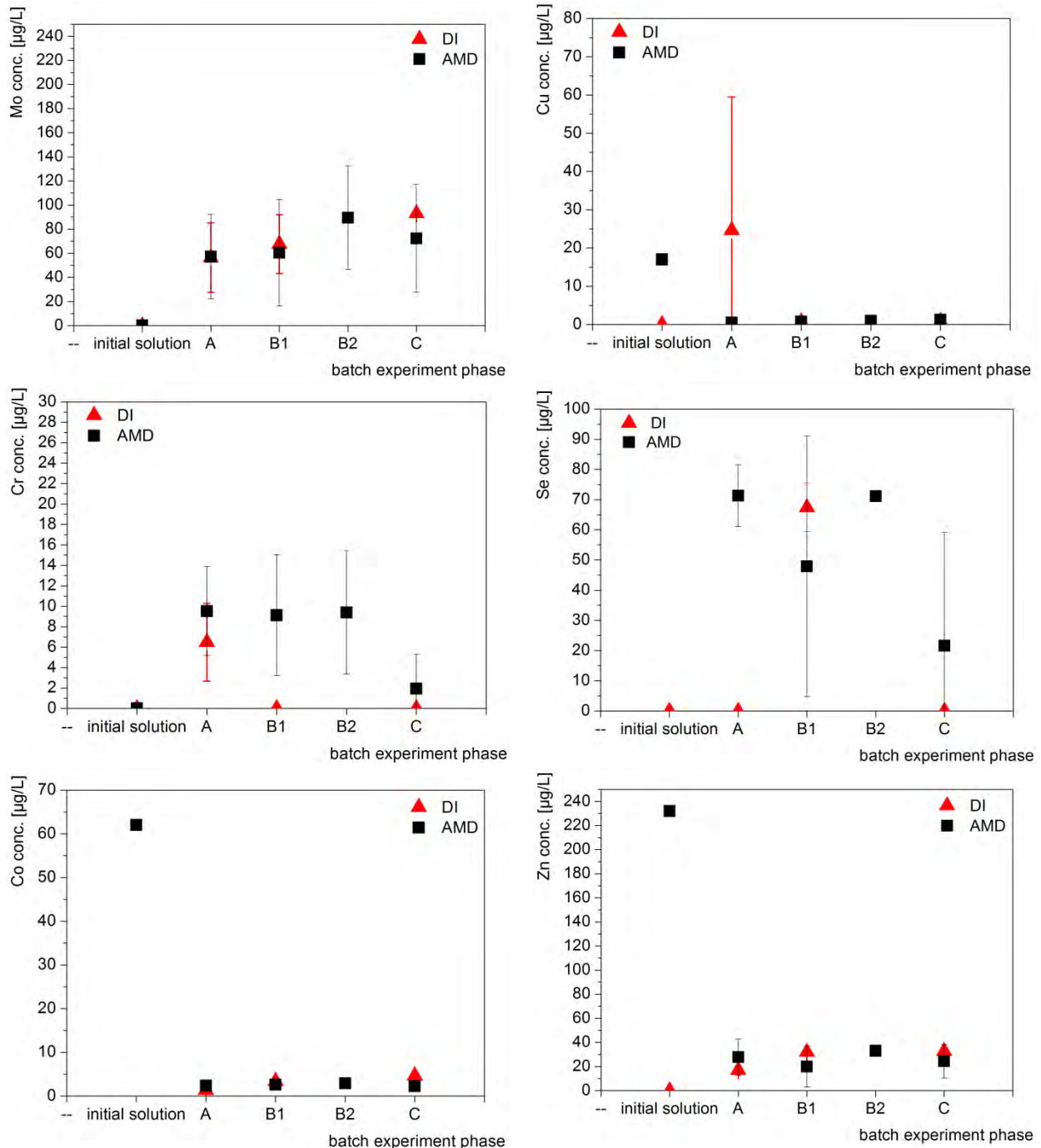


Figure 53. Variation of the trace elements Mo, Cr, Cu, Se, Co and Zn during batch experiments with fresh fly ash (Boxberg). Error bar presents variation between number of experiments ($n_{DI} = 2$; $n_{AMD} = 3$)

4.2.1.2 Summary of conducted batch experiments with settled ash sediment from lake Burghammer

The evolution of pH during batch experiments is presented in Figure 55. The initial pH value of lake water was 2.89. After adding and mixing settled sediment, the pH increases to 8.39 ± 0.55 . CO₂ exposure produces a slight decrease to pH 6.89 ± 0.78 (phase B), or pH 7.29 ± 1.07 (phase C). Conditions for the precipitation of CaCO₃ are given, since calculated

SI indicated oversaturation and the precipitation of calcite in the solid phase was determined. Due to mineralogical investigation, the absence of components like free CaO or MgO was determined. But as cited in literature (Münch, 1996, Zikeli et al., 2004) dissolving calcium from amorphous constituents contributes to increases in pH.

Hence, an increase of calcium is observed, as well. Calcium concentration increased after treatment with fly ash during the first phase of each batch experiment. Geochemical modeling with PhreeqC showed, that the solution after phase A of the batch experiments (mixing of the water phase with settled ash sediment) was undersaturated regarding the following Ca-containing minerals: lime (CaO) (SI -18.37), periclase (MgO) (SI -7.85) and anhydrite (CaSO_4) (SI -0.44). Calcite was calculated to be supersaturated (SI 1.18) and no dissolution of calcite from fly ash sediment was determined. Calculated saturation indices were in the same range like in experiments with fresh fly ash.

Figure 55 represents the **sulfate** concentration during batch reaction with settled ash sediments. In phase A an increase in sulfate concentration to a maximum of $1,349.33 \pm 131.80$ ppm for the reaction with lake water was recorded. During different gas exposure intervals (B1, B2, B3) sulfate concentrations varied between $1,345 \pm 132$ ppm and $1,428 \pm 0$ ppm. After one hour lag time (phase C) sulfate contents were determined to be $1,390 \pm 134$ ppm. In general, sulfate release from settled fly ash sediments is less than release from fresh fly ash. Calculated saturation indices (SI) indicated that gypsum ($\text{CaSO}_4 \cdot 2\text{H}_2\text{O}$) and anhydrite were undersaturated (SI -0.61 / SI -0.87) at all periods during the experiments. Barite (BaSO_4) was saturated during all stages of the experiment (SI +0.85). As mentioned in chapter 1 during an increase of pH in the alkaline range the OH^- ions compete with SO_4^{2-} for adsorption sites on the amorphous iron phases, leading to desorption of sulfate ions (Gitari et al., 2008b).

In general, an increase of **TIC** in the water was determined. Concentrations in phase A were determined to be 31.71 ± 33.77 ppm. In the end of the batch experiments concentrations of 51.79 ± 28.52 ppm were determined. As described in chapter 3.2.4, large variations due to different experiment conditions (e.g. CO_2 partial pressure, gassing time, gassing intervals) occurred.

As seen in experiments with fresh fly ash, the content of **chlorine** remained nearly constant during all phases of batch experiments. On average, a content of 85.55 ± 3.54 ppm was observed.

Strontium concentrations increased from 1.6 ppm to 4.5 ± 0.75 ppm during batch experiments with lake water. CO_2 treatment led to a further increase to 4.49 ± 0.85 ppm. Celestite (SrSO_4) was calculated to be undersaturated (SI -0.92). Saturation indices for Strontianite (SrCO_3) showed undersaturation (SI -1.27), as well as other minerals containing strontium: SrF_2 , SrSeO_3 , SrSeO_4 (SI -7.06, SI -6.15, SI -13.55).

Similar to the batch experiments with fresh fly ash, the removal of **total iron** in AMD was ~94% by treatment with fly ash sediment and CO_2 exposure. The initial concentration of total iron at pH 2.89 was 18.2 ppm. Following the addition of fly ash sediment an increase in pH was observed. At the same time, a decrease of total iron to 807 ± 145 ppb (phase A), or $1,047.47 \pm 278.19$ ppb (phase C, after CO_2 treatment) was observed. Amorphous Fe(OH)_3 (SI +1.76), hematite (Fe_2O_3) (SI +14.72), $\text{Fe(OH)}_{2.7}\text{Cl}_3$ (SI +6.50) and Goethite ($\alpha\text{-FeOOH}$) (SI +6.16) were calculated to be oversaturated. Siderite was undersaturated (SI -2.29) in all batch experiments due to the dominant presence of ferrous iron.

High concentrations of **manganese** in the lake water (5,916 ppb) decreased during ash sediment treatment to concentrations of 882.69 ± 595.85 ppb, and $1,119.19 \pm 1,012.57$ ppb. This equals a reduction of 80 %. In comparison to experiments with fresh fly ash, higher concentrations (factor 50) were determined. PhreeqC calculations showed undersaturation with manganite (MnO(OH)) during all phases of the batch experiments.

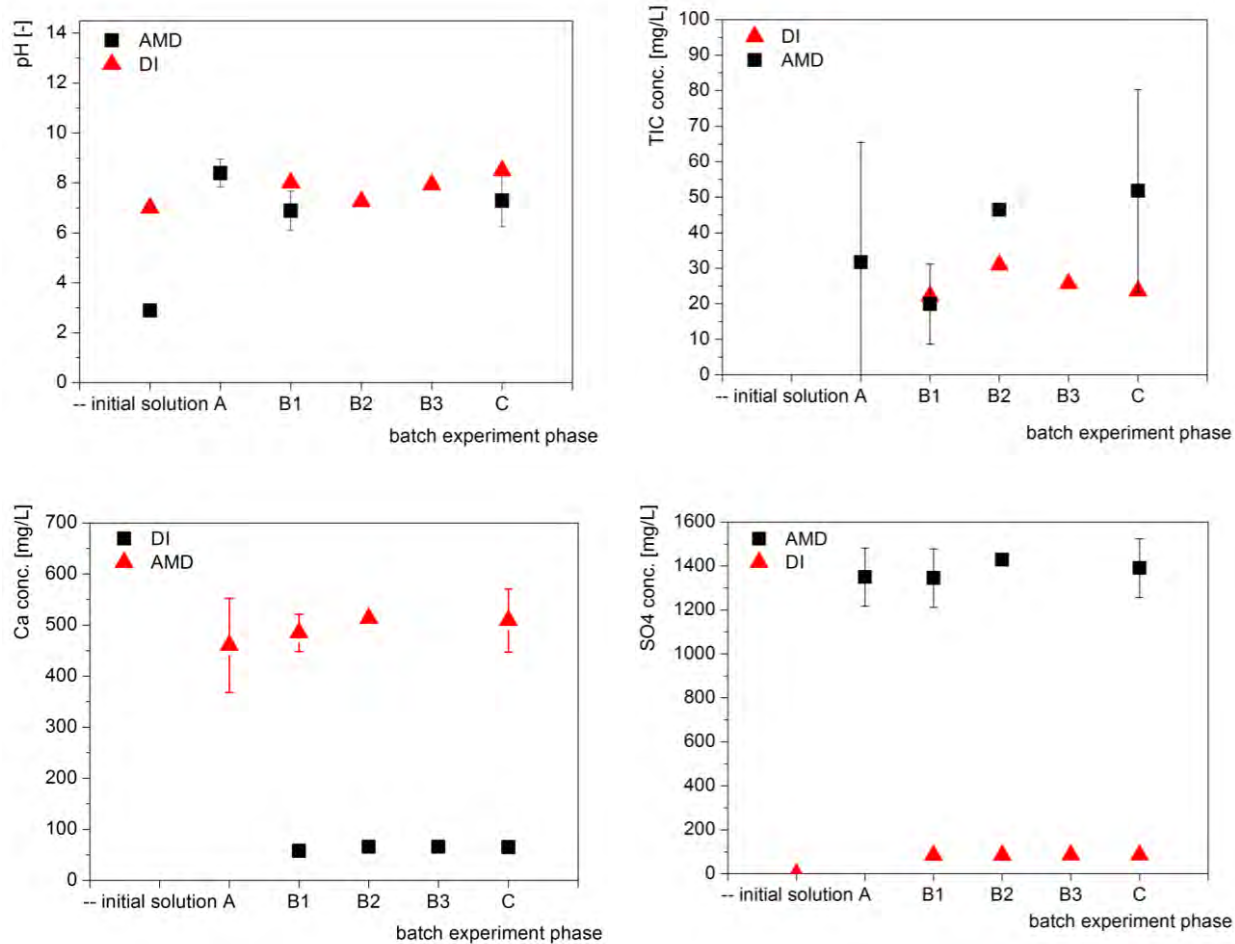


Figure 54. Variation of pH, TIC, Ca^{2+} , SO_4^{2-} during batch experiments with settled fly ash (Lake Burghammer). Error bar presents variation between number of experiments ($n_{\text{DI}} = 1$; $n_{\text{AMD}} = 3$)

Results and discussion

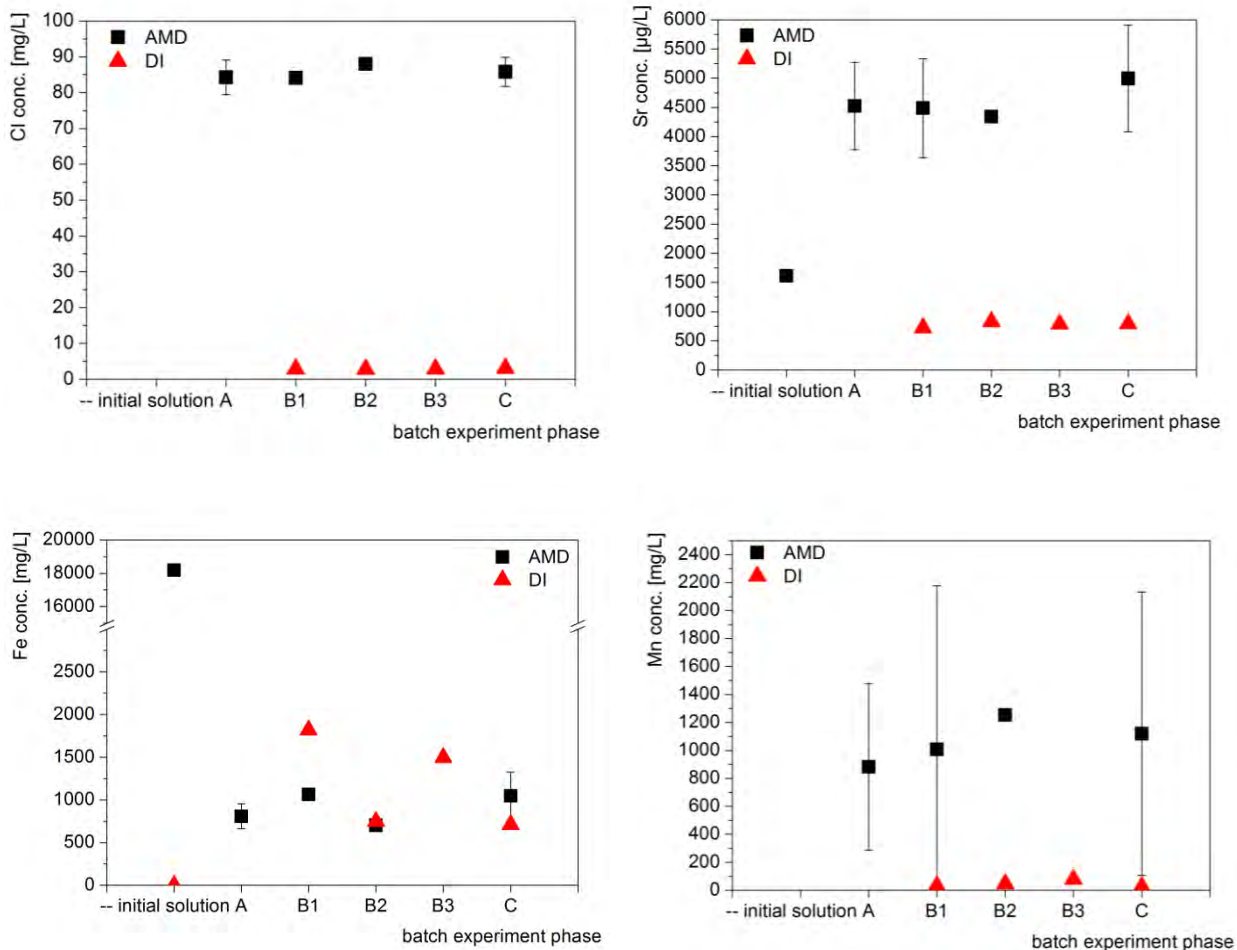


Figure 55. Variation of Cl^- , Sr^{2+} , Fe_{total} and Mn during batch experiments with settled fly ash (Lake Burghammer). Error bar presents variation between number of experiments ($n_{\text{DI}} = 1$; $n_{\text{AMD}} = 3$)

Trace metal release during batch experiments with settled ash sediment and lake water was observed.

Arsenic levels in the lake water were 2.35 ppb. During the batch experiment (phase A, treatment with ash sediment) an increase to 6.69 ± 3.34 ppb occurred. Adding CO_2 led to a further increase (8.13 ± 3.13 ppb). However, the release of arsenic from settled ash sediment was 70 % less than in batch experiments with fresh fly ash.

Antimony in the lake water was below the detection limit (0.0039 ppb). After treatment with ash sediment and CO_2 the content of Sb increased slightly to 0.55 ± 0.46 ppb.

Due to mineral phases like ferric molybdate ($\text{Fe}_2(\text{MoO}_4)_2$) and wulfenite (PbMoO_4) Burghammer lake water is supposed to contain small concentrations of **molybdenum** (0.16 ppb). After batch experiments average Mo concentrations of 1.87 ± 0.90 ppb were determined. The concentrations after phase A and B were much lower than in batch experiments with fresh fly ash. Merkel and Sperling (1998) report co-precipitation on calcium and magnesium hydroxides.

The initial content of **copper** in the lake water was 17 ppb. Like in batch experiments with fresh fly ash, in general, a decrease of copper concentration was observed. After addition of

ash sediment, copper concentrations of 0.68 ± 1.18 ppb were measured and after CO_2 treatment, concentrations increased to 2.90 ± 1.03 ppb. Geochemical calculations resulted in similar saturation indices as reported in chapter 4.2.1.1. Most of the copper minerals available in hydrochemical databases (minteq.4f.dat) were undersaturated: Nantokite (CuCl) ($\text{SI} -6.25$), Cu_2SO_4 ($\text{SI} -20.29$), CuCO_3 ($\text{SI} -2.49$), Cu(OH)_2 ($\text{SI} -1.97$), and Malachite ($\text{Cu}_2(\text{OH})_2\text{CO}_3$) ($\text{SI} -1.98$). Only Cuprous ferrite (Cu_2O) occurred highly saturated ($\text{SI} +13.48$). As mentioned above, the adsorption by Fe-oxides / hydroxides (e.g. hematite) is proposed to be responsible for removal for copper from the lake water.

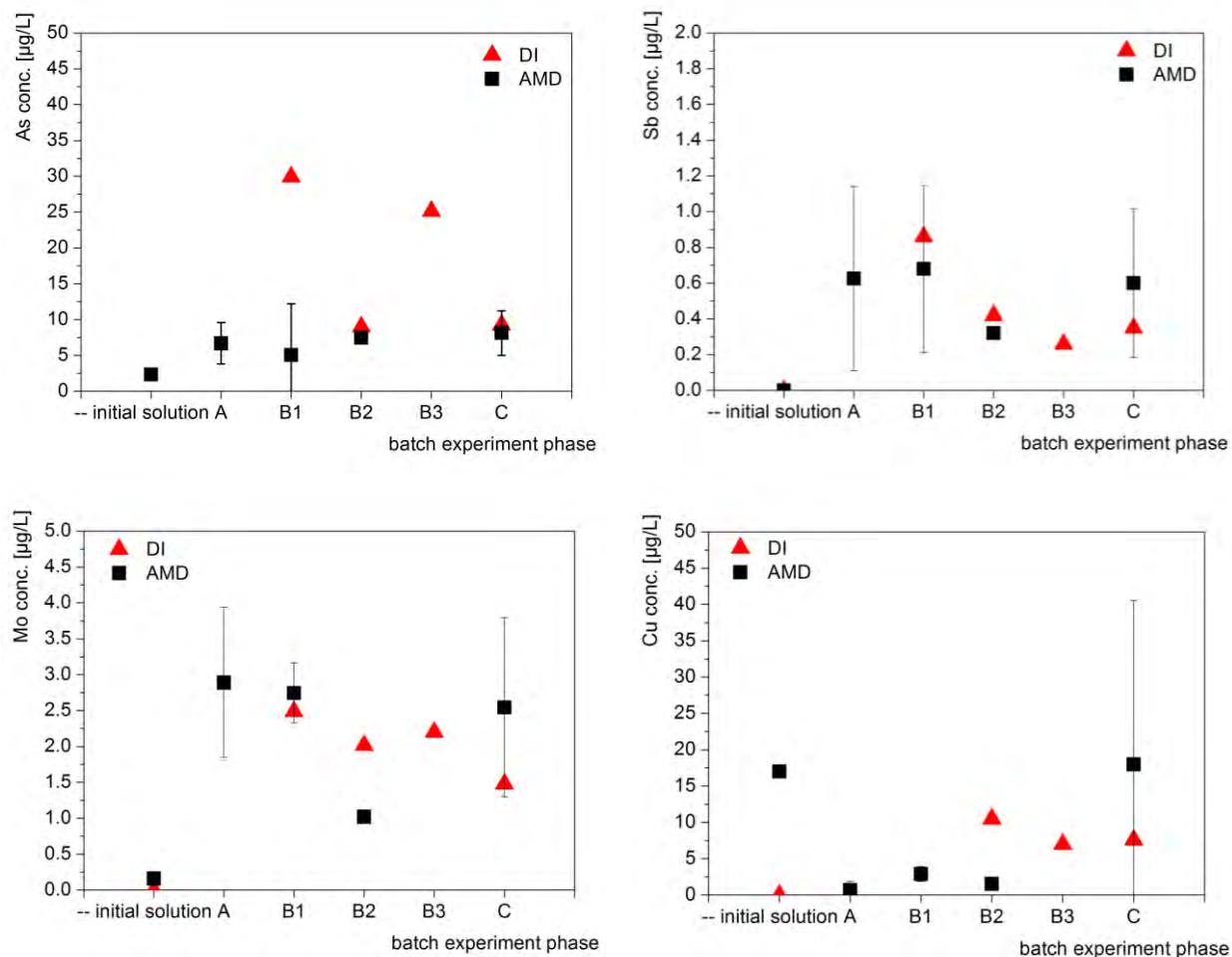


Figure 56. Variation of trace elements As, Sb, Mo, Cu during batch experiments with fly ash sediment (Lake Burghammer). Error bar presents variation between number of experiments ($n_{\text{DI}} = 1$; $n_{\text{AMD}} = 3$)

Results and discussion

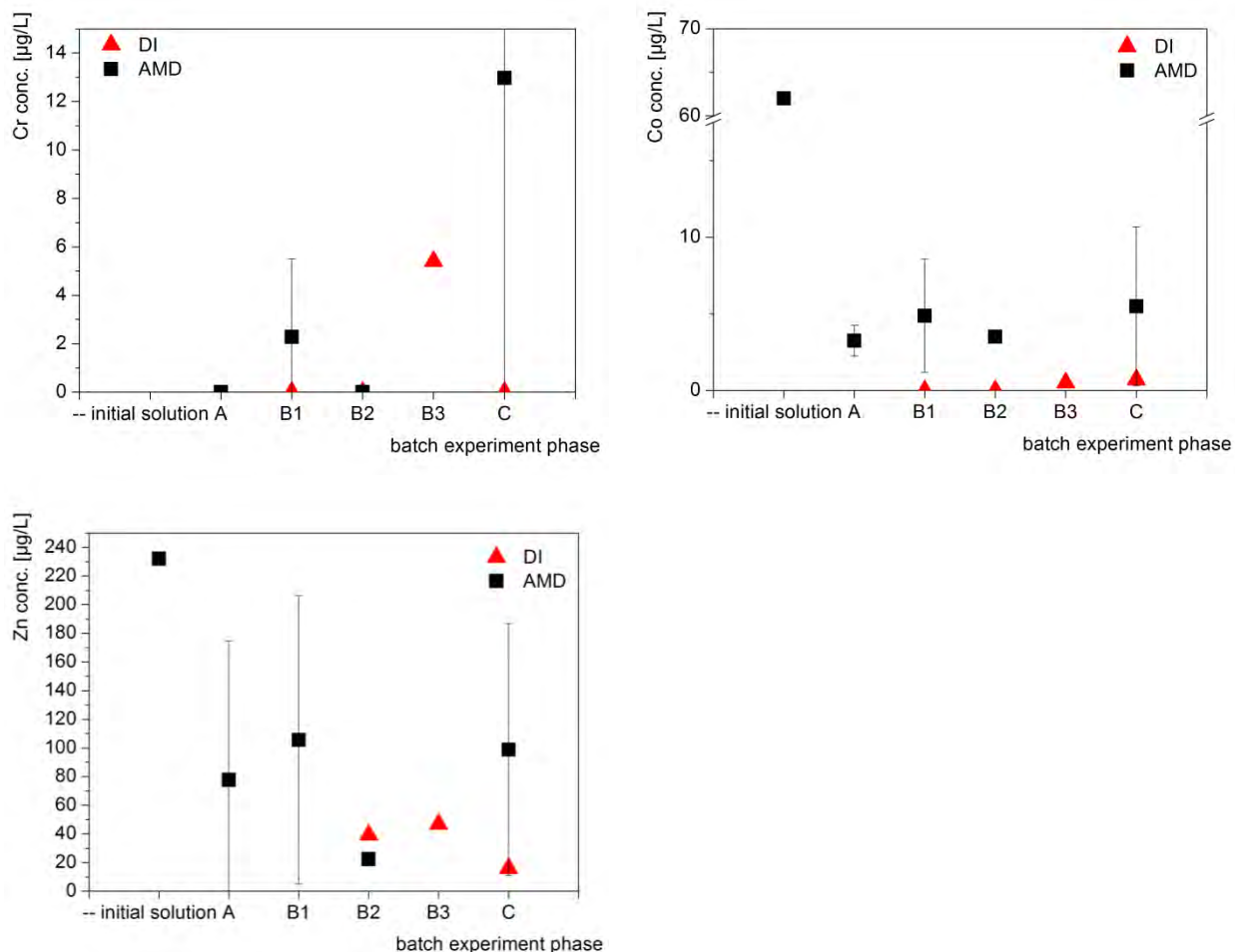


Figure 57. Variation of trace elements Cr, Co, and Zn during batch experiments with fly ash sediment (Lake Burghammer). Error bar presents variation between number of experiments ($n_{DI} = 1$; $n_{AMD} = 3$)

Concentrations of **chromium** in the lake water increased from 0.01 ppb (detection limit) to 2.28 ± 3.22 ppb after treatment with ash sediment and CO_2 (phase B1). Upon finishing the batch experiments, an average content of 12.97 ± 22.47 ppb was measured. Although, chromium was one of the elements with the highest extractability in the range of the S4 elution, the increase of chromium concentration during batch reactions was rather marginal. The sorption on Fe- or Mn-Oxyhydrates (Merkel and Sperling, 1998) limited a further increase.

Cobalt concentration decreased from 62 ppb (lake water) to 5.49 ± 5.18 ppb. The geochemical considerations are discussed in chapter 4.2.1.1.

Treatment of lake water with settled ash sediment and CO_2 led to a decrease from 232 ppb **zinc** to 77.73 ± 87.76 ppb (phase A), and finally to contents in the water phase of 98.79 ± 87.76 ppb Zn. Similar to copper, zinc is supposed to be removed by adsorption on precipitating iron(oxy)hydroxides and mangan oxides which would be in agreement with the results of others (Gitari et al., 2008b, Gitari et al., 2006, Merkel and Sperling, 1998). It is likely that a co-precipitation with calcite ($\text{SI} +0.50$) occurred, as well.

Selenium in Burghammer lake water was as well below detection limit of ~1.12 ppb. During batch experiments with settled ash sediment, no increase was determined. All investigated samples were less than detection limit.

In addition to selenium, a number of trace elements showed low concentrations and no effect to treatment with settled ash sediment in combination with CO₂. The following elements were determined below detection limits (in brackets) Hg (0.12 ppb), Ce (0.01 ppb), Pb (0.0011 ppb), Ti (0.011 ppb), La (0.0035 ppb), Cs (1.82 ppb), Sn (0.0097 ppb), Cd (0.0064 ppb), and Ni (0.212 ppb).

Results from batch experiments showed a general decrease of trace metal concentrations with CO₂ treatment. The elements iron, manganese, cobalt, chromium, copper and zinc decreased significantly, as described above. The proposed treatment technology has no influence on the concentrations of mercury, wolfram, cerium, lead, lanthanum, cesium, tin, cadmium, nickel and selenium. Arsenic, chromium, molybdenum and antimony increased slightly during treatment of the ash-water-suspensions with CO₂.

Sulfate is – besides pH and buffering capacity - one of the most important problems concerning acid mine drainage. During treatment of the ash-water-suspensions with CO₂, an increase of sulfate in the water phase was observed. Removal of sulfate is the objective of a number of R&D projects, however, not an issue in this thesis.

4.2.2 Increase of buffering capacity

The improvement of water-composition in an acidic mining lake can be described by selected results of the conducted batch experiments:

Table 22. Comparison of the buffering capacity of initial lake water and after batch reactions

	lakewater initial	Experiment						
		I231106	D151106	D141106	F161106	G201106	T191206	U191206
Liquid Phase	-	Lake water						
Amount [L]	-	1.1 L						
Solid phase	-	pure CaO	ash	sediment	ash	sediment	ash	sediment
Sample quantity [g]	-	1	20	20	50	50	20	20
Percentage CO ₂ [%]	-	30	30	30	30	30	30	30
Type of test arrangement*	-	A	A	A	A	A	B	B
K _{s4.3} [mmol/L]	-	10.616	0.938	2.288	2.00	6.518	4.840	5.578
K _{s8.2} [mmol/L]	-	-	0.276	-	-	-	-	-
K _{b8.2} [mmol/L]	2.798	0.75	-	0.096	1.584	0.682	0.136	0.3
K _{b4.3} [mmol/L]	2.094	-	-	-	-	-	-	-

* Type of test arrangement, see chapter 3.2.4.2.

Results and discussion

During the sampling campaigns in April and July 2006, the natural buffering capacity of the lake water was determined as shown in (Table 23).

Table 23. Description of the buffering capacity of the original acid mine lake water

	BGH-040406-S1	BGH-040406-S2	BGH-200706-S1
	5701616	5702873	5705164
	33U 0455203	33U 0455976	33U 0454387
pH _{field}	2.89	2.82	2.94
pH _{start titration}	3.24	3.37	2.92
K _{s4.3} [mmol/L]	-	-	-
K _{s8.2} [mmol/L]	-	-	-
K _{b8.2} [mmol/L]	7.926	6.878	3.432
K _{b4.3} [mmol/L]	2.074	1.248	2.522

As shown in Table 23 the lake water is characterized by low pH values and an extremely poor buffering capacity. One aim of the investigations was to produce an increase in the buffering capacity in order to prevent recurrent lake acidification.

Batch experiments have been made analogous to the description in chapter 3.2.4.2. Batch experiment U191206 was performed by test arrangement type B (description see 3.2.4.2).

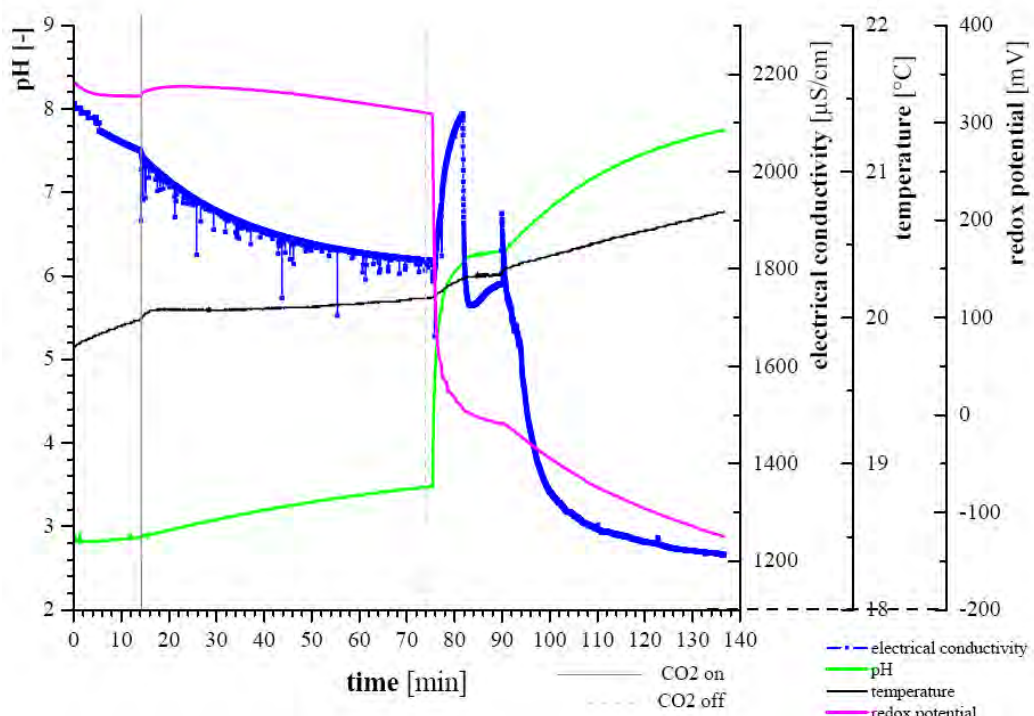


Figure 58. Batch experiment with sediment from Lake Burghammer (experiment U191206, 30 % CO₂, lake water, mixed sediment sample: BGH-1312-P2-6.50 (6.95-7.10), BGH-1312-P2-3.5 (4.25-4.50), BGH-1312-P2-6.5 (6.65-6.80))

During the first experimental step, original lake water was exposed to $p_{CO_2} = 0.3$ for 60 minutes. Following the gas exposure, 20 g of Burghammer sediment were added. Then for a period of 60 minutes, turbulence was generated by stirring. In the end of the experiment, samples were taken.

Figure 59 shows the different buffering capacities / acid neutralization capacity of treated lake water and distilled water. Distilled water shows only a low buffering capacity; the curve decreases very fast in response to the addition of a few mL of hydrochloric acid. The treated water sample of lake Burghammer shows a higher buffering capacity and 5.578 mL of hydrochloric acid was necessary to decrease the initial titration pH of 7.78 (pH after batch experiment). From the sample volume and the concentration of the acid added, the alkalinity or acid neutralization capacity was calculated to be 5.578 mmol/L.

As can be seen in Table 23 in comparison with Table 22, in all batch experiments an increase of the $K_{S4.3}$ could be affected. In general, for fly ash sediment, an increase of the buffering capacity to 4.18 ± 2.51 mmol/L was observed.

Under real conditions, this means that Lake Burghammer will need buffering capacity in order to neutralize incoming potentially acid groundwater inflow, as described in chapter 2.3.

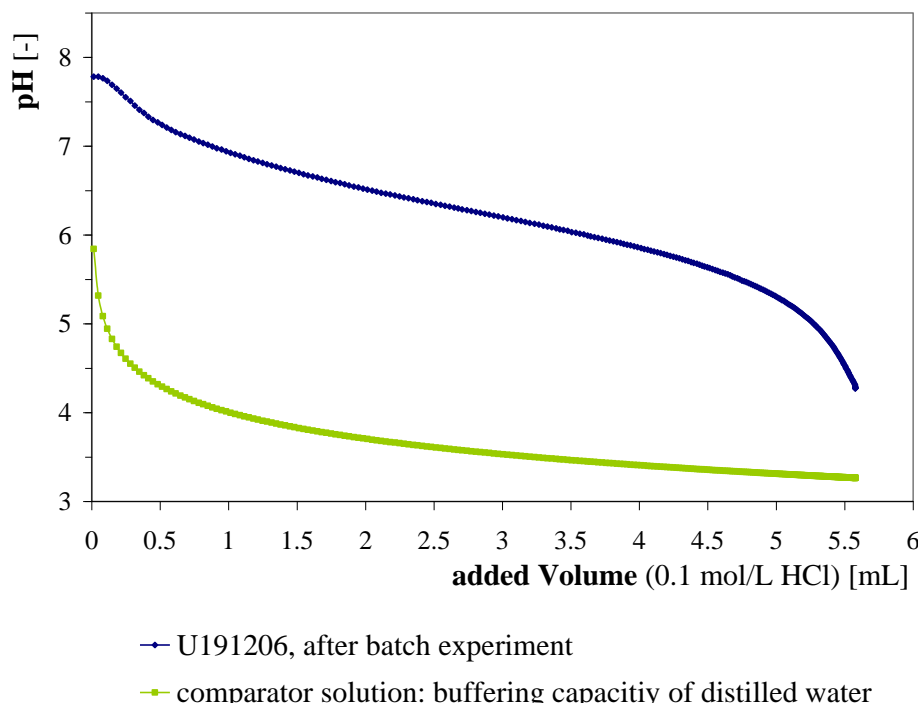


Figure 59. Typical development of the pH during a titration with a strong acid. The green line represents the curve of the titration from distilled water – water with little buffering capacity (modeled by the use of PhreeqC, Version 2.0); the blue line was modeled for the buffering capacity of the treated lake water.

4.2.3 Carbonate Precipitation

The mineralized CO_2 during batch experiments can be calculated from the difference in TIC-content of the solids before and after the experiment. The results are summarized in Table 24.

Table 24. Carbonate precipitation in batch experiments with fly ash (n = 10) and lake sediment (n = 16).

	Fly ash (Boxberg)	Sediment (Burghammer)
TIC [g/kg] before CO ₂	0.01	0.4
Delta TIC [g/kg]	8.9 ± 6.22	4.62 ± 3.94
delta Calcite [g/kg]	74.17 ± 51.85	38.49 ± 32.85
delta Calcite [wt.-%]	7.42 ± 5.19	3.84 ± 3.29
<i>Sequestered CO₂ [wt.-%]</i>		
CO ₂ [mol C/kg]	0.74 ± 0.52	0.38 ± 0.32
CO ₂ [g CO ₂ /kg]	32.63 ± 22.81	16.93 ± 14.46
Min CO ₂ [g CO ₂ /kg]	5.023	0.373
Max CO ₂ [g CO ₂ /kg]	77.697	38.13
Median CO ₂ [g CO ₂ /kg]	31.075	14.043

Approximately 33 g CO₂ per kilogram fresh fly ash (Boxberg) were mineralized within the experiments. In comparison, settled fly ash sediments are less reactive, providing a sequestration rate of 17 g CO₂/kg.

A dependence of the amount of precipitated carbonate on the amount of time after gassing (during Phase C) could not be proven. The carbonate precipitation concluded within minutes and was hardly limited by the technological implementation of the treatment.

4.3 Results of kinetic experiments using liming agents

4.3.1 General results

Kinetic experiments were carried out with synthetic marble powder (Merck, Germany) and an industrial limestone (KSM Beroun) from Rheinkalk GmbH. Figure 60 shows the development of pH over the duration of the experiment. Figure 61 and Figure 62 show the corresponding electrical conductivities, respectively the calcium concentrations.

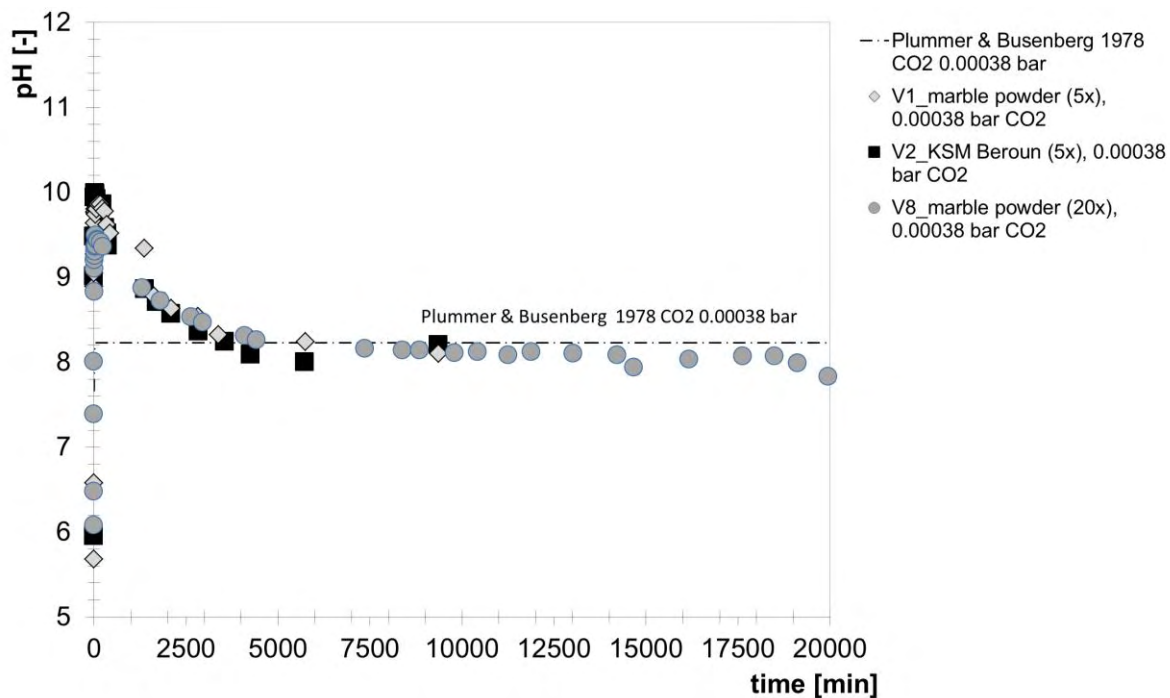


Figure 60. Development of pH over time. Boundary conditions: pure water, $p_{CO_2} 3.8 \times 10^{-4}$ bar.

Noticeable is the significant deviation from the theoretical model after Plummer et al. (1978) (dashed line in Figure 60 and Figure 62). Kinetic modeling according to chapter 3.4.1.2 showed equilibrium conditions after approximately 90 minutes (modeling was performed for 20,000 minutes in 5,000 time steps). Real conditions showed during the initial phase of the experiments a rapid increase of pH from circa 6 to above 10 (Figure 60). Within 4000 minutes, the pH value decreases and reached equilibrium values (pH = 8.2).

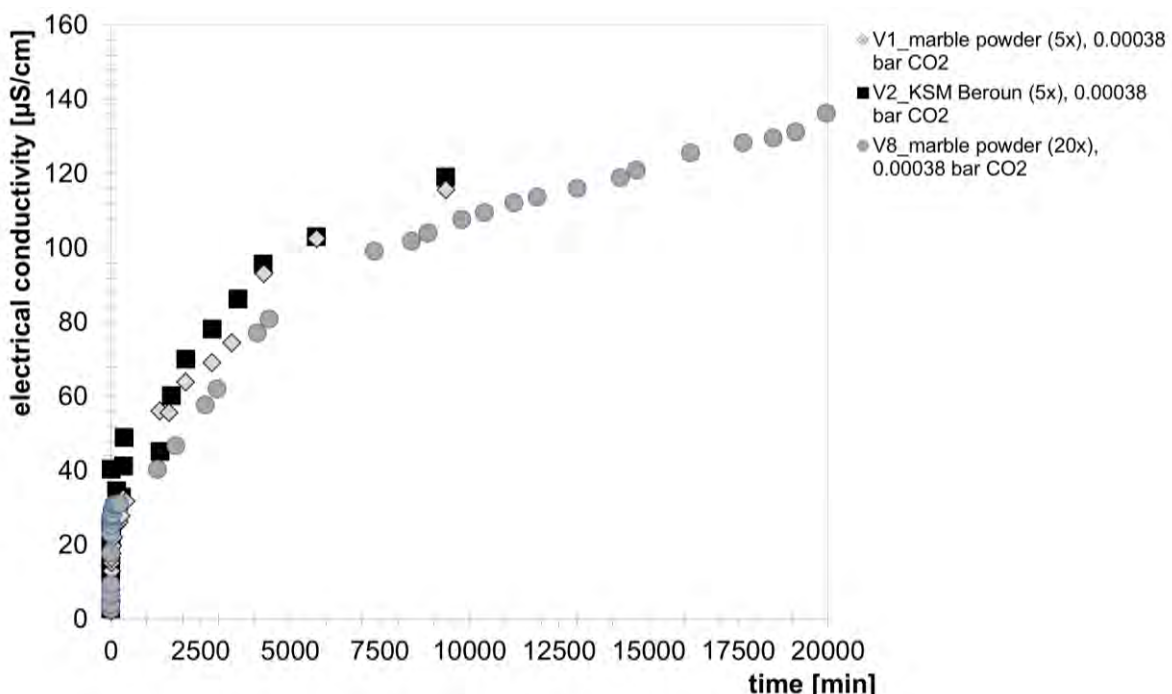


Figure 61. Development of electrical conductivity over time. Boundary conditions: pure water, $p_{CO_2} 3.8 \times 10^{-4}$ bar.

Measurements of the electrical conductivity in experiment V1 and V2 did not result in reaching equilibrium state. Experiment V8 was performed for more than 20,000 minutes, even after this time a further slightly increase of the electrical conductivity cannot be excluded. As described in chapter 1.4.2, most authors dealing with carbonate dissolution kinetics used pH and electrical conductivity as parameter for estimating the equilibrium state of the kinetic reaction. Additionally, in this thesis, the calcium concentration during the course of an experiment was investigated by means of ICP-MS.

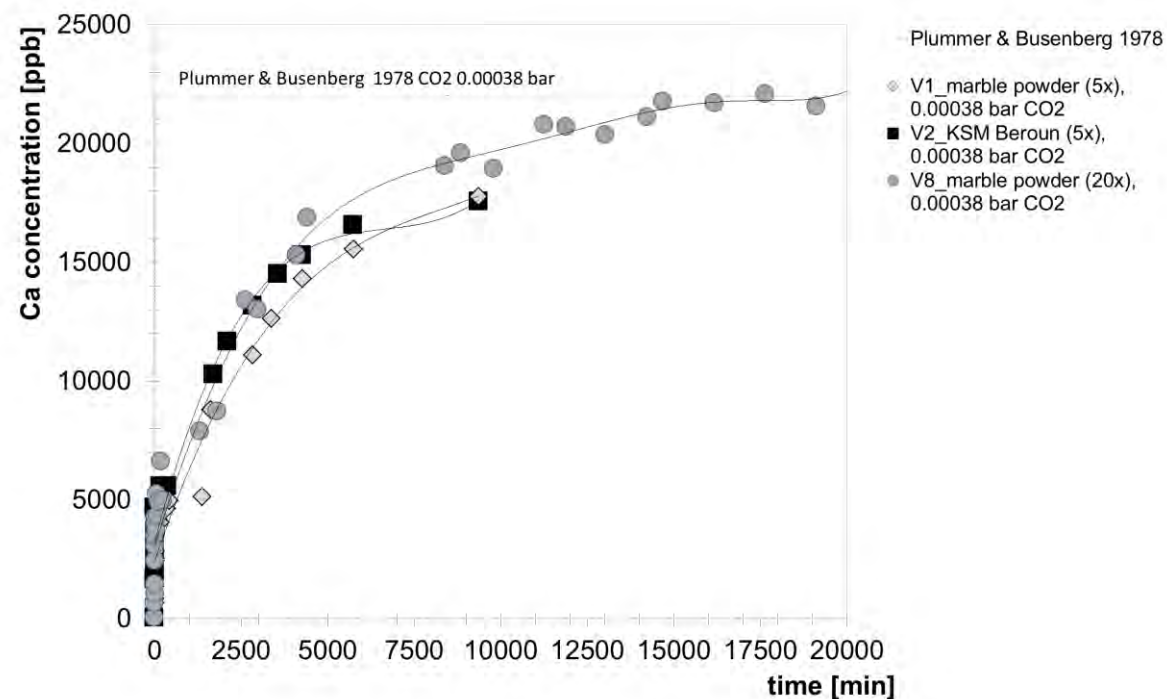


Figure 62. Development of the calcium concentration over time. Boundary conditions: pure water, $p_{CO_2} 3.8 \times 10^{-4}$ bar.

The measured calcium concentration in equilibrium is reached after about 15,000 minutes (Figure 62), significantly later than modeled after Plummer et al. (1978). Differences between the different amounts of liming agents (5 vs. 20 times saturation) and the resulting increased calcium concentrations can be explained by a relatively larger particle surface that is not inhibited by minor constituents of the liming agents. Furthermore, a significant difference between the EC and the calcium concentration compared to the modeled data can be seen. This might be due to the performance of batch experiments in free-drift mode by using calcite powder. Electrical conductivity was measured in the solution with undissolved calcite particles. According to Sjöberg and Rickard (1983) and proofed by own investigation by SEM-EDX, calcite particles represent no ideal spheres and the contribution of convection to the mass transfer is significant. This fact is also shown by the stirring dependence of the dissolution rate of fine powders (Sjöberg, 1976). Thus, hydrodynamics during powder runs might be convection-dominated and difficult to evaluate (Sjöberg and Rickard, 1983), whereas rotating-disc techniques seems to be more well-defined (Levich, 1962, Bircumshaw and Riddiford, 1952).

Based on the elemental contents of the two liming agents (see Table 21), no significant difference between the synthetic marble powder and the industrial product appears.

Considering the course of the kinetic reaction (Figure 61) supports this statement. The final concentrations in equilibrium state for marble powder was measured with 19.44 ppm and 22.06 ppm, the final concentration of KSM Beroun was 17.57 ppm (- 11.72 % / + 0.15 % / - 20.21 % compared to the modeled results (Plummer et al., 1978)). Thermodynamical modeling using equilibrium_phases (see chapter 3.4.1.1) showed consistence (wateq4f.dat: 22.02 ppm, llnl.dat 21.544 ppm). Figure 61 to Figure 63 show that experiment V1 and V2 did not reach the final equilibrium state. Thus, the following experiments considering the influence of CO₂ partial pressure (chapter 4.3.2) and the influence of possible inhibiting ions (chapter 4.3.3) were performed for a significant longer period.

4.3.2 Influence of CO₂ partial pressure

Increased CO₂ partial pressures might be used to suppress the effect of inhibition by material impurities and / or dissolved water constituents. Additionally, a possible increased efficiency ratio by using limestone powder during liming campaigns in the pH range > 6 can be achieved.

Figure 65 and Figure 66 show the calcium concentrations (representative for the dissolution rate) for marble powder and KSM Beroun at different CO₂ partial pressures. Experiment V1 and V2 had been described in chapter 4.3.1.

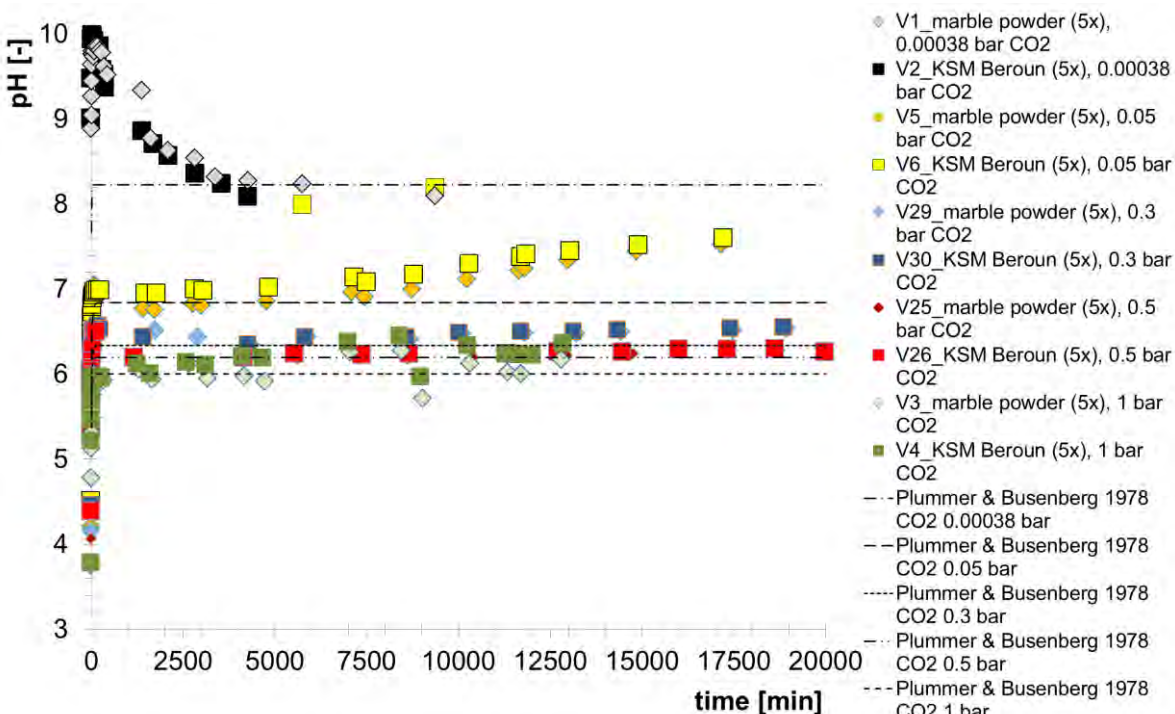


Figure 63. Development of pH in kinetic experiment influenced by different p_{CO₂}. Boundary conditions: pure water, 5-times saturated.

Results and discussion

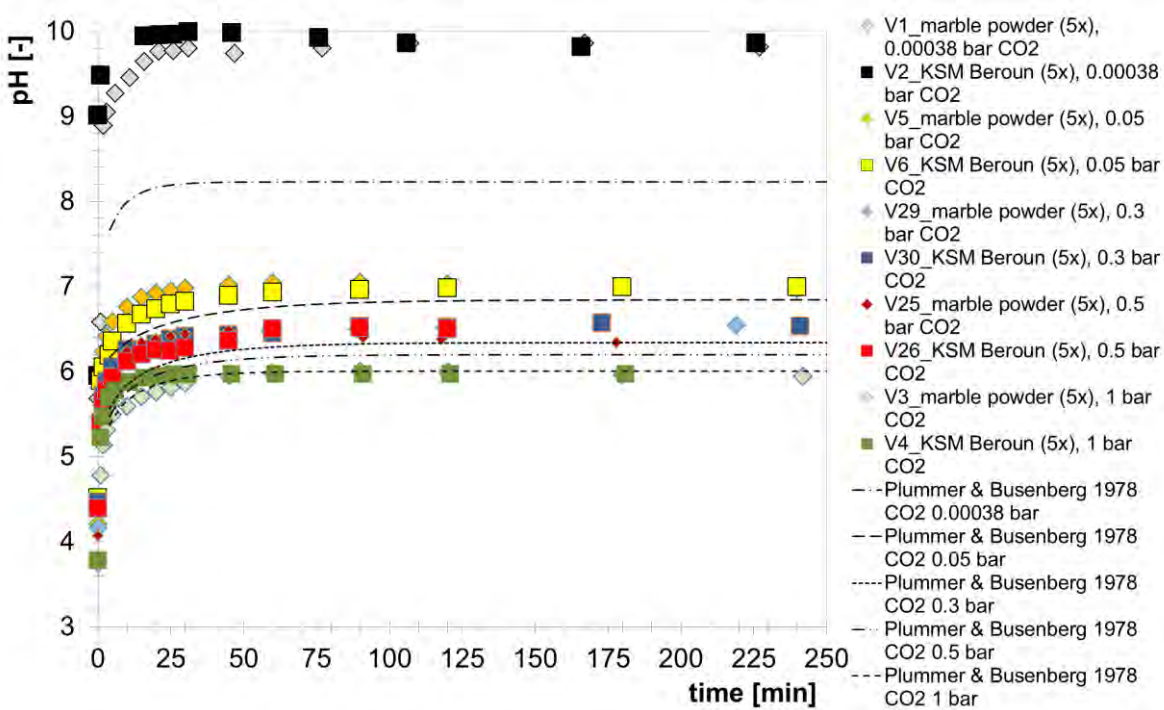


Figure 64. Development of pH in kinetic experiment influenced by different p_{CO_2} . Boundary conditions: pure water, 5-times saturated.

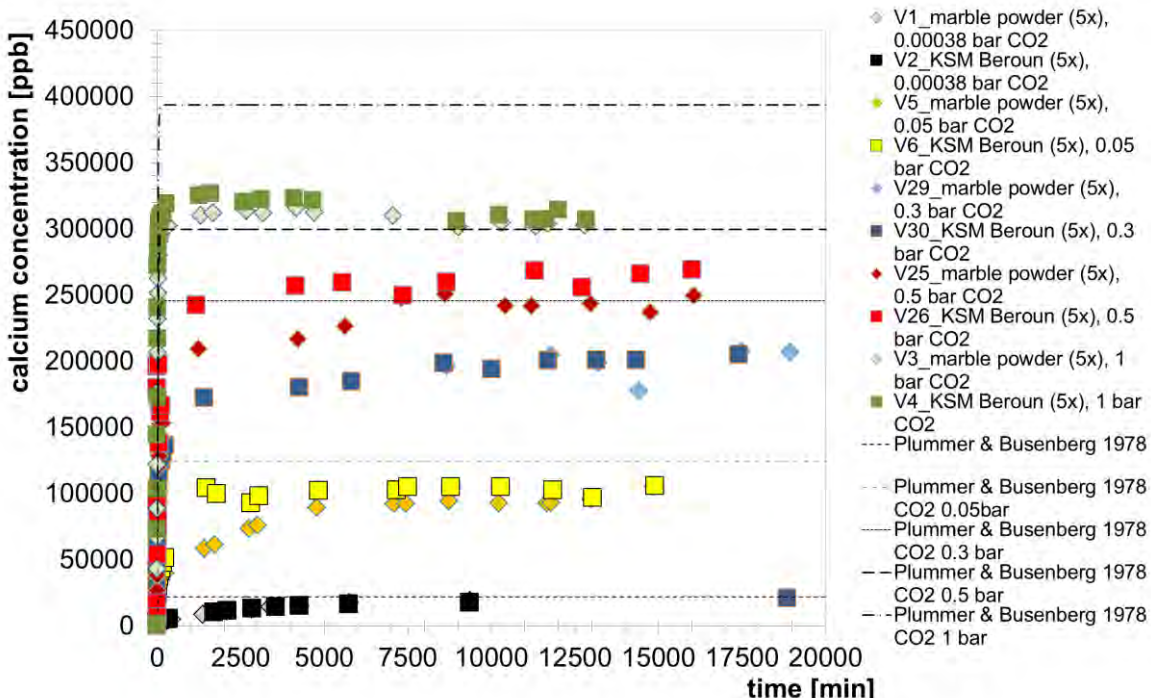


Figure 65. Development of calcium concentration in kinetic experiment influenced by different p_{CO_2} . Boundary conditions: pure water, 5-times saturated.

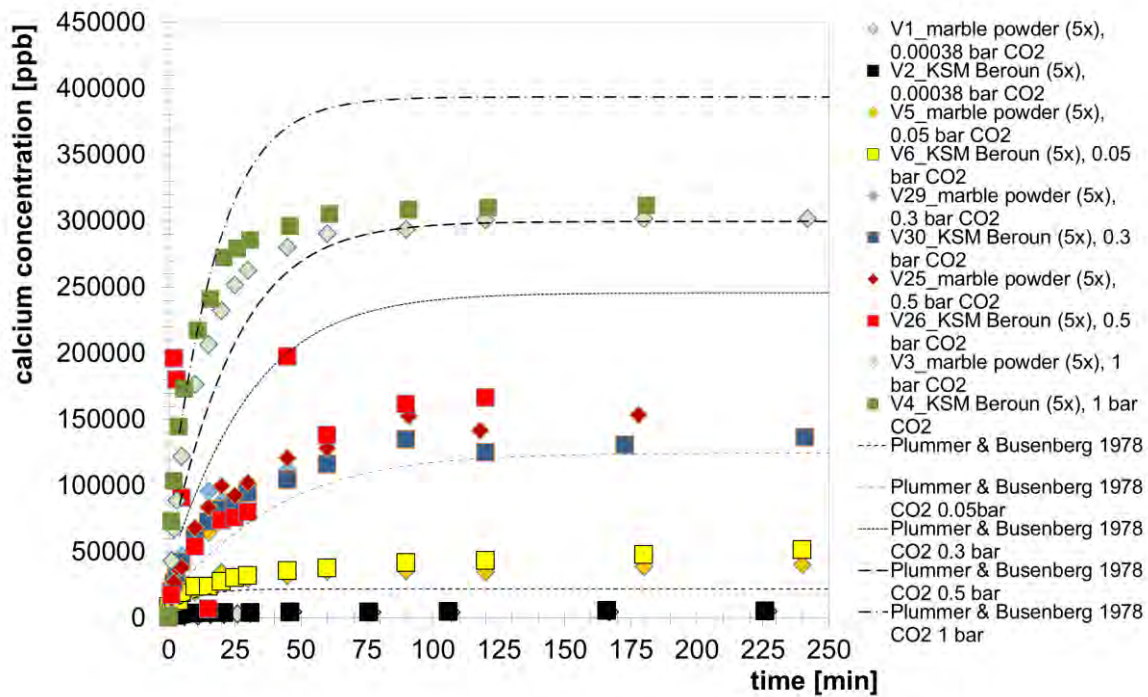


Figure 66. Development of calcium concentration in kinetic experiment influenced by different p_{CO_2} . Boundary conditions: pure water, 5-times saturated.

Regarding the form of the graphs of the calcium concentration, a faster kinetic in relation to the equilibrium state can be stated with increasing p_{CO_2} . The modeled maximum calcium concentrations according to Plummer et al. (1978) were not reached in the experiments. The higher p_{CO_2} the larger the difference between measured and modeled calcium concentration (see Figure 65 and Figure 66, Table 25).

Table 25. Calcium concentrations at the thermodynamic equilibrium state during calcite dissolution

CO_2 partial pressure	Calcium concentration [ppb]				
	0.00038 bar	0.05 bar	0.3 bar	0.5 bar	1 bar
Plummer & Busenberg 1978	22021	124744	245776	299696	393796
equilibrium_phases (wateq4f.dat)	22020	124760	245760	299680	393800
equilibrium_phases (Inll.dat)	21544	121600	239160	291480	382760
lab experiment (marble powder)	19440	105300	198150	244614	303425
lab experiment (KSM Beroun)	17570	105900	201471	261100	308566

Figure 67 A - F illustrate SEM images of marble powder after batch experiments with varying CO_2 partial pressures. A significant influence on the surface of calcite particles can be identified with increasing p_{CO_2} . The smooth surface of calcite particles becomes corroded and shows fissures and dissolution features.

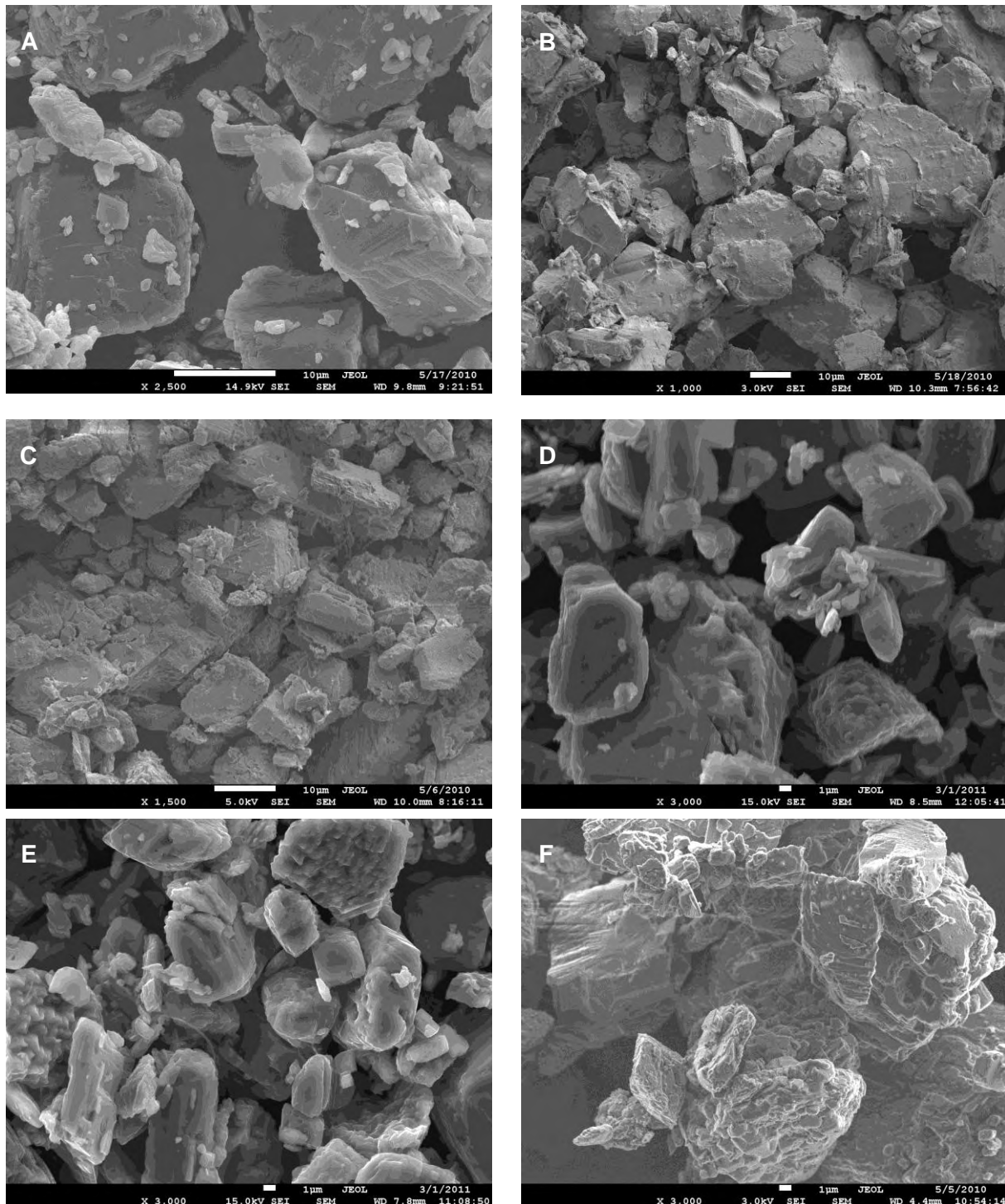


Figure 67. SEM images of marble powder before (A) and after (B - F) experimental use. Boundary conditions: pure water, 5-times saturated, B – $p_{CO_2} 3.8 \times 10^{-4}$ bar, C – $p_{CO_2} 0.05$ bar, D – $p_{CO_2} 0.3$ bar, E – $p_{CO_2} 0.5$ bar, F – $p_{CO_2} 1$ bar.

4.3.3 Influence of inhibiting ions

In addition to occurring inhibition by minor constituents of natural lime products kinetic experiments spiked with external ions (Mn, Cd) were carried out. Dissolved (metal) ions typical for AMD do have different effects on the kinetic of carbonate dissolution. Figure 68 illustrates the influence of manganese ions on carbonate dissolution.

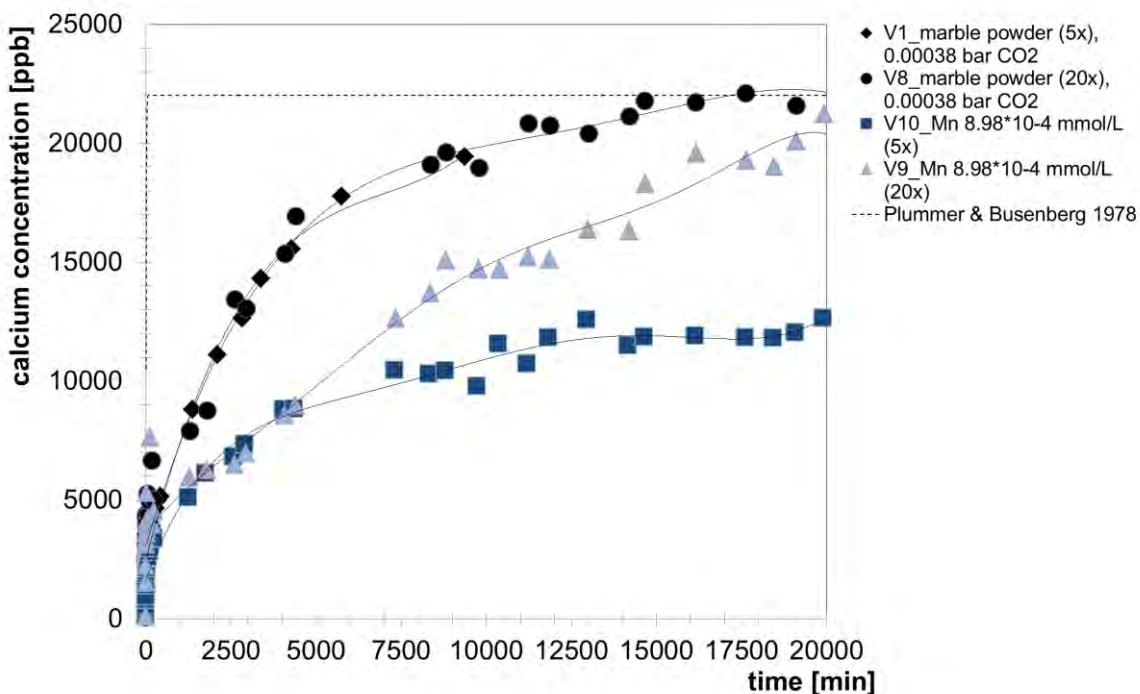


Figure 68. Development of the calcium concentration in kinetic experiment influenced by manganese ions ($c_{Mn^{2+}} = 8.98 \times 10^{-4}$ mmol/L). Boundary conditions: pure water, $p_{CO_2} 3.8 \times 10^{-4}$ bar, 5-times saturated / 20 times saturated. Plotted curves represent best-fit curves (polynomial).

The dissolution rates of the marble powder were inhibited by manganese ions in the solution. In comparison with Figure 62 the reached final concentration of calcium was calculated by 66.4 % compared to the experiment without addition of manganese ions (5-times saturated). The experiment with 20-times saturation and the addition of manganese as inhibitor showed a time shift until equilibrium was reached (20,000 min instead of 12,000 minutes). The fitted curves of the experiments, however, differ significantly.

Dissolved sulfate ions do not inhibit the dissolution rates of marble powder or KSM Beroun. As described in chapter 1.4.2.2 the literature review showed contradictory positions of the authors. Dissolution inhibition was claimed by Mucchi et al. (1989) and Sjöberg et al. (1978), whereas Akin and Lagerwer (1965a) and Dreybrodt and Eisenlohr (2000) didn't find inhibition reactions. The gained results fit with data from Vosbeck (2004) who didn't investigate inhibitor reactions. As Figure 69 shows even higher calcite dissolution rates occurred. Addition of Na_2SO_4 was considered in modeling so that at least the equilibrium state should fit with data modeled.

As can be seen in Figure 70 the effect of Cadmium ions in water has significant influence on carbonate dissolution kinetics. Compared with the general results of calcite dissolution (V1), the final concentration of calcium under consideration of cadmium as inhibitor reached only 12,810 ppb (5-times saturated). This equals approximately 58.2% compared to the dissolution in pure water. 20-times saturated solution showed a slight higher dissolution reaction. Finally, 14,040 ppb calcium had been reached in equilibrium, this equals 63.8%. The orange squares in Figure 70 represents calcium concentrations of V16 (Cd as inhibitor, 5-times saturated). It can be seen that the final equilibrium concentration can be reached

Results and discussion

much faster compared to marble powder in pure water. The curve fits almost the modeled one; without considering the reached equilibrium concentration. The experiment with 20-times saturated conditions is quite different. Here equilibrium seems to be reached within the same period like calcite dissolution in pure water.

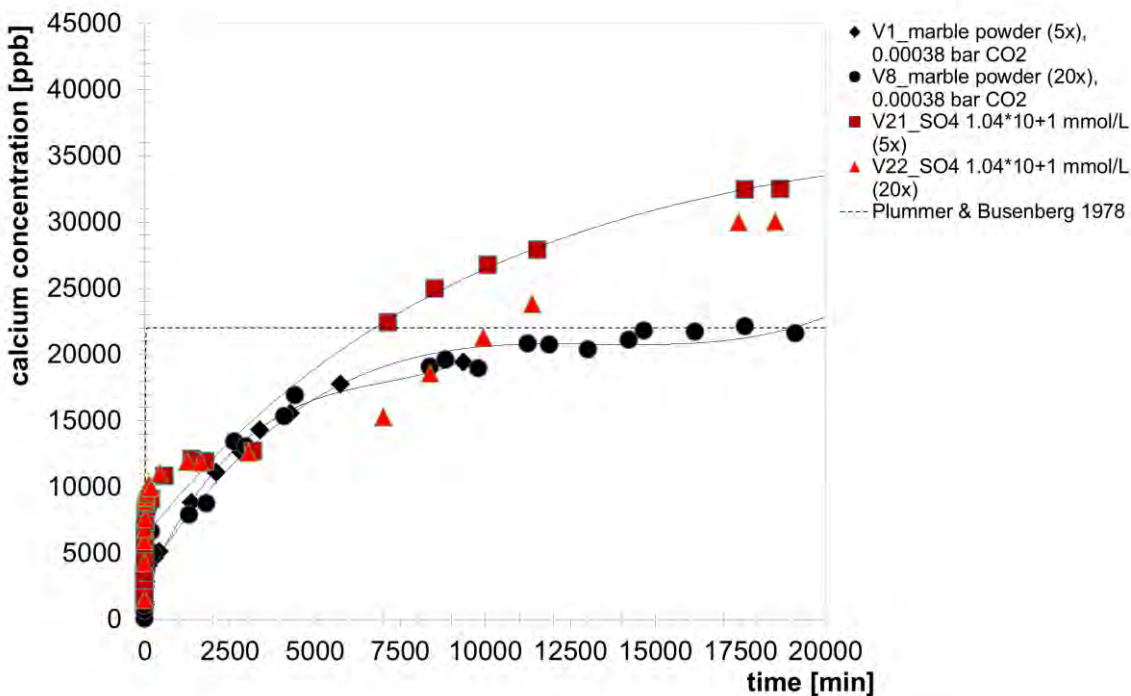


Figure 69. Development of the calcium concentration in kinetic experiment influenced by cadmium ions ($c_{SO_4^{2-}} = 1.04 \times 10^{-1}$ mmol/L). Boundary conditions: pure water, $p_{CO_2} 3.8 \times 10^{-4}$ bar, 5-times saturated / 20 times saturated. Plotted curves represent best-fit curves (polynomial).

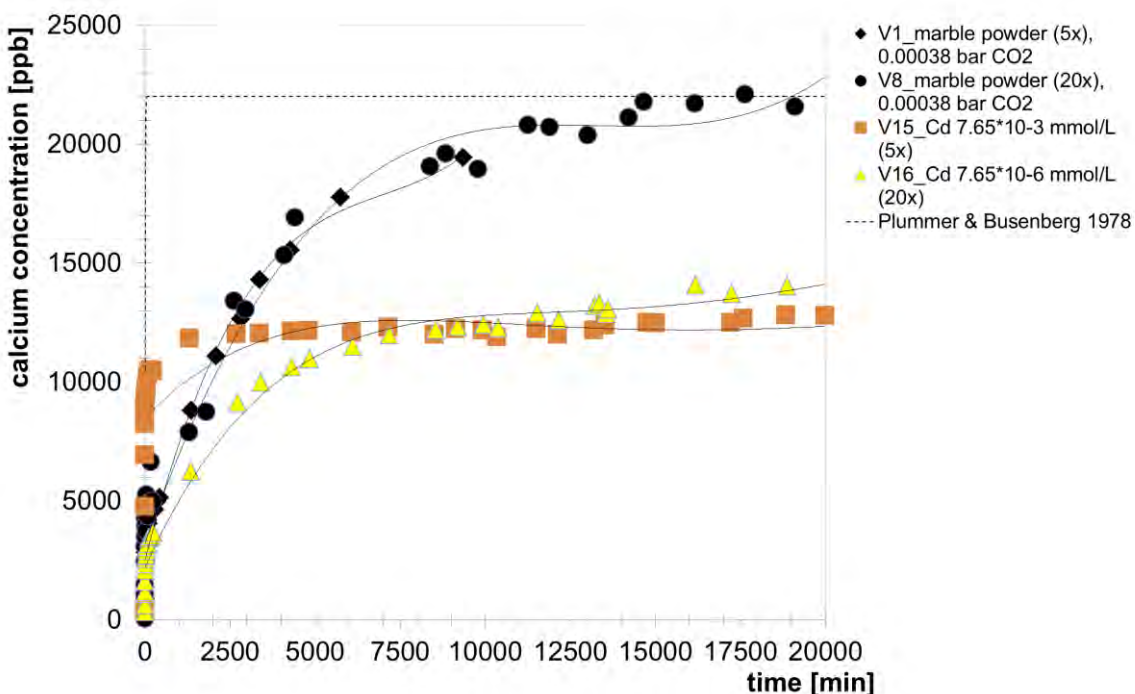


Figure 70. Development of the calcium concentration in kinetic experiment influenced by cadmium ions ($c_{Cd} = 7.65 \times 10^{-6}$ mmol/L). Boundary conditions: pure water, $p_{CO_2} 3.8 \times 10^{-4}$ bar, 5-times saturated / 20 times saturated. Plotted curves represent best-fit curves (polynomial).

As can be seen by the shown examples, water constituents might affect the dissolution rates of possible liming agents. So water composition should be considered if there are ambitious efforts to remediate acidic mine lakes by in-lake liming. The author suggests further experiments with regard to other trace metals in order to estimate the inhibiting effect. Simple batch experiments with the lake water to be neutralized can also help to get results about the reaction on certain liming agents.

4.3.4 Comparision of synthetic marble powder and industrial calcite (KSM Beroun)

As shown in Figure 62 no significant difference in reactivity between the synthetic marble powder and the industrial calcite KSM Beroun was obvious. With increasing CO₂ partial pressure in the experiments larger differences – in particular during the initial phase of the experiments - in electrical conductivity and calcium concentrations were visible (Schipek and Merkel, 2010). This causes a time-shift in the diagram.

Contrary to the expectations, the industrial product turned out to be more reactive. Thus, during the initial phase higher calcium concentrations were reached. Regarding the experiments with p_{CO₂} 0.05 bar, and p_{CO₂} 0.5 bar a lower calcium concentration in the equilibrium phase was reached (- 0.6 %, respectively – 6.3 %).

SEM images of both products are shown in Figure 71 and Figure 72. The typical rhomboedrical structure of the particles can be seen. Moreover, the surface of the synthetic products seems to be smoother than that of the industrial product, resulting in a smaller surface and reactivity. Additionally, it is obvious that the geometry or scale of the particles of the industrial product is entirely different from that of the synthetic material. A significantly larger surface of KSM Beroun can be estimated.

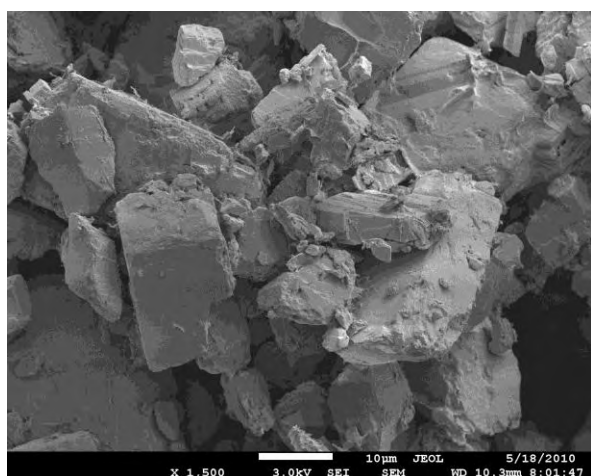


Figure 71. SEM image of synthetic marble powder.

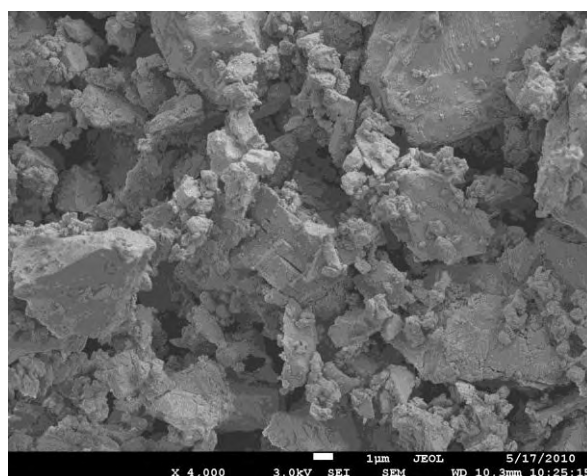


Figure 72. SEM image of an industrial calcite KSM Beroun.

4.4 Column Experiments - Liming

4.4.1 General results

A variety of batch and column experiments with original water from acid mine lakes was carried out. Results showed that a two-stage neutralization, with CaCO_3 and then Ca(OH)_2 having an optimized grain sized distribution, offers neutralization efficiencies close to the theoretical maximum (Schüppel, 2009). Product change should be at pH 4.5 – 5. This strategy marks not only a scientific optimum but also an economic (Schüppel, 2009).

It can be concluded that dissolution behavior of the liming agents and thus, the neutralizing reaction depends on different factors

- The type of product: limestone seems to be more effective than dolomites or mixtures of limestone and dolomites. Differences in the solubility of limestone and dolomite had been already published in literature (Chakrapani et al., 2008, Luttge et al., 2007, Morse and Arvidson, 2002, Pokrovsky et al., 2005, Pokrovsky et al., 2009b, Saldi et al., 2010).
- Grain size distribution of the products: the finer a product the slower is the sinking velocity (in column experiments, or later in lakes). Additionally a larger surface for reaction is provided.

During lake water treatment higher water depths are provided, so there is significantly more time for dissolution processes and mixing.

- pH values in a range of 3 – 5 can be neutralized with the “low-cost” product limestone. Especially the product of the company Rheinkalk GmbH KSM Beroun showed impressive results compared to other limestones.
- In some experiments effects on the hydraulic conductivity had been observed. First results had been described by Schüppel (2009). Hydraulic conductivity changed during column experiments, colimation effects had been observed. Further investigations area necessary in order to gain resilient results.

Three experimental series had been conducted, each with different water types (see chapter 3.2.6.2). By this, experience should be gained if there is a difference in the treatment of lakes with different water composition. As described in chapter 4.3.3 there is significant influence of the water composition. Additionally, different liming agents and strategies (one-stage vs. multi-stage application) had been investigated. Detailed results are shown in chapter 4.4.2 to 4.4.4.

4.4.2 Experimental series 1 (water type: Burghammer)

As described in chapter 3.2.6.2 a first experimental series was conducted by the use of the liming agents KSM Beroun, CaO (Branntkalk, WFK), Branndolomit and KSM Ostrau. As water phase water from Lake Burghammer was used, its composition is shown in Table 7 . Used amounts of liming agents can be found in Table B.10, appendix B.

Figure 73 shows pH values after addition of the liming products. Associated data can be found in Appendix B (Table B.11 – Table B.14). pH values of different sampling depths were prepared using the median, standard deviations of the pH values are shown.

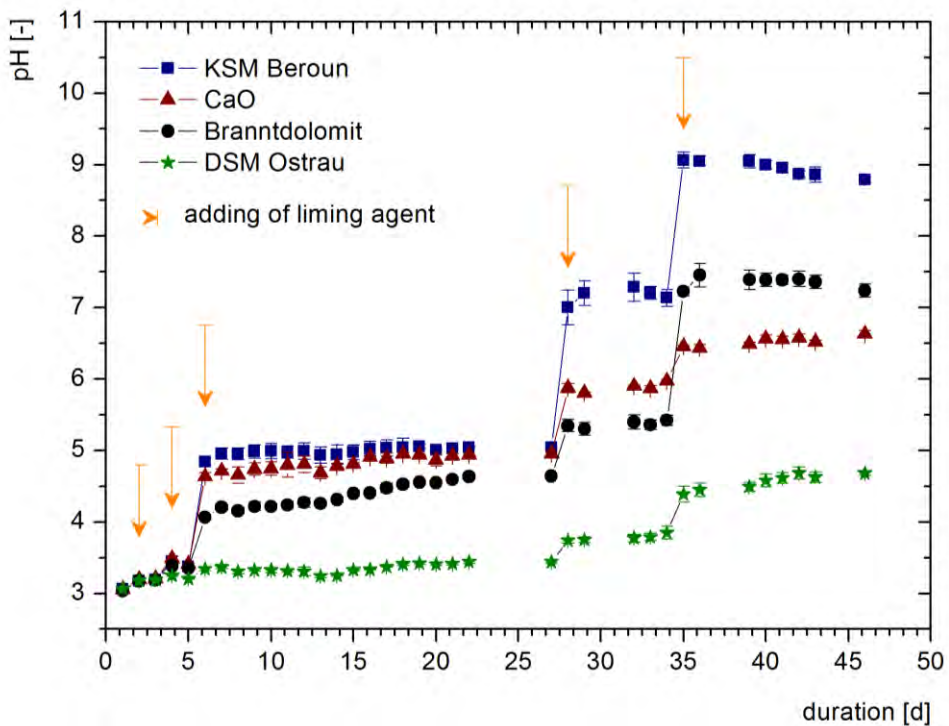


Figure 73. pH curve using different neutralizing agents. The yellow arrows represent the time of adding of the neutralizing agent.

Modeled curves with the stepwise addition of the neutralizing agents are shown in Figure 73. Starting at an initial pH of ca. 3, a slight increase of pH could be measured up to an addition of liming agent of ca. 1.5 mmol/L (Merkel and Schipek, 2008). The first additions of neutralizing agent (see Figure 73) on the first and third day of the experiment are within these areas of slight pH increase. This can be reasoned by existing aluminum and iron buffering systems which are significant up to a pH of 3.5 – 4. This area is followed by an area with high slope, the pH increases with a slope of $6.45 \cdot 10^{-2}$ mmol/L / 2 pH. The modeled curve slabs again and then approaches a constant pH (pH 7.89). Nearly all of the measured pH are below the modeled curve. Based on the modeled data, the efficiency of the neutralizing agent was plotted as a function of pH and the proton activity (Figure 74, Figure 75). For input-file see chapter 3.4.1.1.

Results and discussion

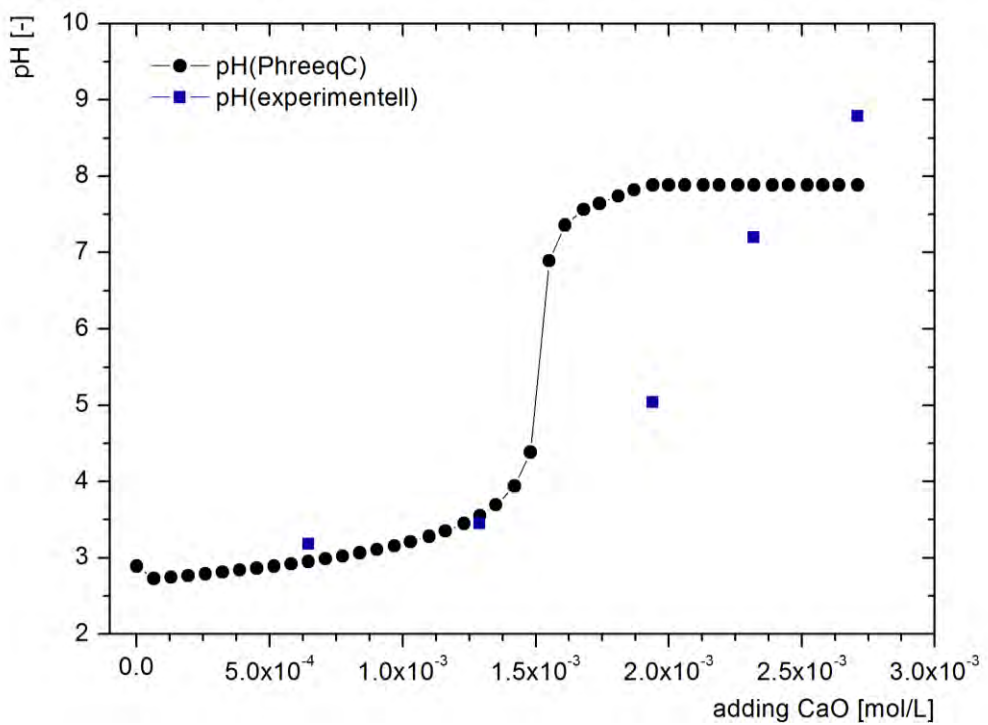


Figure 74. Modeled vs. experimental determined pH values after adding CaO

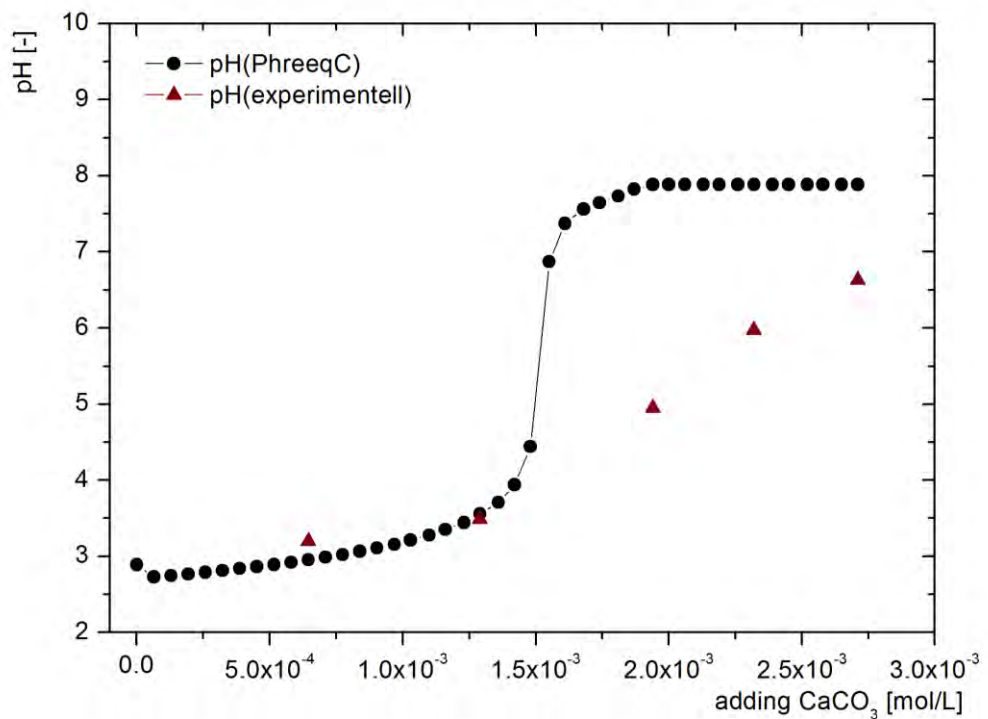


Figure 75. Modeled vs. experimental determined pH values after adding CaCO3

The pH during the experiment is a good indicator for the efficiency of the liming agents, if buffering systems should be considered, the base capacity of the treated water will be more significant. Unfortunately, during this first experimental series no buffering capacity was measured.

Table 26. Efficiency calculation based on experimental and modeled results, liming agent: CaO

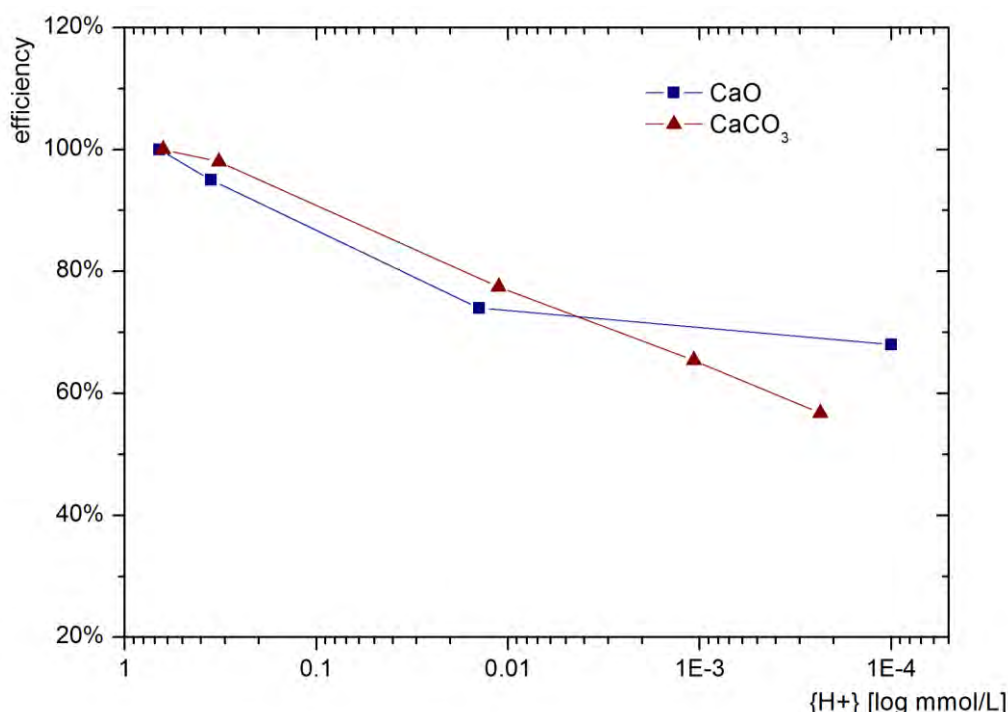
Liming step	amount _{CaO, exp}	Amount ¹ _{CaO, modeled}	pH _{modeled}	pH _{measured}	Efficiency
	mol/L	mol/L	[-]	[-]	[%]
1	6.45E-04	1.03E-03	3.18	1.00E-03	155%
2	1.29E-03	1.27E-03	3.45	1.23E-03	95%
3	1.94E-03	1.50E-03	5.04	1.44E-03	74%
4	2.32E-03	1.52E-03	7.20	1.58E-03	68%
5	2.71E-03	1.54E-03	8.79		

¹ determined by the help of measured pH

Table 27. Efficiency calculation based of experimental and modeled results, liming agent: CaCO₃

Liming step	amount _{CaCO₃, exp}	Amount ² _{CaCO₃, modeled}	pH _{modeled}	pH _{measured}	Efficiency
	mol/L	mol/L	[-]	[-]	[%]
1	6.45E-04	1.03E-03	2.95	3.20	159.58%
2	1.29E-03	1.27E-03	3.55	3.49	98.00%
3	1.94E-03	1.50E-03	7.89	4.95	77.47%
4	2.32E-03	1.52E-03	7.89	5.97	65.42%
5	2.71E-03	1.54E-03	7.89	6.63	56.81%

² determined by the help of measured pH

**Figure 76. Graph of the efficiency in dependence on the existing H⁺-activity.**

Results and discussion

With decreasing H⁺-activity the efficiency of the liming agents decreases from ca. 100% to 57% for CaCO₃ and 68% for CaO (see Figure 76).

4.4.3 Experimental series 2 (water type: Lohsa)

In order to investigate the efficiency of liming products in other lake water compositions, the experimental series 2 and 3 were conducted. During experimental series 2 water from the mining lake Lohsa II was used. Table 28 shows the initial lake water composition (sampling by MOVAB-D GmbH).

Table 28. Chemical composition of the mining lake Lohsa II, 11/2009

In-situ parameters			
pH	[-]	2.95	
Electrical conductivity	µS/cm	160	
redox potential	mV	n.d.	
O ₂ content	[ppm]	n.d.	
Cations [ppm]		Anions [ppm]	
Li ⁺	0.018	F ⁻	0.095
Na ⁺	31.88	Cl ⁻	29.573
K ⁺	34.24	NO ₂ ⁻	n.d.
Ca ²⁺	150.3	Br ⁻	0.0367
Mg ²⁺	25.3	NO ³⁻	0.779
Fe _(total)	8.736	PO ₄ ³⁻	n.d.
Mn ²⁺	2.338	SO ₄ ²⁻	805.7
NH ⁴⁺	1.86		
Al ³⁺	2.049		
TIC	ppm	0.35	
K _{b4.3}	mmol/L	2.952	
K _{b8.2}	mmol/L	4.582	

Calculation of the necessary amounts of liming products was done by using the product-specific neutralization potential and an average base capacity of the Lohsa water of 1.688 mmol/L.

Application of KSM Beroun, KSM Borna, Mischkalk Borna and DSM Borna was done multi-stage (3-stage, time lag of 1 week).

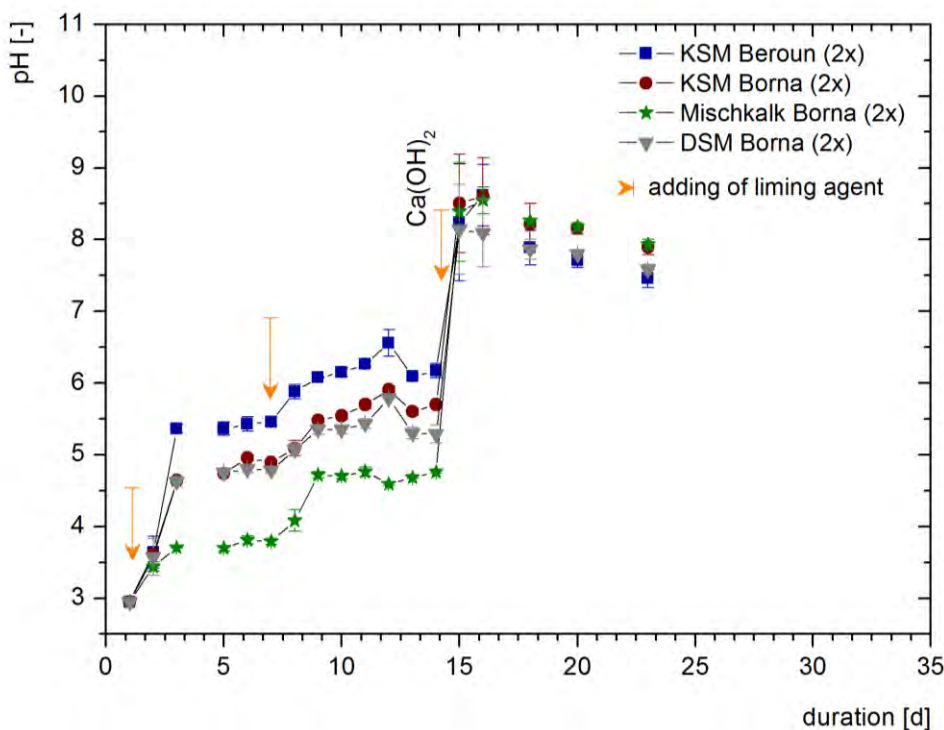


Figure 77. pH curve using different neutralizing agents in experimental series 2. The yellow arrows represent the time of adding of the neutralizing agent.

During series 2 of the column experiments an increase of the pH from 2.95 to neutral pH values (range: 7.5 – 8.0) was observed. The behavior of the tested industrial product KSM Borna was similar to the before used KSM Beroun. Dissolution kinetics of KSM Borna seems to be slightly worse than that of KSM Beroun.

DSM Borna showed the slowest dissolution reaction and thus slowest reactivity. The used product Mischkalk Borna was with its reactivity between KSM Borna and DSM Borna.

Figure 77 shows for each liming agent a rapid increase of pH after product application. The decrease of the ΔpH for the 3 application steps is an indication of a slower reaction kinetic. Above a pH of 5 a slow carbonate dissolution rate occurs. Due to that fact, the final neutralization step was done with $\text{Ca}(\text{OH})_2$ which shows a pH-non-dependent kinetic. According to Schüppel (2009) $\text{Ca}(\text{OH})_2$ has a relatively good solubility. Additionally the extreme fine grain size distribution of the used product has positive effect on sinking velocities (slow compared to larger particles). Thus, the full neutralization potential will be reached within minutes after product application.

In all columns, the acid neutralization capacity was improved in comparison to the initial lake water.

As can be seen in Table B.20, appendix B, metal concentration (miner water constituents) was decreased significantly during liming. Aluminum concentration after treatment was circa 1.78 % of the initial amount before treatment with KSM Beroun/KSM Borna (36.5 ppb versus 2,049 ppb). Chromium was determined after multi-stage treatment in average 0.17 ppb (6.9 %), compared to 2.4 ppb initial concentration. Manganese concentration was reduced by 38 – 53.44 % (Mischkalk Borna, respectively DSM Borna) from 2,388 ppb to 908 ppb,

respectively 1,249 ppb. Contents of iron decreased in average from 8,736 ppb to 3 ppb. This equals a reduction to 0.03 %. Data from further trace metals can be found in Table B.20.

4.4.4 Experimental series 3 (water type: Scheibe)

This third experimental series was conducted with a different type of lake water, mining lake Scheibe. Liming agents were KSM Beroun and DSM Ostrau. Table 29 shows the initial lake water composition of the mining lake Scheibe (sampling by MOVAB-D GmbH, 25.06.2010).

Table 29. Chemical composition of the mining lake Scheibe, 06/2010

In-situ parameters		
pH	[\cdot]	2.4
Electrical conductivity	$\mu\text{S}/\text{cm}$	1642
redox potential	mV	n.d.
O ₂ content	[ppm]	n.d.
Cations [ppm]		Anions [ppm]
Li ⁺	0.00	F ⁻ 0.191
Na ⁺	20.83	Cl ⁻ 36.007
K ⁺	6.28	NO ₂ ⁻ n.d.
Ca ²⁺	119.80	Br ⁻ 0.000
Mg ²⁺	23.74	NO ³⁻ 1.889
Fe _(total)	n.d.	PO ₄ ³⁻ n.d.
Mn ²⁺	n.d.	SO ₄ ²⁻ 692.90
NH ⁴⁺	1.59	
Al ³⁺	n.d.	
TIC		ppm n.d.
K _{b4.3}		mmol/L 2.952
K _{b8.2}		mmol/L 4.582

Input of the liming agents was done in 2 ways: one-stage addition or multi-stage addition, where the product was added in 5 days (1/5). Additionally, CaO and an extremely fine-grained limestone (KSM C20, see also Table 13) was tested

Used amounts of liming agents can be found in Table B.21, Appendix B.

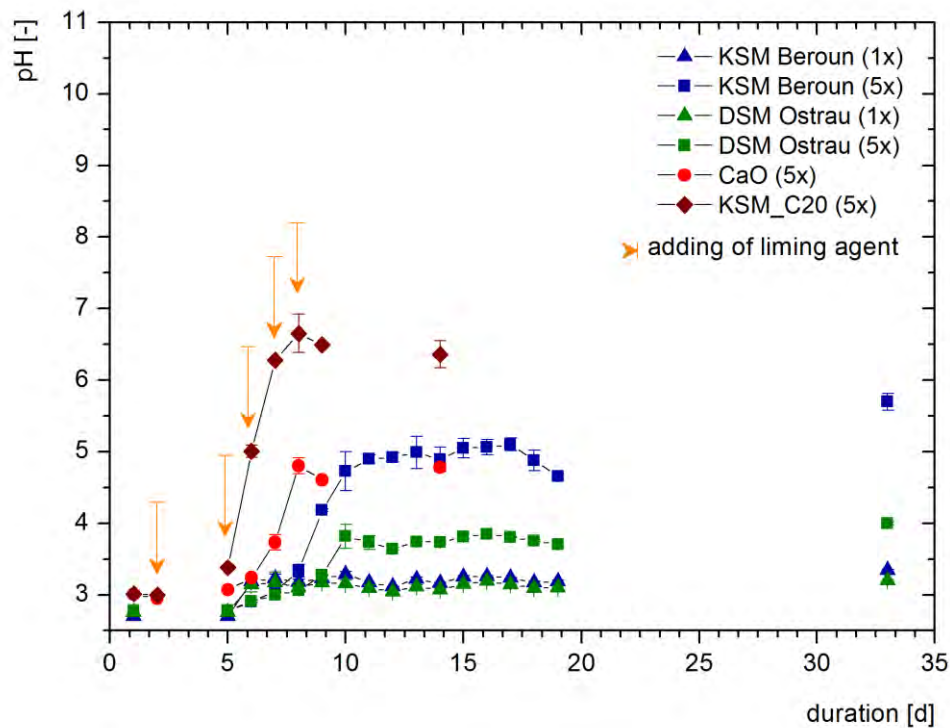


Figure 78. pH curve using different neutralizing agents in experimental series 3. The yellow arrows represent the time of adding of the neutralizing agent.

During the course of the column experiments an increase of pH from 2.7 to 3.2 – 3.4 (one-stage liming, KSM Beroun, respectively DSM Ostrau) was observed. Multi-stage liming resulted in significantly higher pH-values (5.7 for KSM Beroun), respectively 4.0 for DSM Ostrau. Using CaO the pH could be increased from 2.9 – 3.0 to an average pH of 4.78, respectively pH 6.36 for KSM C20. All liming products do not show a further significant increase weeks after product application, so it can be assumed that reaction kinetics are nearly finished.

The amount of used liming agent (KSM Beroun and DSM Ostrau) was calculated by a theoretical efficiency of 70%. For KSM Beroun and DSM Ostrau a neutralization potential of 19 mmoleq/kg was assumed. Table 30 represents the effect on the base neutralization capacity of water from the mining lake Scheibe. In all column experiments, an increase of the acid neutralization capacity was observed.

Results and discussion

Table 30. Calculation of effective efficiencies.

Liming agent		KSM Beroun	KSM Beroun	DSM Ostrau	DSM Ostrau	CaO ²	KSM_C20 ³
K _{b8.2} , before	[mmol/L]	4.244	3.844	3.742	4.834	3.497	3.497
K _{b8.2} , after	[mmol/L]	1.698	0.384	1.996	1.220	0.727	0.433
Δ K _{b8.2}	[mmol/L]	2.546	3.460	1.746	3.614	2.770	3.064
Neutralization potential	[moleq/kg]	19	19	19	19	-	-
amount	[g]	20.7522	20.7546	20.7522	20.7531	9.3397	30.3680
	[mmoleq/92L]	394.29	394.34	394.29	394.31	-	-
	[mmoleq/L]	4.286	4.286	4.286	4.286	-	-
Efficiency _{100%}	[%]	59	81	41	84	77	89
Efficiency ¹ _{70%}	[%]	42	57	29	59	-	-

¹ efficiency under consideration of the theoretical efficiency of 70% (used for calculation of amount of liming agent)

² based on a theoretical efficiency of 95%

³ based on a theoretical efficiency of 55%

Based on the different treatment strategies (one- vs. multi-stage liming) it can be seen, that multi-stage addition of the neutralizing agents effects a higher efficiency (81% / 84% efficiency). Figure 78 shows that the tested dolomite product (DSM Ostrau) is suitable for one-stage liming at low pH; its curve fits with the curve of the previously approved KSM Beroun. No significant difference is recognizable. In general, multi-stage application showed a better reactivity and effectiveness of the KSM Beroun; especially the reached final pH of 5.7 (compared to 4.0 for DSM Ostrau) shows this fact.

Considering the concentrations of trace metals, it can be noted that the application of KSM Beroun and DSM Ostrau leads to significant reductions in concentrations of certain elements. Iron was removed during treatment to 4.12 % (706 ppb, one-stage liming) and below detection limit (< 1 ppb, multi-stage liming). DSM Ostrau leads to a reduced iron concentration of 1,334 ppb one-stage liming (-88.17 %), respectively 113.7 ppb for multi-stage liming (-99.37 %). Cadmium concentration was significantly decreased during one-stage-liming with KSM Beroun (-65.10 %), respectively during multi-stage liming (-96.57 %). DSM Ostrau seems to release cadmium ions during dissolution processes. Concentrations after treatment changed rapidly from 0.13 ppb to approximately 2 ppb after liming. Comparing KSM Beroun and DSM Ostrau, KSM Beroun is more effective in trace metal concentration. Concentrations of aluminum, manganese, cobalt, lead didn't change significant (in average -3.84 %, + 4.08%, -1.30 %, +0.15 %).

Application of CaO leads to a significant reduction of aluminum (-74.0 2%), beryllium (-50.33 %), borum (-19.57 %), cobalt (-14.33 %), nickel (-13.54 %), copper (-12.43 %), zinc (-16.35 %), arsenic (-47.51 %), cadmium (-10.90 %). Iron and chromium have been removed nearly completely (-99.97 %, -86.24 %).

The new product KSM_C20 is characterized by a high surface area compared to commonly used liming products. Following reduction rates could be reached during multi-stage liming: beryllium (-87.75 %), borum (-13.92 %), aluminum (-99.85 %), iron (-99.99 %), copper

(-65.30 %), zinc (-9.10 %), arsenic (-59.93 %). Cobalt and Nickel didn't change significantly (-0.90 %; -0.61 %).

Detailed data (trace metal concentration) are shown in Table B.28, appendix B.

4.5 Field study (CO₂ sequestration)

4.5.1 Aim of the field study

In the context of a field experiment different injection techniques (pure gas or gas-water mixture) were applied and evaluated with respect to the distribution of gas and gas-water-mixture in the sediment and its impact on the adjacent water quality in the lake.

4.5.2 Theoretical considerations

Injecting a gas in water-saturated porous sediment will trigger several processes, depending on the amount of gas injected. As long as the amount of gas is very small, the gas will readily dissolve in the water according to Henry's law. By increasing the amount of gas a coherent or non-coherent multiphase flow will occur, because gas flow in water saturated porous sediments is driven by buoyancy, while flow of water is driven mainly by gravity; thus, pressure opposite the flow direction occurs. Characteristics of the porous medium have significant effects on the gas flow distribution in the ash body (Schipek and Merkel, 2007). "Airflow distributions are directly impacted by air permeability, which is a function of particle size and distribution. Air channels, likely only few grain sizes in diameter and formed by the injected air, make up the extent of the ROI" (Benner et al., 2002). ROI is known here as radius of influence around each injection point.

Horizontal air conductivity represents the relative ease of horizontal gas movement through the ash body. Larger air conductivities represent coarser grained sediment with easier movement of gas, such as gravel or sand, while smaller gas conductivities represent finer grained sediments, such as silt or clay – or relating to lake Burghammer, ash sediments. Different authors state that the radius of influence in finer sediments is larger than in coarser one's under the same injection pressure. This is essentially due to stronger capillarity in finer sediments (Mei et al., 2002, Philip, 1998). The injected gas will move in consequence of the resulting force. This force results from capillary forces, friction forces and lifting forces. Further achievement can be gleaned in Lazik et al. (2002).

As mentioned in section 3.2.1, the evaluation of the grain size distribution was carried out by dry sieving and photosedimentologic methods. By the acquired grain size distribution curve and with the help of formulas for the determination of the hydraulic conductivity, hydraulic conductivities could be calculated in a range from 10^{-5} – 10^{-8} m/s. It must be pointed out that this permeability only shows the permeability of the fluid water. In fact, we had to use the term intrinsic permeability in order to describe the properties of CO₂ transport.

4.5.3 Site description

The experimental site was chosen based on the drillings carried out in December 2005 and the results of the geochemical studies. The location for the passive treatment scheme was situated close to sampling site P2 (drilling core BGH-141205-P2).

Results and discussion

The location of the test site can be described by the coordinates given in Table 31; Figure 79 shows the situation graphically.

Table 31. Coordinates of the different test sites during pilot experiment of passive treatment (Gauß-Krueger-Coordinates, RD 83, Rauenberg, Bessel)

Outline Coordinates	Test site 1*		Test site 2**	
Easting	5456158	5456358	Easting	5456258
Northing	5704128	5704328	Northing	5704228
	5456158	5456358		5704432
	5604328	5704128		

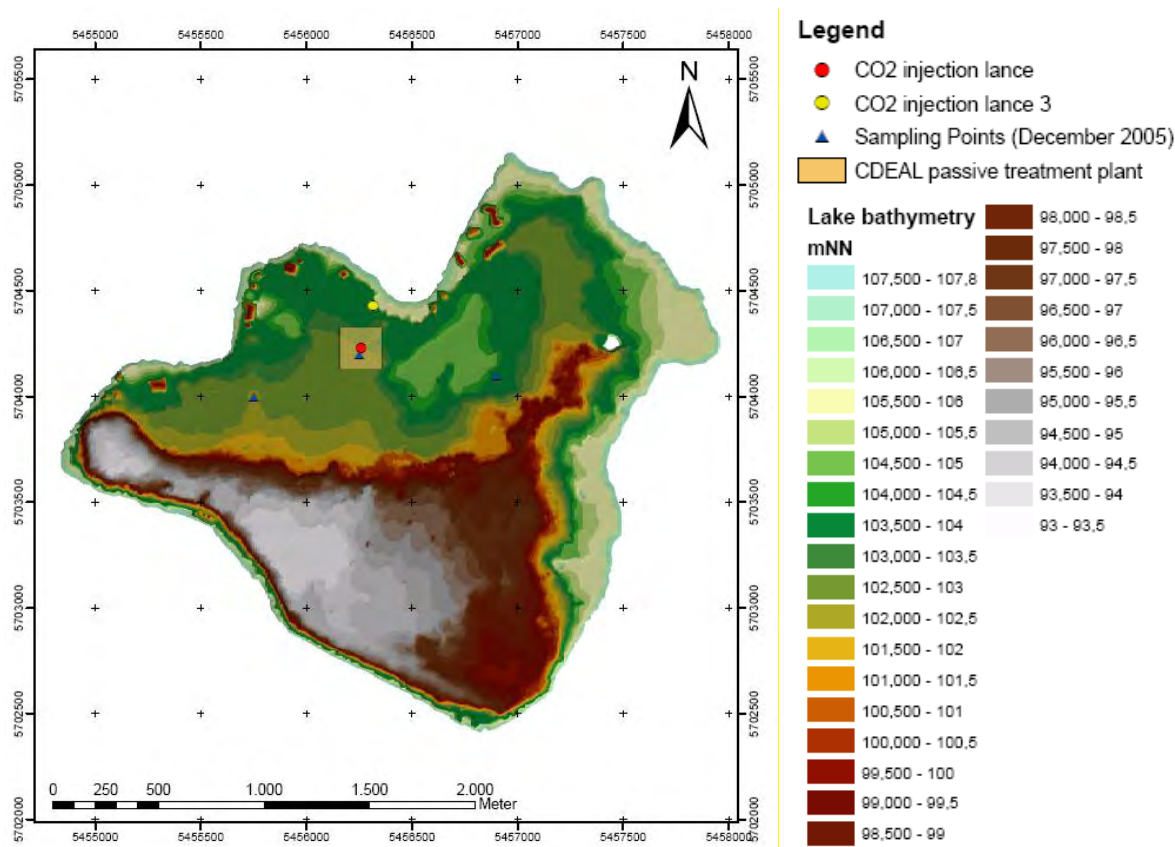


Figure 79. Digital terrain model of the lake bottom from mining Lake Burghammer. The marked square indicated the boundary of the test site (Gauß-Krueger (zones are only 3° apart, as opposed to 6° in UTM), RD 83, Rauenberg, Bessel).

As mentioned in the above, a so-called radius of influence is supposed. The radius of influence amounts to the area where CO₂ is effectively injected. Before starting the pilot experiment a ROI of circa 15 m was assumed (Schipek and Merkel, 2008c).

4.5.4 Results

4.5.4.1 Technical Feasibility

CO₂ was applied with a pressure of 2.2 bar and on average 2.2 m³/h. The duration of the pilot experiment comprised 3 months (05/21/2008 - 07/29/2008) (Schipek and Merkel, 2009c, Schipek and Merkel, 2009b).

Results and discussion

Table 32. Application of CO₂: measured gas flow and applied pressure of CO₂ during the pilot experiment.

	Gas flow ¹⁾ [m ³ /h]	pressure [bar]	Gas flow ¹⁾ [m ³ /d]		Gas flow ¹⁾ [m ³ /h]	pressure [bar]	Gas flow ¹⁾ [m ³ /d]
05/21/2008	2.2	2.4	52.8	06/26/2008	2.4	2.5	57.6
05/22/2008	2.2	2.4	52.8	06/27/2008	2.4	2.5	57.6
05/23/2008	2.2	2.4	52.8	06/28/2008	2.4	2.5	57.6
05/24/2008	2.2	2.4	52.8	06/29/2008	2.4	2.5	57.6
05/25/2008	2.2	2.4	52.8	06/30/2008	2.4	2.5	57.6
05/26/2008	2.2	2.4	52.8	07/01/2008	2.3	2.5	55.2
05/27/2008	2.2	2.4	52.8	07/02/2008	2.3	2.5	55.2
05/28/2008	2.2	2.4	52.8	07/03/2008	2.3	2.5	55.2
05/29/2008	2.2	2.4	52.8	07/04/2008	2.3	2.5	55.2
05/30/2008	-	-	-	07/05/2008	2.3	2.5	55.2
05/31/2008	-	-	-	07/06/2008	-	-	-
06/01/2008	-	-	-	07/07/2008	2.6	2	62.4
06/02/2008	2.2	2.4	52.8	07/08/2008	2.6	2	62.4
06/03/2008	2.2	2.4	52.8	07/09/2008	2.6	2	62.4
06/04/2008	2.2	2.4	52.8	07/10/2008	2.6	2	62.4
06/05/2008	2.2	2.4	52.8	07/11/2008	2.6	2	62.4
06/06/2008	2.2	2.4	52.8	07/12/2008	2.6	2	62.4
06/07/2008	2.2	2.4	52.8	07/13/2008	2.6	2	62.4
06/08/2008	2.2	2.4	52.8	07/14/2008	2	1.8	48
06/09/2008	2.2	1.8	52.8	07/15/2008	2	1.8	48
06/10/2008	2.2	1.8	52.8	07/16/2008	2	1.8	48
06/11/2008	2.2	1.8	52.8	07/17/2008	1.8	2	43.2
06/12/2008	2.3	2.6	55.2	07/18/2008	2.6	2	62.4
06/13/2008	2.2	2.6	52.8	07/19/2008	2.6	2	62.4
06/14/2008	2.2	2.6	52.8	07/20/2008	2.6	2	62.4
06/15/2008	2	2.6	48	07/21/2008	2.6	2	62.4
06/16/2008	2	2.4	48	07/22/2008	2.6	2	62.4
06/17/2008	2	2.4	48	07/23/2008	2.6	2	62.4
06/18/2008	2	2.4	48	07/24/2008	2.6	2	62.4
06/19/2008	2.5	2.5	60	07/25/2008	2.6	2	62.4
06/20/2008	2.5	2.5	60	07/26/2008	2.6	2	62.4
06/21/2008	2.5	2.5	60	07/27/2008	2.6	2	62.4
06/22/2008	2.5	2.5	60	07/28/2008	2.6	2	62.4
06/23/2008	2.5	2.5	60	07/29/2008	2.6	2	62.4
06/24/2008	-	-	-	Total Gas flow [m³]		3,652.8	
06/25/2008	2.5	2.5	60	Total CO₂ amount [kg]		6,750.3744	

¹⁾ the real gas flow was calculated by the measured gas flow, the prevailing temperatures, absolute pressure and gas type (density... 1.848 kg/m³)

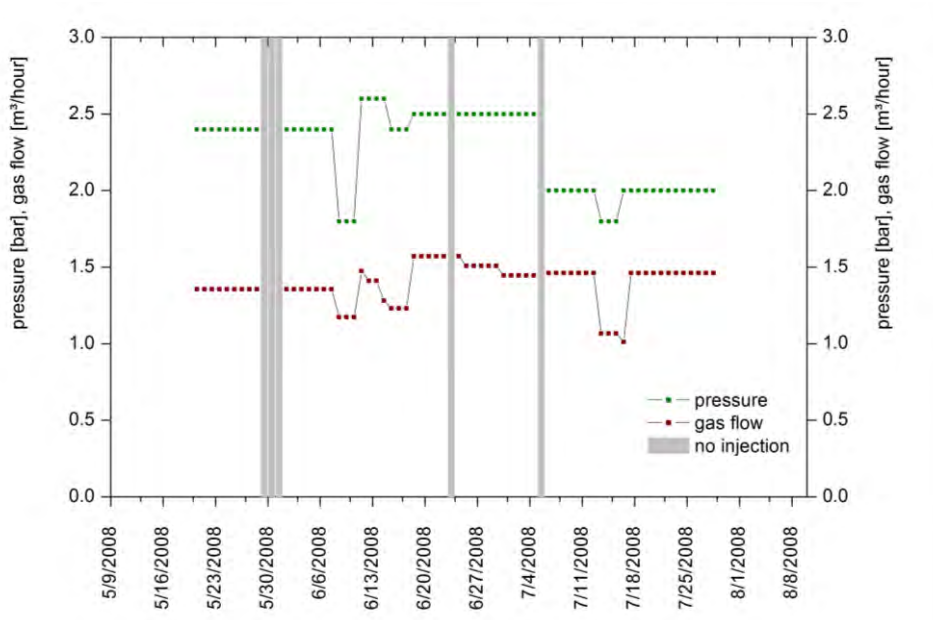


Figure 80. Application of CO₂ during pilot experiment. Grey bars indicate periods of no CO₂ injection through technical problems (05/30/2008 to 06/01/2008; 06/24/2008; 07/06/2008).

In total, an amount of 6,750.4 kg CO₂ was injected within 3 months for 1 injection lance.

4.5.4.2 Effect of CO₂ injection on the water body

Considering the fact that no initial neutralisation of the lake water had been done before CO₂ injection, no effect on pH was determined during the course of the pilot experiment (Figure 81); only within the direct periphery of the injection lances an influence on the total inorganic carbon content was witnessed. This can be reasoned by slight degassing or diffusion of CO₂ out of the sediment body during CO₂ injection.

Results and discussion

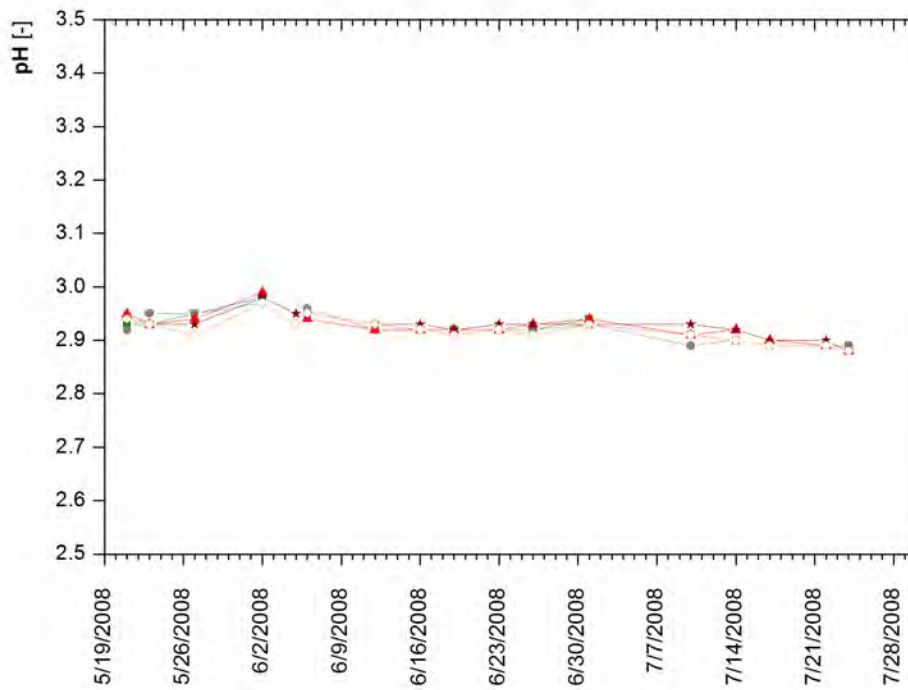


Figure 81. pH-values of Lake Burghammer in the area of CO₂ injection.

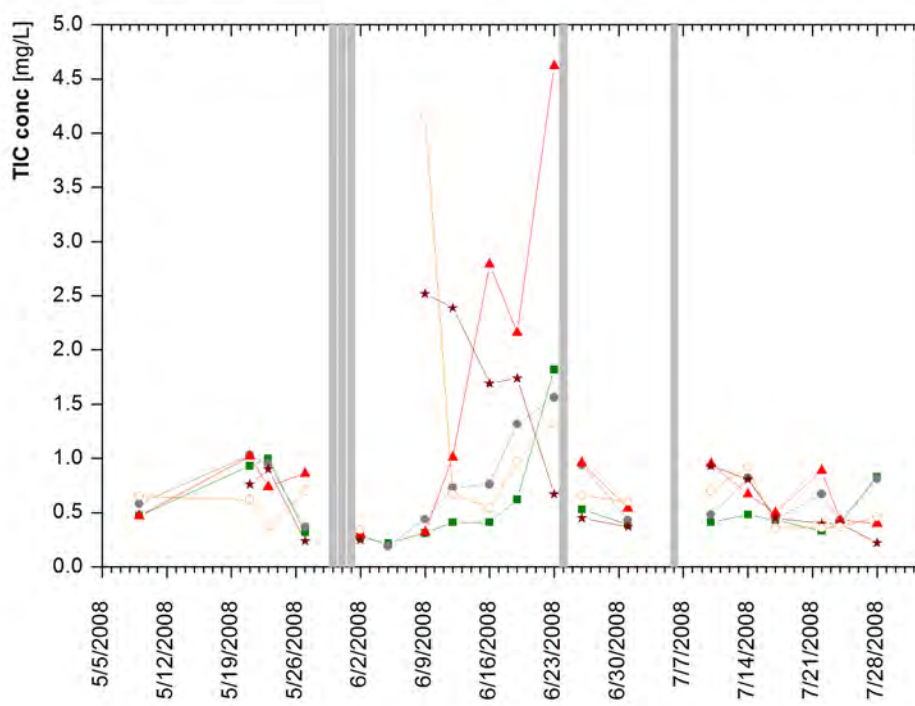


Figure 82. Total inorganic carbon concentration of different sampling sites in Lake Burghammer within the area of CO₂ injection.

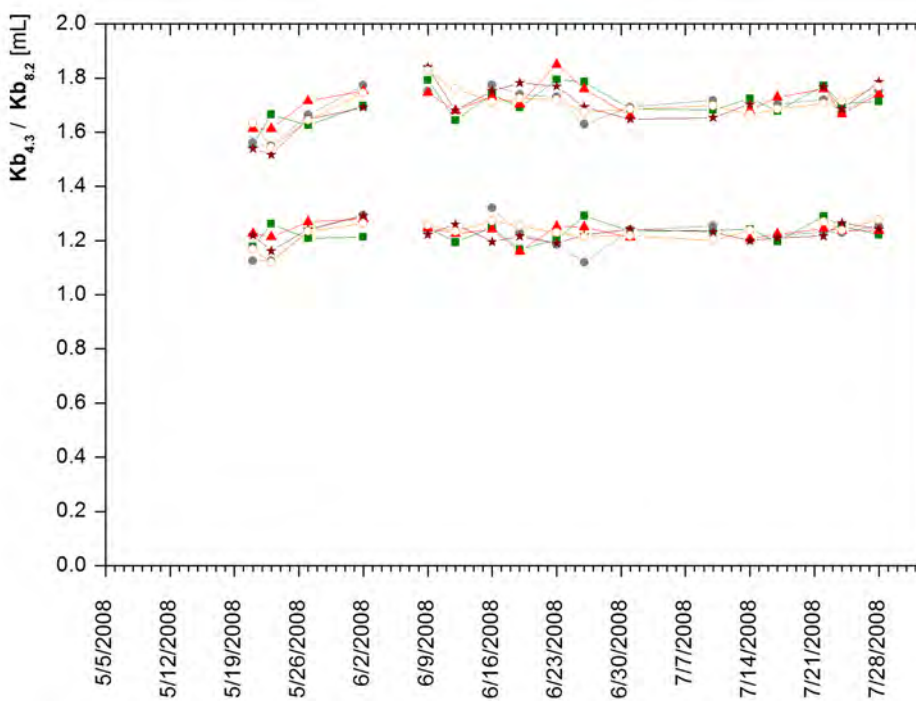


Figure 83. Development of base neutralization capacity in the water body during CO₂ injection.

TIC is shown in Figure 82. In generally, concentrations remained constant during the course of the pilot experiment. Sudden increases can be caused by technical problems, such as the fracturing of the lance due to strong wind and the consequent drift of the platform. 2 times strong winds occurred and the 4 anchors were not able to keep the platform at position. By the drifting of the platform, the injection lance was sheared off and CO₂ escaped directly into the water body for a certain time.

Figure 83 describes variations in base neutralization capacity. Acid neutralization capacity could not be determined due to the low pH (pH 2.9).

Concentrations of main cations (K⁺, Na⁺, Ca²⁺, Mg²⁺), as well as main anions (Cl⁻, SO₄²⁻, NO₃⁻, PO₄³⁻, F⁻, Br⁻), did not change significantly. Corresponding diagrams can be found in appendix A (Figure A.7 – Figure A.12).

4.5.4.3 Effect on Pore water

The ash sediment had water content between 30 and 50 %, with no significant changes before and after CO₂ injection (Figure 84). Water content decreased seemingly with increasing depth; however, no statistical significance was seen ($r^2 = 0.1$)

Chemical data for pore water samples before and after CO₂ treatment can be found in appendix B (Table B.32 – B.35). Before CO₂ injection pH in the pore water of the settled ash body was in the range of 6.8 and 8.9 (Figure 85). After CO₂ injection the pH ranged between 6.5 and 9.7; where no trend with increasing depth was detectable. According to theoretical considerations calcite precipitation may occur. Comparing the pH before CO₂ injection with those of the lake water (in average pH 2.9), it can be assumed that there is no exchange between these two water bodies.

Results and discussion

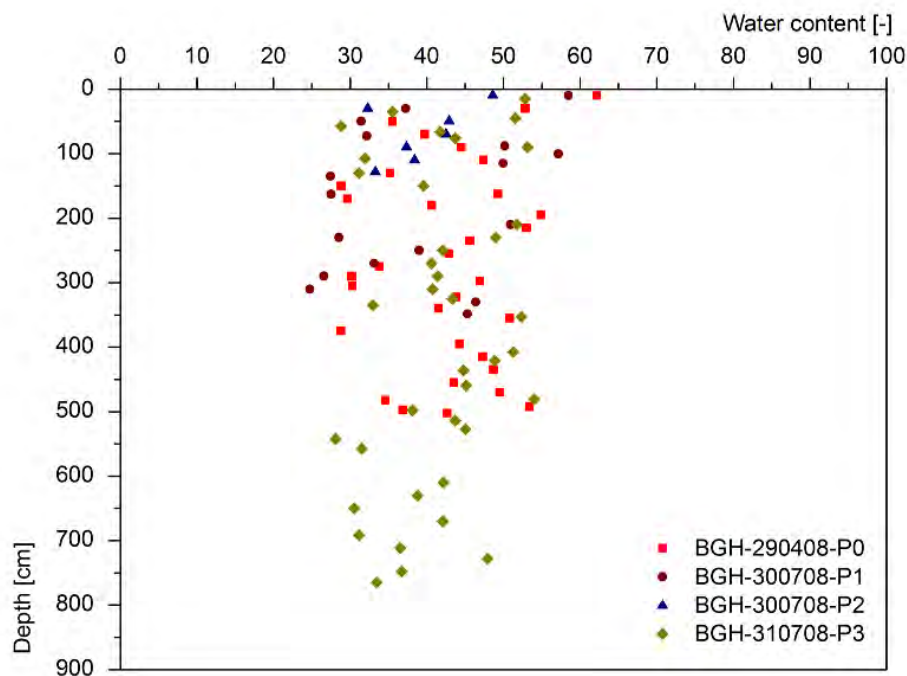


Figure 84. Pore water distribution in sediment cores of Lake Burghammer before and after CO₂ injection. BGH-290408-P0 shows data before CO₂ injection; BGH-300708-P1 / P2 / P3 show data after CO₂ injection.

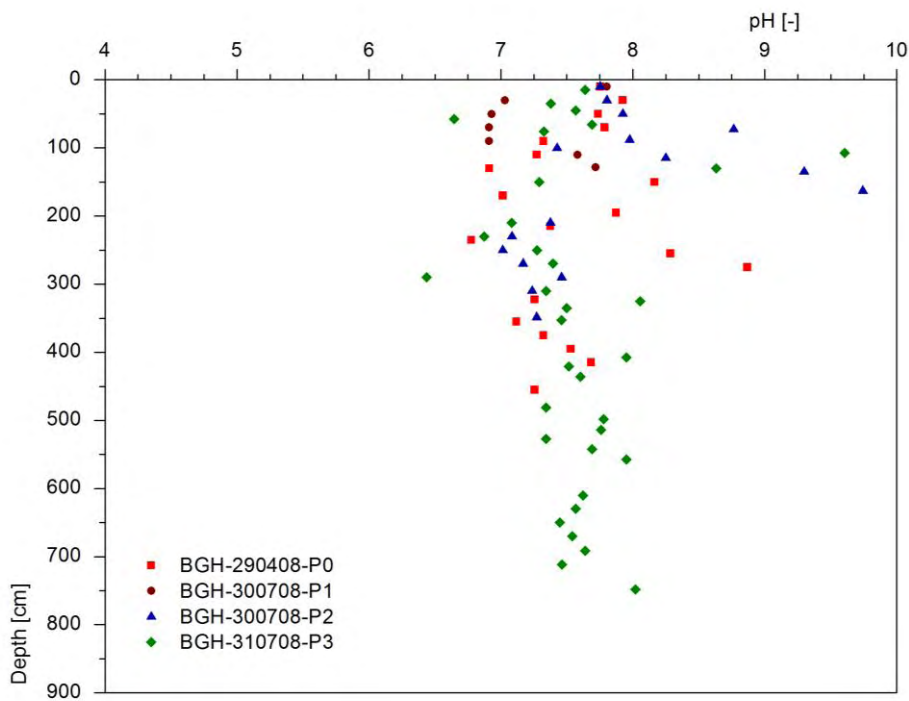
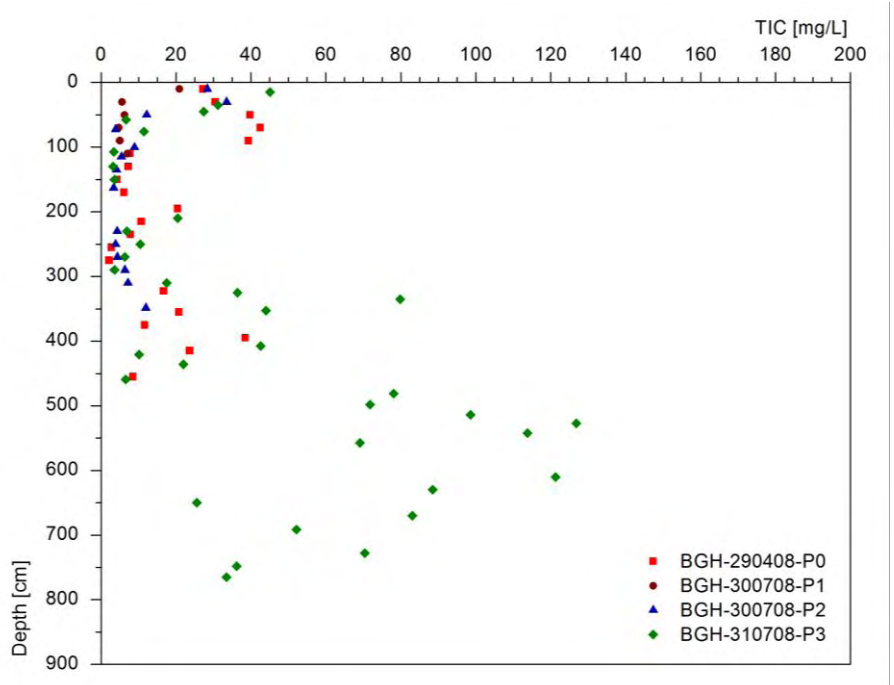


Figure 85. pH of the pore water in sediment cores of Lake Burghammer before and after CO₂. BGH-290408-P0 shows data before CO₂ injection; BGH-300708-P1 / P2 / P3 show data after CO₂ injection.

Associated TIC-contents of the pore water are shown in Figure 86. Before CO₂ treatment the total inorganic carbon decreased from 27.2 ppm at the sediment surface until maximum depth of the drilling core P0-300408-P0 (5 m) to 8.5 ppm. The average content was 18.4

ppm. High contents at the sediment-water boundary layer are reasonable because of the exposure of fly ash before flooding the ash body in the mining lake, and biological activity through microorganism and plant influence.

The TIC content, after CO_2 treatment of the ash sediment, was on average 30.8 ppm. In general, the upper 3 m of the drilling cores (P0, P1, P2, P3) showed a slight decrease in inorganic carbon with increasing depth. BGH-310708-P3 showed higher TIC contents in a range of 3 to 8 m depth, the maximum TIC was 126 ppm as a result of CO_2 injection. This is obviously due to the injection of CO_2 at a sediment depth of about 12 m.



Results and discussion

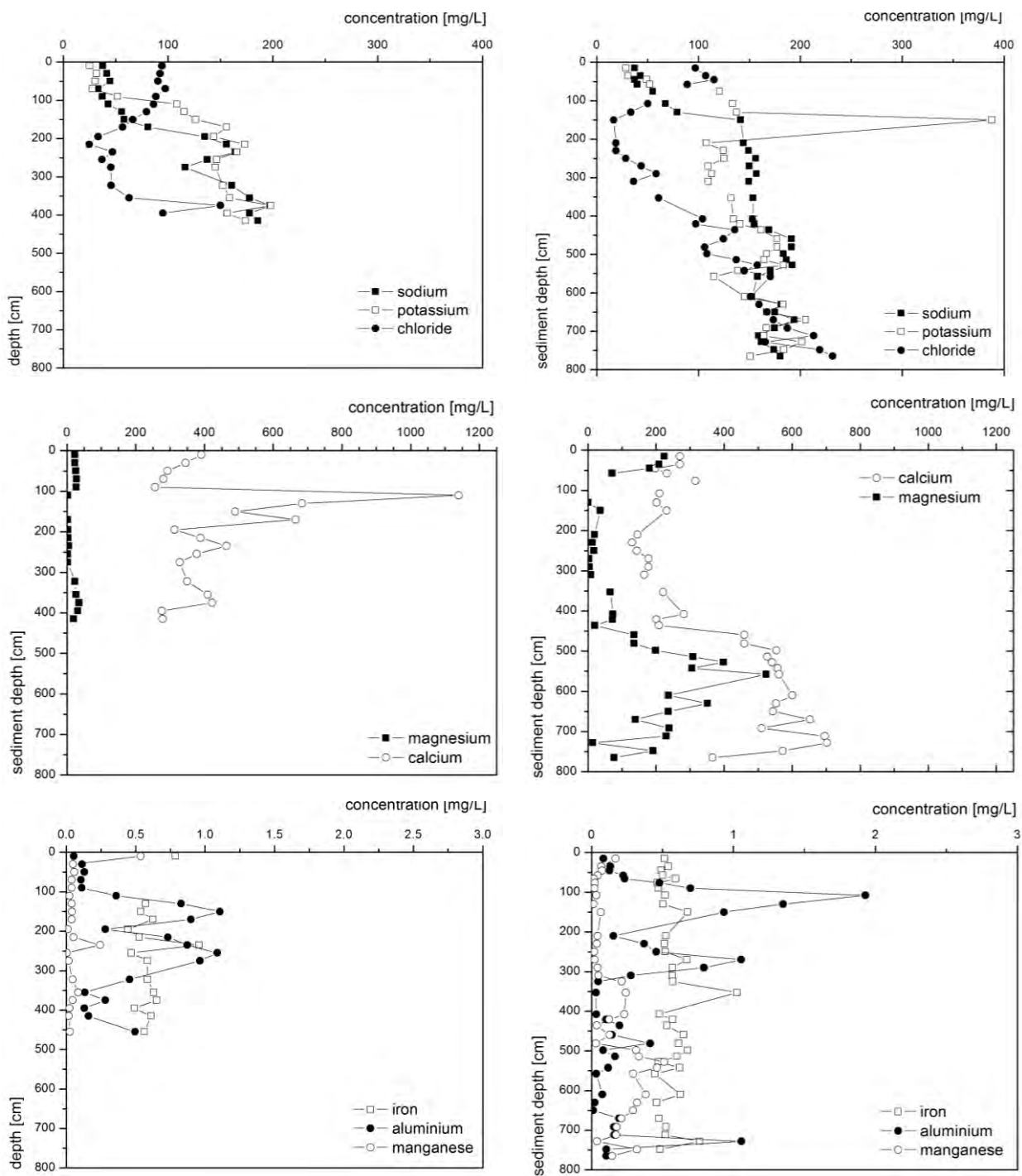


Figure 87. Depth profiles of major ions in the pore water before (left hand, BGH-290408-P1) and after CO₂ treatment (right hand, BGH-310708-P3)

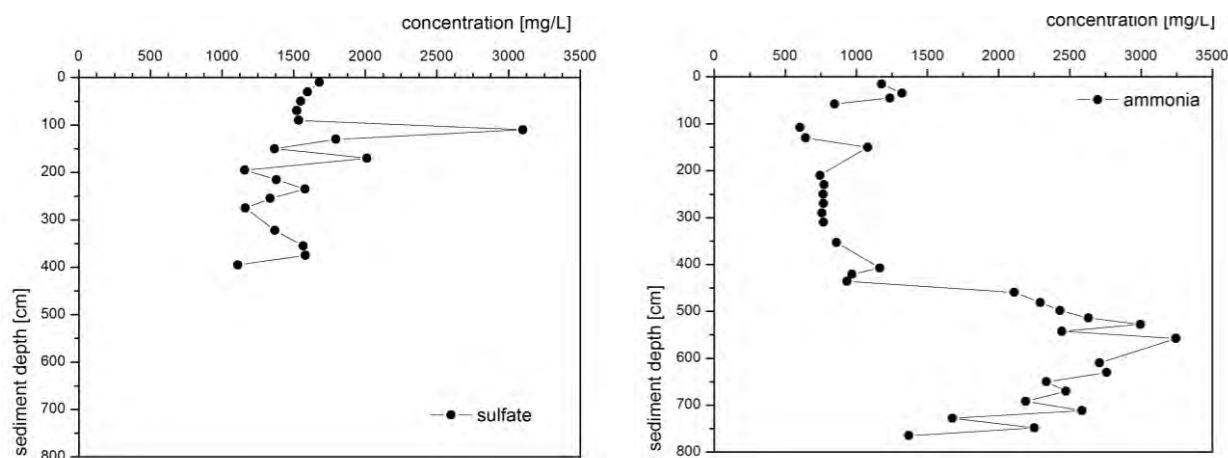


Figure 88. Depth profile of sulfate in the pore water before (left hand, BGH-290408-P1) and after CO₂ treatment (right hand, BGH-310708-P3)

Sodium, potassium and chloride steadily rise with increasing sediment depth.

Sodium increases from 33.22 ppm to 197.47 ppm in 4.65 m depth. After CO₂ treatment, no significant changes were detected; concentrations were determined in a range from 37.15 ppm to 193.89 ppm in 7.70 m depth.

Potassium contents were in average 120.40 ppm (median: 145.28 ppm) before CO₂ treatment. Minimal (25.20 ppm) potassium was found in pore waters, the maximum content was determined to be 198.08 ppm. After CO₂ injection increased values (in average 143.73 ppm; median: 139.66 ppm) were found.

Chloride contents were analyzed in a range from 24.75 to 149.8 ppm (average 71.76 ppm); after the pilot experiment, the average content was 112.90 ppm.

Calcium concentrations were higher than concentrations of other cations. Before CO₂ injection, the average content was 429.10 ppm. In general, there was a large range: 377.82 to 1139.53 ppm. Figure 87 shows a slight decrease of calcium in pore water with increasing depth. With CO₂ treatment, the contents of calcium in the upper part of the fly ash sediment decreased in the pore water. The average content was determined to be 371.56 ppm. From bottom surface to 5 m sediment depth, calcium concentrations were determined on average to be 200 ppm. Below 5 m sediment depth there was an increase to circa 600 ppm.

Magnesium occurred in pore waters, before CO₂ injection, in a range of 16.63 ± 12.49 ppm. After CO₂ injection, magnesium contents increased to 148.02 ± 133 ppm.

Manganese concentrations in pore water did not change by CO₂ treatment. Before, pore waters contained on average 0.07 ± 0.12 ppm; after CO₂ injection the manganese content was 0.15 ± 0.14 ppm.

Ammonia concentrations were in a range from 0.40 to 2.99 ppm before CO₂ injection and 0.69 to 18.82 ppm after CO₂ injection. Before CO₂ injection no trend was observed; after CO₂ injection concentrations increased with increasing sediment depth.

Sulfate was the most dominant anion in the pore water samples. Maximum concentrations of 3,100 ppm and minimum concentrations of 1,110 ppm were observed. The average content before CO₂ treatment was 1,578 ppm (Figure 88). After CO₂ treatment, the average content

Results and discussion

was determined to be 1,633 ppm; the minimum concentration was 603 ppm and the maximum concentration 3,245 ppm. When there is an increase of pH in the alkaline range the OH⁻ ions compete with SO₄²⁻ for adsorption sites, on the amorphous iron phases, leading to desorption of SO₄²⁻ (Gitari et al., 2008b).

The concentrations of **iron** did not change during CO₂ injection. Average contents before were 0.60 ± 0.12 ppm and after CO₂ injection pore water samples contained 0.56 ± 0.11 ppm Fe.

The behavior of **aluminum** in pore water samples is similar: Before CO₂ treatment aluminum concentrations of 0.46 ± 0.37 ppm were detected. After CO₂ treatment, concentrations of 0.35 ± 0.43 ppm were found.

Statistical calculations (Mann-Whitney-Test) were done, in order to prove significant correlation of Ca, Mg and TIC. The difference between these three parameter was significant (n1 = n2 = 31, p < 0.001, two-tailed test).

Table 33. Trace element mobilization before and after pilot experiment [ppb]

	Before CO ₂ treatment		After CO ₂ treatment		Trend
	Mean	Median	Mean	Median	
Li	100.30 ± 33.96	102.27	259.58 ± 234.85	159.66	↑
Co	3.95 ± 1.52	3.56 µg/	3.40 ± 1.71	2.88	↓
Cu	20.79 ± 24.19	10.76	16.17 ± 37.92	0.7351	↓
Zn	49.05 ± 30.22	36.44	55.15 ± 126.36	29.25	→
Se	49.31 ± 39.09	41.86	15.37 ± 17.49	0.74	↓
Rb	454.66 ± 225.29	517.15	503.25 ± 149.95	512.27	→
Sr	6654.9 ± 2266.5	5974.93	5969.1 ± 2679.9	5726.37	↓→
Mo	47.46 ± 19.81	51.67	39.30 ± 14.68	41.20	↓
Cd	0.64 ± 0.44	0.51	0.40 ± 0.60	0.28	↓
Sn	1.77 ± 1.07	1.60	2.66 ± 3.76	1.61	→
Sb	0.64 ± 0.20	0.61	0.69 ± 0.37	0.65	→
Cs	23.59 ± 15.31	21.22	25.03 ± 12.64	22.93	→
Ba	97.70 ± 18.00	94.91	86.95 ± 19.15	82.22	↓
La	0.09 ± 0.06	0.10	0.17 ± 0.61	0.05	→
Ce	0.72 ± 0.51	0.91	0.40 ± 1.25	0.12	↓
W	15.03 ± 11.91	43.34	11.94 ± 12.92	6.11	↓
Hg	0.06 ± 0.05	0.06	0.08 ± 0.07	0.06	→
Tl	0.04 ± 0.10	0.04	0.05 ± 0.05	0.04	→
Pb	0.86 ± 0.97	0.61	1.43 ± 3.09	0.49	→
U	3.09 ± 4.09	1.33	13.41 ± 18.50	2.61	→

As can be seen in Table 33, generally no trace metal mobilization was found during CO₂ treatment of the settled fly ash sediment. Most elements (cobalt, copper, selenium,

molybdenum, cadmium, barium, cesium, wolfram) showed decreasing trends. The concentrations of zinc, rubidium, strontium, tin, antimony, cesium, lanthanum, tellur, lead and uranium did not change significantly. Only lithium was observed to be mobilized by CO₂ treatment.

Besides selenium, a number of trace elements showed very low concentrations and no effect on treatment with settled ash sediment in combination with CO₂. A number of elements were below their respective detection limits: Be (0.0063 ppb), P (35.54 ppb), Cr (< 1.1193 ppb), Ni (< 0.2562 ppb), As (< 0.4340 ppb), Y (0.0229 ppb), Zr < 0.0333 ppb, Ag (0.0867 ppb), Pr (0.0026 ppb), Th (0.0092 ppb).

Elements showing variable concentrations in pore waters as a result of CO₂ treatment can be interpreted with the help of calculated saturation indices and thermodynamic modeling (chapter 5.2).

4.5.4.4 Mineralogical alterations

X-ray diffraction analysis provided only little useful information in this thesis. As seen from the results in Table B.29 (appendix B), the predominant part of the unsettled ash sediment is composed of amorphous, presumably aluminosilicate, glass. Based on X-ray diffraction data untreated ash sediment contained the minerals: quartz, brownmillerite, ferrite, hematite, calcite, microcline and sreboldolskite. The X-ray diffraction pattern for the CO₂-treated ash sediment samples were similar to the pattern for the untreated ash sediment; however, X-ray diffraction is often not sensitive to the development of small, but potentially important, quantities of secondary mineral phases. The normal detection limit of crystalline phases in powdered mounts by X-ray diffraction is on the order of 0.5 wt.-%.

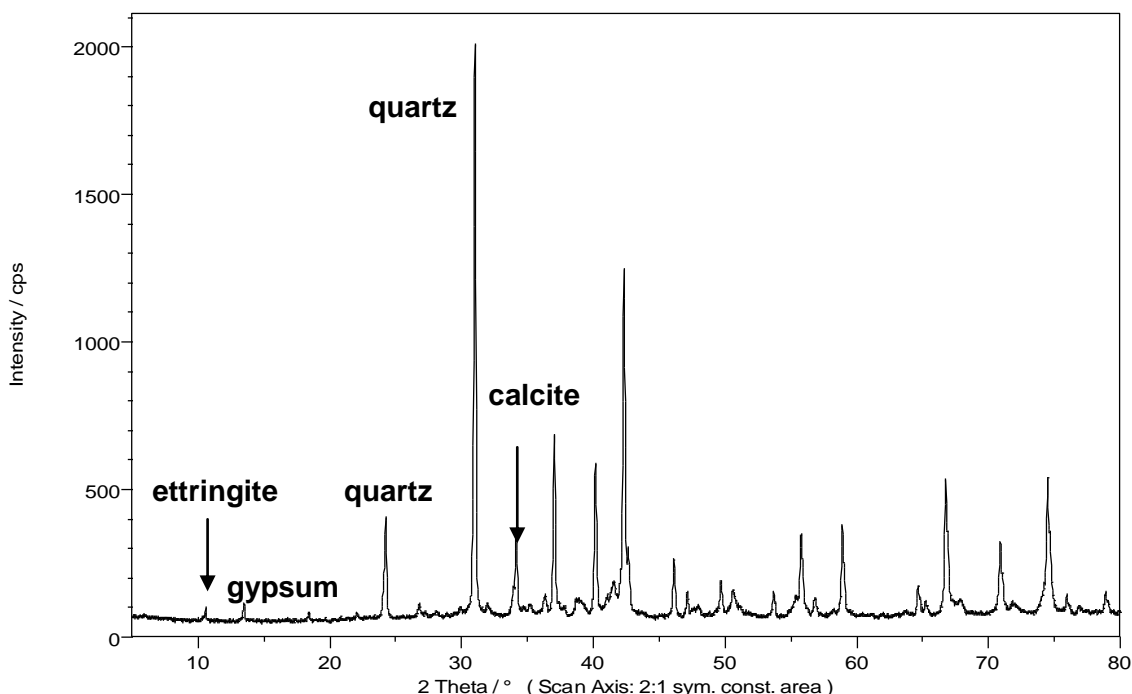


Figure 89. X-ray diffractogram of fly ash before CO₂ treatment (BGH-300408-P0, depth 4.90 – 4.95 m)

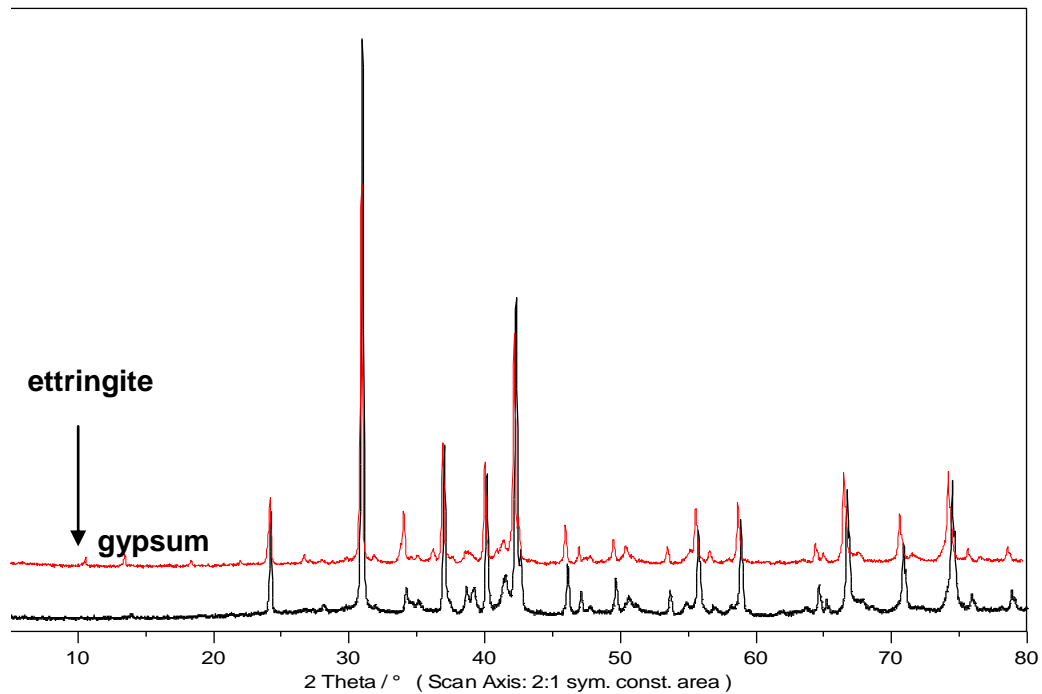


Figure 90. Comparison of X-ray diffractograms of fly ash before CO₂ treatment (BGH-300408-P0, depth 4.90 – 4.95 m, red colored) and after CO₂ treatment (BGH-310708-P3, depth 5.08 – 5.20 m, black colored)

Brownmillerite ($\text{Ca}_2(\text{Al},\text{Fe}^{3+})_2\text{O}_5$) was found in 12 of 32 samples, whereas before CO₂ injection there was only one sample where Brownmillerite could be identified.

The phase ettringite ($\text{Ca}_6\text{Al}_2(\text{SO}_4)_3(\text{OH})_{12}\cdot26\text{H}_2\text{O}$) was identified sporadically throughout the samples. Ettringite is a mineral that is typically found in ash sediments. It was disregarded that ettringite was in the ash sediment in response to the normal environment of its occurrence ($\text{pH} > 10.7$) (Hosseini et al., 1999, Münch, 1996, Myneni et al., 1998). Thermodynamic modelling with PhreeqC (see chapter 5.2.1) showed, that the porewater of all drilling cores was undersaturated concerning the mineral phase ettringite. Hence, the minerals were likely formed during analysis preparation.

Variations were determined in the contents of the mentioned mineral phases. The quartz content before and after CO₂ treatment differed, as did the content of amorphous phases. Table 34 shows mineralogical composition before and after CO₂ treatment.

Table 34. Mineral alterations through CO₂ injection

Mineral	Formula	Before CO ₂	After CO ₂
Amorphous	-	40.4 ± 2.88	35.2 ± 2.91
Calcite	CaCO_3	3.2 ± 0.59	2.8 ± 0.6
Ferrite, magnesian	$\text{MgFe}_2^{3+}\text{O}_4$	3.6 ± 1.11	5.1 ± 0.87
Hematite	Fe_2O_3	1.2 ± 0.45	1.1 ± 0.49
Quartz	SiO_2	41.2 ± 1.7	50.1 ± 1.99
Microcline	$\text{K}(\text{AlSi}_3\text{O}_8)$	2.7 ± 1.14	2.6 ± 1
Srebrodolskite	Ca_2FeO_5	3.6 ± 0.82	3.1 ± 0.76

Due to the standard deviation of about 0.5 wt.-% in calcite, this method was improper for quantification of CO₂ sequestration and carbonation rate.

In addition to XRD investigations, SEM investigations were performed on selected samples. In combination with an energy-dispersive microprobe (EDX), it is possible to determine relative element distributions. In combination with morphological investigations, this element distribution can be helpful for the identification of minerals.

Images of scanning electron microscopy show fly ash particles characterized by a grain size of 5 to 200 µm. Many of the ash particles are spherical with diameters of 5 to 40 µm. Mainly amorphous constituents exist in the form of small spheres of different sizes. A strongly varying chemical composition was determined: magnesium, aluminum, silicon, calcium, iron, sulfur, potassium, sodium and titanium. Appendix B, Table B.36 and B.37 show an abstract of chemical data gained by SEM/EDX.

The ash particles consist mainly of silicon, aluminum, calcium, and iron. All other elements are mostly represented in the trace element field. The outer edge of the ash beads are often iron or calcium oxide. Most of the ash particles are mixed phases and do not form idiomorphic crystals. Occasionally, crystal structures can be identified, e.g. calcite (Figure 92 A).

Results and discussion

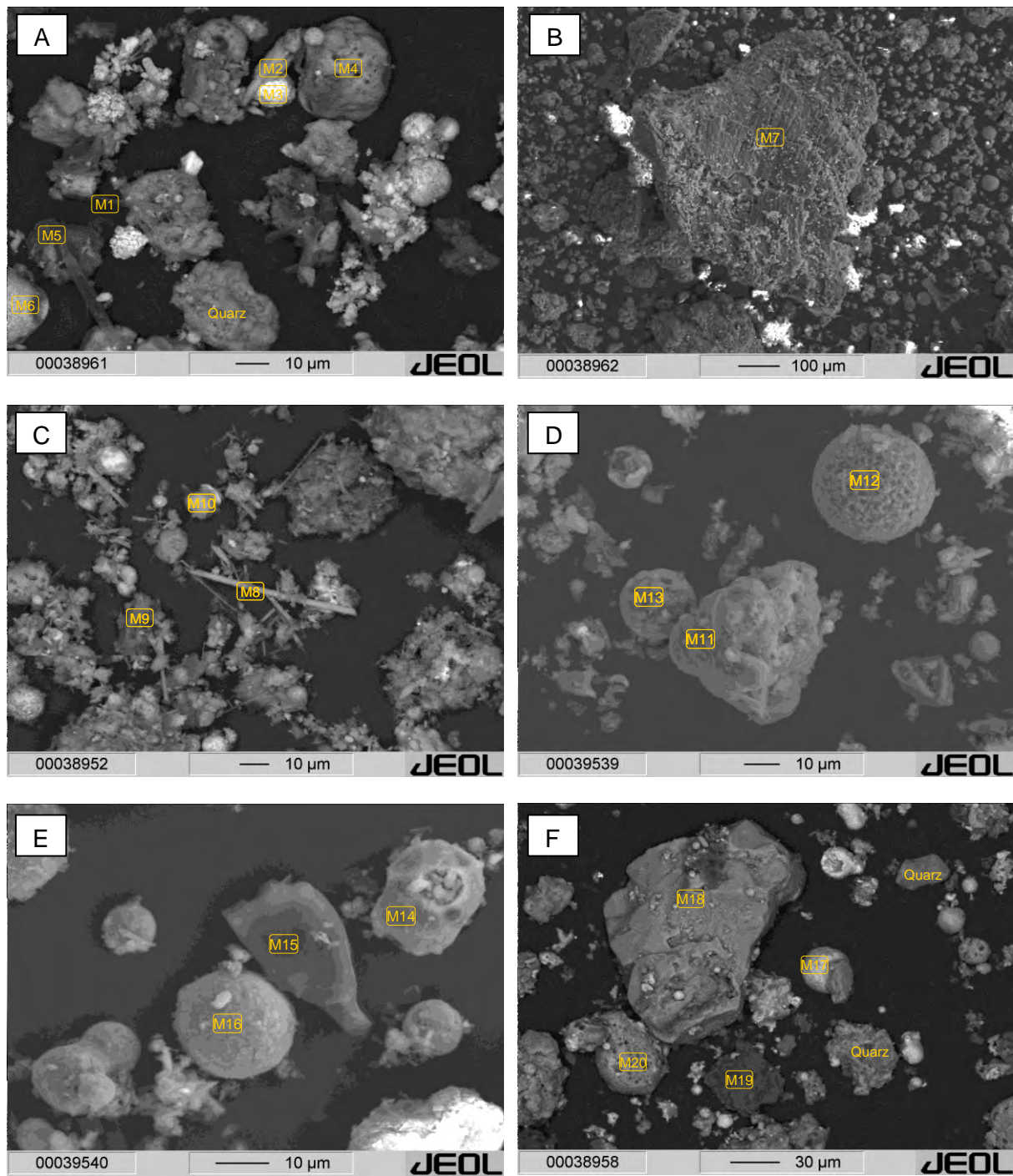


Figure 91 (A – F). Scanning electron micrographs of deposited lignite-ash particles (Sample BGH-290408-P0). Squares mark the areas where EDX microprobe analyses were taken (for element identification cf. appendix B, Table B.36)

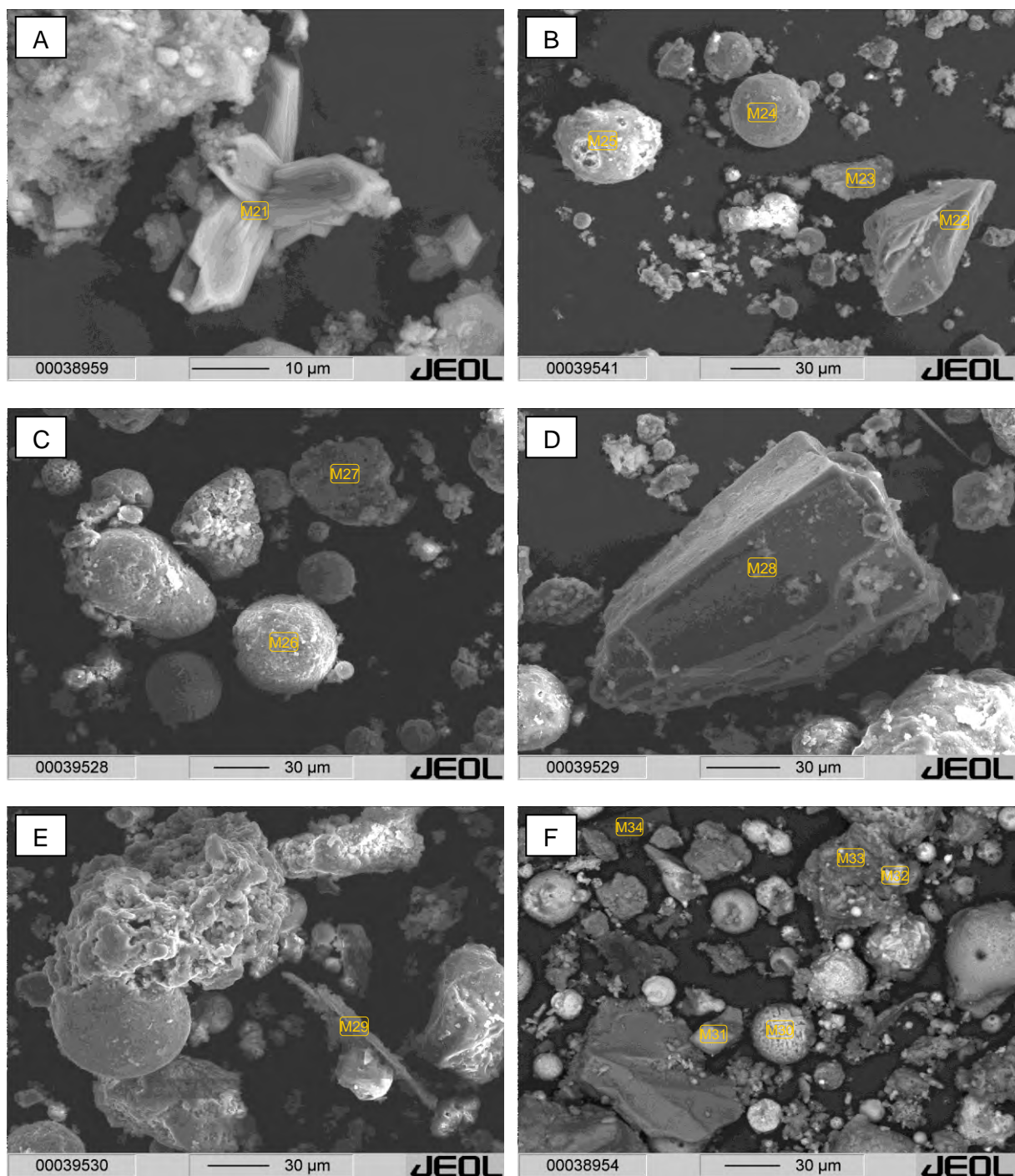


Figure 92 (A – F). Scanning electron micrographs of deposited lignite-ash particles (Sample BGH-290408-P0). Squares mark the areas where EDX microprobe analyses were taken (for element identification cf. Appendix B, Table B.36)

Results and discussion

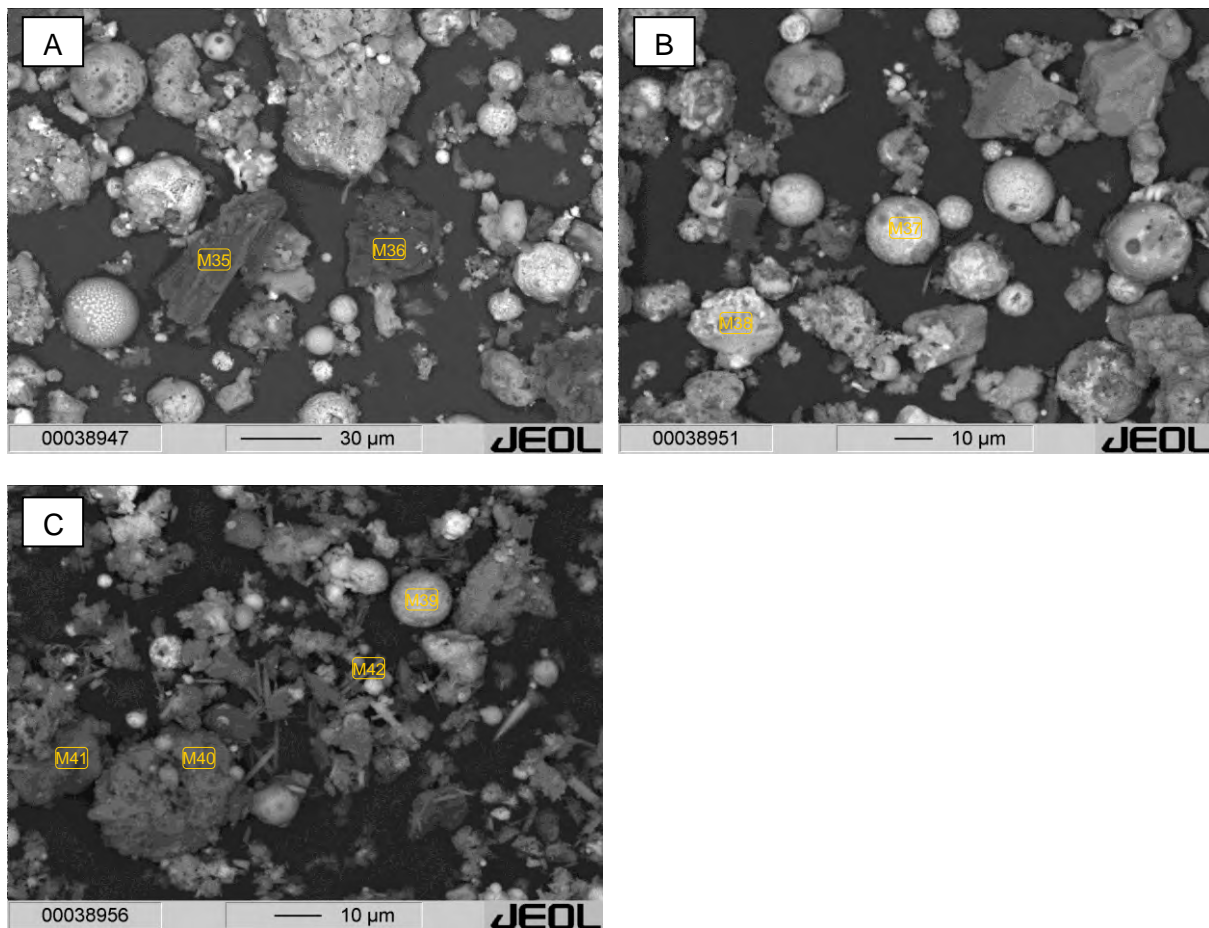


Figure 93 (A – C). Scanning electron micrographs of deposited lignite-ash particles (Sample BGH-290408-P0). Squares mark the areas of which EDX microprobe analyses were taken (for element identification cf. Appendix B, Table B.36)

The following a short description of SEM-EDX graphs of samples before CO₂ treatment was given:

Figure 91

A: BSE-picture (depth 0 – 0.20 m) - M1: Si- and Fe-rich phase, M2: CaCO₃, M3: Fe₂O₃, M4: Si-, Al- and Fe-rich phase, M5: Ca- and Fe-rich phase, M6: Fe- and Si-rich phase

B: SE-picture (depth 0 – 0.20 m) - M7: Fe-, Ca- and S-rich phase

C: BSE-picture (depth 1 – 1.20 m) - M8: ettringite, M9: Ca- and Fe-rich phase, M10: Fe-, Ca- and Si-rich phase

D: SE-picture (depth 1.20 – 1.40 m) - M11: Si-, Al- and Fe-rich phase, M12: Fe₂O₃, M13: Fe-, Ca- and Si-rich phase

E: SE-picture (depth 1.20 – 1.40 m) - M14: SiO₂, M15: Ca-, Fe- and S-rich phase, M16: Fe₂O₃

F: BSE-picture (depth 2.05 – 2.25 m) - M17: Fe- and Ca-rich phase, M18: K-feldspar, M19: thaumasite, M20: illite

Figure 92

- A:** SE-picture (depth 2.05 – 2.25 m) - M21: CaCO₃
- B:** SE-picture (depth 2.45 – 2.65 m) - M22: SiO₂, M23: Si- and Al-rich Phase, M24: Ca-, Fe-, Si- and Al-rich phase, M25: Fe-, Ca- and Si-rich phase
- C:** SE-picture (depth 2.65 – 2.85 m) - M26: Fe-, Ca- and Si-rich phase, M27: Fe- and Si-rich phase
- D:** SE-picture (depth 2.65 – 2.85 m) - M28: SiO₂
- E:** SE-picture (depth 2.65 – 2.85 m) - M29: K-feldspar
- F:** BSE-picture (depth 3 – 3.10 m) - M30: Ca₂Fe₂O₅, M31: Si-, Fe- and Ca-rich phase, M32: Fe₂O₃, M33: Fe- and Si-rich phase, M34: thaumasite

Figure 93

- A:** BSE-picture (depth 4.05 – 4.25 m) - M35: Ca-, Fe- and Si-rich phase, M36: Ca-, Si- and Fe-rich phase)
- B:** BSE-picture (depth 4.05 – 4.25 m) - M37: Ca₂Fe₂O₅, M38: Ca-, Fe- and Si-rich phase
- C:** BSE-picture (depth 5 – 5.05 m) - M39: Ca₂Fe₂O₅, M40: Ca-, Si- and Al-rich phase, M41: Ca- and Fe-rich phase, M42: Ca- and Fe-rich phase

After CO₂ treatment changes in the morphology of fly ash particles were not recognizable. Fly ash particles can be distributed in particles with smooth surface, and particles with structured surfaces (see Figure 94 A, E). Smooth particles seemed to be smaller than structured the ones. The occurrence of quartz particles in the fly ash sediment was shown. Figure 94 F).

Results and discussion

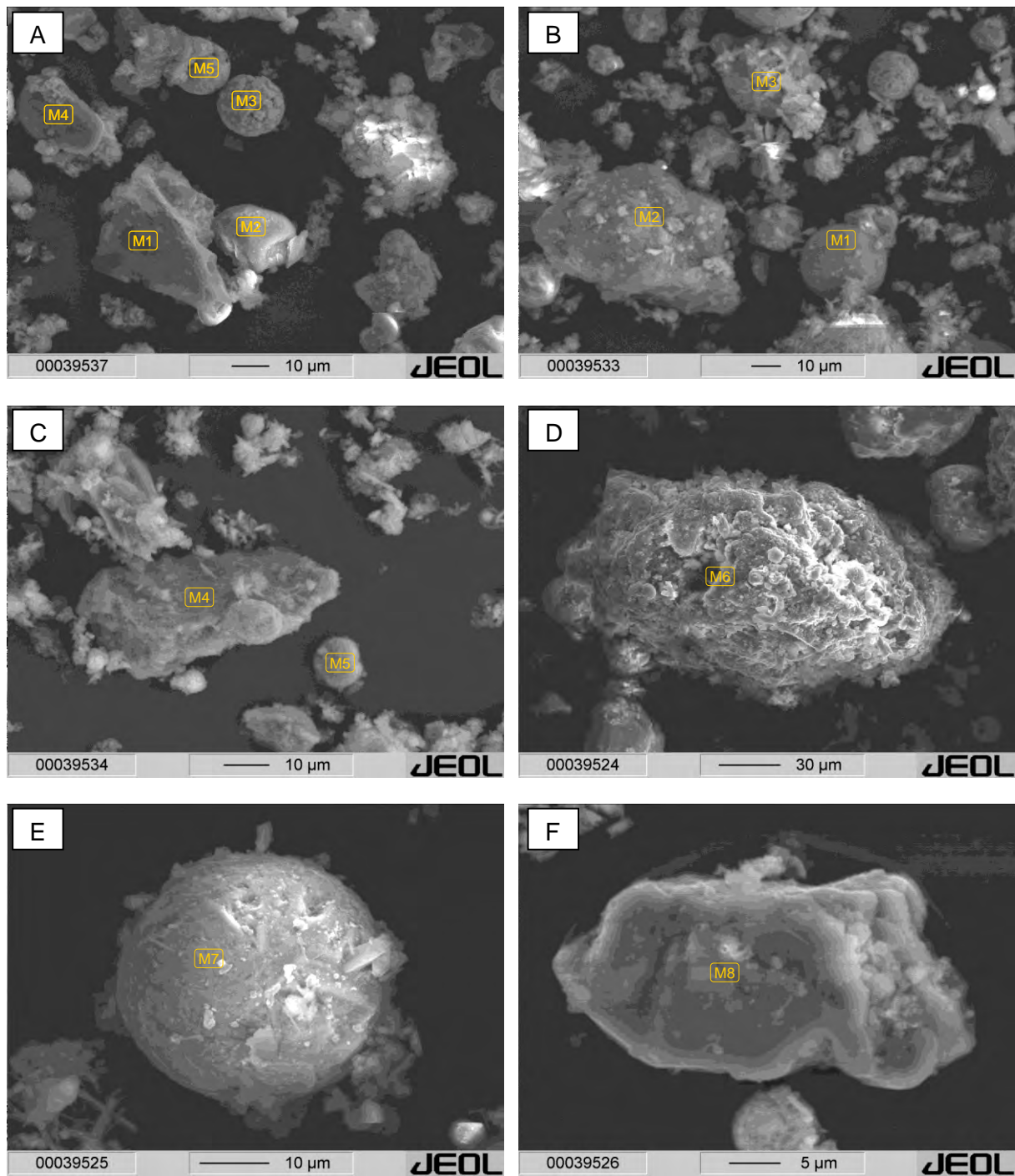


Figure 94 (A – F). Scanning electron micrographs of deposited lignite-ash particles ((A) - Sample BGH-300708-P1; (B – F) – Sample BGH-310708-P3). Squares mark the areas where EDX microprobe analyses were performed (for element identification cf. appendix B, Table B.37).

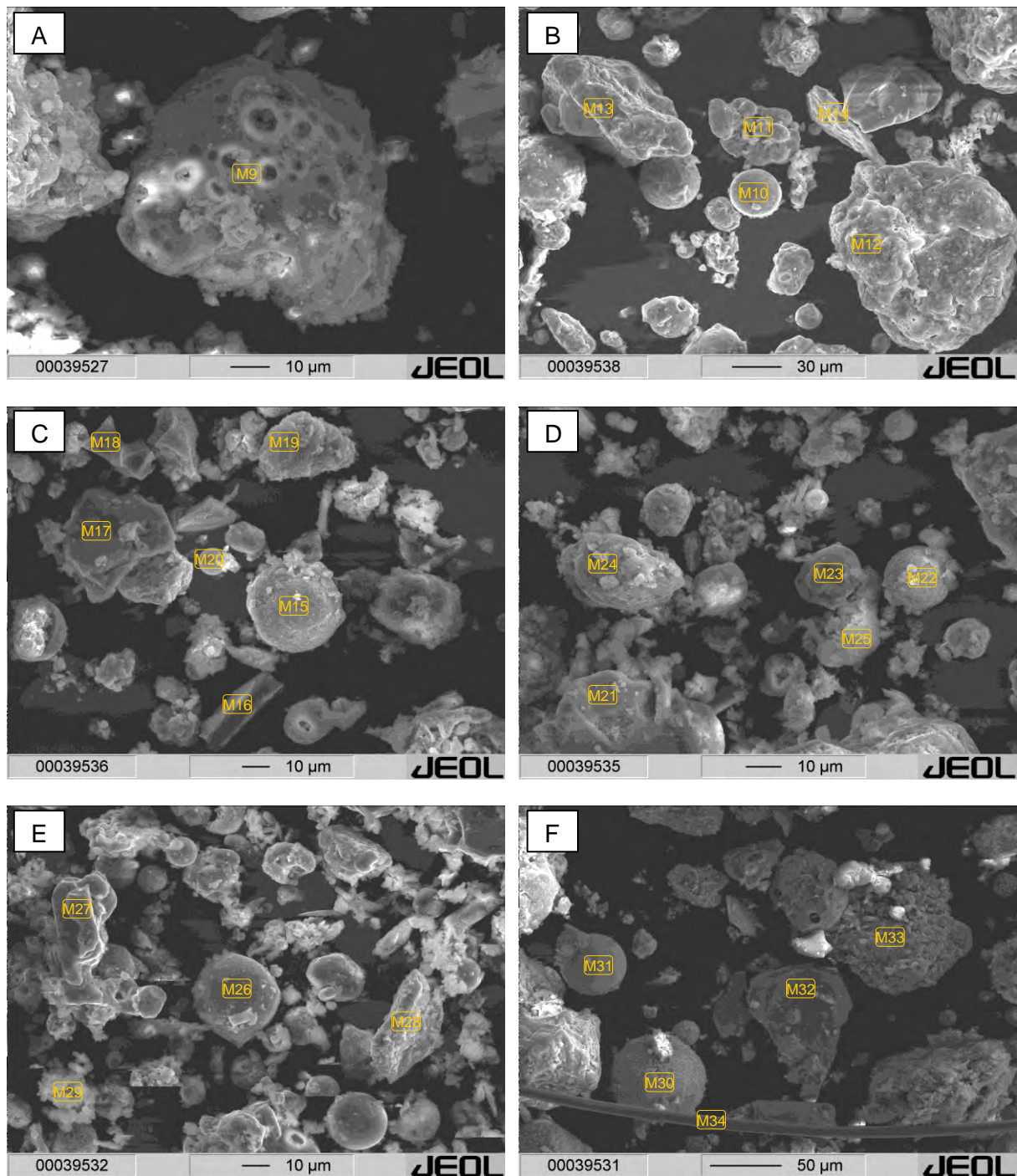


Figure 95 (A – F). Scanning electron micrographs of deposited lignite-ash particles ((B – F) – Sample BGH-310708-P3). Squares mark the areas where EDX microprobe analyses were taken (for element identification cf. appendix B, Table B.37)

Figure 94

A: SE-image (depth 3.40 – 3.57 m) - M1: Ca-, Fe- and Si-rich particles, M2: SiO₂, M3: Fe- and Ca-rich particles, M4: SiO₂, M5: Si-, Fe- und Ca-rich particles

B: SE-image (depth 0.95 – 1.20 m) - M1: Si-, Ca- and Fe-rich particles, M2: Si- and Al-rich particles, M3: Ca- and Si-rich particles

C: SE-image (depth 0.95 – 1.20 m) - M4: SiO₂, M5: Ca- and Fe-rich particles

Results and discussion

D: SE-image (depth 1.20 – 1.40 m) - M6: Si- and Al-rich particles

E: SE-image (depth 1.20 – 1.40 m) - M7: Fe- and Ca-rich particles

F: SE-image (depth 1.20 – 1.40 m) - M8: quartz

Figure 95

A: SE- image (depth 1.20 – 1.40 m) - M9: Si- and Al-rich particles

B: SE-image (depth 3.20 – 3.30 m) - M10: Ca- and Fe containing particle, M11: Fe- and Ca-rich particle, M12: Si- and Al-rich particle, M13: SiO₂, M14: Fe- and Si-rich particle

C: SE- image (depth 3.40 – 3.66) - M15: Ca- and Fe-rich particles, M16: carbon, M17: SiO₂, M18: carbon, M19: Si-, Fe- and Al-rich particle, M20: Si-, Fe- and Al-rich particle

D: SE- image (depth 4.88 – 5.08 m) - M21: SiO₂, M22: Fe-, Ca- and Si-rich particle, M23: Fe-, Si- and Al-rich particle, M24: Si- and Al-rich particle, M25: Fe- and Si-rich particle

E: SE- image (depth 6.20 – 6.40 m) - M26: Si-, Ca- and Fe-containing particle, M27: Ca-, Si- and Fe-containing particle, M28: SiO₂, M29: Ca-, Fe- and Si-containing particle

F: SE- image (depth 7.36 – 7.60 m) - M30: Fe₂O₃, M31: Ca-, Si- and Fe-rich particle, M32: SiO₂, M33: Si- and Al-containing particle, M34: carbon

SEM data before and after CO₂ injection indicates the intermixing of Fe, Ca and Al-Si mineral phases. These results are in agreement with current literature data (Kutchko and Kim, 2006, Münch, 1996, Tishmack and Burns, 2004, EPRI - Electric Power Research Institute & Southern Company Services, 2006, Vassilev and Vassileva, 2007, Vassilev and Vassileva, 2005, Vassilev and Vassileva, 1996). SEM images from fly ash often show hollow cenospheres and irregular shaped unburned carbon particles (M34). As determined by EDS, the predominant elements in Burghammer fly ash sediment were: silicon, aluminum, iron, calcium, and oxygen, in various compounds. Aluminum seems to be associated with silicon. Less amounts of sodium, potassium, titanium, and sulfur were observed. As is typically described in the literature (Kutchko and Kim, 2006), many of the existing spheres consisted of iron oxide mixed with amorphous alumino-silicates. Calcium seems to be associated with iron rich particles and alumino-silicate minerals (e.g. imogolite and allophane). Crystalline minerals containing calcium were rare in sediment samples; thus, the main calcium content is ascribable to the amorphous phase.

Significant effects on sediment after CO₂ treatment were not determined.

Thinsection investigation

Microscopy

Thinsections of fly ash were examined under parallel (Ilpol) and crossed polarized (xpol) light. The excerpts are often photographed in parallel and crossed polarized images in order to better detect within which amorphous or opaque substance the quartz or carbonate minerals can be found. Additional panorama images were shot (xpol) in order to illustrate the general constituents of fly ash.

Figure 96 A shows a micrograph of a thinsection of sample BGH-290408-P0, depth 1.20 – 1.40 m. In parallel polarized light mainly opaque substances (Figure 96 I), ash agglomerates (Figure 96 C), wood fragments (Figure 96 I) and iron –rich ash spheres (Figure 96 G) are visible. Panoramic images show that fly ash consists mainly of quartz fragments of different sizes, with a maximum grain diameter of 500 microns. White, grey and dark gray minerals in Figure 96 A can be recognized as quartz. Feldspars (alkali feldspars) can also be identified under polarized light. Microcline ($KAlSi_3O_8$) was identified (arrow in (D)). Figure 97 (F) indicate the existence of alkali feldspar at a depth of 1.20 – 1.40 m (BGH-290408-P0).

Figure 97 (G) represents an overview of a thinsection from sample BGH-290408 in a depth of 2.45 – 2.65 m. The matrix of ash agglomerates consisted mainly of quartz fragments with grain sizes up to 100 microns in diameter (B + C). Quartz and iron-containing minerals (hematite, magnetite), with brown to red colors, can be identified. (H) and (I) show opaque substances, probably wood fragments.

Microscopical investigations after CO_2 treatment show little difference with those from before CO_2 treatment. The micrographs confirm that fly ash mainly consists of quartz fragments, red to red-brown iron minerals (hematite) and opaque substances. An overview photograph (A) shows the thinsection of sample BGH-300708-P1 (3.40 – 3.57 m): quartz and iron containing minerals (brown to red colored) can be identified. Figure 98 (B) and (C) represent the occurrence of carbonates (carbonate enrichment) within opaque structures.

Sample BGH-300708-P3 is shown in Figure 99 (A) and (B) presenting spherical constituents that are typical for fly ash samples. (C) and (D) refer to incomplete burning processes, either wood or coal fragments were found in various ash sediment samples. Opaque and iron-containing ash spheres were identified (E, F) (sample BGH-300708-P3, 3.20 – 3.30 m).

Results and discussion

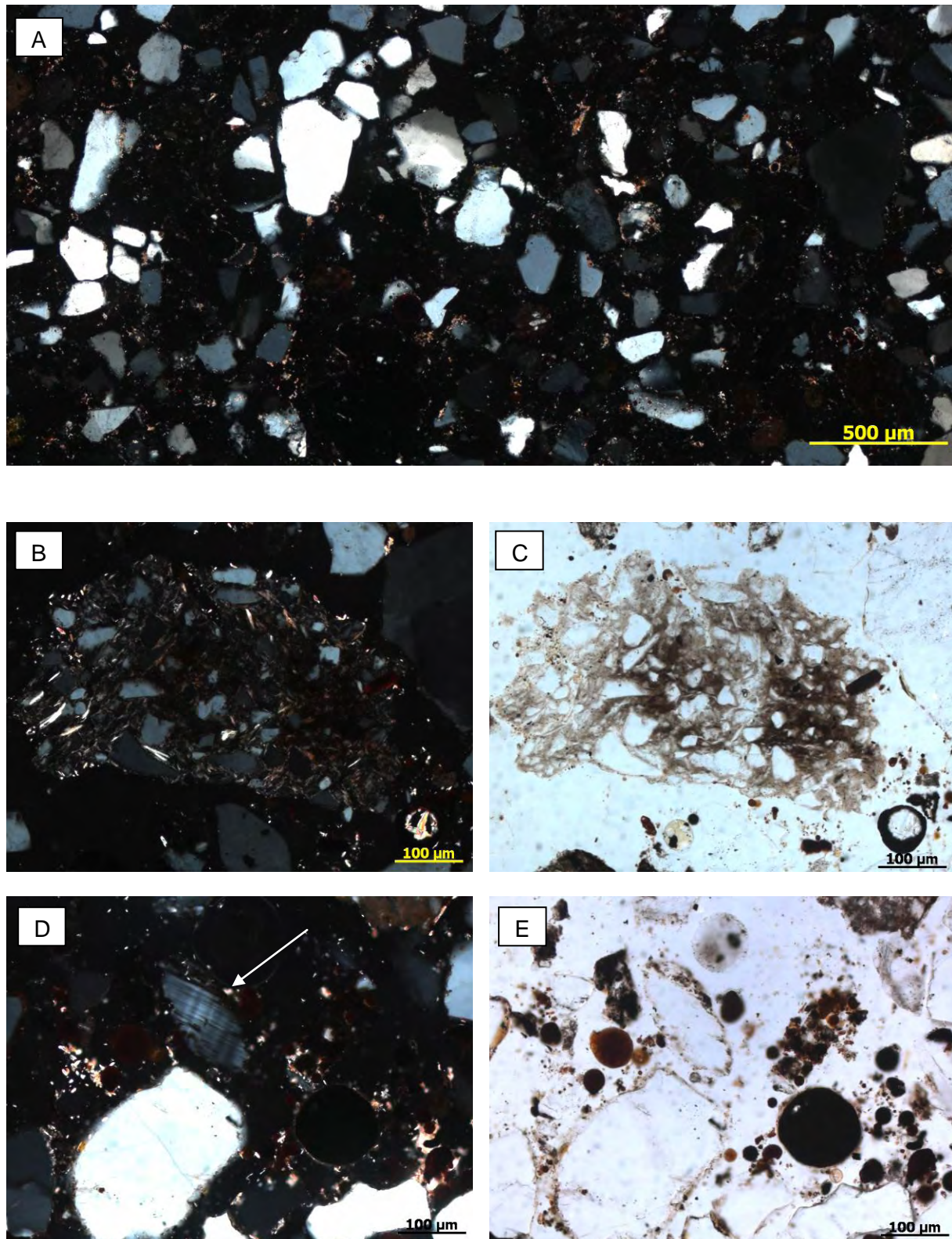


Figure 96. Image made by polarization microscopy (left: xPol, right: IIPol). Sample BGH-290408-P0

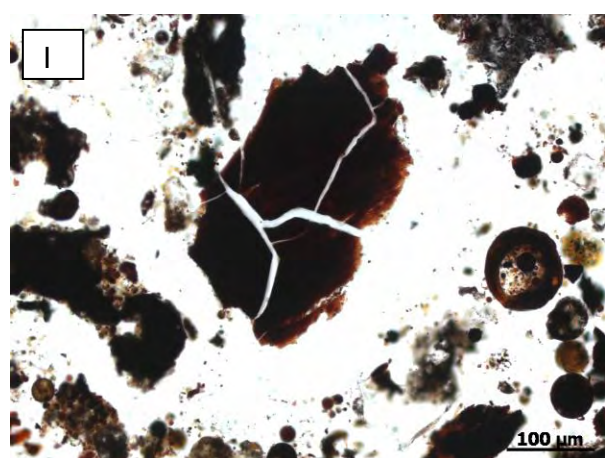
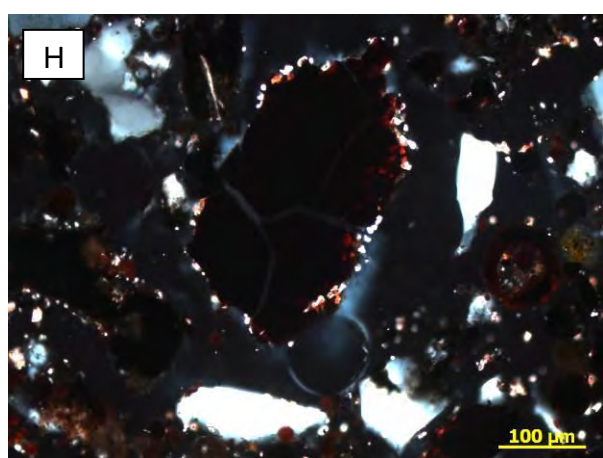
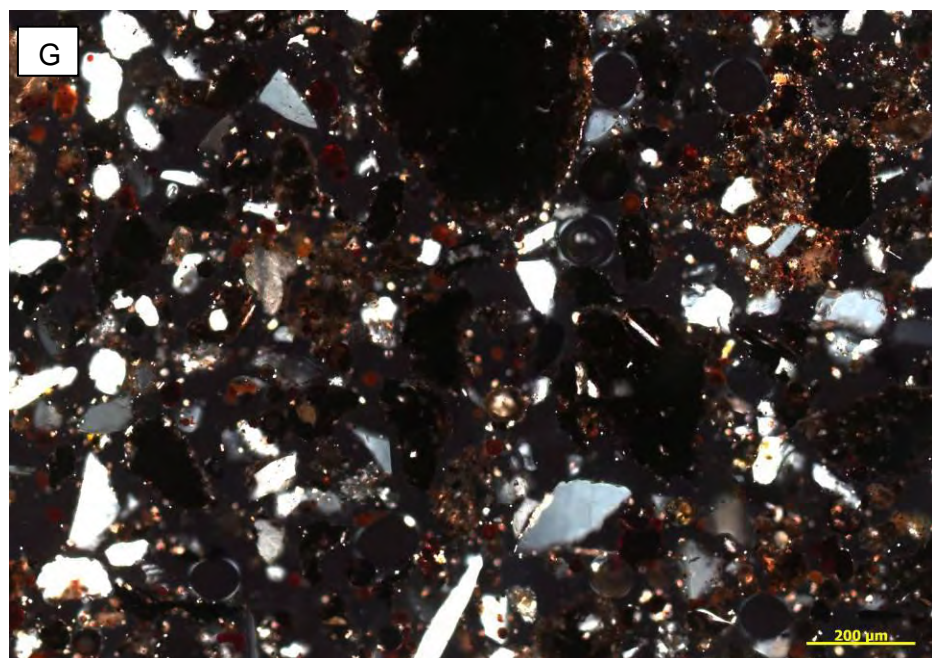
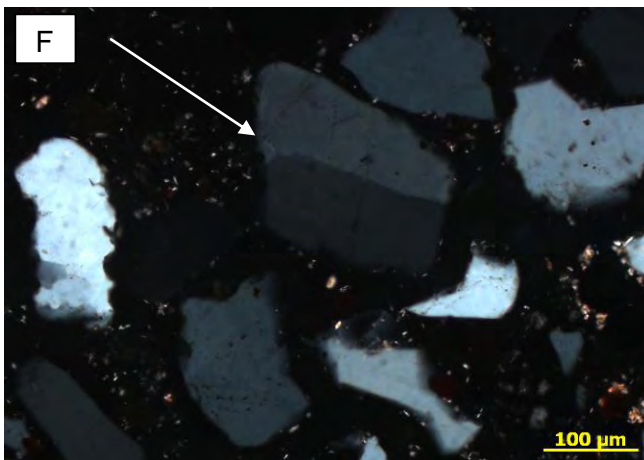


Figure 97. Image made by polarization microscopy (left: xPol, right: IIpol). Sample BGH-290408-P0

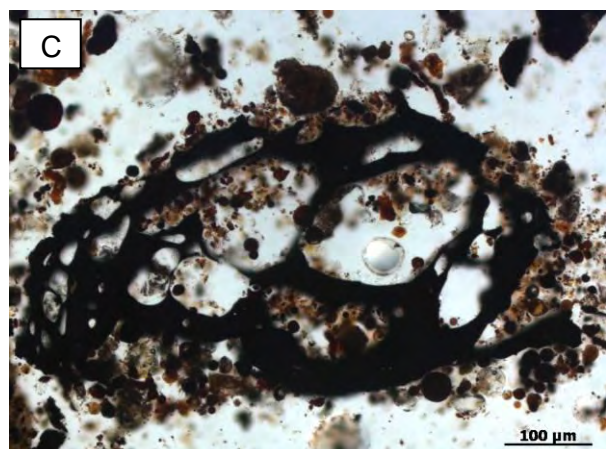
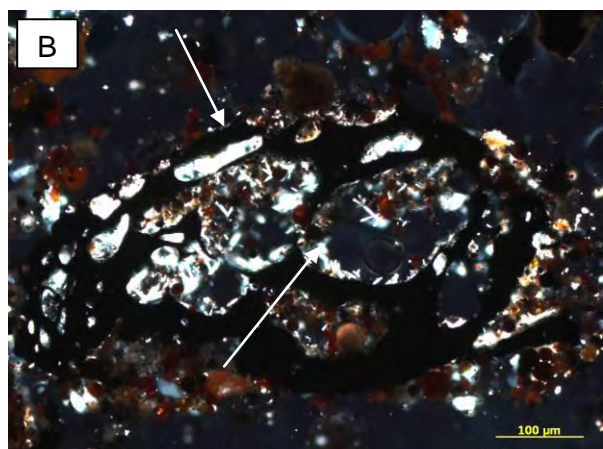
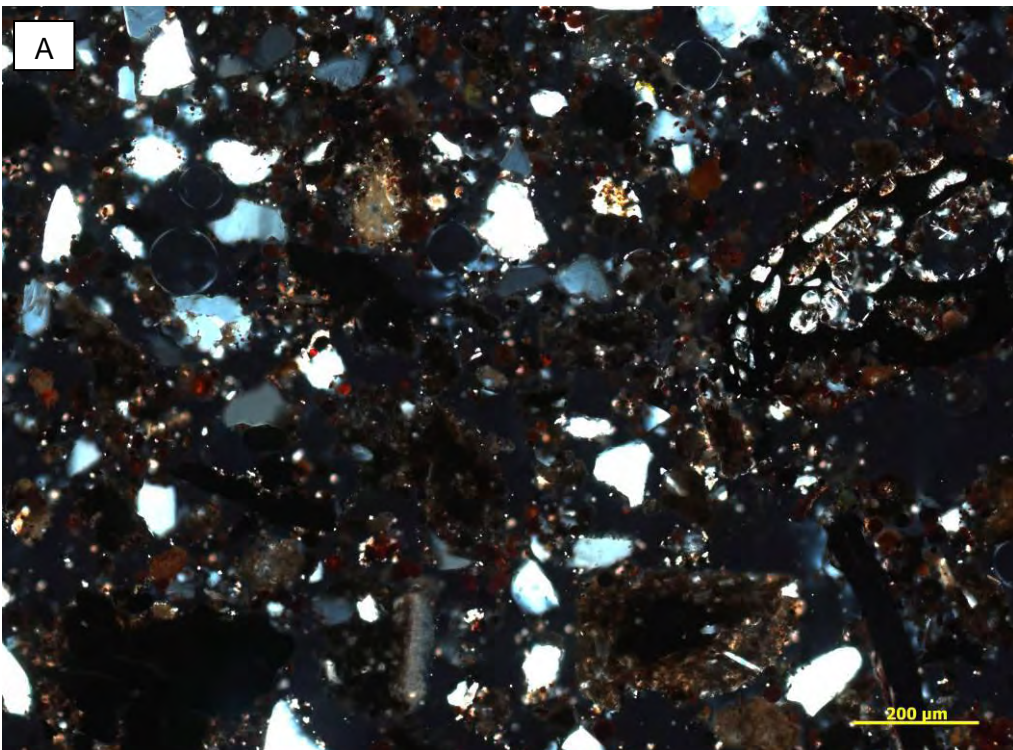


Figure 98. Image made by polarization microscopy (left: xPol, right: IIPol). Sample BGH-300708-P1

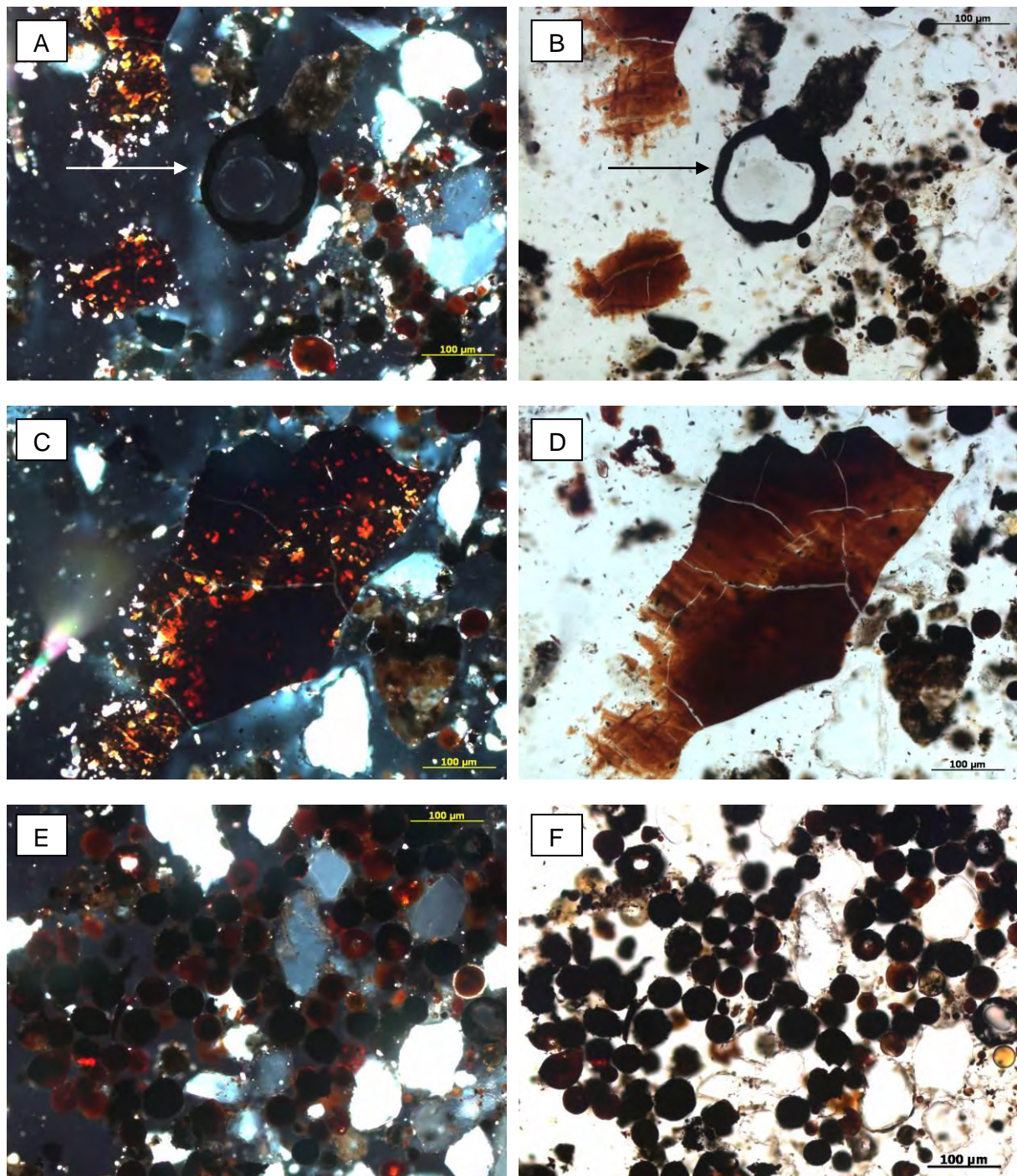


Figure 99. Optical micrographs made by polarization microscopy (left: xPol, right: IIpol). Sample BGH-300708-P3

Cathodoluminescence

Different fly ash components were determined, due to their characteristical luminescence, using cathodoluminescence microscopy.

As can be seen in Figure 100 sample BGH-290408-P2 (before CO₂ treatment), consisted mainly of quartz (qz), whereas the quartz formed out of magmatic rocks is characterized by blue-violet luminescence (Figure 100 C). Quartz developed from metamorphic rocks was distinguished by showing brown luminescence (Figure 100 A). However, mostly opaque, non-luminescent particles existed consisting mainly of Fe₂O₃, SiO₂ and Al₂O₃ (Figure 100 C, D, E, F) (Münch, 1996). Alkali feldspars (fsp) usually have a very light purple to almost white (in case of irradiation) luminescence (Figure 100 A, C, E). No plagioclase was found before the CO₂ injection in the ash sediments.

Orange to red luminescent colors indicated calcium-containing particles (Figure 100 A, C, E). In particular, the Ca/Fe ratio in particles acts as luminescence-determining factor. The higher the share of Fe, the weaker is the occurrence of luminescence of carbonates (Münch, 1996). Carbonate particles were found in a grain size from 10 to 100 microns in diameter.

On contrary to XRD where no significant changes in the qualitative composition of the fly ash sediments were detectable significant differences can be seen by cathodoluminescence before or after the CO₂ treatment (Figure 101 and Figure 102). Sporadic quartz and feldspars were seen as well (Figure 101 A and Figure 102 E).

As mentioned in section 5.2 (with respect to TIC contents), an average increase of 0.5 wt.-% CaCO₃ was observed during CO₂ treatment of the ash sediment. After CO₂ treatment large accumulations of carbonates were found by means of cathodoluminescence in the ash sediments. Comparing the formation of carbonates before and after CO₂ treatment it was observed that carbonates before CO₂ injection occur in the form of isolated carbonate grains (Figure 100 E) and after CO₂ injection the formation of orange to reddish luminescent carbonates were visible as large and massive structures within opaque (partially amorphous) ash agglomerates (Figure 101 A-F and Figure 102 A-F). The different structure likely indicates the new formation of carbonates. The uncertainty regarding carbonate formation can be rationalized by considering the not yet published CL photographs, where new formation of carbonates in fly ash was described. The diameter of ash agglomerates was up to 1 mm, where these ash structures were mostly filled with newly formed carbonates.

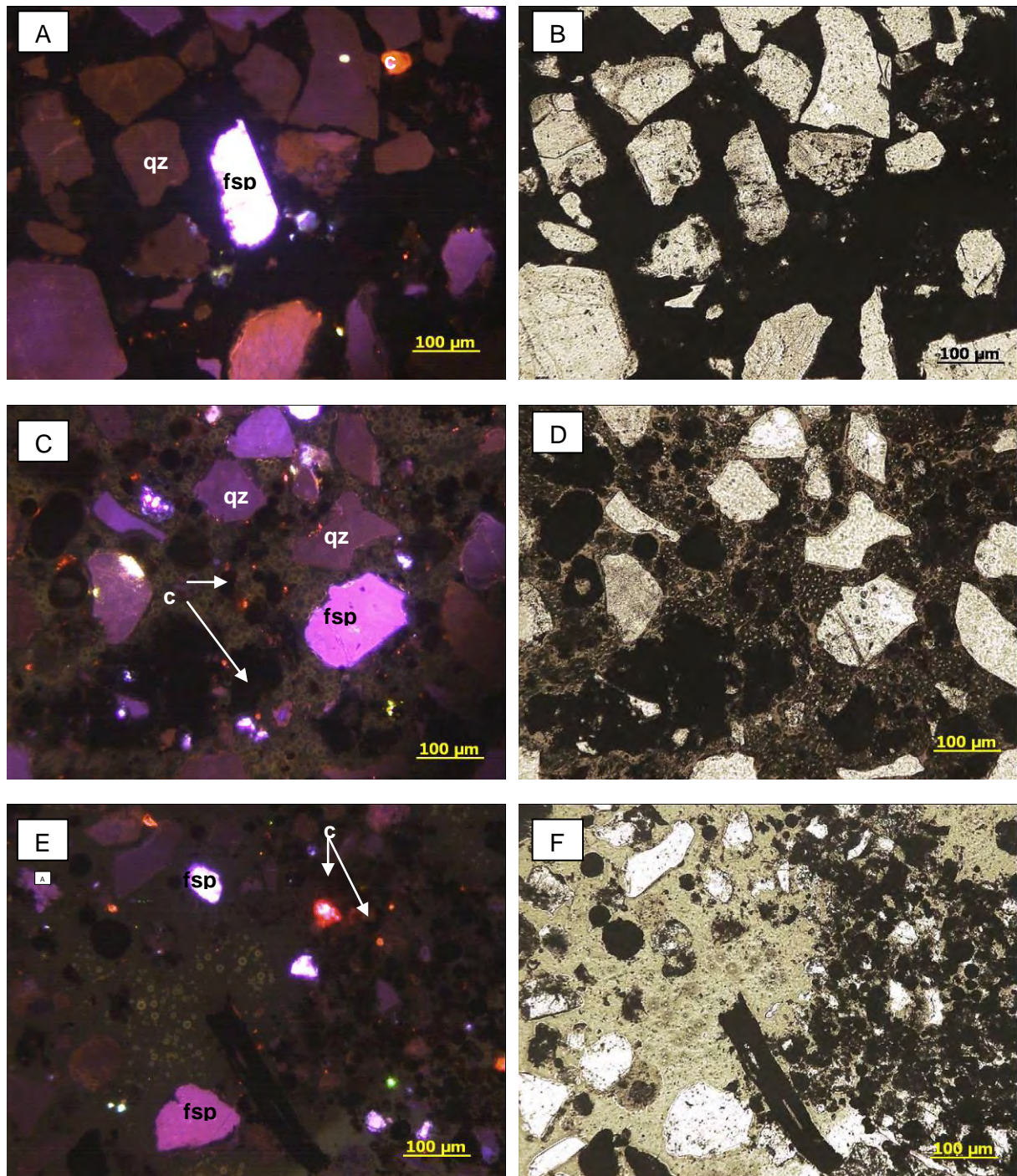


Figure 100 (A – F). Cathodoluminescence (left) and transmission microscopy photographs. Sample BGH-290408-P0 (qz = quarz, fsp = alkali feldspar, c = carbonate)

Results and discussion

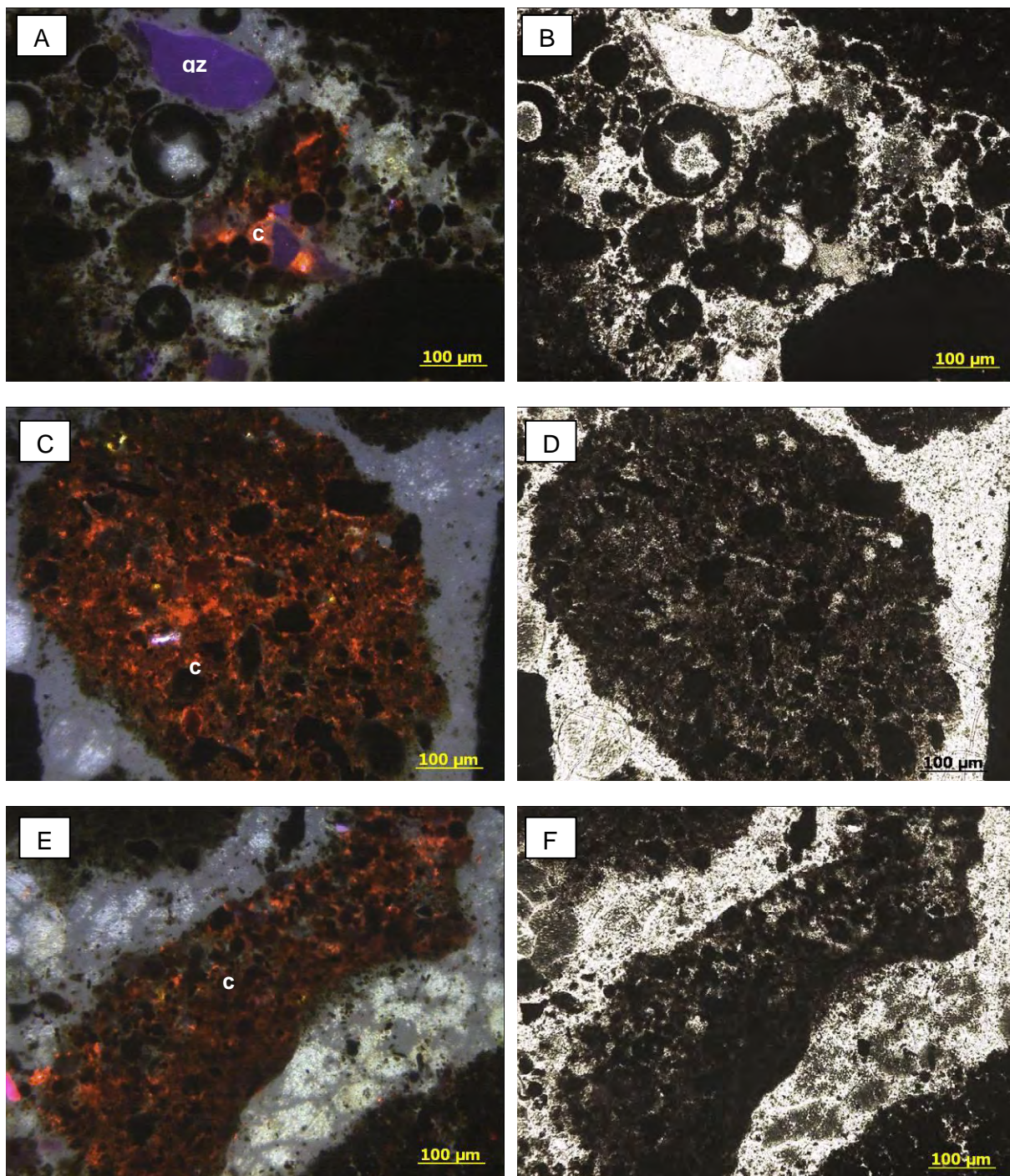


Figure 101 (A – F). Cathodoluminescense (left) and transmission microscopy photographs. Sample BGH-300708-P1 and BGH-310708-P3 (qz = quarz, fsp = alkali feldspar, c = carbonate).

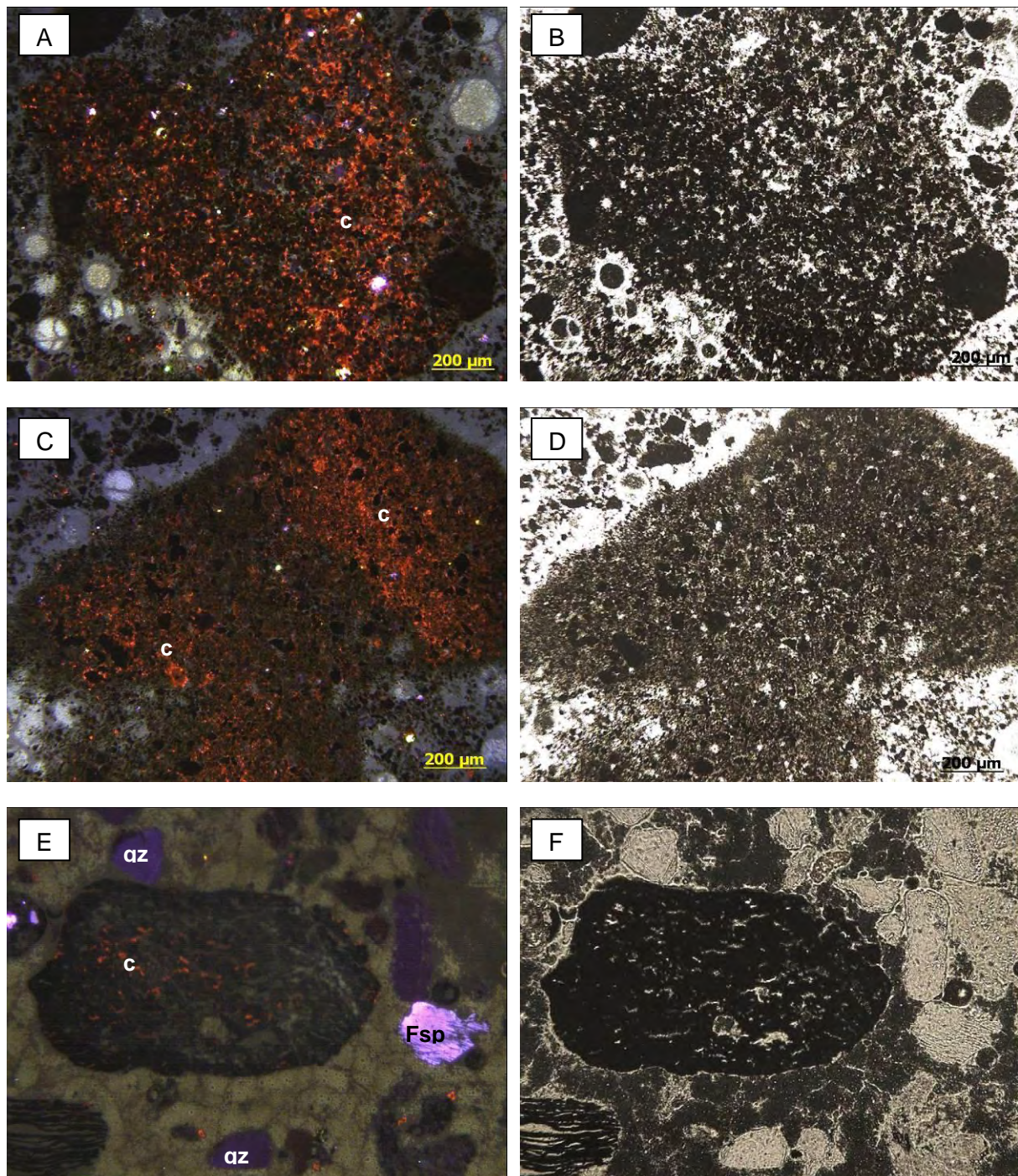


Figure 102 (A – F). Cathodoluminescense (left) and transmission microscopy photographs. Sample BGH-310708-P3 (qz = quarz, fsp = alkali feldspar, c = carbonate).

4.6 Results of Advanced Mobile Inlake Technology within the treatment scheme of Lake Burghammer

In 2009 the following factors forced a neutralization of lake Burghammer in a timely manner: Due to high groundwater levels and, hence, problems with wet basements in the villages near lake Burghammer the owner of lake Burghammer (LMBV – Lausitzer and Mitteldeutsche Braunkohleverwaltungsgesellschaft mbH) was forced to start discharging water in the river Kleine Spree. Additionally the groundwater had low pH-values and high sulfate contents that are aggressive against basements of buildings etc. (Betonaggressivität). Hence, a high need for action existed.

The following data were provided by Rheinkalk GmbH and MOVAB-D GmbH. This chapter will summarize the main results of the liming campaign.

According to theoretical considerations based on primary investigations, modeling and laboratory experiments, a total amount of 36 million m³ lake water with an acidity of 140 Mio. Molq had to be treated within the initial neutralization. Under consideration of a purity of 90% for educts and a neutralization efficiency of 70% the following amounts of liming products were planned: 10,260 t KSM Beroun and 3,200 t Ca(OH)₂. In total, 74 days were planned. For follow-up treatment an amount of Ca(OH)₂ of 4 x 1,000 t (4 x 10 days) was planned for 2009/2010.

Table 35. Temporal course and amounts of liming agents

Type of treatment		Amount of Liming agent
Initial neutralization	03/20 – 06/05/2009	11.010 t CaCO ₃
Initial neutralization	06/12 - 06/26/2009	1.123 t Ca(OH) ₂
1. follow-up treatment	08/28 – 09/10/2009	682 t Ca(OH) ₂
2. follow-up treatment	11/27 – 12/05/2010	363 t Ca(OH) ₂
3. follow-up treatment	03/30 – 04/10/2010	708 t Ca(OH) ₂
4. follow-up treatment	06/30 – 07/08/2010	483 t Ca(OH) ₂
5. follow-up treatment	09/07 – 09/14/2010	427 t Ca(OH) ₂
6. follow-up treatment	12/01 – 12/14/2010	447 t Ca(OH) ₂

The initial neutralization of the lake Burghammer was carried out between 20th of March and 26th of June 2009 (Table 35). About 11,010 tons of limestone and 1.123 tons of Ca(OH)₂ were distributed on the lake with a medium sized special boat rented from Br. Allerts, Sweden. A total of 58 days for initial treatment was required.

The application of the KSM Beroun at the beginning of the initial neutralization was done in areas with large water depth, and thus, larger volume and high acidity potential/area. So a high efficiency was guaranteed, as well as the precipitation of iron hydroxide sludge in larger depths of the lake. With this strategy an immoderate impact on the shore zone was avoided (König and Scholz, 2010). Another advantage of the initial treatment of areas with larger depth was the high kinetic of KSM Beroun in the pH range of 3 – 4 (see experimental results, chapter 4.3 and 4.4). With reaching a pH > 4.0, a more laminar application of the liming

products was applied in order to ensure also a high efficiency in shallow areas of the lake. With reaching a pH > 4.5, the second treatment stage (product change to Ca(OH)₂) started.

The follow-up treatment was done by Ca(OH)₂. A total amount of 3,100 t in 51 days was needed. For technical details, please see (König and Scholz, 2010).

The distribution of the liming products is strongly influenced by wind and lake-internal currents. In total 23 measuring points (MP X 1 – 20, MP Y 1 – 3) had been used to measure in-situ parameters (pH, electrical conductivity, redox potential, O₂ content, turbidity). Within few hours after the application, a rather uniform distribution within the lake body was observed. It can be assumed that the complete lake volume was available as reaction zone. Only in-situ parameters had been used to model the distribution and the efficiency of the liming campaign in Lake Burghammer (see chapter 5.4).

Figure 103 represents pH and alkalinity during the treatment of Lake Burghammer. It can be seen that during the initial neutralization pH increases more rapidly after reaching pH 4 (combined with precipitation processes of dissolved iron – data not shown - and decreasing alkalinity). The rapid decrease of pH due to acidic, iron-containing groundwater (see chapter 2.3.1) required follow-up treatments as shown in Table 35. Additionally in September 2010 flooding water from the river Kleine Spree prevented a fast decrease of pH and improved water quality as sulfate contents decreased from about 1050 ppm to 930 ppm due to dilution (König and Scholz, 2010).

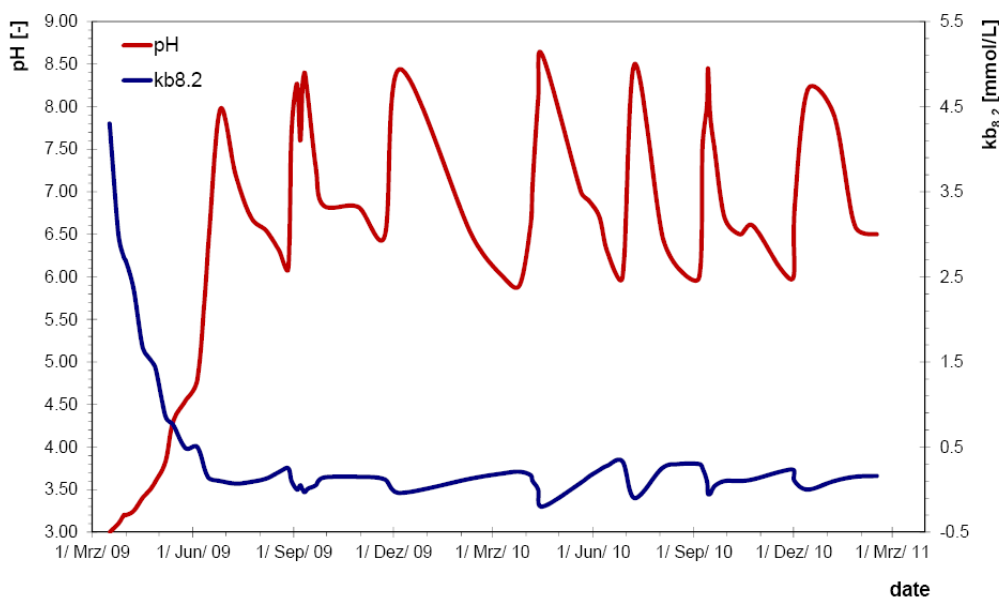


Figure 103. Course of in-situ parameters pH and alkalinity during the water treatment in lake Burghammer.

König and Scholz (2010) reported an efficiency of 65.5% for KSM Beroun and 67.4% for Ca(OH)₂ during the initial neutralization. The follow-up treatments with Ca(OH)₂ reached efficiencies > 90% for Ca(OH)₂.

The pH was increased from ca. 3 up to 8 and metals like iron and aluminum were precipitated. A buffer against re-acidification of $k_{s4.3} = 0.4 \text{ mmol/L}$ was reached.

The monthly net flow of acid into the lake is roughly 3 million moleq H⁺. For as long as the acid groundwater flow remains a follow-up treatment has to be performed every 2 – 6 months to maintain the adjusted water quality.

According to König and Scholz (2010) it can be summarized:

- Large and very acid mining lakes can be treated by mobile inlake technology providing high efficiencies in combination with little time requirement. There is no other technology available to achieve the same results in a comparable time frame.
- The multi-stage neutralization and combination of KSM Beroun in an acid pH range (pH 3 – 5), as well as Ca(OH)₂ in acid up to alkaline area (pH 5 - >7) is feasible, ecological and economical.
- The used Swedish vessels were able to applicate up to 100 t Ca(OH)₂ and 250 t calcite per 8 hours. Even extremely weather conditions (temperatures down to -15 °C) were managed.
- An efficient follow-up treatment in Lake Burghammer by mobile inlake technique should be combined with the usage of flooding water from the river Kleine Spree.

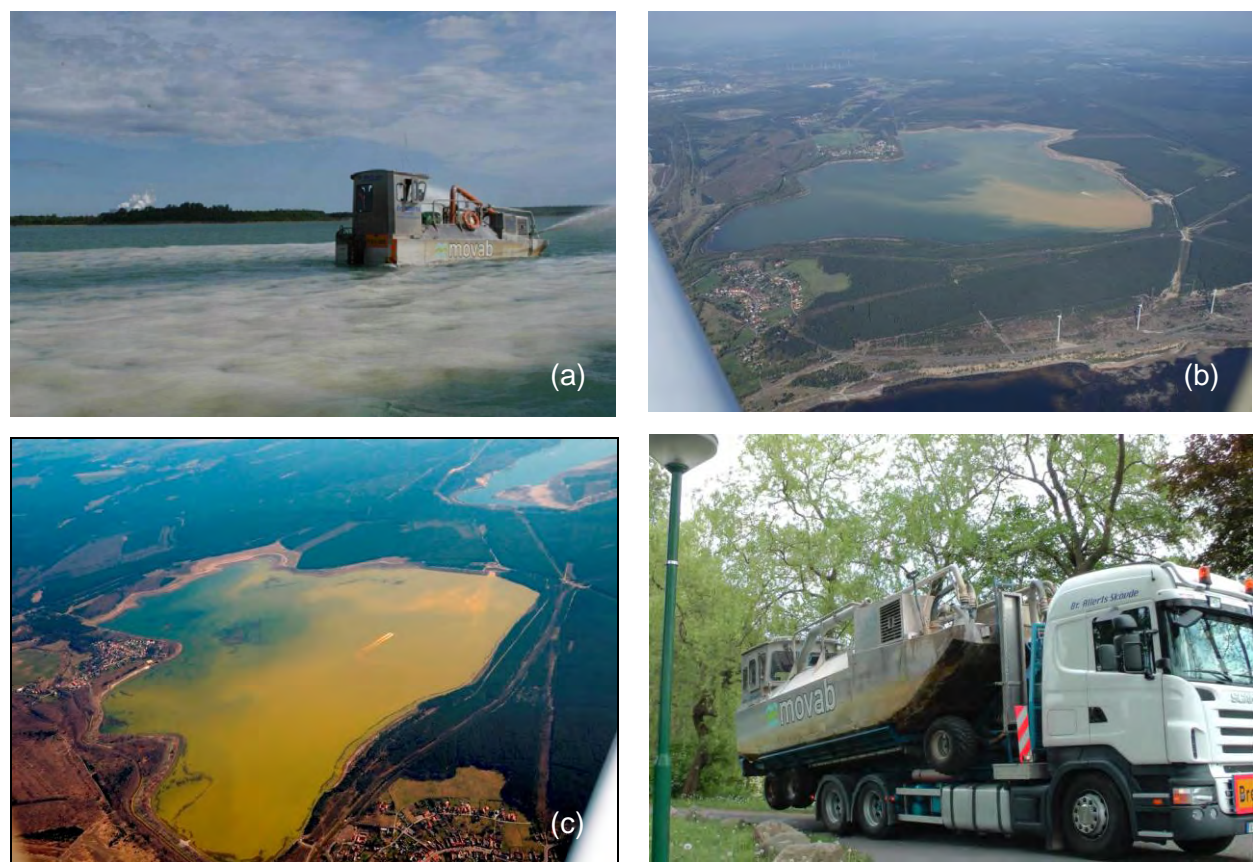


Figure 104. (a) Swedish treatment ship during application of Ca(OH)₂ in Lake Burghammer. (b) Aerial view of Lake Burghammer during the initial neutralization phase. (c) Visual distribution within the lake (copyright: G. Scholz, MOVAB-D GmbH). (d) Transport of the treatment ship.

5 Evaluation and modeling

5.1 Assessment of carbonate precipitation and CO₂ fixation through preliminary investigations and batch experiments

The storage capacity of the investigated mining lake is significant in determining its CO₂ sequestration potential.

In the 20- to 30-year-old fly ash deposits, an average of 1 wt.-% of reactive calcium was detected. CO₂, water and deposits from Lake Burghammer were used in the conducted batch and column experiments. As a result of the experiments, it was proven that reactive cations from fly ash deposits can be used for the second step of the treatment strategy, the carbon precipitation. Reaction times are within minutes. Therefore, it is feasible to use the process technically. The volume of the deposits in Lake Burghammer is approximately 26 Mio. m³ with a grain density of 2.65 g/cm³. If one assumes a water content of about 50% and a reactive calcium content of about 1 wt.-% (dry mass) of the sediments approximately 344,500 t of reactive calcium is available in Lake Burghammer. A mass of 378,950 t of CO₂ could be mineralized, which equals a total mass of 861,250 t precipitated calcium carbonate. For the application of a technical process, which is supposed to treat the entire lake, is reasonable to expect a time of operation of years or even decades.

This assumption is based on the available information regarding the size of the deposited sediment body as well as the batch experiments. The calculated amount of CO₂ depends on the different assumptions made concerning the properties of the ash sediments in Lake Burghammer. Uncertainties are shown in Table 36.

Table 36. Valuation of uncertainties concerning physical and chemical parameters and consequential calculated CO₂ amounts

	dimension		uncertainty	worst / best case
Amount of ash sediments (whole lake)	m ³	26,000,000	-	26,000,000
Grain density	g/cm ³	2.65	(10 %)	2.39 - 2.92
Water content	%	50	± 10 %	45 – 55
Reactive calcium content	%	1	0.5 < ... < 1.5	0.5 – 1.5
Calculated amount of reactive calcium (whole Lake)	t	344,500	-	279,630 – 626,340
Amount of mineralisable CO ₂ (whole Lake)	t	378,950	-	307,593 – 688,974
Calculated amount of precipitated CaCO ₃	t	861,250	-	699,075 – 1,565,850

The amount of ash sediment settled in Lake Burghammer is estimated to contain a volume of 26 million m³. The water content and grain density are two physical parameters that have been determined by laboratory examination.

Based on these facts there is a range of possible sequestration from nearly 300,000 t to 690,000 t of CO₂. These considerations can be supported with the results of the effected

batch experiments. With the help of the batch experiments a range of 150 – 250 mmol TIC/kg (dry substance, sediment) was estimated. This indicates a possible 6.6 – 11 g CO₂ per kg sediment that can be mineralized. In regards to the entire ash body, an estimated CO₂ sequestration potential range is 184,556 – 459,316 t. This approach is assumed to be “conservative”.

5.2 Assessment of carbonate precipitation and CO₂ fixation through the pilot experiment

5.2.1 Hydrochemical modeling

Chemical analysis data of the pore water samples were used as input (Table B.32 B.35, appendix B) to estimate the activities of the aqueous species. The cation / anion balance before CO₂ treatment ranged from -44.5 % to +0.94 % (mean -12.39 %, n = 18), respectively from -7.56 % to 18.97 % (after CO₂ treatment, n = 49, mean +1.03 %). Unbalanced analysis can be reasoned by missing values for e.g. pH, total inorganic carbon due to less sample amount of pore water.

For SI = 0, there is an equilibrium between the mineral and the solution; SI < 0 reflects under-saturation, and SI > 0 super-saturation. For a state of under-saturation dissolution of the solid phase is expected, super-saturation suggests precipitation.

The calculated SI (see Table 37) indicated that gypsum (CaSO₄•2H₂O) and calcite (CaCO₃) were in equilibrium with the pore water. All samples were undersaturated with respect to ettringite (Ca₆Al₂(SO₄)₃(OH)₁₂•26H₂O) and magnesite (MgCO₃).

Simulations indicated that hematite (Fe₂O₃), magnesioferrite (MgFe₂O₄), several Fe/Al-(hydr)oxides (Fe(OH)₃, Fe(OH)_{2.7}Cl₃) and Boehmite AlO(OH)) could all precipitate in leachates.

Table 37. Calculated saturation indices for selected mineral phases before CO₂ treatment

		Average	Median	Maximum	Minimum
Calcite	CaCO ₃	+ 0.11	+ 0.14	+ 0.75	-0.95
Ferrite, magnesian	MgFe ₂ ³⁺ O ₄	+ 7.86	+ 8.20	+ 10.96	+ 4.10
Hematite	Fe ₂ O ₃	+ 14.87	+ 14.85	+ 15.99	+ 13.03
Ettringite	Ca ₆ Al ₂ (SO ₄) ₃ (OH) ₁₂ •26H ₂ O	- 18.93	- 19.59	-13.16	- 21.96
Manganite	MnO(OH)	- 5.34	- 5.70	-1.75	- 7.35
Amorphous iron hydroxide	Fe(OH) ₃	+ 1.84	+ 1.83	+ 2.397	+ 0.937
	Fe(OH) _{2.7} Cl ₃	+ 6.62	+ 6.78	+ 7.13	+ 5.93
Gypsum	CaSO ₄ •2H ₂ O	- 0.18	- 0.21	+ 0.33	- 0.41
Rhodochrosite	MnCO ₃	- 1.97	- 1.96	- 0.35	- 3.00
Anhydrite	CaSO ₄	- 0.43	- 0.46	+ 0.08	- 0.66
Aragonite	CaCO ₃	- 0.07	- 0.04	+ 0.57	- 1.13
Siderite	FeCO ₃	- 2.62	- 2.20	- 1.82	- 5.43
Boehmite	AlO(OH)	+ 1.50	+ 1.34	+ 2.54	+ 0.58
Magnesite	MgCO ₃	-2.20	-2.11	-1.09	-3.95

Figure 105 shows calcite's calculated saturation indices in dependence on sediment depth before CO₂ treatment. Calcite was calculated to be in equilibrium with pore water (SI = + 0.11). Figure 105 shows that pore water in the fly ash offers a great variability with respect to the SI for calcite. This might be due heterogeneities in the ash body or it can be an artifact with respect to the sampling and the sample treatment. The median was 0.14 and thus slightly oversaturated.

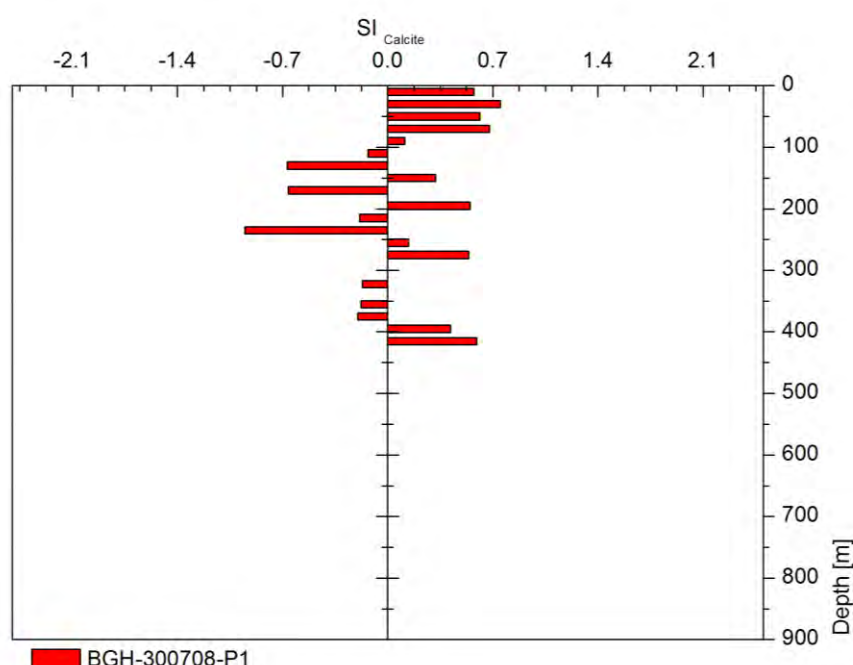
**Figure 105. Calculated saturation indices for calcite (before CO₂ treatment)**

Table 38 shows calculated saturation indices for selected mineral phases after CO₂ treatment. Thermodynamic calculations indicate that after the reaction with CO₂ various pore water samples were super-saturated with respect to calcite. Saturation indices of calcite were in the range of – 0.83 to +1.25; the median of all samples was calculated with + 0.31. These results correlate with measured pH (see above). In comparison to the situation before treatment began, an increase of the median from + 0.14 to + 0.31 is visible, which can be interpreted as a clear effect of CO₂ exposure (the supersaturation was increased and thus the trend and likeliness of calcite formation). For rhodochrosite, the median of SI was increasing from -1.96 to -0.95, for aragonite from -0.04 to + 0.13, and for magnesite from - 2.11 to -1.01. Although rhodochrosite and magnesite are almost equivalent following CO₂ treatment, with undersaturated values, the same trend of greater saturation is evident.

Regarding other minerals no significant changes in the averaged SI could be found: Calculated saturation indices indicated that iron-containing phases magnesioferrite (MgFe₂O₄), hematite (Fe₂O₃), several Fe/Al-(hydr)oxides (Fe(OH)₃, Fe(OH)_{2.7}Cl₃), and Boehmite AlO(OH)) are strongly super-saturated and could precipitate in all leachates. The range of saturation indices is shown in Table 38.

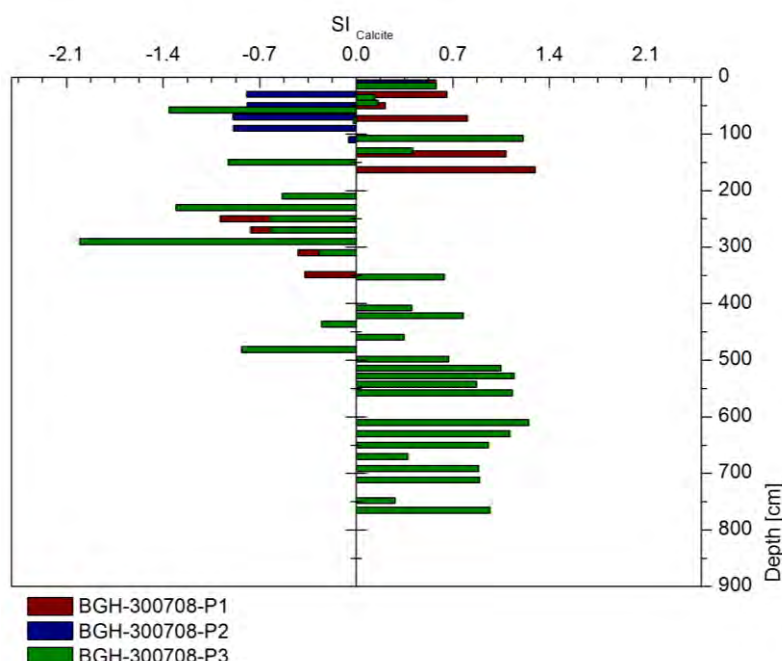
Ettringite (Ca₆Al₂(SO₄)₃(OH)₁₂•26H₂O) was undersaturated in all pore water samples. Besides the saturation index for calcite, other carbonates were considered during thermodynamic modeling. Rhodochrosite (MnCO₃), Siderite (FeCO₃) and Magnesite (MgCO₃) were all calculated to be undersaturated in most of the pore water samples.

Decreased saturation indices of gypsum were calculated after CO₂ treatment of the sediment.

Figure 106 shows calculated saturation indices of calcite's dependence on sediment depth in the drilling cores BGH-300708-P1 / P2 and P3. A stratification of layers where undersaturation or saturation was calculated is visible. Comparing the results of the thermodynamic calculations with determined TIC and XRD investigations showed the conformance of all methods. Figure 106 shows significant oversaturation indices at the depths from 500 to 800 cm; thus, close to the CO₂ injection depth of 12 m. For the depth range from 400 cm to the surface no such clear trend can be seen.

Table 38. Calculated saturation indices for selected mineral phases after CO₂ treatment

		Average	Median	Maximum	Minimum
Calcite	CaCO ₃	+ 0.12	+ 0.31	+ 1.25	- 0.83
Ferrite, magnesian	MgFe ₂ ³⁺ O ₄	+ 8.45	+ 8.72	+ 10.89	+ 6.46
Hematite	Fe ₂ O ₃	+ 14.90	+ 15.12	+ 15.87	+ 13.40
Ettringite	Ca ₆ Al ₂ (SO ₄) ₃ (OH) ₁₂ •26H ₂ O	- 19.68	- 20.48	- 17.00	- 22.94
Manganite	MnO(OH)	-4.77	- 4.88	- 3.35	- 7.24
Amorphous iron hydroxide	Fe(OH) ₃	+ 1.85	+ 1.95	+ 2.34	+ 1.10
	Fe(OH) _{2.7} Cl ₃	+ 6.65	+ 6.79	+ 7.14	+ 6.24
Gypsum	CaSO ₄ •2H ₂ O	- 0.29	- 0.25	+ 0.06	- 0.58
Rhodochrosite	MnCO ₃	- 1.30	- 0.95	- 0.01	- 3.09
Anhydrite	CaSO ₄	- 0.54	- 0.50	- 0.18	- 0.83
Aragonite	CaCO ₃	- 0.07	+ 0.13	+ 1.07	- 1.01
Siderite	FeCO ₃	- 2.61	- 2.11	- 1.19	- 2.41
Boehmite	AlO(OH)	+ 1.27	+ 1.26	+ 2.16	+ 0.09
Magnesite	MgCO ₃	-1.49	- 1.01	+ 0.34	- 2.13

**Figure 106. Calculated saturation indices for calcite (after CO₂ treatment)**

5.2.2 Calculation and Visualisation

The mineralized CO₂ can be calculated from the difference in solid TIC-content before and after the experiment. The results are summarized in Table 39; the results of all samples can be found in Table B.30 and Table B.31, appendix B. Calcite levels were calculated on the

basis of determined TIC-contents on the assumption that all TIC is available as CaCO_3 . To compare, XRD results were considered.

Variations in calcite, as well as TIC contents, before and after CO_2 treatment were calculated by the following equation:

$$\Delta_{\text{CaCO}_3} = \text{CaCO}_3 - \text{conc}_{\text{afterCO}_2}[\text{wt.}\%] - \text{average CaCO}_3 - \text{conc}_{\text{afterCO}_2}[\text{wt.}\%] \quad (5-1)$$

Whereby CaCO_3 -content before CO_2 -treatment was on average 1.50 wt.-%.

Approximately 0.5 wt.-% Calcite was precipitated; this equals 2.2 g of CO_2 per kilogramm of treated ash, which could be mineralized within the field experiment. The maximum rate for carbonate precipitation was determined with +7.4 wt.-% Calcite, according to 32.6 g CO_2 per kilogramm of treated ash.

Investigations of Cathodoluminescence verified the precipitation of calcite in treated ash sediment samples.

Table 39. Precipitated amounts of total carbon (TC), total inorganic carbon (TIC), Calcite during field experiment

	Before CO_2	After CO_2
TC/NPOC [g/kg]	202.7255	159.14823
Min TC/NPOC [g/kg]	32.86	17.13
Max TC/NPOC [g/kg]	453.1	127.45
IC [g/kg]	1.79978	2.31297
Min IC [g/kg]	0.2665	0.3221
Max IC [g/kg]	7.09	1.76
Calcite * [wt.-%]	1.49982	1.92747
Min Calcite * [wt.-%]	0.22208	0.26842
Max Calcite * [wt.-%]	5.90833	8.9333
Average delta Calcite * [wt.-%]	-	+0.42747
Min delta Calcite * [wt.-%]	-	-1.23158
Max delta Calcite * [wt.-%]	-	+7.43333

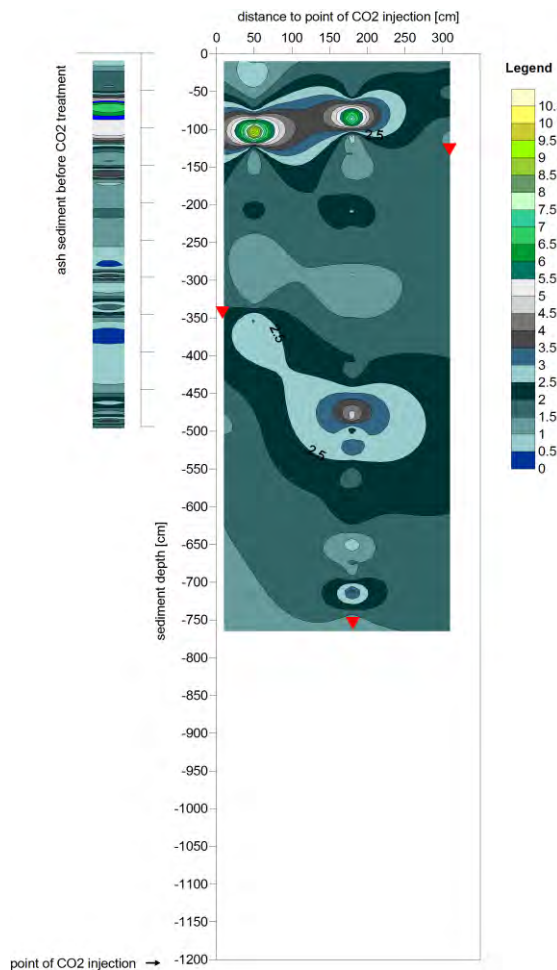


Figure 107. Distribution of TIC in dependency of sediment depth and distance to point of injection. Interpolation method: Kriging, linear (slope = 1, anisotropy = 1, angle = 0)

Figure 107 shows the distribution of TIC's dependence on sediment depth and distance to the point of CO₂ injection. The small graph in the left of the picture visualizes TIC content before the CO₂ injection. As mentioned in Table 39, TIC content was on average 1.79 g/kg. Maximum contents were determined in the upper meter of the sediment core at 7.09 g/kg.

After CO₂ injection, a stratification of zones with lower and higher TIC content was visible. On average, a content of 2.31 g/kg was detected. Figure 108 shows the calcite distribution in the area of CO₂ injections. Values were calculated on the basis of TIC content.

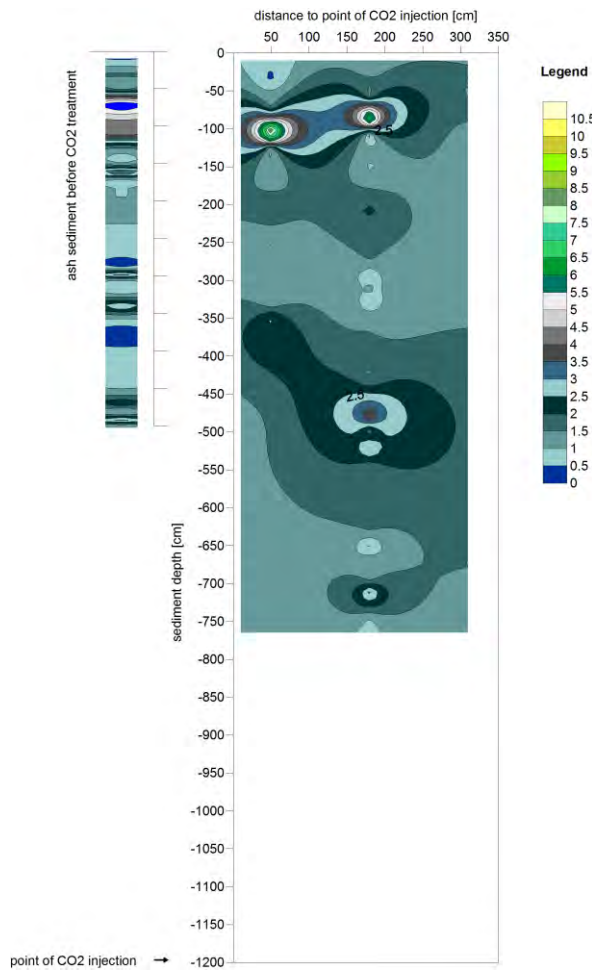


Figure 108. Calcite distribution based on calculations of TIC in dependency of sediment depth and distance to point of injection. Interpolation method: Kriging, linear (slope = 1, anisotropy = 1, angle = 0)

Figure 109 emphasizes the resulting variations in calcite. Red colour describes areas where calcite dissolution occurred.

Gray colour symbolizes equilibrium conditions or areas where calcite content did not change significantly. Besides, overlapping reactions of calcite dissolution and precipitation, gray colour areas may also be caused by interpolation method (insufficient precision of TIC determination). These areas may be unconfident. One also has to consider the different depths of the drilling cores and due to the interpolation method used, areas outside of the data range are extrapolated. Green to brown areas show areas where calcite precipitation occurred during the pilot experiment. It can be noticed clearly that within the sediment body, some areas are more permeable than others. Calcite precipitation seems to occur in preferential channels.

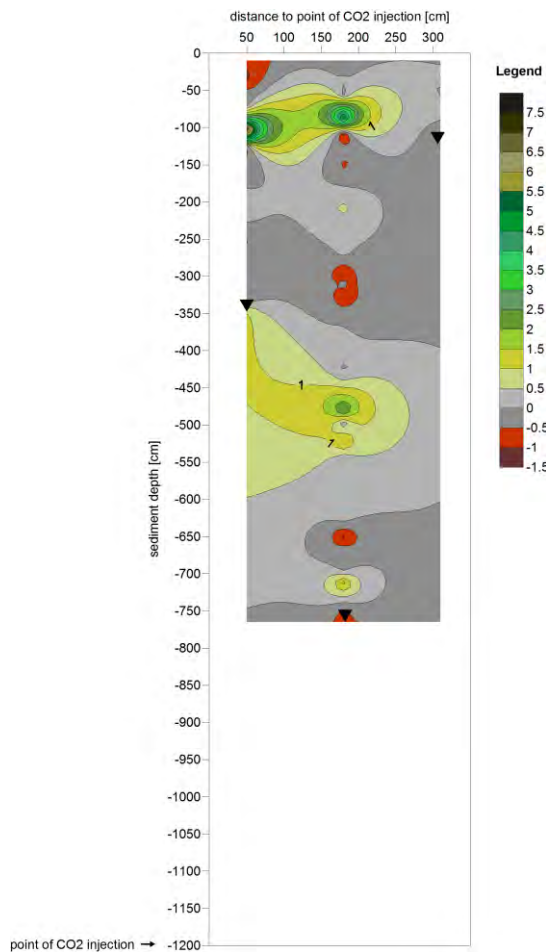


Figure 109. Variation in Calcite contents after CO₂ treatment. Interpolation method: Kriging, linear (slope = 1, anisotropy = 1, angle = 0)

Unfortunately, there were technical problems in the end of the pilot experiment. Due to that fact only 3 drilling cores were taken to describe changes in geochemistry and mineralogy. Based on the field experiment results, an extrapolation of the total CO₂ mineralization for Lake Burghammer is shown in Table 40.

Table 40. Calculation of theoretical captured CO₂ amounts and precipitated CaCO₃ based on the results of the field experiment

dimension	worst / best case	Average
Amount of ash sediments (whole Lake)	m ³	26,000,000
Grain density	g/cm ³	2.65
Water content	%	50
Delta Calcite [wt.-%]	%	1 - 1.23 / + 7.4
Calculated amount of precipitated CaCO ₃	t	861,250 - 423,735 / 2,549,000
Amount of mineralisable CO ₂ (whole Lake)	t	378,950 - 186,443 / 1,121,560

^{1,2} 10 % uncertainty

Based on physical parameters (grain density and water contents), the average calcite precipitation rate was used to calculate the potential amount of CaCO_3 and CO_2 which can be precipitated, and thus sequestered, in lake Burghammer and its ash deposits.

An average of 172,250 t of calcite precipitate was calculated. In the improbable case of dissolution, about 400,000 t Calcite might be dissolve. The maximum precipitation volume was calculated to be 2,549,000 t CaCO_3 . It was recognized that both the worst and best cases are very improbable and are based only on speculations. Regarding the average calcite concentration, there will be a CO_2 mineralization of circa 76,000 t for the whole ash sediment.

It has to be considered, that the conducted pilot experiment affected only a small part of the whole ash body (Schipek and Merkel, 2009a). The uncertainties concerning the amount of ash, exact location, stratification with sandy layers (due to slide processes) and resuspension of ash sediment, should not be overlooked either.

5.3 Risk assessment of re-dissolution of precipitated carbonate due to groundwater and lake water

One of the main questions after the successful realization of the pilot experiment was whether the pH (either in lake water and pore water) could be kept at sufficiently safe levels in order to prevent re-dissolution of precipitated CaCO_3 . In particular, the role of acid rock drainage is of great concern.

The sediment in Lake Burghammer contains an enormous amount of alkaline solids. The lake water is strongly acidic, whereas pore waters are neutral or even in alkaline range. It is suggested, and field experiments lead to the conclusion, that there is no, or only minor, interaction between lake water and lake sediments. It is likely that iron hydroxide precipitation causes mineral capping within the acidic lake Burghammer which reduces the hydraulic permeability and limits lake interaction.

Grain size distributions were used to calculate the hydraulic conductivities to be between $1.1 \cdot 10^{-5}$ and $2.4 \cdot 10^{-9}$ m/s. The layers with hydraulic conductivities between $2.0 \cdot 10^{-6}$ and $2.4 \cdot 10^{-9}$ m/s were dominant.

Before carbon dioxide injection, pH was in the range of 6.8 to 8.9 and after CO_2 injection pH varied from 6.5 to 9.7. From this, it can be concluded that the risk of calcite re-dissolution is very low.

As previously mentioned, an initial neutralisation of the lake water is required. Furthermore, there are plans to use Lake Burghammer as a storage reservoir that includes management. The pH needs to be maintained above 6.5 to fulfil regulation requirements. The aim is to keep the pH above the critical threshold for a long-term perspective.

Due to the following facts, it can be stated that the general risk of calcite re-dissolution is very low:

1. Historical remediation projects (Lake Senftenberg and Lake Koschen) have failed due to the application of too coarsely grained lime which sinks to the bottom of the lake without significant reaction. This lime is still available as alkaline material at the bottom of these lakes but does not react because its' surfaces are covered by lake sediments.

2. Pore water investigations showed neutral to alkaline pH. It is believed that this has been the case for many years. No interaction between lake water and pore water was found.
3. Some preliminary experiments regarding colmation effects due to calcite precipitation were conducted. In general, hydraulic conductivity was decreased by one order of magnitude.

5.4 Lake Liming

As has been described in chapter 4.6 and in Pust et al. (2010) an extensive monitoring was done during lake treatment. Main results showed a strong influence by wind and lake-internal currents on the distribution of the liming products. A measuring net of in total 23 points and data sets of in-situ parameters had been used as basis for the modeling of the distribution within the lake body.

The following figures show an extract of gained data, the whole data set can be found as digital appendix (appendix D).

The whole data set (appendix D) comprises about 3800 figures while interpolation took place each 0.5 m starting from the surface to the lake bottom. Interpreting the modeling results, it can be assumed that the complete lake volume was available as reaction zone. A uniform distribution, especially of pH, was reached within short time (hours to days) after treatment.

Output reserves have been identified with respect to the technology applied. Important aspects regarding navigation tracks of vessels and new techniques applying pipe distribution systems for in-lake liming might be a future aspect. As described in Merkel et al. (2010) and Schipek et al. (2011) the monitoring and real-time modeling of large-scale flow- and transport processes can be essential parameters in treatment of acidic mining lakes. Lake-internal currents and movement of water masses are forced by wind. Lake-internal waves occur in the lake, influenced by temperature-dependent density stratification, the Lake Bathymetry and river banks. Additionally, inflow has an effect on local flow regime.

Further investigations show that the complex three-dimensional flow system must be implemented in a numerical model, where all relevant processes are simulated with sufficient accuracy. First test have been done with ELCOM (Estuary and Lake Computer Model), CWR – Centre for Water Research, Australia). Due to the fact that it would exceed the scale of this thesis, data is not provided here.

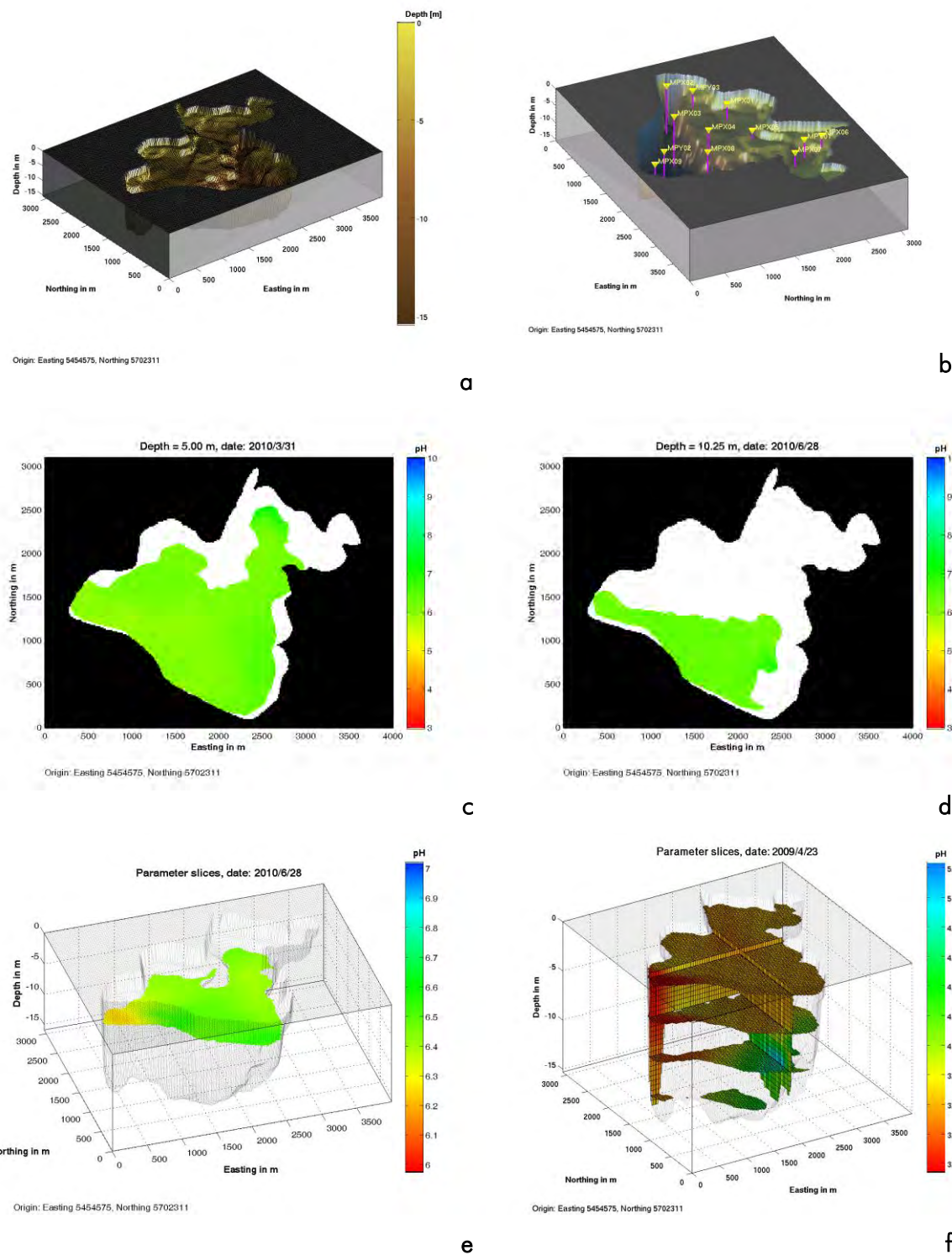


Figure 110. a – Visualization of the lake bathymetry. b – Visualization of the measuring points. c/d – Animated 2D-plots showing the distribution of specified parameters (pH, electrical conductivity, etc.) in time and depth. e – Animated 3D-slices of specified parameters (pH, electrical conductivity, etc.) in time and depth. f – 3D-slices of specified parameters (pH, electrical conductivity, etc.) in specified depths and along user-defined slices through the lake body.

6 Conclusion

Acidification of surface waters is a worldwide problem; major impact areas are rivers, lakes, estuaries, and coastal waters (Gray, 1997). AMD in the Lausitz area (Germany) originates from sulfide weathering taking place during active and inactive periods of the local lignite mining industry. Large open-pits in this district are chiefly being filled with uprising acidic groundwater. Therefore, many lakes in this area are characterized by low pH (< 3), high concentrations of sulfate and iron and a low acid neutralization capacity.

Diverse concepts exist for the remediation of acidified waters; each depending on the geochemical parameters and boundaries as well as on water type. Based on the results in lab and field experiments, as well as thermodynamic modeling, skepticisms about the feasibility of in-lake liming for treatment of acidic mining lakes could be reduced by the help of this thesis.

In-lake treatment can be done by using different neutralizing products: Soda, limestone, hydrated lime, quicklime, or even industrial by-products (e.g. fly ash, LDS). Effectiveness and economics of in-lake treatment depends on adequate alkaline products and adequate distribution. Using fresh fly ash from power plants for treatment of AMD affected waters has been published by different authors (Gitari et al., 2006, Gitari et al., 2008a, Gitari et al., 2008b, Hoffman, 2002, Koch et al., 2008, Perez-Lopez et al., 2007c). Initial aim of the investigations was to proof if "old" industrial by-products (settled fly ash) might be used to improve the water quality in areas seriously affected by lignite mining. Besides, the reactivity of settled fly ash sediments with carbon dioxide, and subsequent precipitation of calcite, was investigated.

Theoretical conclusions (modeling with PhreeqC) and experimental results showed that settled fly ash in combination with carbon dioxide can drastically enhance acidic lake water treatment and can be used to trap carbon dioxide in form of carbonates (e.g. calcite). During laboratory experiments, an increase of pH to 8.39 ± 0.55 in acidic mining lake water ($\text{pH} \sim 3$) could be achieved. Results from batch experiments showed a general decrease of trace metal concentrations with CO_2 treatment. The elements iron, manganese, cobalt, chromium, copper and zinc decreased significantly during treatment of the ash-water suspensions with CO_2 . The proposed treatment technology has no significant influence on the concentrations of mercury, wolfram, cerium, lead, lanthanum, cesium, tin, cadmium, nickel and selenium. Concentrations of these elements were determined to be below the detection limit. Some trace elements (arsenic, chromium, molybdenum, and antimony) contained in the fly ash were slightly mobilized this way. In all batch experiments, an increase of the buffering capacity ($K_{\text{S4.3}}$) could be affected. In general, for fly ash sediment, an increase of the buffering capacity to $4.18 \pm 2.51 \text{ mmol/L}$ was observed.

The predominant part of the ash sediment is composed of amorphous, presumably alumina silicate glass (spheres). Free CaO wasn't detected during mineralogical investigations. Calcium seems to be associated with iron rich particles and alumina silicate glass. Regarding CO_2 sequestration potential, batch experiments showed that settled fly ash sediments are less reactive than fresh fly ash; in average they provide a sequestration rate of 17 g CO_2 per kilogram settled ash sediment whereas 33 g CO_2 / kg fresh fly ash could be mineralized.

Results of the field experiment showed that CO_2 injection in the ash sediment body is possible, too. CO_2 was applied with a pressure of 2.2 bar and 2.2 m^3/h for a period of 3

months. Continuous lake monitoring showed no significant effect on the water quality as no initial neutralization was done before. Only within the direct periphery of the injection lances, an influence on the total inorganic carbon was witnessed. Concentrations of main cations (K^+ , Na^+ , Ca^{2+} , Mg^{2+}), as well as main anions (Cl^- , SO_4^{2-} , NO_2^- , PO_4^{3-} , F^- , Br^-), did not change significantly. Mineralogical and geochemical investigations indicate that calcite precipitation was on average 0.5 wt.-%, while in some areas as well calcite dissolution occurred. Saturation indices of the pore water calculated with PhreeqC were confirmed by TIC measurements. Hence, an average sequestration rate of 2.2 g CO_2 per kilogram settled ash sediment was calculated for the time of the experiment. The maximum rate for carbonate precipitation was determined with +7.4 wt.-% calcite, according to 32.6 g CO_2 per kilogramm of treated ash. Due to the inhomogeneity of the ash sediment body, further estimations are associated with a high uncertainty. The estimated amount of 172,250 t calcite seems to be conservative.

It can be concluded that the use of the industrial by-products (fly ash, CO_2) during the treatment of acid mine lakes in former mining districts can be accounted as a sustainable method for lake water treatment and CO_2 sequestration within appropriate boundaries. CO_2 sequestration occurs in 2 steps: by storage in the water phase and by storage in solid phase; the former is only temporary whereas the latter is permanent.

In further batch and column experiments, more than 23 different neutralization products (synthetic marble powder and industrial products) were tested and investigated. Based on chemical analysis by XRD and SEM-EDX, no significant difference between synthetic material and industrial products appears. Kinetic experiments with marble powder and limestone (KSM Beroun) support this statement.

Ions typical for acid mine drainage (e.g. Mn^{2+} , Cd^{2+} , SO_4^{2-}) have different effects on the kinetic of carbonate dissolution. Manganese concentrations typical for acidic mining lakes inhibit calcite dissolution. Cadmium has as well a significant influence on dissolution and kinetics. Only about 50 % of the calcium concentration was reached with cadmium as inhibitor compared to the dissolution in absence of cadmium. Increased CO_2 partial pressures might be used to suppress the effect of inhibition by material impurities and/or dissolved water constituents. Thus, further experiments considering the influence of CO_2 partial pressure and the influence of possible inhibiting ions were performed. Significant differences in reactivity were obvious at $p_{CO_2} > 3.8 \cdot 10^{-4}$ bar. Additionally, a possible increased efficiency ratio by using limestone powder during liming campaigns in the pH range > 6 can be achieved.

A variety of column experiments with original lake water of mining lakes was carried out. Results showed that a multi-stage neutralization, with $CaCO_3$ and then $Ca(OH)_2$ having an optimized grain size distribution, offers neutralization efficiencies close to the theoretical maximum. This treatment scheme was successfully applied in the open pit lake Burghammer.

For the optimization of lake treatment by vessels a positioning of appropriate sensors at specific points in a lake is obligatory as real water movements (velocities) and significant water quality parameters have to be determined. Additionally weather parameters (wind direction, wind speed) have to be measured. A reduced wind speed will result in a reduction of used liming products, while an increase of wind will lead to higher amounts. Figure 111 shows the main principle of the described technique.

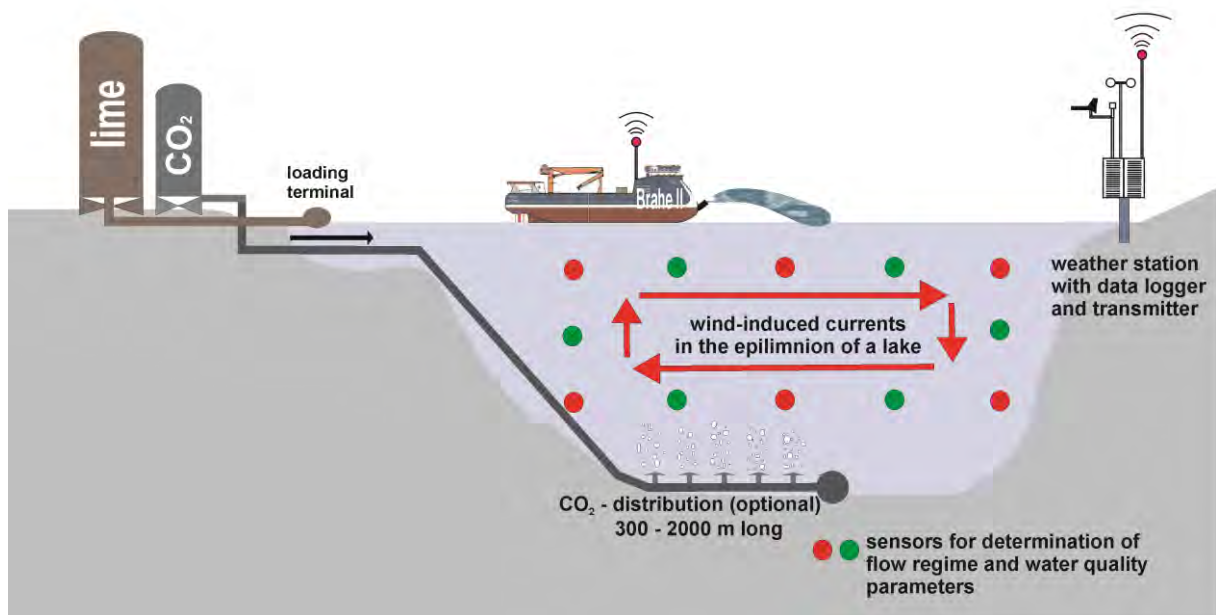


Figure 111. Treatment scheme of an optimized in-lake liming by vessels under consideration of weather conditions and wind-induced currents (Merkel et al., 2010). For further description, see text.

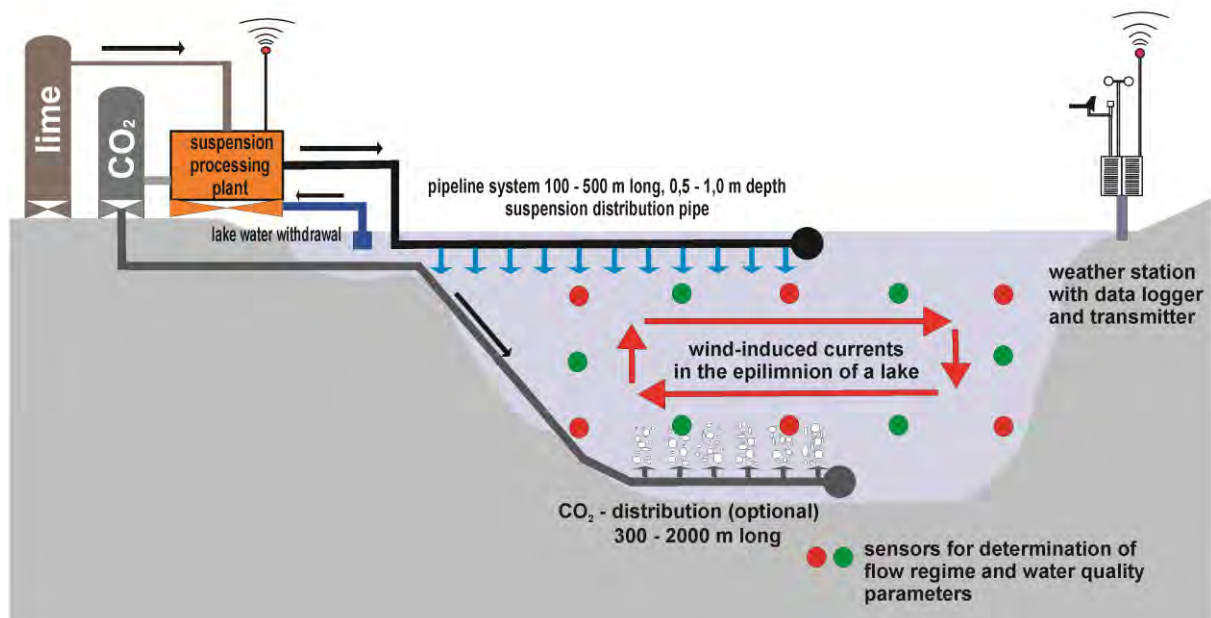


Figure 112. Treatment scheme of an optimized in-lake liming by a pipeline-based system under consideration of weather conditions and wind-induced currents (Merkel et al., 2010). For further description, see text.

In order to minimize the costs for follow-up treatments, these treatments can be done by means of pipeline-systems instead of vessels. Biological communities may react stressed on parameter changes within phases of initial neutralization, re-acidification and follow-up treatments (see Figure 103). This means pH variations should not be in range of 4 to 9, but rather in the range of 6 to maximum 8. Wind-induced currents in combination with pipeline-based treatment might be the solution. Figure 112 shows the concept including its main components.

The development of further strategies and optimization during lake water treatment by in-lake liming can improve the effectiveness of the method. Using calcite instead of NaOH or CaO as liming product will provide advantages in being more economic and ecological. If meteorological parameters (wind) and lake specific characteristics (morphology, currents, etc.) are considered efforts and costs for in-lake liming can be minimized. Both vessel and pipeline based methods promise cost effective solutions for initial neutralization and follow-up treatment. Investigation of the use of CO₂ showed that CO₂ increases the kinetics of dissolution processes. Compared to a multi-stage treatment with limestone and Ca(OH)₂ or other alkaline products, more product is needed using CO₂. Due to the developing buffering system less follow-up treatments are necessary. These are more time-consuming; require larger amounts of neutralization product and require the supply of CO₂ which causes additional costs.

General advantages of in-lake treatment of acidic mining lakes appear as follows:

- avoidance of the construction of mine water treatment systems (end of pipe strategy), and thus, reduced green land area required for treatment plant installation, saving on resources
- lower time, investment costs and products demand in comparison to other techniques (e.g. water treatment plants)
- usage of alkaline substances from existing deposits (fly ash) or sediments (limestone), and thus, reduced chemical consumption

The combination of active (lake water treatment) and passive treatment (CO₂ injection in sediment, e.g. settled fly ash) can provide a sustainable alternative for remediation of acidic mining lakes and for CO₂ sequestration

But it has to be considered that in the moment CO₂ cannot be provided free of charge. Thus, the use of CO₂ to improve sustainability seems to be not economically.

References

- (1983) DIN 38414-7: Deutsche Einheitsverfahren zur Wasser-, Abwasser- und Schlammuntersuchung - Schlamm und Sedimente (Gruppe S) - Aufschluss mit Königswasser zur nachfolgenden Bestimmung des säurelöslichen Anteils von Metallen (S 7). Beuth, 6.
- (1984) DIN 18414-4: Deutsche Einheitsverfahren zur Wasser-, Abwasser und Schlammuntersuchung; Schlamm und Sedimente (Gruppe S); Bestimmung der Eluierbarkeit mit Wasser (S 4). Beuth, 12.
- (1996) DIN 18123: Baugrund, Untersuchung von Bodenproben - Bestimmung der Korngrößenverteilung. Beuth, 12.
- (1997) DIN EN 1484: Wasseranalytik - Anleitungen zur Bestimmung des gesamten organischen Kohlenstoffs (TOC) und des gelösten organischen Kohlenstoffs (DOC). Beuth, 14.
- (2001) DIN EN 12880: Charakterisierung von Schlämmen - Bestimmung des Trockenrückstandes und des Wassergehaltes. Beuth, 7.
- (2007) DIN 18124: Baugrund, Untersuchung von Bodenproben - Bestimmung der Korndichte - Kapillarpyknometer, Weithalspyknometer, Gaspyknometer. Beuth, 14.
- ABANADES, J. C., ANTHONY, E. J., LU, D. Y., SALVADOR, C. & ALVAREZ, D. (2004) Capture of CO₂ from combustion gases in a fluidized bed of CaO. *Aiche Journal*, 50, 1614-1622.
- AHTIAINEN, M., SANDMAN, O. & TYNNI, R. (1983) Sysmajarvi - a Lake Polluted by Mining Waste-Water. *Hydrobiologia*, 103, 303-308.
- AKIN, G. W. & LAGERWER.JV (1965a) Calcium Carbonate Equilibria in Aqueous Solutions Open to Air. I. Solubility of Calcite in Relation to Ionic Strength. *Geochimica et Cosmochimica Acta*, 29, 343-352.
- AKIN, G. W. & LAGERWER.JV (1965b) Calcium Carbonate Equilibria in Solutions Open to Air. 2. Enhanced Solubility of CaCO₃ in Presence of Mg²⁺ and SO₄²⁻. *Geochimica et Cosmochimica Acta*, 29, 353-360.
- AKINFIEV, N. N. & DIAMOND, L. W. (2003) Thermodynamic description of aqueous nonelectrolytes at infinite dilution over a wide range of state parameters. *Geochimica et Cosmochimica Acta*, 67, 613-629.
- AKTIENGESELLSCHAFT, E. (2001) Neutralisation Wasserkörper Burghammer; Aschesedimentumlagerung im Restsee. unpublished report, 12.
- ALKATTAN, M., OELKERS, E. H., DANDURAND, J. L. & SCHOTT, J. (1998) An experimental study of calcite and limestone dissolution rates as a function of pH from -1 to 3 and temperature from 25 to 80 degrees C. *Chemical Geology*, 151, 199-214.

References

- ALKATTAN, M., OELKERS, E. H., DANDURAND, J. L. & SCHOTT, J. (2002) An experimental study of calcite dissolution rates at acidic conditions and 25 degrees C in the presence of NaPO₃ and MgCl₂. *Chemical Geology*, 190, 291-302.
- ANGELER, D. G. & GOEDKOOP, W. (2010) Biological responses to liming in boreal lakes: an assessment using plankton, macroinvertebrate and fish communities. *Journal of Applied Ecology*, 47, 478-486.
- APPELO, C. A. J. & POSTMA, D. (1996) Geochemistry, groundwater and pollution. Rotterdam, Balkema, 536.
- ARVIDSON, R. S., COLLIER, M., DAVIS, K. J., VINSON, M. D., AMONETTE, J. E. & LUTTGE, A. (2006) Magnesium inhibition of calcite dissolution kinetics. *Geochimica et Cosmochimica Acta*, 70, 583-594.
- AYKOL, A., BUDAKOGLU, M., KUMRAL, M., GULTEKIN, A. H., TURHAN, M., ESENLI, V., YAVUZ, F. & ORGUN, Y. (2003) Heavy metal pollution and acid drainage from the abandoned Balya Pb-Zn sulfide Mine, NW Anatolia, Turkey. *Environmental Geology*, 45, 198-208.
- BACHU, S. (2000) Sequestration of CO₂ in geological media: criteria and approach for site selection in response to climate change. *Energy Conversion and Management*, 41, 953-970.
- BACHU, S. & ADAMS, J. J. (2003) Sequestration of CO₂ in geological media in response to climate change: capacity of deep saline aquifers to sequester CO₂ in solution. *Energy Conversion and Management*, 44, 3151-3175.
- BAILEY, S. W., DRISCOLL, C. T. & HORNBECk, J. W. (1995) Acid-Base Chemistry and Aluminum Transport in an Acidic Watershed and Pond in New-Hampshire. *Biogeochemistry*, 28, 69-91.
- BANKS, D., YOUNGER, P. L., ARNESEN, R. T., IVERSEN, E. R. & BANKS, S. B. (1997) Mine-water chemistry: the good, the bad and the ugly. *Environmental Geology*, 32, 157-174.
- BANWART, S. A. & EVANS, K. A. C., S. (2002) Predicting mineral weathering rates at field scale for mine water risk assessment. In: YOUNGER, P. L. & ROBINS, S. (Eds.) In: *Mine Water Hydrogeology and Geochemistry*. London, Geological Society, 137-157.
- BARNES, H. L. & ROMBERGER, S. B. (1968) Chemical Aspects of Acid Mine Drainage. *Journal Water Pollution Control Federation*, 40, 371-384.
- BECCALUVA, L., BIANCHINI, G., COLTORTI, M., PERKINS, W. T., SIENA, F., VACCARO, C. & WILSON, M. (2001) Multistage evolution of the European lithospheric mantle: new evidence from Sardinian peridotite xenoliths. *Contributions to Mineralogy and Petrology*, 142, 284-297.

- BECERRA, C. A., LOPEZ-LUNA, E. L., ERGAS, S. J. & NUSSLEIN, K. (2009) Microcosm-based Study of the Attenuation of an Acid Mine Drainage-Impacted Site through Biological Sulfate and Iron Reduction. *Geomicrobiology Journal*, 26, 9-20.
- BENNER, M. L., MOHTAR, R. H. & LEE, L. S. (2002) Factors affecting air sparging remediation systems using field data and numerical simulations. *Journal of Hazardous Materials*, 95, 305-329.
- BERNER, R. A. (1967) Comparative Dissolution Characteristics of Carbonate Minerals in Presence and Absence of Aqueous Magnesium Ion. *American Journal of Science*, 265, 45-70.
- BERNER, R. A. & MORSE, J. W. (1974) Dissolution Kinetics of Calcium-Carbonate in Seawater. 4. Theory of Calcite Dissolution. *American Journal of Science*, 274, 108-134.
- BEYER, W. (1964) Zur Bestimmung der Wasserdurchlässigkeit von Kiesen und Sanden aus der Kornverteilungskurve. *Wasserwirtschaft - Wassertechnik*, 14, 165-168.
- BIRCUMSHAW, L. L. & RIDDIFORD, A. C. (1952) Transport Control in Heterogeneous Reactions. *Quarterly Reviews*, 6, 157-185.
- BLETTE, V. L. & NEWTON, R. M. (1996) Effects of watershed liming on the soil chemistry of Woods Lake, New York. *Biogeochemistry*, 32, 175-194.
- BLODAU, C. (2006) A review of acidity generation and consumption in acidic coal mine lakes and their watersheds. *Science of the Total Environment*, 369, 307-332.
- BOZAU, E., BECHSTEDT, T., FRIESE, K., FROMMICHEN, R., HEMPRUNG, P., KOSCHORRECK, M., MEIER, J., VOLKNER, C., WENDT-POTTHOFF, K., WIEPRECHT, M. & GELLER, W. (2007a) Biotechnological remediation of an acidic pit lake: Modelling the basic processes in a mesocosm experiment. *Journal of Geochemical Exploration*, 92, 212-221.
- BOZAU, E., BECHSTEDT, T., FRIESE, K., FRÖMMICHEN, R., HERZSPRUNG, P., KOSCHORRECK, M., MEIER, J., VÖLKNER, C., WENDT-POTTHOFF, K., WIEPRECHT, M. & GELLER, W. (2007b) Biotechnological remediation of an acidic pit lake: Modelling the basic processes in a mesocosm experiment. *Journal of Geochemical Exploration*, 92, 212-221.
- BRACCINI, S., BARSOTTI, L., BRADASCHIA, C., CELLA, G., DI VIRGILIO, A., FERRANTE, I., FIDECARO, F., FIORI, I., FRASCONI, F., GENNAI, A., GIAZOTTO, A., PAOLETTI, F., PASSAQUIETI, R., PASSUELLO, D., POGGIANI, R., CAMPAGNA, E., GUIDI, G., LOSURDO, G., MARTELLI, F., MAZZONI, M., PERNIOLA, B., PIERGiovanni, F., STANGA, R., VETRANO, F., VICERE, A., BROCCO, L., FRASCA, S., MAJORANA, E., PAI, A., PALOMBA, C., PUPPO, P., RAPAGNANI, P., RICCI, F., BALLARDIN, G., BARILLE, R., CAVALIERI, R., CUOCO, E., DATTILO, V., ENARD, D., FLAMINIO, R., FREISE, A., HEBRI, S., HOLLOWAY, L., LA PENNA, P., LOUPIAS, M., MARQUE, J., MOINS, C., PASQUALETTI, A., RUGGI, P., TADDEI, R., ZHANG, Z., ACERNESE, F., AVINO, S., BARONE, F., CALLONI, E., DE ROSA, R., DI FIORE, L., ELEUTERI, A., GIORDANO, L., MILANO, L., PARDI, S., QIPIANI, K., RICCIARDI, I., RUSSO, G.,

- SOLIMENO, S., BABUSCI, D., GIORDANO, G., AMICO, P., BOSI, L., GAMMAITONI, L., MARCHESONI, F., PUNTURO, M., TRAVASSO, F., VOCCA, H., BOCCARA, C., MOREAU, J., LORIETTE, V., REITA, V., MACKOWSKI, J. M., MORGADO, N., PINARD, L., REMILLIEUX, A., BARSUGLIA, M., BIZOUARD, M. A., BRISDON, V., CAVALIER, F., CLAPSON, A. C., DAVIER, M., HELLO, P., KRECKLBERGH, S., BEAUVILLE, F., BUSKULIC, D., GOUCATY, R., GROSJEAN, D., MARION, F., MASSEROT, A., MOURS, B., TOURNEFIER, E., TOMBOLATO, D., VERKINDT, D., et al. (2005) Measurement of the seismic attenuation performance of the VIRGO Superattenuator. *Astroparticle Physics*, 23, 557-565.
- BRANTLEY, S. & CONRAD, F. C. (2008) Analysis of Rates of Geochemical Reactions. In: BRANTLEY, S., KUBICKI, J. D. & WHITE, A. F. (Eds.) In: *Kinetics of Water-Rock Interaction*. New York, Springer, 1-35.
- BRANTLEY, S. L. (2008) Kinetics of Mineral Dissolution. In: BRANTLEY, S. L., KUBICKI, J. D. & WHITE, A. F. (Eds.) In: *Kinetics of Water-Rock Interaction*. New York, Springer, 151-210.
- BRASSARD, P., ROSA, F. & MUDROCH, A. (1996) Disposal of acid drainage generating mine tailings in lakes and man-made reservoirs. *Environmental Technology*, 17, 1059-1069.
- BROUWER, E. & ROELOFS, J. G. M. (2002) Oligotrophication of acidified, nitrogen-saturated softwater lakes after dredging and controlled supply of alkaline water. *Archiv Fur Hydrobiologie*, 155, 83-97.
- BRUGAM, R. B., GASTINEAU, J. & RATCLIFF, E. (1995) The neutralization of acidic coal mine lakes by additions of natural organic matter: A mesocosm test. *Hydrobiologia*, 316, 153-159.
- BTU (2005) Gutachten zur Entwicklung der Wasserbeschaffenheit in den Tagebaueen Dreiweibern, Lohsa II und Burghammer. Report, 216.
- BUHMANN, D. & DREYBRODT, W. (1985) The Kinetics of Calcite Dissolution and Precipitation in Geologically Relevant Situations of Karst Areas. 1. Open System. *Chemical Geology*, 48, 189-211.
- BUHMANN, D. & DREYBRODT, W. (1987) Calcite Dissolution Kinetics in the System $H_2O-CO_2-CaCO_3$ with Participation of Foreign Ions. *Chemical Geology*, 64, 89-102.
- BUHRE, B. J. P., ELLIOTT, L. K., SHENG, C. D., GUPTA, R. P. & WALL, T. F. (2005) Oxy-fuel combustion technology for coal-fired power generation. *Progress in Energy and Combustion Science*, 31, 283-307.
- BUNDESVERBAND, B. (2000) Braunkohle - Ein Industriezweig stellt sich vor. Report, 56.
- BUNDESVERBAND, B. (2011) Lignite in Germany - Facts and Figures. Report, 2.

- BURTON, E. A. & WALTER, L. M. (1990) The Role of pH in Phosphate Inhibition of Calcite and Aragonite Precipitation Rates in Seawater. *Geochimica et Cosmochimica Acta*, 54, 797-808.
- BURTON, E. A. & WALTER, L. M. (1991) The Effects of Pco₂ and Temperature on Magnesium Incorporation in Calcite in Seawater and MgCl₂-CaCl₂ Solutions. *Geochimica et Cosmochimica Acta*, 55, 777-785.
- BUSENBERG, E. & PLUMMER, L. N. (1986) A comparative study of the dissolution and precipitation kinetics of calcite and aragonite. In: MUMTON, F. A. (Ed.) In: *Studies in Diagenesis*. U.S. Geol. Surv. bull., 139-168.
- CASTRO, J. M. & MOORE, J. N. (2000) Pit lakes: their characteristics and the potential for their remediation. *Environmental Geology*, 39, 1254-1260.
- CASTRO, J. M., WIELINGA, B. W., GANNON, J. E. & MOORE, J. N. (1999) Stimulation of sulfate-reducing bacteria in lake water from a former open-pit mine through addition of organic wastes. *Water Environment Research*, 71, 218-223.
- CHAFFEE, A. L., KNOWLES, G. P., LIANG, Z., ZHANY, J., XIAO, P. & WEBLEY, P. A. (2007) CO₂ capture by adsorption: Materials and process development. *International Journal of Greenhouse Gas Control*, 1, 11-18.
- CHAKRAPANI, G. J., YADAV, S. K. & GUPTA, M. K. (2008) An experimental study of dissolution kinetics of Calcite, Dolomite, Leucogranite and Gneiss in buffered solutions at temperature 25 and 5 degrees C. *Environmental Geology*, 53, 1683-1694.
- CHEN, M., SOULSBY, C. & YOUNGER, P. L. (1997) Predicting water quality impacts from future minewater outflows in an urbanized Scottish catchment. *Groundwater in the Urban Environment*, 1, 383-388.
- CHOU, L., GARRELS, R. M. & WOLLAST, R. (1989) Comparative-Study of the Kinetics and Mechanisms of Dissolution of Carbonate Minerals. *Chemical Geology*, 78, 269-282.
- CIRMO, C. P. & DRISCOLL, C. T. (1996) The impacts of a watershed CaCO₃ treatment on stream and wetland biogeochemistry in the Adirondack Mountains. *Biogeochemistry*, 32, 265-297.
- CIRMO, C. P., DRISCOLL, C. T. & BOWES, K. (2000) Chemical fluxes from sediments in two Adirondack wetlands: Effects of an acid-neutralization experiment. *Soil Science Society of America Journal*, 64, 790-799.
- CLAUß, D. (2008) Technologie der Gasinjektion und verschiedener Monitoring-Maßnahmen im Rahmen eines Pilotversuches zur CO₂-Sequestrierung. Bachelor Thesis (unpublished), TU Bergakademie Freiberg, 73.
- COMBER, S. D. W., EVANS, D., GARDNER, M. J., GREEN, C. & WHITEHEAD, P. G. (1999) Development of a liming prediction model for Llyn Brianne. *Journal of the Chartered Institution of Water and Environmental Management*, 13, 275-279.

References

- COMPTON, R. G. & BROWN, C. A. (1994) The Inhibition of Calcite Dissolution Precipitation - Mg²⁺ Cations. *Journal of Colloid and Interface Science*, 165, 445-449.
- COMPTON, R. G., DALY, P. J. & HOUSE, W. A. (1986) The Dissolution of Iceland Spar Crystals - the Effect of Surface-Morphology. *Journal of Colloid and Interface Science*, 113, 12-20.
- CRUSIUS, J., PIETERS, R., LEUNG, A., WHITTLE, P., PEDERSEN, T., LAWRENCE, G. & MCNEE, J. J. (2003) Tale of two pit lakes: Initial results of a three-year study of the Main Zone and Waterline pit lakes near Houston, British Columbia, Canada. *Mining Engineering*, 55, 43-48.
- CUBILLAS, P., KOHLER, S., PRIETO, M., CAUSSERAND, C. & OELKERS, E. H. (2005) How do mineral coatings affect dissolution rates? An experimental study of coupled CaCO₃ dissolution - CdCO₃ precipitation. *Geochimica et Cosmochimica Acta*, 69, 5459-5476.
- DAI, J. J., SOKHANSANJ, S., GRACE, J. R., BI, X. T., LIM, C. J. & MELIN, S. (2008) Overview and some issues related to co-firing biomass and coal. *Canadian Journal of Chemical Engineering*, 86, 367-386.
- DANIELS, W. L., STEWART, B. R. & JACKSON, M. L. (1993) Influence of Alkaline Fly-Ash Additions on Acid-Mine Drainage from Coal Refuse. *Abstracts of Papers of the American Chemical Society*, 205, 139.
- DICKSON, W., BORG, H., EKSTROM, C., HORNSTROM, E. & GRONLUND, T. (1995) Reliming and reacidification effects on lakewater, chemistry, plankton and macrophytes. *Water Air and Soil Pollution*, 85, 919-924.
- DIETZSCH, B., DOMKE, R., FLEISCHHAUER, W., LEVEN, V., MÜLLER, W., OHLING, W., SCHÖN, I., SCHWISTER, K. & TARJÁN, I. (2007) Taschenbuch der Verfahrenstechnik. München, Carl Hanser Verlag, 664.
- DIJKSTRA, J. J., VAN DER SLOOT, H. A. & COMANS, R. N. J. (2006a) The leaching of major and trace elements from MSWI bottom ash as a function of pH and time. *Applied Geochemistry*, 21, 335-351.
- DIJKSTRA, J. J., VAN ZOMEREN, A., MEEUSSEN, J. C. L. & COMANS, R. N. J. (2006b) Effect of accelerated aging of MSWI bottom ash on the leaching mechanisms of copper and molybdenum. *Environmental Science & Technology*, 40, 4481-4487.
- DIXON, R. K., BROWN, S., HOUGHTON, R. A., SOLOMON, A. M., TREXLER, M. C. & WISNIEWSKI, J. (1994) Carbon pools and flux of global forest ecosystems. *Science*, 263, 185-190.
- DOMINOK, B. & KILZ, C. (1995) Humantoxikologische Bewertung von Braunkohlefilteraschen. In: AG, R. (Ed.) In: *Verwertung von Filteraschen aus Braunkohlekraftwerken in der Bundesrepublik Deutschland*. Essen, 251 - 260.

- DOWLING, J., ATKIN, S., BEALE, G. & ALEXANDER, G. (2004) Development of the Sleeper pit lake. *Mine Water and the Environment*, 23, 2.
- DREYBRODT, W. & BUHmann, D. (1991) A Mass-Transfer Model for Dissolution and Precipitation of Calcite from Solutions in Turbulent Motion. *Chemical Geology*, 90, 107-122.
- DREYBRODT, W. & EISENLOHR, L. (2000) Limestone dissolution rates in karst environments. In: KLIMCHOUK, A., FORD, D. C., PALMER, A. N. & DREYBRODT, W. (Eds.) In: *Speleogenesis: Evolution of karst aquifers*. Huntsville, Nat. Speleol. Soc., 527.
- DREYBRODT, W., EISENLOHR, L., MADRY, B. & RINGER, S. (1997) Precipitation kinetics of calcite in the system CaCO₃-H₂O-CO₂: The conversion to CO₂ by the slow process H⁺+HCO₃⁻→CO₂+H₂O as a rate limiting step. *Geochimica et Cosmochimica Acta*, 61, 3897-3904.
- DREYBRODT, W. & GABROVSEK, F. (2000) Comments on: Mixed transport/reaction control of gypsum dissolution kinetics in aqueous solutions and initiation of gypsum karst by Michael A. Raines and Thomas A. Dewers in Chemical Geology 140, 29-48, 1997. *Chemical Geology*, 168, 169-172.
- DREYBRODT, W., LAUCKNER, J., LIU, Z. H., SVENSSON, U. & BUHmann, D. (1996) The kinetics of the reaction CO₂+H₂O→H⁺⁺HCO₃⁻ as one of the rate limiting steps for the dissolution of calcite in the system H₂O-CO₂-CaCO₃. *Geochimica et Cosmochimica Acta*, 60, 3375-3381.
- DRISCOLL, C. T., CIRMO, C. P., FAHEY, T. J., BLETTÉ, V. L., BUKAVECKAS, P. A., BURNS, D. A., GUBALA, C. P., LEOPOLD, D. J., NEWTON, R. M., RAYNAL, D. J., SCHOFIELD, C. L., YAVITT, J. B. & PORCELLA, D. B. (1996) The experimental watershed liming study: Comparison of lake and watershed neutralization strategies. *Biogeochemistry*, 32, 143-174.
- DROMGOOLE, E. L. & WALTER, L. M. (1990) Iron and Manganese Incorporation into Calcite - Effects of Growth-Kinetics, Temperature and Solution Chemistry. *Chemical Geology*, 81, 311-336.
- EDENBORN, H. M., MUCCI, A., BELZILE, N., LEBEL, J., SILVERBERG, N. & SUNDBY, B. (1986) A Glove Box for the Fine-Scale Subsampling of Sediment Box Cores. *Sedimentology*, 33, 147-150.
- EISENLOHR, L., BOUZELBOUDJEN, M., KIRALY, L. & ROSSIER, Y. (1997) Numerical versus statistical modelling of natural response of a karst hydrogeological system. *Journal of Hydrology*, 202, 244-262.
- EISENLOHR, L., METEVA, K., GABROVSEK, F. & DREYBRODT, W. (1999) The inhibiting action of intrinsic impurities in natural calcium carbonate minerals to their dissolution kinetics in aqueous H₂O-CO₂ solutions. *Geochimica et Cosmochimica Acta*, 63, 989-1001.

References

- ELONEVA, S., TEIR, S., SALMINEN, J., FOGELHOLM, C. J. & ZEVENHOVEN, R. (2008) Fixation of CO₂ by carbonating calcium derived from blast furnace slag. *Energy*, 33, 1461-1467.
- EPRI - ELECTRIC POWER RESEARCH INSTITUTE & SOUTHERN COMPANY SERVICES, I. (2006) Weathering Processes and Secondary Minerals Formed in Coal Ash. Report, 50.
- ETA (2003) Neutralisation Wasserkörper Burghammer - Weiterführung Monitoring. Report, 30.
- EURACOAL (2005) Coal industry across Europe 2005. Report, 76.
- EURACOAL (2009) An Energy Strategy for Europe: Importance and Best Use of Indigenous Coal. Report, 12.
- FAUVILLE, A., MAYER, B., FROMMICHEN, R., FRIESE, K. & VEIZER, J. (2004) Chemical and isotopic evidence for accelerated bacterial sulphate reduction in acid mining lakes after addition of organic carbon: laboratory batch experiments. *Chemical Geology*, 204, 325-344.
- FISHER, G. L., PRENTICE, B. A., SILBERMAN, D., ONDOV, J. M., BIERMANN, A. H., RAGAINI, R. C. & MCFARLAND, A. R. (1978) Physical and Morphological-Studies of Size-Classified Coal Fly-Ash. *Environmental Science & Technology*, 12, 447-451.
- FRANKLIN, M. L. & MORSE, J. W. (1983) The Interaction of Manganese(II) with the Surface of Calcite in Dilute-Solutions and Seawater. *Marine Chemistry*, 12, 241-254.
- FRIESE, K., WENDT-POTTHOFF, K., ZACHMANN, D. W., FAUVILLE, A., MAYER, B. & VEIZER, J. (1998) Biogeochemistry of iron and sulfur in sediments of an acidic mining lake in Lusatia, Germany. *Water Air and Soil Pollution*, 108, 231-247.
- FROEMMICHEN, R., WENDT-POTTHOFF, K., FRIESE, K. & FISCHER, R. (2004) Microcosm studies for neutralization of hypolimnic acid mine pit lake water (pH 2.6). *Environmental Science & Technology*, 38, 1877-1887.
- FROMMICHEN, R., KELLNER, S. & FRIESE, K. (2003) Sediment conditioning with organic and/or inorganic carbon sources as a first step in alkalinity generation of acid mine pit lake water (pH 2-3). *Environmental Science & Technology*, 37, 1414-1421.
- FROMMICHEN, R., WENDT-POTTHOFF, K., FRIESE, K. & FISCHER, R. (2004) Microcosm studies for neutralization of hypolimnic acid mine pit lake water (pH 2.6). *Environmental Science & Technology*, 38, 1877-1887.
- FYSON, A., NIXDORF, B. & KALIN, M. (2006) The acidic lignite pit lakes of Germany - Microcosm experiments on acidity removal through controlled eutrophication. *Ecological Engineering*, 28, 288-295.

- GIGER, W., REINHARD, M. & SCHAFFNER, C. (1974) Charakterisierung aromatischer Kohlenwasserstoffe. *Vom Wasser*, 25.
- GITARI, M. W., PETRIK, L. F., ETCHEBERS, O., KEY, D. L., IWUOHA, E. & OKUJENI, C. (2006) Treatment of acid mine drainage with fly ash: Removal of major contaminants and trace elements. *Journal of Environmental Science and Health Part a-Toxic/Hazardous Substances & Environmental Engineering*, 41, 1729-1747.
- GITARI, W. M., PETRIK, L. F., ETCHEBERS, O., KEY, D. L., IWUOHA, E. & OKUJENI, C. (2008a) Passive neutralisation of acid mine drainage by fly ash and its derivatives: A column leaching study. *Fuel*, 87, 1637-1650.
- GITARI, W. M., PETRIK, L. F., ETCHEBERS, O., KEY, D. L. & OKUJENI, C. (2008b) Utilization of fly ash for treatment of coal mines wastewater: Solubility controls on major inorganic contaminants. *Fuel*, 87, 2450-2462.
- GLEDHILL, D. K. & MORSE, J. W. (2004) Dissolution kinetics of calcite in NaCl-CaCl₂-MgCl₂ brines at 25 degrees C and 1 bar p_{CO₂}. *Aquatic Geochemistry*, 10, 171-190.
- GLEDHILL, D. K. & MORSE, J. W. (2006a) Calcite dissolution kinetics in Na-Ca-Mg-Cl brines. *Geochimica et Cosmochimica Acta*, 70, 5802-5813.
- GLEDHILL, D. K. & MORSE, J. W. (2006b) Calcite solubility in Na-Ca-Mg-Cl brines. *Chemical Geology*, 233, 249-256.
- GORANSSON, E., BRINGMARK, E., RAPP, L. & WILANDER, A. (2006) Modeling the effect of liming on calcium concentration in Swedish lakes. *Environmental Monitoring and Assessment*, 119, 331-348.
- GRABNER, M., OGRISECK, S. & MEYER, B. (2007) Numerical simulation of coal gasification at circulating fluidised bed conditions. *Fuel Processing Technology*, 88, 948-958.
- GRAY, N. F. (1997) Environmental impact and remediation of acid mine drainage: A management problem. *Environmental Geology*, 30, 62-71.
- GRÜNEWALD, U. (2002) Entwicklung der Wasserbeschaffenheit in den Tagebauseen der Lausitz. Conference Proceedings, Workshop "Biogene Alkalinitätsproduktion und Neutralisierung als ergänzende Strategie für die Restaurierung von extrem sauren Tagebauseen", Cottbus, 25-30.
- GRÜNEWALD, U. (2005) Gutachten zur Entwicklung der Wasserbeschaffenheit in den Tagebauseen Dreiweibern, Lohsa II und Burghammer. Report, 216.
- GUBALA, C. P. & DRISCOLL, C. T. (1991) The Chemical Responses of Acidic Woods Lake, Ny to 2 Different Treatments with Calcium-Carbonate. *Water Air and Soil Pollution*, 59, 7-22.

- GUHRÉN, M., BIGLER, C. & RENBERG, I. (2007) Liming placed in a long-term perspective: A paleolimnological study of 12 lakes in the Swedish liming program. *Journal of Paleolimnology*, 37, 247.
- GUTJAHR, A., DABRINGHAUS, H. & LACMANN, R. (1996a) Studies of the growth and dissolution kinetics of the CaCO₃ polymorphs calcite and aragonite. 1. Growth and dissolution rates in water. *Journal of Crystal Growth*, 158, 310-315.
- GUTJAHR, A., DABRINGHAUS, H. & LACMANN, R. (1996b) Studies of the growth and dissolution kinetics of the CaCO₃ polymorphs calcite and aragonite. 1. Growth and dissolution rates in water. *Journal of Crystal Growth*, 158, 296-309.
- HAENCHEN, M., PRIGIOBBE, V., BACIOCCHI, R. & MAZZOTTI, M. (2008) Precipitation in the Mg-carbonate system - effects of temperature and CO₂ pressure. *Chemical Engineering Science*, 63, 1012-1028.
- HAKANSON, L. (2003) Consequences and correctives related to lake acidification, liming and mercury in fish - A case-study for Lake Huljesjon, Sweden, using the LakeWeb-model. *Environmental Modeling & Assessment*, 8, 275-283.
- HAMELINCK, C. N., FAAIJ, A. P. C., TURKENBURG, W. C., VAN BERGEN, F., PAGNIER, H. J. M., BARZANDJI, O. H. M., WOLF, K. & RUIJG, G. J. (2002) CO₂ enhanced coalbed methane production in the Netherlands. *Energy*, 27, 647-674.
- HÄUSSINGER, P., LOHMÜLLER, R. & WATSON, A. M. (2007) Hydrogen. In: *Ullmann's Encyclopedia of Industrial Chemistry*. Wiley-VCH Verlag GmbH & Co. KGaA, Weinheim, 1-155.
- HAYNES, R. J. (2009) Reclamation and revegetation of fly ash disposal sites - Challenges and research needs. *Journal of Environmental Management*, 90, 43-53.
- HEDIN, R. S., WATZLAF, G. R. & NAIRN, R. W. (1994) Passive Treatment of Acid-Mine Drainage with Limestone. *Journal of Environmental Quality*, 23, 1338-1345.
- HEMINGWAY, B. S., ROBIE, R. A. & APPS, J. A. (1991) Revised values for the thermodynamic properties of boehmite, AlO(OH), and related species and phases in the system Al-H-O. *American Mineralogist*, 76, 445-457.
- HEMM, M., SCHLUNDT, A., KAPFER, M. & NIXDORF, B. (2002) Beispiele für Neutralisierungsversuche am Steinberger See (Bayern) und Zieselsmaar (Nordrhein-Westfalen) - aus der UBA-Studie „Tagebaauseen in Deutschland“. Conference Proceedings, Biogene Neutralisierung, 37-42.
- HENRIKSON, L., HINDAR, A. & THORNELOF, E. (1995) Freshwater liming. *Water Air and Soil Pollution*, 85, 131-142.
- HERMAN, J. (1982) The dissolution kinetics of calcite, dolomite and dolomite rocks in carbon dioxide water systems. PhD Thesis, Pennsylvania State University, 145.

- HERZOG, H., GOLOMB, D. & ZEMBA, S. (1991) FEASIBILITY, MODELING AND ECONOMICS OF SEQUESTERING POWER-PLANT CO₂ EMISSIONS IN THE DEEP OCEAN. *Environmental Progress*, 10, 64-74.
- HIRAI, S., TABE, Y., TANAKA, G. & OKAZAKI, K. (1999) Advanced CO₂ ocean dissolution technology for longer term sequestration with minimum biological impacts. *Greenhouse Gas Control Technologies*, 317-322.
- HOFFERT, J. R. (1947) Acid Mine Drainage. *Industrial and Engineering Chemistry*, 39, 642-646.
- HOFFMAN, G. K. (2002) Fly ash utilization in the Western United States. *Industrial Minerals and Extractive Industry Geology*, 331-339.
- HOSSEIN, M., MOHAMED, A. M. O., HASSANI, F. P. & ELBADRI, H. (1999) Ettringite formation in lime-remediated mine tailings: II. Experimental study. *Cim Bulletin*, 92, 75-80.
- HOWER, J. C., RATHBONE, R. F., ROBERTSON, J. D., PETERSON, G. & TRIMBLE, A. S. (1999) Petrology, mineralogy, and chemistry of magnetically-separated sized fly ash. *Fuel*, 78, 197-203.
- HOWER, J. C., TRIMBLE, A. S. & EBLE, C. F. (2001) Temporal and spatial variations in fly ash quality. *Fuel Processing Technology*, 73, 37-58.
- HUGGINS, F. E., SENIOR, C. L., CHU, P., LADWIG, K. & HUFFMAN, G. P. (2007) Selenium and arsenic speciation in fly ash from full-scale coal-burning utility plants. *Environmental Science & Technology*, 41, 3284-3289.
- HUIJGEN, W. J. J. & COMANS, R. N. J. (2005) Mineral CO₂ sequestration by carbonation of industrial residues. Report, 22.
- HUIJGEN, W. J. J., WITKAMP, G. J. & COMANS, R. N. J. (2005) Mineral CO₂ sequestration by steel slag carbonation. *Environmental Science & Technology*, 39, 9676-9682.
- HUIJTS, N. M. A., MIDDEN, C. J. H. & MEIJNDERS, A. L. (2007) Social acceptance of carbon dioxide storage. *Energy Policy*, 35, 2780-2789.
- HYDROGEOLOGIC, I. (1999) MINTEQA2/PRODEFA2, A Geochemical Assessment Model for Environmental Systems: User Manual Supplement for Version 4.0. Report, 81.
- IIVONEN, P., JARVENPAA, T., LAPPALAINEN, A., MANNIO, J. & RASK, M. (1995) Chemical, biological and socio-economic approaches to the liming of Lake Ainenjarvi in southern Finland. *Water, Air, and Soil Pollution*, 85, 937-942.
- INSKEEP, W. P. & BLOOM, P. R. (1985) An Evaluation of Rate-Equations for Calcite Precipitation Kinetics at p_{CO₂} Less Than 0.01 Atm and pH Greater Than 8. *Geochimica et Cosmochimica Acta*, 49, 2165-2180.

References

- INSKEEP, W. P. & BLOOM, P. R. (1986) Kinetics of Calcite Precipitation in the Presence of Water-Soluble Organic-Ligands. *Soil Science Society of America Journal*, 50, 1167-1172.
- IPCC (2005) Carbon dioxide capture and storage. Report, 53.
- ISHIMATSU, A., HAYASHI, M., KIKKAWA, T. & KITA, J. (2006) Effects of CO₂ ocean sequestration on marine fish. *Proceedings of the 25th International Conference on Offshore Mechanics and Arctic Engineering*, Vol 4, 395-400.
- IVES, M., MUNDY, R. C., FENNELL, P. S., DAVIDSON, J. F., DENNIS, J. S. & HAYHURST, A. N. (2008) Comparison of Different Natural Sorbents for Removing CO₂ from Combustion Gases, as Studied in a Bench-Scale Fluidized Bed. *Energy & Fuels*, 22, 3852-3857.
- IYER, R. (2002) The surface chemistry of leaching coal fly ash. *Journal of Hazardous Materials*, 93, 321-329.
- JEGADEESAN, G., AL-ABED, S. R. & PINTO, P. (2008) Influence of trace metal distribution on its leachability from coal fly ash. *Fuel*, 87, 1887-1893.
- JOHNSON, C. A., KAEPPLEI, M., BRANDENBERGER, S., ULRICH, A. & BAUMANN, W. (1999) Hydrological and geochemical factors affecting leachate composition in municipal solid waste incinerator bottom ash. Part II. The geochemistry of leachate from Landfill Lostorf, Switzerland. *Journal of Contaminant Hydrology*, 40, 239-259.
- JOHNSON, C. A., MOENCH, H., WERSIN, P., KUGLER, P. & WENGER, C. (2005) Solubility of antimony and other elements in samples taken from shooting ranges. *Journal of Environmental Quality*, 34, 248-254.
- KASTURE, M. W., BOKADE, V. V. & JOSHI, P. N. (2005) Conversion of fly ash - An environmentally detrimental waste to zeolite beta (BEA) for commercial catalytic applications. *Journal of the American Ceramic Society*, 88, 3260-3263.
- KAUBISCH, M. (1986) Zur indirekten Ermittlung hydrogeologischer Kennwerte von Kuppenkomplexen, dargestellt am Beispiel des Braunkohlebergbaus. Dissertation, TU Bergakademie Freiberg, 129.
- KAYSER, R., MESECK, H., RÖSCH, A. & HERMANN, R. (1986) Untersuchungen zur Deponierung von Braunkohlenaschen. Braunschweig, Technische Universität Braunschweig, 104.
- KENDRICK, P. J. (1977) Acid Mine Drainage - Old Problem with a New Dimension. *Journal Water Pollution Control Federation*, 49, 1576-1577.
- KEYSER, T. R., NATUSCH, D. F. S., EVANS, C. A. & LINTON, R. W. (1978) Characterizing Surfaces of Environmental Particles. *Environmental Science & Technology*, 12, 768-773.

- KIRBY, C. S. & CRAVOTTA, C. A. (2005a) Net alkalinity and net acidity 1: Theoretical considerations. *Applied Geochemistry*, 20, 1920-1940.
- KIRBY, C. S. & CRAVOTTA, C. A. (2005b) Net alkalinity and net acidity 2: Practical considerations. *Applied Geochemistry*, 20, 1941-1964.
- KLAPPER, H. (2002) Mining Lakes: Generation, Loading and Water Quality Control. In: MUDROCH, A., STOTTMEISTER, U., KENNEDY, C. & KLAPPER, H. (Eds.) In: *Remediation of abandoned surface coal mining sites*. Berlin Heidelberg, Springer, 57 - 110.
- KLAPPER, H. & SCHULTZE, M. (1995) Geogenically acidified mining lakes - Living conditions and possibilities of restoration. *Internationale Revue Der Gesamten Hydrobiologie*, 80, 639-653.
- KLEEBERG, J. & BERGMANN, J. (2002) Quantitative phase analysis using the Rietveld method and a fundamental parameter approach. Conference Proceedings, Powder Diffraction. Proceedings of the II International Shcool on Power Diffraction., New Delhi, 63-76.
- KLEIN, R. T. & WALTER, L. M. (1995) Interactions between Dissolved Silica and Carbonate Minerals - an Experimental-Study at 25-50-Degrees-C. *Chemical Geology*, 125, 29-43.
- KOCH, C., GRAUPNER, B. & WERNER, F. (2008) Pit Lake Treatment Using Fly Ash Deposits and Carbon Dioxide. Conference Proceedings, 10th IMWA Congress, Carlsbad, 579-582.
- KOCH, R. & ZUNDEL, S. (2005) Kosten und Nutzen der Sanierung des Wasserhaushaltes in der Lausitz. Report, unpublished.
- KOLJONEN, T., SIIKAVIRTA, H., ZEVENHOVEN, R. & SAVOLAINEN, I. (2004) CO₂ capture, storage and reuse potential in Finland. *Energy*, 29, 1521-1527.
- KÖNIG, W. & SCHOLZ, G. (2010) Ergebnisdokumentation der Initialneutralisation / Nachsorgebehandlung SB Burghammer 2009/2010. Report, 40.
- KOPACEK, J., HEJZLAR, J., KANA, J., PORCAL, P. & KLEMENTOVA, S. (2003) Photochemical, chemical, and biological transformations of dissolved organic carbon and its effect on alkalinity production in acidified lakes. *Limnology and Oceanography*, 48, 106-117.
- KOSCHORRECK, M., BOZAU, E., FROEMMICHEN, R., GELLER, W., HERZSPRUNG, P. & WENDT-POTTHOFF, K. (2007a) Processes at the sediment water interface after addition of organic matter and lime to an acid mine pit lake mesocosm. *Environmental Science & Technology*, 41, 1608-1614.
- KOSCHORRECK, M., HERZSPRUNG, P., WENDT-POTTHOFF, K., LORKE, A., GELLER, W., LUTHER, G., ELSNER, W. & MUELLER, M. (2002) An In-lake Reactor to Treat

References

- an Acidic Lake: the Effect of Substrate Overdosage. *Mine Water and the Environment*, 21, 137-149.
- KOSCHORRECK, M., WENDT-POTTHOFF, K., BOZAU, E., HERZSPRUNG, P., GELLER, W. & SCHULTZE, M. (2007b) In situ neutralization of acidic pit lakes: Processes in the sediment and limiting factors. Conference Proceedings, IMWA Symposium 2007: Water in Mining Environments, Cagliari, Italy, 215-219.
- KOUKOUZAS, N., HAMALAINEN, J., PAPANIKOLAOU, D., TOURUNEN, A. & JANTTI, T. (2007) Mineralogical and elemental composition of fly ash from pilot scale fluidised bed combustion of lignite, bituminous coal, wood chips and their blends. *Fuel*, 86, 2186-2193.
- KOUKOUZAS, N. K., ZENG, R. S., PERDIKATSIS, V., XU, W. D. & KAKARAS, E. K. (2006) Mineralogy and geochemistry of Greek and Chinese coal fly ash. *Fuel*, 85, 2301-2309.
- KUSHNIR, J. & KASTNER, M. (1985) Adsorption and Desorption of Sulfate on Calcite, Aragonite, Dolomite, and Magnesite - an Experimental-Study. *Abstracts of Papers of the American Chemical Society*, 190, 98.
- KUTCHKO, B. G. & KIM, A. G. (2006) Fly ash characterization by SEM-EDS. *Fuel*, 85, 2537-2544.
- KUYUCAK, N. (1998) Mining, the environment and the treatment of mine effluents. *International Journal of Environment and Pollution*, 10, 315-325.
- LAZIK, D., GEISTLINGER, H., KRAUSS, G., BECKMANN, A. & SCHIRMER, M. (2002) Untersuchungen zum Strömungsverhalten und zur Lösungskinetik von Gasen im Mehrphasensystem "Aquifer". *Grundwasser - Zeitschrift der Fachsektion Hydrogeologie*, 3, 146-155.
- LEA, A. S., AMONETTE, J. E., BAER, D. R., LIANG, Y. & COLTON, N. G. (2001) Microscopic effects of carbonate, manganese, and strontium ions on calcite dissolution. *Geochimica et Cosmochimica Acta*, 65, 369-379.
- LEBRON, I. & SUAREZ, D. L. (1998) Kinetics and mechanisms of precipitation of calcite as affected by p_{CO_2} and organic ligands at 25 degrees C. *Geochimica et Cosmochimica Acta*, 62, 405-416.
- LEE, S. & SPEARS, D. A. (1997) Natural weathering of pulverized fuel ash and porewater evolution. *Applied Geochemistry*, 12, 367-376.
- LEVICH, V. (1962) Physicochemical Hydrodynamics. Longman Higher Education, 700.
- LIANG, Y., HARRISON, D. P., GUPTA, R. P., GREEN, D. A. & MCMICHAEL, W. J. (2004) Carbon dioxide capture using dry sodium-based sorbents. *Energy & Fuels*, 18, 569-575.

- LIN, C. F. & HSI, H. C. (1995) Resource Recovery of Waste Fly-Ash - Synthesis of Zeolite-Like Materials. *Environmental Science & Technology*, 29, 1109-1117.
- LINKE, S. & SCHIFFER, L. (2002) Development Prospects for the Post-Mining Landscape in Central Germany. In: MUDROCH, A., STOTTMEISTER, U., KENNEDY, C. & KLAPPER, H. (Eds.) In: *Remediation of abandoned surface coal mining sites*. Berlin Heidelberg, Springer, 111 - 149.
- LIU, Z. H. & DREYBRODT, W. (1997) Dissolution kinetics of calcium carbonate minerals in H_2O - CO_2 solutions in turbulent flow: The role of the diffusion boundary layer and the slow reaction $H_2O + CO_2 \rightarrow H^+ + HCO_3^-$. *Geochimica et Cosmochimica Acta*, 61, 2879-2889.
- LMBV (2008) Revierkarte Sanierungsbereich Lausitz.
- LOTTERMOSER, B. (2003) Mine Wastes - Characterization, Treatment and Environmental impacts. Berlin, Heidelberg, Springer, 304.
- LUCAS, K., SCHINGNITZ, M. & GOHLER, P. (1988) A Comparison of Technologies for Coal-Gasification under Pressure in an Entrained System. *Chemische Technik*, 40, 277-282.
- LUCKNER, L. (2006a) Lausitz: Sanierung des Wasserhaushalts, Sanierung einer Bergbaufolgelandschaft, Teil 1: Die Lösung des Wassermengen-Problems. *wwt*, 03, 33-37.
- LUCKNER, L. (2006b) Lausitz: Sanierung des Wasserhaushalts, Sanierung einer Bergbaufolgelandschaft, Teil 2: Das Problem mit der Wasserqualität. *wwt*, 04, 10-16.
- LUG (2005) Basisdokumentation CDEAL - Tagebausee (TBS) Burghammer. unpublished report, 15.
- LUTTGE, A., DAVIS, K. J. & NEALSON, K. H. (2007) Calcite and dolomite dissolution rates in the context of microbe-mineral surface interactions. *Geobiology*, 5, 191-205.
- LYDERSEN, E., LOFGREN, S. & ARNESEN, R. T. (2002) Metals in Scandinavian surface waters: Effects of acidification, liming, and potential reacidification. *Critical Reviews in Environmental Science and Technology*, 32, 73-295.
- MANZ, O. E. (1999) Coal fly ash: a retrospective and future look. *Fuel*, 78, 133-136.
- MARCHETTI, C. (1977) On geoengineering and the CO_2 problem. *Climatic Change*, 1, 59-68.
- MARKELS, M. & BARBER, R. T. (2002) Sequestration of carbon dioxide by ocean fertilization. *Environmental Challenges and Greenhouse Gas Control for Fossil Fuel Utilization in the 21st Century*, 119-131.

References

- MBH, R. G. F. F. U. E. & AG, I. I. D. V. V. E. (1995) Abschlussbericht Verbundforschungsvorhaben (VFV) "Verwertung von Filteraschen aus Braunkohlekraftwerken in der Bundesrepublik Deutschland". Report,
- MEI, C. C., CHENG, Z. & NG, C. O. (2002) A model for flow induced by steady air venting and air sparging. *Applied Mathematical Modelling*, 26, 727-750.
- MEIMA, J. A. & COMANS, R. N. J. (1997) Geochemical modeling of weathering reactions in municipal solid waste incinerator bottom ash. *Environmental Science & Technology*, 31, 1269-1276.
- MERKEL, B. (2005) Alkalinitätserhöhung in sauren Grubenwässern durch CO₂-Zugabe. *Wissenschaftliche Mitteilungen*, 28, 51-55.
- MERKEL, B. & SCHIPEK, M. (2008) Prognosewerkzeuge zur Beurteilung der Effizienz von Inlaketechniken für die Neutralisation und Nachsorge saurer Tagebaufolgeseen. *Wissenschaftliche Mitteilungen*, 37, 65-72.
- MERKEL, B., SCHIPEK, M., SCHOLZ, G. & RABE, W. (2010) Optimierung der Kalkung von Tagebauseen. *Wissenschaftliche Mitteilungen*, 42, 51 - 59.
- MERKEL, B. & SPERLING, B. (1998) Hydrogeochemische Stoffsysteme, Teil II. Bonn, Kommisionsvertrieb Wirtschafts- und Verlagsgesellschaft Gas und Wasser mbH, 397.
- MERKEL, B. J. & PLANER-FRIEDRICH, B. (2005) Groundwater Geochemistry -- A Practical Guide to Modeling of Natural and Contaminated Aquatic Systems. Berlin, Heidelberg, Springer, 200.
- MICHIHIRO MIYAKE, C. T. M. M. (2002) Resource Recovery of Waste Incineration Fly Ash: Synthesis of Zeolites A and P. *Journal of the American Ceramic Society*, 85, 1873-1875.
- MONECKE, T., GIORGETTI, G., SCHOLTYSEK, O., KLEEBERG, R., GÖTZE, J., HANNINGTON, M. D. & PETERSEN, S. (2007) Textural and mineralogical changes associated with the incipient hydrothermal alteration of glassy dacite at the submarine PACMANUS hydrothermal system, eastern Manus Basin. *Journal of Volcanology and Geothermal Research*, 160, 23-41.
- MONTES-HERNANDEZ, G., PEREZ-LOPEZ, R., RENARD, F., NIETO, J. M. & CHARLET, L. (2009) Mineral sequestration of CO₂ by aqueous carbonation of coal combustion fly-ash. *Journal of Hazardous Materials*, 161, 1347-1354.
- MORSE, J. W. (1974) Dissolution Kinetics of Calcium-Carbonate in Sea-Water. 5. Effects of Natural Inhibitors and Position of Chemical Lysocline. *American Journal of Science*, 274, 638-647.
- MORSE, J. W. (1978) Dissolution Kinetics of Calcium-Carbonate in Sea-Water. 6. Near-Equilibrium Dissolution Kinetics of Calcium Carbonate-Rich Deep-Sea Sediments. *American Journal of Science*, 278, 344-353.

- MORSE, J. W. & ARVIDSON, R. S. (2002) The dissolution kinetics of major sedimentary carbonate minerals. *Earth-Science Reviews*, 58, 51-84.
- MORSE, J. W., MUCCI, A., WALTER, L. M. & KAMINSKY, M. S. (1979) Magnesium Interaction with the Surface of Calcite in Seawater. *Science*, 205, 904-905.
- MORSE, J. W., WANG, Q. W. & TSIO, M. Y. (1997) Influences of temperature and Mg:Ca ratio on CaCO_3 precipitates from seawater. *Geology*, 25, 85-87.
- MUCCI, A., CANUEL, R. & ZHONG, S. J. (1989) The Solubility of Calcite and Aragonite in Sulfate-Free Seawater and the Seeded Growth-Kinetics and Composition of the Precipitates at 25-Degrees-C. *Chemical Geology*, 74, 309-320.
- MUDROCH, A., STOTTMEISTER, U., KENNEDY, C. & KLAPPER, H. (2002) Remediation of abandoned surface coal mining sites. Berlin, Heidelberg, Springer, 175.
- MÜNCH, U. (1996) Zu Konstitution, Elutionsverhalten und Kathodolumineszenz von Braunkohlenaschen. Dissertation, TU Bergakademie Freiberg, 124.
- MYNENI, S. C. B., TRAINA, S. J. & LOGAN, T. J. (1998) Ettringite solubility and geochemistry of the $\text{Ca}(\text{OH})_2\text{-Al}_2(\text{SO}_4)_3\text{-H}_2\text{O}$ system at 1 atm pressure and 298 K. *Chemical Geology*, 148, 1-19.
- NESTAAS, I. & TERJESEN, S. G. (1969) Inhibiting Effect of Scandium Ions Upon Dissolution of Calcium Carbonate. *Acta Chemica Scandinavica*, 23, 2519-2531.
- NEUSER, R. D., BRUHN, F., GÖTZE, J., HABERMANN, D. & RICHTER, D. K. (1995) Kathodolumineszenz: Methodik und Anwendung. *Zentralblatt für Geologie und Paläontologie*, 1, 287-306.
- NOWEL, W., BÖNISCH, R., SCHNEIDER, W. & SCHULZE, H. (1994) Geologie des Lausitzer Braunkohlenreviers. Lausitzer Braunkohle Aktiengesellschaft, 102.
- NYBERG, P. & THORNELOF, E. (1988) Operational liming of surface waters in Sweden. *Water, Air, and Soil Pollution*, 41, 3.
- OELKERS, E. H., SCHOTT, J. & DEVIDAL, J. L. (2001) On the interpretation of closed system mineral dissolution experiments: Comment on "Mechanism of kaolinite dissolution at room temperature and pressure Part II: Kinetic study" by Huertas et al. (1999). *Geochimica et Cosmochimica Acta*, 65, 4429-4432.
- OHSUMI, T. (1995) CO_2 storage options in the deep sea. *Marine Technology Society Journal*, 29, 58-66.
- PALANDRI, J. L., ROSENBAUER, R. J. & KHARAKA, Y. K. (2005) Ferric iron in sediments as a novel CO_2 mineral trap: $\text{CO}_2\text{-SO}_2$ reaction with hematite. *Applied Geochemistry*, 20, 2038-2048.

References

- PALMER, A. N. (1991) Origin and Morphology of Limestone Caves. *Geological Society of America Bulletin*, 103, 1-21.
- PARK, A. H. A., JADHAV, R. & FAN, L. S. (2003) CO₂ mineral sequestration: Chemically enhanced aqueous carbonation of serpentine. *Canadian Journal of Chemical Engineering*, 81, 885-890.
- PARKHURST, D. L. & APPELO, C. A. J. (1999) User's guide to PHREEQC (Version 2) -- a computer program for speciation, batch reaction, one-dimensional transport, and inverse geochemical calculations. Report, 312.
- PENILLA, R. P., BUSTOS, A. G. & ELIZALDE, S. G. (2003) Zeolite synthesized by alkaline hydrothermal treatment of bottom ash from combustion of municipal solid wastes. *Journal of the American Ceramic Society*, 86, 1527-1533.
- PEREZ-LOPEZ, R., CAMA, J., NIETO, J. M. & AYORA, C. (2007a) The iron-coating role on the oxidation kinetics of a pyritic sludge doped with fly ash. *Geochimica et Cosmochimica Acta*, 71, 1921-1934.
- PEREZ-LOPEZ, R., NIETO, J. M., ALVAREZ-VALERO, A. M. & DE ALMODOVAR, G. R. (2007b) Mineralogy of the hardpan formation processes in the interface between sulfide-rich sludge and fly ash: Applications for acid mine drainage mitigation. *American Mineralogist*, 92, 1966-1977.
- PEREZ-LOPEZ, R., NIETO, J. M. & DE ALMODOVAR, G. R. (2007c) Utilization of fly ash to improve the quality of the acid mine drainage generated by oxidation of a sulphide-rich mining waste: Column experiments. *Chemosphere*, 67, 1637-1646.
- PHILIP, J. R. (1998) Full and boundary-layer solutions of the steady air sparging problem. *Journal of Contaminant Hydrology*, 33, 337-345.
- PICHLER, H. & HECTOR, A. (1965) Synthesegas. In: *Ullmann's Enzyklopädie der Technischen Chemie*. Wiley-VCH Verlag GmbH & Co. KGaA, Weinheim, 599.
- PLUMMER, L. N. & BUSENBERG, E. (1982) The Solubilities of Calcite, Aragonite and Vaterite in CO₂-H₂O Solutions between 0-Degrees-C and 90-Degrees-C, and an Evaluation of the Aqueous Model for the System CaCO₃-CO₂-H₂O. *Geochimica et Cosmochimica Acta*, 46, 1011-1040.
- PLUMMER, L. N. & WIGLEY, T. M. L. (1976) Dissolution of Calcite in CO₂-Saturated Solutions at 25Degrees C and 1 Atmosphere Total Pressure. *Geochimica et Cosmochimica Acta*, 40, 191-202.
- PLUMMER, L. N., WIGLEY, T. M. L. & PARKHURST, D. L. (1978) Kinetics of Calcite Dissolution in CO₂-Water Systems at 5-Degrees-C to 60-Degrees-C and 0.0 to 1.0 Atm CO₂. *American Journal of Science*, 278, 179-216.
- POKROVSKY, O. S., GOLUBEV, S. V. & JORDAN, G. (2009a) Effect of organic and inorganic ligands on calcite and magnesite dissolution rates at 60 degrees C and 30 atm p_{CO₂}. *Chemical Geology*, 265, 33-43.

- POKROVSKY, O. S., GOLUBEV, S. V. & SCHOTT, J. (2005) Dissolution kinetics of calcite, dolomite and magnesite at 25 degrees C and 0 to 50 atm p_{CO_2} . *Chemical Geology*, 217, 239-255.
- POKROVSKY, O. S., GOLUBEV, S. V., SCHOTT, J. & CASTILLO, A. (2009b) Calcite, dolomite and magnesite dissolution kinetics in aqueous solutions at acid to circumneutral pH, 25 to 150 degrees C and 1 to 55 atm p_{CO_2} : New constraints on CO_2 sequestration in sedimentary basins. *Chemical Geology*, 265, 20-32.
- PRASHANTH, J. P., SIVAPULLAIAH, P. V. & SRIDHARAN, A. (2001) Pozzolanic fly ash as a hydraulic barrier in land fills. *Engineering Geology*, 60, 245-252.
- PRATT, A. R., NESBITT, H. W. & MUIR, I. J. (1994) Generation of Acids from Mine Waste - Oxidative Leaching of Pyrrhotite in Dilute H_2SO_4 Solutions at pH 3.0. *Geochimica et Cosmochimica Acta*, 58, 5147-5159.
- PRUSTY, B. K. (2008) Sorption of methane and CO_2 for enhanced coalbed methane recovery and carbon dioxide sequestration. *Journal of Natural Gas Chemistry*, 17, 29-38.
- PUST, C., SCHÜPPEL, B., MERKEL, B., SCHIPEK, M., LILJA, G., RABE, W. & SCHOLZ, G. (2010) Advanced Mobile Inlake Technology (AMIT) - An efficient Process for Neutralisation of Acid Open Pit Lakes. Conference Proceedings, International Mine Water Association Symposium - Mine Water and Innovative Thinking, Sydney, Nova Scotia, Canada, 175 - 179.
- QUEROL, X., UMANA, J. C., ALASTUEY, A., AYORA, C., LOPEZ-SOLER, A. & PLANAS, F. (2001) Extraction of soluble major and trace elements from fly ash in open and closed leaching systems. *Fuel*, 80, 801-813.
- RAM, L. C., SRIVASTAVA, N. K., TRIPATHI, R. C., THAKUR, S. K., SINHA, A. K., JHA, S. K., MASTO, R. E. & MITRA, S. (2007) Leaching behavior of lignite fly ash with shake and column tests. *Environmental Geology*, 51, 1119-1132.
- RAO, M. V. B. B. G., KOLAY, P. K. & SINGH, D. N. (1998) Thermal characteristics of a class F fly ash. *Cement and Concrete Research*, 28, 841-846.
- RAUCH, H. W. & WHITE, W. B. (1977) Dissolution Kinetics of Carbonate Rocks. 1. Effects of Lithology on Dissolution Rate. *Water Resources Research*, 13, 381-394.
- REDDY, M. M. (1980) Kinetic Inhibition of Mineral Formation - Magnesium-Ion Reduction of Calcite Crystallization at pH 8.8 and 25-Degrees-C. *Abstracts of Papers of the American Chemical Society*, 179, 19.
- RICKARD, D. & SJÖBERG, E. L. (1983) Mixed Kinetic Control of Calcite Dissolution Rates. *American Journal of Science*, 283, 815-830.
- RITSCHARD, R. L. (1992) Marine algae as a CO_2 sink. *Water Air and Soil Pollution*, 64, 289-303.

References

- ROBB, G. A. & ROBINSON, J. D. F. (1995) Acid Drainage from Mines. *Geographical Journal*, 161, 47-54.
- ROSTAMI, H. & BRENDLEY, W. (2003) Alkali ash material: A novel fly ash-based cement. *Environmental Science & Technology*, 37, 3454-3457.
- RWE (2011) Braunkohlenabbau im rheinischen Revier. Electronic Source: <http://www.rwe.com/web/cms/de/494542/rheinbraun-brennstoff/produktion/rheinisches-revier/>
- RWE & IFK (1995) Verwertung von Filteraschen aus Braunkohlekraftwerken in der Bundesrepublik Deutschland. Report, .
- SABBIDES, T. G. & KOUTSOUKOS, P. G. (1994) The Dissolution of Calcium-Carbonate in the Presence of Magnesium and Inorganic Orthophosphate. *Abstracts of Papers of the American Chemical Society*, 208, 38.
- SABBIDES, T. G. & KOUTSOUKOS, P. G. (1996) The effect of surface treatment with inorganic orthophosphate on the dissolution of calcium carbonate. *Journal of Crystal Growth*, 165, 268-272.
- SALDI, G. D., SCHOTT, J., POKROVSKY, O. S. & OELKERS, E. H. (2010) An experimental study of magnesite dissolution rates at neutral to alkaline conditions and 150 and 200 degrees C as a function of pH, total dissolved carbonate concentration, and chemical affinity. *Geochimica et Cosmochimica Acta*, 74, 6344-6356.
- SCHIPEK, M. (2009) Carbon dioxide mineralisation by using acid mine lakes and industrial by-products: A specific solution for abandoned mining areas. Conference Proceedings, International Forum-Competition of Young Researchers "Topical Issues of subsoil usage", St. Petersburg, Russia, 18-19.
- SCHIPEK, M., GRAUPNER, B., MERKEL, B., WOLKERSDORFER, C. & WERNER, F. (2006a) Neutralisationspotential von Flugaschen - Restseesanierung Burghammer. *Wissenschaftliche Mitteilungen*, 31, 125-132.
- SCHIPEK, M. & MERKEL, B. (2007) Carbon dioxide elimination in post-mining lakes by using industrial by-products - design of a pilot scale field experiments (using injection technology). Conference Proceedings, Geotechnologien Status-Seminar "Investigation, Utilization and Protection of the Underground", RWE DEA Hamburg, 1-5.
- SCHIPEK, M. & MERKEL, B. (2008a) Carbon dioxide sequestration by using acid mine lakes and industrial by-products: Applicability of a niche solution. Conference Proceedings, International Conference "Geo2008 – Resources and Risks in the Earth System" and 160th annual meetig of the Deutsche Gesellschaft für Geowissenschaften e.V. (DGG) and 98th annual meeting of the Geologische Vereinigung e.V. (GV), Aachen, Germany, 127.

- SCHIPEK, M. & MERKEL, B. (2008b) CDEAL - Results using CO₂ and dumped fly ash in AMD affected lakes. Conference Proceedings, Geotechnologien Status-Seminar "Investigation, Utilization and Protection of the Underground", Stuttgart, 1-6.
- SCHIPEK, M. & MERKEL, B. (2008c) Pilotversuch zur CO₂-Injektion in alkalische Sedimente eines Tagebaufolgesees – Erste Ergebnisse. *Wissenschaftliche Mitteilungen*, 37, 25-30.
- SCHIPEK, M. & MERKEL, B. (2009a) CO₂ sequestration in AMD affected areas: A case study. *Geochemica et Cosmochimica Acta*, 73, 1174.
- SCHIPEK, M. & MERKEL, B. (2009b) Combined carbon dioxide sequestration and mine water treatment as a specific solution for abandoned mining areas - Results of a case study. Conference Proceedings, GeoDresden 2009, 161. Jahrestagung der Deutschen Gesellschaft für Geowissenschaften (DGG) Dresden, 301.
- SCHIPEK, M. & MERKEL, B. (2009c) Mine water treatment - Results using CO₂ and dumped fly ash in AMD affected lakes. *Wissenschaftliche Mitteilungen*, 38-43.
- SCHIPEK, M. & MERKEL, B. (2010) Betrachtung der Carbonatlösungskinetik und möglichen Inhibitoren bei der Anwendung von Inlake-Verfahren - Erste Ergebnisse. *Wissenschaftliche Mitteilungen*, 42, 61 - 70.
- SCHIPEK, M., MERKEL, B., UNGER, Y. & WOLKERSDORFER, C. (2006b) CO₂ inlake treatment - a challenge for different tasks. Conference Proceedings, Geotechnologien Status-Seminar "Investigation, Utilization and Protection of the Underground", TU Bergakademie Freiberg, 4.
- SCHIPEK, M., RABE, W., SCHOLZ, G., CLAUß, D., MERKEL, B. & LILJA, G. (2011) Recent results of the research project OILL (Optimizing In-Lake Liming) Conference Proceedings, 11th IMWA Congress, Aachen, Germany, 457-462.
- SCHIPEK, M., SCHULZ, S. & MERKEL, B. (2010) Continuous monitoring of dissolved CO₂ and H₂S: Technical application in the submarine hydrothermal system of Panarea, Italy. Conference Proceedings, Second International Workshop on Research in Shallow Marine and Fresh Water Systems, Milazzo, Italy, 72 - 75.
- SCHIPEK, M., UNGER, Y. & MERKEL, B. (2007) Alkalitätsverbessernde Maßnahmen in Tagebaufolgeseen: Nutzung von CO₂ und anderen industriellen "Abfallprodukten". *Wissenschaftliche Mitteilungen*, 35, 125-132.
- SCHRECK, P. & GLÄSSER, W. (1998) Regional Geology of the Lignite Mining Districts in Eastern Germany. In: GELLER, W., KLAPPER, H. & SALOMONS, W. (Eds.) In: *Acidic Mining Lakes*. Berlin, Heidelberg, Springer, 15 - 21.
- SCHROEDER, P. & LADD, L. (1991) Slowing the increase of atmospheric carbon dioxide - A biological approach. *Climatic Change*, 19, 283-290.

References

- SCHROETER, L. & GLASSER, C. (2011) Analyses and monitoring of lignite mining lakes in Eastern Germany with spectral signatures of Landsat TM satellite data. *International Journal of Coal Geology*, 86, 27-39.
- SCHÜLER, V. H. W. & COENEN, M. (2005) Rheinische Brikettfabriken 1877 - 2004. Electronic Source: <http://www.dbhverlag.de/brikettherstellung.html>
- SCHÜPPEL, B. (2009) Entwicklung von Modellen zur Optimierung der Sanierung saurer Tagebaurestseen und der Validierung im Labormaßstab. unpublished diploma thesis, Technische Universität Dresden, 106.
- SCHULTZE, M., POKRANDT, K. H. & HILLE, W. (2010) Pit lakes of the Central German lignite mining district: Creation, morphometry and water quality aspects. *Limnologica*, 40, 148-155.
- SHEORAN, A. S. & SHEORAN, V. (2006) Heavy metal removal mechanism of acid mine drainage in wetlands: A critical review. *Minerals Engineering*, 19, 105-116.
- SIBRELL, P. L., WATTEN, B. J., HAINES, T. A. & SPAULDING, B. W. (2006) Limestone fluidized bed treatment of acid-impacted water at the Craig Brook National Fish Hatchery, Maine, USA. *Aquacultural Engineering*, 34, 61-71.
- SIGG, L. & STUMM, W. (1996) Aquatische Chemie: eine Einführung in die Chemie wässriger Lösungen und natürlicher Gewässer. Zürich, vdf Hochschulverlag AG, ETH Zürich, 498.
- SIMS, R. C. & OVERCASH, M. R. (1983) Fate of Polynuclear Aromatic-Compounds (Pnas) in Soil-Plant Systems. *Residue Reviews*, 88, 1-68.
- SINGH, D. N. & KOLAY, P. K. (2002) Simulation of ash-water interaction and its influence on ash characteristics. *Progress in Energy and Combustion Science*, 28, 267-299.
- SJOBERG, E. L. (1976) Fundamental Equation for Calcite Dissolution Kinetics. *Geochimica et Cosmochimica Acta*, 40, 441-447.
- SJOBERG, E. L. (1978) Kinetics and mechanism of calcite dissolution in aqueous solutions at low temperatures. *Stockholm Contrib. Geol.*, 32, 92
- SJOBERG, E. L. & RICKARD, D. (1983) The Influence of Experimental-Design on the Rate of Calcite Dissolution. *Geochimica et Cosmochimica Acta*, 47, 2281-2285.
- SJOBERG, E. L. & RICKARD, D. T. (1985) The Effect of Added Dissolved Calcium on Calcite Dissolution Kinetics in Aqueous-Solutions at 25-Degrees-C. *Chemical Geology*, 49, 405-413.
- SKOUSEN, J., ROSE, A., GEIDEL, G., FOREMAN, J., EVANS, R. & HELLIER, W. (1998) Handbook of Technologies for Avoidance and Remediation of Acid Mine Drainage. Morgantown, West Virginia, West Virginia Water Research Institute, West Virginia University, 131.

- STEENARI, B. M., SCHELANDER, S. & LINDQVIST, O. (1999) Chemical and leaching characteristics of ash from combustion of coal, peat and wood in a 12 MW CFB - a comparative study. *Fuel*, 78, 249-258.
- STEVENS, S. H., KUUSKRAA, V. A. & GALE, J. (2001) Sequestration of CO₂ in depleted oil & gas fields: Global capacity, costs, and barriers. *Greenhouse Gas Control Technologies*, 278-283.
- STEVENS, S. H., KUUSKRAA, V. A., SPECTOR, D. & RIEMER, P. (1999) CO₂ sequestration in deep coal seams: Pilot results and worldwide potential. *Greenhouse Gas Control Technologies*, 175-180.
- STEWART, B. R., DANIELS, W. L. & JACKSON, M. L. (1997) Evaluation of leachate quality from codisposed coal fly ash and coal refuse. *Journal of Environmental Quality*, 26, 1417-1424.
- STEWART, B. R., DANIELS, W. L., ZELAZNY, L. W. & JACKSON, M. L. (2001) Evaluation of leachates from coal refuse blended with fly ash at different rates. *Journal of Environmental Quality*, 30, 1382-1391.
- STOLAROFF, J. K., LOWRY, G. V. & KEITH, D. W. (2005) Using CaO- and MgO-rich industrial waste streams for carbon sequestration. *Energy Conversion and Management*, 46, 687-699.
- STOTTMEISTER, U., MUDROCH, A., KENNEDY, C., MATIOVA, Z., SANECKI, J. & SVOBODA, I. (2002) Reclamation and Regeneration of Landscapes after Brown Coal Opencast Mining in Six Different Countries. In: MUDROCH, A., STOTTMEISTER, U., KENNEDY, C. & KLAPPER, H. (Eds.) In: *Remediation of abandoned surface coal mining sites*. Berlin Heidelberg, Springer, 4 - 36.
- STUMM, W. & MORGAN, J. J. (1996) Aquatic Chemistry: Chemical Equilibria and Rates in Natural Waters. New York, Wiley, 1040.
- SU, C. M. & HARSH, J. B. (1994) Gibbs Free-Energies of Formation at 298-K for Imogolite and Gibbsite from Solubility Measurements. *Geochimica et Cosmochimica Acta*, 58, 1667-1677.
- SULLIVAN, P. J. & YELTON, J. L. (1988) An Evaluation of Trace-Element Release Associated with Acid-Mine Drainage. *Environmental Geology and Water Sciences*, 12, 181-186.
- SUPP, E. (2007) Gas Production. In: *Ullmann's Encyclopedia of Industrial Chemistry*. Wiley-VCH Verlag GmbH & Co. KGaA, Weinheim, 1-169.
- SVENSON, T., DICKSON, W., HELLBERG, J., MOBERG, G. & MUNTHE, N. (1995) The Swedish liming programme. *Water Air and Soil Pollution*, 85, 1003-1008.
- SVENSSON, U. & DREYBRODT, W. (1992) Dissolution Kinetics of Natural Calcite Minerals in CO₂-Water Systems Approaching Calcite Equilibrium. *Chemical Geology*, 100, 129-145.

References

- SVERDRUP, H. U. (1985) Calcite dissolution kinetics and Lake neutralization. Lund Institute of Technology, 170.
- TAN, Y., DOUGLAS, M. A. & THAMBIMUTHU, K. V. (2002) CO₂ capture using oxygen enhanced combustion strategies for natural gas power plants. *Fuel*, 81, PII S0016-2361(0002)00014-00015.
- TAUBER, C. (1988) Spurenelemente in Flugaschen. Köln, Verlag TÜV Rheinland GmbH, 469.
- TEIEN, H. C., KROGLUND, F., SALBU, B. & ROSSELAND, B. O. (2006) Gill reactivity of aluminium-species following liming. *Science of the Total Environment*, 358, 206-220.
- TEIR, S., ELONEVA, S., FOGELHOLM, C. J. & ZEVENHOVEN, R. (2009) Fixation of carbon dioxide by producing hydromagnesite from serpentinite. *Applied Energy*, 86, 214-218.
- TEIR, S., KUUSIK, R., FOGELHOHN, C. J. & ZEVENHOVEN, R. (2007) Production of magnesium carbonates from serpentinite for long-term storage of CO₂. *International Journal of Mineral Processing*, 85, 1-15.
- TEMPLE, K. L. & COLMER, A. R. (1951) The Formation of Acid Mine Drainage. *Transactions of the American Institute of Mining and Metallurgical Engineers*, 190, 1090-1092.
- TERJESEN, S. G., ERGA, O., THORSEN, G. & VE, A. (1961) Phase Boundary Processes as Rate Determining Steps in Reactions between Solids and Liquids - the Inhibitory Action of Metal Ions on the Formation of Calcium Bicarbonate by the Reaction of Calcite with Aqueous Carbon Dioxide. *Chemical Engineering Science*, 14, 277-289.
- THISTLE, D., SEDLACEK, L., CARMAN, K. R., FLEEGER, J. W., BREWER, P. G. & BARRY, J. P. (2007) Exposure to carbon dioxide-rich seawater is stressful for some deep-sea species: an in situ, behavioral study. *Marine Ecology-Progress Series*, 340, 9-16.
- TISHMACK, J. K. & BURNS, P. E. (2004) The chemistry and mineralogy of coal and coal combustion products. *Geological Society Special Publication*, 223.
- TOTSCHE, O., FYSON, A. & STEINBERG, C. (2006) Microbial Alkalinity Production to Prevent Reacidification of Neutralized Mining Lakes. *Mine Water and the Environment*, 25, 204-213.
- TRAUTH, H. M. (2007) MATLAB(R) Recipes for Earth Sciences. Berlin Heidelberg New York, Springer, 288.
- TRAVAR, I. (2006) Assessing the environmental impact of ashes used in a landfill cover construction. Licentiate Thesis, Luleå University of Technology, 87.
- UFER, K., ROTH, G., KLEEBERG, R., STANJEK, H., DOHRMANN, R. & BERGMANN, J. (2004) Description of X-ray powder pattern of turbostratically disordered layer

- structures with a Rietveld compatible approach. *Zeitschrift fuer Kristallographie*, 219, 519-527.
- UIBU, M., UUS, M. & KUUSIK, R. (2009) CO₂ mineral sequestration in oil-shale wastes from Estonian power production. *Journal of Environmental Management*, 90, 1253-1260.
- VADAPALLI, V. R. K., KLINK, M. J., ETCHEBERS, O., PETRIK, L. F., GITARI, W., WHITE, R. A., KEY, D. & IWUOHA, E. (2008) Neutralization of acid mine drainage using fly ash, and strength development of the resulting solid residues. *South African Journal of Science*, 104, 317-322.
- VAN DER SLOOT, H. A., WIJKSTRA, J., VAN DALEN, A., DAS, H. A., SLANINA, J., DEKKERS, J. & WALS, G. D. (1982) Leaching of trace elements from coal solid waste. Report, 105.
- VASSILEV, S. V. & VASSILEVA, C. G. (1996) Mineralogy of combustion wastes from coal-fired power stations. *Fuel Processing Technology*, 47, 261-280.
- VASSILEV, S. V. & VASSILEVA, C. G. (2005) Methods for characterization of composition of fly ashes from coal-fired power stations: A critical overview. *Energy & Fuels*, 19, 1084-1098.
- VASSILEV, S. V. & VASSILEVA, C. G. (2007) A new approach for the classification of coal fly ashes based on their origin, composition, properties, and behaviour. *Fuel*, 86, 1490-1512.
- VASSILEV, S. V., VASSILEVA, C. G., KARAYIGIT, A. I., BULUT, Y., ALASTUEY, A. & QUEROL, X. (2005) Phase-mineral and chemical composition of fractions separated from composite fly ashes at the Soma power station, Turkey. *International Journal of Coal Geology*, 61, 65-85.
- VERBURG, R., BEZUIDENHOUT, N., CHATWIN, T. & FERGUSON, K. (2009) The Global Acid Rock Drainage Guide (GARD Guide). *Mine Water and the Environment*, 28, 305-310.
- VILE, M. A. & WIEDER, R. K. (1993) Alkalinity Generation by Fe(III) Reduction Versus Sulfate Reduction in Wetlands Constructed for Acid-Mine Drainage Treatment. *Water Air and Soil Pollution*, 69, 425-441.
- VINSON, M. D., ARVIDSON, R. S. & LUTTGE, A. (2007) Kinetic inhibition of calcite (104) dissolution by aqueous manganese(II). *Journal of Crystal Growth*, 307, 116-125.
- VOSBECK, K. (2004) Experimentelle Bestimmung der Lösungskinetik synthetischen Calciumcarbonats und natürlicher Kalkgesteine. Dissertation, Universität Bremen, 117.
- WALLIN, M. & BJERLE, I. (1989a) A Mass-Transfer Model for Limestone Dissolution from a Rotating Cylinder. *Chemical Engineering Science*, 44, 61-67.

References

- WALLIN, M. & BJERLE, I. (1989b) Rate Models for Limestone Dissolution - a Comparison. *Geochimica et Cosmochimica Acta*, 53, 1171-1176.
- WALTER, L. M. & BURTON, E. A. (1986) The Effect of Ortho-Phosphate on Carbonate Mineral Dissolution Rates in Seawater. *Chemical Geology*, 56, 313-323.
- WALTER, L. M. & HANOR, J. S. (1979) Effect of Ortho-Phosphate on the Dissolution Kinetics of Biogenic Magnesian Calcites. *Geochimica et Cosmochimica Acta*, 43, 1377-1385
- WANG, C. B., JIA, L. F., TAN, Y. W. & ANTHONY, E. J. (2008) Carbonation of fly ash in oxy-fuel CFB combustion. *Fuel*, 87, 1108-1114.
- WARREN, C. J. & DUDAS, M. J. (1985) Formation of Secondary Minerals in Artificially Weathered Fly-Ash. *Journal of Environmental Quality*, 14, 405-410.
- WATTEN, B. J., LEE, P. C., SIBRELL, P. L. & TIMMONS, M. B. (2007) Effect of temperature, hydraulic residence time and elevated P-CO₂ on acid neutralization within a pulsed limestone bed reactor. *Water Research*, 41, 1207-1214.
- WATTEN, B. J., SIBRELL, P. L. & SCHWARTZ, M. F. (2004) Effect of acidity and elevated P-CO₂ on acid neutralization within pulsed limestone bed reactors receiving coal mine drainage. *Environmental Engineering Science*, 21, 786-802.
- WATTEN, B. J., SIBRELL, P. L. & SCHWARTZ, M. F. (2005) Acid neutralization within limestone sand reactors receiving coal mine drainage. *Environmental Pollution*, 137, 295-304.
- WEINBERG, A. & HEMMINGS, R. (1997) Hydration and weathering reactions in by-products from clean coal technologies: Effects on material properties. *Fuel*, 76, 705-709.
- WEYL, P. K. (1958) The Solution Kinetics of Calcite. *Journal of Geology*, 66, 163-176.
- WHITE, C. M., SMITH, D. H., JONES, K. L., GOODMAN, A. L., JIKICH, S. A., LACOUNT, R. B., DUBOSE, S. B., OZDEMIR, E., MORSI, B. I. & SCHROEDER, K. T. (2005) Sequestration of carbon dioxide in coal with enhanced coalbed methane recovery - A review. *Energy & Fuels*, 19, 659-724.
- WILSON, M., MOBERG, R., STEWART, B. & THAMBIMUTHU, K. (2001) CO₂ sequestration in oil reservoirs - A monitoring and research opportunity. *Greenhouse Gas Control Technologies*, 243-247.
- YANG, H. Q., XU, Z. H., FAN, M. H., GUPTA, R., SLIMANE, R. B., BLAND, A. E. & WRIGHT, I. (2008) Progress in carbon dioxide separation and capture: A review. *Journal of Environmental Sciences-China*, 20, 14-27.
- YAVITT, J. B. & FAHEY, T. J. (1996) Peat and solution chemistry responses to CaCO₃ application in wetlands next to Woods Lake, New York. *Biogeochemistry*, 32, 245-263.

- ZEIEN, H. (1995) Chemische Extraktionen zur Bestimmung der Bindungsformen von Schwermetallen in Böden. *Bonner bodenkundliche Abhandlungen*, 17, 284.
- ZEVENBERGEN, C., BRADLEY, J. P., VAN REEUWIJK, L. P., SHYAM, A. K., HJELMAR, O. & COMANS, R. N. J. (1999) Clay formation and metal fixation during weathering of coal fly ash. *Environmental Science & Technology*, 33, 3405-3409.
- ZEVENBERGEN, C., BRADLEY, J. P., VANDERWOOD, T., BRWON, R. S., VAN REEUWIJK, L. P. & SCHUILING, R. D. (1994) Microanalytical investigation of mechanisms of MSWI bottom ash weathering. *Microbeam Analysis*, 3, 125–135.
- ZEVENBERGEN, C., VANREEUWIJK, L. P., BRADLEY, J. P., BLOEMEN, P. & COMANS, R. N. J. (1996) Mechanism and conditions of clay formation during natural weathering of MSWI bottom ash. *Clays and Clay Minerals*, 44, 546-552.
- ZHANG, Y. P. & DAWE, R. A. (2000) Influence of Mg²⁺ on the kinetics of calcite precipitation and calcite crystal morphology. *Chemical Geology*, 163, 129-138.
- ZIELINSKI, R. A. & BUDAHN, J. R. (2007) Mode of occurrence and environmental mobility of oil-field radioactive material at US Geological Survey research site B, Osage-Skiatook Project, northeastern Oklahoma. *Applied Geochemistry*, 22, 2125-2137.
- ZIKELI, S., KASTLER, M. & JAHN, R. (2004) Cation exchange properties of soils derived from lignite ashes. *Journal of Plant Nutrition and Soil Science*, 167, 439-448.
- ZSCHIEDRICH, K. (2011) Wasserwirtschaftliche Sanierung unter sich ändernden Rahmenbedingungen. Conference Proceedings, Flutungswasserkonferenz 2011, Hoyerswerda, 1-37.
- ZSCHIEDRICH, K., BENTHAUS, F.-C., KAISER, J., GOCKEL, G., LUCKNER, L. & VOGT, A. (2007) LMBV Flutungs- und Wasserbehandlungskonzept, Lausitz 12/2006. Report,
- ZSCHIEDRICH, K., GOCKEL, G., SCHOLZ, G., RABE, W., APPELT, J., JESCHKE, A., MÖNCH, W., JAHN, M. & JANY, S. (2000) Abschlussbericht "Einsatz von Kraftwerkssaschen der Lausitz zur Verbesserung der Wassergüte des Tagebaurestsees Burghammer". Report, 54.

APPENDIX A: Additional Figures

Figure A. 1. Zinc release from deposited ash sediment	194
Figure A. 2. Nickel release from deposited ash sediment	194
Figure A. 3. Molybdenum release from deposited ash sediment	195
Figure A. 4. Arsenic release from deposited ash sediment.....	195
Figure A. 5. Chromium release from deposited ash sediment	196
Figure A. 6. Iron release from deposited ash sediment.....	196
Figure A. 7. Sodium concentration in lake water during pilot experiment	197
Figure A. 8. Potassium concentration in lake water during pilot experiments	197
Figure A. 9. Calcium concentration in lake water during pilot experiment.....	198
Figure A. 10. Magnesium concentration in lake water during pilot experiment	198
Figure A. 11. Chloride concentration in lake water during pilot experiment	199
Figure A. 12. Sulfate concentration in lake water during pilot experiment	199
Figure A. 13. SEM image of Dolomitfeinkalk_DL85. Main components of this liming agent contain Mg (wide range 23.17 (1) – 79.27 (5) wt.-%), average 53.75 wt.-%), Si (0 – 38.26 (1) wt.-%, average 12.85 wt.-%) and K (2.97 (5) – 15.93 (1) wt.-%, average 9.93 wt.-%). Further constituents are Al (average 0.97 wt.-%), Ca (average 1.08 wt.-%) and Fe (0.37 wt.-%). Traces of S, Ti and Mn were found.	200
Figure A. 14. SEM image of Dolomitsteinmehl_913. Main elements are Ca (in average 33.90 wt.-%) and Mg (in average 14.92 wt.-%). Further constituents contain Fe (in average 1.41 wt.-%) and Si (in average 1.28 wt.-%). Al was found as minor element (0.46 wt.-%).	200
Figure A. 15. SEM image of Dünger_Ostrau. Main elements are Ca (in average 29.31 wt.-%) and Mg (in average 15.19 wt.-%). Fe was found with 1.72 wt.-%. Some areas contained Al (1.39 wt.-%, (14)), Si (in average 1.67 wt.-%, (2)/(4)/(14), and Mn (in average 1.28 wt.-%, (3) & (10)).	200
Figure A. 16. SEM image of Kalk_Hoehnetal. Ca was dominant in all areas (in average 45.67 wt.-%). Besides, Mg and Si (both in average 1.00 wt.-%), Fe (0.81 wt.-%) and Al (in average 0.44 wt.-%) was found.....	201
Figure A. 17. SEM image of Kalkhydrat_6132-5. Ca was main constituent with 55.0 wt.-%. Minor constituents were S (wide range 0.27 (7) – 11.25 (6) wt.-%, in average 2.29 wt.-%), Fe (in average 0.88 wt.-%), Mg (in average 0.39 wt.-%) and Si (in average 0.33 wt.-%).....	201

Figure A. 18. SEM-image of Kalksteinmehl_0-0.09. Main elements are Ca (in average 25.77 wt.-%) and Mg (in average 15.04 wt.-%). Minor constituents are Si (in average 4.19 wt.-%), Al (in average 2.90 wt.-%), Fe (in average 1.40 wt.-%). Mn was found as trace element (in average 0.73 wt.-%) 201

Figure A. 19. SEM image of Kalksteinsand. Calcium was found in a range from 34.90 (8) – 79.35 (7) wt.-%. Average content was 49.28 wt.-%. Other elements had low concentrations, e.g. Mg (in average 0.56 wt.-%), Fe (in average 0.75 wt.-%), Mn (in average 0.45 wt.-%), Si (in average 0.32 wt.-%) and Al (in average 0.20 wt.-%) 202

Figure A. 20. SEM image of KSM 10-90. Main constituent of KSM 10-90 was Ca (in average 47.44 wt.-%). Less concentrations were found from Si (in average 0.85 wt.-%), Fe (in average 0.84 wt.-%), Mg (in average 0.61 wt.-%) and Al (in average 0.33 wt.-%) 202

Figure A. 21. SEM image of KSM 40-3. Calcium was found as main element (in average 38.35 wt.-%). Fe was the second most element in the sample (in average 7.86 wt.-%). Other elements were in lower concentrations: Si (in average 1.22 wt.-%), Na (in average 1.17 wt.-%), Mg (in average 0.72 wt.-%), Al (in average 0.51 wt.-%) and Mn (in average 1.57 wt.-%) 202

Figure A. 22. SEM image of Rheinkalk WFK CL90. Main element is Ca (in average 42.93 wt.-%). Si and Mg were minor elements, in average 1.73 wt.-%, respectively 1.57 wt.-%). Traces of Fe (in average 0.78 wt.-%), Al (in average 0.66 wt.-%) and Mn (in average 0.50 wt.-%) were found 203

Figure A. 23. SEM image of Rüdersdorfer Kalk WKH_u12. Most of the areas had high concentrations of Ca (in average 47.57 wt.-%). Minor constituents were Si (in average 1.01 wt.-%), Mg (in average 0.80 wt.-%), Fe (in average 0.65 wt.-%), Al (in average 0.44 wt.-%), Mn (in average 0.35 wt.-%) and K (in average 0.15 wt.-%) 203

Figure A. 24. SEM image of Rügener Schlämmkreide. Rügener Schlämmkreide mainly consists of Calcium (in average 36.55 wt.-%). Minor constituents are Si (in average 1.53 wt.-%), Mg (in average 0.90 wt.-%), Fe (in average 0.69 wt.-%), Al (in average 0.60 wt.-%), Mn (in average 0.42 wt.-%) and K (0.17 wt.-%) 203

Figure A. 25. SEM image of Saxocarb_300F. Ca and Mg were main elements in the sample Saxocarb_300F, in average 32.05 and 14.47 wt.-%. Minor elements were Si (in average 3.73 wt.-%), Fe (in average 1.17 wt.-%), Na (in average 0.82 wt.-%), Al (in average 0.63 wt.-%), Mn (in average 0.63 wt.-%) and K (in average 0.16 wt.-%) 204

Figure A. 26. SEM image of Saxolith_C1. Calcium was detected as main element (in average 48.14 wt.-%). Besides, the elements Si (in average 4.79 wt.-%), Fe (in average 2.68 wt.-%), Al (in average 2.45 wt.-%), Mg (in average 1.75 wt.-%), K (in average 0.86 wt.-%) and Mn (in average 0.57 wt.-%) 204

Figure A. 27. SEM image of Wasserkalk, reaktionsverzögert. Main constituent was Calcium with in average 42.18 wt.-%. Other elements found were Si (2.61 wt.-%), Al (1.23 wt.-%), Mg (in average 0.92 wt.-%), Fe (in average 0.86 wt.-%), Mn (in average 0.46 wt.-%), and K (in average 0.17 wt.-%) 204

Figure A. 28. SEM image of WFK (Weissfeinkalk) CaO. WFK CaO mainly consists of Ca (52.67 wt.-%). Further elements were Fe (in average 0.56 wt.-%), Mg (in average 0.43 wt.-%), Si (in average 0.28 wt.-%) and Al (in average 0.24 wt.-%). 205

Figure A. 29. SEM image of Weisskalkhydrat WKH 2-4. Calcium was detected with in average 45.33 wt.-%. Si and Mg were minor constituents with 1.42 and 1.13 wt.-%. Lower concentrations of Fe (in average 0.74 wt.-%), Al (in average 0.57 wt.-%), and Mn (in average 0.43 wt.-%) had been measured. 205

Figure A. 30. SEM image of WKH ultralight. Calcium was the main element in this sample (46.25 wt.-%). Minor elements were Si (1.61 wt.-%), Mg (1.26 wt.-%), Fe (0.74 wt.-%), Al (0.60 wt.-%) and Mn (0.51 wt.-%)..... 205

Figure A. 31. SEM image of Wünschendorfer Dolomitfeinkalk. Ca and Mg were main elements in this sample (in average 34.83, respectively 18.07 wt.-%). Other elements had been determined in minor concentrations, e.g. Fe (in average 0.72 wt.-%), Si (0.59 wt.-%), Mn (0.43 wt.-%), K (0.36 wt.-%), Ti (0.24 wt.-%), Al (0.22 wt.-%). 206

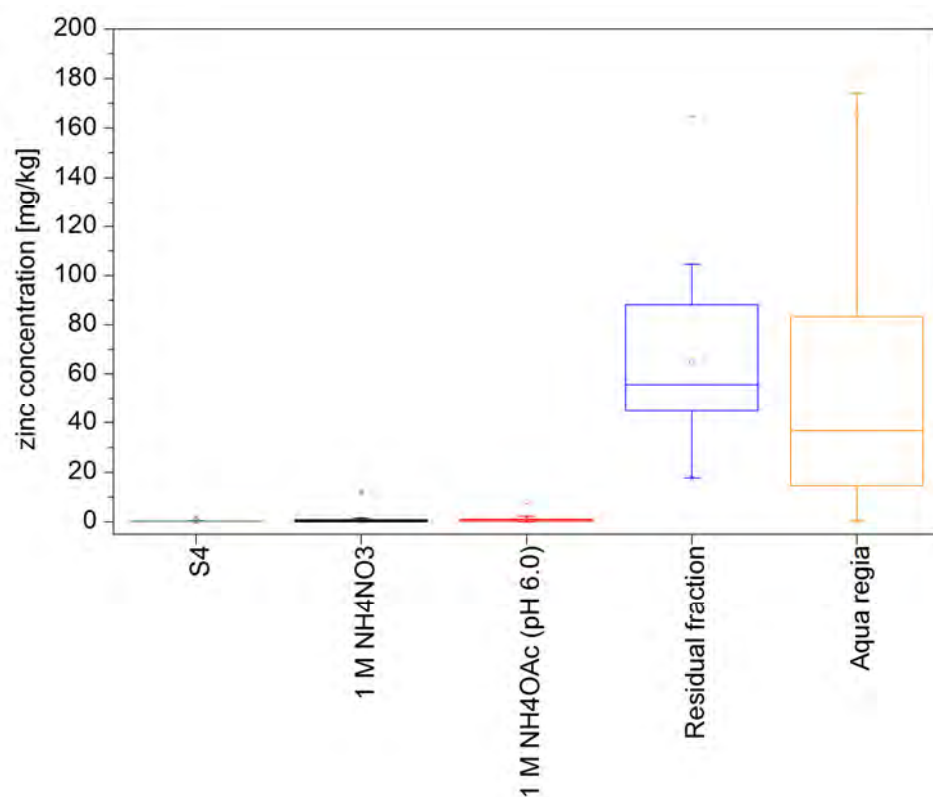


Figure A. 1. Zinc release from deposited ash sediment

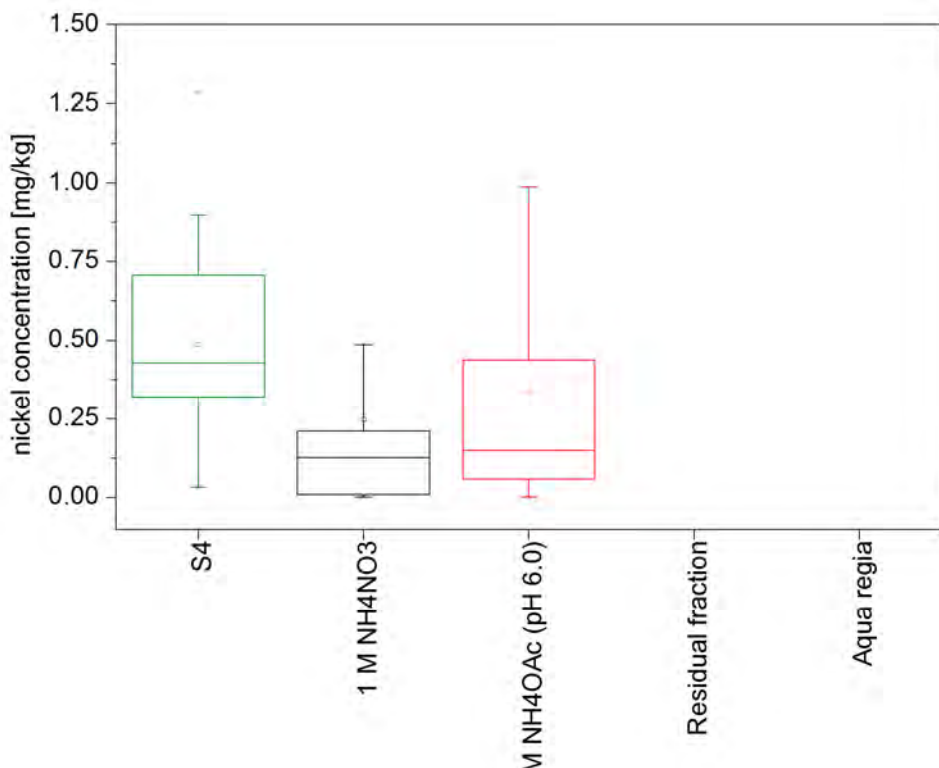


Figure A. 2. Nickel release from deposited ash sediment

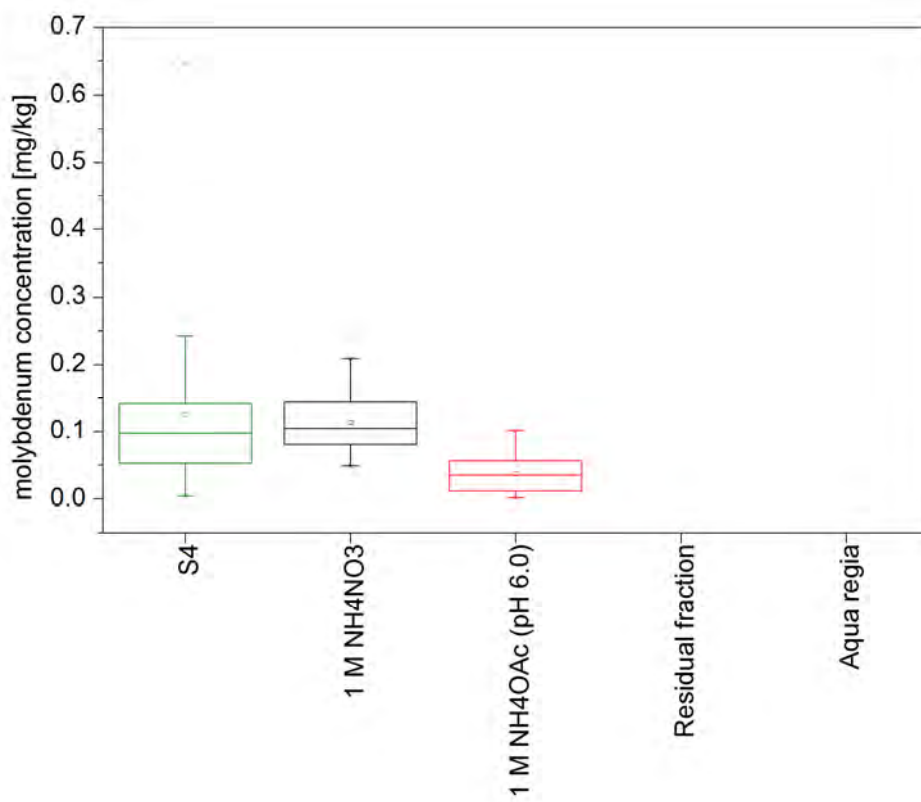


Figure A. 3. Molybdenum release from deposited ash sediment

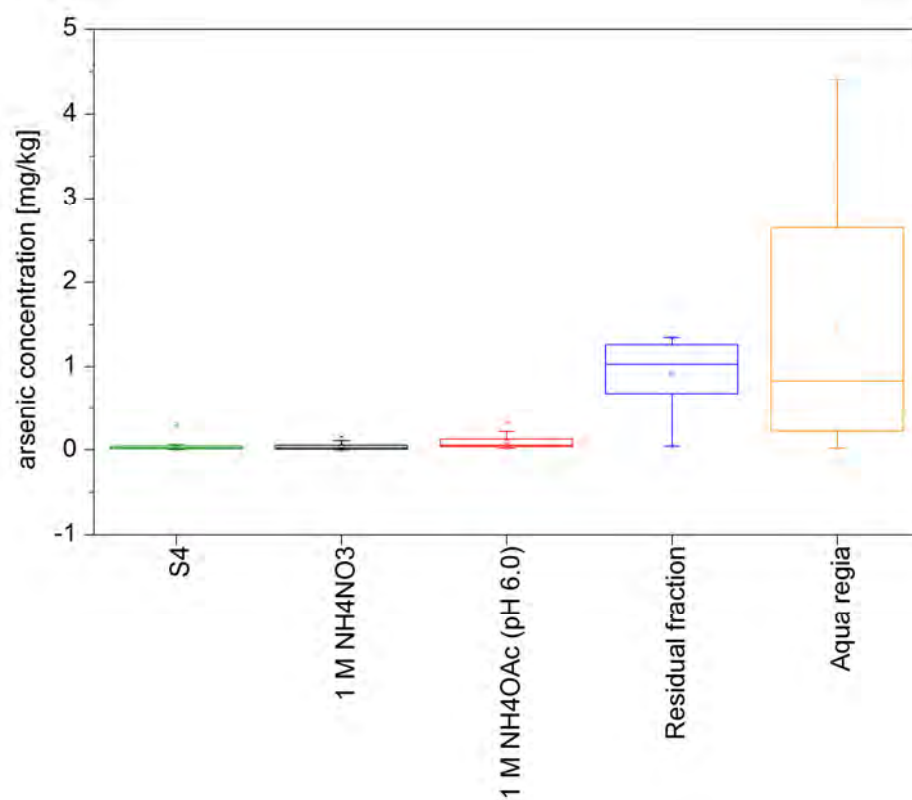


Figure A. 4. Arsenic release from deposited ash sediment

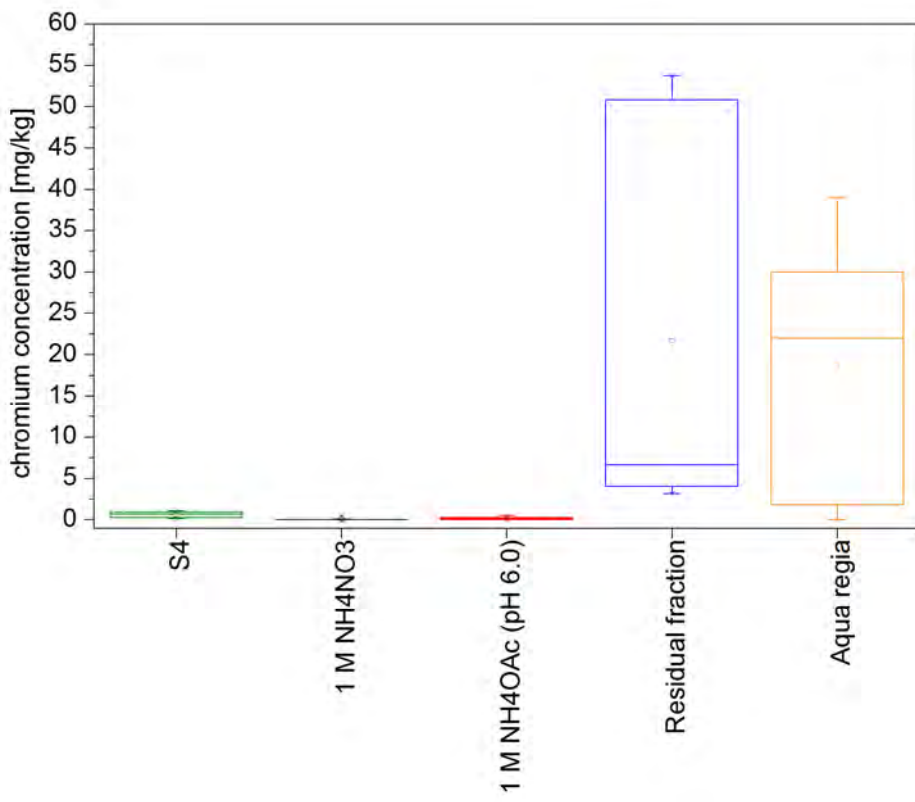


Figure A. 5. Chromium release from deposited ash sediment

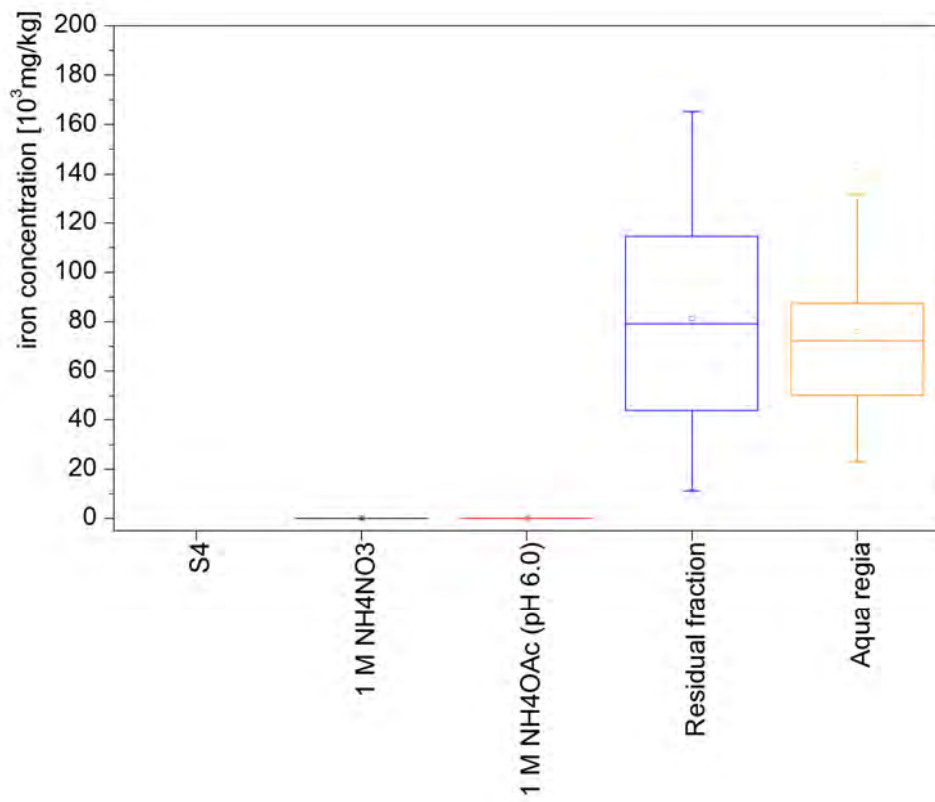


Figure A. 6. Iron release from deposited ash sediment

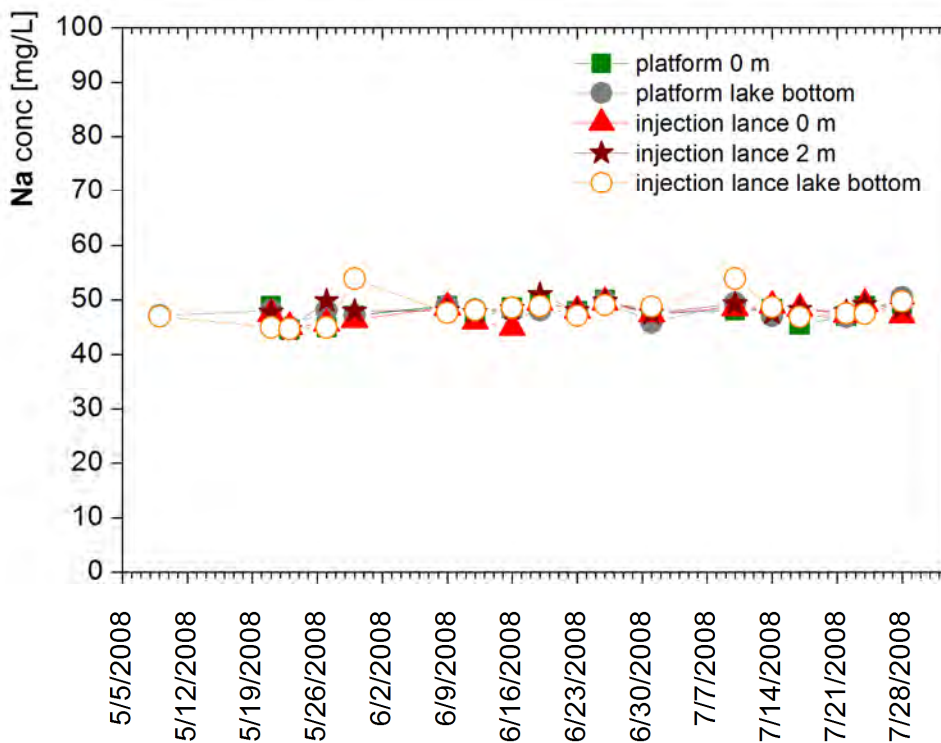


Figure A. 7.Sodium concentration in lake water during pilot experiment

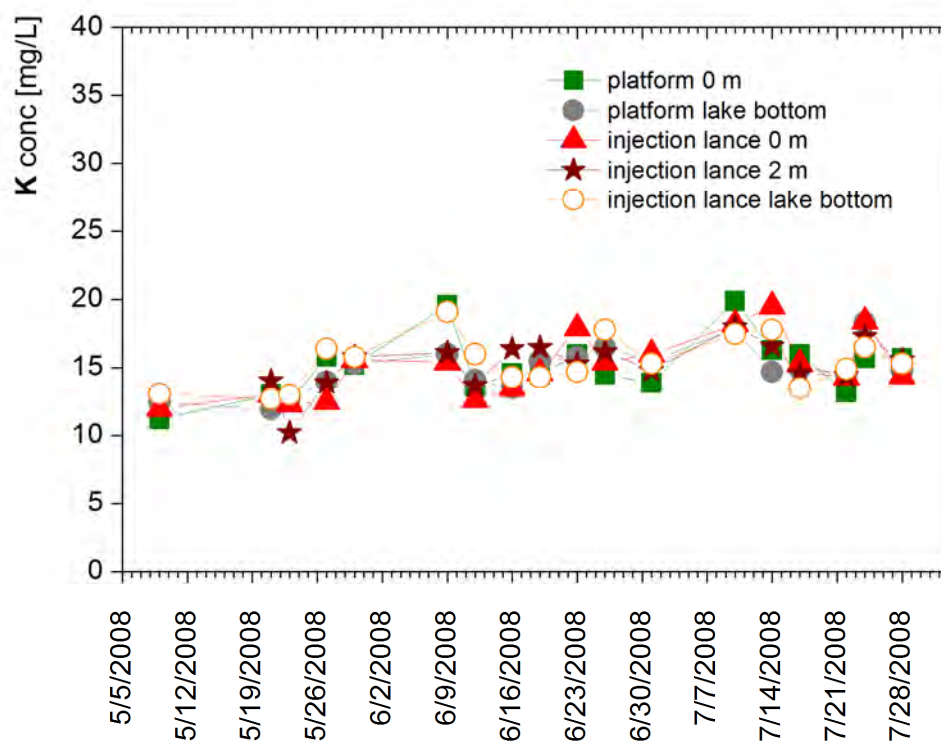


Figure A. 8.Potassium concentration in lake water during pilot experiments

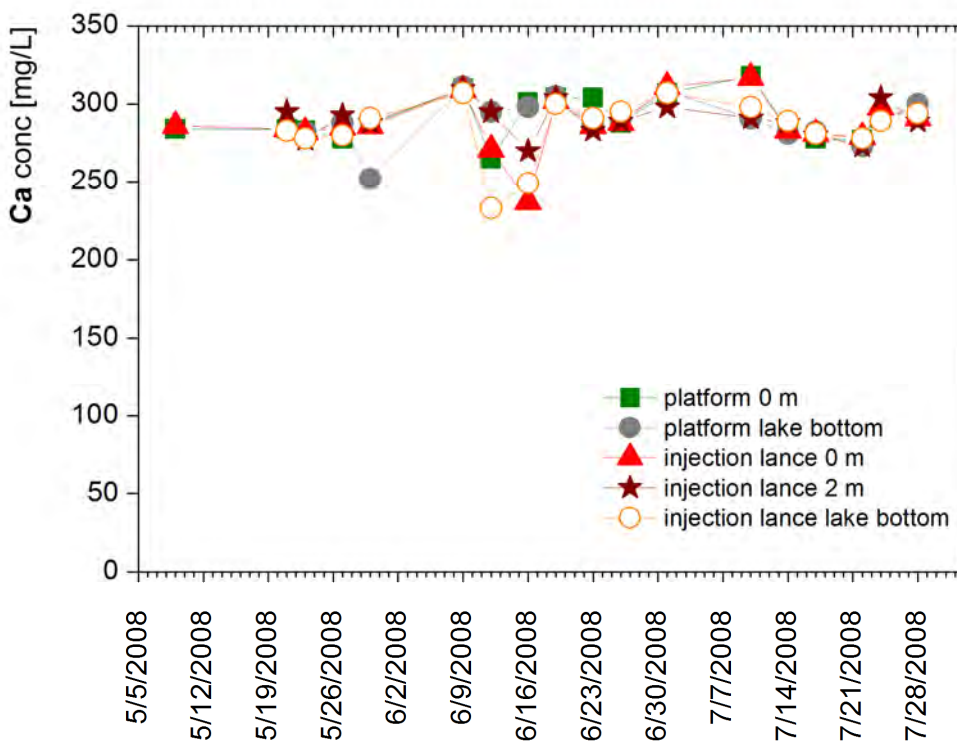


Figure A. 9.Calcium concentration in lake water during pilot experiment

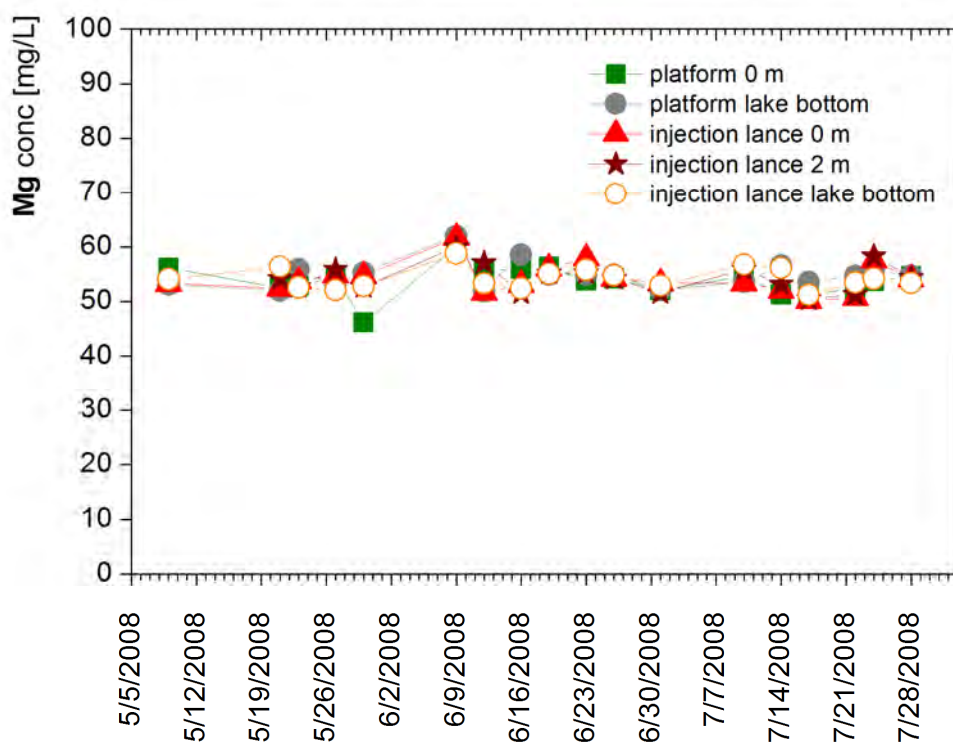


Figure A. 10.Magnesium concentration in lake water during pilot experiment

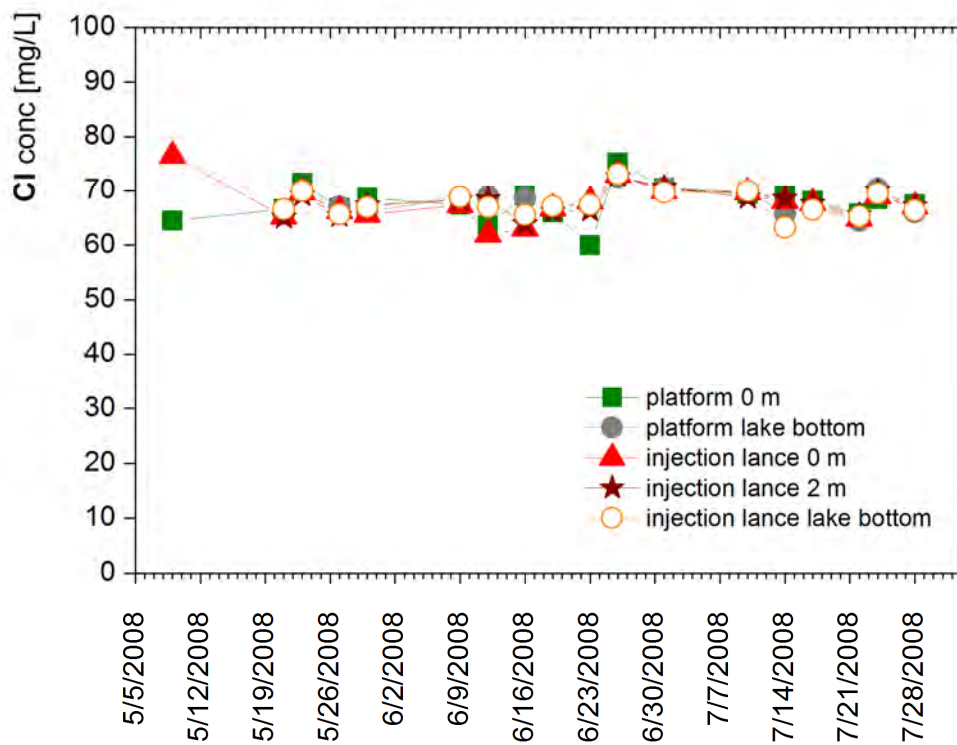


Figure A. 11. Chloride concentration in lake water during pilot experiment

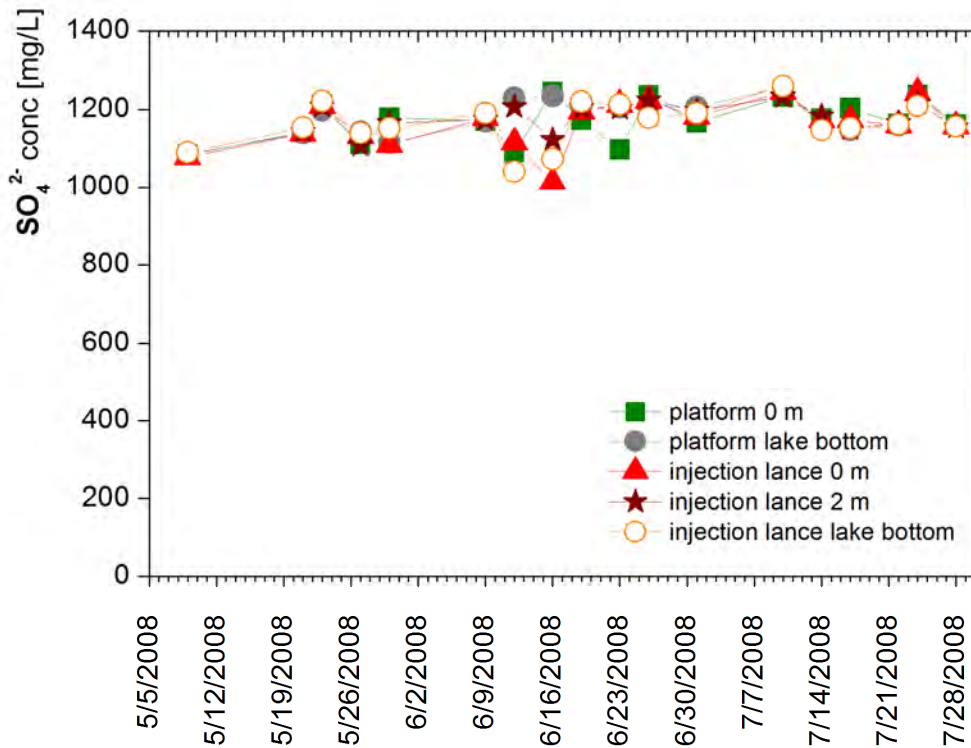


Figure A. 12. Sulfate concentration in lake water during pilot experiment

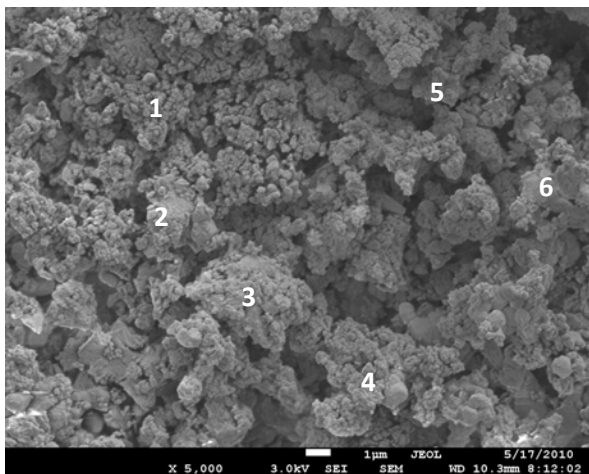


Figure A. 13. SEM image of Dolomitfeinkalk_DL85. Main components of this liming agent contain Mg (wide range 23.17 (1) – 79.27 (5) wt.-%), average 53.75 wt.-%), Si (0 – 38.26 (1) wt.-%, average 12.85 wt.-%) and K (2.97 (5) – 15.93 (1) wt.-%, average 9.93 wt.-%). Further constituents are Al (average 0.97 wt.-%), Ca (average 1.08 wt.-%) and Fe (0.37 wt.-%). Traces of S, Ti and Mn were found.

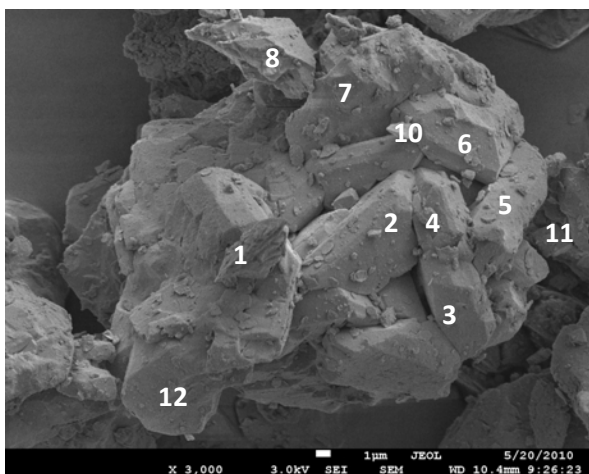


Figure A. 14. SEM image of Dolomitsteinmehl_913. Main elements are Ca (in average 33.90 wt.-%) and Mg (in average 14.92 wt.-%). Further constituents contain Fe (in average 1.41 wt.-%) and Si (in average 1.28 wt.-%). Al was found as minor element (0.46 wt.-%).

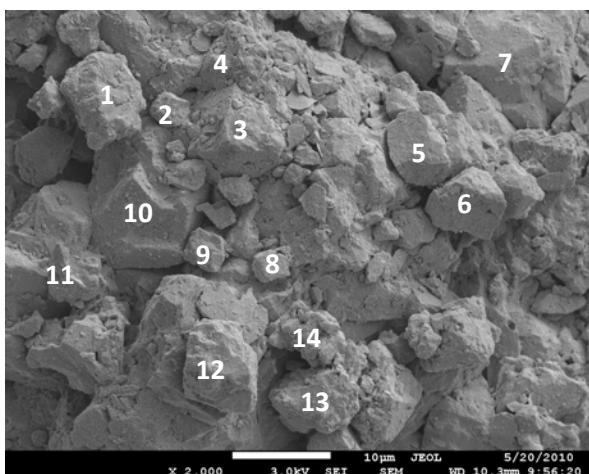


Figure A. 15. SEM image of Dünger_Ostrau. Main elements are Ca (in average 29.31 wt.-%) and Mg (in average 15.19 wt.-%). Fe was found with 1.72 wt.-%. Some areas contained Al (1.39 wt.-%, (14)), Si (in average 1.67 wt.-%, (2)/(4)/(14)), and Mn (in average 1.28 wt.-%, (3) & (10)).

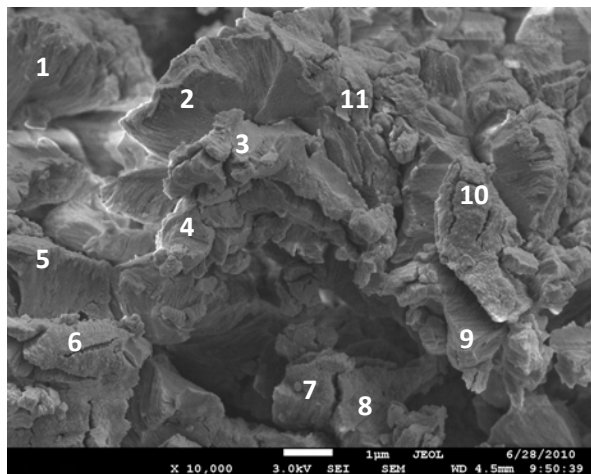


Figure A. 16. SEM image of Kalk_Hoehnetal. Ca was dominant in all areas (in average 45.67 wt.-%). Besides, Mg and Si (both in average 1.00 wt.-%), Fe (0.81 wt.-%) and Al (in average 0.44 wt.-%) was found.

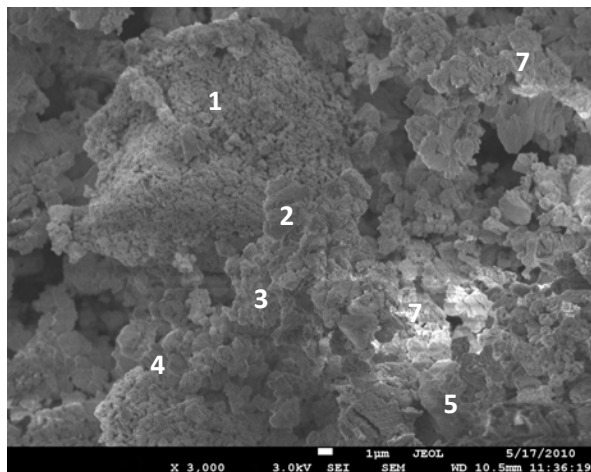


Figure A. 17. SEM image of Kalkhydrat_6132-5. Ca was main constituent with 55.0 wt.-%. Minor constituents were S (wide range 0.27 (7) – 11.25 (6) wt.-%, in average 2.29 wt.-%), Fe (in average 0.88 wt.-%), Mg (in average 0.39 wt.-%) and Si (in average 0.33 wt.-%).

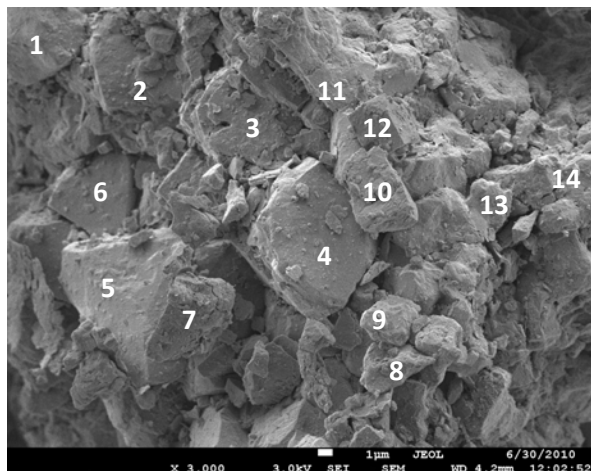


Figure A. 18. SEM-image of Kalksteinmehl_0-0.09. Main elements are Ca (in average 25.77 wt.-%) and Mg (in average 15.04 wt.-%). Minor constituents are Si (in average 4.19 wt.-%), Al (in average 2.90 wt.-%), Fe (in average 1.40 wt.-%). Mn was found as trace element (in average 0.73 wt.-%).

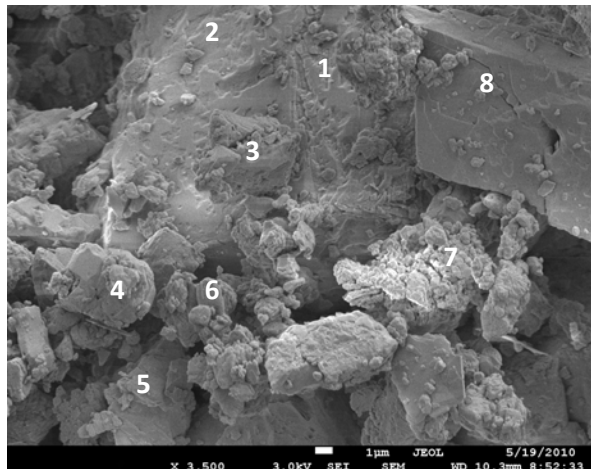


Figure A. 19. SEM image of Kalksteinsand. Calcium was found in a range from 34.90 (8) – 79.35 (7) wt.-%. Average content was 49.28 wt.-%. Other elements had low concentrations, e.g. Mg (in average 0.56 wt.-%), Fe (in average 0.75 wt.-%), Mn (in average 0.45 wt.-%), Si (in average 0.32 wt.-%) and Al (in average 0.20 wt.-%).

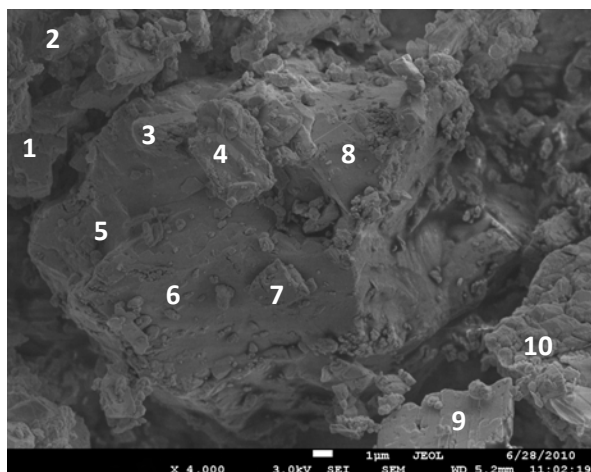


Figure A. 20. SEM image of KSM 10-90. Main constituent of KSM 10-90 was Ca (in average 47.44 wt.-%). Less concentrations were found from Si (in average 0.85 wt.-%), Fe (in average 0.84 wt.-%), Mg (in average 0.61 wt.-%) and Al (in average 0.33 wt.-%).

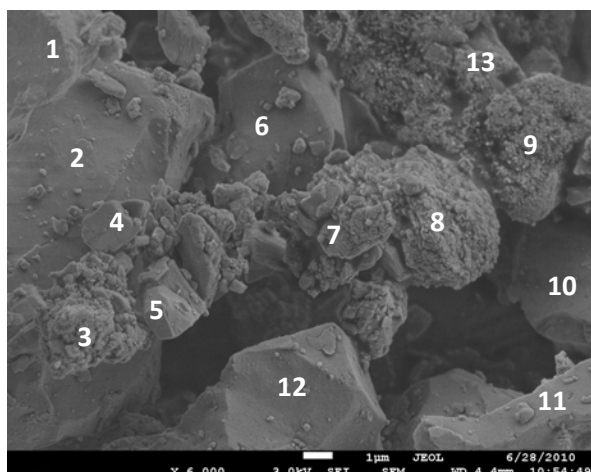


Figure A. 21. SEM image of KSM 40-3. Calcium was found as main element (in average 38.35 wt.-%). Fe was the second most element in the sample (in average 7.86 wt.-%). Other elements were in lower concentrations: Si (in average 1.22 wt.-%), Na (in average 1.17 wt.-%), Mg (in average 0.72 wt.-%), Al (in average 0.51 wt.-%) and Mn (in average 1.57 wt.-%).

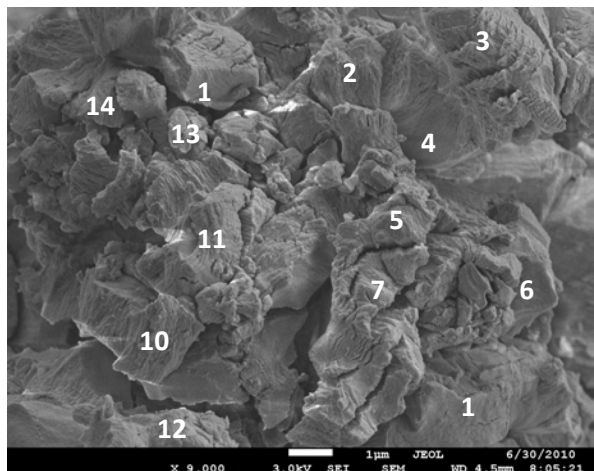


Figure A. 22. SEM image of Rheinkalk WFK CL90. Main element is Ca (in average 42.93 wt.-%). Si and Mg were minor elements, in average 1.73 wt.-%, respectively 1.57 wt.-%). Traces of Fe (in average 0.78 wt.-%), Al (in average 0.66 wt.-%) and Mn (in average 0.50 wt.-%) were found.

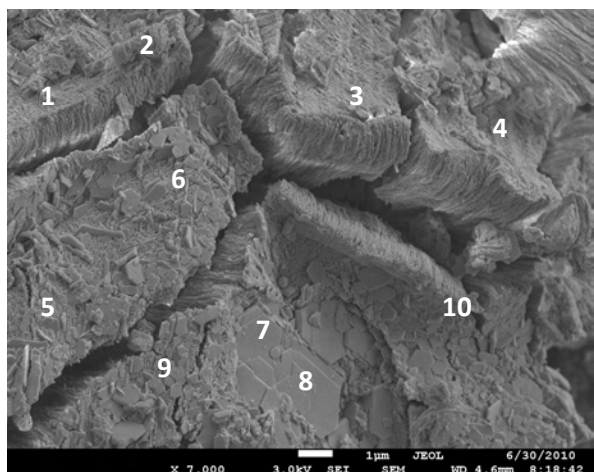


Figure A. 23. SEM image of Rüdersdorfer Kalk WKH_u12. Most of the areas had high concentrations of Ca (in average 47.57 wt.-%). Minor constituents were Si (in average 1.01 wt.-%), Mg (in average 0.80 wt.-%), Fe (in average 0.65 wt.-%), Al (in average 0.44 wt.-%), Mn (in average 0.35 wt.-%) and K (in average 0.15 wt.-%).

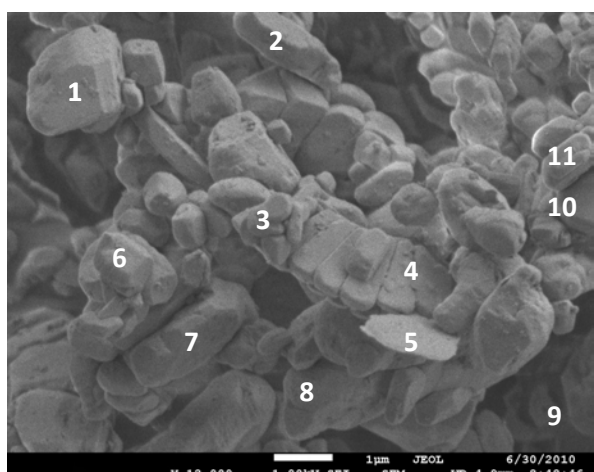


Figure A. 24. SEM image of Rügener Schlämmkreide. Rügener Schlämmkreide mainly consists of Calcium (in average 36.55 wt.-%). Minor constituents are Si (in average 1.53 wt.-%), Mg (in average 0.90 wt.-%), Fe (in average 0.69 wt.-%), Al (in average 0.60 wt.-%), Mn (in average 0.42 wt.-%) and K (0.17 wt.-%).

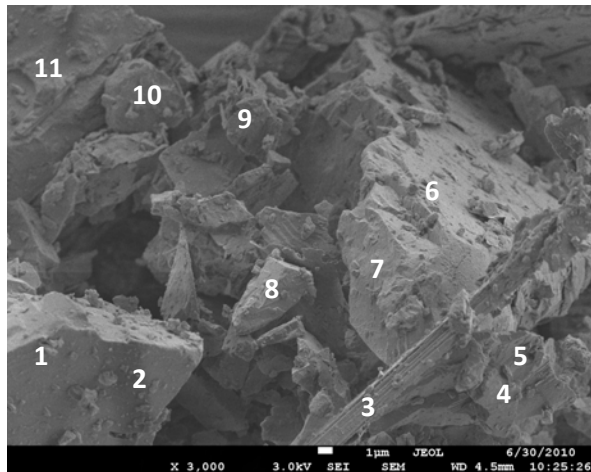


Figure A. 25. SEM image of Saxocarb_300F. Ca and Mg were main elements in the sample Saxocarb_300F, in average 32.05 and 14.47 wt.-%. Minor elements were Si (in average 3.73 wt.-%), Fe (in average 1.17 wt.-%), Na (in average 0.82 wt.-%), Al (in average 0.63 wt.-%), Mn (in average 0.63 wt.-%) and K (in average 0.16 wt.-%).

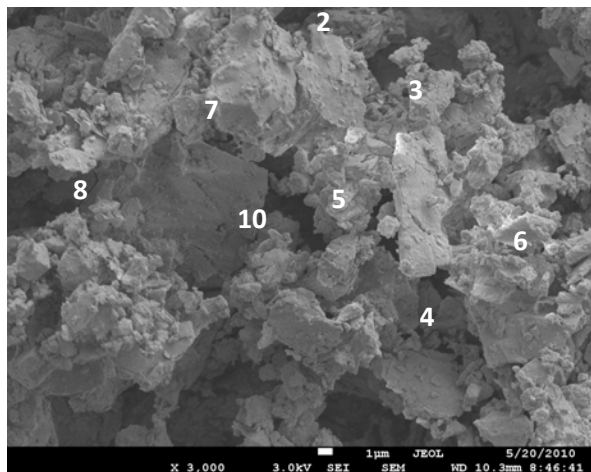


Figure A. 26. SEM image of Saxolith_C1. Calcium was detected as main element (in average 48.14 wt.-%). Besides, the elements Si (in average 4.79 wt.-%), Fe (in average 2.68 wt.-%), Al (in average 2.45 wt.-%), Mg (in average 1.75 wt.-%), K (in average 0.86 wt.-%) and Mn (in average 0.57 wt.-%).

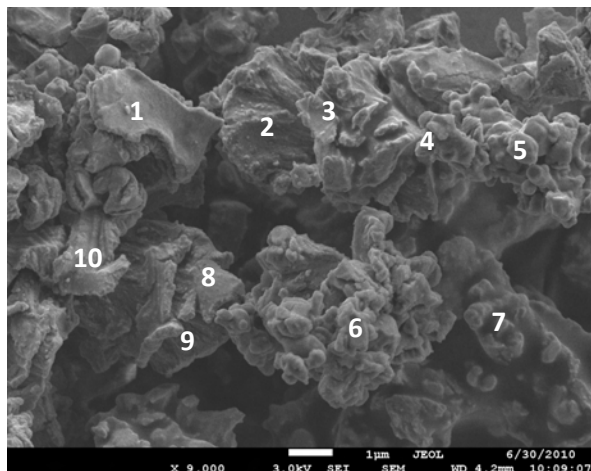


Figure A. 27. SEM image of Wasserkalk, reaktionsverzögert. Main constituent was Calcium with in average 42.18 wt.-%. Other elements found were Si (2.61 wt.-%), Al (1.23 wt.-%), Mg (in average 0.92 wt.-%), Fe (in average 0.86 wt.-%), Mn (in average 0.46 wt.-%), and K (in average 0.17 wt.-%).

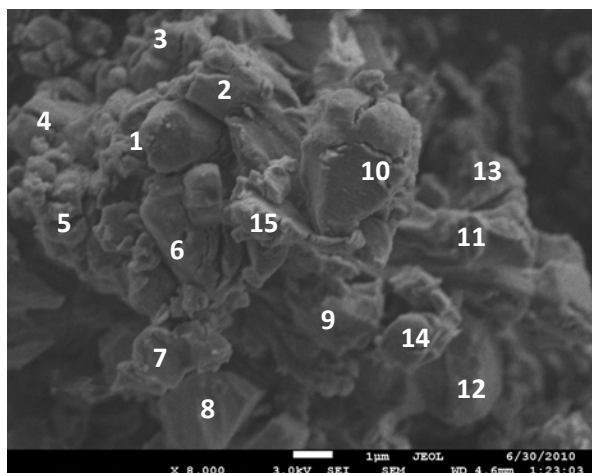


Figure A. 28. SEM image of WFK (Weissfeinkalk) CaO. WFK CaO mainly consists of Ca (52.67 wt.-%). Further elements were Fe (in average 0.56 wt.-%), Mg (in average 0.43 wt.-%), Si (in average 0.28 wt.-%) and Al (in average 0.24 wt.-%).

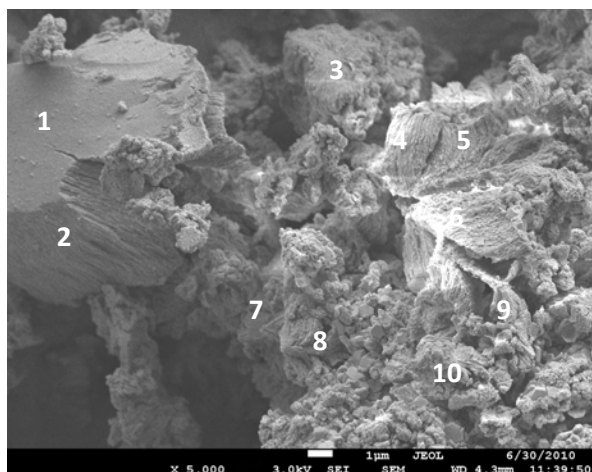


Figure A. 29. SEM image of Weisskalkhydrat WKH 2-4. Calcium was detected with in average 45.33 wt.-%. Si and Mg were minor constituents with 1.42 and 1.13 wt.-%. Lower concentrations of Fe (in average 0.74 wt.-%), Al (in average 0.57 wt.-%), and Mn (in average 0.43 wt.-%) had been measured.

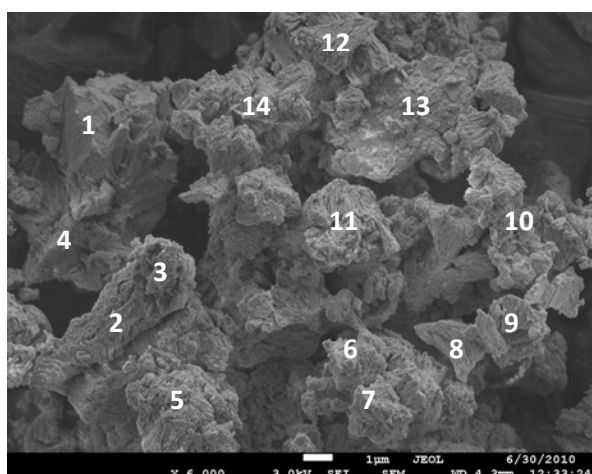


Figure A. 30. SEM image of WKH ultralight. Calcium was the main element in this sample (46.25 wt.-%). Minor elements were Si (1.61 wt.-%), Mg (1.26 wt.-%), Fe (0.74 wt.-%), Al (0.60 wt.-%) and Mn (0.51 wt.-%).

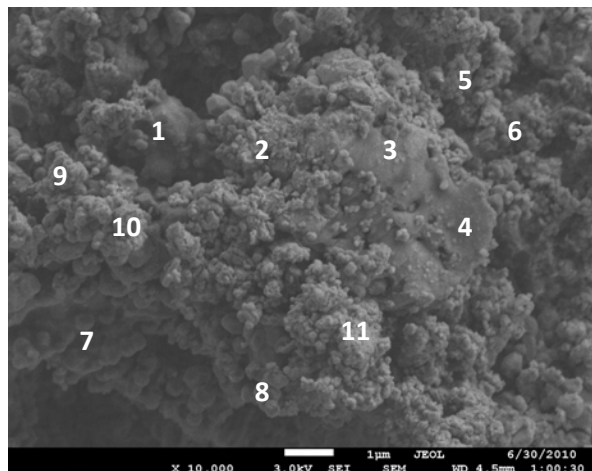


Figure A. 31. SEM image of Wünschendorfer Dolomitfeinkalk. Ca and Mg were main elements in this sample (in average 34.83, respectively 18.07 wt.-%). Other elements had been determined in minor concentrations, e.g. Fe (in average 0.72 wt.-%), Si (0.59 wt.-%), Mn (0.43 wt.-%), K (0.36 wt.-%), Ti (0.24 wt.-%), Al (0.22 wt.-%).

APPENDIX B: Tables

Table B.1 Measuring parameters (detected isotopes, used modi, detection limits) for trace metal determination with ICP-MS XSERIES 2 (Thermo Fisher Scientific)	211
Table B.2 Mineralogical composition of the settled ash sediments (results in wt.-%); preliminary investigations	212
Table B.3. TIC and calculated CaCO ₃ contents of the settled ash sediments (results in wt.-%); preliminary investigations	214
Table B.4. Leachate concentration, S4-elution, [units mg/kg]	215
Table B.4. Leachate concentration, S4-elution, [units mg/kg], continued	216
Table B.4. Leachate concentration, S4-elution, [units mg/kg], continued	217
Table B.4. Leachate concentration, S4-elution, [units mg/kg], continued	218
Table B.4. Leachate concentration, S4-elution, [units mg/kg], continued	219
Table B.4. Leachate concentration, S4-elution, [units mg/kg], continued	220
Table B.4. Leachate concentration, S4-elution, [units mg/kg], continued	221
Table B.4. Leachate concentration, S4-elution, [units mg/kg], continued	222
Table B.5. Leachate concentration, NH ₄ NO ₃ , [units mg/kg]	223
Table B.5. Leachate concentration, NH ₄ NO ₃ , [units mg/kg], continued	224
Table B.5. Leachate concentration, NH ₄ NO ₃ , [units mg/kg], continued	225
Table B.5. Leachate concentration, NH ₄ NO ₃ , [units mg/kg], continued	226
Table B.5. Leachate concentration, NH ₄ NO ₃ , [units mg/kg], continued	227
Table B.5. Leachate concentration, NH ₄ NO ₃ , [units mg/kg], continued	228
Table B.5. Leachate concentration, NH ₄ NO ₃ , [units mg/kg], continued	229
Table B.6. Leachate concentration, NH ₄ -Acetate, [units mg/kg], continued	230
Table B.6. Leachate concentration, NH ₄ -Acetate, [units mg/kg], continued	231
Table B.6. Leachate concentration, NH ₄ -Acetate, [units mg/kg], continued	232
Table B.6. Leachate concentration, NH ₄ -Acetate, [units mg/kg], continued	233
Table B.6. Leachate concentration, NH ₄ -Acetate, [units mg/kg], continued	234
Table B.6. Leachate concentration, NH ₄ -Acetate, [units mg/kg], continued	235
Table B.6. Leachate concentration, NH ₄ -Acetate, [units mg/kg], continued	236
Table B.7. Leachate concentration, Aqua regia, [units mg/kg]	237
Table B.7. Leachate concentration, Aqua regia, [units mg/kg], continued	238
Table B.7. Leachate concentration, Aqua regia, [units mg/kg], continued	239

Table B.7. Leachate concentration, Aqua regia, [units mg/kg], continued	240
Table B.8. Content of polycyclic aromatic hydrocarbons of the drilling core BGH-1412-P2 [$\mu\text{g}/\text{kg}$]	241
Table B.9. Trace metal concentration gained by X-ray fluorescence in different liming products. Precision and detection limits are shown for each element (contents and error in wt.-%).	242
Table B.9. Trace metal concentration gained by X-ray fluorescence in different liming products. Precision and detection limits are shown for each element (contents and error in wt.-%), contin.	244
Table B.9. Trace metal concentration gained by X-ray fluorescence in different liming products. Precision and detection limits are shown for each element (contents and error in wt.-%), contin.	246
Table B.9. Trace metal concentration gained by X-ray fluorescence in different liming products. Precision and detection limits are shown for each element (contents and error in wt.-%), contin.	248
Table B.9. Trace metal concentration gained by X-ray fluorescence in different liming products. Precision and detection limits are shown for each element (contents and error in wt.-%), contin.	250
Table B.9. Trace metal concentration gained by X-ray fluorescence in different liming products. Precision and detection limits are shown for each element (contents and error in wt.-%), contin.	252
Table B.9. Trace metal concentration gained by X-ray fluorescence in different liming products. Precision and detection limits are shown for each element (contents and error in wt.-%), contin.	254
Table B.10. Amounts of liming products, experimental series 1 (BGH water).	256
Table B.11. Development of in-situ parameters (pH, EC) in Column 1; experimental series 1 (neutralizing product KSM Beroun).	257
Table B.12. Development of in-situ parameters (pH, EC) in Column 2; experimental series 1 (neutralizing product CaO).	258
Table B.13. Development of in-situ parameters (pH, EC) in Column 3; experimental series 1 (neutralizing product Branndolomit)	259
Table B.14. Development of in-situ parameters (pH, EC) in Column 4; experimental series 1 (neutralizing product DSM Ostrau)	260
Table B.15. Amounts of liming products, experimental series 2 (Lohsa).	261
Table B.16. Development of in-situ parameters (pH, EC) in Column 1; experimental series 2 (neutralizing product KSM Beroun).	262
Table B.17. Development of in-situ parameters (pH, EC) in Column 2; experimental series 2 (neutralizing product KSM Borna).	263
Table B.18. Development of in-situ parameters (pH, EC) in Column 3; experimental	

series 2 (neutralizing product Mischkalk Borna).	264
Table B.19. Development of in-situ parameters (pH, EC) in Column 4; experimental series 2 (neutralizing product DSM Borna).	265
Table B.20. Determined trace metal concentration variation during experimental series 2.	266
Table B.20. Determined trace metal concentration variation during experimental series 2, continued.	267
Table B.21. Trace element reduction during experimental series 2.	268
Table B.21. Trace element reduction during experimental series 2, continued.	269
Table B.22. Amounts of liming products, experimental series 3 (Scheibe).	270
Table B.23. Development of in-situ parameters (pH, EC) in column 1; experimental series 3 (neutralizing product KSM Beroun (1x))	271
Table B.24. Development of in-situ parameters (pH, EC) in column 2; experimental series 3 (neutralizing product KSM Beroun (5x))	272
Table B.25. Development of in-situ parameters (pH, EC) in column 3; experimental series 3 (neutralizing product DSM Ostrau (1x))	273
Table B.26. Development of in-situ parameters (pH, EC) in column 4; experimental series 3 (neutralizing product DSM Ostrau (5x))	274
Table B.27. Development of in-situ parameters (pH, EC) in column 5; experimental series 3 (neutralizing product CaO, 5x)	274
Table B.28. Development of in-situ parameters (pH, EC) in column 6; experimental series 3 (neutralizing product KSM_C20, 5x)	275
Table B.29. Determined trace metal concentration variation during experimental series 3, neutralizing product KSM Beroun, DSM Ostrau.	276
Table B.29. Det. trace metal concentration variation during experimental series 2, neutralizing product KSM Beroun, DSM Ostrau, continued.	277
Table B.30. Determined trace metal concentration variation during experimental series 3, neutralizing product CaO.	278
Table B.30. Determined trace metal concentration variation during experimental series 3, neutralizing product CaO, continued.	279
Table B.30. Determined trace metal concentration variation during experimental series 3, neutralizing product CaO, continued.	280
Table B.31. Determined trace metal concentration variation during experimental series 3, neutralizing product KSM_C20.	281
Table B.31. Determined trace metal concentration variation during experimental series 3, neutralizing product KSM_C20, continued.	282
Table B.31. Determined trace metal concentration variation during experimental series 3, neutralizing product KSM_C20, continued.	283

Appendix B - Tables

Table B.32. Mineralogical analysis of settled ash sediments before and after pilot experiment (results in wt.-%)	284
Table B.33. TIC and calculated CaCO ₃ contents of settled ash sediments before CO ₂ treatment	286
Table B.34. TIC and calculated CaCO ₃ contents of settled ash sediments after CO ₂ treatment	287
Table B.35. Chemical composition of Burghammer pore water (main anions and cations, pH) of drilling core BGH-290408-P0 (ash sediment before CO ₂ treatment)	289
Table B.36. Chemical composition of Burghammer pore water (metals / metalloids) of drilling core BGH-290408-P0 (ash sediment before CO ₂ treatment)	290
Table B.37. Chemical composition of Burghammer pore water (main anions and cations, pH) of drilling cores BGH-300708-P1 / P2 / P3 (after CO ₂ treatment)	293
Table B.38. Chemical composition of Burghammer pore water (metals / metalloids) of drilling cores BGH-300708-P1 /P2 / P3 (ash sediment after CO ₂ treatment)	296
Table B.39. Results of SEM-EDX investigations before CO ₂ injection	302
Table B.40. Results of SEM-EDX investigations after CO ₂ injection	304
Table B.41. Content of polycyclic aromatic hydrocarbons of the drilling cores before and after CO ₂ injection [µg/kg]	306

Table B.1 Measuring parameters (detected isotopes, used modi, detection limits) for trace metal determination with ICP-MS XSERIES 2 (Thermo Fisher Scientific)

Detected isotope	Used modi	DL [ppb]	Detected isotope	Used modi	DL [ppb]	Detected isotope	Used modi	DL [ppb]
6Li	Standard	0.1	63Cu	KED-2V	1	139La	Standard	0.001
7Li	Standard	0.1	66Zn	KED-2V	1	140Ce	Standard	0.001
9Be	Standard	0.01	71Ga	Standard	0.01	141Pr	Standard	0.001
10B	Standard	1	75As	KED-2V	0.2	146Nd	Standard	0.001
23Na	KED-2V	2	78Se	KED-1V	2	147Sm	Standard	0.001
24Mg	KED-2V	1	81Br	Standard	2	153Eu	Standard	0.001
27Al	KED-2V	1	85Rb	Standard	0.005	159Gd	Standard	0.001
29Si	KED-2V	100	88Sr	Standard	0.02	159Tb	Standard	0.001
31P	KED-2V	10	89Y	Standard	0.001	163Dy	Standard	0.001
34S	KED-2V	300	95Mo	Standard	0.01	165Ho	Standard	0.001
39K	KED-2V	20	107Ag	Standard	0.005	166Er	Standard	0.001
43Ca	Standard	20	114Cd	KED-2V	0.01	169Tm	Standard	0.001
45Sc	KED-2V	0.1	115In	Standard	0.001	172Yb	Standard	0.001
51V	KED-2V	0.1	118Sn	Standard	0.05	175Lu	Standard	0.001
52Cr	KED-2V	0.1	121Sb	Standard	0.01	205Tl	Standard	0.001
55Mn	KED-2V	0.05	125Te	Standard	0.01	208Pb	Standard	0.01
56Fe	KED-2V/3V	1	127I	Standard	0.05	209Bi	Standard	0.001
59Co	KED-2V	0.01	133Cs	Standard	0.001	232Th	Standard	0.001
60Ni	KED-2V	0.1	137Ba	Standard	0.1	238U	Standard	0.003

Table B.2 Mineralogical composition of the settled ash sediments (results in wt.-%); preliminary investigations

Sample	Amorphous	Akermanite	Brownmillerite	Calcite	Diopside	Ettringite	Ferrite, magnesian	Hematite	Periclase	Quartz	Rutile
BGH-1312-P1-4.00-4.50	64.8	-	5.0	8.6	-	-	7.4	1.3	-	12.9	0.1
BGH-1312-P1-4.50-5.00	65.5	-	4.6	8.4	-	-	7.6	1.3	-	12.6	-
BGH-1312-P1-5.10-5.25	68.5	0.5	5.7	3.6	1.1	-	5.4	1.0	-	14.2	-
BGH-1312-P1-6.00-7.00	73.0	0.3	3.6	2.4	1.0	-	4.9	1.0	-	13.8	-
BGH-1312-P1-7.20-7.35	60.5	0.8	4.6	2.7	2.5	-	5.8	1.4	0.5	21.2	-
BGH-1312-P1-7.50-7.65	69.3	0.8	1.3	7.9	1.0	-	8.5	0.8	-	10.3	-
BGH-1312-P1-8.40-8.60	57.7	1.2	4.3	4.5	1.7	6.0	9.2	1.1	-	14.3	-
BGH-1312-P1-9.17-9.30	92.1	-	0.9	0.6	-	-	0.6	-	-	5.8	-
BGH-1312-P1-9.60-9.75	50.8	1.1	3.2	1.6	-	-	4.1	0.9	-	38.3	-
BGH-1412-P2-4.25-4.50	50.4	0.4	5.6	2.6	1.6	1.4	3.8	1.1	0.4	32.6	-
BGH-1412-P2-4.55-4.70	48.8	0.7	6.8	1.1	-	-	4.8	1.2	0.4	36.3	-
BGH-1412-P2-5.07-5.22	59.6	0.3	3.9	0.7	1.2	-	3.6	0.8	-	29.9	-
BGH-1412-P2-5.85-6.00	73.9	-	1.8	0.7	1.1	-	3.5	0.8	-	18.2	-
BGH-1412-P2-6.65-6.80	80.7	-	0.6	0.7	-	-	1.8	0.3	-	15.9	-
BGH-1412-P2-6.95-7.10	44.8	-	1.6	1.7	1.5	-	3.6	1.2	-	45.7	-
BGH-1412-P2-7.70-7.85	54.2	1.1	7.2	2.0	2.2	-	5.8	1.3	0.4	25.6	-
BGH-1412-P2-8.20-8.35	52.6	0.6	3.6	1.9	1.9	-	3.6	0.8	-	34.9	0.3
BGH-1412-P2-8.80-8.95	35.4	1.6	5.5	2.1	1.4	-	4.0	0.9	-	48.9	0.3
BGH-1412-P3-2.70-2.80	36.1	-	2.5	3.0	2.3	-	4.3	1.0	-	50.8	-
BGH-1412-P3-3.15-3.25	98.2	-	-	1.0	-	-	-	-	-	0.8	-
BGH-1412-P3-3.85-4.00	53.7	-	7.1	3.7	1.9	0.8	11.2	2.3	0.9	18.5	-
BGH-1412-P3-5.10-5.25	53.6	1.1	5.0	4.1	1.9	8.6	10.9	2.2	1.3	11.4	-
BGH-1412-P3-5.80-6.00	60.4	0.9	7.2	8.5	1.3	-	10.9	1.5	0.5	8.8	-

Sample	Amorphous	Akermanite	Brownmillerite	Calcite	Diopside	Ettringite	Ferrite, magnesian	Hematite	Periclase	Quartz	Rutile
BGH-1412-P3-6.15-6.30	58.3	0.8	6.8	4.2	1.3	-	9.3	1.6	0.6	17.1	-
BGH-1412-P3-6.90-7.10	66.7	1.1	3.0	4.1	1.2	5.0	7.3	0.7	-	10.9	-
BGH-1412-P3-7.70-7.90	63.5	0.7	2.9	1.7	1.1	-	2.9	0.7	-	26.3	0.3
BGH-1412-P3-8.15-8.35	65.6	1.1	3.7	2.8	1.2	5.8	5.2	0.7	-	13.9	0.3
BGH-1412-P3-8.80-9.00	68.6	0.8	2.7	2.6	1.1	1.3	5.9	0.9	-	16.1	-
BGH-1412-P3-9.65-9.85	64.1	-	3.2	2.5	1.9	-	3.7	0.9	-	23.6	0.3
BGH-1412-P3-10.10-10.30	60.8	-	3.9	2.4	2.2	4.4	3.9	1.1	-	21.5	-

Table B.3. TIC and calculated CaCO₃ contents of the settled ash sediments (results in wt.-%); preliminary investigations

Sample	depth	TIC [wt.-%]	CaCO₃ [wt.-%]
BGH-1312-P1-4.0	Disturbed	0.95	7.9
BGH-1312-P1-4.5	dist.	1.00	8.3
BGH-1312-P1-5.0	5.10 - 5.25	0.52	4.3
BGH-1312-P1-6.0	Disturbed	0.30	2.5
BGH-1312-P1-7.0	7.20 - 7.35	0.29	2.4
BGH-1312-P1-7.0	7.50 - 7.65	0.99	8.3
BGH-1312-P1-8.0	8.40 - 8.60	0.40	3.3
BGH-1312-P1-9.0	9.17 - 9.30	0.23	1.9
BGH-1312-P1-9.0	9.60 - 9.75	0.17	1.4
BGH-1312-P2-3.50	3.76 - 3.98	0.82	6.8
BGH-1312-P2-3.50	4.25 - 4.50	0.35	2.9
BGH-1312-P2-4.50	4.55 - 4.70	0.18	1.5
BGH-1312-P2-4.50	5.07 - 5.22	0.17	1.4
BGH-1312-P2-5.50	5.85 - 6.00	0.13	1.1
BGH-1312-P2-6.50	6.65 - 6.80	0.18	1.5
BGH-1312-P2-6.50	6.95 - 7.10	0.13	1.1
BGH-1312-P2-7.50	7.70 - 7.85	0.19	1.6
BGH-1312-P2-7.50	8.20 - 8.35	0.12	1.0
BGH-1312-P2-8.50	8.80 - 8.95	0.13	1.1
BGH-1312-P3-2.50	2.70 - 2.80	0.42	3.5
BGH-1312-P3-2.50	3.15 - 3.25	0.11	0.9
BGH-1312-P3-3.5	3.85 - 4.00	0.41	3.4
BGH-1312-P3-4.50	5.10 - 5.25	0.44	3.7
BGH-1312-P3-5.50	5.85 - 6.00	0.87	7.3
BGH-1312-P3-5.50	6.15 - 6.30	0.51	4.3
BGH-1312-P3-6.50	6.90 - 7.10	0.43	3.6
BGH-1312-P3-7.50	7.70 - 7.80	0.17	1.4
BGH-1312-P3-7.50	8.15 - 8.35	0.38	3.2
BGH-1312-P3-8.50	8.80 - 9.00	0.34	2.8
BGH-1312-P3-9.50	9.65 - 9.85	0.25	2.1
BGH-1312-P3-9.50	10.10 - 10.30	0.27	2.3

Table B.4. Leachate concentration, S4-elution, [units mg/kg]

ID	BGH-1312-P1-4.0	BGH-1312-P1-4.5	BGH-1312-P1-5.0	BGH-1312-P1-6.0	BGH-1312-P1-7.0	BGH-1312-P1-7.0
Depth [m]	Dist.	Dist.	5.10 – 5.25	Dist.	7.20 – 7.35	7.50 – 7.65
Depth _{average} [m]	4.25	4.75	5.18	6.25	7.28	7.58
Li	0.0747	0.0803	0.0666	0.0927	0.1135	0.1090
Be	0.0006	0.0003	0.0002	0.0002	0.0001	0.0004
Na	144.5323	156.3693	182.2275	190.5084	210.1526	317.2825
Mg	285.5898	303.0407	11.7941	6.0711	3.7291	17.7546
P	0.7401	0.4383	0.5053	0.0201	0.1310	1.2934
K	117.5463	131.8886	232.9313	327.1523	416.3946	382.3704
Ca	914.3926	977.7594	3118.9625	738.3837	379.0842	955.8595
V	0.0889	0.0502	0.7231	1.3371	3.3212	0.4334
Cr	0.7186	0.1437	0.2566	0.2360	1.0798	1.0677
Mn	0.4838	0.4551	0.0779	0.0745	0.0336	0.0078
Co	0.0051	0.0061	0.0153	0.0107	0.0153	0.0172
Ni	0.7053	0.5331	0.7883	0.0681	1.2868	0.3724
Cu	0.0056	0.0187	0.0044	0.0846	0.0042	0.0566
Zn	0.0985	0.1645	0.2263	0.2542	0.1921	0.1271
As	0.0152	0.0124	0.0193	0.0439	0.0653	0.0446
Se	0.0484	0.0484	0.1358	0.1306	0.1855	0.2131
Sr	36.5167	16.6667	37.6765	12.8070	7.5294	16.1412
Y	0.0003	0.0003	0.0006	0.0003	0.0003	0.0003
Mo	0.0740	0.0334	0.0599	0.0817	0.0212	0.1298
Cd	0.0010	0.0007	0.0014	0.0007	0.0006	0.0013
Sn	0.0031	0.0007	0.0001	0.0011	0.0009	0.0011
Sb	0.0609	0.0582	0.0112	0.0074	0.0099	0.0106
Cs	0.0318	0.0193	0.0634	0.0492	0.1471	0.0262
La	0.0007	0.0001	0.0007	0.0000	0.0003	0.0005
Ce	0.0005	0.0003	0.0007	0.0004	0.0003	0.0003
Hg	0.0025	0.0017	0.0024	0.0022	0.0047	0.0034
Tl	0.0013	0.0001	0.0011	0.0012	0.0009	0.0010
Pb	0.0101	0.0038	0.0076	0.0059	0.0033	0.0089
Th	0.0002	0.0001	0.0001	0.0002	0.0001	0.0001
U	0.0271	0.0362	0.0021	0.0027	0.0043	0.0031

Table B.4. Leachate concentration, S4-elution, [units mg/kg], continued

ID	BGH-1312-P1-8.00	BGH-1312-P1-9.0	BGH-1312-P1-9.0	BGH-1312-P2-3.50	BGH-1312-P2-3.50	BGH-1312-P2-4.50
Depth[m]	8.40 - 8.60	9.17 - 9.30	9.60 - 9.75	3.76 - 3.98	4.25 - 4.50	4.55 - 4.70
Depth _{average} [m]	8.50	9.25	9.68	3.87	4.40	4.60
Li	0.0927	0.1046	0.2678	0.2249	0.1554	0.1672
Be	0.0003	0.0002	0.0006	0.0003	0.0003	0.0004
Na	342.3447	448.1295	296.4005	83.9403	127.2806	150.0233
Mg	5.8701	2.4951	6.5278	436.0503	4.6472	9.4279
P	1.1810	0.5863	0.7847	0.1412	0.5754	1.1974
K	465.7565	817.4561	621.4832	95.5115	264.2833	284.0048
Ca	3903.8375	519.1024	953.2372	488.5279	2312.4131	2710.0494
V	1.4822	0.8084	2.3774	0.0601	1.4786	1.6381
Cr	1.0388	1.0625	1.0554	0.7813	0.1290	1.1004
Mn	0.0868	0.0240	0.0565	0.0524	0.0103	0.0965
Co	0.0170	0.0018	0.0071	0.0076	0.0118	0.0157
Ni	0.5045	0.0768	0.1385	0.6034	0.3404	0.8971
Cu	0.0478	0.0164	0.0759	0.0877	0.0058	0.0774
Zn	0.2807	0.4779	0.1886	0.0753	0.0905	0.1369
As	0.0413	0.1404	0.0240	0.0056	0.0226	0.0270
Se	0.3222	0.1024	0.1186	0.0410	0.2344	0.1332
Sr	45.0630	22.0460	14.3623	9.9949	31.8598	33.5370
Y	0.0006	0.0005	0.0004	0.0004	0.0004	0.0003
Mo	0.1306	0.1278	0.0936	0.0707	0.0287	0.0753
Cd	0.0003	0.0012	0.0001	0.0009	0.0004	0.0015
Sn	0.0001	0.0004	0.0005	0.0005	0.0011	0.0014
Sb	0.0057	0.0097	0.0121	0.0034	0.0073	0.0059
Cs	0.0081	0.2078	0.0838	0.0366	0.0850	0.0666
La	0.0002	0.0020	0.0004	0.0000	0.0006	0.0008
Ce	0.0006	0.0010	0.0005	0.0004	0.0009	0.0006
Hg	0.0037	0.0067	0.0032	0.0009	0.0019	0.0019
Tl	0.0015	0.0009	0.0011	0.0012	0.0017	0.0010
Pb	0.0055	0.0026	0.0087	0.0169	0.0011	0.0020
Th	0.0001	0.0001	0.0001	0.0001	0.0002	0.0001
U	0.0014	0.0030	0.0059	0.0028	0.0026	0.0015

Table B.4. Leachate concentration, S4-elution, [units mg/kg], continued

ID	BGH-1312-P2-4.50	BGH-1312-P2-5.50	BGH-1312-P2-6.50	BGH-1312-P2-6.50	BGH-1312-P2-7.50	BGH-1312-P2-7.50
Depth [m]	5.07 - 5.22	5.85 - 6.00	6.65 - 6.80	6.95 - 7.10	7.70 - 7.85	8.20 - 8.35
Depth_{average} [m]	5.15	5.93	6.73	7.03	7.78	8.28
Li	0.3382	0.3058	0.2676	0.2180	0.2252	0.3053
Be	0.0002	0.0005	0.0000	0.0002	0.0002	0.0003
Na	220.2644	296.9787	233.7967	101.3538	294.3524	222.4345
Mg	7.9452	23.5086	33.0064	24.2744	6.3062	5.4997
P	0.9747	0.4673	1.2426	0.4724	0.9627	1.3202
K	359.3039	382.8797	321.0033	179.0957	492.0379	413.0486
Ca	937.0471	571.5222	619.7014	346.4394	2279.0132	861.3745
V	1.7878	0.3861	0.4345	0.6593	3.3353	3.0096
Cr	0.2555	0.2977	0.1576	0.1272	1.0226	1.0480
Mn	0.0385	0.0832	0.0758	0.0573	0.0438	0.1021
Co	0.0165	0.0029	0.0032	0.0067	0.0161	0.0080
Ni	0.3402	0.1380	0.1387	0.6093	0.8821	0.8600
Cu	0.0782	0.0497	0.0037	0.0125	0.0522	0.0526
Zn	0.0899	0.1196	0.1003	0.0723	0.4022	0.2464
As	0.0337	0.0422	0.0548	0.0228	0.0202	0.0335
Se	0.0967	0.0825	0.0614	0.0984	0.1976	0.1134
Sr	15.8875	8.8749	9.4902	15.1197	26.0710	13.6132
Y	0.0003	0.0004	0.0004	0.0005	0.0003	0.0003
Mo	0.0856	0.1115	0.1115	0.0187	0.0972	0.0771
Cd	0.0003	0.0001	0.0014	0.0012	0.0011	0.0000
Sn	0.0007	0.0018	0.0016	0.0003	0.0007	0.0004
Sb	0.0094	0.0064	0.0096	0.0065	0.0172	0.0126
Cs	0.1007	0.0473	0.0508	0.0250	0.1083	0.1631
La	0.0006	0.0007	0.0006	0.0006	0.0000	0.0004
Ce	0.0003	0.0004	0.0005	0.0013	0.0002	0.0005
Hg	0.0022	0.0023	0.0016	0.0011	0.0014	0.0010
Tl	0.0009	0.0003	0.0008	0.0008	0.0009	0.0008
Pb	0.0063	0.0081	0.0006	0.0095	0.0029	0.0053
Th	0.0001	0.0001	0.0001	0.0001	0.0000	0.0001
U	0.0039	0.0156	0.0138	0.0078	0.0024	0.0027

Table B.4. Leachate concentration, S4-elution, [units mg/kg], continued

ID	BGH-1312-P2-8.50	BGH-1312-P3-2.50	BGH-1312-P3-2.50	BGH-1312-P3-3.5	BGH-1312-P3-4.50	BGH-1312-P3-5.50
Depth [m]	8.80 - 8.95	2.70 - 2.80	3.15 - 3.25	3.85 - 4.00	5.10 - 5.25	5.85 - 6.00
Depth _{average} [m]	8.88	2.85	3.20	3.93	5.18	5.93
Li	0.2514	0.3373	0.2768	0.2386	0.0951	0.0693
Be	0.0003	0.0001	0.0003	0.0003	0.0002	0.0004
Na	114.4619	54.6062	122.3672	257.6917	350.8141	471.6570
Mg	4.0123	240.8276	366.2262	7.3343	2.5383	2.5546
P	1.2846	0.9890	0.5395	0.0174	0.7358	1.0271
K	285.7698	63.3889	144.8040	838.0097	1162.1376	1268.3591
Ca	2346.0612	395.0749	1194.5970	2317.3344	1205.5085	435.8108
V	1.7003	0.0335	0.0704	4.2650	1.0792	5.8126
Cr	0.6315	0.7142	0.5215	0.9491	0.4169	0.7873
Mn	0.0136	0.3013	1.3896	0.0437	0.0050	0.0564
Co	0.0142	0.0092	0.0108	0.0154	0.0123	0.0128
Ni	0.3746	0.5552	0.2128	0.2159	0.3963	0.0323
Cu	0.0123	0.0904	0.0379	0.0513	0.0894	0.0827
Zn	0.1159	0.1621	0.1652	0.1198	0.0857	1.7217
As	0.0198	0.0063	0.0073	0.0607	0.0322	0.1153
Se	0.0982	0.0335	0.0297	0.4441	0.1743	0.4081
Sr	29.8480	15.7387	16.8617	38.1411	33.4525	20.2929
Y	0.0010	0.0003	0.0003	0.0005	0.0003	0.0004
Mo	0.0526	0.0177	0.1313	0.1476	0.3166	0.6460
Cd	0.0012	0.0007	0.0012	0.0006	0.0014	0.0018
Sn	0.0005	0.0003	0.0015	0.0006	0.0011	0.0025
Sb	0.0045	0.0072	0.0052	0.0443	0.0045	0.0298
Cs	0.0578	0.0173	0.0224	0.1626	0.1951	0.1506
La	0.0004	0.0007	0.0005	0.0002	0.0000	0.0006
Ce	0.0015	0.0003	0.0002	0.0007	0.0001	0.0008
Hg	0.0021	0.0006	0.0002	0.0041	0.0031	0.0064
Tl	0.0009	0.0008	0.0009	0.0001	0.0010	0.0012
Pb	0.0053	0.0081	0.0111	0.0116	0.0058	0.0038
Th	0.0001	0.0001	0.0001	0.0001	0.0001	0.0001
U	0.0013	0.0158	0.0050	0.0046	0.0006	0.0040

Table B.4. Leachate concentration, S4-elution, [units mg/kg], continued

ID	BGH-1312-P3-5.50	BGH-1312-P3-6.50	BGH-1312-P3-7.50	BGH-1312-P3-7.50	BGH-1312-P3-8.50	BGH-1312-P3-9.50
Depth [m]	6.15 - 6.30	6.90 - 7.10	7.70 - 7.80	8.15 - 8.35	8.80 - 9.00	10.10 - 10.30
Depth_{average} [m]	6.23	7	7.75	8.25	8.90	10.2
Li	0.1326	0.0803	0.4269	0.2137	0.1835	0.3171
Be	0.0006	0.0003	0.0000	0.0002	0.0002	0.0004
Na	424.4712	479.2128	297.3473	381.2744	317.1604	386.9965
Mg	1.9252	3.6220	7.1795	7.2081	6.1794	5.7756
P	1.0526	0.6120	1.2895	1.6203	1.0709	1.5186
K	1197.9152	800.3488	747.6895	907.0476	872.7515	1028.9764
Ca	179.2739	3120.7387	1230.0504	2382.9088	1623.6462	3202.1409
V	10.3962	2.5739	1.4111	3.0403	3.5359	5.6335
Cr	0.2754	0.5249	0.9906	0.1691	0.9651	0.7490
Mn	0.0961	0.0528	0.0130	0.0939	0.0279	0.0073
Co	0.0159	0.0071	0.0029	0.0022	0.0020	0.0056
Ni	0.7321	0.6252	0.7866	0.5835	0.2861	0.7661
Cu	0.0857	0.0358	0.0091	0.0797	0.0758	0.0367
Zn	0.3763	0.1760	0.2532	0.2758	0.2458	0.1500
As	0.3030	0.0470	0.0347	0.0381	0.0456	0.0466
Se	0.3157	0.4120	0.1896	0.4046	0.2954	0.1717
Sr	6.8996	53.1015	20.9104	36.5175	25.8973	51.5964
Y	0.0007	0.0006	0.0003	0.0004	0.0004	0.0006
Mo	0.4123	0.3805	0.1415	0.2426	0.2208	0.2096
Cd	0.0018	0.0008	0.0015	0.0012	0.0000	0.0008
Sn	0.0039	0.0008	0.0007	0.0000	0.0012	0.0002
Sb	0.0293	0.0085	0.0151	0.0155	0.0178	0.0079
Cs	0.1386	0.0321	0.1439	0.0510	0.1090	0.1660
La	0.0009	0.0001	0.0007	0.0002	0.0006	0.0172
Ce	0.0017	0.0003	0.0003	0.0004	0.0003	0.0005
Hg	0.0060	0.0036	0.0043	0.0036	0.0035	0.0037
Tl	0.0008	0.0011	0.0009	0.0011	0.0009	0.0020
Pb	0.0026	0.0076	0.0029	0.0036	0.0074	0.0024
Th	0.0002	0.0001	0.0001	0.0001	0.0000	0.0001
U	0.0272	0.0031	0.0085	0.0051	0.0079	0.0064

Appendix B - Tables

Table B.4. Leachate concentration, S4-elution, [units mg/kg], continued

ID	BGH-1312- P3-9.50	PCD1-L1- S2(1)	PCD1-L1- S2(2)	PCD1-L1-S3	PCD1-L1- S4(1)	PCD1-L1- S4(2)
Depth [m]	9.65 - 9.85					
Depth_{average} [m]	9.75					
Li	0.2590	0.21425828	0.19128589	0.19222228	0.25931088	0.26620639
Be	0.0001	0.00019966	0.00035753	0.00096835	0.00019165	0.00027676
Na	325.4581	103.946302	105.932367	120.620079	161.025883	151.141765
Mg	6.3712	169.567434	166.409418	238.301636	392.863971	362.180305
P	0.4773	0.22389547	0.48895768	0.6877148	1.10822309	0.31716879
K	906.6630	99.8221275	106.5527	118.725991	95.4024339	98.463454
Ca	4498.9375	1058.78757	986.094273	1047.47377	1275.59069	1224.86762
V	2.6844	0.05528239	0.04492085	0.04575068	0.03350658	0.03501246
Cr	0.6816	0.55989427	0.99336207	1.12523753	0.6256926	0.17137153
Mn	0.0496	0.56610804	0.64610232	0.74526363	0.71711323	0.67661442
Co	0.0197	0.01161657	0.01484052	0.00950555	0.0052598	0.0170087
Ni	0.1876	0.42846611	0.34545946	0.81277424	0.50032337	0.87982479
Cu	0.0352	0.02095962	0.04065479	0.06460983	0.08177226	0.0120771
Zn	0.2511	0.23478252	0.25735935	0.14954622	0.18087105	0.13278107
As	0.0360	0.02318128	0.01428951	0.01402791	0.01023485	0.01040808
Se	0.2312	0.05637529	0.04121329	0.0562103	0.02780738	0.04564768
Sr	51.6329	26.9597709	11.0704913	14.383304	17.9630799	16.6993635
Y	0.0006	0.00044714	0.00072833	0.00622819	0.00059382	0.00065742
Mo	0.1896	0.03916649	0.01297218	0.04413947	0.03526029	0.00413969
Cd	0.0002	8.2948E-05	0.00127195	0.00010515	0.00071203	0.00024467
Sn	0.0015	0.00052088	0.00137659	0.00121181	0.0011325	0.000632
Sb	0.0058	0.01802995	0.01954374	0.01445617	0.01077475	0.01110962
Cs	0.1396	0.01614767	0.00631966	0.0033363	0.01222797	0.01777154
La	0.0006	0.00090144	0.00136538	0.00868169	0.00050082	0.00059934
Ce	0.0012	0.00045383	0.00084599	0.01430874	0.00031166	0.00065136
Hg	0.0027	0.00073381	0.00034598	0.00016009	0.00043789	0.0003735
Tl	0.0010	0.00041869	0.00095567	0.00057512	0.00042257	0.00053945
Pb	0.0072	0.00206591	0.00620112	0.00663503	0.0110612	0.00073365
Th	0.0002	0.00014461	0.00015666	0.00046632	8.5011E-05	0.00013955
U	0.0030	0.02030535	0.02326146	0.03852316	0.04203238	0.0358442

Table B.4. Leachate concentration, S4-elution, [units mg/kg], continued

ID	PCD3-B2	PCD4-B1	PCD5-B1	PCD5-B2(1)	PCD5-B2(2)	PCD5-B3(1)
Depth [m]						
Depth _{average} [m]						
Li	0.23273744	0.17985897	0.19947395	0.17943921	0.25016891	0.0471039
Be	0.00017563	0.00013569	0.00217778	0.00036985	0.00036249	0.00021839
Na	101.654109	12.7799252	41.2070433	53.4804592	54.9033685	106.512925
Mg	252.541975	162.734347	361.998292	831.367638	875.029418	61.2094715
P	0.70546924	1.35753904	1.58244399	0.96615221	1.23819253	0.03677439
K	99.3335819	47.1676011	61.5874158	94.8376331	98.9800174	151.507044
Ca	545.847621	219.423089	583.544407	3270.71102	2181.62453	9810.75359
V	0.03573481	0.08238212	0.07724642	0.02659858	0.03291555	0.03817137
Cr	0.53825417	0.8757933	0.87288936	0.16032131	0.40547972	0.76269922
Mn	0.23326072	0.03817198	1.12220931	0.18986264	0.283805	0.06607182
Co	0.01026133	0.00328527	0.01469488	0.00550396	0.00587389	0.04047281
Ni	0.63528072	0.31850173	0.33566665	0.39887706	0.15406758	0.52626995
Cu	0.01033207	0.00681986	0.08795918	0.0533751	0.07240419	0.09482788
Zn	0.10575255	0.19098186	0.21005365	0.94069667	0.51920459	0.18010612
As	0.00826083	0.01309305	0.02878058	0.01110971	0.01286302	0.0106347
Se	0.04665939	0.04587158	0.04380889	0.08536241	0.07956285	0.20936216
Sr	10.0517847	8.01879811	17.7957538	43.983216	33.1723265	94.582377
Y	0.00044789	0.00026729	0.0138352	0.00067673	0.00064361	0.00068852
Mo	0.08185892	0.00796644	0.07346168	0.13159066	0.13404212	0.10406506
Cd	0.00016284	0.0004266	0.00234755	0.00121159	0.00068993	0.00020759
Sn	0.00085258	0.0010876	0.0118693	0.00140589	0.00137828	0.00069768
Sb	0.01562901	0.00718579	0.02078412	0.00537395	0.00627771	0.0056882
Cs	0.02002783	0.0074699	0.01546558	0.01191318	0.0148143	0.01053666
La	0.00024401	9.8455E-05	0.01804379	0.00314841	0.00108961	0.00038222
Ce	0.00026567	0.00037519	0.03295866	0.00049877	0.00044522	0.00016127
Hg	0.00073078	0.00017967	3.0187E-05	0.00033622	0.00011968	0.00145513
Tl	0.00064855	0.00045889	0.00018157	0.00030721	0.00159201	0.00079058
Pb	0.00190115	0.00482533	0.04667049	0.00572763	0.00840476	0.01116289
Th	7.5595E-05	7.57E-05	0.00045916	6.6101E-05	0.00010595	9.7309E-05
U	0.01031335	0.00329103	0.01958369	0.04403275	0.04227706	0.00245031

Table B.4. Leachate concentration, S4-elution, [units mg/kg], continued

ID	PCD5-B3(2)	PCD5-B4(1)	PCD5-B4(2)
Depth [m]			
Depth _{average} [m]			
Li	0.05491636	0.22219548	0.19281333
Be	0.0006813	0.00038836	0.00029649
Na	115.291633	148.108802	129.54228
Mg	78.8419515	613.561703	550.122995
P	0.86375316	1.32336206	0.41728279
K	174.706717	232.686902	200.14505
Ca	9791.37563	2417.61344	2212.02458
V	0.0365584	0.04502949	0.04415893
Cr	1.08807762	0.33390335	0.84984784
Mn	0.00853128	1.39825787	1.23768524
Co	0.03943179	0.01323801	0.01562805
Ni	0.85928514	0.37662547	0.32744633
Cu	0.09375291	0.05595479	0.055946
Zn	0.33240455	0.17746784	0.23991495
As	0.01014352	0.01580807	0.01634987
Se	0.19055983	0.04511376	0.05502845
Sr	96.3295246	47.3082789	44.5776152
Y	0.0006918	0.00079115	0.0007565
Mo	0.11391552	0.15782155	0.1623507
Cd	0.000629	0.0007587	0.00056655
Sn	0.00148175	0.0015836	0.00059928
Sb	0.0056938	0.00381586	0.00420331
Cs	0.01278693	0.01074224	0.0128428
La	0.00126275	0.00026313	0.00185485
Ce	0.00013822	0.00045796	0.00096004
Hg	0.0016425	0.00106541	0.00093316
Tl	0.000631	0.0004896	0.00042191
Pb	0.00795363	0.00763698	0.00669538
Th	4.9627E-05	6.3048E-05	0.00011367
U	0.00299022	0.02879662	0.02295394

Table B.5. Leachate concentration, NH₄NO₃, [units mg/kg]

ID	BGH-1312-P1-4.0	BGH-1312-P1-4.5	BGH-1312-P1-5.0	BGH-1312-P1-6.0	BGH-1312-P1-7.0	BGH-1312-P1-7.0
Depth [m]	Dist.	Dist.	5.10 – 5.25	Dist.	7.20 – 7.35	7.50 – 7.65
Depth _{average} [m]	4.25	4.75	5.18	6.25	7.28	7.58
Li	0.4995	0.4868	1.4824	1.3984	1.5990	2.8053
Be	0.0009	0.0010	0.0005	0.0006	0.0007	0.0008
Na	255.5173	251.1161	268.0641	320.0207	354.2440	511.5905
Mg	2297.5903	2027.2955	1516.1535	840.2040	1182.8236	1674.9784
P	3.4955	0.8572	3.8730	3.2846	3.9714	3.8382
K	434.9774	420.9461	658.5769	1043.5250	1214.9268	1566.9247
Ca	14405.173	14161.332	28129.792	22303.334	17750.283	24503.633
V	0.0656	0.0648	0.3669	0.4771	0.4065	0.2370
Cr	0.0224	0.5107	0.0350	0.0514	0.0495	0.0604
Mn	11.3256	11.4853	2.0558	1.5436	2.1651	2.2361
Co	0.0717	0.0711	0.1372	0.1122	0.0987	0.1192
Ni	0.0975	0.6944	0.2860	0.6619	0.3016	0.1473
Cu	0.1452	0.1191	0.1837	0.2273	0.1820	0.1751
Zn	0.6488	11.8571	1.4555	0.8664	0.3809	1.3984
As	0.0251	0.0266	0.0323	0.0478	0.0567	0.0698
Se	0.0780	0.1509	0.1779	0.1925	0.1625	0.2361
Sr	237.1475	245.9177	351.2674	347.2489	289.6968	420.9610
Y	0.0036	0.0032	0.0034	0.0030	0.0031	0.0073
Mo	0.0610	0.0551	0.0907	0.0899	0.1041	0.1457
Cd	0.0130	0.0125	0.0013	0.0047	0.0037	0.0124
Sn	0.0029	0.0024	0.0009	0.0010	0.0042	0.0021
Sb	0.1498	0.1308	0.0290	0.0198	0.0157	0.0284
Cs	0.5037	0.5042	1.5221	0.9605	1.6643	1.1638
La	0.0035	0.0033	0.0014	0.0020	0.0017	0.0159
Ce	0.0019	0.0033	0.0008	0.0013	0.0013	0.0098
Hg	0.0003	0.0009	0.0034	0.0020	0.0010	0.0025
Tl	0.0261	0.0318	0.0310	0.0310	0.0194	0.0602
Pb	0.0053	0.0904	0.0188	0.0096	0.0067	0.0096
Th	0.0001	0.0002	0.0005	0.0007	0.0006	0.0003
U	0.1287	0.1021	0.1183	0.1320	0.1332	0.1789

Table B.5. Leachate concentration, NH₄NO₃, [units mg/kg], continued

ID	BGH-1312-P1-8.00	BGH-1312-P1-9.0	BGH-1312-P1-9.0	BGH-1312-P2-3.50	BGH-1312-P2-3.50	BGH-1312-P2-4.50
Depth [m]	8.40 - 8.60	9.17 - 9.30	9.60 - 9.75	3.76 - 3.98	4.25 - 4.50	4.55 - 4.70
Depth _{average} [m]	8.50	9.25	9.68	3.87	4.40	4.63
Li	1.5398	0.6997	1.8057	1.2522	1.8124	1.5080
Be	0.0016	0.0000	0.0000	0.0011	0.0011	0.0006
Na	431.6089	663.2730	386.3861	147.3285	225.3498	213.4024
Mg	683.2425	201.6524	909.3641	4503.8378	952.7739	1357.0798
P	4.6476	3.7836	3.7484	3.8366	3.9530	3.5873
K	1555.1335	1800.0138	1400.9515	303.6749	683.3031	691.9970
Ca	41725.356	25676.129	18668.187	12482.205	29267.612	20760.593
V	0.4860	0.4227	0.4959	0.0832	0.0825	0.3968
Cr	0.0716	0.0521	0.0620	0.0144	0.0705	0.0504
Mn	0.8465	1.3614	2.4558	4.7912	1.5932	2.0171
Co	0.1893	0.1221	0.0900	0.0583	0.1283	0.0954
Ni	0.1877	0.1596	0.1914	0.1279	0.4867	0.3259
Cu	0.1896	0.1325	0.1880	0.0945	0.1528	0.2488
Zn	0.8130	0.6814	0.4203	0.5309	0.5512	0.6451
As	0.0672	0.1619	0.0601	0.0068	0.0182	0.0576
Se	0.3130	0.1534	0.1952	0.1332	0.2733	0.2462
Sr	341.4551	352.1814	252.4939	220.0233	281.4737	240.0366
Y	0.0028	0.0027	0.0025	0.0036	0.0026	0.0030
Mo	0.1599	0.1215	0.1436	0.1426	0.0827	0.0802
Cd	0.0057	0.0024	0.0051	0.0056	0.0045	0.0052
Sn	0.0008	0.0007	0.0012	0.0071	0.0030	2.2771
Sb	0.0853	0.0128	0.0238	0.0093	0.0302	0.0289
Cs	0.5866	1.5522	0.6071	0.6887	0.9345	1.0582
La	0.0013	0.0027	0.0011	0.0047	0.0021	0.0023
Ce	0.0008	0.0011	0.0007	0.0034	0.0018	0.0029
Hg	0.0047	0.0033	0.0037	0.0014	0.0043	0.0036
Tl	0.1034	0.0094	0.0309	0.0230	0.0264	0.0263
Pb	0.0041	0.0098	0.0071	0.0036	0.0105	0.0086
Th	0.0007	0.0006	0.0004	0.0007	0.0007	0.0003
U	0.1709	0.0460	0.1718	0.0363	0.0529	0.1068

Table B.5. Leachate concentration, NH₄NO₃, [units mg/kg], continued

ID	BGH-1312-P2-4.50	BGH-1312-P2-5.50	BGH-1312-P2-6.50	BGH-1312-P2-6.50	BGH-1312-P2-7.50	BGH-1312-P2-7.50
Depth [m]	5.07 - 5.22	5.85 - 6.00	6.65 - 6.80	6.95 - 7.10	7.70 - 7.85	8.20 - 8.35
Depth_{average} [m]	5.15	5.93	6.73	7.03	7.78	8.28
Li	1.4942	0.7834	0.7895	1.0164	2.3342	2.0542
Be	0.0005	0.0003	0.0006	0.0007	0.0002	0.0006
Na	308.1074	310.0340	366.6310	175.1806	416.5039	347.9225
Mg	932.9912	500.3491	676.1102	709.3743	1321.6510	947.9492
P	4.2785	2.8744	3.4546	1.5295	4.2892	2.7281
K	878.4247	668.4464	704.9527	611.7596	1207.7737	1165.4532
Ca	17567.648	12818.581	18129.642	7978.0012	24522.654	13650.209
V	0.5015	0.1573	0.1894	0.0898	0.5857	0.2249
Cr	0.0380	0.0043	0.0281	0.0225	0.0532	0.0228
Mn	1.8702	2.8085	3.8821	3.3852	2.1829	1.5836
Co	0.0865	0.0582	0.0878	0.0350	0.1086	0.0611
Ni	0.1821	0.0889	0.0568	0.0589	0.1382	0.3410
Cu	0.1411	0.1087	0.0985	0.1126	0.2415	0.0948
Zn	0.4046	0.3783	0.8976	0.2860	1.1442	0.8362
As	0.0683	0.0560	0.1047	0.0311	0.0838	0.0487
Se	0.2162	0.1382	0.1621	0.1393	0.2018	0.1496
Sr	266.7739	163.9356	225.9126	125.6557	279.5494	215.9870
Y	0.0025	0.0014	0.0022	0.0014	0.0032	0.0019
Mo	0.0805	0.0672	0.0952	0.0487	0.1552	0.1373
Cd	0.0030	0.0026	0.0050	0.0034	0.0022	0.0012
Sn	0.0103	0.0013	0.0014	0.0069	0.0017	0.0009
Sb	0.0143	0.0069	0.0121	0.0098	0.0379	0.0182
Cs	0.9761	0.3596	0.4037	0.4091	0.9019	1.5465
La	0.0015	0.0028	0.0014	0.0019	0.0032	0.0020
Ce	0.0008	0.0011	0.0006	0.0014	0.0018	0.0019
Hg	0.0026	0.0002	0.0002	0.0014	0.0012	0.0047
Tl	0.0153	0.0096	0.0098	0.0128	0.0610	0.0149
Pb	0.0068	0.0041	0.0054	0.0203	0.0241	0.0154
Th	0.0001	0.0005	0.0002	0.0003	0.0004	0.0002
U	0.0886	0.0107	0.0507	0.0480	0.2386	0.1244

Appendix B - Tables

Table B.5. Leachate concentration, NH₄NO₃, [units mg/kg], continued

ID	BGH-1312-P2-8.50	BGH-1312-P3-2.50	BGH-1312-P3-2.50	BGH-1312-P3-3.5	BGH-1312-P3-4.50	BGH-1312-P3-5.50
Depth [m]	8.80 - 8.95	2.70 - 2.80	3.15 - 3.25	3.85 - 4.00	5.10 - 5.25	5.85 - 6.00
Depth_{average} [m]	8.88	2.85	3.20	3.90	5.18	5.93
Li	1.5972	-	-	-	-	-
Be	0.0009	-	-	-	-	-
Na	174.5297	215.82	226.48	-	511.88	675.97
Mg	1156.1905	1006.35	1890.35	-	234.60	505.29
P	3.2301	0.15	0.12	-	0.39	
K	649.7927	222.10	390.10	-	1887.70	2668.80
Ca	19518.962	4459.90	12269.90	-	34469.90	14668.78
Cr	0.0066	0.00	0.01	-	0.01	0.00
Mn	3.0693	3.00	9.70	-	0.0061	0.10
Co	0.0859	0.01	0.01	-	0.00	0.00
Ni	0.1898	0.00	0.00	-	0.00	0.00
Cu	0.1320	0.01	0.01	-	0.00	0.01
Zn	0.3729	0.00	0.00	-	0.01	0.00
As	0.0437	0.0060	0.0074	-	0.0035	0.00
Se	0.1519	-	-	-	-	-
Sr	223.5678	-	-	-	-	-
Y	0.0021	-	-	-	-	-
Mo	0.1303	-	-	-	-	-
Cd	0.0047	0.00	0.01	-	0.01	0.00
Sn	0.0030	-	-	-	-	-
Sb	0.0262	-	-	-	-	-
Cs	0.3901	-	-	-	-	-
La	0.0029	-	-	-	-	-
Ce	0.0017	-	-	-	-	-
Hg	0.0046	-	-	-	-	-
Tl	0.0397	-	-	-	-	-
Pb	0.0070	0.01	0.00	-	0.00	0.01
Th	0.0005	-	-	-	-	-
U	0.1393	-	-	-	-	-
Fe	-	0.85	0.02	-	4.10	19.74
S	-	439.70	1207.70	-	10418.70	900.08
Si	-	12.65	37.80	-	1.00	20.19

Table B.5. Leachate concentration, NH₄NO₃, [units mg/kg], continued

ID	BGH-1312-P3-5.50	BGH-1312-P3-6.50	BGH-1312-P3-7.50	BGH-1312-P3-7.50	BGH-1312-P3-8.50	BGH-1312-P3-9.50
Depth [m]	6.15 - 6.30	6.90 - 7.10	7.70 - 7.80	8.15 - 8.35	8.80 - 9.00	10.10 - 10.30
Depth _{average} [m]	6.2300	7	7.7500	8.25	8.9000	10.2
Li	-	-	-	-	-	-
Be	-	-	-	-	-	-
Na	614.14	629.08	364.72	502.81	429.90	523.63
Mg	441.65	257.95	517.31	266.29	303.05	255.70
P	0.10	0.42	-	-	0.31	0.26
K	2541.70	1682.50	990.76	1680.64	1633.30	1791.70
Ca	10929.90	32239.90	13781.18	24312.35	14689.90	28729.90
V	-	-	-	-	-	-
Cr	0.01	0.00	0.00	0.00	0.01	0.01
Mn	0.0053	0.0030	0.51	0.0085	0.0018	0.0099
Co	0.01	0.00	0.00	0.00	0.00	0.01
Ni	0.00	0.01	0.01	0.01	0.01	0.00
Cu	0.01	0.01	0.01	0.01	0.01	0.01
Zn	0.01	0.01	0.01	0.00	0.01	0.00
As	0.0011	0.0002	0.00	0.01	0.0022	0.0024
Se	-	-	-	-	-	-
Sr	-	-	-	-	-	-
Y	-	-	-	-	-	-
Mo	-	-	-	-	-	-
Cd	0.00	0.00	0.00	0.01	0.00	0.00
Sn	-	-	-	-	-	-
Sb	-	-	-	-	-	-
Cs	-	-	-	-	-	-
La	-	-	-	-	-	-
Ce	-	-	-	-	-	-
Hg	-	-	-	-	-	-
Tl	-	-	-	-	-	-
Pb	0.00	0.01	0.00	0.00	0.01	0.01
Th	-	-	-	-	-	-
U	-	-	-	-	-	-

Table B.5. Leachate concentration, NH₄NO₃, [units mg/kg], continued

ID	BGH-1312- P3-9.50	PCD1-L1- S2	PCD1-L1- S3	PCD1-L1- S4	PCD3-B2	PCD5-B1
Depth [m]	9.65 - 9.85					
Depth_{average} [m]	9.7500					
Li	-	0.6577	0.5633	0.6712	0.8017	0.5848
Be	-	0.0007	0.0004	0.0004	0.0014	0.0012
Na	413.14	194.6300	215.4051	219.4312	201.4091	182.1427
Mg	574.53	887.5905	1170.1588	1836.1088	1805.9354	2313.9905
P	-	3.2499	2.4489	2.5350	5.1982	4.5922
K	1430.46	386.2749	376.3041	274.8240	387.3282	220.7567
Ca	21472.52	14465.935	11278.484	13203.927	12656.416	10953.474
V	-	0.0220	0.0311	0.0255	0.0072	0.0152
Cr	0.01	0.0469	0.0196	0.0189	0.1232	0.0089
Mn	0.61	11.7088	5.8749	7.4623	6.2117	11.6039
Co	0.00	0.0651	0.0524	0.0592	0.0692	0.0588
Ni	0.01	2.9409	0.0978	0.1268	0.1212	0.2101
Cu	0.00	0.1194	0.2169	0.0891	0.1363	0.3169
Zn	0.00	0.4280	0.5874	1.0050	1.0143	1.0330
As	0.01	0.0310	0.0131	0.0140	0.1523	0.0263
Se	-	0.0858	0.0660	0.0617	0.0799	0.0751
Sr	-	192.4975	195.2990	228.8715	223.9806	150.8954
Y	-	0.0033	0.0024	0.0024	0.0044	0.0047
Mo	-	0.0862	0.0671	0.0705	0.1294	0.1071
Cd	0.01	0.0012	0.0025	0.0099	0.0222	0.3337
Sn	-	0.0049	0.0046	0.0024	0.0041	0.0031
Sb	-	0.0350	0.0162	0.0163	0.0308	0.0358
Cs	-	0.3192	0.3221	0.1859	0.4843	0.2182
La	-	0.0028	0.0030	0.0023	0.0086	0.0040
Ce	-	0.0028	0.0014	0.0010	0.0056	0.0049
Hg	-	0.0056	0.0028	0.0013	0.0034	0.0080
Tl	-	0.0234	0.0150	0.0115	0.0234	0.0174
Pb	0.01	0.0365	0.0648	0.0277	0.0969	0.2487
Th	-	0.0008	0.0003	0.0003	0.0006	0.0007
U	-	0.1058	0.1224	0.1139	0.0627	0.1036

Table B.5. Leachate concentration, NH₄NO₃, [units mg/kg], continued

ID	PCD5-B2	PCD5-B4	PCD5-B4(A)	Ash
Depth [m]				
Depth _{average} [m]				
Li	1.4657	0.4137	0.5617	-
Be	0.0008	0.0010	0.0012	-
Na	103.2254	213.5643	223.4855	404.31
Mg	4573.9636	1984.1253	2210.6240	5856.35
P	2.4750	3.2077	4.0637	0.25
K	377.8407	493.0139	597.0845	700.90
Ca	19892.401	19442.642	20687.775	39299.90
V	0.1317	0.0183	0.0881	-
Cr	0.0563	0.0343	0.0075	0.00
Mn	10.3793	9.3464	9.9498	0.20
Co	0.0862	0.0830	0.0894	0.01
Ni	0.1210	0.8095	0.1654	0.32
Cu	0.3029	0.1040	0.1642	0.01
Zn	0.8775	0.9359	0.4089	0.01
As	0.1105	0.0379	0.0277	5.80
Se	0.2506	0.0786	0.0696	-
Sr	331.8339	331.5574	394.7370	-
Y	0.0042	0.0049	0.0039	-
Mo	0.1871	0.2036	0.2094	-
Cd	0.0027	0.0043	0.0037	0.00
Sn	0.0025	0.0062	0.0027	-
Sb	0.0233	0.0095	0.0093	-
Cs	0.4958	0.5740	0.6048	-
La	0.0034	0.0057	0.0026	-
Ce	0.0021	0.0038	0.0030	-
Hg	0.0050	0.0027	0.0004	-
Tl	0.0568	0.0159	0.0188	-
Pb	0.2583	0.0813	0.0931	0.01
Th	0.0009	0.0002	0.0006	-
U	0.0714	0.0756	0.0973	-
U	0.0714	0.0756	0.0973	-

Table B.6. Leachate concentration, NH₄-Acetate, [units mg/kg], continued

ID	BGH-1312-P1-4.0	BGH-1312-P1-4.5	BGH-1312-P1-5.0	BGH-1312-P1-6.0	BGH-1312-P1-7.0	BGH-1312-P1-7.0
Depth [m]	Dist.	Dist.	5.10 – 5.25	Dist.	7.20 – 7.35	7.50 – 7.65
Depth _{average} [m]	4.25	4.75	5.18	6.25	7.28	7.58
Li	0.6636	0.5613	1.3840	1.1065	0.9319	3.3855
Be	0.0048	0.0027	0.0032	0.0049	0.0069	0.0019
Na	56.6658	19.2708	23.4068	14.3743	37.0111	78.9424
Mg	1604.2774	1261.9885	2168.4228	1565.0240	1556.4434	1896.2108
P	4.0441	3.0470	0.2260	0.8870	0.7470	2.9222
K	328.7382	70.9339	95.2361	117.0511	123.6766	190.2833
Ca	30479.817	26330.695	23425.801	15762.354	13321.944	28412.677
V	0.0937	0.0607	0.0382	0.0976	0.1084	0.2199
Cr	0.4668	0.4423	0.3301	0.3334	0.3108	0.3231
Mn	112.9321	79.7130	44.3141	36.0064	44.0622	23.5578
Co	0.2147	0.1717	0.1225	0.0825	0.0806	0.1475
Ni	0.2023	0.4495	0.3936	0.0674	0.2982	0.0809
Cu	0.1870	0.1963	0.3596	0.3217	0.2637	0.2435
Zn	1.0103	1.1892	1.0816	0.9741	0.7377	1.2058
As	0.0402	0.0459	0.0287	0.0402	0.0353	0.0926
Se	0.0738	0.0733	0.0007	0.1166	0.1160	0.0467
Sr	219.7209	185.4443	167.9272	129.3102	119.8146	239.9347
Y	0.1760	0.1161	0.0581	0.0589	0.0727	0.0816
Mo	0.0094	0.0440	0.0562	0.0485	0.0642	0.0437
Cd	0.3176	0.1898	0.0060	0.0079	0.0073	0.0160
Sn	0.0014	0.0003	0.0025	0.0001	0.0019	0.0046
Sb	0.1382	0.1161	0.0210	0.0160	0.0117	0.0259
Cs	0.0771	0.0718	0.2173	0.1330	0.2016	0.2212
La	0.2106	0.1411	0.0717	0.0743	0.1047	0.1206
Ce	0.3196	0.2101	0.1089	0.1209	0.1662	0.1880
Hg	0.0023	0.0027	0.0041	0.0033	0.0028	0.0034
Tl	0.0461	0.0417	0.0420	0.0494	0.0406	0.0775
Pb	0.0562	0.0434	0.0421	0.0498	0.0496	0.0336
Th	0.0003	0.0014	0.0013	0.0007	0.0001	0.0005
U	0.3086	0.2402	0.1038	0.0296	0.0350	0.3404

Table B.6. Leachate concentration, NH₄-Acetate, [units mg/kg], continued

ID	BGH-1312-P1-8.00	BGH-1312-P1-9.0	BGH-1312-P1-9.0	BGH-1312-P2-3.50	BGH-1312-P2-3.50	BGH-1312-P2-4.50
Depth [m]	8.40 - 8.60	9.17 - 9.30	9.60 - 9.75	3.76 - 3.98	4.25 - 4.50	4.55 - 4.70
Depth average [m]	8.50	9.25	9.68	3.87	4.40	4.63
Li	2.0633	0.4546	1.0087	0.9634	1.2547	0.8743
Be	0.0095	0.0034	0.0079	0.0080	0.0149	0.0128
Na	77.2003	113.5349	46.4032	43.6742	13.1760	17.6247
Mg	2102.2421	456.5670	1138.1795	4115.4544	2687.3229	2159.2108
P	0.9599	1.5988	2.7971	1.0711	1.5155	1.1667
K	424.3585	494.3462	147.4928	282.1033	304.0385	76.2098
Ca	27483.980	14883.505	10133.795	23776.964	17920.057	9996.9103
V	0.1780	0.0984	0.1008	0.0800	0.1166	0.0237
Cr	0.1919	0.2611	0.2592	0.1050	0.1266	0.0985
Mn	42.2027	22.9089	49.0802	63.9954	67.3689	53.8110
Co	0.1486	0.0814	0.0682	0.1147	0.1176	0.0927
Ni	0.3406	0.0097	0.2307	0.2197	0.5074	0.6057
Cu	0.2546	0.1504	0.2435	0.3125	0.2774	0.2672
Zn	0.8573	0.5508	0.8636	0.8986	0.9693	2.3493
As	0.0743	0.1295	0.0343	0.0221	0.0273	0.0287
Se	0.1538	0.0206	0.0494	0.0494	0.1234	0.0590
Sr	199.1197	136.4261	93.0393	285.5940	128.2386	87.5479
Y	0.2339	0.0286	0.0992	0.2725	0.1882	0.1260
Mo	0.0349	0.0052	0.0465	0.0413	0.0018	0.0214
Cd	0.0251	0.0011	0.0062	0.0138	0.0119	0.0077
Sn	0.0025	0.0002	0.0025	0.0023	0.0062	0.0020
Sb	0.0478	0.0089	0.0155	0.0114	0.0213	0.0139
Cs	0.1220	0.2644	0.0935	0.0859	0.1482	0.1583
La	0.2835	0.0403	0.1303	0.3420	0.2170	0.1475
Ce	0.4425	0.0673	0.2100	0.5226	0.3304	0.2324
Hg	0.0032	0.0019	0.0023	0.0037	0.0027	0.0030
Tl	0.1226	0.0179	0.0386	0.0350	0.0447	0.0428
Pb	0.0516	0.0364	0.0531	0.0403	0.0510	0.0527
Th	0.0016	0.0000	0.0014	0.0003	0.0018	0.0013
U	0.3797	0.0009	0.0460	0.0806	0.0892	0.0425

Table B.6. Leachate concentration, NH₄-Acetate, [units mg/kg], continued

ID	BGH-1312-P2-4.50	BGH-1312-P2-5.50	BGH-1312-P2-6.50	BGH-1312-P2-6.50	BGH-1312-P2-7.50	BGH-1312-P2-7.50
Depth [m]	5.07 - 5.22	5.85 - 6.00	6.65 - 6.80	6.95 - 7.10	7.70 - 7.85	8.20 - 8.35
Depth_{average} [m]	5.1500	5.9300	6.7300	7.0300	7.7800	8.2800
Li	0.6295	0.6878	0.4479	0.6775	1.6516	1.2846
Be	0.0101	0.0079	0.0057	0.0224	0.0337	0.0133
Na	50.2283	125.9220	54.8391	34.7575	46.4473	52.9291
Mg	1350.0906	909.9780	674.5437	832.8330	2497.6256	1572.0828
P	3.2647	1.1751	1.2384	1.3182	1.9504	0.6409
K	77.9837	437.6295	327.6700	239.3327	349.2411	286.1421
Ca	7268.5630	9616.3465	10107.330	4270.0129	13256.963	8681.3043
V	0.0983	0.1207	0.1183	0.0869	0.1133	0.0935
Cr	0.1499	0.2853	0.0689	0.2526	0.3650	0.2331
Mn	34.5543	32.6275	34.4254	40.7435	81.0092	42.8986
Co	0.0540	0.0638	0.0714	0.0836	0.1392	0.0793
Ni	0.4054	0.1134	0.3260	0.9875	1.2311	0.1483
Cu	0.2181	0.2076	0.1666	0.2054	0.2886	0.1426
Zn	1.0566	0.9633	0.6837	0.8330	0.8258	0.5609
As	0.0315	0.0561	0.0969	0.0265	0.0391	0.0221
Se	0.0197	0.0988	0.1126	0.0357	0.1109	0.0138
Sr	68.5566	103.6895	76.1723	40.4685	120.6744	92.0715
Y	0.0686	0.0795	0.0527	0.2284	0.3946	0.1801
Mo	0.0510	0.0621	0.0739	0.0317	0.0094	0.0083
Cd	0.0028	0.0028	0.0011	0.0075	0.0223	0.0082
Sn	0.0016	0.0027	0.0016	0.0018	0.0308	0.0010
Sb	0.0092	0.0084	0.0083	0.0081	0.0196	0.0096
Cs	0.1287	0.1602	0.0812	0.0769	0.1346	0.2247
La	0.0786	0.0954	0.0598	0.2777	0.4652	0.2677
Ce	0.1347	0.1596	0.1042	0.4969	0.7880	0.4426
Hg	0.0024	0.0026	0.0024	0.0025	0.0055	0.0019
Tl	0.0258	0.0185	0.0161	0.0183	0.0759	0.0378
Pb	0.0480	0.0751	0.0623	0.1775	0.4387	0.0618
Th	0.0002	0.0009	0.0010	0.0035	0.0040	0.0020
U	0.0137	0.0109	0.0038	0.0327	0.0865	0.0350

Table B.6. Leachate concentration, NH₄-Acetate, [units mg/kg], continued

ID	BGH-1312-P2-8.50	BGH-1312-P3-2.50	BGH-1312-P3-2.50	BGH-1312-P3-3.5	BGH-1312-P3-4.50	BGH-1312-P3-5.50
Depth [m]	8.80 - 8.95	2.70 - 2.80	3.15 - 3.25	3.85 - 4.00	5.10 - 5.25	5.85 - 6.00
Depth_{average} [m]	8.88	2.85	3.20	3.93	5.18	5.93
Li	0.8450	-	-	-	-	-
Be	0.0507	-	-	-	-	-
Na	16.3205	24.14	60.38	-	116.66	165.94
Mg	1542.8041	547.00	832.00	-	3898.00	844.40
P	2.1271	0.03	0.10	-	0.05	-
K	296.2547	36.33	95.16	-	299.33	497.74
Ca	8341.8571	5377.38	7029.92	-	14302.58	12164.03
Cr	0.5393	0.08	0.06	-	0.05	0.01
Mn	73.5629	22.79	21.76	-	0.76	2.93
Co	0.1812	0.07	0.05	-	0.01	0.06
Ni	2.0593	0.01	0.00	-	0.05	0.03
Cu	0.2473	0.05	0.07	-	0.07	0.01
Zn	1.2194	0.06	0.06	-	0.07	0.03
As	0.0667	0.40	0.28	-	0.11	0.17
Se	0.0970	-	-	-	-	-
Sr	89.7953	-	-	-	-	-
Y	0.5301	-	-	-	-	-
Mo	0.0266	-	-	-	-	-
Cd	0.0124	0.02	0.06	-	0.01	0.03
Sn	0.0049	-	-	-	-	-
Sb	0.0133	-	-	-	-	-
Cs	0.0756	-	-	-	-	-
La	0.5986	-	-	-	-	-
Ce	1.0544	-	-	-	-	-
Hg	0.0019	-	-	-	-	-
Tl	0.0409	-	-	-	-	-
Pb	0.1076	0.01	0.04	-	0.05	0.01
Th	0.0116	-	-	-	-	-
U	0.2103	-	-	-	-	-
Fe	-	2.12	0.65	-	6.79	4.28
S	-	0.98	0.07	-	3.95	3.04
Si	-	180.00	318.00	-	2047.00	476.20

Table B.6. Leachate concentration, NH₄-Acetate, [units mg/kg], continued

ID	BGH-1312-P3-5.50	BGH-1312-P3-6.50	BGH-1312-P3-7.50	BGH-1312-P3-7.50	BGH-1312-P3-8.50	BGH-1312-P3-9.50
Depth [m]	6.15 - 6.30	6.90 - 7.10	7.70 - 7.80	8.15 - 8.35	8.80 - 9.00	10.10 - 10.30
Depth _{average} [m]	6.2300	7	7.7500	8.25	8.9000	10.2
Li	-	-	-	-	-	-
Be	-	-	-	-	-	-
Na	156.73	167.11	75.75	125.15	121.32	126.82
Mg	1178.00	867.00	615.42	492.93	842.00	880.00
P	0.04	0.08	-	-	0.07	0.08
K	451.84	329.86	157.02	303.20	306.65	296.91
Ca	11204.20	15225.84	10191.81	14696.83	13004.08	14512.46
V	-	-	-	-	-	-
Cr	0.00	0.06	0.06	0.01	0.08	0.03
Mn	5.40	1.73	9.19	1.92	3.67	3.02
Co	0.04	0.09	0.08	0.07	0.04	0.08
Ni	0.07	0.02	0.08	0.09	0.05	0.02
Cu	0.05	0.09	0.06	0.02	0.08	0.04
Zn	0.08	0.05	0.05	0.01	0.06	0.02
As	0.47	0.17	0.06	0.24	0.36	0.41
Se	-	-	-	-	-	-
Sr	-	-	-	-	-	-
Y	-	-	-	-	-	-
Mo	-	-	-	-	-	-
Cd	0.09	0.03	0.08	0.08	0.06	0.02
Sn	-	-	-	-	-	-
Sb	-	-	-	-	-	-
Cs	-	-	-	-	-	-
La	-	-	-	-	-	-
Ce	-	-	-	-	-	-
Hg	-	-	-	-	-	-
Tl	-	-	-	-	-	-
Pb	0.07	0.07	0.05	0.03	0.03	0.02
Th	-	-	-	-	-	-
U	-	-	-	-	-	-

Table B.6. Leachate concentration, NH₄-Acetate, [units mg/kg], continued

ID	BGH-1312- P3-9.50	PCD1-L1- S2	PCD1-L1- S3	PCD1-L1- S4	PCD3-B2	PCD5-B1
Depth [m]	9.65 - 9.85					
Depth_{average} [m]	9.7500					
Li	-	0.3838	0.5135	0.5047	0.3655	0.2229
Be	-	0.0034	0.0012	0.0011	0.0028	0.0033
Na	79.97	12.1234	6.7609	47.1318	19.6971	60.7195
Mg	735.89	386.4979	797.1731	1224.0647	739.4298	694.6991
P	-	2.5700	6.0285	1.5571	0.2475	1.2376
K	181.18	83.6038	114.1585	81.2737	68.3054	46.2002
Ca	12782.74	8250.5964	20377.161	19039.478	11601.466	5261.965
V	-	0.1370	0.0893	0.0723	0.0146	0.0217
Cr	0.03	0.1578	0.0140	0.0749	0.3050	0.1124
Mn	6.01	34.0912	36.8842	26.8854	14.6180	23.7877
Co	0.07	0.0385	0.0891	0.0900	0.0650	0.0446
Ni	0.10	0.5888	0.4378	0.0298	0.2639	0.5274
Cu	0.01	0.1639	0.2113	0.1571	0.1659	0.2022
Zn	0.02	2.0887	0.9333	0.9286	1.1593	0.9620
As	0.44	0.0547	0.0599	0.0549	0.0509	0.0281
Se	-	0.0833	0.1142	0.1068	0.0495	0.0872
Sr	-	71.6019	181.8479	196.5970	127.0199	49.5389
Y	-	0.0305	0.0381	0.0260	0.0519	0.0279
Mo	-	0.0118	0.0041	0.0119	0.0117	0.0201
Cd	0.07	0.0166	0.0102	0.0084	0.0326	0.0515
Sn	-	0.0035	0.0039	0.0032	0.0034	0.0040
Sb	-	0.0244	0.0243	0.0291	0.0253	0.0270
Cs	-	0.0465	0.0724	0.0514	0.0610	0.0351
La	-	0.0337	0.0383	0.0246	0.0641	0.0274
Ce	-	0.0489	0.0587	0.0360	0.0855	0.0436
Hg	-	0.0019	0.0034	0.0051	0.0036	0.0009
Tl	-	0.0285	0.0283	0.0228	0.0255	0.0169
Pb	0.07	0.0382	0.0210	0.0428	0.0828	0.0874
Th	-	0.0018	0.0004	0.0006	0.0014	0.0007
U	-	0.0348	0.2941	0.2957	0.1128	0.0191

Appendix B - Tables

Table B.6. Leachate concentration, NH₄-Acetate, [units mg/kg], continued

ID	PCD5-B2	PCD5-B4	PCD5-	Ash
			B4(A)	
Depth [m]				
Depth _{average} [m]				
Li	0.6006	0.1790	0.2456	-
Be	0.0008	0.0016	0.0008	-
Na	63.0901	34.3690	42.6841	57.44
Mg	1306.5508	695.9794	742.7660	9704.00
P	3.1017	2.8132	2.2533	6.85
K	85.4711	80.1539	85.6211	95.22
Ca	25940.510	9113.000	13050.031	13207.60
V	0.0306	0.0591	0.0448	-
Cr	0.2824	0.1487	0.0179	0.01
Mn	27.2868	18.5570	18.2768	9.40
Co	0.1109	0.0435	0.0691	0.04
Ni	0.1444	1.5757	0.0579	0.10
Cu	0.3063	0.1279	0.1723	0.07
Zn	2.0987	0.8325	7.4331	0.03
As	0.0509	0.0671	0.0703	1.70
Se	0.0540	0.0153	0.0579	-
Sr	184.3420	89.9323	120.5829	-
Y	0.0511	0.0176	0.0183	-
Mo	0.0710	0.0899	0.1014	-
Cd	0.0426	0.0197	0.0285	0.08
Sn	0.0083	0.0009	0.0047	-
Sb	0.0211	0.0103	0.0097	-
Cs	0.0510	0.1007	0.0899	-
La	0.0589	0.0214	0.0235	-
Ce	0.0775	0.0361	0.0365	-
Hg	0.0069	0.0017	0.0022	-
Tl	0.0460	0.0190	0.0184	-
Pb	0.0627	0.0463	0.0432	0.03
Th	0.0023	0.0004	0.0014	-
U	0.0940	0.0142	0.0497	-

Table B.7. Leachate concentration, Aqua regia, [units mg/kg]

ID	BGH-1312-P1-4.0	BGH-1312-P1-4.5	BGH-1312-P1-5.0	BGH-1312-P1-6.0	BGH-1312-P1-7.0	BGH-1312-P1-7.0
Depth [m]	Dist.	Dist.	5.10 – 5.25	Dist.	7.20 – 7.35	7.50 – 7.65
Depth _{average} [m]	4.25	4.75	5.18	6.25	7.28	7.58
Li	-	-	-	-	-	-
Al	23576	27890	23612	21667	24539	26939
Na	589	637	626	621	892	761
Mg	18452	22437	18897	15228	16954	21168
Fe	-	-	87419	66558	76028	-
P	180	252	109	83	92	150
K	1959	2005	1494	2219	3095	1717
Ba	429	358	310	255	312	327
Ca	64053	74969	80151	53897	56783	65075
Cr	32	39	28	39	32	32
Mn	879	1063	917	683	722	888
Co	12	14	6	5	6	9
Ni	21	24	10	12	12	13
Cu	13	14	6	5	5	6
Zn	90	102	29	8	4	1965
S	6477	6395	7188	46333	3866	6134
As	-	-	0.00480474	0.00945136	0.00313891	-
B	274	328	327	234	269	281
Si	4542	5027	3006	2544	3332	6445
Se	-	-	-	-	-	-
Sr	587	695	682	574	681	591
Y	-	-	-	-	-	-
Mo	-	-	-	-	-	-
Cd	4	5	3	1	2	12
Sn	-	-	-	-	-	-
Sb	-	-	-	-	-	-
Cs	-	-	-	-	-	-
La	-	-	-	-	-	-
Ce	-	-	-	-	-	-
Hg	-	-	-	-	-	-
Tl	-	-	-	-	-	-
Pb	43	47	20	18	19	24

Appendix B - Tables

Table B.7. Leachate concentration, Aqua regia, [units mg/kg], continued

ID	BGH-1312-P1-8.00	BGH-1312-P1-9.0	BGH-1312-P1-9.0	BGH-1312-P2-3.50	BGH-1312-P2-3.50	BGH-1312-P2-4.50
Depth [m]	8.40 - 8.60	9.17 - 9.30	9.60 - 9.75	3.76 - 3.98	4.25 - 4.50	4.55 - 4.70
Depth _{average} [m]	8.50	9.25	9.68	3.87	4.40	4.63
Li	-	-	-	-	-	-
Al	30800	10360	25232	24689	27435	23786
Be	-	-	-	-	-	-
Na	807	957	904	518	626	610
Mg	21999	3067	11147	30551	18417	15603
Fe	-	-	48412	-	-	72250
P	159	39	131	226	115	100
K	2430	2106	3435	1575	2265	2389
Ba	354	106	203	312	291	274
Ca	84537	48022	51423	69553	74371	62347
V	-	-	-	-	-	-
Cr	36	10	30	30	28	30
Mn	940	213	596	951	788	732
Co	7	2	6	5	6	4
Ni	16	4	10	15	11	10
Cu	8	1	5	5	4	5
Zn	81	13	2	36	15	3
S	11655	6801	4151	5421	8717	5868
As	-	-	0.00110989	-	-	0.00858406
B	482	151	216	374	378	314
Si	7337	1409	2526	4504	6539	4542
Se	-	-	-	-	-	-
Sr	617	450	561	766	643	642
Y	-	-	-	-	-	-
Mo	-	-	-	-	-	-
Cd	3	0.0040207	0.00657137	3	1	2
Pb	28	5	17	23	21	18
Th	-	-	-	-	-	-
U	-	-	-	-	-	-

Table B.7. Leachate concentration, Aqua regia, [units mg/kg], continued

ID	BGH-1312-P2-4.50	BGH-1312-P2-5.50	BGH-1312-P2-6.50	BGH-1312-P2-6.50	BGH-1312-P2-7.50	BGH-1312-P2-7.50
Depth [m]	5.07 - 5.22	5.85 - 6.00	6.65 - 6.80	6.95 - 7.10	7.70 - 7.85	8.20 - 8.35
Depth _{average} [m]	5.1500	5.9300	6.7300	7.0300	7.7800	8.2800
Li	-	-	-	-	-	-
Al	19244	47549	13964	26088	32369	30434
Na	608	741	632	728	998	936
Mg	10585	8444	4682	10316	19603	13517
Fe	49392	-	-	-	87197	56246
P	70	66	55	90	123	107
K	2339	2396	1997	4132	3465	4253
Ba	203	173	145	211	376	259
Ca	42189	39294	32785	32467	72535	47693
Cr	22	21	15	29	34	30
Mn	482	361	225	403	930	574
Co	3	4	3	5	6	7
Ni	9	8	9	12	17	14
Cu	3	2	5	4	8	6
Zn	0.09307143	9	174	18	20	47
S	3674	4893	6306	2674	4618	3086
As	0.00791925	-	-	-	0.00304979	0.00053096
B	180	235	201	166	336	195
Si	2127	740	1636	1934	4055	6968
Se	-	-	-	-	-	-
Sr	496	404	348	374	700	546
Y	-	-	-	-	-	-
Mo	-	-	-	-	-	-
Cd	0.00208204	0.00800328	0.00103278	0.00812411	0.00654136	0.00233015
Sn	-	-	-	-	-	-
Sb	-	-	-	-	-	-
Cs	-	-	-	-	-	-
La	-	-	-	-	-	-
Ce	-	-	-	-	-	-
Hg	-	-	-	-	-	-
Tl	-	-	-	-	-	-
Pb	13	11	12	21	27	20

Table B.7. Leachate concentration, Aqua regia, [units mg/kg], continued

ID	BGH-1312-P2-8.50
Depth [m]	8.80 - 8.95
Depth _{average} [m]	8.8800
Li	-
Al	25070
Na	666
Mg	10836
Fe	-
P	138
K	2833
Ba	204
Ca	54198
Cr	27
Mn	666
Co	7
Ni	0.00352849
Cu	5
Zn	1722
S	4975
As	-
B	234
Si	3478
Se	-
Sr	588
Y	-
Mo	-
Cd	12
Sn	-
Sb	-
Cs	-
La	-
Ce	-
Hg	-
Tl	-
Pb	18

Table B.8. Content of polycyclic aromatic hydrocarbons of the drilling core BGH-1412-P2 [µg/kg]

Probenbezeichnung	Nap	2-MNap	1-MNap	Any	Ace	Fln	Phe	Ant	Fth	Py	BaA	Chr	Bbf-BkF	BaP	Indeno	DahA	BghiP	Sum
BGH-1412-P2-7.5 (8.25-8.5)	1894	349	177	107	27	68	386	68	127	108	30	37	25	9.6	< 0.2	< 0.2	< 0.2	3413
BGH-1412-P2-8.5 (9.25-9.5)	1218	352	173	53	22	59	264	56	77	74	27	32	21	5.2	< 0.2	< 0.2	< 0.2	2434
BGH-1412-P2-6.5 (6.75-8.0)	1593	378	207	79	30	111	524	112	209	223	73	76	68	31	< 0.2	< 0.2	< 0.2	3715
BGH-1412-P2-3.5 (3.75-4.0)	1899	308	180	57	29	64	440	70	161	145	33	45	39	17	< 0.2	< 0.2	< 0.2	3489
BGH-1412-P2-4.5 (4.5-4.75)	1377	383	217	67	31	86	390	83	119	105	26	33	22	9.4	< 0.2	< 0.2	< 0.2	2950
BGH-1412-P2-4.5 (5.25-5.5)	1031	320	176	44	24	80	320	69	95	100	25	31	21	9.3	< 0.2	< 0.2	< 0.2	2346
Nap	Naphthalin		Ace	Acenaphthen		Fth	Fluoranthen			Bbf-BkF	Benzo(b)fluoranthen / Benzo(k)fluoranthen							
2-MNap	2-Methylnaphthalin		Fln	Fluoren		Py	Pyren			BaP	Benzo(a)pyren							
1-MNap	1-Methylnaphthalin		Phe	Phenanthren		BaA	Benzo(a)anthracen			Indeno	Indeno(1.2.3-cd)pyren							
Any	Acenaphthylen		Ant	Anthracen		Chr	Chrysene			DahA	Dibenz(a,h)anthracen							
BghiP	Benzo(g,h,i)perylene																	

Appendix B - Tables

Table B.9. Trace metal concentration gained by X-ray fluorescence in different liming products. Precision and detection limits are shown for each element (contents and error in wt.-%).

	Bornia DSM 90		Bornia KSM 90		Dolomitfeinkalk DL85	
	Content	Error	Content	Error	Content	Error
Mg	9.982	0.018	3.518	0.011	19.29	0.02
Al	0.7719	0.0026	0.9508	0.0027	0.4358	0.0023
Si	4.842	0.004	5.648	0.004	1.279	0.002
P	0.01178	0.00028	0.01191	0.00028	0.00912	0.00036
S	0.05405	0.00016	0.04222	0.00014	0.2993	0.0004
Cl	0.00405	0.00003	0.00516	0.00003	0.0636	0.00013
K	0.0957	0.0018	0.2008	0.002	0.2991	0.0025
Ca	25.04	0.02	30.3	0.02	36.29	0.02
Ti	0.0452	0.0012	0.0535	0.0013	0.0388	0.0015
V	0.0032	0.001	< 0.0024	-0.0024	< 0.0015	-0.0015
Cr	< 0.00010	-	< 0.00010	-	< 0.00010	-
Mn	0.03309	0.00037	0.1212	0.0007	0.1132	0.0007
Fe	0.5045	0.001	0.5293	0.0011	1.384	0.002
Co	< 0.00030	-	< 0.00030	-	< 0.00030	-
Ni	0.00023	0.00003	0.00101	0.00007	< 0.00005	-
Cu	0.00068	0.00006	0.00067	0.00007	0.00112	0.00008
Zn	0.00496	0.00006	0.04446	0.00016	0.00898	0.00009
Ga	0.00019	0.00004	0.00047	0.00004	0.0007	0.00005
Ge	< 0.00005	-	< 0.00005	-	< 0.00005	-
As	0.00022	0.00002	0.00016	0.00002	0.00107	0.00005
Se	< 0.00005	-	< 0.00005	-	< 0.00005	-
Br	0.00006	0.00001	< 0.00005	-	0.00108	0.00002
Rb	0.00058	0.00001	0.0009	0.00002	0.00156	0.00002
Sr	0.02077	0.00005	0.03113	0.00006	0.01555	0.00005
Y	0.00023	0.00002	0.00029	0.00002	0.00046	0.00002
Zr	0.00134	0.0001	0.00216	0.00013	0.0013	0.00011
Nb	< 0.00010	-	< 0.00001	-0.00001	< 0.00010	-
Mo	0.00062	0.00005	0.00069	0.00005	0.00099	0.00006
Ag	< 0.00020	-	< 0.00020	-	< 0.00020	-
Cd	< 0.00020	-	< 0.00020	-	< 0.00020	-
Sn	< 0.00030	-	0.00053	0.00005	0.00095	0.00007
Sb	< 0.00030	-	0.0003	0.00005	0.00169	0.00011
Te	< 0.00030	-	0.00025	0.00003	0.00154	0.00009
I	0.00018	0.00009	0.00075	0.00016	< 0.00030	-
Cs	< 0.00040	-	< 0.00040	-	< 0.00040	-
Ba	0.00576	0.00052	0.00327	0.00045	0.01246	0.00069
La	< 0.00020	-	< 0.00020	-	< 0.00020	-
Ce	< 0.00020	-	< 0.00020	-	< 0.00020	-
Er	< 0.00051	-	< 0.00051	-	< 0.00051	-
Yb	< 0.00020	-	< 0.00020	-	< 0.00020	-

Hf	< 0.00010	-	< 0.00010	-	< 0.00010	-
Ta	0.00613	0.00013	0.006	0.00014	0.00647	0.00017
W	0.00004	0.00001	0.00015	0.00004	< 0.00010	-
Hg	< 0.00010	-	< 0.00010	-	< 0.00010	-
Tl	0.00004	0.00002	< 0.00010	-	< 0.00001	-0.00001
Pb	0.00072	0.00004	0.00068	0.00004	0.00496	0.00008
Bi	< 0.00010	-	< 0.00010	-	< 0.00010	-
Th	0.00018	0.00003	0.00023	0.00003	0.0003	0.00003
U	< 0.00010	-	< 0.00010	-	< 0.00010	-

Table B.9. Trace metal concentration gained by X-ray fluorescence in different liming products. Precision and detection limits are shown for each element (contents and error in wt.-%), contin.

Fertilizer DSM Ostrau		Hydrophobierter Kalk		Kalkhydrat 6132-5		
Content	Error	Content	Error	Content	Error	
Mg	< 0.0020	-	< 0.0020	-	0.4124	0.0051
Al	< 0.0020	-	< 0.0020	-	0.00172	0.00007
Si	< 0.00051	-	< 0.00051	-	0.04905	0.00046
P	0.00028	-	0.00074	-	0.00265	0.00026
S	< 0.00020	-	< 0.00020	-	0.04795	0.00014
Cl	< 0.00020	-	< 0.00020	-	0.00462	0.00003
K	0.0025	-	0.00791	-	< 0.0010	-
Ca	< 0.0010	-	< 0.0010	-	51.06	0.03
Ti	0.0458	0.0012	< 0.0016	-0.0016	< 0.00020	-
V	< 0.0026	-0.0026	0.0089	0.0018	< 0.0018	-0.0018
Cr	< 0.00010	-	< 0.00010	-	< 0.00010	-
Mn	0.2358	0.0009	0.02947	0.00054	0.007	0.00031
Fe	0.9372	0.0014	0.1293	0.0007	0.02676	0.00024
Co	< 0.00030	-	0.0252	0.0012	< 0.00030	-
Ni	0.00166	0.00005	0.00932	0.0002	< 0.00005	-
Cu	0.00611	0.00008	0.00073	0.0001	< 0.00005	-
Zn	0.03761	0.00013	0.00172	0.00006	0.00108	0.00005
Ga	< 0.00005	-	0.00045	0.00006	0.00036	0.00006
Ge	< 0.00005	-	< 0.00005	-	< 0.00005	-
As	0.00157	0.00012	< 0.00005	-	< 0.00005	-
Se	< 0.00005	-	< 0.00004	-0.00004	< 0.00005	-
Br	0.0006	0.00002	0.00016	0.00002	0.00012	0.00002
Rb	0.00177	0.00002	0.00022	0.00002	0.00013	0.00002
Sr	0.0116	0.00003	0.02612	0.00007	0.01965	0.00006
Y	0.00053	0.00002	0.00023	0.00003	0.00034	0.00002
Zr	0.00202	0.00009	< 0.00010	-	< 0.00010	-
Nb	< 0.00010	-	< 0.00010	-	< 0.00010	-
Mo	0.00064	0.00005	0.00114	0.00007	0.00102	0.00006
Ag	0.00049	0.00018	< 0.00020	-	0.00407	0.00015
Cd	< 0.00020	-	< 0.00020	-	0.00281	0.00011
Sn	< 0.00030	-	0.00529	0.00014	0.00491	0.00011
Sb	< 0.00030	-	0.00657	0.00016	0.0054	0.00012
Te	< 0.00030	-	0.00639	0.00017	0.00718	0.00013
I	0.00126	0.00028	0.00596	0.00031	0.00691	0.00021
Cs	< 0.00040	-	0.00183	0.00087	< 0.00040	-
Ba	0.00207	0.00052	0.00102	0.00026	0.0146	0.00067
La	< 0.00020	-	< 0.00020	-	< 0.00020	-
Ce	< 0.00020	-	< 0.00020	-	< 0.00020	-
Er	< 0.00051	-	< 0.00051	-	< 0.00051	-
Yb	< 0.00020	-	< 0.00020	-	< 0.00020	-

Hf	< 0.00010	-	< 0.00010	-	< 0.00010	-
Ta	0.00496	0.00017	0.00567	0.0002	0.00653	0.00017
W	< 0.00010	-	< 0.00010	-	< 0.00010	-
Hg	0.00003	0.00001	< 0.00010	-	< 0.00010	-
Tl	0.00014	0.00001	0.00012	0.00003	0.00015	0.00003
Pb	0.06977	0.00016	0.00073	0.00005	0.00037	0.00004
Bi	< 0.00010	-	< 0.00010	-	< 0.00010	-
Th	0.00071	0.00005	0.00038	0.00004	0.00032	0.00004
U	< 0.00010	-	< 0.00010	-	< 0.00010	-

Table B.9. Trace metal concentration gained by X-ray fluorescence in different liming products. Precision and detection limits are shown for each element (contents and error in wt.-%), contin.

	Kalksteinsand		KSM 10/90		KSM 40/30	
	Content	Error	Content	Error	Content	Error
Mg	0.226	0.0037	0.3299	0.0043	0.2439	0.0037
Al	0.06903	0.00088	0.1092	0.001	0.1959	0.0013
Si	0.2216	0.0007	0.2864	0.0008	0.3588	0.0009
P	0.00168	0.00024	0.00354	0.00023	0.01117	0.00023
S	0.00525	0.00005	0.0068	0.00006	0.00243	0.00003
Cl	0.00878	0.00004	0.00852	0.00004	0.00553	0.00003
K	< 0.0010	-	< 0.0010	-	0.0254	0.0016
Ca	38.87	0.02	38.82	0.02	39.19	0.02
Ti	0.0041	0.0011	< 0.0018	-0.0018	0.0045	0.0011
V	< 0.0023	-	< 0.0031	-0.0031	< 0.0028	-
Cr	< 0.00010	-	< 0.00010	-	< 0.00010	-
Mn	0.02833	0.0004	0.03002	0.0004	0.02402	0.00037
Fe	0.08172	0.00044	0.0751	0.00042	0.1164	0.0005
Co	< 0.00030	-	< 0.00030	-	< 0.00030	-
Ni	< 0.00005	-	< 0.00005	-	< 0.00005	-
Cu	< 0.00009	-	< 0.00014	-	< 0.00005	-
Zn	0.00245	0.00005	0.00232	0.00005	0.00083	0.00004
Ga	0.00027	0.00005	0.00031	0.00005	0.00017	0.00005
Ge	< 0.00005	-	< 0.00005	-	< 0.00005	-
As	< 0.00005	-	< 0.00005	-	< 0.00005	-
Se	< 0.00005	-	< 0.00005	-	< 0.00005	-
Br	0.00019	0.00002	0.00018	0.00002	0.0001	0.00002
Rb	0.00021	0.00001	0.00025	0.00001	0.00041	0.00001
Sr	0.01621	0.00005	0.01625	0.00005	0.01792	0.00005
Y	0.00019	0.00002	0.00022	0.00002	0.00039	0.00002
Zr	< 0.00010	-	< 0.00010	-	< 0.00004	-
Nb	< 0.00010	-	< 0.00010	-	< 0.00010	-
Mo	0.00087	0.00005	0.00072	0.00005	0.00084	0.00006
Ag	< 0.00020	-	< 0.00028	-	< 0.00020	-
Cd	< 0.00020	-	< 0.00020	-	< 0.00020	-
Sn	0.00113	0.00008	0.00139	0.00009	0.00124	0.00008
Sb	0.00163	0.00011	0.00184	0.00011	0.00123	0.0001
Te	0.00129	0.00008	0.00156	0.00009	0.00098	0.00007
I	0.00161	0.00019	0.00201	0.00021	0.00164	0.0002
Cs	< 0.00040	-	< 0.00040	-	< 0.00040	-
Ba	0.00527	0.00058	< 0.00020	-	0.00061	0.00018
La	< 0.00020	-	< 0.00020	-	< 0.00020	-
Ce	< 0.00020	-	< 0.00020	-	0.00521	0.0009
Er	< 0.00051	-	< 0.00051	-	< 0.00051	-
Yb	< 0.00020	-	< 0.00020	-	< 0.00020	-

Hf	< 0.00010	-	< 0.00010	-	< 0.00010	-
Ta	0.0064	0.00015	0.00605	0.00014	0.00599	0.00015
W	< 0.00010	-	0.00014	0.00002	< 0.00010	-
Hg	< 0.00010	-	< 0.00010	-	< 0.00010	-
Tl	0.00006	0.00002	0.00008	0.00002	0.00007	0.00002
Pb	0.00265	0.00005	0.003	0.00005	0.00035	0.00003
Bi	< 0.00010	-	< 0.00010	-	< 0.00010	-
Th	0.00022	0.00003	0.00025	0.00003	0.00017	0.00003
U	< 0.00010	-	< 0.00010	-	< 0.00010	-

Table B.9. Trace metal concentration gained by X-ray fluorescence in different liming products. Precision and detection limits are shown for each element (contents and error in wt.-%), contin.

KSM Beroun		Marmorpulver		Mischkalk Borna			
	Content		Error		Content		Error
Mg	0.2747	0.004		0.2497	0.0038	2.772	0.01
Al	0.01392	0.00036		0.03757	0.00064	1.144	0.003
Si	0.05579	0.00043		0.08777	0.00049	3.93	0.003
P	0.00321	0.00023		0.00132	0.00023	0.02011	0.00028
S	0.00136	0.00002	< 0.00020	-	-	0.05308	0.00015
Cl	0.00726	0.00003		0.00298	0.00002	0.00302	0.00002
K	< 0.0010	-		< 0.0010	-	0.2349	0.002
Ca	39.4	0.02		39.1	0.02	31.61	0.02
Ti	< 0.00020	-		0.0049	0.0011	0.065	0.0015
V	< 0.0037	-		< 0.0025	-	0.0028	0.0012
Cr	< 0.00010	-		< 0.00010	-	< 0.00010	-
Mn	0.00524	0.00023		0.00703	0.00025	0.02627	0.00037
Fe	0.01979	0.00018		0.02013	0.00018	0.5691	0.0012
Co	< 0.00030	-		< 0.00030	-	< 0.00030	-
Ni	< 0.00005	-		< 0.00005	-	< 0.00005	-
Cu	0.00022	0.00007		0.00023	0.00007	0.00058	0.00007
Zn	0.00086	0.00004		0.0008	0.00004	0.00346	0.00006
Ga	0.00026	0.00005		0.00028	0.00005	0.00048	0.00004
Ge	< 0.00005	-		< 0.00005	-	< 0.00005	-
As	< 0.00005	-		< 0.00005	-	0.00009	0.00003
Se	< 0.00005	-		< 0.00005	-	< 0.00005	-
Br	0.00014	0.00002		0.0001	0.00002	0.00008	0.00002
Rb	0.00013	0.00001		0.0002	0.00001	0.00123	0.00002
Sr	0.01546	0.00005		0.01545	0.00005	0.04012	0.00007
Y	0.00018	0.00002		0.00032	0.00002	0.00026	0.00002
Zr	< 0.00010	-		< 0.00010	-	0.00282	0.00014
Nb	< 0.00010	-		< 0.00010	-	< 0.00010	-
Mo	0.00086	0.00005		0.00096	0.00005	0.00045	0.00005
Ag	0.00095	0.00015		< 0.00020	-	< 0.00020	-
Cd	< 0.00020	-		< 0.00020	-	< 0.00020	-
Sn	0.00149	0.00009		0.00116	0.00008	0.00004	0.00001
Sb	0.00158	0.00011		0.00102	0.00009	0.00018	0.00003
Te	0.00141	0.00008		0.00059	0.00005	< 0.00030	-
I	0.00261	0.00021		0.0015	0.0002	< 0.00030	-
Cs	< 0.00040	-		< 0.00040	-	< 0.00040	-
Ba	< 0.00020	-		0.00287	0.00043	0.00947	0.00059
La	< 0.00020	-		< 0.00020	-	0.00445	0.0006
Ce	< 0.00020	-		< 0.00020	-	< 0.00020	-
Er	< 0.00051	-		< 0.00051	-	< 0.00051	-
Yb	< 0.00020	-		< 0.00020	-	< 0.00020	-

Hf	< 0.00010	-	< 0.00010	-	< 0.00010	-
Ta	0.00612	0.00014	0.00611	0.00014	0.00583	0.00014
W	0.00019	0.00003	0.00009	0.00002	0.00012	0.00002
Hg	< 0.00007	-	< 0.00010	-	< 0.00010	-
Tl	0.00006	0.00002	0.00009	0.00002	< 0.00010	-
Pb	0.0004	0.00003	0.00029	0.00003	0.00104	0.00004
Bi	< 0.00010	-	< 0.00010	-	< 0.00010	-
Th	0.0003	0.00003	0.00031	0.00003	0.00028	0.00003
U	< 0.00010	-	< 0.00010	-	< 0.00010	-

Table B.9. Trace metal concentration gained by X-ray fluorescence in different liming products. Precision and detection limits are shown for each element (contents and error in wt.-%), contin.

Rheinkalk WFK CL90		Rüdersdorfer WKH u/12		Ruegener Schlämmkreide		
	Content	Error	Content	Error	Content	Error
Mg	0.7416	0.0059	< 0.0020	-	< 0.0020	-
Al	0.0902	0.001	< 0.0020	-	< 0.0020	-
Si	0.4701	0.001	< 0.00051	-	< 0.00051	-
P	0.00448	0.00026	0.00103	-	0.00065	-
S	0.03248	0.00012	< 0.00020	-	< 0.00020	-
Cl	0.00168	0.00002	< 0.00020	-	< 0.00020	-
K	< 0.0010	-	0.008	-	0.006	-
Ca	61.94	0.04	< 0.0010	-	< 0.0010	-
Ti	< 0.00016	-0.00016	0.0131	0.0019	< 0.00075	-
V	< 0.0047	-0.0047	< 0.0057	-	< 0.0038	-
Cr	< 0.00010	-	< 0.00010	-	< 0.00010	-
Mn	0.0462	0.00062	0.00704	0.00036	0.00881	0.0003
Fe	0.1961	0.0009	0.2839	0.001	0.04682	0.00033
Co	< 0.00030	-	0.01398	0.00085	0.00857	0.00059
Ni	< 0.00005	-	0.00546	0.00015	0.00356	0.0001
Cu	< 0.00005	-	0.00079	0.00009	0.00068	0.00007
Zn	0.00296	0.00007	0.00108	0.00005	0.00241	0.00005
Ga	0.00029	0.00007	0.0006	0.00006	0.00045	0.00004
Ge	< 0.00005	-	< 0.00005	-	< 0.00005	-
As	< 0.00005	-	0.00006	0.00003	< 0.00005	-
Se	< 0.00005	-	< 0.00005	-	< 0.00005	-
Br	0.00014	0.00002	0.00024	0.00002	0.00017	0.00002
Rb	0.00022	0.00002	0.00052	0.00002	0.00016	0.00002
Sr	0.02642	0.00007	0.2246	0.0002	0.06972	0.0001
Y	0.00047	0.00003	0.0004	0.00003	0.00067	0.00002
Zr	< 0.00010	-	< 0.00010	-	< 0.00010	-
Nb	< 0.00010	-	< 0.00010	-	< 0.00010	-
Mo	0.00187	0.00008	0.00142	0.00007	0.00108	0.00006
Ag	0.00132	0.0002	< 0.00020	-	< 0.00020	-
Cd	< 0.00020	-	< 0.00020	-	0.00012	0.00003
Sn	0.00375	0.00012	0.00304	0.00014	0.00244	0.00014
Sb	0.0044	0.00014	0.00441	0.00018	0.00423	0.00019
Te	0.0047	0.00014	0.00406	0.00016	0.0035	0.00017
I	0.00443	0.00026	0.00444	0.00033	0.00412	0.00036
Cs	< 0.00040	-	< 0.00069	-0.00068	0.00413	0.00099
Ba	< 0.00020	-	< 0.00020	-	0.00139	0.00037
La	< 0.00020	-	< 0.00020	-	0.0022	0.0005
Ce	< 0.00020	-	0.00106	0.00035	0.00043	0.00017
Er	< 0.00051	-	< 0.00051	-	< 0.00051	-
Yb	< 0.00020	-	< 0.00020	-	< 0.00020	-

Hf	< 0.00010	-	< 0.00010	-	< 0.00010	-
Ta	0.00747	0.00022	0.00679	0.0002	0.00528	0.00016
W	< 0.00010	-	< 0.00010	-	< 0.00010	-
Hg	< 0.00010	-	0.00005	0.00002	< 0.00010	-
Tl	< 0.00002	-	0.00006	0.00003	< 0.00010	-
Pb	0.00257	0.00006	0.00037	0.00005	0.00023	0.00003
Bi	< 0.00010	-	< 0.00010	-	< 0.00010	-
Th	0.00028	0.00004	< 0.00008	-0.00008	0.00012	0.00003
U	< 0.00010	-	0.00015	0.00001	< 0.00010	-

Table B.9. Trace metal concentration gained by X-ray fluorescence in different liming products. Precision and detection limits are shown for each element (contents and error in wt.-%), contin.

	Saxocarb 300 F		Saxolith C1		Wasserkalk, reaktionsverzögert	
	Content	Error	Content	Error	Content	Error
Mg	13.09	0.02	1.888	0.009	< 0.0020	-
Al	0.5343	0.0021	0.7088	0.0024	< 0.0020	-
Si	1.967	0.002	5.289	0.004	< 0.00051	-
P	0.03469	0.00027	0.00914	0.00028	0.00081	-
S	0.01037	0.00007	< 0.00014	-	< 0.00020	-
Cl	0.00726	0.00004	0.00343	0.00003	< 0.00020	-
K	0.0333	0.0015	0.1159	0.0019	0.00701	-
Ca	21.92	0.01	32.85	0.02	< 0.0010	-
Ti	0.02163	0.00093	0.0259	0.0012	0.0712	0.0025
V	< 0.0018	-	< 0.0019	-	0.009	0.0022
Cr	< 0.00010	-	< 0.00010	-	< 0.00010	-
Mn	0.07266	0.00047	0.02463	0.00036	0.1378	0.001
Fe	0.4275	0.0009	0.3039	0.0009	0.5761	0.0014
Co	< 0.00030	-	< 0.00030	-	0.01092	0.00071
Ni	0.00009	0.00002	< 0.00005	-	0.00618	0.00013
Cu	0.00013	0.00006	0.00037	0.00007	0.00142	0.00008
Zn	0.00968	0.00007	0.00336	0.00006	0.00353	0.00006
Ga	0.00024	0.00004	0.00047	0.00004	0.00075	0.00005
Ge	< 0.00005	-	< 0.00005	-	< 0.00005	-
As	< 0.00005	-	< 0.00005	-	< 0.00001	-
Se	< 0.00005	-	< 0.00005	-	< 0.00005	-
Br	0.00014	0.00001	< 0.00005	-	0.00007	0.00002
Rb	0.00046	0.00001	0.00173	0.00002	0.00174	0.00003
Sr	0.00611	0.00003	0.0221	0.00005	0.1159	0.0002
Y	0.00016	0.00002	0.00022	0.00002	0.00152	0.00003
Zr	0.00133	0.00007	0.00101	0.00011	< 0.00010	-
Nb	< 0.00010	-	< 0.00010	-	< 0.00010	-
Mo	0.00242	0.00006	0.00043	0.00005	0.00115	0.00007
Ag	< 0.00020	-	< 0.00020	-	0.00191	0.00022
Cd	< 0.00020	-	< 0.00020	-	< 0.00020	-
Sn	< 0.00030	-	0.00075	0.00006	0.00482	0.00014
Sb	< 0.00030	-	0.00134	0.0001	0.00657	0.00017
Te	< 0.00030	-	< 0.00030	-	0.0062	0.00017
I	< 0.00030	-	0.00141	0.00018	0.00577	0.00032
Cs	< 0.00040	-	0.00399	0.00054	< 0.00040	-
Ba	0.00182	0.00035	0.00568	0.00053	0.00043	0.00013
La	< 0.00020	-	0.00806	0.00073	0.00003	0.00001
Ce	0.00327	0.00071	< 0.00020	-	0.0053	0.0011
Er	< 0.00051	-	< 0.00051	-	< 0.00051	-
Yb	< 0.00020	-	< 0.00020	-	< 0.00020	-

Hf	< 0.00010	-	< 0.00010	-	< 0.00010	-
Ta	0.00593	0.00011	0.00583	0.00013	0.00467	0.00018
W	< 0.00010	-	0.01165	0.00014	< 0.00010	-
Hg	< 0.00010	-	< 0.00010	-	0.00013	0.00003
Tl	0.00003	0.00001	0.00007	0.00002	0.00006	0.00003
Pb	0.00448	0.00005	0.0009	0.00004	0.00093	0.00004
Bi	< 0.00010	-	< 0.00010	-	< 0.00010	-
Th	0.00018	0.00003	0.00022	0.00003	0.00027	0.00004
U	< 0.00004	-	< 0.00010	-	< 0.00010	-

Table B.9. Trace metal concentration gained by X-ray fluorescence in different liming products. Precision and detection limits are shown for each element (contents and error in wt.-%), contin.

	Weissfeinkalk CaO	Weisskalkhydrat WKH 2/4	Wünschendorfer Dolomitfeinkalk		
Mg	0.4814	0.0056	0.4103	0.005	< 0.0020
Al	0.01298	0.00038	0.05333	0.00083	< 0.0020
Si	0.06115	0.00052	0.1781	0.0007	< 0.00051
P	0.00347	0.00029	0.00617	0.00026	0.00049
S	0.04493	0.00014	0.03415	0.00012	< 0.00020
Cl	0.00297	0.00003	0.00499	0.00003	< 0.00020
K	< 0.0010	-	< 0.0010	-	0.00379
Ca	57.78	0.04	51.22	0.03	< 0.0010
Ti	< 0.00020	-	< 0.00020	-	0.0352
V	< 0.0046	-0.0045	< 0.00093	-0.00092	0.0052
Cr	< 0.00010	-	< 0.00010	-	< 0.00010
Mn	0.00703	0.00034	0.01811	0.0004	0.06997
Fe	0.04187	0.00034	0.1335	0.0006	0.7324
Co	< 0.00030	-	< 0.00030	-	0.00163
Ni	< 0.00005	-	< 0.00005	-	0.00309
Cu	< 0.00005	-	< 0.00005	-	0.00195
Zn	0.00122	0.00006	0.00226	0.00006	0.00437
Ga	0.00052	0.00006	0.00038	0.00006	0.00063
Ge	< 0.00005	-	< 0.00005	-	< 0.00005
As	< 0.00005	-	< 0.00005	-	0.00101
Se	< 0.00005	-	< 0.00005	-	0.00004
Br	0.00021	0.00002	< 0.00005	-	0.001
Rb	0.00013	0.00002	0.00022	0.00002	0.00207
Sr	0.02246	0.00007	0.01633	0.00005	0.01112
Y	0.0004	0.00003	0.00049	0.00002	0.0006
Zr	< 0.00010	-	< 0.00010	-	0.00153
Nb	< 0.00010	-	< 0.00010	-	< 0.00010
Mo	0.00118	0.00007	0.00144	0.00007	0.00083
Ag	< 0.00020	--	0.00477	0.00014	< 0.00020
Cd	0.00021	0.00004	0.0046	0.00012	< 0.00020
Sn	0.0044	0.00012	0.00599	0.00011	0.00193
Sb	0.00486	0.00014	0.00629	0.00013	0.00348
Te	0.00541	0.00014	0.00854	0.00013	0.0015
I	0.00456	0.00025	0.00767	0.00021	0.00305
Cs	< 0.00040	-	< 0.00040	-	0.00415
Ba	0.00427	0.00054	0.02338	0.00075	0.0178
La	< 0.00020	-	< 0.00020	-	< 0.00020
Ce	< 0.00020	-	< 0.00020	-	< 0.00020
Er	< 0.00051	-	< 0.00051	-	< 0.00051
Yb	< 0.00020	-	< 0.00020	-	< 0.00020
Hf	< 0.00010	-	< 0.00010	-	< 0.00010

Ta	0.00676	0.0002	0.00644	0.00018	0.00497	0.00017
W	0.00016	0.00003	< 0.00010	-	< 0.00010	-
Hg	< 0.00010	-	< 0.00010	-	0.00019	0.00003
Tl	0.00016	0.00003	0.00009	0.00003	0.00009	0.00002
Pb	0.00061	0.00005	0.00045	0.00004	0.00452	0.00007
Bi	< 0.00010	-	< 0.00010	-	< 0.00010	-
Th	0.00048	0.00004	0.00029	0.00004	0.00043	0.00003
U	< 0.00010	-	< 0.00010	-	< 0.00010	-

Table B.10. Amounts of liming products, experimental series 1 (BGH water).

Column	1	2	3	4
Neutralizing product	KSM Beroun	CaO	Brannt-Dolomite	DSM Ostrau
Chemical formula	CaCO ₃	CaO	CaO / MgO	CaCO ₃ / MgCO ₃
Amount, 1st treatment [g]	6.0002	3.3614	2.8920	5.4545
Date, 1st treatment	12/21/2007	12/21/2007	12/21/2007	12/21/2007
Amount, 2nd treatment [g]	6.0000	3.3613	2.8923	5.4545
Date, 2nd treatment [g]	12/23/2007	12/23/2007	12/23/2007	12/23/2007
Amount, 3rd treatment [g]	6.0003	3.3612	2.8921	3.4545
Date, 3rd treatment	12/25/2007	12/25/2007	12/25/2007	12/25/2007
Amount of suspension	300 mL	167 mL	143 mL	273 mL

Table B.11. Development of in-situ parameters (pH, EC) in Column 1; experimental series 1 (neutralizing product KSM Beroun).

No. of day	Date	Sampling port – Height above bottom													
		VI - 200		V - 600		IV - 1100		III - 1500		II - 1800		I - 1950		Temp °C	
		pH [-]	EC µS/cm	pH [-]	EC µS/cm	pH [-]	EC µS/cm	pH [-]	EC µS/cm	pH [-]	EC µS/cm	pH [-]	EC µS/cm		
1	21.12.2007	3.05	2270	-	-	3.06	2285	-	-	3.06	2270	-	-	-	
2	22.12.2007	3.21	2180	3.17	2224	3.17	2200	3.17	2208	3.2	2192	3.25	2192	-	
3	23.12.2007	3.23	2174	3.19	2196	3.19	2244	3.2	2232	3.21	2200	3.24	2192	19.3	
4	24.12.2007	3.55	2082	3.51	2116	3.47	2110	3.46	2118	3.45	2120	3.47	2090	18.5	
5	25.12.2007	3.39	2112	3.4	2108	3.4	2128	3.4	2345	3.41	2150	3.45	2176	18.9	
6	26.12.2007	4.7	1992	4.58	1992	4.58	1996	4.59	2008	4.63	2000	4.73	2100	18.7	
7	27.12.2007	4.7	2010	4.69	2024	4.7	2016	4.7	2026	4.71	1986	4.78	1984	19	
8	28.12.2007	4.88	2036	4.64	1944	4.58	1980	4.67	1970	4.67	1978	4.51	1988	17.7	
9	29.12.2007	4.91	2016	4.68	1964	4.68	1984	4.67	1980	4.72	1954	4.79	1956	18.6	
10	30.12.2007	4.93	2022	4.67	1972	4.67	1984	4.68	1994	4.78	1968	4.75	1968	19.1	
11	31.12.2007	5.11	2036	4.7	1988	4.68	1982	4.65	1964	4.69	1980	4.95	2014	17.3	
12	01.01.2008	5.05	2004	4.8	1984	4.77	1952	4.76	1994	4.68	1956	4.78	2016	18.2	
13	02.01.2008	4.75	1996	4.75	1992	4.74	1984	4.69	1984	4.67	1988	4.52	1988	18.3	
14	03.01.2008	4.74	2000	4.76	1994	4.76	1996	4.77	1996	4.78	1990	4.87	1994	18.1	
15	04.01.2008	4.81	1996	4.83	1996	4.82	1996	4.81	1996	4.81	1996	4.78	1996	18.7	
16	05.01.2008	4.89	2002	4.9	2002	4.89	2000	4.93	1998	4.91	2004	4.93	2000	17.3	
17	06.01.2008	4.94	2000	4.92	1996	4.92	2004	4.92	2000	4.9	1998	4.73	1998	16.8	
18	07.01.2008	4.96	2000	4.95	1996	4.92	2000	4.94	1996	4.95	1996	4.98	1998	17.4	
19	08.01.2008	4.93	1996	4.94	1992	4.93	1992	4.93	1992	4.94	1992	4.96	1992	19.3	
20	09.01.2008	4.91	1994	4.89	1990	4.91	1988	4.92	1996	4.87	1992	4.69	1994	18.8	
21	10.01.2008	4.93	1996	4.91	2000	4.94	1996	4.9	1996	4.92	1996	4.97	1992	19.9	
22	11.01.2008	4.95	2000	4.92	2004	4.93	1996	4.95	1996	4.94	2000	4.94	2000	19.3	

Table B.12. Development of in-situ parameters (pH, EC) in Column 2; experimental series 1 (neutralizing product CaO).

No. of day	Date	Sampling port – Height above bottom													
		VI - 200		V - 600		IV - 1100		III - 1500		II - 1800		I - 1950		Temp °C	
		pH [-]	EC µS/cm	pH [-]	EC µS/cm	pH [-]	EC µS/cm	pH [-]	EC µS/cm	pH [-]	EC µS/cm	pH [-]	EC µS/cm		
1	21.12.2007	3.06	2278	-	-	3.06	2270	-	-	3.06	2285	-	-	-	
2	22.12.2007	3.19	2212	3.17	2212	3.17	2224	3.17	2228	3.18	2188	3.19	2224	-	
3	23.12.2007	3.21	2180	3.17	2198	3.18	2204	3.18	2220	3.2	2156	3.21	2100	19.4	
4	24.12.2007	3.46	2096	3.45	2132	3.46	2098	3.43	2120	3.43	2096	3.44	2100	18.4	
5	25.12.2007	3.38	2120	3.38	2040	3.38	2068	3.38	2054	3.38	2060	3.37	2094	19.5	
6	26.12.2007	4.93	1980	4.86	1976	4.85	1978	4.84	1972	4.83	1980	4.76	1940	18.9	
7	27.12.2007	5.11	1958	4.96	1948	4.92	2008	4.92	1946	4.92	1992	4.91	1960	18.9	
8	28.12.2007	5.12	2040	4.94	1980	4.91	1986	4.91	1990	4.92	1986	4.91	1980	18.0	
9	29.12.2007	5.17	2040	4.97	1976	4.95	1974	4.96	1984	4.96	1980	4.9	1968	20.2	
10	30.12.2007	5.2	2049	4.99	1978	4.96	1970	4.96	1986	4.93	1980	4.91	1970	19.1	
11	31.12.2007	5.14	2032	4.95	2012	4.97	2012	4.97	1964	4.9	1974	4.93	1972	18.7	
12	01.01.2008	5.21	2000	5.03	1978	4.93	1964	4.89	1976	4.93	1940	4.97	1956	18.2	
13	02.01.2008	5.17	2024	4.88	1978	4.89	1984	4.88	1988	4.91	1980	4.89	1984	18.9	
14	03.01.2008	5.22	2024	4.89	1988	4.89	1984	4.89	1988	4.88	1984	4.89	1992	17.9	
15	04.01.2008	5.18	2016	4.93	1992	4.93	1988	4.93	1988	4.93	1988	4.94	1988	19.1	
16	05.01.2008	5.24	2020	4.98	1996	4.98	1996	4.96	1996	4.98	2000	4.97	2000	17.5	
17	06.01.2008	5.27	2018	5.00	1996	4.99	1998	4.99	1992	4.98	1996	4.98	1996	17.2	
18	07.01.2008	5.3	2016	4.96	1992	5.00	1992	4.99	1994	4.99	1996	5.01	1992	17.9	
19	08.01.2008	5.09	2004	5.01	1992	5.04	1992	5.05	1992	5.06	1992	5.08	1996	19.4	
20	09.01.2008	5.02	1994	5.00	1992	5.02	1996	5.02	1988	4.99	1996	4.99	1996	19.8	
21	10.01.2008	5.03	1994	5.01	1994	5.02	1996	5.02	1994	5.02	1992	5.05	1996	20.0	
22	11.01.2008	5.02	1996	5.04	1998	5.05	2000	5.05	2002	5.05	2000	5.03	2000	19.5	

Table B.13. Development of in-situ parameters (pH, EC) in Column 3; experimental series 1 (neutralizing product Branndolomit)

No. of day	Date	Sampling port – Height above bottom												
		VI - 200		V - 600		IV - 1100		III - 1500		II - 1800		I - 1950		Temp °C
		pH [-]	EC µS/cm	pH [-]	EC µS/cm	pH [-]	EC µS/cm	pH [-]	EC µS/cm	pH [-]	EC µS/cm	pH [-]	EC µS/cm	
1	21.12.2007	3.02	2280	-	-	3.06	2278	-	-	3.04	2285	-	-	-
2	22.12.2007	3.19	2192	3.16	2236	3.17	2255	3.17	2204	3.17	2230	3.19	2172	-
3	23.12.2007	3.2	2200	3.17	2210	3.18	2232	3.19	2230	3.18	2224	3.21	2104	-
4	24.12.2007	3.37	2022	3.38	2124	3.39	2112	3.39	2120	3.38	2132	3.39	2140	18.4
5	25.12.2007	3.35	2124	3.35	2092	3.35	2118	3.36	2060	3.36	2092	3.36	2048	19.2
6	26.12.2007	4.01	1988	4.04	2008	4.06	2020	4.07	2020	4.1	2012	4.11	2014	18.5
7	27.12.2007	4.17	2008	4.17	1978	4.2	1972	4.21	1928	4.21	2006	4.27	2008	18.9
8	28.12.2007	4.08	2022	4.17	2008	4.17	1966	4.17	2008	4.19	2020	4.16	2032	18.1
9	29.12.2007	4.16	2008	4.21	2012	4.18	2020	4.19	2008	4.26	2004	4.31	2008	18.7
10	30.12.2007	4.2	2000	4.23	2011	4.18	2009	4.19	2006	4.25	1999	4.26	2003	19
11	31.12.2007	4.17	2020	4.22	2014	4.24	2024	4.2	2018	4.3	2008	4.3	2010	18.1
12	01.01.2008	4.25	1976	4.2	1962	4.3	1984	4.23	1928	4.38	1952	4.27	1960	18.6
13	02.01.2008	4.22	2010	4.26	2008	4.25	2020	4.24	2006	4.28	2002	4.3	2000	19.5
14	03.01.2008	4.27	2008	4.29	2008	4.29	2008	4.3	2008	4.35	2008	4.37	2012	18.1
15	04.01.2008	4.34	2010	4.39	2006	4.4	2008	4.39	2004	4.43	2004	4.45	2002	19.2
16	05.01.2008	4.35	2012	4.38	2012	4.41	2012	4.41	2012	4.42	2016	4.46	2012	17.6
17	06.01.2008	4.41	2016	4.39	2010	4.49	2008	4.53	2010	4.52	2016	4.53	2008	17.6
18	07.01.2008	4.46	2010	4.52	2008	4.53	2008	4.52	2004	4.55	2002	4.58	2002	18.1
19	08.01.2008	4.51	2012	4.56	2004	4.56	2004	4.54	2006	4.58	2004	4.59	2004	19.3
20	09.01.2008	4.52	2000	4.53	2002	4.55	2004	4.52	2004	4.57	2008	4.6	2000	19.1
21	10.01.2008	4.55	2004	4.59	2000	4.58	2000	4.61	2000	4.63	1992	4.62	2004	19.9
22	11.01.2008	4.61	2008	4.62	2004	4.63	2004	4.63	2004	4.66	2004	4.66	2012	20.3

Table B.14. Development of in-situ parameters (pH, EC) in Column 4; experimental series 1 (neutralizing product DSM Ostrau)

No. of day	Date	Sampling port – Height above bottom												
		VI - 200		V - 600		IV - 1100		III - 1500		II - 1800		I - 1950		Temp °C
		pH [-]	EC µS/cm	pH [-]	EC µS/cm	pH [-]	EC µS/cm	pH [-]	EC µS/cm	pH [-]	EC µS/cm	pH [-]	EC µS/cm	
1	21.12.2007	3.06	2285	-	-	3.08	2288	-	-	3.06	2285	-	-	-
2	22.12.2007	3.19	2196	3.18	2198	3.17	2196	3.18	2192	3.18	2172	3.18	2196	-
3	23.12.2007	3.21	2148	3.2	2140	3.19	2206	3.17	2216	3.19	2164	3.19	2160	-
4	24.12.2007	3.26	2128	3.26	2144	3.25	2136	3.24	2114	3.24	2112	3.24	2116	18.8
5	25.12.2007	3.2	2140	3.2	2174	3.2	2168	3.21	2168	3.21	2148	3.21	2166	18.6
6	26.12.2007	3.33	2118	3.33	2124	3.33	2114	3.33	2120	3.34	2106	3.39	2132	18.5
7	27.12.2007	3.35	2120	3.35	2128	3.37	2104	3.36	2130	3.38	2082	3.4	2100	19.5
8	28.12.2007	3.35	2112	3.29	2140	3.29	2128	3.28	2136	3.29	2156	3.33	2166	18.5
9	29.12.2007	3.31	2126	3.33	2110	3.31	2132	3.34	2100	3.32	2120	3.35	2098	20.5
10	30.12.2007	3.29	2130	3.32	2102	3.31	2130	3.35	2098	3.3	2135	3.38	2078	19.1
11	31.12.2007	3.3	2156	3.3	2144	3.31	2136	3.32	2116	3.32	2140	3.34	2108	18.4
12	01.01.2008	3.36	2092	3.3	2054	3.35	2134	3.28	2080	3.36	2104	3.2	2084	18.6
13	02.01.2008	3.22	2128	3.23	2126	3.23	2132	3.23	2132	3.27	2124	3.27	2120	18.8
14	03.01.2008	3.24	2130	3.24	2124	3.25	2132	3.25	2128	3.26	2132	3.26	2136	18.1
15	04.01.2008	3.31	2132	3.32	2132	3.32	2120	3.33	2120	3.35	2120	3.34	2132	19.0
16	05.01.2008	3.33	2130	3.33	2138	3.33	2136	3.33	2136	3.34	2140	3.34	2140	17.7
17	06.01.2008	3.37	2134	3.38	2128	3.37	2128	3.36	2132	3.38	2136	3.38	2144	17.5
18	07.01.2008	3.39	2116	3.39	2118	3.41	2114	3.42	2104	3.44	2100	3.41	2120	18.2
19	08.01.2008	3.41	2108	3.41	2112	3.42	2108	3.41	2114	3.43	2100	3.45	2104	19.2
20	09.01.2008	3.39	2112	3.39	2116	3.4	2096	3.41	2116	3.41	2108	3.44	2106	19.2
21	10.01.2008	3.39	2116	3.4	2112	3.41	2108	3.41	2108	3.43	2096	3.45	2096	19.9
22	11.01.2008	3.43	2104	3.42	2108	3.43	2112	3.44	2096	3.45	2112	3.49	2088	19.8

Table B.15. Amounts of liming products, experimental series 2 (Lohsa).

Column Neutralizing product Efficiency	1 KSM Beroun 70 % [g]	2 Kalksteinmehl Borna 70 % [g]	3 Mischkalk Borna 70 % [g]	4 Dolomitsteinmehl Borna 70 % [g]
1. step, pH to be reached 4.3				
19.11.2009 09:00	3.8127	4.1910	4.1925	4.1919
19.11.2009 09:00	3.8100	4.1920	4.1900	4.1903
19.11.2009 09:00	3.8127	4.1900	4.1921	4.1920
2. step, pH to be reached 5.0				
25.11.2009 09:00	0.8400	0.9220	0.9200	0.9200
25.11.2009 09:00	0.8392	0.9200	0.9210	0.9196
25.11.2009 09:00	0.8400	0.9210	0.9214	0.9206
3. step, pH to be reached 7.5 – 8				
02.12.2009 09:00	2.2543	2.2529	2.2516	2.2564
02.12.2009 09:00	2.2616	2.2457	2.2518	2.2418
02.12.2009 09:00	2.2558	2.2475	2.2470	2.2481

Table B.16. Development of in-situ parameters (pH, EC) in Column 1; experimental series 2 (neutralizing product KSM Beroun).

No. of day	Date	Sampling port – Height above bottom						
		II - 1800		IV - 1100		VI - 200		
		pH [-]	LF μS/cm	pH [-]	LF μS/cm	pH [-]	LF μS/cm	Temp °C
1	11/18/09 12:00	2.95	1600	2.95	1600	2.95	1600	21.2
2	11/19/09 10:30	3.41	2080	3.4	1418	3.34	1854	22.2
2	11/19/09 12:00	3.83	1389	3.93	1320	3.69	1344	22.3
3	11/20/09 11:00	5.42	1263	5.36	1257	5.31	1272	21.9
4	-	-	-	-	-	-	-	-
5	11/22/09 9:00	5.26	1269	5.43	1258	5.4	1272	20.9
6	11/23/09 9:00	5.39	1275	5.35	1260	5.54	1257	21.3
7	11/24/09 9:00	5.4	1230	5.44	1238	5.53	1231	21.1
8	11/25/09 9:00	5.32	1238	5.37	1230	5.02	1277	21.7
8	11/25/09 11:00	5.77	1219	5.76	1234	5.51	1222	23.1
8	11/25/09 12:30	5.9	1242	5.97	1214	5.77	1248	22.6
9	11/26/09 13:00	6.08	1228	6.07	1244	6.08	1228	22.7
9	11/27/09 9:00	6.15	1204	6.08	1266	6.21	1262	21.4
10	11/28/09 10:00	6.25	1269	6.23	1254	6.31	1231	21.2
11	11/29/09 14:00	6.77	1235	6.48	1266	6.42	1263	20.9
12	11/30/09 8:00	6.1	1271	6.07	1280	6.11	1308	20.9
13	12/1/09 9:00	6.06	1248	6.2	1257	6.2	1254	20.8
14	12/2/09 10:00	6.1	1275	6.07	1278	6.03	1280	21.3
14	12/2/09 13:00	7.78	1284	7.88	1298	6.56	1245	21.8
14	12/2/09 17:00	8.58	1272	8.61	1260	7.31	1319	20.8
15	12/3/09 8:00	8.9	1271	8.83	1290	8.12	1311	20.2
16	-	-	-	-	-	-	-	-
17	12/5/09 20:00	7.78	1280	8.16	1263	7.72	1278	20
18	-	-	-	-	-	-	-	-
19	12/7/09 11:00	7.59	1281	7.76	1280	7.78	1283	20.8
20	-	-	-	-	-	-	-	-
21	-	-	-	-	-	-	-	-
22	12/10/09 13:00	7.38	1292	7.39	1271	7.6	1272	20.4

Table B.17. Development of in-situ parameters (pH, EC) in Column 2; experimental series 2 (neutralizing product KSM Borna).

No. of day	Date	Sampling port – Height above bottom							
		II - 1800		IV - 1100		VI - 200		LF [μS/cm]	Temp °C
		pH [-]	LF [μS/cm]	pH [-]	LF [μS/cm]	pH [-]	LF [μS/cm]		
1	11/18/09 12:00	2.95	1600	2.95	1600	2.95	1600	21.2	
2	11/19/09 10:30	3.27	1740	3.31	1460	3.29	1421	22.3	
2	11/19/09 12:00	3.62	1332	3.63	1470	3.6	1434	22.1	
3	11/20/09 11:00	4.65	1281	4.66	1240	4.61	1256	21.9	
4	-	-	-	-	-	-	-	-	
5	11/22/09 9:00	4.75	1271	4.73	1265	4.73	1251	21.1	
6	11/23/09 9:00	4.91	1269	4.96	1263	5	126	21.7	
7	11/24/09 9:00	4.9	1234	4.85	1232	4.92	1236	21.1	
8	11/25/09 9:00	4.79	1257	4.81	1228	4.24	1296	21.4	
8	11/25/09 11:00	4.89	1224	5.04	1224	4.92	1232	22.7	
8	11/25/09 12:30	5.17	1228	5.13	1238	4.97	1222	22.8	
9	11/26/09 13:00	5.52	1226	5.46	1201	5.47	1226	22.5	
9	11/27/09 9:00	5.59	1271	5.49	1251	5.55	1244	21.5	
10	11/28/09 10:00	5.71	1266	5.75	1235	5.64	1263	21.4	
11	11/29/09 14:00	5.9	1254	5.96	1269	5.86	1275	20.7	
12	11/30/09 8:00	5.62	1257	5.54	1254	5.64	1278	20.5	
13	12/1/09 9:00	5.7	1263	5.68	1263	5.72	1272	20.7	
14	12/2/09 10:00	5.57	1260	5.52	1275	5.51	1278	21.3	
14	12/2/09 13:00	7.61	1275	7.64	1262	6.25	1225	21.6	
14	12/2/09 17:00	8.86	1246	8.94	1269	7.71	1272	20.9	
15	12/3/09 8:00	8.93	1266	8.9	1272	7.98	1290	20.3	
16	-	-	-	-	-	-	-	-	
17	12/5/09 20:00	8.39	1286	8.37	1280	7.88	1302	20.1	
18	-	-	-	-	-	-	-	-	
19	12/7/09 11:00	8.22	1302	8.17	128	8.07	1287	20.7	
20	-	-	-	-	-	-	-	-	
21	-	-	-	-	-	-	-	-	
22	12/10/09 13:00	7.8	1299	7.87	1290	8.01	1302	20.8	

Appendix B - Tables

Table B.18. Development of in-situ parameters (pH, EC) in Column 3; experimental series 2 (neutralizing product Mischkalk Borna).

No. of day	Date	Sampling port – Height above bottom						
		II - 1800		IV - 1100		VI - 200		
		pH [-]	LF μS/cm	pH [-]	LF μS/cm	pH [-]	LF μS/cm	Temp °C
1	11/18/09 12:00	2.95	1600	2.95	1600	2.95	1600	21.2
2	11/19/09 10:30	3.2	1872	3.27	1440	3.18	1461	22.3
2	11/19/09 12:00	3.46	1830	3.49	1314	3.37	1587	22.2
3	11/20/09 11:00	3.72	1812	3.71	1292	3.7	1305	22.1
4	-	-	-	-	-	-	-	-
5	11/22/09 9:00	3.74	1284	3.68	1284	3.68	1299	21.2
6	11/23/09 9:00	3.88	1287	3.78	1302	3.78	1314	21.8
7	11/24/09 9:00	3.78	1281	3.76	1301	3.84	1281	22.2
8	11/25/09 9:00	3.75	1296	3.73	1278	3.79	1263	21.5
8	11/25/09 11:00	4.02	1246	4.04	1209	3.8	1260	22.3
8	11/25/09 12:30	4.19	1220	4.15	1222	3.91	1232	22.7
9	11/26/09 13:00	4.77	1194	4.68	1198	4.71	1200	22.8
9	11/27/09 9:00	4.72	1225	4.66	1234	4.73	1216	21.8
10	11/28/09 10:00	4.76	1240	4.77	1206	4.83	1204	21.3
11	11/29/09 14:00	4.6	1246	4.57	1228	4.62	1233	21.1
12	11/30/09 8:00	4.68	1212	4.67	1248	4.7	1226	20.7
13	12/1/09 9:00	4.74	1226	4.77	1228	4.77	1230	21.1
14	12/2/09 10:00	4.86	1224	4.74	1269	4.78	1254	21
14	12/2/09 13:00	6.69	1269	6.98	1271	5.09	1232	21.4
14	12/2/09 17:00	8.68	1256	8.88	1272	7.6	1266	20.9
15	12/3/09 8:00	8.65	1260	8.66	1284	8.33	1281	20.5
16	-	-	-	-	-	-	-	-
17	12/5/09 20:00	8.24	1278	8.26	1298	8.27	1266	20.2
18	-	-	-	-	-	-	-	-
19	12/7/09 11:00	8.24	1254	8.15	1266	8.14	1281	20.9
20	-	-	-	-	-	-	-	-
21	-	-	-	-	-	-	-	-
22	12/10/09 13:00	7.99	1314	7.86	1281	7.95	1287	20.9

Table B.19. Development of in-situ parameters (pH, EC) in Column 4; experimental series 2 (neutralizing product DSM Borna).

No. of day	Date	Sampling port – Height above bottom						
		II - 1800		IV - 1100		VI - 200		
		pH [-]	LF µS/cm	pH [-]	LF µS/cm	pH [-]	LF µS/cm	Temp °C
1	11/18/09 12:00	2.95	1600	2.95	1600	2.95	1600	21.2
2	11/19/09 10:30	3.27	1677	3.27	1448	3.28	1437	22.0
2	11/19/09 12:00	3.72	1728	3.72	1360	3.57	1692	22.3
3	11/20/09 11:00	4.56	1956	4.62	1208	4.7	1200	22.1
4	-	-	-	-	-	-	-	-
5	11/22/09 9:00	4.71	1242	4.76	1236	4.79	1269	21.3
6	11/23/09 9:00	4.84	1251	4.81	1251	4.75	1251	21.4
7	11/24/09 9:00	4.75	1210	4.77	1237	4.83	1236	22.5
8	11/25/09 9:00	4.55	1220	4.75	1221	4.81	1224	21.6
8	11/25/09 11:00	5.04	1210	5.02	1205	4.92	1199	22
8	11/25/09 12:30	5.13	1211	5.11	1208	4.98	1184	22.5
9	11/26/09 13:00	5.43	1218	5.31	1222	5.32	1218	22.7
9	11/27/09 9:00	5.28	1224	5.38	1238	5.39	1226	22
10	11/28/09 10:00	5.38	1238	5.41	1188	5.51	1238	21.1
11	11/29/09 14:00		1229	5.78	1240	5.79	1238	20.7
12	11/30/09 8:00	5.22	1230	5.38	1250	5.31	1240	20.5
13	12/1/09 9:00	5.15	1236	5.39	1224	5.33	1240	21.4
14	12/2/09 10:00	5.34	1251	5.31	1248	5.4	1246	21.1
14	12/2/09 13:00	7.8	1272	7.03	1269	5.76	1230	20.4
14	12/2/09 17:00	8.55	1278	8.45	1263	7.42	1272	20.9
15	12/3/09 8:00	8.44	1269	8.29	1262	7.55	1300	20.5
16	-	-	-	-	-	-	-	-
17	12/5/09 20:00	8.02	1284	7.82	1266	7.75	1263	20.8
18	-	-	-	-	-	-	-	-
19	12/7/09 11:00	7.81	1278	7.83	1293	7.75	1280	21.2
20	-	-	-	-	-	-	-	-
21	-	-	-	-	-	-	-	-
22	12/10/09 13:00	7.56	1293	7.53	1302	7.66	1296	20.7

Appendix B - Tables

Table B.20. Determined trace metal concentration variation during experimental series 2.

Ident	B ppb	Al ppb	Cr ppb	Mn ppb	Fe ppb	Co ppb	Ni ppb	Cu ppb	Zn ppb	As ppb	Rb ppb
Lohsa II, initial solution	137.40	2049.00	2.40	2338.00	8736.00	56.99	69.05	11.16	117.80	1.22	94.63
Average concentration											
Column 1	10.12.2009	142.20	38.25	0.21	1231.23	3.08	23.15	81.32	4.42	107.96	0.49
Column 1	19.11.2009	133.33	2398.67	1.05	2241.33	1068.20	52.28	81.67	38.70	208.57	0.71
Column 1	23.11.2009	149.63	495.57	0.44	2523.00	285.50	57.55	119.53	28.26	265.87	0.80
Column 1	25.11.2009	129.27	466.80	0.57	2197.00	235.80	49.77	116.23	49.30	277.40	1.01
Column 1	02.12.2009	130.47	60.07	0.26	2218.00	139.53	48.01	135.33	50.38	404.33	0.95
Column 2	10.12.2009	149.80	34.67	0.13	927.70	1.99	11.58	36.84	3.12	39.48	0.33
Column 2	19.11.2009	133.13	2834.67	1.46	2283.67	2618.67	53.69	67.73	52.76	225.13	0.84
Column 2	23.11.2009	138.00	2572.33	0.63	2347.33	306.50	51.84	83.75	40.13	331.30	0.89
Column 2	25.11.2009	131.40	2400.00	0.42	2251.00	152.92	49.28	81.45	50.29	341.90	0.74
Column 2	02.12.2009	137.43	329.90	0.27	2315.67	155.37	46.81	95.48	53.78	546.77	1.01
Column 3	10.12.2009	138.50	94.46	0.20	908.17	4.90	5.84	83.33	14.15	65.65	0.33
Column 3	19.11.2009	134.77	2981.33	1.91	2293.00	5285.67	53.73	74.31	48.44	314.53	1.12
Column 3	23.11.2009	139.93	3274.00	1.38	2337.33	663.07	53.11	105.83	58.54	434.00	0.75
Column 3	25.11.2009	139.57	3332.00	1.22	2384.67	555.70	52.80	124.53	65.15	468.77	0.77
Column 3	02.12.2009	141.27	3067.33	0.75	2417.33	213.97	50.20	198.93	96.25	729.20	0.92
Column 4	10.12.2009	138.73	70.81	0.13	1249.33	2.07	18.90	51.99	6.79	223.83	0.19
Column 4	19.11.2009	138.23	2072.59	1.14	2008.33	2111.75	43.34	62.63	28.92	437.17	0.61
Column 4	23.11.2009	141.13	3086.67	1.25	2447.33	1791.47	55.22	68.07	69.02	707.27	0.84
Column 4	25.11.2009	136.90	2688.67	0.56	2340.67	222.37	52.16	66.30	72.35	774.27	0.95
Column 4	02.12.2009	142.77	624.97	0.33	2373.33	137.38	50.71	83.50	76.04	1127.33	1.16

Table B.20. Determined trace metal concentration variation during experimental series 2, continued.

Ident	Cd ppb	Sb ppb	I ppb	Cs ppb	Ba ppb	Re ppb	Tl ppb	Pb ppb	U ppb	
Lohsa II, initial solution	0.91	0.02	1.82	1.11	31.60	0.84	0.23	8.34	1.00	
Average concentration										
Column 1	10.12.2009	0.12	0.14	6.69	0.86	67.58	0.84	0.15	0.42	0.43
Column 1	19.11.2009	1.18	0.15	2.72	0.98	67.25	0.82	0.12	6.28	0.85
Column 1	23.11.2009	0.80	0.10	3.51	1.07	80.09	0.79	0.13	2.27	0.62
Column 1	25.11.2009	0.47	0.13	2.98	0.94	72.91	0.86	0.11	3.13	0.54
Column 1	02.12.2009	0.43	0.09	2.95	0.91	79.32	0.84	0.11	1.50	0.35
Column 2	10.12.2009	0.12	0.11	4.12	0.86	81.32	0.78	0.14	0.18	0.38
Column 2	19.11.2009	1.30	0.10	1.84	1.00	83.41	0.82	0.12	7.24	0.85
Column 2	23.11.2009	0.63	0.09	2.83	0.95	92.91	0.83	0.12	4.83	0.79
Column 2	25.11.2009	0.69	0.12	1.53	0.91	89.29	0.84	0.11	4.90	0.73
Column 2	02.12.2009	0.65	0.15	1.96	0.87	92.41	0.80	0.12	4.66	0.58
Column 3	10.12.2009	0.13	0.11	3.14	0.85	82.46	0.80	0.13	0.43	0.49
Column 3	19.11.2009	1.31	0.18	2.38	1.00	84.75	0.80	0.12	13.53	3.39
Column 3	23.11.2009	0.51	0.14	3.98	0.99	91.92	0.81	0.13	12.83	0.88
Column 3	25.11.2009	0.48	0.09	2.95	0.98	94.64	0.80	0.13	12.44	0.89
Column 3	02.12.2009	0.54	0.14	2.23	0.92	96.21	0.78	0.12	12.02	0.83
Column 4	10.12.2009	0.14	0.07	2.66	0.85	91.91	0.80	0.12	0.21	0.43
Column 4	19.11.2009	0.29	0.05	1.92	0.97	89.62	0.81	0.13	7.51	0.81
Column 4	23.11.2009	0.41	0.09	1.78	1.02	105.58	0.79	0.13	10.72	0.91
Column 4	25.11.2009	0.47	0.13	2.50	0.95	99.78	0.80	0.12	7.98	0.83
Column 4	02.12.2009	0.49	0.15	2.10	0.93	106.57	0.78	0.12	6.81	0.67

Table B.21. Trace element reduction during experimental series 2.

Ident		B	Al	Cr	Mn	Fe	Co	Ni	Cu	Zn	As	Rb
Column 1	10.12.2009	103.49	1.87	8.82	52.7	0.0	40.6	117.8	39.6	91.6	39.9	99.1
Column 1	19.11.2009	97.04	117.07	43.76	95.9	12.2	91.7	118.3	346.7	177.1	57.8	92.9
Column 1	23.11.2009	108.90	24.19	18.12	107.9	3.3	101.0	173.1	253.2	225.7	65.4	104.7
Column 1	25.11.2009	94.08	22.78	23.91	94.0	2.7	87.3	168.3	441.8	235.5	82.3	91.3
Column 1	02.12.2009	94.95	2.93	10.63	94.9	1.6	84.2	196.0	451.5	343.2	77.7	94.6
Column 2	10.12.2009	109.02	1.69	5.23	39.7	0.0	20.3	53.3	27.9	33.5	26.9	103.5
Column 2	19.11.2009	96.89	138.34	60.79	97.7	30.0	94.2	98.1	472.8	191.1	68.5	95.6
Column 2	23.11.2009	100.44	125.54	26.14	100.4	3.5	91.0	121.3	359.6	281.2	73.1	96.2
Column 2	25.11.2009	95.63	117.13	17.37	96.3	1.8	86.5	118.0	450.6	290.2	60.9	92.9
Column 2	02.12.2009	100.02	16.10	11.15	99.0	1.8	82.1	138.3	481.9	464.1	83.0	95.1
Column 3	10.12.2009	100.80	4.61	8.26	38.8	0.1	10.3	120.7	126.8	55.7	27.3	100.8
Column 3	19.11.2009	98.08	145.50	79.74	98.1	60.5	94.3	107.6	434.0	267.0	91.4	96.9
Column 3	23.11.2009	101.84	159.79	57.50	100.0	7.6	93.2	153.3	524.6	368.4	60.9	98.3
Column 3	25.11.2009	101.58	162.62	51.01	102.0	6.4	92.7	180.4	583.8	397.9	62.6	99.2
Column 3	02.12.2009	102.81	149.70	31.06	103.4	2.4	88.1	288.1	862.5	619.0	75.4	101.0
Column 4	10.12.2009	100.97	3.46	5.30	53.4	0.0	33.2	75.3	60.9	190.0	15.2	96.9
Column 4	19.11.2009	100.61	101.15	47.31	85.9	24.2	76.1	90.7	259.1	371.1	49.6	98.9
Column 4	23.11.2009	102.72	150.64	52.09	104.7	20.5	96.9	98.6	618.4	600.4	68.4	99.7
Column 4	25.11.2009	99.64	131.22	23.52	100.1	2.5	91.5	96.0	648.3	657.3	78.0	94.7
Column 4	02.12.2009	103.91	30.50	13.58	101.5	1.6	89.0	120.9	681.4	957.0	94.6	98.0

Table B.21. Trace element reduction during experimental series 2, continued.

Ident		Cd	Sb	I	Cs	Ba	Re	Tl	Pb	U
Column 1	10.12.2009	12.8	593.1	368.1	76.8	213.9	100.0	66.7	5.1	42.8
Column 1	19.11.2009	129.1	604.2	149.5	88.3	212.8	98.6	53.6	75.3	85.3
Column 1	23.11.2009	87.3	409.7	192.9	96.0	253.4	94.7	57.4	27.2	62.4
Column 1	25.11.2009	51.6	547.2	163.9	84.7	230.7	102.7	49.5	37.5	54.7
Column 1	02.12.2009	47.2	370.8	162.3	81.4	251.0	100.2	50.5	17.9	35.3
Column 2	10.12.2009	13.3	477.8	226.9	77.0	257.4	93.1	63.7	2.1	38.5
Column 2	19.11.2009	142.6	422.2	101.3	89.8	264.0	97.6	54.8	86.8	85.6
Column 2	23.11.2009	69.4	370.8	155.9	85.5	294.0	99.7	53.6	58.0	79.5
Column 2	25.11.2009	75.2	493.1	83.9	81.9	282.6	100.3	49.8	58.8	73.0
Column 2	02.12.2009	71.5	630.6	107.8	78.2	292.4	95.2	51.4	55.9	58.2
Column 3	10.12.2009	14.0	455.6	172.7	76.5	261.0	95.9	58.4	5.2	49.2
Column 3	19.11.2009	143.5	731.9	131.1	90.1	268.2	95.5	54.8	162.2	
Column 3	23.11.2009	55.4	575.0	219.2	89.0	290.9	97.0	55.1	153.8	88.1
Column 3	25.11.2009	52.7	370.8	162.3	88.3	299.5	96.0	55.1	149.2	89.7
Column 3	02.12.2009	58.8	568.1	122.9	82.9	304.5	93.6	54.8	144.1	83.3
Column 4	10.12.2009	15.6	286.1	146.3	76.3	290.8	96.1	54.8	2.5	43.0
Column 4	19.11.2009	32.1	216.7	105.9	87.2	283.6	96.4	55.2	90.0	81.4
Column 4	23.11.2009	44.6	368.1	97.9	91.2	334.1	94.4	55.4	128.6	91.4
Column 4	25.11.2009	51.7	531.9	137.7	85.1	315.8	95.5	53.6	95.7	83.0
Column 4	02.12.2009	53.5	609.7	115.6	83.2	337.2	93.8	53.0	81.6	67.3

Table B.22. Amounts of liming products, experimental series 3 (Scheibe).

Column	1 KSM Beroun	2 KSM Beroun	3 DSM Ostrau	4 DSM Ostrau	5 CaO	6 KSM_C20
Neutralizing product	19	19	19	19	19	19
Neutralizing potential [moleq/kg]	70 %	70 %	70 %	70 %	95 %	55 %
Efficiency	[g]	[g]	[g]	[g]	[g]	[g]
1. Treatment 29.06.2010	20.7522	4.1512	20.7522	4.1507	-	-
2. Treatment 30.06.2010	-	4.1506	-	4.1509	-	-
3. Treatment 01.07.2010	-	4.1511	-	4.1504	-	-
4. Treatment 02.07.2010	-	4.1508	-	4.1506	-	-
5. Treatment 03.07.2010	-	4.1509	-	4.1505	-	-
1. Treatment 17.02.2011	-	-	-	-	1.8679	6.0735
2. Treatment 18.02.2011	-	-	-	-	1.8679	6.0725
3. Treatment 21.02.2011	-	-	-	-	1.8681	6.0725
4. Treatment 22.02.2011	-	-	-	-	1.8698	6.0730
5. Treatment 23.02.2011	-	-	-	-	1.8675	6.0734
Total amount	20.7522	20.7546	20.7522	20.7531	9.3397	30.3680

Table B.23. Development of in-situ parameters (pH, EC) in column 1; experimental series 3 (neutralizing product KSM Beroun (1x))

Datum	Sampling port – Height above bottom						
	II - 1800		IV - 1100		VI - 200		
	pH [-]	LF µS/cm	pH [-]	LF µS/cm	pH [-]	LF µS/cm	Temp °C
6/25/2010 9:00	2.7	1635	2.7	1635	2.7	1635	26.3
6/29/2010 9:00	2.7	1635	2.7	1635	2.7	1635	26.5
6/30/2010 13:30	3.16	1422	3.15	1422	3.25	1389	27.7
7/1/2010 11:55	3.2	1410	3.19	1404	3.3	1383	28.6
7/2/2010 10:05	3.17	1404	3.15	1394	3.22	1374	29
7/3/2010 18:35	3.23	1380	3.23	1392	3.23	1385	30.9
7/4/2010 12:02	3.32	1359	3.25	1350	3.3	1332	31.7
7/5/2010 10:30	3.17	1410	3.17	1404	3.17	1395	29.4
7/6/2010 14:00	3.11	1413	3.11	1416	3.12	1422	27.3
7/7/2010 10:00	3.25	1422	3.21	1416	3.2	1428	25.8
7/8/2010 10:00	3.18	1410	3.15	1418	3.16	1419	27
7/9/2010 10:00	3.27	1410	3.25	1428	3.24	1452	28.5
7/10/2010 17:00	3.25	1374	3.25	1386	3.27	1395	29.8
7/11/2010 15:10	3.23	1375	3.24	1374	3.24	1380	30.7
7/12/2010 10:00	3.17	1389	3.19	1386	3.15	1407	31.7
7/13/2010 9:50	3.19	1389	3.2	1386	3.17	1388	30.9
7/27/2010 10:00	3.36	1342	3.34	1347	3.33	1360	27.8

Table B.24. Development of in-situ parameters (pH, EC) in column 2; experimental series 3 (neutralizing product KSM Beroun (5x))

Datum	Sampling port – Height above bottom						
	II - 1800		IV - 1100		VI - 200		
	pH [-]	LF μS/cm	pH [-]	LF μS/cm	pH [-]	LF μS/cm	Temp °C
6/25/2010 9:00	2.77	1602	2.77	1602	2.77	1602	26.3
6/29/2010 9:00	2.77	1602	2.77	1602	2.77	1602	26.5
6/30/2010 13:30	2.91	1557	2.89	1557	2.92	1547	29.5
7/1/2010 11:55	3.05	1464	3.07	1446	3.04	1464	28.7
7/2/2010 10:05	3.39	1316	3.39	1314	3.23	1364	29
7/3/2010 18:20	4.16	1253	4.18	1242	4.2	1268	31.2
7/4/2010 12:59	4.56	1282	5.04	1284	4.58	1260	31.7
7/5/2010 10:30	4.83	1246	4.93	1254	4.93	1240	29.6
7/6/2010 14:10	4.85	1260	4.95	1269	4.97	1260	27.4
7/7/2010 10:10	4.74	1274	5.06	1263	5.17	1269	25.6
7/8/2010 10:10	4.71	1263	4.91	1260	5.05	1275	26.9
7/9/2010 10:10	4.9	1280	5.08	1278	5.17	1281	28.5
7/10/2010 17:00	4.95	1240	5.07	1260	5.17	1246	29.9
7/11/2010 15:20	5.01	1242	5.11	1246	5.19	1248	30.9
7/12/2010 10:10	4.72	1281	4.91	1253	5	1266	31.5
7/13/2010 10:10	4.62	1260	4.65	1254	4.7	1266	31.1
7/27/2010 10:00	5.76	1233	5.56	1227	5.77	1239	25.7

Table B.25. Development of in-situ parameters (pH, EC) in column 3; experimental series 3 (neutralizing product DSM Ostrau (1x))

Datum	Sampling port – Height above bottom							
	II - 1800		IV - 1100		VI - 200		Temp °C	
	pH [-]	LF µS/cm	pH [-]	LF µS/cm	pH [-]	LF µS/cm		
6/25/2010 9:00	2.76	1655	2.76	1655	2.76	1655	26.3	
6/29/2010 9:00	2.76	1655	2.76	1655	2.76	1655	26.5	
6/30/2010 13:45	3.1	1447	3.07	1440	3.26	1386	28.3	
7/1/2010 11:05	3.11	1440	3.08	1443	3.34	1370	28.9	
7/2/2010 10:05	3.07	1430	3.06	1431	3.18	1388	29.3	
7/3/2010 18:25	3.19	1403	3.14	1416	3.2	1413	31	
7/4/2010 12:47	3.16	1404	3.11	1401	3.2	1413	31	
7/5/2010 10:30	3.14	1434	3.1	1440	3.05	1449	29.5	
7/6/2010 14:20	3.04	1455	3.03	1466	3.06	1470	27.3	
7/7/2010 10:20	3.1	1470	3.11	1455	3.14	1455	25.6	
7/8/2010 10:20	3.06	1458	3.07	1449	3.09	1445	26.9	
7/9/2010 10:20	3.17	1451	3.15	1449	3.14	1467	28.4	
7/10/2010 17:00	3.21	1428	3.18	1436	3.18	1426	30	
7/11/2010 15:30	3.15	1410	3.14	1422	3.14	1422	30.8	
7/12/2010 10:20	3.15	1437	3.07	1424	3.07	1443	31.5	
7/13/2010 10:10	3.09	1416	3.12	1418	3.09	1416	31.6	
7/27/2010 10:00	3.21	1400	3.19	1398	3.2	1401	26.3	

Table B.26. Development of in-situ parameters (pH, EC) in column 4; experimental series 3 (neutralizing product DSM Ostrau (5x))

Datum	Sampling port – Height above bottom						
	II - 1800		IV - 1100		VI - 200		
	pH [-]	LF µS/cm	pH [-]	LF µS/cm	pH [-]	LF µS/cm	Temp °C
6/25/2010 9:00	2.78	1603	2.78	1603	2.78	1603	26.3
6/29/2010 9:00	2.78	1603	2.78	1603	2.78	1603	26.5
6/30/2010 13:30	2.93	1548	2.89	1547	2.92	1550	28.3
7/1/2010 11:55	2.99	1512	2.98	1506	3.02	1491	29.1
7/2/2010 10:05	3.07	1440	3.05	1433	3.07	1430	29.4
7/3/2010 18:35	3.28	1386	-	1377	3.27	1353	31.1
7/4/2010 12:40	3.73	1278	3.71	1275	4.01	1260	31.4
7/5/2010 10:30	3.66	1290	3.69	1287	3.84	1233	29.7
7/6/2010 14:30	3.62	1302	3.65	1299	3.66	1304	27.3
7/7/2010 10:30	3.74	1293	3.74	1287	3.75	1296	25.6
7/8/2010 10:30	3.71	1290	3.76	1296	3.73	1296	26.8
7/9/2010 10:30	3.78	1311	3.8	1305	3.85	1305	28.4
7/10/2010 17:00	3.85	1268	3.85	1278	3.85	1281	30.2
7/11/2010 15:40	3.80	1269	3.81	1266	3.81	1261	31.2
7/12/2010 10:30	3.74	1293	3.75	1278	3.77	1281	31.6
7/13/2010 10:20	3.74	1263	3.69	1272	3.69	1265	31.6
7/27/2010 10:00	3.99	1249	3.98	1240	4.02	1244	25.8

Table B.27. Development of in-situ parameters (pH, EC) in column 5; experimental series 3 (neutralizing product CaO, 5x)

Datum	Sampling port – Height above bottom						
	II - 1800		IV - 1100		VI - 200		
	pH [-]	LF µS/cm	pH [-]	LF µS/cm	pH [-]	LF µS/cm	Temp °C
2/15/2011 15:00	2.97	1266	3.06	1311	2.99	1319	
2/18/2011 13:00	2.94	1248	2.95	1251	2.96	1278	21
2/18/2011 14:45	2.97	1266	3.42	1127	2.98	1278	21
2/21/2011 10:15	3.09	1233	3.06	1248	3.06	1269	20
2/21/2011 13:00	3.42	1122	3.23	1184	3.1	1225	21
2/22/2011 10:30	3.23	1170	3.23	1192	3.26	1196	20
2/23/2011 10:20	3.83	1074	3.62	1082	3.75	1096	20
2/24/2011 11:00	4.88	1054	4.85	1056	4.68	1052	21
2/25/2011 10:00	4.63	1056	4.61	1057	4.58	1058	21
3/2/2011 9:45			4.82	1026	4.74	1035	21

Table B.28. Development of in-situ parameters (pH, EC) in column 6; experimental series 3 (neutralizing product KSM_C20, 5x)

Datum	Sampling port – Height above bottom						
	II - 1800		IV - 1100		VI - 200		
	pH [-]	LF µS/cm	pH [-]	LF µS/cm	pH [-]	LF µS/cm	Temp °C
2/15/2011 15:00	2.99	1172	3.02	1298	3.03	1331	
2/18/2011 13:00	3.01	1256	2.99	1290	2.99	1275	21
2/18/2011 14:45	4.32	1056	3.65	1090	3	1284	21
2/21/2011 10:20	3.34	1160	3.41	1152	3.39	1131	20
2/21/2011 13:00	6.01	1066	5.68	1052	3.47	1134	21
2/22/2011 10:40	4.91	1064	5.07	1050	5.04	1061	20
2/23/2011 10:25	6.24	1126	6.29	1139	6.3	1125	20
2/24/2011 11:00	6.35	1151	6.85	1144	6.76	1150	20
2/25/2011 10:00	6.45	1144	6.5	1150	6.53	1150	21
3/2/2011 9:45	6.16	1119	6.38	1086	6.54	1118	21

Appendix B - Tables

Table B.29. Determined trace metal concentration variation during experimental series 3, neutralizing product KSM Beroun, DSM Ostrau.

Ident	mg/L	ppb	ppb	ppb	ppb	ppb	ppb	ppb	ppb	ppb	ppb	ppb
	Mn	Al	Cr	Fe	Co	Ni	Cu	Zn	Rb	Pb	Cd	
Column 1, Port IV 25.06.2010 (initial solution)	2.43	7099.00	2.97	17130.00	144.30	145.80	367.90	269.40	13.51	621.30	0.15	
Column 1, Port IV 05.07.2010	2.46	6710.00	1.34	799.90	140.90	143.80	476.00	263.40	13.23	618.10	0.08	
Column 1, Port IV 06.07.2010	2.49	6828.00	1.15	706.20	143.20	145.40	481.10	264.10	13.51	627.90	0.05	
Column 1, Port IV 13.07.2010	2.44	-	-	-	-	-	-	-	-	-	-	
Column 1, Port IV 27.07.2010	-	-	-	-	-	-	-	-	-	-	-	
Column 2, Port IV 25.06.2010 (initial solution)	2.47	7244.00	2.95	14430.00	142.80	152.60	414.70	428.10	13.71	631.40	3.12	
Column 2, Port IV 05.07.2010	2.52	655.80	-0.22	-0.57	142.40	152.40	521.80	367.70	13.76	655.30	0.10	
Column 2, Port IV 06.07.2010	2.45	685.00	-0.48	-4.70	140.60	151.20	528.60	377.80	13.41	652.80	0.11	
Column 2, Port IV 13.07.2010	2.51	-	-	-	-	-	-	-	-	-	-	
Column 2, Port IV 27.07.2010	-	-	-	-	-	-	-	-	-	-	-	
Column 3, Port IV 25.06.2010 (initial solution)	2.73	7088.00	2.65	11280.00	145.20	148.00	184.30	272.60	13.45	636.90	0.15	
Column 3, Port IV 05.07.2010	2.70	6922.00	2.09	1512.00	140.00	141.80	271.70	304.30	13.22	607.60	1.74	
Column 3, Port IV 06.07.2010	2.74	6861.00	2.10	1334.00	140.80	144.40	267.30	305.30	13.43	615.30	1.86	
Column 3, Port IV 13.07.2010	2.69	-	-	-	-	-	-	-	-	-	-	
Column 3, Port IV 27.07.2010	-	-	-	-	-	-	-	-	-	-	-	
Column 4, Port IV 25.06.2010 (initial solution)	2.45	6884.00	2.77	18190.00	141.80	145.60	6.97	268.70	13.38	623.10	0.11	
Column 4, Port IV 05.07.2010	2.74	6794.00	1.42	213.70	141.10	144.70	34.88	331.40	13.31	623.70	1.67	
Column 4, Port IV 06.07.2010	2.87	6683.00	0.92	113.70	142.00	142.20	11.50	309.20	13.48	620.20	1.71	
Column 4, Port IV 13.07.2010	2.71	-	-	-	-	-	-	-	-	-	-	
Column 4, Port IV 27.07.2010	-	-	-	-	-	-	-	-	-	-	-	
Trace element content [%] before / after												
Column1 (KSM Beroun, 1 x)	102.48	96.18	38.54	4.12	99.24	99.73	130.77	98.03	100.00	101.06	34.90	
Column 2 (KSM Beroun, 5x)	99.23	94.56	16.11	-0.03	98.46	99.08	127.47	88.25	97.81	103.39	3.43	
Column 3 (DSM Ostrau, 1 x)	100.34	96.80	79.21	11.83	96.97	97.57	145.04	112.00	99.85	96.61	1204.55	
Column 4 (DSM Ostrau, 5x)	117.16	97.08	33.16	0.63	100.14	97.66	165.04	115.07	100.75	99.53	1515.93	

Table B.29. Det. trace metal concentration variation during experimental series 2, neutralizing product KSM Beroun, DSM Ostrau, continued.

Ident	ppb	ppb	ppb	ppb	ppb	ppb	ppb
	Sn	Ba	Re	Tl	Pb	Bi	U
Column 1, Port IV 25.06.2010 (initial solution)	0.96	46.53	0.89	0.08	6.13	0.35	1.82
Column 1, Port IV 05.07.2010	0.90	55.21	0.88	0.05	5.39	0.33	1.73
Column 1, Port IV 06.07.2010	0.88	47.59	0.87	0.06	5.71	0.33	1.79
Column 1, Port IV 13.07.2010	-	-	-	-	-	-	-
Column 1, Port IV 27.07.2010	-	-	-	-	-	-	-
Column 2, Port IV 25.06.2010 (initial solution)	1.11	56.90	0.88	0.05	15.08	0.33	1.81
Column 2, Port IV 05.07.2010	0.85	45.76	0.87	0.05	6.54	0.32	1.84
Column 2, Port IV 06.07.2010	0.87	50.00	0.87	0.06	6.54	0.32	1.52
Column 2, Port IV 13.07.2010	-	-	-	-	-	-	-
Column 2, Port IV 27.07.2010	-	-	-	-	-	-	-
Column 3, Port IV 25.06.2010 (initial solution)	0.84	53.83	0.86	0.06	6.13	0.32	1.82
Column 3, Port IV 05.07.2010	0.86	57.53	0.87	0.06	53.80	0.32	1.86
Column 3, Port IV 06.07.2010	0.87	50.20	0.87	0.07	54.38	0.32	1.88
Column 3, Port IV 13.07.2010	-	-	-	-	-	-	-
Column 3, Port IV 27.07.2010	-	-	-	-	-	-	-
Column 4, Port IV 25.06.2010 (initial solution)	0.80	70.23	0.85	0.04	5.53	0.32	1.84
Column 4, Port IV 05.07.2010	0.89	54.34	0.86	0.06	60.07	0.32	1.92
Column 4, Port IV 06.07.2010	0.86	45.43	0.86	0.05	58.34	0.32	1.91
Column 4, Port IV 13.07.2010	-	-	-	-	-	-	-
Column 4, Port IV 27.07.2010	-	-	-	-	-	-	-
Trace element content [%] before / after							
Column1 (KSM Beroun, 1 x)	92.47	102.28	97.46	71.25	93.11	94.20	98.62
Column 2 (KSM Beroun, 5x)	78.84	87.87	98.93	120.41	43.39	97.25	84.17
Column 3 (DSM Ostrau, 1 x)	103.59	93.26	100.55	114.04	887.26	100.31	103.19
Column 4 (DSM Ostrau, 5x)	107.46	64.69	101.41	123.08	1055.93	99.68	104.14

Appendix B - Tables

Table B.30. Determined trace metal concentration variation during experimental series 3, neutralizing product CaO.

Ident		ppb	ppb	ppb	ppb	ppb	ppb	ppb	ppb	ppb	ppb	ppb
		Be	B	Al	Si	V	Cr	Fe	Co	Ni	Cu	Zn
Column 5, Port II	15.02.2011	2.991	51.15	7454	17000	0.339	3.247	28480	132.4	157.9	518.7	496.3
Column 5, Port IV	15.02.2011	2.887	49.59	7083	16400	0.357	3.132	27980	130.0	152.8	469.3	490.3
Column 5, Port VI	15.02.2011	2.800	47.37	6828	15940	0.354	3.056	27670	128.3	150.1	417.9	484.3
Column 5, Port II	22.02.2011	2.341	42.69	5528	16580	< 0.1	2.280	2570	133.1	161.4	537.2	493.8
Column 5, Port IV	22.02.2011	2.287	42.02	5540	16630	< 0.1	2.316	2816	133.1	161.3	536.9	495.0
Column 5, Port VI	22.02.2011	2.225	41.55	5341	15940	< 0.1	2.206	2522	129.4	156.3	523.2	480.7
Column 5, Port II	23.02.2011	2.148	40.86	5102	16130	< 0.1	1.309	241.3	126.3	152.9	512.9	472.3
Column 5, Port IV	23.02.2011	2.178	40.67	5256	16050	< 0.1	1.418	297.60	129.2	155.7	527.1	471.7
Column 5, Port VI	23.02.2011	2.173	41.19	5200	16230	< 0.1	1.446	423.7	128.0	154.7	523.7	477.8
Column 5, Port II	25.02.2011	1.578	42.51	2295	15000	< 0.1	0.502	9.15	119.5	141.9	433.0	428.0
Column 5, Port IV	25.02.2011	1.554	42.10	2257	15050	< 0.1	0.493	6.67	120.2	143.6	428.2	430.3
Column 5, Port VI	25.02.2011	1.779	41.50	2929	15400	< 0.1	0.579	7.15	125.4	148.5	487.8	462.9
Column 5, Port II	02.03.2011	1.420	39.28	1880	14540	< 0.1	0.442	10.39	110.6	131.7	405.9	393.6
Column 5, Port IV	02.03.2011	1.421	39.21	1792	14470	< 0.1	0.393	7.21	109.6	130.1	404.5	410.8
Column 5, Port VI	02.03.2011	1.469	40.63	1879	14750	< 0.1	0.463	8.83	114.5	136.6	420.7	426.0
Average concentration												
Column 5	15.02.2011	2.89	49.37	7121.67	16446.67	-	3.15	28043.33	130.23	153.60	468.63	490.30
Column 5	22.02.2011	2.28	42.09	5469.67	16383.33	-	2.27	2636.00	131.87	159.67	532.43	489.83
Column 5	23.02.2011	2.17	40.91	5186.00	16136.67	-	1.39	320.87	127.83	154.43	521.23	473.93
Column 5	25.02.2011	1.64	42.04	2493.67	15150.00	-	0.52	7.66	121.70	144.67	449.67	440.40
Column 5	02.03.2011	1.44	39.71	1850.33	14586.67	-	0.43	8.82	111.57	132.80	410.37	410.13
Trace element content [%] before / after												
		49.67	80.43	25.98	88.69	-	13.76	0.03	85.67	86.46	87.57	83.65

Table B.30. Determined trace metal concentration variation during experimental series 3, neutralizing product CaO, continued.

Ident		ppb	ppb	ppb	ppb	ppb	ppb	ppb	ppb	ppb	ppb	ppb
		Ga	As	Se	Rb	Sr	Mo	Ag	Cd	Sn	Sb	Te
Column 5, Port II	15.02.2011	0.251	2.417	< 2	14.31	581.1	0.023	0.009	0.780	0.116	0.023	< 0.01
Column 5, Port IV	15.02.2011	0.237	2.382	< 2	14.32	583.6	0.023	0.008	0.799	0.276	0.021	< 0.01
Column 5, Port VI	15.02.2011	0.225	2.421	< 2	14.17	580.5	0.022	0.008	0.816	0.121	0.019	< 0.01
Column 5, Port II	22.02.2011	0.232	1.504	1.287	13.950	668.400	<0.01	0.010	0.820	< 0.05	< 0.01	< 0.01
Column 5, Port IV	22.02.2011	0.233	1.372	1.521	14.070	670.600	<0.01	0.009	0.810	< 0.05	< 0.01	< 0.01
Column 5, Port VI	22.02.2011	0.222	1.440	1.304	13.830	665.200	<0.01	0.008	0.799	< 0.05	< 0.01	< 0.01
Column 5, Port II	23.02.2011	0.216	1.313	1.424	13.750	674.700	<0.01	0.007	0.782	< 0.05	< 0.01	< 0.01
Column 5, Port IV	23.02.2011	0.220	1.313	1.391	13.890	681.000	<0.01	0.009	0.787	< 0.05	< 0.01	< 0.01
Column 5, Port VI	23.02.2011	0.216	1.348	1.238	13.930	682.200	<0.01	0.008	0.790	< 0.05	< 0.01	< 0.01
Column 5, Port II	25.02.2011	0.197	1.293	1.069	13.860	706.500	<0.01	0.009	0.753	< 0.05	< 0.01	< 0.01
Column 5, Port IV	25.02.2011	0.193	1.236	1.155	14.040	719.300	<0.01	0.006	0.766	< 0.05	< 0.01	< 0.01
Column 5, Port VI	25.02.2011	0.209	1.374	1.299	14.160	724.000	<0.01	0.007	0.794	< 0.05	< 0.01	< 0.01
Column 5, Port II	02.03.2011	0.191	1.249	1.025	13.580	709.400	<0.01	0.006	0.705	< 0.05	0.020	< 0.01
Column 5, Port IV	02.03.2011	0.182	1.279	0.973	13.490	709.100	<0.01	< 0.005	0.702	< 0.05	0.019	< 0.01
Column 5, Port VI	02.03.2011	0.189	1.269	1.112	14.250	741.200	<0.01	< 0.005	0.727	< 0.05	0.025	< 0.01
Average concentration												
Column 5	15.02.2011	0.24	2.41	-	14.27	581.73	-	0.01	0.80	0.17	0.02	-
Column 5	22.02.2011	0.23	1.44	1.37	13.95	668.07	-	0.01	0.81	-	-	-
Column 5	23.02.2011	0.22	1.32	1.35	13.86	679.30	-	0.01	0.79	-	-	-
Column 5	25.02.2011	0.20	1.30	1.17	14.02	716.60	-	0.01	0.77	-	-	-
Column 5	02.03.2011	0.19	1.27	1.04	13.77	719.90	-	0.01	0.71	-	0.02	-
Trace element content [%] before / after												
		78.82	52.59	-	96.54	123.75	-	72.00	89.10	-	101.59	-

Table B.30. Determined trace metal concentration variation during experimental series 3, neutralizing product CaO, continued.

Ident		ppb						
		I	Cs	Ba	Tl	Pb	Bi	U
Column 5, Port II	15.02.2011	2.698	0.054	33.09	0.123	6.414	0.003	1.400
Column 5, Port IV	15.02.2011	2.633	0.055	33.46	0.123	6.410	0.002	1.397
Column 5, Port VI	15.02.2011	2.497	0.054	33.54	0.124	6.366	0.001	1.397
Column 5, Port II	22.02.2011	1.251	0.071	38.920	0.147	7.331	< 0.001	1.347
Column 5, Port IV	22.02.2011	1.221	0.069	37.640	0.145	7.220	< 0.001	1.332
Column 5, Port VI	22.02.2011	1.230	0.066	37.870	0.144	6.964	< 0.001	1.311
Column 5, Port II	23.02.2011	1.179	0.066	34.320	0.142	6.000	< 0.001	1.277
Column 5, Port IV	23.02.2011	1.261	0.068	35.190	0.143	6.304	< 0.001	1.304
Column 5, Port VI	23.02.2011	1.040	0.068	35.100	0.143	6.145	< 0.001	1.302
Column 5, Port II	25.02.2011	0.903	0.064	45.570	0.140	3.443	0.012	1.050
Column 5, Port IV	25.02.2011	0.843	0.067	40.930	0.142	3.274	0.004	1.032
Column 5, Port VI	25.02.2011	0.888	0.067	41.190	0.142	4.062	0.002	1.162
Column 5, Port II	02.03.2011	0.834	0.069	31.340	0.134	3.245	0.001	0.973
Column 5, Port IV	02.03.2011	0.833	0.065	31.560	0.133	3.177	< 0.001	0.970
Column 5, Port VI	02.03.2011	0.875	0.076	33.290	0.139	3.241	< 0.001	1.016
Average concentration								
Column 5	15.02.2011	2.61	0.05	33.36	0.12	6.40	0.00	1.40
Column 5	22.02.2011	1.23	0.07	38.14	0.15	7.17	-	1.33
Column 5	23.02.2011	1.16	0.07	34.87	0.14	6.15	-	1.29
Column 5	25.02.2011	0.88	0.07	42.56	0.14	3.59	0.01	1.08
Column 5	02.03.2011	0.85	0.07	32.06	0.14	3.22	0.00	0.99
Trace element content [%] before / after								
		32.47	128.83	96.10	109.73	50.35	50.00	70.55

Table B.31. Determined trace metal concentration variation during experimental series 3, neutralizing product KSM_C20.

Ident		ppb	ppb	ppb	ppb	ppb	ppb	ppb	ppb	ppb	ppb	ppb
		Be	B	Al	Si	V	Cr	Fe	Co	Ni	Cu	Zn
Column 6, Port II	15.02.2011	2.849	48.97	6811	16160	0.386	3.150	28220	129.90	136.2	257.5	267.7
Column 6, Port IV	15.02.2011	2.855	47.42	6774	16130	0.437	3.075	28710	130.50	129.7	287.6	265.1
Column 6, Port VI	15.02.2011	2.835	47.81	6701	16030	0.435	3.047	28570	129.50	127.8	261.0	265.7
Column 6, Port II	22.02.2011	1.516	42.22	1177	16420	< 0.1	0.311	12.240	135.00	138.3	249.4	273.4
Column 6, Port IV	22.02.2011	1.494	42.25	1066	16230	< 0.1	0.331	11.160	134.40	137.4	246.9	268.7
Column 6, Port VI	22.02.2011	1.634	41.83	1590	16460	< 0.1	0.375	13.710	136.10	138.9	254.2	273.6
Column 6, Port II	23.02.2011	0.546	41.66	19.73	16010	< 0.1	< 0.1	2.375	134.10	136.4	137.6	260.0
Column 6, Port IV	23.02.2011	0.599	42.21	21.66	16310	< 0.1	< 0.1	2.681	135.90	138.3	152.7	262.8
Column 6, Port VI	23.02.2011	0.585	41.87	30.80	16120	< 0.1	< 0.1	7.040	134.70	136.2	155.2	258.7
Column 6, Port II	25.02.2011	0.403	42.46	10.38	16270	< 0.1	< 0.1	2.211	135.30	137.5	109.7	256.5
Column 6, Port IV	25.02.2011	0.408	42.34	9.90	16370	< 0.1	< 0.1	< 1	135.10	137.3	109.1	260.5
Column 6, Port VI	25.02.2011	0.420	40.89	10.91	15760	< 0.1	0.101	3.237	132.20	134.0	118.0	244.5
Column 6, Port II	02.03.2011	0.335	40.81	10.19	15780	< 0.1	< 0.1	3.897	126.60	128.4	91.02	238.2
Column 6, Port IV	02.03.2011	0.360	42.91	10.96	16680	< 0.1	< 0.1	3.928	133.50	134.9	95.20	250.0
Column 6, Port VI	02.03.2011	0.351	40.41	9.73	15650	< 0.1	< 0.1	3.011	126.30	128.0	93.47	237.6
Average concentration												
Column 6	15.02.2011	2.85	48.07	6762.00	16106.67	-	3.09	28500.00	129.97	131.23	268.70	266.17
Column 6	22.02.2011	1.55	42.10	1277.67	16370.00	-	0.34	12.37	135.17	138.20	250.17	271.90
Column 6	23.02.2011	0.58	41.91	24.06	16146.67	-	-	4.03	134.90	136.97	148.50	260.50
Column 6	25.02.2011	0.41	41.90	10.40	16133.33	-	0.10	2.72	134.20	136.27	112.27	253.83
Column 6	02.03.2011	0.35	41.38	10.30	16036.67	-	-	3.61	128.80	130.43	93.23	241.93
Trace element content [%] before / after												
		12.25	86.08	0.15	99.57	-	-	0.01	99.10	99.39	34.70	90.90

Table B.31. Determined trace metal concentration variation during experimental series 3, neutralizing product KSM_C20, continued.

Ident		ppb										
		Ga	As	Se	Rb	Sr	Mo	Ag	Cd	Sn	Sb	Te
Column 6, Port II	15.02.2011	0.222	2.357	< 2	14.52	589.2	0.021	0.005	0.772	< 0.05	0.019	< 0.01
Column 6, Port IV	15.02.2011	0.221	2.569	< 2	14.54	593.1	0.017	< 0.005	0.778	0.053	0.013	< 0.01
Column 6, Port VI	15.02.2011	0.215	2.431	< 2	14.50	591.2	0.019	< 0.005	0.770	0.050	0.011	< 0.01
Column 6, Port II	22.02.2011	0.209	1.318	1.172	13.950	807.1	<0.01	0.003	0.802	< 0.05	< 0.01	< 0.01
Column 6, Port IV	22.02.2011	0.214	1.327	1.287	13.890	804.2	<0.01	0.003	0.805	< 0.05	< 0.01	< 0.01
Column 6, Port VI	22.02.2011	0.213	1.284	1.326	14.010	809.7	<0.01	0.005	0.811	< 0.05	< 0.01	< 0.01
Column 6, Port II	23.02.2011	0.170	1.094	0.871	13.950	883.1	<0.01	< 0.005	0.803	< 0.05	< 0.01	< 0.01
Column 6, Port IV	23.02.2011	0.174	1.122	0.929	14.130	893.0	<0.01	< 0.005	0.818	< 0.05	< 0.01	< 0.01
Column 6, Port VI	23.02.2011	0.173	1.127	0.896	13.980	887.0	<0.01	< 0.005	0.793	< 0.05	< 0.01	< 0.01
Column 6, Port II	25.02.2011	0.158	1.039	0.639	14.300	954.5	<0.01	< 0.005	0.792	< 0.05	< 0.01	< 0.01
Column 6, Port IV	25.02.2011	0.142	1.093	0.628	14.230	954.4	<0.01	< 0.005	0.813	< 0.05	< 0.01	< 0.01
Column 6, Port VI	25.02.2011	0.159	1.036	0.709	13.970	936.0	<0.01	< 0.005	0.767	< 0.05	< 0.01	< 0.01
Column 6, Port II	02.03.2011	0.145	0.964	0.680	13.510	925.5	<0.01	< 0.005	0.764	< 0.05	0.015	< 0.01
Column 6, Port IV	02.03.2011	0.153	0.989	0.741	14.320	978.3	<0.01	< 0.005	0.798	< 0.05	0.016	< 0.01
Column 6, Port VI	02.03.2011	0.149	0.995	0.706	13.440	922.8	<0.01	< 0.005	0.753	< 0.05	0.015	< 0.01
Average concentration												
Column 6	15.02.2011	0.22	2.45	-	14.52	591.17	-	0.01	0.77	0.05	0.01	-
Column 6	22.02.2011	0.21	1.31	1.26	13.95	807.00	-	0.00	0.81	-	-	-
Column 6	23.02.2011	0.17	1.11	0.90	14.02	887.70	-	-	0.80	-	-	-
Column 6	25.02.2011	0.15	1.06	0.66	14.17	948.30	-	-	0.79	-	-	-
Column 6	02.03.2011	0.15	0.98	0.71	13.76	942.20	-	-	0.77	-	0.02	-
Trace element content [%] before / after												
		67.93	40.07	-	94.74	159.38	-	-	99.78	-	106.98	-

Table B.31. Determined trace metal concentration variation during experimental series 3, neutralizing product KSM_C20, continued.

Ident		ppb						
		I	Cs	Ba	Tl	Pb	Bi	U
Column 6, Port II	15.02.2011	2.536	0.054	34.11	0.122	4.762	0.001	1.352
Column 6, Port IV	15.02.2011	2.389	0.052	33.94	0.121	4.701	0.001	1.366
Column 6, Port VI	15.02.2011	1.949	0.053	34.17	0.123	4.713	0.001	1.368
Column 6, Port II	22.02.2011	1.174	0.065	39.910	0.145	2.981	< 0.001	0.995
Column 6, Port IV	22.02.2011	1.404	0.065	41.580	0.144	3.075	< 0.001	0.985
Column 6, Port VI	22.02.2011	1.502	0.065	41.920	0.144	3.306	< 0.001	1.032
Column 6, Port II	23.02.2011	1.104	0.065	40.120	0.144	0.789	< 0.001	0.576
Column 6, Port IV	23.02.2011	1.186	0.067	40.600	0.143	0.956	< 0.001	0.596
Column 6, Port VI	23.02.2011	1.018	0.065	39.460	0.143	1.154	< 0.001	0.571
Column 6, Port II	25.02.2011	1.008	0.065	46.880	0.144	0.342	0.001	0.637
Column 6, Port IV	25.02.2011	0.994	0.065	38.930	0.143	0.324	< 0.001	0.640
Column 6, Port VI	25.02.2011	1.263	0.062	52.110	0.139	0.423	0.001	0.613
Column 6, Port II	02.03.2011	0.962	0.065	36.980	0.134	0.196	< 0.001	0.623
Column 6, Port IV	02.03.2011	1.020	0.066	39.280	0.142	0.191	< 0.001	0.653
Column 6, Port VI	02.03.2011	0.917	0.062	36.720	0.135	0.227	< 0.001	0.614
Average concentration								
Column 6	15.02.2011	2.29	0.05	34.07	0.12	4.73	0.00	1.36
Column 6	22.02.2011	1.36	0.07	41.14	0.14	3.12	-	1.00
Column 6	23.02.2011	1.10	0.07	40.06	0.14	0.97	-	0.58
Column 6	25.02.2011	1.09	0.06	45.97	0.14	0.36	0.00	0.63
Column 6	02.03.2011	0.97	0.06	37.66	0.14	0.20	-	0.63
Trace element content [%] before / after								
		42.17	121.38	110.53	112.30	4.33	-	46.26

Table B.32. Mineralogical analysis of settled ash sediments before and after pilot experiment (results in wt.-%)

Sample	Amorphous	Brown-millerite	Calcite	Ettringite	Ferrite, magnesian	Hematite	Quartz	Gypsum	Microcline	Magnetite	Srebro-dolskite
BGH-290408-P0-0.80-1.00	43.1	5	4.1	-	-	1.1	36.2	-	4.3	5.1	1.1
BGH-290408-P0-1.00-1.20	46	-	6.7	3.5	5.4	1	24.1	4.3	1.5	1	6.5
BGH-290408-P0-1.20-1.40	25.2	-	2.7	-	4.1	1	61.1	-	2.6	-	3.3
BGH-290408-P0-1.40-1.60	14	-	0.9	-	3.7	0.8	76.1	-	2	-	2.5
BGH-290408-P0-1.60-1.65	41.6	-	3.4	2.5	--	0.9	40.7	2.2	1.7	3.3	3.7
BGH-290408-P0-2.45-2.65	39.4	-	1.3	-	4.6	1	48	-	3.1	-	2.6
BGH-290408-P0-2.65-2.85	28.9	-	1.2	-	4.8	1.4	56.6	-	4.3	-	2.8
BGH-290408-P0-4.45-4.65	52.4	-	1.8	-	7	1.4	30.9	-	2.5	-	4
BGH-290408-P0-4.65-4.75	57.4	-	3.9	-	6.9	1.1	23.5	-	2.5	-	4.7
BGH-290408-P0-4.90-4.95	52.5	-	5.8	4	-	0.8	24	4.1	2	4.4	2.4
BGH-290408-P0-4.95-5.00	31.6	-	2.5	-	-	2	48.6	2.2	2.9	4.8	5.4
BGH-290408-P0-5.00-5.05	52.7	-	4.3	-	7.2	1.3	25.1	2.4	2.4	-	4.6
BGH-300708-P1-0.60-0.85	20.9	-	2	-	7.4	1.9	59.9	-	3.2	-	4.7
BGH-300708-P1-1.10-1.20	48.6	-	8.5	1.8	-	0.7	26.9	3.4	1.9	4.4	3.8
BGH-300708-P1-1.20-1.50	23.1	-	1.4	-	4.6	1	64.1	-	2.3	-	3.5
BGH-300708-P1-1.50-1.76	21.3	-	1.2	-	4.1	0.7	67.4	-	2.4	-	2.9
BGH-300708-P1-3.20-3.40	25.6	-	1.9	-	6.1	1.5	57.8	-	2.8	-	4.3
BGH-300708-P1-3.40-3.57	52.7	-	3.8	-	6.9	1.4	29.1	-	2.2	-	3.9
BGH-300708-P2-0.00-0.20	47.9	-	3.2	-	8	1.7	32.3	-	2.3	-	4.6
BGH-300708-P2-1.20-1.37	21.8	-	2.5	-	4.4	0.9	64.7	-	2.5	-	3.2
BGH-310708-P3-0.00-0.30	55.1	5	3.7	-	6.6	1.3	26	-	2.3	-	-
BGH-310708-P3-0.30-0.40	19.2	-	1.2	-	7.5	1.6	64.4	-	2.1	-	4
BGH-310708-P3-0.40-0.50	50.5	-	4.8	-	6.8	1.2	31.1	--	1.5	-	4.1

Sample	Amorphous	Brown-millerite	Calcite	Ettringite	Ferrite, magnesian	Hematite	Quartz	Gypsum	Microcline	Magnetite	Srebro-dolskite
BGH-310708-P3-0.95-1.20	22.1	-	3.2	-	4.5	0.9	63.7	-	2.2	-	3.4
BGH-310708-P3-1.20-1.40	22.8	-	1.6	-	5.2	1	63.2	-	2.3	-	3.9
BGH-310708-P3-2.80-3.00	39.6	2	1.2	-	6	1.3	47.3	-	2.5	-	0.1
BGH-310708-P3-3.00-3.20	44.2	1.9	1.2	-	5.7	1.4	42.5	-	3.1	-	-
BGH-310708-P3-3.20-3.30	41.8	-	1.5	-	5	1.1	46.8	-	2.3	-	1.5
BGH-310708-P3-3.30-3.40	25.6	2	1.1	-	5.6	1.3	61.5	-	2.9	-	-
BGH-310708-P3-3.40-3.66	30.8	1	1.6	-	4.3	0.8	59.3	-	2.2	-	-
BGH-310708-P3-4.88-5.08	35.5	-	3.3	-	3.9	0.9	51.5	-	3.1	-	1.8
BGH-310708-P3-5.08-5.20	45.8	-	6.2	-	6.6	1.3	32.4	-	3	-	4.7
BGH-310708-P3-5.20-5.35	42.8	-	4.6	-	5.8	1.1	38.5	-	3.1	-	4.1
BGH-310708-P3-5.35-5.50	27.6	-	2.5	-	3	0.9	60.9	1.1	2.5	-	1.5
BGH-310708-P3-5.50-5.65	19	2.8	3.3	-	4.8	1.2	66.3	-	2.6	-	-
BGH-310708-P3-6.00-6.20	51.5	2	4.6	-	3.9	0.8	33.9	0.8	2.5	-	-
BGH-310708-P3-6.20-6.40	39.4	1.5	3.2	-	3.9	1	47	1.1	2.9	-	-
BGH-310708-P3-6.40-6.60	29.4	1.8	1.4	-	4.3	0.9	59.4	-	2.8	-	-
BGH-310708-P3-6.60-6.80	43.3	1.8	3.2	-	5.2	1.2	42.5	-	2.8	-	-
BGH-310708-P3-6.80-7.03	26.1	1.2	1	-	4.4	1	63.5	-	2.8	-	-
BGH-310708-P3-7.03-7.20	31.9	1.6	3.3	-	2.6	1.1	54.1	1.6	2.7	1.1	-
BGH-310708-P3-7.20-7.36	46	-	4	1.4	4.4	1.3	34.9	2.6	3.1	-	2.3
BGH-310708-P3-7.36-7.60	39.2	-	1.7	-	3.8	1	51.9	-	2.4	-	-
BGH-310708-P3-7.60-7.70	34.1	-	1.1	-	3.9	1.1	57.1	-	2.7	-	-

Table B.33. TIC and calculated CaCO₃ contents of settled ash sediments before CO₂ treatment

	TC/NPOC [g/kg]	IC [g/kg]	CaCO₃ [wt.-%]
BGH-290408-P0-0.00-0.20	406.9	0.5002	0.42
BGH-290408-P0-0.20-0.40	331.6	1.92	1.60
BGH-290408-P0-0.40-0.60	55.93	1.59	1.33
BGH-290408-P0-0.60-0.80	104.2	7.09	5.91
BGH-290408-P0-0.80-1.00	122.2	5.34	4.45
BGH-290408-P0-1.00-1.20	125.5	5.13	4.28
BGH-290408-P0-1.20-1.40	32.86	1.62	1.35
BGH-290408-P0-1.40-1.60	37.49	1.16	0.97
BGH-290408-P0-1.60-1.65	112.1	4.68	3.90
BGH-290408-P0-1.65-1.75	50.79	0.7601	0.63
BGH-290408-P0-1.75-1.85	92.08	1.24	1.03
BGH-290408-P0-1.85-2.05	453.1	1.2	1.00
BGH-290408-P0-2.05-2.25	393.1	1.64	1.37
BGH-290408-P0-2.25-2.45	287.8	1.05	0.88
BGH-290408-P0-2.45-2.65	169.9	1.08	0.90
BGH-290408-P0-2.65-2.85	38.61	0.6345	0.53
BGH-290408-P0-2.85-2.95	14.46	0.5579	0.46
BGH-290408-P0-2.95-3.00	181.5	4.52	3.77
BGH-290408-P0-3.00-3.10	100	0.8712	0.73
BGH-290408-P0-3.10-3.35	271.5	1.06	0.88
BGH-290408-P0-3.35-3.45	157	3.39	2.83
BGH-290408-P0-3.45-3.65	381.6	1.27	1.06
BGH-290408-P0-3.65-3.85	71.33	0.2665	0.22
BGH-290408-P0-3.85-4.05	297.8	0.6333	0.53
BGH-290408-P0-4.05-4.25	253.6	0.641	0.53
BGH-290408-P0-4.25-4.45	193.8	0.8	0.67
BGH-290408-P0-4.45-4.65	168.7	1.41	1.18
BGH-290408-P0-4.65-4.75	143.9	2.85	2.38
BGH-290408-P0-4.75-4.90	88.22	0.8563	0.71
BGH-290408-P0-4.90-4.95	112.4	4.39	3.66
BGH-290408-P0-4.95-5.00	40.54	1.23	1.03
BGH-290408-P0-5.00-5.05	127	1.54	1.28

Table B.34. TIC and calculated CaCO₃ contents of settled ash sediments after CO₂ treatment

	TC/NPOC [g/kg]	IC [g/kg]	CaCO₃ [wt.-%]
BGH-300708-P1-0.00-0.20	361.5	1.1	0.92
BGH-300708-P1-0.20-0.40	115.4	0.3734	0.31
BGH-300708-P1-0.40-0.60	67.45	1.25	1.04
BGH-300708-P1-0.60-0.85	48.78	1.79	1.49
BGH-300708-P1-0.85-0.91	251.5	5.57	4.64
BGH-300708-P1-0.91-1.10	98.44	10.72	8.93
BGH-300708-P1-1.10-1.20	140.8	7.96	6.63
BGH-300708-P1-1.20-1.50	60.03	1	0.83
BGH-300708-P1-1.50-1.76	55.19	1.52	1.27
BGH-300708-P1-2.00-2.20	392.2	2.22	1.85
BGH-300708-P1-2.20-2.40	318	1.74	1.45
BGH-300708-P1-2.40-2.60	247.7	1.12	0.93
BGH-300708-P1-2.60-2.80	90.36	1.45	1.21
BGH-300708-P1-2.80-3.00	44.24	1.44	1.20
BGH-300708-P1-3.00-3.20	35.79	1.21	1.01
BGH-300708-P1-3.20-3.40	90.91	1.27	1.06
BGH-300708-P1-3.40-3.57	151.9	3.1	2.58
BGH-300708-P2-0.00-0.20	133.6	1.49	1.24
BGH-300708-P2-0.20-0.40	42.33	2.55	2.13
BGH-300708-P2-0.40-0.60	204.4	1.55	1.29
BGH-300708-P2-0.60-0.80	97.92	2.34	1.95
BGH-300708-P2-0.80-1.00	146.5	1.8	1.50
BGH-300708-P2-1.00-1.20	67.61	1.25	1.04
BGH-300708-P2-1.20-1.37	60.76	1.53	1.28
BGH-310708-P3-0.00-0.30	206	1.55	1.29
BGH-310708-P3-0.30-0.40	32.91	1.87	1.56
BGH-310708-P3-0.40-0.50	349.5	1.78	1.48
BGH-310708-P3-0.50-0.65	84.97	1.64	1.37
BGH-310708-P3-0.65-0.67	24.18	4.05	3.38
BGH-310708-P3-0.67-0.85	79.9	6.58	5.48
BGH-310708-P3-0.85-0.95	171.8	8.27	6.89
BGH-310708-P3-0.95-1.20	38.16	0.3221	0.27
BGH-310708-P3-1.20-1.40	46.66	1.58	1.32
BGH-310708-P3-1.40-1.60	121.3	1.07	0.89
BGH-310708-P3-2.00-2.20	412.8	2.62	2.18
BGH-310708-P3-2.20-2.40	407.1	1.85	1.54

Appendix B - Tables

BGH-310708-P3-2.40-2.60	184.6	2.02	1.68
BGH-310708-P3-2.60-2.80	159.7	1.93	1.61
BGH-310708-P3-2.80-3.00	241.7	0.8922	0.74
BGH-310708-P3-3.00-3.20	385.3	1.28	1.07
BGH-310708-P3-3.20-3.30	441.1	1.08	0.90
BGH-310708-P3-3.30-3.40	110	0.9595	0.80
BGH-310708-P3-3.40-3.66	160.5	1.69	1.41
BGH-310708-P3-4.00-4.15	414.1	2.05	1.71
BGH-310708-P3-4.15-4.27	291.9	1.67	1.39
BGH-310708-P3-4.27-4.45	262	2.17	1.81
BGH-310708-P3-4.45-4.74	148.1	3.34	2.78
BGH-310708-P3-4.74-4.88	98.31	5.05	4.21
BGH-310708-P3-4.88-5.08	221.1	1.94	1.62
BGH-310708-P3-5.08-5.20	65.16	3.28	2.73
BGH-310708-P3-5.20-5.35	203.6	3.46	2.88
BGH-310708-P3-5.35-5.50	62.76	2.08	1.73
BGH-310708-P3-5.50-5.65	17.13	1.78	1.48
BGH-310708-P3-6.00-6.20	239.2	2.42	2.02
BGH-310708-P3-6.20-6.40	169.9	1.82	1.52
BGH-310708-P3-6.40-6.60	86.28	0.5067	0.42
BGH-310708-P3-6.60-6.80	137.4	1.63	1.36
BGH-310708-P3-6.80-7.03	71.36	1.24	1.03
BGH-310708-P3-7.03-7.20	66.26	3.81	3.18
BGH-310708-P3-7.20-7.36	51.14	2.61	2.18
BGH-310708-P3-7.36-7.60	110.4	1.09	0.91
BGH-310708-P3-7.60-7.70	169.6	1.08	0.90

Table B.35. Chemical composition of Burghammer pore water (main anions and cations, pH) of drilling core BGH-290408-P0 (ash sediment before CO₂ treatment)

Sample	pH	cations							anions				TIC mg/L
		Li ⁺ mg/L	Na ⁺ mg/L	K ⁺ mg/L	Ca ²⁺ mg/L	Mg ²⁺ mg/L	Mn ²⁺ mg/L	NH ₄ ⁺ mg/L	NO ₃ ⁻ mg/L	F ⁻ mg/L	Cl ⁻ mg/L	SO ₄ ²⁻ mg/L	
BGH-290408-P0-0.00-0.20	7.75	-	37.7	25.2	391	23.2	1.11	1.82	-	-	94.2	1680	27.21
BGH-290408-P0-0.20-0.40	7.92	-	41.7	31.8	345	23.2	-	0.56	-	-	92.3	1597	30.51
BGH-290408-P0-0.40-0.60	7.74	0.09	44.6	30.7	292	25.8	-	0.40	-	-	90.5	1550	39.78
BGH-290408-P0-0.60-0.80	7.79	0.08	33.2	28.0	281	27.8	-	3.00	-	-	97.4	1522	42.49
BGH-290408-P0-0.80-1.00	7.32	0.24	37.3	51.8	256	27.3	-	2.32	-	-	88.5	1535	39.35
BGH-290408-P0-1.00-1.20	7.27	-	42.8	109	1140	1.98	-	0.68	-	4.16	86.1	3100	7.78
BGH-290408-P0-1.20-1.40	6.91	-	55.8	115	684	-	-	2.47	-	-	79.5	1795	7.26
BGH-290408-P0-1.40-1.60	8.16	-	58.1	127	489	-	-	2.33	-	-	66.3	1366	4.25
BGH-290408-P0-1.65-1.75	7.01	-	80.9	156	666	2.02	-	0.71	-	-	56.6	2012	6.15
BGH-290408-P0-1.85-2.05	7.87	-	135.1	144	313	2.57	-	1.90	-	3.55	33.2	1158	20.47
BGH-290408-P0-2.05-2.25	7.37	0.18	155.8	173	388	3.24	2.02	0.58	25.3	-	24.8	1380	10.73
BGH-290408-P0-2.25-2.45	6.77	-	164.3	166	464	4.97	3.40	1.70	-	1.48	46.8	1580	7.87
BGH-290408-P0-2.45-2.65	8.28	-	137.4	146	378	2.19	-	1.21	-	-	37.0	1336	2.75
BGH-290408-P0-2.65-2.85	8.87	-	116.4	145	328	2.19	-	1.29	-	-	45.3	1162	2.14
BGH-290408-P0-3.10-3.35	7.25	-	160.9	152	350	23.3	0.80	0.78	-	0.35	45.8	1368	16.71
BGH-290408-P0-3.45-3.65	7.12	-	177.9	159	410	26.7	-	1.10	-	5.03	62.7	1567	20.74
BGH-290408-P0-3.65-3.85	7.32	0.10	197.5	198	422	35.2	-	1.36	-	3.25	150	1581	11.62
BGH-290408-P0-3.85-4.05	7.53	-	177.8	156	276	31.9	-	1.15	-	-	95.0	1110	38.46
BGH-290408-P0-4.05-4.25	7.68	-	185.7	174	278	19.3	-	1.12	-	-	-	-	23.67
BGH-290408-P0-4.45-4.65	7.25	-	-	-	-	-	-	-	-	-	-	-	8.53

Table B.36. Chemical composition of Burghammer pore water (metals / metalloids) of drilling core BGH-290408-P0 (ash sediment before CO₂ treatment)

Sample	Li	Be	Mg	Al	P	Ca	Cr	Mn	Fe	Co	Ni	Cu	Zn
	µg/L	µg/L	µg/L	µg/L	µg/L	µg/L	µg/L	µg/L	µg/L	µg/L	µg/L	µg/L	µg/L
BGH-290408-P0-0.00-0.20	56.77	<DL	237565	54	<DL	363747	<DL	535.63	785.28	3.48	<DL	20.17	43.28
BGH-290408-P0-0.20-0.40	82.11	<DL	235845	114	<DL	330815	<DL	47.37	<DL	2.88	8.72	9.40	37.19
BGH-290408-P0-0.40-0.60	135.34	<DL	252479	130	<DL	265105	<DL	56.84	<DL	3.05	10.28	34.81	39.49
BGH-290408-P0-0.60-0.80	131.98	<DL	285335	106	<DL	259944	<DL	38.32	<DL	2.73	7.95	13.81	33.47
BGH-290408-P0-0.80-1.00	150.62	<DL	283682	111	<DL	246028	<DL	39.74	<DL	2.37	8.07	6.71	33.81
BGH-290408-P0-1.00-1.20	24.24	<DL	6815	359	<DL	693387	<DL	22.71	<DL	6.47	10.17	10.18	53.81
BGH-290408-P0-1.20-1.40	58.53	<DL	3069	826	<DL	650793	<DL	38.79	572.97	6.24	12.56	33.00	89.78
BGH-290408-P0-1.40-1.60	59.88	<DL	2274	1106	<DL	466640	<DL	40.05	535.79	4.61	<DL	107.13	84.46
BGH-290408-P0-1.65-1.75	80.57	<DL	4096	897	<DL	635306	<DL	39.38	623.87	6.39	7.46	7.83	35.70
BGH-290408-P0-1.85-2.05	139.19	<DL	7806	280	<DL	283026	<DL	10.72	443.41	2.86	<DL	6.71	34.37
BGH-290408-P0-2.05-2.25	134.31	<DL	5098	732	<DL	371916	<DL	52.78	524.34	3.63	<DL	10.01	27.24
BGH-290408-P0-2.25-2.45	125.42	0.09	7459	870	<DL	429380	<DL	244.36	955.98	7.61	28.41	43.66	126.08
BGH-290408-P0-2.45-2.65	88.19	<DL	2420	1087	<DL	345121	<DL	3.43	468.17	3.27	<DL	8.95	24.23
BGH-290408-P0-2.65-2.85	87.37	<DL	1059	963	<DL	317732	<DL	16.72	585.48	2.96	<DL	<DL	22.56
BGH-290408-P0-3.10-3.35	99.29	<DL	23350	456	<DL	337023	<DL	45.16	585.13	3.76	7.96	47.30	46.87
BGH-290408-P0-3.45-3.65	109.98	<DL	30002	133	<DL	397454	<DL	86.11	629.93	3.99	11.56	10.14	34.42
BGH-290408-P0-3.65-3.85	138.78	<DL	36903	280	<DL	385683	<DL	45.20	650.32	3.64	<DL	4.79	49.99
BGH-290408-P0-3.85-4.05	107.66	<DL	34344	130	<DL	252690	<DL	24.69	490.03	2.52	9.71	11.35	28.28
BGH-290408-P0-4.05-4.25	105.26	<DL	19306	161	<DL	253267	<DL	19.38	610.55	2.61	<DL	11.33	22.27
BGH-290408-P0-4.45-4.65	90.45	<DL	18849	495	<DL	378355	<DL	25.45	563.46	3.95	11.39	18.39	113.77

Sample	As µg/L	Se µg/L	Rb µg/L	Sr µg/L	Y µg/L	Zr µg/L	Mo µg/L	Ag µg/L	Cd µg/L	Sn µg/L	Sb µg/L	Cs µg/L	Ba µg/L
BGH-290408-P0-0.00-0.20	<DL	<DL	63.42	5899.46	<DL	<DL	7.65	<DL	0.41	0.29	0.53	2.03	86.17
BGH-290408-P0-0.20-0.40	<DL	<DL	90.54	5317.18	<DL	<DL	14.86	<DL	0.55	0.90	0.66	4.61	91.12
BGH-290408-P0-0.40-0.60	<DL	8.08	94.41	5291.20	<DL	<DL	22.23	<DL	0.61	2.29	0.55	3.97	113.66
BGH-290408-P0-0.60-0.80	<DL	11.88	98.19	5866.17	<DL	<DL	33.90	<DL	0.74	1.89	0.56	4.18	96.10
BGH-290408-P0-0.80-1.00	<DL	16.82	142.25	6239.27	<DL	<DL	35.65	<DL	0.62	0.55	0.37	6.05	70.06
BGH-290408-P0-1.00-1.20	<DL	55.77	453.56	11472.69	<DL	<DL	63.05	<DL	0.48	3.65	0.32	48.36	120.28
BGH-290408-P0-1.20-1.40	<DL	52.28	519.22	11046.68	0.36	<DL	53.43	<DL	0.57	1.26	0.51	43.52	131.78
BGH-290408-P0-1.40-1.60	<DL	90.15	597.33	8560.72	<DL	<DL	53.43	<DL	0.40	1.74	0.83	32.83	115.16
BGH-290408-P0-1.65-1.75	3.43	42.80	681.32	11737.67	<DL	<DL	62.78	<DL	0.45	4.14	0.69	42.30	124.29
BGH-290408-P0-1.85-2.05	<DL	32.07	626.71	4602.77	<DL	<DL	35.02	<DL	0.22	1.47	0.62	40.72	78.91
BGH-290408-P0-2.05-2.25	<DL	38.37	754.48	6229.64	<DL	<DL	49.90	<DL	0.53	1.76	0.73	43.55	105.66
BGH-290408-P0-2.25-2.45	<DL	24.43	721.57	6819.23	0.77	<DL	72.54	<DL	2.24	2.50	0.89	34.43	91.69
BGH-290408-P0-2.45-2.65	<DL	42.49	578.94	6133.46	<DL	<DL	62.24	<DL	0.33	2.41	0.62	24.47	93.92
BGH-290408-P0-2.65-2.85	<DL	41.23	507.74	6050.40	<DL	<DL	58.92	<DL	0.44	3.10	0.44	17.44	82.20
BGH-290408-P0-3.10-3.35	<DL	99.56	579.07	5172.86	<DL	<DL	59.72	<DL	0.47	2.84	0.79	27.68	111.29
BGH-290408-P0-3.45-3.65	<DL	26.38	546.99	5839.13	<DL	<DL	33.99	<DL	0.50	0.95	0.54	17.97	84.36
BGH-290408-P0-3.65-3.85	<DL	116.40	515.08	6602.28	<DL	<DL	63.70	<DL	0.67	0.83	0.90	15.78	95.91
BGH-290408-P0-3.85-4.05	<DL	70.82	469.28	4317.14	<DL	<DL	34.22	<DL	0.30	0.72	0.52	14.36	73.39
BGH-290408-P0-4.05-4.25	<DL	75.11	502.34	4106.92	<DL	<DL	47.10	<DL	1.18	1.06	0.64	17.86	76.90
BGH-290408-P0-4.45-4.65	<DL	141.28	550.68	5792.50	<DL	<DL	84.77	<DL	1.15	1.17	1.19	29.74	111.21

Appendix B - Tables

Sample	La µg/L	Ce µg/L	Pr µg/L	W µg/L	Hg µg/L	Tl µg/L	Pb µg/L	Th µg/L	U µg/L
BGH-290408-P0-0.00-0.20	0.08	0.74	<DL	0.70	<DL	<DL	1.28	<DL	2.23
BGH-290408-P0-0.20-0.40	0.04	0.64	<DL	1.65	0.05	<DL	0.64	<DL	6.16
BGH-290408-P0-0.40-0.60	0.12	0.91	0.02	1.54	<DL	0.04	0.30	<DL	13.54
BGH-290408-P0-0.60-0.80	0.10	0.97	<DL	1.44	<DL	0.03	0.67	<DL	11.99
BGH-290408-P0-0.80-1.00	0.15	1.22	<DL	1.68	<DL	<DL	0.65	<DL	9.58
BGH-290408-P0-1.00-1.20	<DL	0.18	<DL	14.93	0.04	<DL	0.34	<DL	0.14
BGH-290408-P0-1.20-1.40	0.18	1.12	0.02	16.59	0.08	<DL	1.65	<DL	0.21
BGH-290408-P0-1.40-1.60	0.13	1.50	0.03	25.02	0.09	0.04	4.61	<DL	0.23
BGH-290408-P0-1.65-1.75	0.13	0.98	0.02	28.12	0.09	0.05	0.46	<DL	0.19
BGH-290408-P0-1.85-2.05	0.07	<DL	<DL	11.63	0.06	0.04	0.49	<DL	0.95
BGH-290408-P0-2.05-2.25	0.10	1.53	0.02	19.30	0.10	0.04	0.35	<DL	0.68
BGH-290408-P0-2.25-2.45	0.23	0.97	0.04	27.37	0.13	0.46	0.63	<DL	0.44
BGH-290408-P0-2.45-2.65	<DL	<DL	<DL	27.84	0.12	<DL	0.50	<DL	0.25
BGH-290408-P0-2.65-2.85	0.06	0.50	<DL	25.04	0.09	<DL	0.40	<DL	0.07
BGH-290408-P0-3.10-3.35	0.08	1.02	<DL	20.24	0.07	0.05	1.63	<DL	2.26
BGH-290408-P0-3.45-3.65	0.11	0.92	0.02	6.43	<DL	<DL	0.59	<DL	1.70
BGH-290408-P0-3.65-3.85	0.12	1.13	0.03	43.34	0.18	0.05	0.38	<DL	2.64
BGH-290408-P0-3.85-4.05	<DL	0.04	<DL	6.03	0.04	0.04	0.64	<DL	3.94
BGH-290408-P0-4.05-4.25	<DL	<DL	<DL	7.19	<DL	<DL	0.33	<DL	3.78
BGH-290408-P0-4.45-4.65	0.10	0.08	<DL	14.50	0.06	0.06	0.63	<DL	0.79

Table B.37. Chemical composition of Burghammer pore water (main anions and cations, pH) of drilling cores BGH-300708-P1 / P2 / P3 (after CO₂ treatment)

	pH	cations							anions				TIC mg/L
		Li ⁺ mg/L	Na ⁺ mg/L	K ⁺ mg/L	Ca ²⁺ mg/L	Mg ²⁺ mg/L	Mn ²⁺ mg/L	NH ₄ ⁺ mg/L	NO ₃ ⁻ mg/L	F ⁻ mg/L	Cl ⁻ mg/L	SO ₄ ²⁻ mg/L	
BGH-300708-P1-0.00-0.20	7.75	-	47.2	22.8	342	170	-	2.99	-	-	85.4	1332	28.38
BGH-300708-P1-0.20-0.40	7.80	-	50.2	26.0	314	210	1.58	-	-	-	94.2	1351	33.51
BGH-300708-P1-0.40-0.60	7.92	-	42.9	37.7	217	193	0.78	0.85	-	-	93.7	1206	12.21
BGH-300708-P1-0.60-0.85	8.76	-	43.6	97.0	404	11.0	-	1.60	-	-	93.2	1038	3.90
BGH-300708-P1-0.85-0.91	7.98	-	88.5	234	395	-	-	7.10	-	-	-	-	-
BGH-300708-P1-0.91-1.10	-	-	-	-	-	-	-	-	-	-	-	-	8.93
BGH-300708-P1-1.10-1.20	-	-	-	-	-	-	-	-	-	-	-	-	5.46
BGH-300708-P1-1.20-1.50	9.30	-	71.5	148	209	-	-	3.63	-	-	49.6	646	4.15
BGH-300708-P1-1.50-1.76	9.74	-	83.1	149	260	-	-	2.73	-	-	36.8	787	3.39
BGH-300708-P1-2.00-2.20	7.37	-	154.8	159	352	31.4	-	3.81	-	-	18.7	1351	-
BGH-300708-P1-2.20-2.40	7.08	-	144.3	152	383	28.3	-	3.13	-	-	16.8	1432	4.30
BGH-300708-P1-2.40-2.60	7.01	-	141.9	146	463	36.8	1.16	5.42	-	-	15.5	1714	3.88
BGH-300708-P1-2.60-2.80	7.17	-	135.3	144	463	52.1	-	4.62	-	-	20.6	1778	4.34
BGH-300708-P1-2.80-3.00	-	-	-	-	-	-	-	-	-	-	-	-	6.38
BGH-300708-P1-3.00-3.20	7.24	-	118.7	130	554	60.9	-	4.37	-	-	37.0	2067	7.20
BGH-300708-P1-3.20-3.40	-	-	-	-	-	-	-	-	-	-	-	-	-
BGH-300708-P1-3.40-3.57	7.27	-	126.9	107	253	23.6	-	5.51	-	-	31.7	1015	11.95
BGH-300708-P2-0.00-0.20	7.80	0.09	60.7	56.6	386	165	-	1.68	-	-	93.1	1493	20.88
BGH-300708-P2-0.20-0.40	7.03	-	62.6	83.4	431	68.3	-	1.69	-	-	94.4	1428	5.66
BGH-300708-P2-0.40-0.60	6.93	-	60.2	95.6	534	32.1	-	0.82	-	-	79.5	1573	6.25
BGH-300708-P2-0.60-0.80	6.91	-	58.9	115	614	15.2	-	1.16	-	-	79.5	1715	4.72

Appendix B - Tables

	pH	cations								anions				TIC	
		Li ⁺ mg/L	Na ⁺ mg/L	K ⁺ mg/L	Li ⁺ mg/L	Na ⁺ mg/L	K ⁺ mg/L	Li ⁺ mg/L	Na ⁺ mg/L	K ⁺ mg/L	Li ⁺ mg/L	Na ⁺ mg/L	K ⁺ mg/L	TIC K ⁺ mg/L	
BGH-300708-P2-0.80-1.00	6.91	-	66.1	128	551	4.04	-	1.02	-	-	75.1	1546	-	5.05	
BGH-300708-P2-1.00-1.20	7.58	0.14	67.3	169	490	7.37	0.00	4.61	-	-	122	1436	-	7.01	
BGH-300708-P2-1.20-1.37	-	-	-	-	-	-	-	-	-	-	-	-	-	-	
BGH-310708-P3-0.00-0.30	7.64	-	37.2	28.6	270	224	-	0.74	-	-	96.8	1176	-	45.05	
BGH-310708-P3-0.30-0.40	7.38	-	42.9	30.7	270	209	2.01	0.69	-	-	107	1320	-	31.20	
BGH-310708-P3-0.40-0.50	7.57	-	37.1	49.0	198	181	1.85	1.81	1.32	-	115	1235	-	27.33	
BGH-310708-P3-0.50-0.65	6.65	0.47	39.8	52.1	232	70.7	-	4.08	-	-	88.8	847	-	6.65	
BGH-310708-P3-0.65-0.67	-	-	-	-	-	-	-	-	-	-	-	-	-	-	
BGH-310708-P3-0.67-0.85	7.32	-	55.1	121	316	-	-	2.16	-	-	-	-	-	11.48	
BGH-310708-P3-0.85-0.95	-	-	-	-	-	-	-	-	-	-	-	-	-	-	
BGH-310708-P3-0.95-1.20	9.60	-	67.6	133	210	-	-	1.26	-	-	50.1	603	-	3.47	
BGH-310708-P3-1.20-1.40	8.63	-	79.0	137	202	0.63	-	-	-	-	33.3	642	-	3.22	
BGH-310708-P3-1.40-1.60	7.29	-	141.4	388	231	35.9	-	18.8	-	-	16.6	1079	-	3.56	
BGH-310708-P3-2.00-2.20	7.08	-	144.1	107	145	19.2	-	1.94	-	-	18.8	745	-	20.47	
BGH-310708-P3-2.20-2.40	6.87	0.28	149.2	124	130	12.7	-	1.32	-	-	18.8	774	-	6.89	
BGH-310708-P3-2.40-2.60	7.27	0.04	156.2	125	143	17.3	-	3.87	-	-	28.5	766	-	10.50	
BGH-310708-P3-2.60-2.80	7.39	-	149.8	110	178	2.86	-	4.16	-	-	43.7	769	-	6.32	
BGH-310708-P3-2.80-3.00	6.44	-	156.9	113	178	4.59	-	-	-	-	58.2	758	-	3.59	
BGH-310708-P3-3.00-3.20	7.34	-	149.4	110	165	8.17	-	4.65	-	-	36.2	769	-	17.49	
BGH-310708-P3-3.20-3.30	-	-	-	-	-	-	-	-	-	-	-	-	-	36.40	
BGH-310708-P3-3.40-3.66	7.50	-	153.6	132	221	65.5	-	6.34	4.12	-	60.7	860	-	79.78	
BGH-310708-P3-4.00-4.15	7.46	0.17	153.1	134	281	73.3	-	10.68	11.2	-	104	1164	-	43.97	
BGH-310708-P3-4.15-4.27	7.95	0.22	154.7	141	201	71.8	-	7.54	-	-	97.2	968	-	42.60	

	pH	cations							anions				TIC mg/L
		Li ⁺ mg/L	Na ⁺ mg/L	K ⁺ mg/L	Ca ²⁺ mg/L	Mg ²⁺ mg/L	Mn ²⁺ mg/L	NH ₄ ⁺ mg/L	NO ₃ ⁻ mg/L	F ⁻ mg/L	Cl ⁻ mg/L	SO ₄ ²⁻ mg/L	
BGH-310708-P3-4.27-4.45	7.52	-	169.2	162	209	19.7	-	3.97	3.97	-	136	934	10.11
BGH-310708-P3-4.45-4.74	7.60	0.17	191.3	177	459	135	-	8.35	1.29	-	124	2109	21.94
BGH-310708-P3-4.74-4.88	-	0.17	191.3	177	459	135	-	8.35	-	-	106	2291	6.62
BGH-310708-P3-4.88-5.08	7.34	0.52	183.3	167	554	199	-	5.00	3.04	2.23	108	2431	78.14
BGH-310708-P3-5.08-5.20	7.78	0.21	186.3	164	526	308	-	6.72	1.38	3.19	137	2630	71.83
BGH-310708-P3-5.20-5.35	7.76	0.51	192.0	183	540	398	-	4.52	-	3.46	158	2996	98.61
BGH-310708-P3-5.35-5.50	7.34	0.66	170.6	138	557	306	-	8.37	-	1.99	145	2444	126.78
BGH-310708-P3-5.50-5.65	7.69	0.88	158.0	115	561	524	-	5.44	-	4.43	171	3245	113.81
BGH-310708-P3-6.00-6.20	7.95	0.38	152.4	145	601	237	-	5.61	-	0.89	151	2708	69.03
BGH-310708-P3-6.20-6.40	7.62	0.48	180.9	183	552	351	-	6.11	-	3.71	159	2759	121.26
BGH-310708-P3-6.40-6.60	7.57	0.65	175.0	167	543	236	3.27	8.33	-	2.29	167	2336	88.44
BGH-310708-P3-6.60-6.80	7.45	0.28	193.9	205	653	139	-	6.60	-	3.12	173	2473	25.49
BGH-310708-P3-6.80-7.03	7.54	0.64	174.6	167	510	239	-	6.54	-	2.09	187	2189	83.07
BGH-310708-P3-7.03-7.20	7.64	0.81	158.9	164	696	230	-	4.80	-	4.39	213	2585	52.16
BGH-310708-P3-7.20-7.36	7.46	-	161.6	201	702	13.7	-	9.21	2.60	4.29	166	1675	-
BGH-310708-P3-7.36-7.60	-	0.41	174.0	184	573	191	-	8.95	-	-	219	2250	70.31
BGH-310708-P3-7.60-7.70	8.02	0.13	180.2	151	366	76.7	-	9.73	-	-	232	1370	36.15

Table B.38. Chemical composition of Burghammer pore water (metals / metalloids) of drilling cores BGH-300708-P1 /P2 / P3 (ash sediment after CO₂ treatment)

	Li µg/L	Be µg/L	Mg µg/L	Al µg/L	P µg/L	Ca µg/L	Cr µg/L	Mn µg/L	Fe µg/L	Co µg/L	Ni µg/L	Cu µg/L	Zn µg/L
BGH-300708-P1-0.60-0.85	47.10	<DL	14332	443	<DL	367584	<DL	19.75	512.46	3.22	<DL	<DL	16.07
BGH-300708-P1-1.10-1.20	<DL	<DL	335	791	<DL	340590	<DL	<DL	572.53	2.96	<DL	<DL	10.98
BGH-300708-P1-1.20-1.50	32.91	<DL	807	2004	<DL	198924	<DL	23.40	595.29	1.98	<DL	<DL	20.47
BGH-300708-P1-1.50-1.76	46.00	<DL	398	1494	<DL	247062	<DL	17.28	575.81	2.18	<DL	<DL	16.31
BGH-300708-P1-3.20-3.40	113.28	<DL	168424	291	<DL	405375	<DL	38.42	572.42	3.71	<DL	<DL	24.66
BGH-300708-P1-3.40-3.57	132.21	<DL	23759	221	<DL	231411	<DL	69.91	588.62	1.92	<DL	8.75	25.78
BGH-300708-P2-0.00-0.20	55.57	<DL	162364	101	<DL	342973	<DL	158.57	1231.65	3.28	<DL	429.37	274.19
BGH-300708-P2-1.20-1.37	44.91	<DL	2834	781	<DL	459246	<DL	14.51	<DL	4.15	<DL	117.59	85.11
BGH-310708-P3-0.00-0.30	109.30	<DL	233677	84	<DL	212657	<DL	169.25	514.60	1.91	<DL	<DL	18.07
BGH-310708-P3-0.30-0.40	107.04	<DL	223220	131	<DL	245970	<DL	68.91	541.03	2.15	<DL	4.55	23.39
BGH-310708-P3-0.40-0.50	132.77	<DL	190514	126	<DL	166830	<DL	74.06	490.54	1.45	<DL	11.50	28.35
BGH-310708-P3-0.50-0.65	122.38	<DL	77345	224	<DL	221794	<DL	43.19	501.21	1.95	<DL	<DL	14.69
BGH-310708-P3-0.65-0.67	35.25	<DL	4960	232	<DL	524696	<DL	14.93	591.01	4.72	<DL	13.60	25.99
BGH-310708-P3-0.67-0.85	17.72	<DL	2326	479	<DL	306473	<DL	24.12	463.47	2.79	<DL	<DL	14.05
BGH-310708-P3-0.85-0.95	13.08	<DL	8336	697	<DL	320026	<DL	20.45	472.38	2.89	<DL	6.80	20.62
BGH-310708-P3-0.95-1.20	18.14	<DL	1730	1930	<DL	211597	<DL	33.73	517.86	2.02	<DL	<DL	12.41
BGH-310708-P3-1.20-1.40	43.37	<DL	1047	1350	<DL	199860	<DL	14.59	504.38	1.76	<DL	19.43	26.00
BGH-310708-P3-1.40-1.60	78.42	0.21	15925	934	<DL	291303	<DL	64.26	677.31	3.02	<DL	21.64	791.10
BGH-310708-P3-2.00-2.20	202.57	<DL	20552	154	<DL	132792	<DL	43.06	522.75	1.19	<DL	19.92	26.43
BGH-310708-P3-2.20-2.40	242.14	<DL	13709	371	<DL	122358	<DL	35.92	513.24	1.16	<DL	74.76	70.29
BGH-310708-P3-2.40-2.60	142.03	<DL	15258	456	<DL	135700	<DL	17.62	519.62	1.32	<DL	212.42	143.08

Sample	Li µg/L	Be µg/L	Mg µg/L	Al µg/L	P µg/L	Ca µg/L	Cr µg/L	Mn µg/L	Fe µg/L	Co µg/L	Ni µg/L	Cu µg/L	Zn µg/L
BGH-310708-P3-2.60-2.80	56.76	<DL	3351	1054	<DL	175338	<DL	22.30	669.33	1.71	<DL	<DL	17.90
BGH-310708-P3-2.80-3.00	77.70	<DL	3030	792	<DL	165063	<DL	42.71	570.33	1.53	<DL	4.40	19.86
BGH-310708-P3-3.00-3.20	118.38	<DL	11115	277	<DL	164973	<DL	48.09	569.97	1.64	<DL	<DL	24.01
BGH-310708-P3-3.20-3.30	59.70	<DL	37279	45	<DL	215565	<DL	211.38	573.67	1.95	<DL	<DL	22.61
BGH-310708-P3-3.40-3.66	174.14	<DL	64516	31	<DL	208154	<DL	241.67	1024.99	2.07	<DL	<DL	24.38
BGH-310708-P3-4.00-4.15	192.22	<DL	70420	33	<DL	257072	<DL	229.84	478.36	2.44	<DL	<DL	21.83
BGH-310708-P3-4.15-4.27	233.84	<DL	78513	103	<DL	192117	<DL	124.81	572.38	1.83	<DL	<DL	24.21
BGH-310708-P3-4.27-4.45	144.89	<DL	21315	197	<DL	198633	<DL	37.84	530.37	1.98	<DL	40.10	39.64
BGH-310708-P3-4.45-4.74	289.02	<DL	144125	143	<DL	437666	<DL	126.41	649.47	4.10	<DL	<DL	31.14
BGH-310708-P3-4.74-4.88	73.78	<DL	6126	413	<DL	575503	<DL	31.19	613.26	5.39	<DL	75.20	67.98
BGH-310708-P3-4.88-5.08	438.87	<DL	206391	82	<DL	522772	<DL	313.91	677.69	5.17	<DL	<DL	36.22
BGH-310708-P3-5.08-5.20	365.84	<DL	321938	165	<DL	505869	<DL	332.99	600.80	4.70	<DL	<DL	29.45
BGH-310708-P3-5.20-5.35	661.64	<DL	415444	<DL	<DL	531138	<DL	512.58	471.65	5.37	<DL	7.70	50.21
BGH-310708-P3-5.35-5.50	767.97	<DL	333842	117	<DL	598287	<DL	461.91	621.50	5.88	<DL	10.91	45.76
BGH-310708-P3-5.50-5.65	848.39	<DL	560619	33	<DL	533844	<DL	294.24	446.69	5.14	<DL	<DL	41.00
BGH-310708-P3-6.00-6.20	376.26	<DL	242457	76	<DL	565137	<DL	380.86	625.85	5.41	<DL	<DL	38.52
BGH-310708-P3-6.20-6.40	623.37	<DL	373914	23	<DL	542237	<DL	319.42	458.57	5.18	<DL	<DL	39.08
BGH-310708-P3-6.40-6.60	657.50	<DL	237114	12	<DL	542322	<DL	291.88	<DL	5.31	<DL	<DL	43.74
BGH-310708-P3-6.60-6.80	399.82	<DL	143360	193	<DL	591129	<DL	209.45	475.55	5.34	<DL	<DL	29.53
BGH-310708-P3-6.80-7.03	390.45	<DL	247586	158	<DL	485592	<DL	176.42	522.47	4.53	<DL	14.83	37.84
BGH-310708-P3-7.03-7.20	698.41	<DL	242714	159	<DL	633925	<DL	172.46	519.19	5.85	<DL	<DL	33.22
BGH-310708-P3-7.20-7.36	159.66	<DL	16585	1056	<DL	635494	<DL	38.88	760.19	6.04	11.33	27.41	42.47
BGH-310708-P3-7.36-7.60	390.41	<DL	193135	104	<DL	576172	<DL	319.77	483.87	5.69	<DL	<DL	29.58
BGH-310708-P3-7.60-7.70	141.24	<DL	75821	104	<DL	338883	<DL	145.28	<DL	3.33	<DL	25.75	36.02

Appendix B - Tables

	As	Se	Rb	Sr	Y	Zr	Mo	Ag	Cd	Sn	Sb	Cs	Ba
	µg/L	µg/L	µg/L	µg/L	µg/L	µg/L	µg/L	µg/L	µg/L	µg/L	µg/L	µg/L	µg/L
BGH-300708-P1-0.60-0.85	<DL	64.82	424.17	6973.87	<DL	<DL	45.56	<DL	<DL	1.92	0.48	14.45	97.41
BGH-300708-P1-1.10-1.20	<DL	27.28	411.32	9615.99	<DL	<DL	59.61	<DL	0.26	2.55	0.11	47.41	99.51
BGH-300708-P1-1.20-1.50	<DL	39.64	627.24	6265.84	<DL	<DL	49.15	<DL	0.30	2.85	0.58	36.09	94.08
BGH-300708-P1-1.50-1.76	4.46	85.25	689.41	7265.19	<DL	<DL	52.32	<DL	<DL	1.22	0.68	30.14	105.57
BGH-300708-P1-3.20-3.40	<DL	16.63	387.17	8157.69	<DL	<DL	42.55	<DL	0.45	1.88	0.51	20.43	110.85
BGH-300708-P1-3.40-3.57	<DL	20.18	440.51	3733.72	<DL	<DL	33.40	<DL	0.21	1.50	0.63	22.84	71.56
BGH-300708-P2-0.00-0.20	<DL	<DL	157.82	5526.36	<DL	0.56	20.28	<DL	0.37	1.52	0.59	8.75	79.31
BGH-300708-P2-1.20-1.37	<DL	52.08	514.81	9012.48	<DL	<DL	48.21	<DL	0.36	2.51	0.58	25.40	118.85
BGH-310708-P3-0.00-0.30	<DL	<DL	86.65	4170.03	<DL	<DL	39.60	<DL	0.20	0.55	0.30	4.10	70.70
BGH-310708-P3-0.30-0.40	<DL	5.26	100.39	4374.80	<DL	<DL	41.96	<DL	0.34	2.18	0.89	4.12	77.38
BGH-310708-P3-0.40-0.50	<DL	5.24	205.98	4037.19	<DL	<DL	45.24	<DL	0.29	1.01	0.50	14.95	63.30
BGH-310708-P3-0.50-0.65	<DL	<DL	314.39	5035.04	<DL	<DL	35.02	<DL	0.26	2.42	0.41	14.41	73.42
BGH-310708-P3-0.65-0.67	<DL	24.05	468.52	10038.05	<DL	<DL	51.17	<DL	0.20	22.40	0.17	14.67	120.86
BGH-310708-P3-0.67-0.85	<DL	18.16	470.69	6298.20	<DL	<DL	44.15	<DL	<DL	8.48	0.17	23.54	73.48
BGH-310708-P3-0.85-0.95	<DL	25.25	589.03	8589.03	<DL	<DL	56.17	<DL	0.18	3.81	0.19	65.70	119.58
BGH-310708-P3-0.95-1.20	3.11	33.14	674.06	6484.87	<DL	<DL	51.84	<DL	0.43	2.42	0.39	51.48	94.07
BGH-310708-P3-1.20-1.40	<DL	85.77	634.49	3721.78	<DL	<DL	58.25	<DL	<DL	2.81	0.74	23.76	75.86
BGH-310708-P3-1.40-1.60	<DL	18.99	669.84	4153.81	4.32	<DL	53.72	<DL	3.54	6.06	0.86	36.88	105.78
BGH-310708-P3-2.00-2.20	<DL	4.37	494.64	2549.07	<DL	<DL	27.85	<DL	0.22	2.12	0.48	22.93	69.85
BGH-310708-P3-2.20-2.40	<DL	4.21	512.27	2410.12	<DL	<DL	37.95	<DL	1.79	4.91	0.63	19.52	69.17
BGH-310708-P3-2.40-2.60	<DL	38.20	522.75	2687.41	<DL	<DL	44.39	<DL	0.25	1.33	0.73	20.89	70.97
BGH-310708-P3-2.60-2.80	<DL	23.03	502.58	2787.20	<DL	<DL	62.28	<DL	0.28	1.30	0.65	22.35	54.28
BGH-310708-P3-2.80-3.00	3.43	25.05	420.82	2650.96	<DL	<DL	59.36	<DL	0.27	2.66	0.62	12.83	53.34

Sample	As	Se	Rb	Sr	Y	Zr	Mo	Ag	Cd	Sn	Sb	Cs	Ba
	µg/L	µg/L	µg/L	µg/L	µg/L	µg/L	µg/L	µg/L	µg/L	µg/L	µg/L	µg/L	µg/L
BGH-310708-P3-3.00-3.20	<DL	14.29	456.30	2796.55	<DL	<DL	41.20	<DL	0.28	0.96	0.69	17.82	78.89
BGH-310708-P3-3.20-3.30	<DL	5.09	364.14	3446.19	<DL	<DL	15.26	<DL	<DL	0.66	0.33	12.53	65.99
BGH-310708-P3-3.40-3.66	<DL	<DL	439.99	3491.96	<DL	<DL	11.34	0.26	<DL	0.67	0.39	13.42	69.21
BGH-310708-P3-4.00-4.15	<DL	<DL	443.44	4740.13	<DL	<DL	7.30	<DL	0.22	1.05	0.22	15.83	77.76
BGH-310708-P3-4.15-4.27	<DL	<DL	471.68	4088.24	<DL	<DL	21.58	<DL	0.28	1.09	0.37	16.51	84.84
BGH-310708-P3-4.27-4.45	<DL	38.76	510.94	3385.34	<DL	<DL	41.95	<DL	0.26	2.48	0.64	16.79	79.52
BGH-310708-P3-4.45-4.74	<DL	11.31	626.84	7210.66	<DL	<DL	30.22	<DL	0.43	0.84	0.60	34.31	95.72
BGH-310708-P3-4.74-4.88	<DL	57.53	749.17	11756.00	<DL	<DL	46.74	<DL	0.21	2.23	0.47	40.01	89.59
BGH-310708-P3-4.88-5.08	<DL	<DL	554.81	7130.96	<DL	<DL	14.65	<DL	<DL	2.60	0.60	38.56	101.41
BGH-310708-P3-5.08-5.20	<DL	9.87	543.62	7063.90	<DL	0.69	41.15	<DL	0.31	0.97	0.73	37.55	81.56
BGH-310708-P3-5.20-5.35	<DL	<DL	547.64	6445.43	<DL	<DL	32.04	<DL	0.31	0.36	0.75	35.33	82.22
BGH-310708-P3-5.35-5.50	<DL	9.51	470.77	5726.37	<DL	1.45	41.22	<DL	0.38	1.83	1.18	26.11	107.02
BGH-310708-P3-5.50-5.65	<DL	11.06	393.58	5636.11	<DL	<DL	66.01	<DL	0.42	0.52	1.24	20.11	88.78
BGH-310708-P3-6.00-6.20	<DL	6.43	537.55	7339.32	<DL	<DL	24.13	<DL	0.50	1.32	0.65	36.05	102.43
BGH-310708-P3-6.20-6.40	<DL	9.87	615.56	7073.53	<DL	0.51	26.66	<DL	0.18	1.21	0.80	37.85	100.25
BGH-310708-P3-6.40-6.60	<DL	8.41	626.39	8051.77	<DL	<DL	27.21	<DL	0.62	0.63	1.11	27.71	98.91
BGH-310708-P3-6.60-6.80	<DL	10.20	757.98	9920.18	<DL	<DL	24.95	<DL	0.35	3.48	0.93	29.94	107.73
BGH-310708-P3-6.80-7.03	<DL	15.64	609.49	8688.11	<DL	0.49	55.64	<DL	0.36	0.73	1.70	22.18	101.56
BGH-310708-P3-7.03-7.20	<DL	10.89	569.74	7961.51	<DL	<DL	41.60	<DL	0.44	1.61	1.29	26.14	116.49
BGH-310708-P3-7.20-7.36	<DL	18.08	625.47	10922.32	<DL	<DL	52.87	<DL	0.40	4.02	0.82	30.69	128.68
BGH-310708-P3-7.36-7.60	<DL	8.55	582.97	11256.32	<DL	<DL	40.29	<DL	0.31	0.45	1.08	25.19	66.44
BGH-310708-P3-7.60-7.70	<DL	11.28	455.15	6738.36	<DL	<DL	41.18	<DL	0.33	4.21	1.43	13.30	100.03

Appendix B - Tables

Sample	La µg/L	Ce µg/L	Pr µg/L	W µg/L	Hg µg/L	Tl µg/L	Pb µg/L	Th µg/L	U µg/L
BGH-300708-P1-0.60-0.85	0.09	0.20	<DL	23.30	0.10	<DL	0.44	<DL	0.44
BGH-300708-P1-1.10-1.20	<DL	<DL	<DL	14.86	0.09	0.04	0.22	<DL	0.04
BGH-300708-P1-1.20-1.50	0.07	0.31	<DL	28.05	0.14	<DL	0.31	<DL	0.06
BGH-300708-P1-1.50-1.76	0.06	0.34	<DL	33.94	0.16	0.03	0.80	<DL	0.08
BGH-300708-P1-3.20-3.40	<DL	0.17	<DL	6.99	0.06	<DL	0.44	<DL	4.47
BGH-300708-P1-3.40-3.57	0.04	0.10	<DL	10.60	0.06	<DL	0.93	<DL	0.48
BGH-300708-P2-0.00-0.20	<DL	0.07	<DL	1.94	<DL	0.03	20.60	0.06	5.87
BGH-300708-P2-1.20-1.37	0.08	0.14	<DL	28.34	0.10	<DL	4.07	<DL	0.16
BGH-310708-P3-0.00-0.30	0.11	0.31	0.02	3.19	<DL	<DL	0.24	<DL	10.58
BGH-310708-P3-0.30-0.40	0.06	0.15	<DL	2.83	0.06	<DL	0.49	<DL	14.35
BGH-310708-P3-0.40-0.50	0.05	0.18	0.05	9.77	0.06	<DL	0.90	<DL	2.61
BGH-310708-P3-0.50-0.65	<DL	0.20	<DL	12.24	0.05	<DL	0.20	<DL	1.62
BGH-310708-P3-0.65-0.67	<DL	<DL	<DL	19.88	0.34	<DL	1.11	<DL	0.15
BGH-310708-P3-0.67-0.85	0.09	0.34	0.02	22.24	0.12	<DL	0.30	<DL	0.16
BGH-310708-P3-0.85-0.95	0.11	0.18	<DL	25.73	0.14	<DL	0.55	<DL	0.61
BGH-310708-P3-0.95-1.20	0.16	0.90	0.03	37.43	0.16	<DL	0.18	<DL	0.09
BGH-310708-P3-1.20-1.40	<DL	0.11	<DL	46.57	0.26	<DL	1.18	<DL	0.08
BGH-310708-P3-1.40-1.60	3.77	7.56	0.96	22.37	0.12	<DL	17.20	<DL	0.33
BGH-310708-P3-2.00-2.20	<DL	<DL	<DL	6.24	0.06	<DL	1.09	<DL	0.95
BGH-310708-P3-2.20-2.40	<DL	<DL	<DL	11.62	0.08	<DL	4.14	<DL	0.32
BGH-310708-P3-2.40-2.60	<DL	<DL	<DL	15.42	0.10	0.03	8.89	<DL	0.85
BGH-310708-P3-2.60-2.80	0.09	0.45	<DL	41.82	0.17	0.03	0.49	<DL	0.26
BGH-310708-P3-2.80-3.00	0.13	1.69	0.02	36.76	0.14	<DL	0.72	<DL	0.28
BGH-310708-P3-3.00-3.20	0.04	0.12	<DL	8.93	0.06	<DL	0.71	<DL	1.08

Sample	La µg/L	Ce µg/L	Pr µg/L	W µg/L	Hg µg/L	Tl µg/L	Pb µg/L	Th µg/L	U µg/L
BGH-310708-P3-3.20-3.30	0.10	0.09	<DL	1.45	<DL	<DL	1.64	<DL	2.12
BGH-310708-P3-3.40-3.66	0.06	0.07	<DL	1.56	<DL	0.04	0.57	<DL	4.51
BGH-310708-P3-4.00-4.15	<DL	0.09	<DL	1.01	0.05	<DL	0.24	<DL	1.02
BGH-310708-P3-4.15-4.27	0.32	0.42	<DL	1.90	<DL	0.07	0.36	<DL	5.63
BGH-310708-P3-4.27-4.45	0.42	0.16	<DL	7.66	0.05	0.05	1.80	<DL	1.20
BGH-310708-P3-4.45-4.74	<DL	0.11	<DL	3.62	0.06	0.07	0.37	<DL	4.08
BGH-310708-P3-4.74-4.88	0.10	0.16	<DL	18.94	0.07	0.10	2.32	<DL	0.24
BGH-310708-P3-4.88-5.08	<DL	0.06	<DL	1.94	<DL	0.09	0.39	<DL	16.36
BGH-310708-P3-5.08-5.20	0.03	0.10	<DL	3.71	0.04	0.10	0.21	0.08	24.91
BGH-310708-P3-5.20-5.35	<DL	<DL	<DL	0.87	<DL	0.08	<DL	<DL	22.92
BGH-310708-P3-5.35-5.50	0.06	0.09	<DL	3.95	0.12	0.13	1.35	<DL	44.79
BGH-310708-P3-5.50-5.65	<DL	<DL	<DL	6.11	<DL	0.06	<DL	<DL	46.52
BGH-310708-P3-6.00-6.20	0.05	0.13	<DL	2.65	<DL	0.09	0.18	<DL	15.09
BGH-310708-P3-6.20-6.40	<DL	<DL	<DL	3.58	<DL	0.09	<DL	<DL	39.81
BGH-310708-P3-6.40-6.60	<DL	<DL	<DL	2.87	<DL	0.15	0.11	<DL	43.26
BGH-310708-P3-6.60-6.80	0.10	0.14	<DL	4.98	0.08	0.14	0.17	<DL	12.63
BGH-310708-P3-6.80-7.03	<DL	0.11	<DL	4.64	<DL	0.11	0.95	<DL	72.78
BGH-310708-P3-7.03-7.20	0.10	0.20	0.03	8.48	0.09	0.14	0.27	<DL	36.83
BGH-310708-P3-7.20-7.36	0.04	0.39	<DL	33.85	0.14	0.07	1.81	<DL	0.65
BGH-310708-P3-7.36-7.60	0.06	0.07	<DL	2.64	0.05	0.13	0.29	<DL	44.83
BGH-310708-P3-7.60-7.70	0.05	0.13	<DL	2.58	0.07	0.09	1.50	<DL	22.01

Appendix B - Tables

Table B.39. Results of SEM-EDX investigations before CO₂ injection

Sample	Depth [cm]	Label	Element content [wt.-%]								Oxide contents [wt.-%]										
			Mg	Al	Si	Ca	Fe	S	K	Na	Ti	O	MgO	Al ₂ O ₃	SiO ₂	CaO	Fe ₂ O ₃	SO ₃	K ₂ O	Na ₂ O	TiO ₂
P0	0 - 20	M1	1.04	4.56	25.21	5.3	16.88	1.48	0.4	-	-	45.13	1.73	8.61	53.94	7.41	24.14	3.69	0.48	-	-
		M2	0.2	0.54	0.93	62.07	6.11	0.35	0.13	-	-	51.63	0.32	1.02	1.99	86.85	8.74	0.86	0.22	-	-
		M3	0.1	0.99	1.29	0.65	36.6	0.06	0.26	-	-	60.04	0.13	1.63	2.5	1.17	94.02	0.15	0.4	-	-
		M4	0.77	12.95	23.84	2.76	9.47	0.23	3.21	-	0.85	45.92	1.28	24.46	50.99	3.86	13.54	0.58	3.87	-	1.42
		M5	2.05	1.15	2.42	45.29	10.02	4.38	0.49	-	-	34.19	3.4	2.18	5.18	63.37	14.33	10.95	0.59	-	-
		M6	1.38	8.13	14.64	7.27	25.63	0.1	1.6	-	1.22	40.03	2.29	15.36	31.31	10.18	36.64	0.25	1.93	-	2.04
		M7	4.28	1.96	4	17.02	29.41	5.88	0.09	-	-	37.37	7.1	3.7	8.55	23.81	42.05	14.68	0.11	-	-
P0	100 - 120	M8	0.73	4.14	1.74	37.64	3.43	11.88	0.03	-	-	40.43	1.21	7.82	3.72	52.66	4.9	29.66	0.04	-	-
		M9	1.55	1.36	3.26	44.15	7.19	6.22	0.24	-	-	36.03	2.57	2.57	6.98	61.77	10.28	15.54	0.29	-	-
		M10	2.19	1.55	9.4	17.85	29.77	2.28	0.09	-	-	36.87	3.63	2.92	20.1	24.98	42.56	5.7	0.11	-	-
P0	120 - 140	M11	1.79	11.44	21.04	5.72	10.3	0.13	5.15	-	0.68	43.74	2.97	21.61	45.02	8.01	14.73	0.33	6.2	-	1.13
		M12	5.8	2.86	2.99	5.65	49.33	-	0.11	0.02	-	33.25	9.62	5.41	6.39	7.9	70.53	0.13	0.02	-	-
		M13	1	1.59	5.46	18.13	39.82	0.17	0.07	0.13	0.4	33.23	1.66	3.01	11.69	25.36	56.94	0.42	0.09	0.17	0.66
		M14	0.59	0.78	42.52	2.29	2.04	0.04	0.28	0.02	-	51.44	0.97	1.47	90.95	3.2	2.92	0.11	0.34	0.03	-
		M15	3.72	5.33	2.2	25.28	17.95	7.22	-	-	-	38.3	-	10.07	4.7	35.37	25.67	18.02	-	-	-
		M16	0.18	0.3	0.97	0.57	66.69	0.1	0.04	0.44	-	30.7	0.3	0.57	2.07	0.8	95.34	0.26	0.05	0.6	-
P0	205 - 225	M17	1.94	2.97	3.92	10.43	47.28	-	0.47	-	-	32.97	3.22	5.62	8.39	14.6	67.6	-	0.57	-	-
		M18	0.62	6.79	24.33	1.36	1.46	-	24.99	-	-	40.45	1.03	12.82	52.06	1.91	2.09	-	30.1	-	-
		M19	1.88	3.86	7.89	32.19	6.99	6.28	1.66	-	-	39.26	3.11	7.3	16.88	45.03	9.99	15.69	2	-	-
		M20	0.84	14.04	25.38	1.56	4.59	0.06	6.13	-	0.91	46.5	1.4	26.53	54.31	2.18	6.56	0.14	7.38	-	1.51
		M21	0.16	0.19	67.64	0.42	1.56	0.13	-	-	-	29.9	-	0.29	0.41	94.65	0.6	3.89	0.15	-	-
P0	245 - 265	M22	0.41	0.79	44.09	0.78	1.33	-	0.11	0.23	0.06	52.22	0.68	1.48	94.31	1.09	1.9	-	0.13	0.31	0.1
		M23	0.62	12.11	28.17	3.22	2.46	0.3	1.51	0.14	3.04	48.44	1.02	22.87	60.26	4.51	3.52	0.74	1.82	0.19	5.07
		M24	0.84	6.62	5.74	31.76	19.65	0.44	-	-	0.11	34.84	1.39	12.52	12.29	44.44	28.09	1.1	-	-	0.19
		M25	1.68	5.51	10.17	14.33	29.39	0.19	0.66	0.25	0.81	37	2.79	10.41	21.76	20.06	42.02	0.49	0.79	0.33	1.35

Sample	Depth	Label	Element content										Oxide contents								
			[wt.-%]										[wt.-%]								
			Mg	Al	Si	Ca	Fe	S	K	Na	Ti	O	MgO	Al ₂ O ₃	SiO ₂	CaO	Fe ₂ O ₃	SO ₃	K ₂ O	Na ₂ O	TiO ₂
P0	265 - 285	M26	4.88	5.43	7.82	15.23	30.06	-	0.28	-	0.17	36.12	8.09	10.26	16.73	21.31	42.98	-	0.34	-	0.29
		M27	0.47	6.3	9.32	1.59	44.65	-	0.67	0.25	0.12	36.65	0.78	11.9	19.93	2.22	63.83	-	0.81	0.33	0.2
		M28	0.24	0.2	45.92	0.23	0.08	-	0.21	0.21	-	52.9	0.4	0.37	98.24	0.33	0.12	-	0.25	0.29	-
		M29	1.38	9.32	19.17	8.66	11.02	-	8.4	0.05	0.62	41.38	-	17.6	41	-	15.76	-	10.12	0.06	1.04
P0	300 - 310	M30	0.9	1.76	1.44	30.37	34.47	0.12	-	-	-	30.92	1.5	3.33	3.09	42.5	49.28	0.3	-	-	-
		M31	1.11	1.97	22.21	13.68	18.8	-	0.74	-	-	41.48	1.84	3.73	47.51	19.15	26.88	-	0.89	-	-
		M32	0.51	1.33	3.9	0.79	60.9	-	0.09	-	-	32.47	0.85	2.52	8.34	1.1	87.07	-	0.11	-	-
		M33	0.92	5.15	18.86	1.5	30.67	0.2	1.61	-	-	41.09	1.52	9.74	40.34	2.1	43.85	0.51	1.94	-	-
		M34	1.3	2.7	8.9	31.52	4.78	8.91	0.44	-	-	41.46	2.16	5.11	19.03	44.1	6.83	22.24	0.52	-	-
P0	405 - 425	M35	2.84	5.43	12.53	23.49	13.22	2.59	-	-	-	39.91	4.71	10.27	26.81	32.86	18.9	6.46	-	-	-
		M36	0.75	2.65	8.98	29.37	12.12	6.45	-	-	-	39.67	1.25	5.01	19.2	41.1	17.33	16.11	-	-	-
		M37	1.82	2.55	2.75	21.5	38.7	0.31	0.06	-	-	32.3	3.03	4.82	5.89	30.08	55.34	0.78	0.07	-	-
		M38	2.71	1.08	16.58	19.59	21.05	0.12	0.16	-	-	38.71	4.5	2.04	35.46	27.41	30.09	0.3	0.2	-	-
P0	500 - 505	M39	2.4	3.02	4.56	23.7	32.74	0.17	0.12	-	-	33.28	3.98	5.71	9.76	33.17	46.8	0.43	0.15	-	-
		M40	4	8.27	15.79	20.38	7.38	1.49	0.98	-	-	41.71	6.63	15.62	33.77	28.52	10.56	3.72	1.18	-	-
		M41	0.98	2.34	5.37	44.77	9.65	2.15	0.54	-	-	34.19	1.63	4.41	11.5	62.64	13.8	5.36	0.65	-	-
		M42	1.12	4	8.21	28.68	10.56	7.07	0.12	-	-	40.24	1.86	7.56	17.56	40.12	15.1	17.65	0.14	-	-

Appendix B - Tables

Table B.40. Results of SEM-EDX investigations after CO₂ injection

Sample	Depth [cm]	Label	Element content [wt.-%]								Oxide contents [wt.-%]										
			Mg	Al	Si	Ca	Fe	S	K	Na	Ti	O	MgO	Al ₂ O ₃	SiO ₂	CaO	Fe ₂ O ₃	SO ₃	K ₂ O	Na ₂ O	TiO ₂
P1	340 - 357	M1	1.98	4.6	10.97	18.01	14.54	7.05	0.8	-	-	42.05	3.28	8.69	23.47	25.2	20.79	17.61	0.96	-	-
		M2	0.22	0.56	45.48	0.36	0.46	-	0.1	-	-	52.82	0.36	1.06	97.3	0.5	0.65	-	0.12	-	-
		M3	6.38	5.03	2.86	8.22	42.53	0.3	0.06	0.49	-	34.13	10.58	9.5	6.13	11.5	60.81	0.76	0.08	0.66	-
		quartz																			
		M5	2.03	5.86	21.88	10.56	12.87	0.07	2.93	0.82	0.46	42.52	3.37	11.06	46.81	14.77	18.41	0.18	-	1.1	0.77
P3	95 - 120	M1	2.06	6.2	18.55	16.68	13.68	-	1.1	0.12	0.47	41.13	3.42	11.72	39.69	23.34	19.56	-	1.32	0.16	0.78
		M2	0.93	11.99	27.25	4.95	4.16	--	0.63	0.38	2.01	47.69	1.54	22.66	58.29	6.93	5.95	-	0.76	0.51	3.35
		M3	3.95	6.51	15.36	21.02	10.7	0.87	0.47	0.31	0.25	40.56	6.55	12.3	32.86	29.41	15.3	2.18	0.57	0.42	0.42
		M4	0.54	0.44	42.1	3.15	1.65	0.56	0.05	-	-	51.52	0.89	0.83	90.07	4.4	2.35	1.4	0.06	-	-
		M5	1.71	7.87	4.27	28.7	21.39	0.63	0.08	0.33	0.18	34.84	2.84	14.88	9.14	40.15	30.58	1.57	0.1	0.44	0.3
P3	120 - 140	M6	0.67	15.94	25.43	3.1	4.04	-	2.61	0.18	0.51	47.51	1.11	30.12	54.41	4.33	5.78	-	3.14	0.25	0.85
		M7	0.97	1.15	1.8	18.73	46.12	-	-	0.01	0.12	31.09	1.61	2.17	3.85	26.21	65.94	-	--	0.02	0.2
		M8	0.14	0.47	45.38	0.19	0.72	-	0.08	0.12	0.14	52.76	0.23	0.88	97.09	0.26	1.03	-	0.09	0.16	0.24
		M9	1.05	11.12	22.76	7.52	7.17	-	2.45	0.14	2.78	45.01	1.75	21.02	48.69	10.52	10.25	-	2.95	0.18	4.64
P3	320 - 330	M10	3.24	1.49	2.17	31.09	29.77	0.18	0.16	-	0.28	31.62	5.37	2.82	4.63	43.49	42.56	0.45	0.2	-	0.47
		M11	2.37	2.08	2.34	15.34	45.44	-	0.36	0.02	0.14	31.91	3.94	3.94	5.02	21.46	64.96	-	0.43	0.02	0.23
		M12	0.52	15.84	26.69	0.75	4.57	-	3.12	-	0.46	48.05	0.85	29.94	57.1	1.05	6.53	-	3.76	-	0.77
		M13	0.09	0.55	44.94	0.76	0.43	0.15	-	0.37	0.07	52.64	0.16	1.05	96.15	1.06	0.61	0.37	-	0.5	0.11
		M14	1.24	4.31	17.51	8.19	27.78	-	0.63	0.29	-	40.04	2.06	8.15	37.46	11.46	39.72	-	0.76	0.39	-
P3	340 - 366	M15	1.66	6.63	5.99	28.31	22.13	0.06	0.16	0.24		34.83	2.76	12.52	12.81	39.62	31.64	0.15	0.19	0.32	-
		carbon																			
		M16	-	0.02	46.07	0.12	0.44	-	-	0.09	0.29	52.97	-	0.04	98.55	0.17	0.63	-	-	0.12	0.49
		M17																			
		M18																			
		M19	1.18	8.49	20.08	5.45	10.25	4.97	1.82	0.32	1.05	46.4	1.95	16.03	42.95	7.62	14.66	12.42	2.19	0.43	1.75
		M20	1.29	10.28	21.41	6.05	11.73	-	2.92	0.12	2.23	43.97	2.13	19.42	45.8	8.47	16.77	-	3.51	0.17	3.72

Sample	Depth [cm]	Label	Element content [wt.-%]										Oxide contents [wt.-%]									
			Mg	Al	Si	Ca	Fe	S	K	Na	Ti	O	MgO	Al ₂ O ₃	SiO ₂	CaO	Fe ₂ O ₃	SO ₃	K ₂ O	Na ₂ O	TiO ₂	
P3	620 - 640	M22	1.11	4.67	7.55	22.72	27.81	0.19	0.4	0.5	-	35.05	1.84	8.82	16.16	31.79	39.76	0.48	0.48	0.67	-	-
		M23	1.4	10.62	13.8	4.67	26.2	0.13	2.15	-	0.7	40.32	2.33	20.07	29.52	6.53	37.46	0.33	2.59	-	1.16	
		M24	0.99	13.89	23.18	4.14	5.92	0.5	2.66	0.07	2.25	46.42	1.63	26.24	49.59	5.79	8.46	1.25	3.2	0.09	3.76	
		M25	2.21	6.02	15	8.2	27	0.71	0.61	0.2	-	40.04	3.67	11.38	32.09	11.47	38.61	1.78	0.73	0.27	-	
		M26	0.44	6.9	20.58	12.16	10.97	-	6.18	0.24	1.03	41.49	0.73	13.04	44.04	17.02	15.69	-	7.44	0.32	1.72	
		M27	0.78	3.92	15.66	23.04	14.39	-	0.37	-	2.73	39.12	1.29	7.4	33.5	32.24	20.57	-	0.44	-	4.56	
		M28	0.5	0.81	43.44	1.86	1.1	-	0.24	-	0.15	51.9	0.83	1.53	92.93	2.6	1.57	-	0.29	-	0.26	
		M29	1.75	6.08	10.21	26.07	14.06	2.31	0.86	0.02	0.22	38.42	2.9	11.48	21.84	36.48	20.1	5.76	1.04	0.03	0.37	
P3	736 - 760	M30	0.32	0.69	1.67	0.48	64.91	-	0.23	0.61	-	31.08	0.53	1.3	3.58	0.68	92.8	-	0.28	0.83	-	
		M31	1.94	3.92	17.23	20.66	15.32	-	0.43	-	0.72	39.79	3.21	7.41	36.86	28.91	21.9	-	0.52	-	1.2	
		M32	0.11	-	46.41	-	0.26	-	-	0.13	-	53.1	0.18	-	99.28	-	0.38	-	-	0.17	-	
		M33	0.48	13.06	27.57	1.85	4.39	-	3.93	0.2	1.01	47.51	0.8	24.68	58.97	2.59	6.27	-	4.74	0.27	1.68	
		M34	carbon																			

Appendix B - Tables

Table B.41. Content of polycyclic aromatic hydrocarbons of the drilling cores before and after CO₂ injection [µg/kg]

Labeling	Nap	2-MNap	1-MNap	Any	Ace	Fln	Phe	Ant	Fth	Py	BaA	Chr	Bbf-BkF	BaP	Indeno	DahA	BghiP	Sum
TUBAF-1	2151	920	462	26	51	14	214	32	59	58	16	16	9	3.7	0.9	0.3	1.0	4035
TUBAF-2	2484	607	343	109	54	71	678	144	209	197	53	61	32	11.8	2.0	1.1	3.4	5061
TUBAF-3	802	217	116	17	23	14	143	24	42	42	10	11	7	2.5	0.6	< 0.2	0.7	1471
TUBAF-4	1029	270	154	43	29	36	301	62	112	138	25	26	17	6.9	1.7	0.7	3.5	2255
TUBAF-5	1181	305	168	35	31	25	229	39	75	73	15	17	11	3.8	1.1	0.4	1.6	2212
TUBAF-6	1373	373	214	39	37	35	243	43	74	73	15	18	12	3.5	1.4	0.4	1.4	2557
Nap	Naphthalin		Ace	Acenaphthen		Fth	Fluoranthen			Bbf-BkF	Benzo(b)fluoranthen / Benzo(k)fluoranthen							
2-MNap	2-Methylnaphthalin		Fln	Fluoren		Py	Pyren			BaP	Benzo(a)pyren							
1-MNap	1-Methylnaphthalin		Phe	Phenanthren		BaA	Benzo(a)anthracen			Indeno	Indeno(1.2.3-cd)pyren							
Any	Acenaphthylen		Ant	Anthracen		Chr	Chrysene			DahA	Dibenz(a,h)anthracen							
BghiP	Benzo(g.h.i)perylene																	

APPENDIX C: Matlab© Scripts

Executable Scripts

Hydro_topo.m

```

close all, clc, clear all;

%=====
% EXECUTABLE SCRIPT
% This script plots the surface of the lake.
%=====

%% Input
surface_height = 108.3; % height of the lake surface in m
resampling = 20; % resampling of the areal grid, use every X'th pixel of the map
app_medfilt = 1; % apply median filter in case of unexpected gaps in the plot

show_grid = 1; % 0=none, 1=lines, 2=dots
alpha_face = 0.75; % transparency of the bounding areas of the 3D block
% range: 0...1
ambient_strength = 0.4; % strength of the ambient light source
% range: 0...1

saveimage = 0; % save the plot to an image file

% =====

%% Load files
load_mapfile;
load_topofile;

%% Generate the 2D grid
[XI,YI] = meshgrid(xvec',yvec');

%% Compute topography
fprintf('Computing topography.\n\n');
warning off;

% convert heights to depths
topo_z = surface_height - topo_h;

% expand topography to the edges of the model area
nxv = length(xvec);
nyv = length(yvec);
topo_rw = [topo_rw; xvec'; ones(nyv,1)*xvec(1);...
           xvec'; ones(nyv,1)*xvec(end)];
topo_hw = [topo_hw; ones(nxv,1)*yvec(1); yvec';...
           ones(nxv,1)*yvec(1); yvec'];
topo_z = [topo_z; zeros(2*nxv+2*nyv,1)];

% interpolate data to the 2D grid
[XI,YI,TOPO] = griddata(topo_rw, topo_hw, topo_z,XI,YI,'cubic');
ibad = find(TOPO < min(topo_z));
TOPO(ibad) = min(topo_z);
ibad = find(TOPO > max(topo_z));
TOPO(ibad) = max(topo_z);
if app_medfilt
    TOPO = medfilt2D(TOPO,5);

```

```

end

% apply mask to topography
imapbad = find(MAP(:,:,1) > 128);
TOPO(imapbad) = 0;

warning on;

%% Plot topography
if ishandle(31),close(31);end
figure(31);

xvec = linspace(map_xmin, map_xmax, xpix);
yvec = linspace(map_ymin, map_ymax, ypix);

minx = min(xvec);
miny = min(yvec);
XI2 = XI - minx;
YI2 = YI - miny;
dx = xvec(end)-xvec(1);
dy = yvec(end)-yvec(1);

sh = surf(XI2,YI2,-TOPO);
fcol = [0.5 0.5 0.5];
cmap = f_colpal(2,'linear',0,256);
cmap = [[1 1 1]; cmap; fcol];
colormap(cmap);
ch = f_colorbar([], 'Depth [m]',[],'top');

hold on;
box on;
grid on;

dz = abs(diff(zlim));
xlim([min(XI2(:)) max(XI2(:))]);
ylim([min(YI2(:)) max(YI2(:))]);
zlim([(min(-TOPO(:))-dz/127) 0]);
caxis([(min(-TOPO(:))-dz/127) 0]);

xlabel('Easting in m', 'fontweight','bold');
ylabel('Northing in m', 'fontweight','bold');
zlabel('Depth in m', 'fontweight','bold');

xae = xlim;
xea = fliplr(xlim);
yae = ylim;
yea = fliplr(ylim);
zae = zlim;
zea = fliplr(zlim);

fh(1) = fill3([xae xea], ones(1,4)*yae(1), [zae(1) zae(1) zae(2) zae(2)], fcol);
fh(2) = fill3([xae xea], ones(1,4)*yae(2), [zae(1) zae(1) zae(2) zae(2)], fcol);
fh(3) = fill3(ones(1,4)*xae(1), [yae yea], [zae(1) zae(1) zae(2) zae(2)], fcol);
fh(4) = fill3(ones(1,4)*xae(2), [yae yea], [zae(1) zae(1) zae(2) zae(2)], fcol);
fh(5) = fill3([xae xea], [yae(1) yae(1) yae(2) yae(2)], ones(1,4)*zae(1), fcol);

% format colors
set(sh, 'edgecolor', [0 0 0],...
    'facecolor', 'interp',...
    'FaceLighting', 'phong',...
    'AmbientStrength', ambient_strength,...
    'specularcolorreflectance', 0.2,...
    'diffusestrength', 0.25);

if show_grid==1
    set(sh, 'linestyle', '',...
        'marker','none');

```

```
elseif show_grid==2
    set(sh, 'linestyle','none',...
        'marker','.',...
        'markersize',4);
else
    set(sh, 'linestyle','none',...
        'marker','none');
end
light('Position',[1 0 0],'Style','infinite');
for n=1:length(fh)
    set(fh(n), 'facealpha', alpha_face);
end
camlight;
camlight('right');

ax = gca;
axis equal
set(ax, 'dataaspectratio', [1 1 0.02]);

% text: origin
ax0 = axes('position',[0 0 1 1], 'visible','off');
torigin = sprintf('Origin: Easting %s, Northing %s',...
    num2str(uint32(floor(minx))),num2str(uint32(floor(miny))));
text(0.07,0.02, torigin,'fontsize',10);

axes(ax);

%% save it
if saveimage
    saveas(31,'./images/hydro_topo.tiff','tiffn');
end
```

Hydro_plot_mp.m

```
close all, clc, clear all;

%=====
% EXECUTABLE SCRIPT
% This script plots the surface of the lake and the measurement profiles
% for a certain date.
%=====

%% Input
surface_height = 108.3; % height of the water surface above sea level in m
resampling = 10; % resampling of the areal grid, grid spacing in m
app_medfilt = 1; % apply median filter in case of unexpected gaps in the plot
show_topo = 2; % 0: none 1: transparent surface 2: transparent grid
show_grid = 1; % 0: no 1: yes
alpha_face = 0.75; % transparency of the bounding areas of the 3D block
    % range: 0...1
ambient_strength = 0.4; % strength of the ambient light source
    % range: 0...1

saveimage = 0; % save the plot to an image file

%=====

%% Load files
load_datafiles;
load_coordfile;
load_mapfile;
load_topofile;

%% plot map and measuring points
plot_map;

%% Generate the 2D grid
[XI,YI] = meshgrid(xvec',yvec');
zvec = 0.5:0.5:surface_height-topo_h;
NY = length(yvec);
NX = length(xvec);
NZ = length(zvec);

%% Compute topography
fprintf('Computing topography.\n\n');
warning off;

% convert heights to depths
topo_z = surface_height - topo_h;

% expand topography to the edges of the model area
nxv = length(xvec);
nyv = length(yvec);
topo_rw = [topo_rw; xvec'; ones(nyv,1)*xvec(1);...
           xvec'; ones(nyv,1)*xvec(end)];
topo_hw = [topo_hw; ones(nxv,1)*yvec(1); yvec';...
           ones(nxv,1)*yvec(1); yvec'];
topo_z = [topo_z; zeros(2*nxv+2*nyv,1)];

% interpolate data to the 2D grid
[XI,YI,TOPO] = griddata(topo_rw, topo_hw, topo_z,XI,YI,'cubic');
ibad = find(TOPO < min(topo_z));
TOPO(ibad) = min(topo_z);
ibad = find(TOPO > max(topo_z));
TOPO(ibad) = max(topo_z);
if app_medfilt
```

```

TOPO = medfilt2D(TOPO,5);
end

% apply mask to topography
imapbad = find(MAP(:,:,1) > 128);
TOPO(imapbad) = 0;

warning on;

%% Plot topography
if ishandle(51),close(51);end
figure(51);

xvec = linspace(map_xmin, map_xmax, xpix);
yvec = linspace(map_ymin, map_ymax, ypix);

minx = min(xvec);
miny = min(yvec);
XI2 = XI - minx;
YI2 = YI - miny;
xvec = xvec - minx;
yvec = yvec - miny;
dx = xvec(end)-xvec(1);
dy = yvec(end)-yvec(1);

sh = surf(XI2,YI2,-TOPO);
fcol = [0.5 0.5 0.5];
cmap = f_colpal(2,'linear',0,256);
cmap = [[1 1 1]; cmap; fcol];
colormap(cmap);

hold on;
box on;
grid on;

dz = abs(diff(zlim));
xlim([min(XI2(:)) max(XI2(:))]);
ylim([min(YI2(:)) max(YI2(:))]);
zlim([(min(-TOPO(:))-dz/127) 0]);
caxis([(min(-TOPO(:))-dz/127) 0]);

xlabel('Easting in m', 'fontweight','bold');
ylabel('Northing in m', 'fontweight','bold');
zlabel('Depth in m', 'fontweight','bold');

xae = xlim;
xea = fliplr(xlim);
yae = ylim;
yea = fliplr(ylim);
zae = zlim;
zea = fliplr(zlim);

fh(1) = fill3([xae xea], ones(1,4)*yae(1), [zae(1) zae(1) zae(2) zae(2)], fcol);
fh(2) = fill3([xae xea], ones(1,4)*yae(2), [zae(1) zae(1) zae(2) zae(2)], fcol);
fh(3) = fill3(ones(1,4)*xae(1), [yae yea], [zae(1) zae(1) zae(2) zae(2)], fcol);
fh(4) = fill3(ones(1,4)*xae(2), [yae yea], [zae(1) zae(1) zae(2) zae(2)], fcol);
fh(5) = fill3([xae xea], [yae(1) yae(1) yae(2) yae(2)], ones(1,4)*zae(1), fcol);

% format colors
set(sh, 'edgecolor', [0 0 0],...
    'facecolor', 'interp',...
    'FaceLighting', 'phong',...
    'AmbientStrength', ambient_strength,...
    'specularcolorreflectance', 0.2,...
    'diffusestrength', 0.25,...
    'edgealpha', show_grid);

```

```

light('Position',[1 0 0],'Style','infinite');
for n=1:length(fh)
    set(fh(n), 'facealpha', alpha_face);
end
camlight;
camlight('right');

ax = gca;
axis equal
set(ax, 'dataaspectratio', [1 1 0.02]);

% text: origin
ax0 = axes('position',[0 0 1 1], 'visible','off');
torigin = sprintf('Origin: Easting %s, Northing %s',...
    num2str(uint32(floor(minx))),num2str(uint32(floor(miny))));
text(0.07,0.02, torigin,'fontsize',10);

drawnow;
axes(ax);

%% plot measuring points and profiles
menu(sprintf('Rotate the image to the desired\nposition and press OK.'), 'OK');

for n = 1:numfiles
    th = text(F(n).rw-minx+dx/100, F(n).hw-miny+dy/100, F(n).mp_id,...
        'horizontalalignment','left',...
        'verticalalignment','bottom',...
        'color', [1 1 0.5],...
        'clipping','off');

    mx = F(n).rw-minx;
    my = F(n).hw-miny;
    plot3([mx mx], [my my], [0 -F(n).dep100(end)],...
        'marker', 'none',...
        'linestyle', '-',...
        'linewidth', 2,...
        'color', [1 0 1]);
    plot3(mx, my, 0,...
        'marker', 'v',...
        'markerfacecolor', [1 1 0],...
        'markeredgecolor', [1 1 0],...
        'markersize', 8,...
        'color', [1 0.2 0]);
end

drawnow;

TMP = double(MAP(:,:,1));
ig = find(TMP<128);
TMP = 0*TMP;
TMP(ig) = 1;
TMP2 = 0*TMP;
for ny = 2:NY-1
    for nx = 2:NX-1
        if (TMP(ny,nx)==1)
            TMP2(ny-1:ny+1,nx-1:nx+1) = 1;
        end
    end
end
ib = find(~TMP2);
shs = surf(XI2,YI2,0*TMP2,TMP2/max(TMP2(:)));
XD = get(shs, 'xdata');
YD = get(shs, 'ydata');
XD(ib) = nan;
YD(ib) = nan;
set(shs, 'xdata', XD,...
```

```
'ydata', YD,...  
'edgecolor', 'none',...  
'facecolor', [0 0.5 1],...  
'facealpha', 0.25);  
  
clear TMP TMP2  
  
%% save it  
if saveimage  
    saveas(51,'./images/hydro_topo_mp.tiff','tiffn');  
end
```

Hydro_depth.m

```
close all, clc, clear all;

%=====
% EXECUTABLE SCRIPT
% This script creates animated 2D-plots of parameter distributions for one
% date and different depths.
%=====

%% Input
depth_min    = 0.5; % minimum depth for computation of vertical profiles
depth_spacing = 0.25; % interpolation of the profile using this spacing
plot_parameter = 2; % parameter: 1=temperature, 2=pH, 3=ORP, 4=SpCond,
                     % 5=Depth, 6=Turbidity, 7=LDO%, 8=LDO
clim         = [3 10]; % limits of the parameter range, [ ]=auto
newlabel      = ""; % replace the colorbar label by this one,
                     % ""=use the name from the excel file
surface_height = 108.9; % height of the water surface above sea level in m
resampling    = 10; % resampling of the areal grid, use every X'th pixel of the map
app_medfilt   = 1; % apply median filter in case of unexpected gaps in the plot
delay         = 0.1; % delay time in s for animated display

saveimage     = 1; % save all 2D-plots to image files
framerate    = 1; % framerate of the animated gif file (Linux only)

% =====

%% Load files
load_datafiles;
load_coordfile;
load_mapfile;
load_topofile;

%% Prepare data
preparedata;
set_labels;

%% plot map and measuring points
plot_map;

%% Generate the 2D grid
[XI,YI] = meshgrid(xvec',yvec');

%% Compute the 2D images for all depths
clear data2D;

% collect all values (measuring points) of 1 measured parameter to
% 2D matrices which belong to the same depth
izmax = length(zvec);
% loop over depths
for iz = 1:izmax
    fprintf('Computing 2D slice %d of %d.\n', iz, izmax);
    % loop over measuring points per depth
    for n=1:numfiles
        % coordinates of measuring points
        data2D.z(iz).rw(n) = F(n).rw;
        data2D.z(iz).hw(n) = F(n).hw;
        % data
        data2D.z(iz).param(n) = F(n).data_interp(iz);
    end
end
```

```

% date and units
data2D.z(iz).year = F(n).year;
data2D.z(iz).month = F(n).month;
data2D.z(iz).day = F(n).day;

% remove NaN from the data
igood = isnan(data2D.z(iz).param);
data2D.z(iz).param = data2D.z(iz).param(igood)';
data2D.z(iz).rw = data2D.z(iz).rw(igood)';
data2D.z(iz).hw = data2D.z(iz).hw(igood)';

% expand data to the edges of the model area
data2D.z(iz).rw = [data2D.z(iz).rw; [xvec(1) xvec(1) xvec(end) xvec(end)']];
data2D.z(iz).hw = [data2D.z(iz).hw; [yvec(1) yvec(end) yvec(1) yvec(end)']];
mparam = mean(data2D.z(iz).param);
data2D.z(iz).param = [data2D.z(iz).param; [mparam mparam mparam mparam]];

% interpolate data to the 2D grid
[XI,YI,ZI] = griddedInterpolant(data2D.z(iz).rw,data2D.z(iz).hw,data2D.z(iz).param,...
    XI,YI,'cubic');
data2D.z(iz).ZI = single(ZI);
end
data2D.label_unit = F(1).label_unit;
fprintf('\n');

%% Compute topography
fprintf('Computing topography.\n\n');
warning off;

% convert heights to depths
topo_z = surface_height - topo_h;

% expand topography to the edges of the model area
nxv = length(xvec);
nyv = length(yvec);
topo_rw = [topo_rw; xvec'; ones(nyv,1)*xvec(1);...
    xvec'; ones(nyv,1)*xvec(end)];
topo_hw = [topo_hw; ones(nxv,1)*yvec(1); yvec';...
    ones(nxv,1)*yvec(1); yvec'];
topo_z = [topo_z; zeros(2*nxv+2*nyv,1)];

% interpolate data to the 2D grid
[XI,YI,TOPO] = griddedInterpolant(topo_rw,topo_hw,topo_z,XI,YI,'linear');
TOPO = single(TOPO);
ibad = find(TOPO < min(topo_z));
TOPO(ibad) = min(topo_z);
ibad = find(TOPO > max(topo_z));
TOPO(ibad) = max(topo_z);
if app_medfilt
    TOPO = medfilt2D(TOPO,5);
end

% apply mask to topography
imapbad = find(MAP(:,:,1) > 128);
imapgood = find(MAP(:,:,1) < 128);
TOPO(imapbad) = nan;

warning on;

%% Apply mask (l) - map
fprintf('Applying masks to slices.\n\n');
for iz = 1:izmax
    data2D.z(iz).ZI(imapbad) = inf;
end

```

```

%% Apply mask (II) - topography
for iz = 1:izmax
    ibad = find(zvec(iz) > TOPO);
    data2D.z(iz).ZI(ibad) = -inf;
end

%% caxis limits
for iz = 1:izmax
    iok = find(isfinite(data2D.z(iz).ZI));
    if isempty(iok)
        continue
    end
    minv(iz) = min(data2D.z(iz).ZI(iok));
    maxv(iz) = max(data2D.z(iz).ZI(iok));
end
fprintf('\nMinimum and maximum values of the data:\n');
fprintf(' min = %.3e\n max = %.3e\n',min(minv), max(maxv));

if isempty(clim)
    clim = [min(minv) max(maxv)];
else
    for iz = 1:izmax
        ibad = find((data2D.z(iz).ZI < clim(1)) & isfinite(data2D.z(iz).ZI));
        data2D.z(iz).ZI(ibad) = clim(1);
        ibad = find((data2D.z(iz).ZI > clim(2)) & isfinite(data2D.z(iz).ZI));
        data2D.z(iz).ZI(ibad) = clim(2);
    end
end
dc = diff(clim);
cv = linspace(clim(1), clim(2), 254);
dcv = diff(cv(1:2));
clim = [clim(1)-dcv clim(2)+dcv];

%% 2D animation
if ishandle(2),close(2);end
figure(2);

box on;
grid on;

colours;
cmap = [[1 1 1]; cmap; [0 0 0]];

minx = min(xvec);
miny = min(yvec);
xvec = xvec - minx;
yvec = yvec - miny;
dx = xvec(end)-xvec(1);
dy = yvec(end)-yvec(1);

torigin = sprintf('Origin: Easting %s, Northing %s',...
    num2str(uint32(floor(minx))),num2str(uint32(floor(miny))));;
text(xvec(1),yvec(1)-dy/6, torigin,'fontsize',10);
hold on;

lrun = 1;
while lrun
    n = 0;
    for iz = 1:izmax
        n = n + 1;

        imagesc(xvec,yvec,data2D.z(iz).ZI);

        axis equal tight;
    end
end

```

```

set(gca, 'ydir','normal');
caxis(clim);
colormap(cmap);
ch = colorbar;
f_colorbar([],data2D.label_unit,ch,'top');

xlabel('Easting in m', 'fontweight','bold');
ylabel('Northing in m', 'fontweight','bold');
tstr = sprintf('Depth = %1.2f m, date: %d/%d/%d',zvec(iz),...
    data2D.z(iz).year,data2D.z(iz).month,data2D.z(iz).day);
title(tstr, ...
    'fontsize',12, ...
    'fontweight','bold');

pause(delay);

%-----
% save image
if saveimage
    savfig = gcf;
    drawnow;
    if n < 10
        imgfile = ['..../images/anim00' sprintf('%d',n) '.tiff'];
    elseif n < 100
        imgfile = ['..../images/anim0' sprintf('%d',n) '.tiff'];
    elseif n < 1000
        imgfile = ['..../images/anim' sprintf('%d',n) '.tiff'];
    end
    saveas(savfig,imgfile,'tiffn');
    fprintf(' Saving image: %s\n', imgfile);
end
if saveimage
    lrun = 0;
end
end

%% save it
cd('../images/');
if saveimage & isunix
    eval(['!tif2gif.sh ' num2str(izmax) '' num2str(1/framerate*100) ...
        '' num2str(1024) '' num2str(768) '' num2str(0)]);
end
cd('../matlab/');

```

Hydro_time.m

```
close all, clc, clear all;

%=====
% EXECUTABLE SCRIPT
% This script creates animated 2D-plots of parameter distributions in
% dependence of the date of measurement and for an user-defined depth.
%=====

%% Input
depth_min    = 0.5; % minimum depth for computation of vertical profiles
depth_spacing = 0.25; % interpolation of the profile using this spacing
plot_depth_2D = 14; % compute the 2D-plot for this depth in m
plot_parameter = 2; % parameter: 1=temperature, 2=pH, 3=ORP, 4=SpCond,
                     %      5=Depth, 6=Turbidity, 7=LDO%, 8=LDO
clim         = [3 10]; % limits of the parameter range, [ ]=auto
newlabel     = ""; % replace the colorbar label by this one,
                     % ""=use the name from the excel file
surface_height = 108.9; % height of the water surface above sea level in m
resampling    = 10; % resampling of the areal grid, use every X'th pixel of the map
app_medfilt   = 1; % apply median filter in case of unexpected gaps in the plot
delay         = 0.1; % delay time in s for animated display

saveimage    = 1; % save all 2D-plots to image files
framerate   = 1; % framerate of the animated gif file (Linux only)

% =====

%% Load files
load_datafiles;
load_coordfile;
load_mapfile;
load_topofile;

%% Prepare data
preparedata;
set_labels;

%% plot map and measuring points
plot_map;

%% Sort data by date. Which measuring points belong to 1 date?
sort_data_date;

%% Generate the 2D grid
[XI,YI] = meshgrid(xvec',yvec');

%% Get user-defined depth
sel_depth = round(plot_depth_2D/depth_spacing)*depth_spacing;
depth_index = find(abs(sel_depth-zvec) <= 1e-4);

%% Compute the 2D images for all times and 1 depth
clear data2D;

n = 0;
% loop over dates
for it = 1:numdates
    fprintf('\nComputing 2D slice %d of %d:\n', it, numdates);
    % loop over measurements per date
```

```

for impd = 1:mp_per_date(it)
    % file counter
    n = n + 1;
    fprintf('\tMeasuring point: %s (date: %i)\n', F(n).mp_id,mp_datevec(it));
    % coordinates of measuring points
    data2D.t(it).rw(impd) = F(n).rw;
    data2D.t(it).hw(impd) = F(n).hw;
    % data
    data2D.t(it).param(impd) = F(n).data_interp(depth_index);
end
% date and units
data2D.t(it).year = F(n).year;
data2D.t(it).month = F(n).month;
data2D.t(it).day = F(n).day;

% remove NaN from the data
igood = isnan(data2D.t(it).param);
data2D.t(it).param = data2D.t(it).param(igood)';
data2D.t(it).rw = data2D.t(it).rw(igood)';
data2D.t(it).hw = data2D.t(it).hw(igood)';

% expand data to the edges of the model area
data2D.t(it).rw = [data2D.t(it).rw; [xvec(1) xvec(1) xvec(end) xvec(end)']];
data2D.t(it).hw = [data2D.t(it).hw; [yvec(1) yvec(end) yvec(1) yvec(end)']];
mparam = mean(data2D.t(it).param);
data2D.t(it).param = [data2D.t(it).param; [mparam mparam mparam mparam]];

% interpolate data to the 2D grid
warning off
[XI,YI,ZI] = griddata(data2D.t(it).rw,data2D.t(it).hw,data2D.t(it).param,...
    XI,YI,'cubic');
warning on
data2D.t(it).ZI = single(ZI);
end
data2D.label_unit = F(1).label_unit;
fprintf('\n');

%% Compute topography
fprintf('Computing topography.\n\n');
warning off;

% convert heights to depths
topo_z = surface_height - topo_h;

% expand topography to the edges of the model area
nxv = length(xvec);
nyv = length(yvec);
topo_rw = [topo_rw; xvec'; ones(nyv,1)*xvec(1);...
    xvec'; ones(nyv,1)*xvec(end)];
topo_hw = [topo_hw; ones(nxv,1)*yvec(1); yvec';...
    ones(nxv,1)*yvec(1); yvec'];
topo_z = [topo_z; zeros(2*nxv+2*nyv,1)];

% interpolate data to the 2D grid
[XI,YI,TOPO] = griddata(topo_rw, topo_hw, topo_z,XI,YI,'linear');
TOPO = single(TOPO);
ibad = find(TOPO < min(topo_z));
TOPO(ibad) = min(topo_z);
ibad = find(TOPO > max(topo_z));
TOPO(ibad) = max(topo_z);
if app_medfilt
    TOPO = medfilt2D(TOPO,5);
end

% apply mask to topography
imapbad = find(MAP(:,:,1) > 128);

```

```

TOPO(imapbad) = nan;
warning on;

%% Apply mask (I) - map
fprintf('Applying masks to slices.\n');
for it = 1:numfiles
    data2D.t(it).ZI(imapbad) = inf;
end

%% Apply mask (II) - topography
ibad = find(zvec(depth_index) > TOPO);
for it = 1:numfiles
    data2D.t(it).ZI(ibad) = -inf;
end

%% caxis limits
for it = 1:numdates
    iok = find(isfinite(data2D.t(it).ZI));
    if isempty(iok)
        continue
    end
    minv(it) = min(data2D.t(it).ZI(iok));
    maxv(it) = max(data2D.t(it).ZI(iok));
end
fprintf('\nMinimum and maximum values of the data:\n');
fprintf(' min = %.3e\n max = %.3e\n',min(minv), max(maxv));
if isempty(clim)
    clim = [min(minv) max(maxv)];
else
    for it = 1:numdates
        ibad = find((data2D.t(it).ZI < clim(1)) & isfinite(data2D.t(it).ZI));
        data2D.t(it).ZI(ibad) = clim(1);
        ibad = find((data2D.t(it).ZI > clim(2)) & isfinite(data2D.t(it).ZI));
        data2D.t(it).ZI(ibad) = clim(2);
    end
end
dc = diff(clim);
cv = linspace(clim(1), clim(2), 254);
dcv = diff(cv(1:2));
clim = [clim(1)-dcv clim(2)+dcv];

%% 2D animation
figure(21);

box on;
grid on;

colours;
cmap = [[1 1 1]; cmap; [0 0 0]];

minx = min(xvec);
miny = min(yvec);
xvec = xvec - minx;
yvec = yvec - miny;
dx = xvec(end)-xvec(1);
dy = yvec(end)-yvec(1);

torigin = sprintf('Origin: Easting %s, Northing %s',...
    num2str(uint32(floor(minx))),num2str(uint32(floor(miny))));
text(xvec(1),yvec(1)-dy/6, torigin,'fontsize',10);
hold on;

```

```

lrun = 1;
while lrun
    n = 0;
    for it = 1:numdates
        n = n + 1;

        ih = imagesc(xvec,yvec,data2D.t(it).ZI);

        axis equal tight;
        set(gca, 'ydir','normal');
        caxis(clim);
        colormap(cmap);
        ch = colorbar;
        f_colorbar([],data2D.label_unit,ch,'top');

        xlabel('Easting in m', 'fontweight','bold');
        ylabel('Northing in m', 'fontweight','bold');
        tstr = sprintf('Depth = %1.2f m, date: %d/%d/%d',zvec(depth_index),...
            data2D.t(it).year,data2D.t(it).month,data2D.t(it).day);
        title(tstr,...
            'fontsize',12,...
            'fontweight','bold');
        hold on;

        drawnow;
        pause(delay);

        %-----
        % save image
        if saveimage
            savfig = gcf;
            drawnow;
            if n < 10
                imgfile = ['..../images/anim00' sprintf('%d',n) '.tiff'];
            elseif n < 100
                imgfile = ['..../images/anim0' sprintf('%d',n) '.tiff'];
            elseif n < 1000
                imgfile = ['..../images/anim' sprintf('%d',n) '.tiff'];
            end
            saveas(savfig,imgfile,'tiffn');
            fprintf(' Saving image: %s\n', imgfile);
        end
        if saveimage
            lrun = 0;
        end
    end

    %% save it
    cd('..../images/');
    if saveimage & isunix
        eval(['!tif2gif.sh ' num2str(numdates) '' num2str(1/framerate*100) ...
            '' num2str(1024) '' num2str(768) '' num2str(0)]);
    end
    cd('..../matlab/');

```

Hydro_surface.m

```
clear all, close all, clc;

%=====
% EXECUTABLE SCRIPT
% This script creates a 3D-plot of parameter distributions for the bottom
% of the lake.
%=====

%% Input
depth_min    = 0.5; % minimum depth for computation of vertical profiles
depth_spacing = 0.25; % interpolation of the profile using this spacing

plot_parameter = 2; % parameter: 1=temperature, 2=pH, 3=ORP, 4=SpCond,
%                   5=Depth, 6=Turbidity, 7=LDO%, 8=LDO

newlabel      = ""; % replace the colorbar label by this one,
% "use the name from the excel file
surface_height = 108.3; % height of the lake surface in m
resampling    = 10; % resampling of the areal grid, use every X'th pixel of the map
app_medfilt   = 1; % apply median filter in case of unexpected gaps in the plot
clim         = [];% limits of the parameter range, [ ]=auto

show_grid     = 1; % 0=no, 1=yes
alpha_face    = 0.75; % transparency of the bounding areas of the 3D block
% range: 0...1

saveimage     = 1; % save the plot to an image file

%=====

%% Load files
load_datafiles;
load_coordfile;
load_mapfile;
load_topofile;

%% Prepare data
preparedata;
set_labels;

%% plot map and measuring points
plot_map;

%% Generate the 2D grid
[XI,YI] = meshgrid(xvec',yvec');

%% Compute the 2D image for maximum depth
clear data2Db;

% collect all values (measuring points) of 1 measured parameter to
% 2D matrices which belong to the same depth
```

```

for n=1:numfiles
    % coordinates of measuring points
    data2Db.rw(n) = F(n).rw;
    data2Db.hw(n) = F(n).hw;
    data2Db.z(n) = F(n).dep100(end);
    data2Db.year = F(n).year;
    data2Db.month = F(n).month;
    data2Db.day = F(n).day;
    % data
    data2Db.param(n) = F(n).data(end,plot_parameter);
end
data2Db.label_unit = F(1).label_unit;

% remove NaN from the data
igood = isnan(data2Db.param);
data2Db.param = data2Db.param(igood)';
data2Db.rw = data2Db.rw(igood)';
data2Db.hw = data2Db.hw(igood)';

% expand data to the edges of the model area
data2Db.rw = [data2Db.rw; [xvec(1) xvec(1) xvec(end) xvec(end)']];
data2Db.hw = [data2Db.hw; [yvec(1) yvec(end) yvec(1) yvec(end)']];
data2Db.z = [data2Db.z [0 0 0 0]];
mparam = mean(data2Db.param);
data2Db.param = [data2Db.param; [mparam mparam mparam mparam]];

[XI,YI] = meshgrid(xvec',yvec');

% interpolate data to the 2D grid
% w = griddata3(data2Db.rw,data2Db.hw,data2Db.z,data2Db.param, ...
%                 XI,YI,ZI,'linear');
[XI,YI,ZI] = griddata(data2Db.rw,data2Db.hw,data2Db.param, ...
                      XI,YI,'linear');
data2Db.ZI = single(ZI);
fprintf('\n');

%% Compute topography
fprintf('Computing topography.\n\n');
warning off;

% convert heights to depths
topo_z = surface_height - topo_h;

% expand topography to the edges of the model area
nxv = length(xvec);
nyv = length(yvec);
topo_rw = [topo_rw; xvec'; ones(nyv,1)*xvec(1); ...
           xvec'; ones(nyv,1)*xvec(end)];
topo_hw = [topo_hw; ones(nxv,1)*yvec(1); yvec'; ...
           ones(nxv,1)*yvec(1); yvec'];
topo_z = [topo_z; zeros(2*nxv+2*nyv,1)];

% interpolate data to the 2D grid
[XI,YI,TOPO] = griddata(topo_rw,topo_hw,topo_z,XI,YI,'linear');
TOPO = single(TOPO);
ibad = find(TOPO < min(topo_z));
TOPO(ibad) = min(topo_z);

```

```

ibad = find(TOPO > max(topo_z));
TOPO(ibad) = max(topo_z);
if app_medfilt
    TOPO = medfilt2D(TOPO,5);
end

% apply mask to topography
imapbad = find(MAP(:,:,1) > 128);
TOPO(imapbad) = 0;

warning on;

%% caxis limits
iok = find(isfinite(data2Db.ZI));
minv = [];
maxv = [];
if ~isempty(iok)
    minv = min(data2Db.ZI(iok));
    maxv = max(data2Db.ZI(iok));
end
fprintf('\nMinimum and maximum values of the data:\n');
fprintf(' min = %.3e\n max = %.3e\n',minv, maxv);

if isempty(clim)
    clim = [minv maxv];
else
    ibad = find((data2Db.ZI < clim(1)) & isfinite(data2Db.ZI));
    data2Db.ZI(ibad) = clim(1);
    ibad = find((data2Db.ZI > clim(2)) & isfinite(data2Db.ZI));
    data2Db.ZI(ibad) = clim(2);
end
dc = diff(clim);
cv = linspace(clim(1), clim(2), 254);
dcv = diff(cv(1:2));
clim = [clim(1)-dcv clim(2)+dcv];

%% Apply mask (I) - map
fprintf('Applying mask to slices.\n\n');
data2Db.ZI(imapbad) = 0;

%% Surface plot 2D
if ishandle(11),close(11);end
figure(11);
hold on;

xvec = linspace(map_xmin, map_xmax, xpix);
yvec = linspace(map_ymin, map_ymax, ypix);

minx = min(xvec);
miny = min(yvec);
xvec = xvec - minx;
yvec = yvec - miny;
dx = xvec(end)-xvec(1);
dy = yvec(end)-yvec(1);

```

```

sh = imagesc(xvec,yvec,data2Db.ZI);
shading flat;
axis equal tight;

colours;
cmap = [[0 0 0]; cmap; [1 1 1]];
colormap(cmap);
ch = colorbar;
f_colorbar([],data2Db.label_unit,ch,'top');
hold on;
box on;
grid on;

torigin = sprintf('Origin: Easting %s, Northing %s',...
    num2str(uint32(floor(minx))),num2str(uint32(floor(miny)))); 
text(xvec(1),yvec(1)-dy/6, torigin,'fontsize',10);

xlabel('Easting in m', 'fontweight','bold');
ylabel('Northing in m', 'fontweight','bold');
tstr = sprintf('Lake bottom, date: %d/%d/%d',...
    data2Db.year,data2Db.month,data2Db.day);
title(tstr,'fontsize',12,'fontweight','bold');

%% Surface plot 3D
if ishandle(12),close(12);end
figure(12);

xvec = linspace(map_xmin, map_xmax, xpix);
yvec = linspace(map_ymin, map_ymax, ypix);

minx = min(xvec);
miny = min(yvec);
xvec = xvec - minx;
yvec = yvec - miny;
XI2 = XI - minx;
YI2 = YI - miny;
dx = xvec(end)-xvec(1);
dy = yvec(end)-yvec(1);

sh = surf(XI2,YI2,-TOPO,double(data2Db.ZI));

colours;
fcol = [0.5 0.5 0.5];
cmap = [fcol; cmap; [1 1 1]];
colormap(cmap);
ch = colorbar;
f_colorbar([],'pH',ch,'top');

hold on;
box on;
grid on;

dz = abs(diff(zlim));
xlim([min(XI2(:)) max(XI2(:))]);
ylim([min(YI2(:)) max(YI2(:))]);
zlim([(min(-TOPO(:))-dz/127) 0]);

```

```
xlabel('Easting in m', 'fontweight','bold');
ylabel('Northing in m', 'fontweight','bold');
zlabel('Depth in m', 'fontweight','bold');
tstr = sprintf('Lake bottom, date: %d/%d/%d',...
    data2Db.year,data2Db.month,data2Db.day);
title(tstr,'fontsize',12,'fontweight','bold');

xae = xlim;
xea = fliplr(xlim);
yae = ylim;
yea = fliplr(ylim);
zae = zlim;
zea = fliplr(zlim);

fh(1) = fill3([xae xea], ones(1,4)*yae(1), [zae(1) zae(1) zae(2) zae(2)], fcol);
fh(2) = fill3([xae xea], ones(1,4)*yae(2), [zae(1) zae(1) zae(2) zae(2)], fcol);
fh(3) = fill3(ones(1,4)*xae(1), [yae yea], [zae(1) zae(1) zae(2) zae(2)], fcol);
fh(4) = fill3(ones(1,4)*xae(2), [yae yea], [zae(1) zae(1) zae(2) zae(2)], fcol);
fh(5) = fill3([xae xea], [yae(1) yae(1) yae(2) yae(2)], ones(1,4)*zae(1), fcol);

% format colors
set(sh, 'edgecolor', [0 0 0],...
    'facecolor', 'interp',...
    'edgealpha', show_grid);
for n=1:length(fh)
    set(fh(n), 'facealpha', alpha_face);
end

ax = gca;
axis equal
set(ax, 'dataaspectratio', [1 1 0.02]);

% text: origin
ax0 = axes('position',[0 0 1 1], 'visible','off');
torigin = sprintf('Origin: Easting %s, Northing %s',...
    num2str(uint32(floor(minx))),num2str(uint32(floor(miny))));
text(0.07,0.02, torigin,'fontsize',10);

axes(ax);

%% save it
if saveimage
    saveas(gcf,'..../bilder/hydro_surface.tiff','tiffn');
end
```

Hydro_surface_time.m

```

close all, clc, clear all;

%=====
% EXECUTABLE SCRIPT
% This script creates animated 3D-plots of parameter distributions in
% dependence of the date of measurement and for the bottom of the lake.
%=====

%% Input
depth_min    = 0.5; % minimum depth for computation of vertical profiles
depth_spacing = 0.5; % interpolation of the profile using this spacing

plot_parameter = 2; % parameter: 1=temperature, 2=pH, 3=ORP, 4=SpCond,
%                      5=Depth, 6=Turbidity, 7=LDO%, 8=LDO

newlabel      = ""; % replace the colorbar label by this one,
%                      "% use the name from the excel file
surface_height = 108.3; % height of the lake surface in m
resampling    = 20; % resampling of the areal grid, use every X'th pixel of the map
app_medfilt   = 1; % apply median filter in case of unexpected gaps in the plot
clim         = []; % limits of the parameter range, [ ]=auto

show_grid     = 1; % 0=no, 1=yes
alpha_face    = 0.75; % transparency of the bounding areas of the 3D block
% range: 0...1
delay        = 0.1; % delay time in s for animated display

saveimage     = 0; % save all 3D plots to image files
framerate    = 1; % framerate of the animated gif file (Linux only)

% =====

%% Load files
load_datafiles;
load_coordfile;
load_mapfile;
load_topofile;

%% Prepare data
preparedata;
set_labels;

%% plot map and measuring points
plot_map;

%% Sort data by date. Which measuring points belong to 1 date?
sort_data_date;

%% Generate the 2D grid
[XI,YI] = meshgrid(xvec',yvec');

%% Compute the 2D images for all times and maximum depth
clear data2D;

n = 0;
% loop over dates
for it = 1:numdates
    fprintf('\nComputing 2D slice %d of %d:\n', it, numdates);
    % loop over measurements per date

```

```
for impd = 1:mp_per_date(it)
    % file counter
    n = n + 1;
    fprintf('\tMeasuring point: %s (date: %i)\n', F(n).mp_id,mp_datevec(it));
    % coordinates of measuring points
    data2D.t(it).rw(impd) = F(n).rw;
    data2D.t(it).hw(impd) = F(n).hw;
    % data
    data2D.t(it).param(impd) = F(n).data(end,plot_parameter);
end
% date and units
data2D.t(it).year = F(n).year;
data2D.t(it).month = F(n).month;
data2D.t(it).day = F(n).day;

% remove NaN from the data
igood = isnan(data2D.t(it).param);
data2D.t(it).param = data2D.t(it).param(igood)';
data2D.t(it).rw = data2D.t(it).rw(igood)';
data2D.t(it).hw = data2D.t(it).hw(igood)';

% expand data to the edges of the model area
data2D.t(it).rw = [data2D.t(it).rw; [xvec(1) xvec(1) xvec(end) xvec(end)']];
data2D.t(it).hw = [data2D.t(it).hw; [yvec(1) yvec(end) yvec(1) yvec(end)']];
mparam = mean(data2D.t(it).param);
data2D.t(it).param = [data2D.t(it).param; [mparam mparam mparam mparam]];

% interpolate data to the 2D grid
warning off
[XI,YI,ZI] = griddata(data2D.t(it).rw,data2D.t(it).hw,data2D.t(it).param,...
    XI,YI,'cubic');
warning on
data2D.t(it).ZI = single(ZI);
end
data2D.label_unit = F(1).label_unit;
fprintf('\n');

%% Compute topography
fprintf('Computing topography.\n\n');
warning off;

% convert heights to depths
topo_z = surface_height - topo_h;

% expand topography to the edges of the model area
nxv = length(xvec);
nyv = length(yvec);
topo_rw = [topo_rw; xvec'; ones(nyv,1)*xvec(1);...
    xvec'; ones(nyv,1)*xvec(end)];
topo_hw = [topo_hw; ones(nxv,1)*yvec(1); yvec';...
    ones(nxv,1)*yvec(1); yvec'];
topo_z = [topo_z; zeros(2*nxv+2*nyv,1)];

% interpolate data to the 2D grid
[XI,YI,TOPO] = griddata(topo_rw, topo_hw, topo_z,XI,YI,'linear');
TOPO = single(TOPO);
ibad = find(TOPO < min(topo_z));
TOPO(ibad) = min(topo_z);
ibad = find(TOPO > max(topo_z));
TOPO(ibad) = max(topo_z);
if app_medfilt
    TOPO = medfilt2D(TOPO,5);
end

% apply mask to topography
imapbad = find(MAP(:,:,1) > 128);
```

```

TOPO(imapbad) = 0;
warning on;

%% caxis limits
for it = 1:numdates
    iok = find(isfinite(data2D.t(it).ZI));
    if isempty(iok)
        continue
    end
    minv(it) = min(data2D.t(it).ZI(iok));
    maxv(it) = max(data2D.t(it).ZI(iok));
end
fprintf('\nMinimum and maximum values of the data:\n');
fprintf(' min = %.3e\n max = %.3e\n',min(minv), max(maxv));
if isempty(clim)
    clim = [min(minv) max(maxv)];
else
    for it = 1:numdates
        ibad = find((data2D.t(it).ZI < clim(1)) & isfinite(data2D.t(it).ZI));
        data2D.t(it).ZI(ibad) = clim(1);
        ibad = find((data2D.t(it).ZI > clim(2)) & isfinite(data2D.t(it).ZI));
        data2D.t(it).ZI(ibad) = clim(2);
    end
    dc = diff(clim);
    cv = linspace(clim(1), clim(2), 254);
    dcv = diff(cv(1:2));
    clim = [clim(1)-dcv clim(2)+dcv];
end
dc = diff(clim);
cv = linspace(clim(1), clim(2), 254);
dcv = diff(cv(1:2));
clim = [clim(1)-dcv clim(2)+dcv];

%% Apply mask (l) - map
fprintf('Applying mask to slices.\n\n');
for it = 1:numfiles
    data2D.t(it).ZI(imapbad) = 0;
end

%% 3D animation
if ishandle(41),close(41);end
figure(41);

box on;
grid on;

xvec = linspace(map_xmin, map_xmax, xpix);
yvec = linspace(map_ymin, map_ymax, ypix);
minx = min(xvec);
miny = min(yvec);
xvec = xvec - minx;
yvec = yvec - miny;
XI2 = XI - minx;
YI2 = YI - miny;
dx = xvec(end)-xvec(1);
dy = yvec(end)-yvec(1);

dz = abs(diff(zlim));
xlim([min(XI2(:)) max(XI2(:))]);
ylim([min(YI2(:)) max(YI2(:))]);
zlim([(min(-TOPO(:))-dz/127) 0]);
xae = xlim;
xeal = fliplr(xlim);
yae = ylim;
yeal = fliplr(ylim);
zae = zlim;
zeal = fliplr(zlim);

```

```

ax = gca;

% text: origin
ax0 = axes('position',[0 0 1 1], 'visible','off');
torigin = sprintf('Origin: Easting %s, Northing %s',...
    num2str(uint32(floor(minx))),num2str(uint32(floor(miny)))); 
text(0.07,0.02, torigin,'fontsize',10);

axes(ax);

lrun = 1;
while lrun
    n = 0;
    for it = 1:numdates
        n = n + 1;

        sh = surf(XI2,YI2,-TOPO,double(data2D.t(it).ZI));

        colours;
        fcol = [0.5 0.5 0.5];
        cmap = [fcol; cmap; [1 1 1]];
        colormap(cmap);
        f_colorbar([],data2D.label_unit,[],'top');
        hold on;

        xlabel('Easting in m', 'fontweight','bold');
        ylabel('Northing in m', 'fontweight','bold');
        zlabel('Depth in m', 'fontweight','bold');
        tstr = sprintf('Lake bottom, date: %d/%d/%d',...
            data2D.t(it).year,data2D.t(it).month,data2D.t(it).day);
        title(tstr,...
            'fontsize',12,...
            'fontweight','bold');

        fh(1) = fill3([xae xea], ones(1,4)*yae(1), [zae(1) zae(1) zae(2) zae(2)], fcol);
        fh(2) = fill3([xae xea], ones(1,4)*yae(2), [zae(1) zae(1) zae(2) zae(2)], fcol);
        fh(3) = fill3(ones(1,4)*xae(1), [yae yea], [zae(1) zae(1) zae(2) zae(2)], fcol);
        fh(4) = fill3(ones(1,4)*xae(2), [yae yea], [zae(1) zae(1) zae(2) zae(2)], fcol);
        fh(5) = fill3([xae xea], [yae(1) yae(2) yae(2)], ones(1,4)*zae(1), fcol);

        set(sh, 'edgecolor', [0 0 0],...
            'facecolor', 'interp',...
            'edgealpha', show_grid);
        for k=1:length(fh)
            set(fh(k), 'facealpha', alpha_face);
        end

        axis equal
        set(ax, 'dataaspectratio', [1 1 0.02]);

        if it==1 & lrun==1
            menu(sprintf('Rotate the image to the desired\nposition and press OK.'), 'OK');
        end

%-----
% save image
if saveimage
    savfig = gcf;
    drawnow;
    if n < 10
        imgfile = ['..../images/anim00' sprintf('%d',n) '.tiff'];
    elseif n < 100
        imgfile = ['..../images/anim0' sprintf('%d',n) '.tiff'];
    elseif n < 1000
        imgfile = ['..../images/anim' sprintf('%d',n) '.tiff'];
    end
end

```

```
fprintf(' Saving image: %s\n', imgfile);
saveas(savfig,imgfile,'tiffn');
end

pause(delay);
delete(fh);
delete(sh);
end
lrun = lrun + 1;
if saveimage
    lrun = 0;
end
end

%% save it
cd('../images/');
if saveimage & isunix
    eval(['!tif2gif.sh ' num2str(numdates) ' ' num2str(1/framerate*100) ...
        ' ' num2str(1024) ' ' num2str(768) ' ' num2str(0)]);
end
cd('../matlab/');
```

Hydro_slice.m

```
close all, clc, clear all;

%=====
% EXECUTABLE SCRIPT
% This script creates 3D-slices of parameter distributions across the lake
% different user-defined directions.
%=====

%% Input
% Vertical data interpolation
depth_min    = 0.5; % minimum depth for computation of vertical profiles
depth_spacing = 0.25; % interpolation of the profile using this spacing

% Slices
% type: 1=horizontal, 2=vertical (North-South), 3=vertical (East-West)
slice_type    = [1 1 1 1 2      3];
% position of the slice in m
% type=1: pos=depth, type=2: -> pos=Easting, type=3: pos=Northing
slice_pos     = [1 5 9 13 2000 1500];
show_grid     = 1; % 0: none 1: add grid to the slices

% Additional plots
show_topo     = 1; % 0: none 1: transparent surface 2: transparent grid
show_lines    = 1; % 0: none 1: auxiliary lines along the boundary of the 3D block

% Parameter:
% 1=temperature, 2=pH, 3=ORP, 4=SpCond, 5=Depth, 6=Turbidity, 7=LDO%, 8=LDO
plot_parameter = 2;

% Misc.
newlabel      = ""; % replace the colorbar label by this one,
% "use the name from the excel file
surface_height = 108.3; % height of the lake surface in m
resampling    = 10; % resampling of the areal grid, use every X'th pixel of the map
app_medfilt   = 1; % apply median filter in case of unexpected gaps in the plot
clim         = [];% limits of the parameter range, [ ]=auto

saveimage     = 1; % save the plot to an image file

% =====

%% Load files
load_datafiles;
load_coordfile;
load_mapfile;
load_topofile;

%% Prepare data
preparedata;
set_labels;

%% plot map and measuring points
plot_map;

%% Generate the 2D grid
[XI,YI] = meshgrid(xvec',yvec');
NY = length(yvec);
NX = length(xvec);
NZ = length(zvec);
```

```

%% Compute the 2D images for all depths
clear data3D;

% collect all values (measuring points) of 1 measured parameter to
% 2D matrices which belong to the same depth

% 3D matrix
data3D.D3D = single(zeros(NY,NX,NZ));
% loop over depths
for iz = 1:NZ
    fprintf('Computing 2D slice %d of %d.\n', iz, NZ);
    % loop over measuring points per depth
    for n=1:numfiles
        % coordinates of measuring points
        data3D.z(iz).rw(n) = F(n).rw;
        data3D.z(iz).hw(n) = F(n).hw;
        % data
        data3D.z(iz).param(n) = F(n).data_interp(iz);
    end

    % date and units
    data3D.z(iz).year = F(n).year;
    data3D.z(iz).month = F(n).month;
    data3D.z(iz).day = F(n).day;

    % remove NaN from the data
    igood = isnan(data3D.z(iz).param);
    data3D.z(iz).param = data3D.z(iz).param(igood)';
    data3D.z(iz).rw = data3D.z(iz).rw(igood)';
    data3D.z(iz).hw = data3D.z(iz).hw(igood)';

    % expand data to the edges of the model area
    data3D.z(iz).rw = [data3D.z(iz).rw; [xvec(1) xvec(1) xvec(end) xvec(end)']];
    data3D.z(iz).hw = [data3D.z(iz).hw; [yvec(1) yvec(end) yvec(1) yvec(end)']];
    mparam = mean(data3D.z(iz).param);
    data3D.z(iz).param = [data3D.z(iz).param; [mparam mparam mparam mparam]];

    % interpolate data to the 2D grid
    [XI,YI,ZI] = griddedInterpolant(data3D.z(iz).rw,data3D.z(iz).hw,data3D.z(iz).param,...
        XI,YI,'cubic');
    data3D.D3D(:,:,iz) = single(ZI);
end
data3D.label_unit = F(1).label_unit;
fprintf('\n');

%% Get positions of the slices
xslice = [];
yslice = [];
zslice = [];
% number of slices
numsllices = length(slice_type);
% spacings
dx = diff(xvec(1:2));
dy = diff(yvec(1:2));
dz = depth_spacing;
for isl = 1:numsllices
    slice2d(isl).type = slice_type;
    % metric position and position index of the slices
    switch slice_type(isl)
        case 1 % horizontal
            slice2d(isl).x = [];
            slice2d(isl).y = [];
            slice2d(isl).z = slice_pos(isl);

        case 2 % vertical North-South
            slice2d(isl).x = slice_pos(isl);
    end
end

```

```

slice2d(isl).y = [];
slice2d(isl).z = [];

case 3 % vertical East-West
    slice2d(isl).x = [];
    slice2d(isl).y = slice_pos(isl);
    slice2d(isl).z = [];
end

xslice = [xslice slice2d(isl).x];
yslice = [yslice slice2d(isl).y];
zslice = [zslice slice2d(isl).z];

slice_types_sort = [ones(1,length(zslice)) * 1, ...
    ones(1,length(xslice)) * 2, ...
    ones(1,length(yslice)) * 3];
end

ixslice = [];
iyslice = [];
izslice = [];

for k = 1:length(zslice)
    coord = round(zslice(k)/dz)*dz;
    izslice(k) = find(abs(coord-zvec+min(zvec)) <= 1e-4);
end
for k = 1:length(xslice)
    coord = round(xslice(k)/dx)*dx;
    ixslice(k) = find(abs(coord-xvec+min(xvec)) <= 1e-4);
end
for k = 1:length(yslice)
    coord = round(yslice(k)/dy)*dy;
    iyslice(k) = find(abs(coord-yvec+min(yvec)) <= 1e-4);
end

slice_index_sort = [izslice ixslice iyslice];

%% Compute topography
fprintf('Computing topography.\n\n');
warning off;

% convert heights to depths
topo_z = surface_height - topo_h;

% expand topography to the edges of the model area
nxv = length(xvec);
nyv = length(yvec);
topo_rw = [topo_rw; xvec'; ones(nyv,1)*xvec(1); ...
    xvec'; ones(nyv,1)*xvec(end)];
topo_hw = [topo_hw; ones(nxv,1)*yvec(1); yvec'; ...
    ones(nxv,1)*yvec(1); yvec'];
topo_z = [topo_z; zeros(2*nxv+2*nyv,1)];

% interpolate data to the 2D grid
[XI,YI,TOPO] = griddata(topo_rw, topo_hw, topo_z, XI, YI, 'linear');
TOPO = single(TOPO);
ibad = find(TOPO < min(topo_z));
TOPO(ibad) = min(topo_z);
ibad = find(TOPO > max(topo_z));
TOPO(ibad) = max(topo_z);
if app_medfilt
    TOPO = medfilt2D(TOPO,5);
end

% apply mask to topography
imapbad = find(MAP(:,:,1) > 128);

```

```

TOPO(imapbad) = 0;

TOPO3D = zeros(NY,NX,NZ);
TMP = zeros(NY,NX);
for iz = 1:NZ
    TMP = nan*TMP;
    ii = find(zvec(iz) < TOPO);
    TMP(ii) = 1;
    TOPO3D(:,:,iz) = TMP;
end

warning on;
clear TMP ii

%% 3D grid
[XI,YI,ZI] = meshgrid(xvec',yvec',zvec');

%% Apply mask (II) - topography
data3D.D3D = data3D.D3D .* TOPO3D;

%% caxis limits
if isempty(clim)
    clim = [min(data3D.D3D(:)) max(data3D.D3D(:))];
    dc = diff(clim);
    clim = [clim(1)-dc/128 clim(2)+dc/128];
end

%% Plot slices
if ishandle(41),close(41);end
figure(41);

% grid stuff
[XI,YI,ZI] = meshgrid(xvec',yvec',zvec');
minx = min(xvec);
miny = min(yvec);
XI = XI - minx;
YI = YI - miny;
dx = xvec(end)-xvec(1);
dy = yvec(end)-yvec(1);

% slices

% sha = slice(XI,YI,-ZI,double(data3D.D3D),xslice,yslice,-zslice);
m = 0;
for k = 1:length(zslice)
    m = m + 1;
    sha(m) = slice(XI,YI,-ZI,double(data3D.D3D),[],[],-zslice(k));
    if k==1
        hold on;
    end
end
for k = 1:length(xslice)
    m = m + 1;
    sha(m) = slice(XI,YI,-ZI,double(data3D.D3D),xslice(k),[],[]);
end
for k = 1:length(yslice)
    m = m + 1;
    sha(m) = slice(XI,YI,-ZI,double(data3D.D3D),[],yslice(k),[]);
end

box on;
grid on;
shading faceted;

```

```

for isl = 1:numsllices
    XD = get(sha(isl),'xdata');
    YD = get(sha(isl),'ydata');
    ZD = get(sha(isl),'zdata');

    switch slice_types_sort(isl)
        case 1
            TMP = TOPO3D(:, :, slice_index_sort(isl));
            XD = XD .* TMP;
            YD = YD .* TMP;
            ZD = ZD .* TMP;
        case 2
            TMP = squeeze(TOPO3D(:, :, slice_index_sort(isl), :));
            XD = XD .* TMP;
            YD = YD .* TMP;
            ZD = ZD .* TMP;
        case 3
            TMP = squeeze(TOPO3D(slice_index_sort(isl), :, :));
            XD = XD .* TMP;
            YD = YD .* TMP;
            ZD = ZD .* TMP;
    end

    set(sha(isl),'xdata',XD, 'ydata',YD, 'zdata',ZD, ...
        'facelighting', 'none');

    if show_grid
        set(sha(isl), 'edgecolor', [0 0 0]);
    else
        set(sha(isl), 'edgecolor', 'none');
    end
end

colours;
cmap = [[0 0 0]; cmap; [1 1 1]];
colormap(cmap);
f_colorbar([], data3D.label_unit, [], 'top');
drawnow;

% bottom of the lake
if show_topo
    [XI1, YI1] = meshgrid(xvec', yvec');
    XI1 = XI1 - minx;
    YI1 = YI1 - miny;
    shb = surf(XI1, YI1, -double(TOPO));
    drawnow;

    if show_topo==1
        set(shb,'edgecolor', 'none',...
            'facecolor', [0.3 0.3 0.3],...
            'FaceLighting', 'flat',...
            'AmbientStrength', 1,....
            'specularcolorreflectance', 1,....
            'specularexponent', 20,....
            'specularstrength', 1,....
            'diffusestrength', 0.5,....
            'facealpha', 0.25);
        light('Position',[0 -1 0], 'Style','infinite');
    elseif show_topo==2
        set(shb,'edgecolor', [0 0 0],...
            'facecolor', 'none');
    end
end

menu(sprintf('Rotate the image to the desired\nposition and press OK.'), 'OK');
if show_topo==2

```

```

    set(shb,'edgealpha', 0.1);
end

% labels etc.
xlabel('Easting in m', 'fontweight','bold');
ylabel('Northing in m', 'fontweight','bold');
zlabel('Depth in m', 'fontweight','bold');
tstr = sprintf('Parameter slices, date: %d/%d/%d',...
    data3D.z(1).year,data3D.z(1).month,data3D.z(1).day);
title(tstr,...
    'fontsize',12,...
    'fontweight','bold');

ax = gca;
axis tight

% auxiliary lines
if show_lines
    axlim = axis;
    xa = axlim(1);
    xe = axlim(2);
    ya = axlim(3);
    ye = axlim(4);
    za = axlim(5);
    ze = axlim(6);
    for isl = 1:numsllices
        switch slice_types_sort(isl)
            case 1 % horizontal
                line([xa xe xe xa xa], [ya ya ye ye ya], -slice_pos(isl)*ones(5,1),...
                    'linestyle', '--', 'color', [0 0 0]);
            case 2 % vertical North-South
                line( slice_pos(isl)*ones(5,1), [ya ye ye ya ya], [za za ze ze za],...
                    'linestyle', '--', 'color', [0 0 0]);
            case 3 % vertical East-West
                line([xa xe xe xa xa], slice_pos(isl)*ones(5,1), [za za ze ze za],...
                    'linestyle', '--', 'color', [0 0 0]);
        end
    end
end

% text: origin
ax0 = axes('position',[0 0 1 1], 'visible','off');
torigin = sprintf('Origin: Easting %s, Northing %s',...
    num2str(uint32(floor(minx))),num2str(uint32(floor(miny))));;
text(0.07,0.02, torigin,'fontsize',10);

axes(ax);

%% save it
if saveimage
    saveas(gcf,'..//images/hydro_slice_3D.tiff','tiffn');
end

```

Hydro_slice_anim.m

```
close all, clc, clear all;

%=====
% EXECUTABLE SCRIPT
% This script creates animated 3D-slices of parameter distributions across
% the lake and along a user-defined direction.
%=====

%% Input
% Vertical data interpolation
depth_min    = 0.5; % minimum depth for computation of vertical profiles
depth_spacing = 0.5; % interpolation of the profile using this spacing

% Slices
% type: 1=horizontal, 2=vertical (North-South), 3=vertical (East-West)
slice_animtype = 1;
num_sliceanim = 100; % number of slices, only vertical slices!
show_grid     = 0; % 0: none 1: add grid to the slices

% Additional plots
show_topo     = 2; % 0: none 1: transparent surface 2: grid
show_lines    = 0; % 0: none 1: auxiliary lines along the boundary of the 3D block

% Parameter:
% 1=temperature, 2=pH, 3=ORP, 4=SpCond, 5=Depth, 6=Turbidity, 7=LDO%, 8=LDO
plot_parameter = 2;

% Misc.
newlabel      = ""; % replace the colorbar label by this one,
                     % "use the name from the excel file
surface_height = 108.9; % height of the lake surface in m
resampling    = 20; % resampling of the areal grid, use every X'th pixel of the map
app_medfilt   = 1; % apply median filter in case of unexpected gaps in the plot
clim         = [];% limits of the parameter range, [ ]=auto

saveimage     = 1; % save all slices to image files
framerate    = 1; % framerate of the animated gif file (Linux only)

%=====

%% Load files
load_datafiles;
load_coordfile;
load_mapfile;
load_topofile;

%% Prepare data
preparedata;
set_labels;

%% plot map and measuring points
plot_map;

%% Generate the 2D grid
[XI,YI] = meshgrid(xvec',yvec');
NY = length(yvec);
NX = length(xvec);
NZ = length(zvec);

%% Compute the 2D images for all depths
clear data3D;
```

```
% collect all values (measuring points) of 1 measured parameter to
% 2D matrices which belong to the same depth

% 3D matrix
data3D.D3D = single(zeros(NY,NX,NZ));
% loop over depths
for iz = 1:NZ
    fprintf('Computing 2D slice %d of %d.\n', iz, NZ);
    % loop over measuring points per depth
    for n=1:numfiles
        % coordinates of measuring points
        data3D.z(iz).rw(n) = F(n).rw;
        data3D.z(iz).hw(n) = F(n).hw;
        % data
        data3D.z(iz).param(n) = F(n).data_interp(iz);
    end

    % date and units
    data3D.z(iz).year = F(n).year;
    data3D.z(iz).month = F(n).month;
    data3D.z(iz).day = F(n).day;

    % remove NaN from the data
    igood = isnan(data3D.z(iz).param);
    data3D.z(iz).param = data3D.z(iz).param(igood)';
    data3D.z(iz).rw = data3D.z(iz).rw(igood)';
    data3D.z(iz).hw = data3D.z(iz).hw(igood)';

    % expand data to the edges of the model area
    data3D.z(iz).rw = [data3D.z(iz).rw; [xvec(1) xvec(1) xvec(end) xvec(end)']];
    data3D.z(iz).hw = [data3D.z(iz).hw; [yvec(1) yvec(end) yvec(1) yvec(end)']];
    mparam = mean(data3D.z(iz).param);
    data3D.z(iz).param = [data3D.z(iz).param; [mparam mparam mparam mparam]];

    % interpolate data to the 2D grid
    [XI,YI,ZI] = griddata(data3D.z(iz).rw,data3D.z(iz).hw,data3D.z(iz).param, ...
                           XI,YI,'cubic');
    data3D.D3D(:,:,iz) = single(ZI);
end
data3D.label_unit = F(1).label_unit;
fprintf('\n');

%% Compute topography
fprintf('Computing topography.\n\n');
warning off;

% convert heights to depths
topo_z = surface_height - topo_h;

% expand topography to the edges of the model area
nxv = length(xvec);
nyv = length(yvec);
topo_rw = [topo_rw; xvec'; ones(nyv,1)*xvec(1); ...
           xvec'; ones(nyv,1)*xvec(end)];
topo_hw = [topo_hw; ones(nxv,1)*yvec(1); yvec'; ...
           ones(nxv,1)*yvec(1); yvec'];
topo_z = [topo_z; zeros(2*nxv+2*nyv,1)];

% interpolate data to the 2D grid
[XI,YI,TOPO] = griddata(topo_rw, topo_hw, topo_z,XI,YI,'linear');
TOPO = single(TOPO);
ibad = find(TOPO < min(topo_z));
TOPO(ibad) = min(topo_z);
ibad = find(TOPO > max(topo_z));
TOPO(ibad) = max(topo_z);
```

```

if app_medfilt
    TOPO = medfilt2D(TOPO,5);
end

% apply mask to topography
imapbad = find(MAP(:,:,1) > 128);
TOPO(imapbad) = 0;

TOPO3D = zeros(NY,NX,NZ);
TMP = zeros(NY,NX);
for iz = 1:NZ
    TMP = nan*TMP;
    ii = find(zvec(iz) < TOPO);
    TMP(ii) = 1;
    TOPO3D(:,:,:,iz) = TMP;
end

warning on;
clear TMP ii

%% 3D grid
[XI,YI,ZI] = meshgrid(xvec',yvec',zvec');

%% Apply mask (II) - topography
data3D.D3D = data3D.D3D .* TOPO3D;

%% caxis limits
% if isempty(clim)
%     clim = [min(data3D.D3D(:)) max(data3D.D3D(:))];
%     dc = diff(clim);
%     clim = [clim(1)-dc/128 clim(2)+dc/128];
% end

minv = min(data3D.D3D(:));
maxv = max(data3D.D3D(:));
fprintf('\nMinimum and maximum values of the data:\n');
fprintf(' min = %.3e\n max = %.3e\n',minv, maxv);
if isempty(clim)
    clim = [min(minv) max(maxv)];
else
    for it = 1:numdates
        ibad = find((data3D.D3D(:) < clim(1)));
        data3D.D3D(ibad) = clim(1);
        ibad = find((data3D.D3D(:) > clim(2)));
        data3D.D3D(ibad) = clim(2);
    end
end
dc = diff(clim);
cv = linspace(clim(1), clim(2), 254);
dcv = diff(cv(1:2));
clim = [clim(1)-dcv clim(2)+dcv];

%% Plot slices
if ishandle(41),close(41);end
figure(41);

% grid stuff
[XI,YI,ZI] = meshgrid(xvec',yvec',zvec');
minx = min(xvec);
miny = min(yvec);
XI = XI - minx;
YI = YI - miny;
xvec2 = xvec - minx;

```

```

yvec2 = yvec - miny;

% bottom of the lake
if show_topo
    [XI1,YI1] = meshgrid(xvec',yvec');
    XI1 = XI1 - minx;
    YI1 = YI1 - miny;
    shb = surf(XI1,YI1,-double(TOPO));

    if show_topo==1
        set(shb,'edgecolor', 'none',...
            'facecolor', [0.3 0.3 0.3],...
            'FaceLighting', 'flat',...
            'AmbientStrength', 1,...
            'specularcolorreflectance', 1,...
            'specularexponent', 20,...
            'specularstrength', 1,...
            'diffusestrength', 0.5,...
            'facealpha', 0.25);
        light('Position',[0 -1 0],'Style','infinite');
    elseif show_topo==2
        set(shb,'edgecolor', [0 0 0],...
            'facecolor', 'none');
    end
end
drawnow;
hold on;
grid on;
box on;

% labels etc.
xlabel('Easting in m', 'fontweight','bold');
ylabel('Northing in m', 'fontweight','bold');
zlabel('Depth in m', 'fontweight','bold');
tstr = sprintf('Parameter slices, date: %d/%d/%d',...
    data3D.z(1).year,data3D.z(1).month,data3D.z(1).day);
title(tstr, ...
    'fontsize',12, ...
    'fontweight','bold');

ax = gca;
axis tight
set(ax, 'dataaspectratio', [1 1 0.01]);

% text: origin
ax0 = axes('position',[0 0 1 1], 'visible','off');
torigin = sprintf('Origin: Easting %s, Northing %s',...
    num2str(uint32(floor(minx))),num2str(uint32(floor(miny))));;
text(0.07,0.02, torigin,'fontsize',10);

axes(ax);

axlim = axis;
xa = axlim(1);
xe = axlim(2);
ya = axlim(3);
ye = axlim(4);
za = axlim(5);
ze = axlim(6);

% spacings
dx = diff(xvec(1:2));
dy = diff(yvec(1:2));
dz = depth_spacing;

% -----
% slices

```

```
% -----
% number of slices: z: length(zvec)
%           x,y: user-defined

switch slice_animtype
    case 1
        svec = -zvec;
    case 2
        svec = linspace(xvec2(1),xvec2(end), num_sliceanim);
    case 3
        svec = linspace(yvec2(1),yvec2(end), num_sliceanim);
end

for m = 1:length(svec)
    switch slice_animtype
        case 1
            coord = round(svec(m)/dz)*dz;
            isvec(m) = find(abs(coord-svec) < dz,1);
        case 2
            coord = round(svec(m)/dx)*dx;
            isvec(m) = find(abs(coord-xvec2) < dx,1);
        case 3
            coord = round(svec(m)/dy)*dy;
            isvec(m) = find(abs(coord-yvec2) < dy,1);
    end
end

for m = 1:length(svec)
    switch slice_animtype
        case 1
            sha = slice(XI,YI,-ZI,double(data3D.D3D),[],[],svec(m));
            TMP = TOPO3D(:, :, isvec(m));
        case 2
            sha = slice(XI,YI,-ZI,double(data3D.D3D),svec(m),[],[]);
            TMP = squeeze(TOPO3D(:, :, isvec(m), :));
        case 3
            sha = slice(XI,YI,-ZI,double(data3D.D3D),[],svec(m),[]);
            TMP = squeeze(TOPO3D(isvec(m), :, :));
    end
    XD = get(sha,'xdata');
    YD = get(sha,'ydata');
    ZD = get(sha,'zdata');

    XD = XD .* TMP;
    YD = YD .* TMP;
    ZD = ZD .* TMP;

    set(sha,'xdata',XD, 'ydata',YD, 'zdata',ZD, ...
        'facelighting', 'none',...
        'facecolor', 'flat');

    if show_grid
        set(sha, 'edgecolor', [0 0 0]);
    else
        set(sha, 'edgecolor', 'none');
    end

    colours;
    cmap = [[0 0 0]; cmap; [1 1 1]];
    colormap(cmap);
    f_colorbar([],data3D.label_unit,[],'top');

    % auxiliary lines
    if show_lines
        switch slice_animtype

```

```

case 1 % horizontal
    lh = line([xa xe xe xa xa], [ya ya ye ye ya], svec(m)*ones(5,1),...
        'linestyle', '--', 'color', [0 0 0]);
case 2 % vertical North-South
    lh = line( svec(m)*ones(5,1), [ya ye ye ya ya], [za za ze ze za],...
        'linestyle', '--', 'color', [0 0 0]);
case 3 % vertical East-West
    lh = line([xa xe xe xa xa], svec(m)*ones(5,1), [za za ze ze za],...
        'linestyle', '--', 'color', [0 0 0]);
end
end

if m==1
    menu(sprintf('Rotate the image to the desired\nposition and press OK.'), 'OK');
    if show_topo==2
        set(shb,'edgealpha', 0.15);
    end
end

%-----
% save image
if saveimage
    savfig = gcf;
    drawnow;
    if m < 10
        imgfile = ['..../images/anim00' sprintf('%d',m) '.tiff'];
    elseif m < 100
        imgfile = ['..../images/anim0' sprintf('%d',m) '.tiff'];
    elseif m < 1000
        imgfile = ['..../images/anim' sprintf('%d',m) '.tiff'];
    end
    fprintf(' Saving image: %s\n', imgfile);
    saveas(savfig,imgfile,'tiffn');
end

pause(0.1);
delete(sha);
if show_lines
    delete(lh);
end
end

%% save it
cd('../images/');
if saveimage & isunix
    eval(['!tif2gif.sh ' num2str(length(svec)) ' ' num2str(1/framerate*100) ...
        ' ' num2str(1024) ' ' num2str(768) ' ' num2str(0)]);
end
cd('../matlab/');

```

AUXILIARY SCRIPTS

Load_topofile.m

```
%=====
% AUXILIARY SCRIPT
% This script loads the topography data from a text file.
%=====

% ****
% Topography
currdir = pwd;
cd('../topography');
[topofile topopath] = uigetfile({'*.txt','Text file'},...
    'Load topography',...
    'multiselect','off');
cd(currdir);

% =====
% Load files

%% Load topography and remove zero-values
[topo_rw,topo_hw,topo_h] = textread([topopath '/ topofile],...
    '%f %f %f',...
    'commentstyle', 'c++');

l1 = length(topo_h);
igood = find(topo_h>0);
topo_h = topo_h(igood);
topo_rw = topo_rw(igood);
topo_hw = topo_hw(igood);
l2 = length(topo_h);

fprintf('Topography has been loaded successfully!\n');
fprintf(' Valid data points: %d of %d\n\n', l2,l1);
pause(2);
```

Load_mapfile.m

```
%=====
% AUXILIARY SCRIPT
% This script loads the map (image file) and its coordinates ('.txt' file).
%=====

% ****
% Image file (map), coordinates of map will be loaded automatically
currdir = pwd;
cd('../map');
mapfile = uigetfile({'*.tiff;*.tif','Tiff image'},...
    'Load map',...
    'multiselect','off');
cd(currdir);

% =====
% Load files

%% Load map file and coordinates of the image
MAP = imread(['../map/' mapfile]);
MAP(:,:,1) = flipud(MAP(:,:,1));
MAP(:,:,2) = flipud(MAP(:,:,2));
MAP(:,:,3) = flipud(MAP(:,:,3));
fprintf('Map file has been loaded successfully!\n');

[map_rw,map_hw] = textread(['../map/' mapfile(1:end-3) 'txt'],...
    '%f %f',...
    'commentstyle', 'c++');

map_xmin = mean(map_rw([1 3]));
map_xmax = mean(map_rw([2 4]));
map_ymin = mean(map_hw([3 4]));
map_ymax = mean(map_hw([1 2]));

[ypix0,xpix0,col] = size(MAP);
MAP = MAP(1:resampling:end,1:resampling:end,:);
[ypix,xpix,col] = size(MAP);
xvec = linspace(map_xmin, map_xmax, xpix);
yvec = linspace(map_ymin, map_ymax, ypix);

fprintf('Coordinates of the map have been loaded successfully!\n\n');
fprintf(' Original size of the map grid: %d x %d pixels\n', ypix0, xpix0);
fprintf(' Size after resampling: %d x %d pixels\n\n', ypix, xpix);
fprintf(' Minimum and maximum Easting: %.0f, %.0f\n', map_xmin, map_xmax);
fprintf(' Minimum and maximum Northing: %.0f, %.0f\n\n', map_ymin, map_ymax);
```

Load_coordfile.m

```
%=====
% AUXILIARY SCRIPT
% This script loads the coordinates of the measuring points.
%=====

% ****
% Coordinates of measuring points
currdir = pwd;
cd('../coordinates');
geomfile = uigetfile({'*.txt'},'Load coordinates of measuring points', 'multiselect','off');
cd(currdir);

% =====
% Load files

%% Load geometry and associate coordinates to measuring points
[mp_name,hw,rw,z_grund,max_tiefe] = textread(['../coordinates/' geomfile],...
    '%s %f %f %f %f');

numgeo = length(hw);
for n = 1:numfiles
    for k = 1:numgeo
        if lower(F(n).mp_id) == lower(mp_name{k})
            F(n).hw = hw(k);
            F(n).rw = rw(k);
            F(n).z_grund = z_grund(k);
            F(n).max_tiefe = max_tiefe(k);
            break
        end
    end
end

fprintf('Coordinates of the measuring points have been loaded successfully!\n');
for n = 1:numfiles
    fprintf(' ID = %s\tNorthing = %.0f\tEasting = %.0f\n',...
        F(n).mp_id,F(n).hw,F(n).rw);
end
fprintf('\n');
```

Load_datafiles.m

```
%=====
% AUXILIARY SCRIPT
% This script loads the Excel files.
%=====

% ****
% Data
currdir = pwd;
cd('../data');
[filelist,pathname] = uigetfile({'*.xls','Excel file'},...
    'Load data',...
    'multiselect','on');

if isnumeric(filelist)
    error('No files have been selected!');
end

cd(currdir);

if iscell(filelist)
    numfiles = length(filelist);
    for n=1:numfiles
        F(n).name = filelist{n};
        F(n).path = pathname;
    end
else
    numfiles = 1;
    F(1).name = filelist;
    F(1).path = pathname;
end

% =====
% Load files
%% Load data files
warning off all;
for n=1:numfiles
    file = [F(n).path F(n).name];
    [dnum,dtxt,draw] = xlsread(file, ",",'basic');
    F(n).mp_id    = F(n).name(1:5);
    F(n).day      = str2num(F(n).name(13:14));
    F(n).month    = str2num(F(n).name(11:12));
    F(n).year     = str2num(F(n).name(7:10));
    F(n).fulldate = uint32(10000*F(n).year + 100*F(n).month + F(n).day);
    F(n).hour     = 0;
    F(n).minute   = 0;
    F(n).temp     = [draw{2:end,2}'];
    F(n).ph       = [draw{2:end,3}'];
    F(n).orp      = [draw{2:end,4}'];
    F(n).spcond   = [draw{2:end,5}'];
    F(n).turbidity = [draw{2:end,7}'];
    F(n).ldo1     = [draw{2:end,8}'];
    F(n).ldo2     = [draw{2:end,9}'];
    F(n).dep100   = [draw{2:end,6}'];
    for p = 1:8
        F(n).label_unit(p) = draw(1,p+1);
    end
    % find bad depths
    badz = find((F(n).dep100 > 1e3) | isnan(F(n).dep100));
    F(n).dep100(badz,:) = [];
    F(n).temp(badz,:)  = [];
    F(n).ph(badz,:)   = [];
    F(n).orp(badz,:)  = [];
    F(n).spcond(badz,:) = [];
    F(n).turbidity(badz,:) = [];

```

```
F(n).ldo1(badz,:)=[];  
F(n).ldo2(badz,:)=[];  
end  
warning on;  
  
% sum up all data to 1 matrix  
for n=1:numfiles  
    F(n).data = [F(n).temp F(n).ph F(n).orp F(n).spcond F(n).dep100 ...  
        F(n).turbidity F(n).ldo1 F(n).ldo2];  
end  
  
fprintf('\n%d data files have been loaded successfully!\n\n', numfiles);
```

preparedata.m

```
%=====
% AUXILIARY SCRIPT
% This script prepares the data:
% - sorting, removing duplicates and invalid values
% - computing the depth profiles for a user-defined parameter
%=====

pause(1);

%% sort data by depth
for n=1:numfiles
    [zz,idx] = sort(F(n).dep100);

    F(n).data(:, :) = F(n).data(idx,:);
    F(n).dep_sort = F(n).dep100(idx);
end

%% remove duplicates
for n=1:numfiles
    z = F(n).dep_sort;
    idx = find(z(1:end-1)==z(2:end));
    F(n).data(idx,:) = [];
    F(n).dep_sort(idx) = [];
end

%% Check if the parameter column is empty == NaN
for n=1:numfiles
    idx = find(isnan(F(n).data(:,plot_parameter)));
    if length(idx) == length(F(n).data(:,plot_parameter))
        F(n).ok = 0;
        numfiles = numfiles - 1;
    else
        F(n).ok = 1;
    end
end

n = 1;
while n <= length(F)
    if ~F(n).ok
        F(n) = [];
    end
    n = n + 1;
end

%% interpolate data along the depth profiles
fprintf('Interpolating depth profiles.\n\n');
for n=1:numfiles
    z = F(n).dep_sort;
    F(n).depth_interp = depth_min:depth_spacing:max(z);
    F(n).data_interp = zeros(length(F(n).depth_interp),1);

    F(n).data_interp(:,1) = interp1(z,F(n).data(:,plot_parameter),F(n).depth_interp,...
        'linear','extrap');
    minp = min(F(n).data(:,plot_parameter));
    maxp = max(F(n).data(:,plot_parameter));
    ibad = find(min(F(n).data_interp)<minp);
    ZI(ibad) = minp;
    ibad = find(max(F(n).data_interp)>maxp);
    ZI(ibad) = maxp;
end
```

```
%% adapt data matrices
% the length of short depth profiles will be increased to the length of the
% longest profile and filled with NaN
maxsamples = 0;
for n = 1:numfiles
    if length(F(n).depth_interp) > maxsamples
        maxsamples = length(F(n).depth_interp);
        zvec = F(n).depth_interp';
    end
end
for n = 1:numfiles
    addnan = maxsamples - length(F(n).depth_interp);
    F(n).data_interp = [F(n).data_interp; nan*zeros(addnan,1)];
    F(n).depth_interp = zvec;
end

%%
clear s addnan n maxsamples npar idx
```

sort_data_date.m

```
%=====
% AUXILIARY SCRIPT
% This script sorts the data by date of measurement.
%=====

%% Sort data in dependence of the date (for time slices)

mp_datevec = cell2mat({F(:,fulldate)})';
[ds, idx] = sort(mp_datevec);
FF = F;
F(1:numfiles) = FF(idx);

%% Which measuring points belong to 1 date?
dds = diff([0; ds]);
fds = find(dds);
mp_per_date = diff([fds; numfiles+1]);
numdates = length(mp_per_date);

mp_datevec = ds(fds);

%%%
clear idx mp_date FF fds ds dds
```

Colours.m

```
%=====
% AUXILIARY SCRIPT
% This script chooses the colormap.
%=====

%% Colormap

switch plot_parameter
    case 1
        cmap = flipud(f_colpal(19,'linear',0,254));
        colormap(cmap);
    case 2
        cmap = f_colpal(19,'linear',0,254);
        colormap(cmap);
    case 3
        cmap = f_colpal(19,'linear',0,254);
        colormap(cmap);
    case 4
        cmap = f_colpal(19,'linear',0,254);
        colormap(cmap);
    case 5
        cmap = f_colpal(19,'linear',0,254);
        colormap(cmap);
    case 6
        cmap = f_colpal(19,'linear',0,254);
        colormap(cmap);
    case 7
        cmap = f_colpal(19,'linear',0,254);
        colormap(cmap);
end

if diff(clim)==0
    clim(1) = clim(1)-0.1*clim(1);
    clim(2) = clim(2)+0.1*clim(2);
end

caxis(clim);
```

set_labels.m

```
%=====
% AUXILIARY SCRIPT
% This script creates the default labels for the colorbar.
%=====

for n = 1:numfiles
    if isempty(newlabel)
        switch plot_parameter
            case 1
                F(n).label_unit = {'T [°C]'};;
            case 2
                F(n).label_unit = {'pH'};;
            case 3
                F(n).label_unit = {'ORP [mV]'};;
            case 4
                F(n).label_unit = {'SpCond [\mu S/cm]'};;
            case 5
                F(n).label_unit = {'Depth [m]'};;
            case 6
                F(n).label_unit = {'Turbidity [NTU]'};;
            case 7
                F(n).label_unit = {'LDO% [Sat]'};;
            case 8
                F(n).label_unit = {'LDO [mg/l]'};;
        end
    else
        F(n).label_unit = {sprintf(newlabel)};
    end
end
```

Plot_map.m

```
%=====
% AUXILIARY SCRIPT
% This script plots the map of the lake incl. the measuring points.
%=====

minx = min(xvec);
miny = min(yvec);
xvec2 = xvec - minx;
yvec2 = yvec - miny;
dxx = xvec(end)-xvec(1);
dy = yvec(end)-yvec(1);

%% plot map
figure(1);
box on;

image(xvec2, yvec2, MAP);
axis equal tight;
set(gca, 'ydir','normal');
hold on;

%% plot measuring points
for n = 1:numfiles
    plot(F(n).rw-minx, F(n).hw-miny, '+', 'color', [0 1 0]);
    text(F(n).rw-minx, F(n).hw-miny, F(n).mp_id, 'color', [0 1 0],...
        'horizontalalignment','left',...
        'verticalalignment','bottom',...
        'backgroundcolor',[0 0 0.95]);
end

%% text
torigin = sprintf('Origin: Easting %s, Northing %s',...
    num2str(uint32(floor(minx))),num2str(uint32(floor(miny))));;
text(xvec2(1),yvec2(1)-dy/8, toigin,'fontsize',10);

clear minx miny xvec2 yvec2 dxx dy
```

Functions

Medfilt2D.m

```
function C = medfilt2D(A,n)

%=====
% FUNCTION
% This function applies a 2D median filter to a 2D array to remove
% artificial peaks in the interpolated data created by 'griddata'.
%=====

[ny,nx] = size(A);

nh = floor(n/2);

for n=1:nh
    A = [A(:,1) A A(:,end)];
end
for n=1:nh
    A = [A(1,:); A; A(end,:)];
end

C = 0*A;

for y = 1+nh:ny+nh
    for x = 1+nh:nx+nh
        B = A(y-nh:y+nh,x-nh:x+nh);
        igood = find(isfinite(B));
        C(y-nh:y+nh,x-nh:x+nh) = median(B(igood));
    end
end

C = C(1+nh:end-nh, 1+nh:end-nh);
```

F_colpal.m

```
function [fpal] = f_colpal(palmd,cmode,sca,ncol)

%=====
% FUNCTION
% This function computes the colormap.
%=====

% IN
% palmd ... which colormap
% cmode ... 'linear'=linear color scaling
%         'nonlin1', 'nonlin2'=nonlinear (not recommended)
% sca ..... scaling in case of nonlin1/2
% ncol .... number of colors

% OUT
% fpal ... colormap

if nargin == 1
    nonlin = 0;
end
if nargin >= 2
    switch lower(cmode)
        case 'nonlin'
            nonlin = 1;
        case 'nonlin2'
            nonlin = 2;
        otherwise
            nonlin = 0;
    end
end
if nonlin & (nargin == 2)
    sca = 1;
end
if nargin < 4
    ncol = 64;
end

switch palmd
    % pH
    case 19
        rv = [1.0 1.0 0.0 0.0 0.0];
        gv = [0.0 1.0 1.0 1.0 0.2];
        bv = [0.0 0.0 0.0 1.0 1.0];
        ci = [ 1 20 39 55 64];
    % Topography
    case 2
        rv = [0.3 0.6 0.9];
        gv = [0.2 0.4 0.9];
        bv = [0.1 0.2 0.3];
        ci = [ 1 32 64];
end

% Skalierung der Palettengröße
ci = round((ci-1)*(ncol-1)/63) + 1;

kend = length(ci)-1;
for k = 1:kend
    dr = rv(k+1) - rv(k);
    dg = gv(k+1) - gv(k);
    db = bv(k+1) - bv(k);

    civ = ci(k):ci(k+1);
    di = ci(k+1) - ci(k);
```

```

if dr == 0
    fr(civ) = rv(k);
else
    fr(civ) = rv(k):dr/di:rv(k+1);
end
fr(civ) = fr(civ);

if dg == 0
    fg(civ) = gv(k);
else
    fg(civ) = gv(k):dg/di:gv(k+1);
end
fg(civ) = fg(civ);

if db == 0
    fb(civ) = bv(k);
else
    fb(civ) = bv(k):db/di:bv(k+1);
end
fb(civ) = fb(civ);
end

fpal = [fr' fg' fb'];

lf = length(fr);

if nonlin==1 & (sca > 0)
    nold = (0:(ncol-1))';
    scal = (atan(sca))/pi*2;
    t = tan(nold/(ncol-1)*scal*pi-pi*scal/2);
    t = t - min(t);
    nvec = floor(t/max(t)*1279)+1;
    ipvec = 1:(ncol-1)/1279:ncol;
    for k = 1:3
        cc = interp1(1:lf,fpal(:,k),ipvec,'linear');
        fpnew(1:ncol,k) = cc(nvec);
    end
    fpal = fpnew;
elseif nonlin==2 & (sca > 0)
    nold = (0:(ncol-1))';
    scal = tan(sca);
    t = atan((nold/(ncol-1)-0.5)*scal);
    t = t - min(t);
    nvec = floor(t/max(t)*1279)+1;
    ipvec = 1:(ncol-1)/1279:ncol;
    for k = 1:3
        cc = interp1(1:lf,fpal(:,k),ipvec,'linear');
        fpnew(1:ncol,k) = cc(nvec);
    end
    fpal = fpnew;
end

badf = find(fpal<0);
fpal(badf) = 0;
badf = find(fpal>1);
fpal(badf) = 1;

dlmwrite('palette.asc', 255*fpal, 'precision', '%.0f', 'delimiter', ' ');

```

f_colorbar.m

```
function [cbar] = f_colorbar(cposneu,clabel,...  
    cbar,clabposv)  
  
%=====  
% FUNCTION  
% This function creates an advanced colorbar incl. label.  
%=====  
  
% =====  
if nargin < 4  
    clabposv = 'bottom';  
end  
if nargin < 3 || isempty(cbar)  
    cbar = colorbar;  
end  
if nargin < 2  
    clabel = " ";  
end  
  
% =====  
% Position  
if length(cposneu) == 4  
    cbar = colorbar;  
    cbarpos = get(cbar, 'position');  
    cposnew(1:2) = cbarpos(1:2) + cposneu(1:2);  
    cposnew(3:4) = cposneu(3:4);  
    % NaN's durch aktuellen Wert ersetzen  
    cpnan = find(isnan(cposneu));  
    cposnew(cpnan) = cbarpos(cpnan);  
    set(cbar, 'position', cposnew);  
end  
  
if nargin == 1  
    return  
end  
  
% =====  
% Label  
if ~isempty(clabel)  
    cprop = get(cbar);  
    set(cprop.XLabel,...  
        'String', clabel,...  
        'HorizontalAlignment','left',...  
        'FontWeight','bold');  
  
    set(cbar,'XAxisLocation',clabposv);  
end
```